RECENT ADVANCES IN THE TUMORIGENIC MECHANISM AND CLINICAL MANAGEMENT OF PITUITARY TUMORS

EDITED BY: Zhixiong Liu, Zhifeng Kou, Zhe Bao Wu and Qun Wu

PUBLISHED IN: Frontiers in Oncology and Frontiers in Neurology

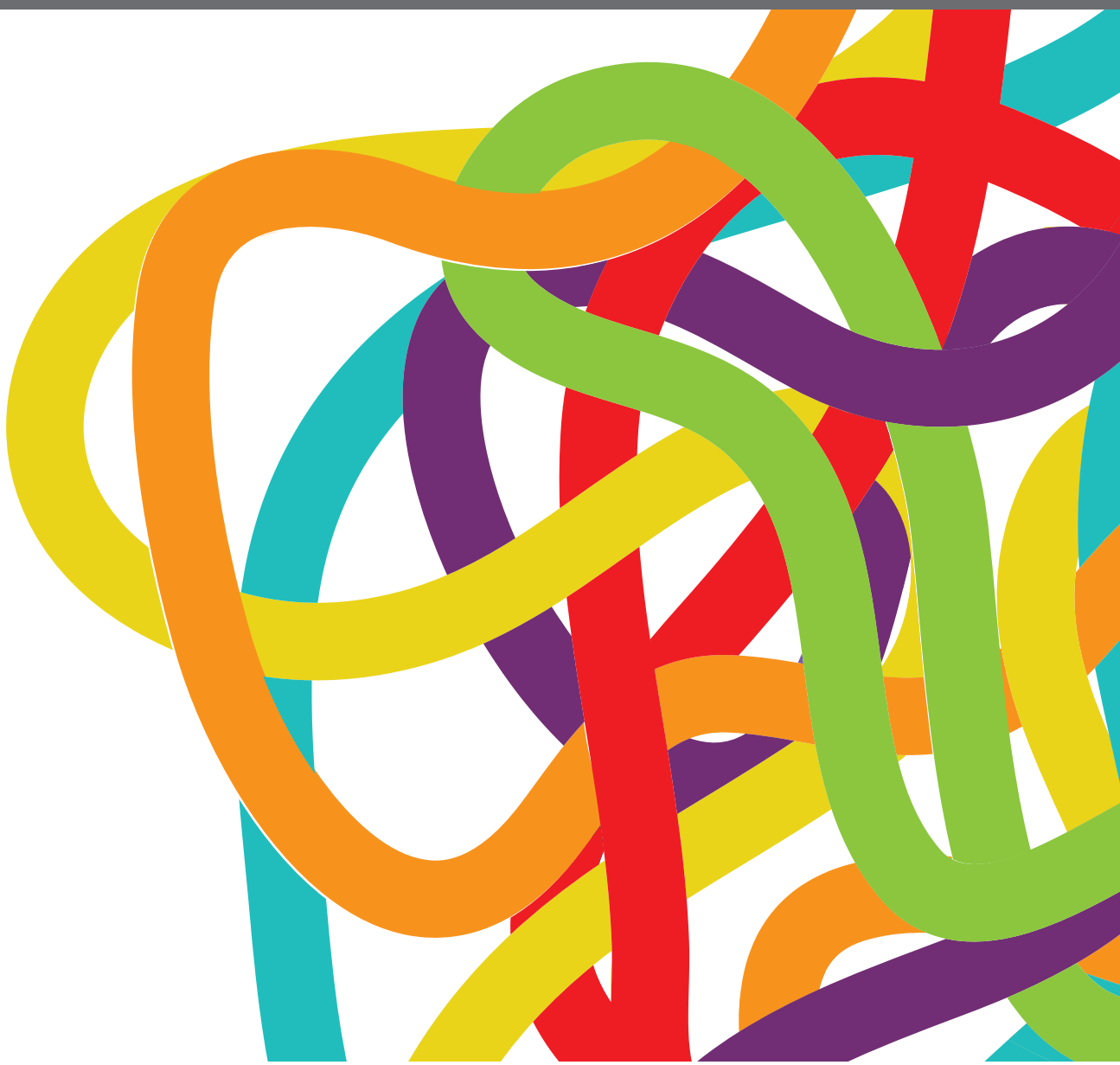

frontiers Research Topics

frontiers

ISSN 1664-8714
ISBN 978-2-88976-741-0
DOI 10.3389/978-2-88976-741-0

About Frontiers

Frontiers is more than just an open-access publisher of scholarly articles: it is a pioneering approach to the world of academia, radically improving the way scholarly research is managed. The grand vision of Frontiers is a world where all people have an equal opportunity to seek, share and generate knowledge. Frontiers provides immediate and permanent online open access to all its publications, but this alone is not enough to realize our grand goals.

Frontiers Journal Series

The Frontiers Journal Series is a multi-tier and interdisciplinary set of open-access, online journals, promising a paradigm shift from the current review, selection and dissemination processes in academic publishing. All Frontiers journals are driven by researchers for researchers; therefore, they constitute a service to the scholarly community. At the same time, the Frontiers Journal Series operates on a revolutionary invention, the tiered publishing system, initially addressing specific communities of scholars, and gradually climbing up to broader public understanding, thus serving the interests of the lay society, too.

Dedication to Quality

Each Frontiers article is a landmark of the highest quality, thanks to genuinely collaborative interactions between authors and review editors, who include some of the world's best academicians. Research must be certified by peers before entering a stream of knowledge that may eventually reach the public - and shape society; therefore, Frontiers only applies the most rigorous and unbiased reviews.
Frontiers revolutionizes research publishing by freely delivering the most outstanding research, evaluated with no bias from both the academic and social point of view. By applying the most advanced information technologies, Frontiers is catapulting scholarly publishing into a new generation.

What are Frontiers Research Topics?

Frontiers Research Topics are very popular trademarks of the Frontiers Journals Series: they are collections of at least ten articles, all centered on a particular subject. With their unique mix of varied contributions from Original Research to Review Articles, Frontiers Research Topics unify the most influential researchers, the latest key findings and historical advances in a hot research area! Find out more on how to host your own Frontiers Research Topic or contribute to one as an author by contacting the Frontiers Editorial Office: frontiersin.org/about/contact

RECENT ADVANCES IN THE TUMORIGENIC MECHANISM AND CLINICAL MANAGEMENT OF PITUITARY TUMORS

Topic Editors:
Zhixiong Liu, Central South University, China
Zhifeng Kou, Wayne State University, United States
Zhe Bao Wu, Shanghai Jiao Tong University, China
Qun Wu, Zhejiang University, China

Citation: Liu, Z., Kou, Z., Wu, Z. B., Wu, Q., eds. (2022). Recent Advances in the Tumorigenic Mechanism and Clinical Management of Pituitary Tumors. Lausanne: Frontiers Media SA. doi: 10.3389/978-2-88976-741-0

Table of Contents

frontiers in Oncology

ORIGINAL RESEARCH
published: 20 July 2021
doi: 10.3389/fonc.2021.723513

Identification of the Extradural and Intradural Extension of Pituitary Adenomas to the Suprasellar Region: Classification, Surgical Strategies, and Outcomes

*YouQing Yang†, YouYuan Bao†, ShenHao Xie†, Bin Tang, Xiao Wu, Le Yang, Jie Wu, Han Ding, ShaoYang Li, SuYue Zheng and Tao Hong**

Department of Neurosurgery, The First Affiliated Hospital of Nanchang University, Nanchang, China

OPEN ACCESS

Edited by:
Qun Wu,
Zhejiang University, China

Reviewed by:
Qingfang Sun,
Shanghai Jiao Tong University, China
Zhenyan Li,
Central South University, China
Songbai Gui,
Capital Medical University, China

****Correspondence:***
Tao Hong
ht2000@vip.sina.com

†These authors have contributed equally to this work

Specialty section:
This article was submitted to Neuro-Oncology and Neurosurgical Oncology, a section of the journal Frontiers in Oncology

Received: *10 June 2021*
Accepted: *05 July 2021*
Published: *20 July 2021*

Citation:
Yang Y, Bao Y, Xie S, Tang B, Wu X, Yang L, Wu J, Ding H, Li S, Zheng S and Hong T (2021) Identification of the Extradural and Intradural Extension of Pituitary Adenomas to the Suprasellar Region: Classification, Surgical Strategies, and Outcomes. Front. Oncol. 11:723513. doi: 10.3389/fonc.2021.723513

Objective: Suprasellar pituitary adenomas (PAs) can be located in either extradural or intradural spaces, which impacts surgical strategies and outcomes. This study determined how to distinguish these two different types of PAs and analyzed their corresponding surgical strategies and outcomes.

Methods: We retrospectively analyzed 389 patients who underwent surgery for PAs with suprasellar extension between 2016 to 2020 at our center. PAs were classified into two main grades according to tumor topography and their relationships to the diaphragm sellae (DS) and DS-attached residual pituitary gland (PG). Grade 1 tumors were located extradurally and further divided into grades 1a and 1b, while grade 2 tumors were located intradurally.

Results: Of 389 PAs, 292 (75.1%) were surrounded by a bilayer structure formed by the DS and the residual PG and classified as grade 1a, 63 (16.2%) had lobulated or daughter tumors resulting from the thinning or absence of the residual PG and subsequently rendering the bilayer weaker were classified as Grade 1b, and the remaining 34 (8.7%) PAs that broke through the DS or traversed the diaphragmic opening and encased suprasellar neurovascular structures were classified as Grade 2. We found that the gross total removal of the suprasellar part of grade 1a, 1b, and 2 PAs decreased with grading (88.4%, 71.4%, and 61.8%, respectively). The rate of major operative complications, including cerebrospinal fluid leakage, hemorrhage, and death, increased with grading.

Conclusions: It is essential to identify whether PAs with suprasellar extension are located extradurally or intradurally, which depends on whether the bilayer structure is intact. PAs with an intact bilayer structure were classified as grade 1. These were extradural and

usually had good surgical outcomes and lower complications. PAs with no bilayer structure surrounding them were classified as grade 2. These were intradural, connected to the cranial cavity, and had increased surgical complications and a lower rate of gross total removal. Different surgical strategies should be adopted for extradural and intradural PAs.

Keywords: pituitary adenoma, suprasellar extension, extradural space, intradural space, classification, diaphragma sellae

INTRODUCTION

Pituitary adenomas (PAs) account for approximately 15% of all intracranial tumors that originate in the anterior pituitary gland (1–3). As the tumor increases in size, it often grows beyond the confines of the sella turcica (4). Since the lateral and superior surfaces of the sella turcica lack bony structural support, PAs are likely to extend into the parasellar and suprasellar regions (5). In past studies, approximately 80% of the macroadenomas reported were observed to extend into the suprasellar space (6–8).

PAs that significantly extend into the suprasellar region are considered invasive on imaging (9, 10). This definition of an invasive PA, with the criteria that the tumor invades into the suprasellar region, leads to confusion in diagnosis and treatment. Some PAs that significantly extend into the suprasellar region still have a bilayer structure formed by the diaphragm sellae (DS) and the thinning residual pituitary gland after tumor removal. Thus, the tumor cavity is not connected to the intracranial cavity and it seems unreasonable to classify these as invasive PAs. Other tumors create cavities that are in direct contact with the cranial cavity after excision. These tumors often encircle vital neurovascular structures. The surgical approach to and complications of such PAs are markedly different from those with unconnected tumor cavities.

Distinguishing between the two types of PA with differential suprasellar extension (SSE) is crucial to surgical strategy, though there is currently no method to distinguish between them.

There is also still no convincing theory on how PAs extend into the suprasellar space. Some suggest that they extend through the large diaphragmatic opening (5, 11) but fail to explain how an intact DS and DS-attached residual pituitary gland can still be visible without cerebrospinal fluid (CSF) leakage after tumor resection.

The purpose of this study was to determine how to objectively identify these two different forms of PA, their differential extension into the suprasellar region, and their corresponding surgical strategies, and to present our hypotheses on how the adenomas extend into the suprasellar space.

MATERIALS AND METHODS

Patient Selection

Included in this study were 389 patients with PAs with SSE who underwent tumor removal surgery performed by lead investigator, Hong Tao, M.D. between 2016 and 2020. Patients with recurrent tumors were excluded to avoid confounding bias. Patients without preoperative magnetic resonance imaging (MRI) or with PAs lacking SSE were also excluded.

This retrospective study was approved by the University of Nanchang Institutional Review Board. Clinical and pathological characteristics were obtained from the institutional database and medical records. All patients routinely underwent endocrine and ophthalmic examinations just before surgery and 7 days post-surgery.

MRI Evaluation and Tumor Classification

An MRI was performed on each patient just before surgery and 3 days post-surgery using a standard 3.0-T scanner. Two independent neurosurgeons classified the adenomas with guidance from senior professors (T.H. and B.T.); any divergence was discussed and resolved.

Tumors were classified into two main grades based on the configuration of the suprasellar portion of the tumor and its relationship to the DS, DS-attached residual pituitary gland, and major intracranial neurovascular structure. Grade 1a: PAs presented as "inflated balloons" with expansive growth toward the suprasellar region and pushed the DS and DS-attached residual pituitary gland (**Figure 1A**). The suprasellar aspects of the tumors were regularly shaped and smooth with clear borders. A thick, uneven layer of residual pituitary was often observed below the DS. The arteries of the circle of Willis were located at the edge of these tumors and still outside the DS. Grade 1b: The suprasellar portion of the adenomas had an asymmetrically lobulated appearance, with clear borders (**Figure 1B**). 1b tumors elevated the DS and its attached residual pituitary gland. In some areas beneath the DS, the residual pituitary gland was flattened by the tumor, causing an extremely thin or even absent pituitary, leading to the formation of a daughter tumor, as if a tire had thinned and formed a bulb. Blood vessels were also often located at the edges of the tumor and still outside the DS. Grade 2: The tumor broke through the DS growing into the suprasellar region. These tumors grew along the suprasellar cistern and encircled the neurovascular structures (**Figure 1C**). In these tumors, the shape of the suprasellar adenoma was irregular and matched the suprasellar cistern morphology.

The extent of tumor removal was confirmed by intraoperative findings and postoperative contrast enhanced MRI acquired within 72 hours after surgery. Gross total removal (GTR) was confirmed if no suprasellar adenoma was identified by postoperative MRI, and cases in which there were any small residual tumors were classified as subtotal resection (STR).

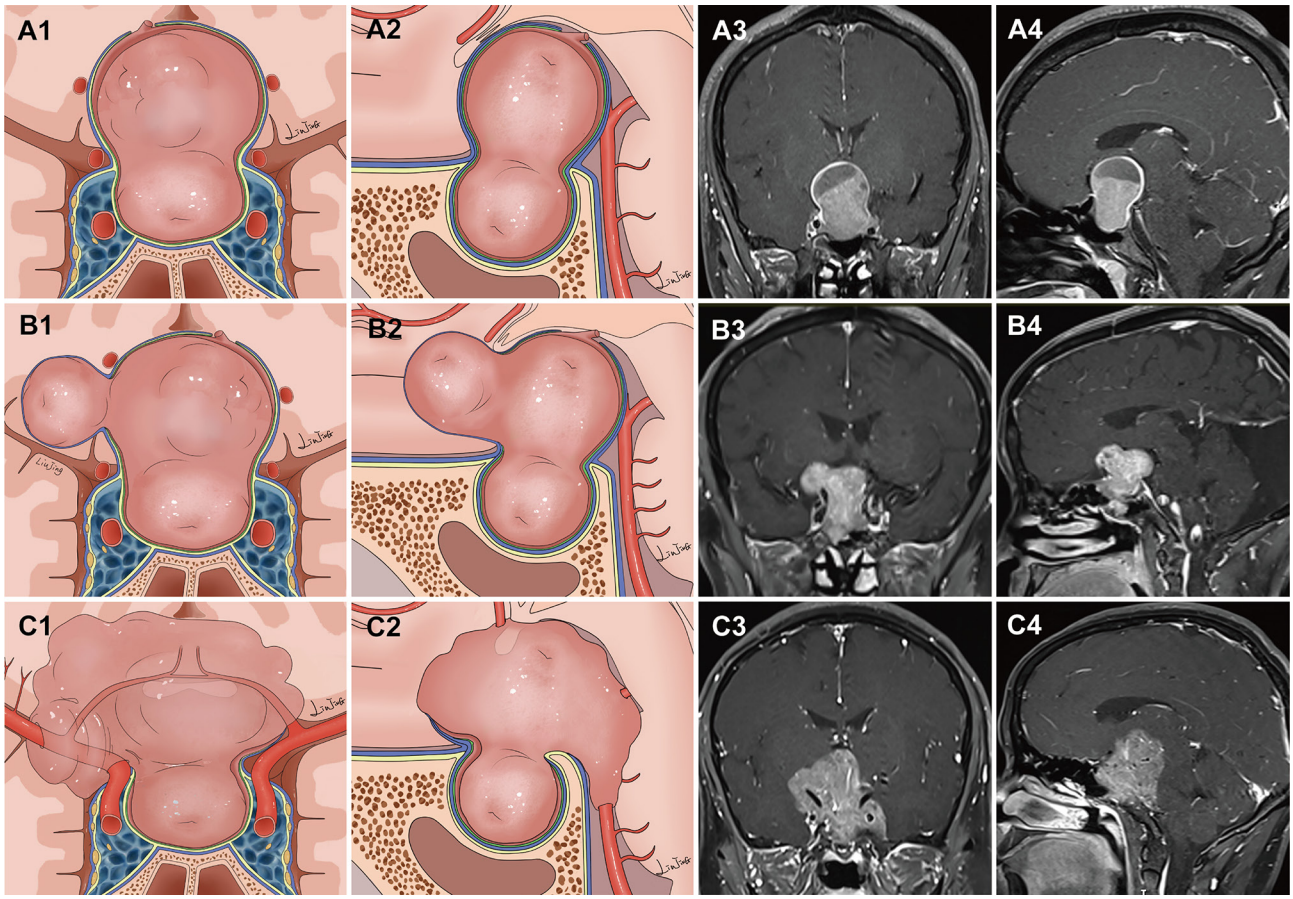

FIGURE 1 | Classification of pituitary adenomas (PAs) with suprasellar extensions (SSE). Each horizontal panel represents an illustration of coronal and sagittal sectional views, and preoperative and postoperative magnetic resonance images for each type of PA. **(A1–A4)** Grade 1a PAs presented as an "inflated balloon" with expansive growth toward the suprasellar region that pushed the DS and DS-attached residual pituitary gland. **(B1–B4)** Grade 1b PAs elevated the DS and DS-attached residual pituitary gland. In some areas beneath the DS, the residual pituitary gland was compressed by the tumor, resulting in it become extremely thin or even absent. The thinning or even absence of the residual pituitary caused the bilayer to become weaker, leading to an inability to resist the intratumoral pressure. This led to the formation of daughter tumors, like a thinning tire forming a bulge. The suprasellar portion of the PAs had an asymmetrically lobulated appearance with clear border. **(C1–C4)** Grade 2 PAs broke through the DS to reach the subarachnoid space.

Radical resection of the tumor from within the cavernous sinus was not involved as the focus of the study was on resection of suprasellar adenomas.

Surgical Approach

All patients underwent surgical treatment *via* the endoscopic endonasal approach (EEA). The expanded endoscopic endonasal approach (EEEA), transsphenoidal transtuberculum approach, is a valuable treatment option for PAs with significant SSE (12–16). However, it remains unclear how deep a tumor must extend into the suprasellar region to require EEEA. Therefore, on the mid-sagittal image, the degree of SSE (17, 18) and the maximum vertical height (H1) of the upper surface of the tumor to the line joining the inferior border of the nostril and the inferior border of the tuberculum sellae were measured (**Figure 2**). A receiver operating characteristic curve (ROC) was used to evaluate the cutoff values of SSE and H1 as predictive factors for EEEA.

Operative Technique

The standard EEA for PAs has been described previously (13, 19, 20). A 2-surgeon 4-handed technique with binostril access was employed as previously described (21, 22). Briefly, in situations where the DS descended asymmetrically, care was taken to avoid tumor residue (23). For lobulated tumors, special attention was paid to the management of the daughter tumor. Because grade 2 tumors encircled vital neurovascular structures, surgeons took particular care to avoid damaging non-tumor structures such as the perforators. After tumor removal, a multilayered reconstruction technique was performed to repair the skull base defect, as described in previous publications (24).

Statistical Analysis

Differences between groups were assessed by Chi-square analysis (or Fisher's exact test where appropriate). A p-value <0.05 was considered statistically significant by using SPSS software (SPSS

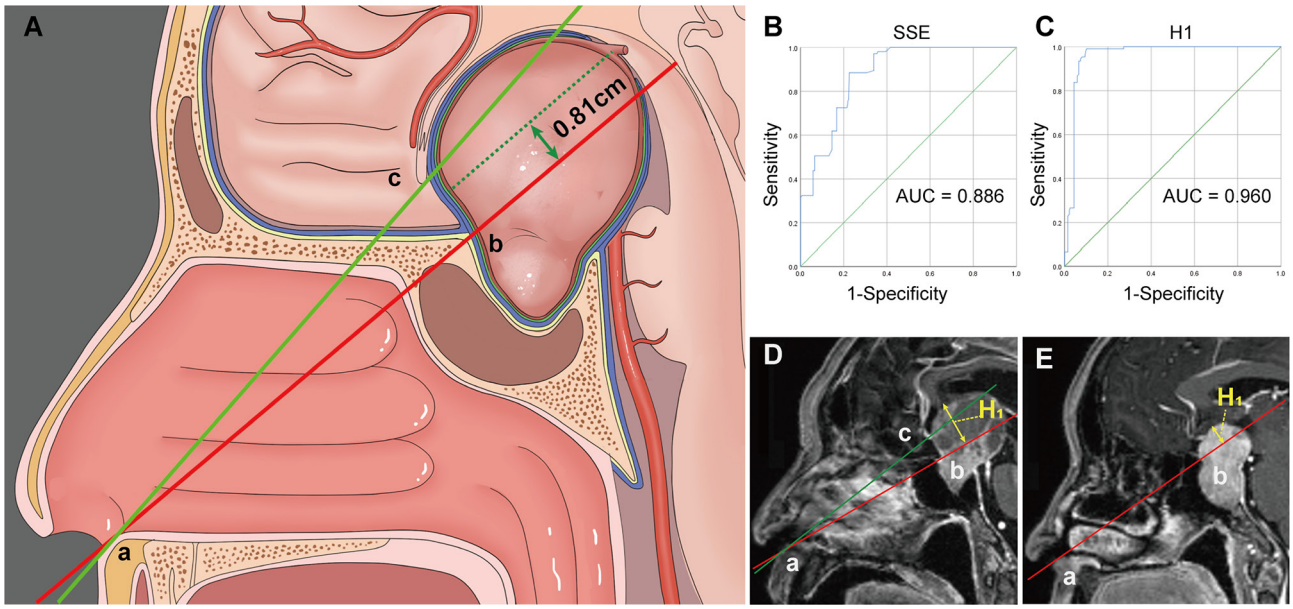

FIGURE 2 | **(A)** Illustration demonstrating the "two points and one line" method. **(B, C)** Receiver operating characteristic (ROC) curves for evaluating the predictive power of the SSE **(B)** and H1 **(C)** for the expand endoscopic endonasal approach. **(D)** The vertical height (H1) from the upper surface of the tumor to the AB line is within 8.1 mm and often a standard endoscopic endonasal approach can remove the tumor. **(E)** Tumors that exceed the AB line by 8.1 mm often require an extended endoscopic endonasal approach. Point A, the inferior border of the nostril. Point B, the inferior border of the tuberculum sellae. Point C, the inferior border of the optic chiasm. H1, the vertical height from the upper surface of the tumor to the AB line.

version 25). ROC curves were generated to determine the sensitivities and specificities of the cut-off values of H1 and SSE for the prediction of EEEA.

RESULTS

Patient Demographics, Tumor Characteristics, and Grading

There were 389 patients with PAs with SSEs who received surgical treatment. The mean age was 51.6 ± 13.1 years, and 52.2% (n = 203) of patients were male. The mean follow-up time was 16.2 months (range 3–54 months). Nonfunctioning PA was the most frequent tumor type (n=263, 67.4%). There were 52 (13.4%) growth hormone secreting adenomas, 34 (8.7%) prolactinomas, 12 (3.1%) ACTH secreting adenomas, 6 (1.5%) TSH-secreting adenomas, and 22 (5.7%) mixed adenomas. The prolactinomas in this study were treated surgically in patients who had either serious side effects or no reaction to a dopamine agonist. The most common clinical manifestations were visual complaints (n = 286, 73.5%) and headaches (n = 160, 41.1%), while 58 (14.9%) cases were asymptomatic (incidental detection). Anterior hypopituitarism was detected in 51 cases (13.1%). According to the criteria described above, there were 292 (75.1%), 63 (16.2%), and 34 (8.7%) patients with grade 1a, 1b, and 2 tumors, respectively (**Table 1**).

TABLE 1 | Patient and tumor characteristics.

Characteristic	Value
Sex, male	203(52.2%)
Age (median ± SD [range]) (yrs)	51.6 ± 13.1 (17–79)
Suprasellar extension (According to the degree of SSE) (no. [%])	389
0mm < SSE ≤ 10mm	127 (32.6%)
10mm < SSE ≤ 20mm	149 (38.3%)
20mm < SSE ≤ 30mm	74 (19.1%)
30mm < SSE	39 (10%)
Suprasellar extension (Our suprasellar grading) (no. [%])	389
Grade 1a	292 (75.1%)
Grade 1b	63 (16.2%)
Grade 2	34 (8.7%)
Pathological types	
Nonfunctional	263 (67.6%)
GH	52 (13.4%)
PRL	34 (8.7%)
ACTH	12 (3.1%)
TSH	6 (1.5%)
Mix	22 (5.7%)

SSE, suprasellar extension; PRL, prolactin; ACTH, adrenocorticotropic hormone; GH, growth hormone; TSH, thyroid stimulating hormone.

Surgical Outcomes

As this study focused on removal of suprasellar adenomas, radicality of tumor removal from within the cavernous sinus was not addressed. Based on the intraoperative assessment and postoperative MRI, GTR of the suprasellar adenoma was achieved in 258 (88.4%), 45 (71.4%) and 21 (61.8%) grade 1a, 1b, and 2 adenomas, respectively. The rate of GTR declined with increasing grade ($p < 0.05$) (**Table 2**).

Postoperative CSF leakage occurred in 13 (3.3%) patients: grade 1a, 6 (2.1%); grade 1b, 4 (6.3%); and grade 2, 3 (8.8%). The rate of CSF leakage was significantly higher in grade 2 than in grade 1a ($p < 0.05$) (**Table 2**).

For the patients with preoperative visual dysfunction, approximately 70% reported improvement after surgery. A total of 9 patients experienced worsening vision: grade 1a, 4 (1.4%); grade 1b, 2 (3.2%); and grade 2, 3 (8.8%). The rate of worsening vision was significantly higher in grade 2 than in grade 1a ($p < 0.05$) (**Table 2**).

Out of our cohort, 5 (1.7%) patients in grade 1a, 3 (4.7%) in grade 1b, and 4 (11.8%) in grade 2 experienced postoperative hematomas. There were no cases of intracranial ischemia or death in grade 1a and grade 1b tumors. Among those with grade 2 tumors, cerebral ischemia occurred in 2 cases and death occurred in 1 case.

Sensitivities and Specificities of Cut-Off Values of H1 and SSE on Sagittal Views

In our cohort, 67 (22.9%) patients in grade 1a, 19 (30.2%) in grade 1b, and 25 (73.5%) in grade 2 experienced EEEA. The ROC curves for the sagittal H1 and SSE that were used to predict the need for an EEEA are shown in **Figure 2**. The area under the curve (AUC) of the ROC curve for the sagittal SSE was 0.886 (95% CI: 0.855-0.917). When the Youden index reached a maximum, the optimal cut-off value was 17.4 mm. The AUC for H1 was 0.960 (95% CI: 0.941-0.980). We found the optimal relationship between sensitivity and specificity for EEA at the cut-off value of 8.1 mm.

DISCUSSION

PAs with significant extension into the suprasellar region are a huge challenge for neurosurgeons. Identifying whether PAs with SSE are located extradural or intradural is essential for surgical strategies and outcomes, though there is currently no method to distinguish between them. The DS is an important barrier between the intrasellar and the suprasellar region (25–27). Hence, we established a classification system that can identify these two PAs preoperatively according to tumor topography and its relationship to the DS, DS-attached residual pituitary gland, and major intracranial neurovascular structures.

Grade 1a PAs pushed and stretched the DS and the residual pituitary gland up toward the suprasellar region. Due to the restriction of the DS and DS-attached residual pituitary gland, these tumors grew expansively into the suprasellar region like an inflated balloon (**Figure 3**). The clear border and smoothly rounded superior wall of the tumors we observed suggests that the DS was intact (28). A thin, uneven layer of residual pituitary was usually observed beneath the DS (**Figure 1A3**). Intraoperatively, the intact DS and DS-attached residual pituitary gland were observed to herniate into the intrasellar space after tumor resection (**Figure 3A3**). Even in some PAs that grew significantly toward the suprasellar region, we were still able to observe an intact DS and its attached residual gland after adenomas resection (**Figure 3B3**). Therefore, we suggest that the surfaces of grade 1a suprasellar tumors are often surrounded by the DS and a thin, uneven layer of residual pituitary. The intact bilayer structure formed by the DS and the residual pituitary gland act as a barrier between the tumor and the cranial cavity, so this type of PA is located in the extradural space. Theoretically, these tumors are located in the intrasellar/subdiaphragmatic space. The bilayer structure is the key to determining whether a PA is located in the extradural or intradural region.

Compared to Grade 1a, Grade 1b PAs grew further and stretched the DS and DS- attached residual gland into the suprasellar region. The relatively thin residual pituitary gland beneath the DS was compressed and stretched so much by the tumor that it became extremely thin or even absent, leading to weakness in this area and an inability to resist the intratumoral pressure (**Figure 4**). This led to the formation of daughter tumors (**Figure 5A**). Despite being thin, the walls of the daughter tumors remained continuous with the DS. Thus, theoretically, these tumors were still located in the intrasellar/subdiaphragmatic space and classified as grade 1. When the area

TABLE 2 | Clinical outcomes in patients with suprasellar pituitary adenomas.

	Grade 1a (n = 292)	Grade 1b (n = 63)	Grade 2 (n = 34)	*p* Value
Gross total resection, n (%)	258 (88.4)	45 (71.4)	21 (61.8)	**0.004***
Visual dysfunction				
Improved, n (%)†	158 (73.4)	32 (71.1)	18 (69.2)	0.868
Unchanged, n (%)	130 (44.5)	29 (46)	12 (35.3)	0.553
Worsened, n (%)	4 (1.4)	2 (3.2)	3 (8.8)	**0.023***
Postop Endocrine				
Posterior pituitary insufficiency				
Temporary DI, n (%)	30 (10.3)	8 (12.7)	4 (11.8)	0.838
Permanent DI, n (%)	13 (4.4)	3 (4.7)	2 (5.9)	0.930
New or worse anterior pituitary insufficiency, n (%)	38 (13)	9 (14.3)	5 (14.7)	0.937
CSF leak, n (%)	6 (2.1)	4 (6.3)	3 (8.8)	**0.016***
Meningitis, n (%)	4 (1.4)	3 (4.7)	2 (5.9)	0.067
Intracranial hematoma, n (%)	5 (1.7)	3 (4.7)	4 (11.8)	**0.006***
Intracranial ischemia, n (%)	0	0	2 (5.9)	NA
Death, n (%)	0	0	1 (2.9)	NA

DI, Diabetes insipidus; CSF, Cerebrospinal fluid.
*†, % means "% of Pre-op abnormal." *p < 0.05 vs. grade 1a group.*
All the indicators (P < 0.05) are highlighted in bold values.
NA, not available.

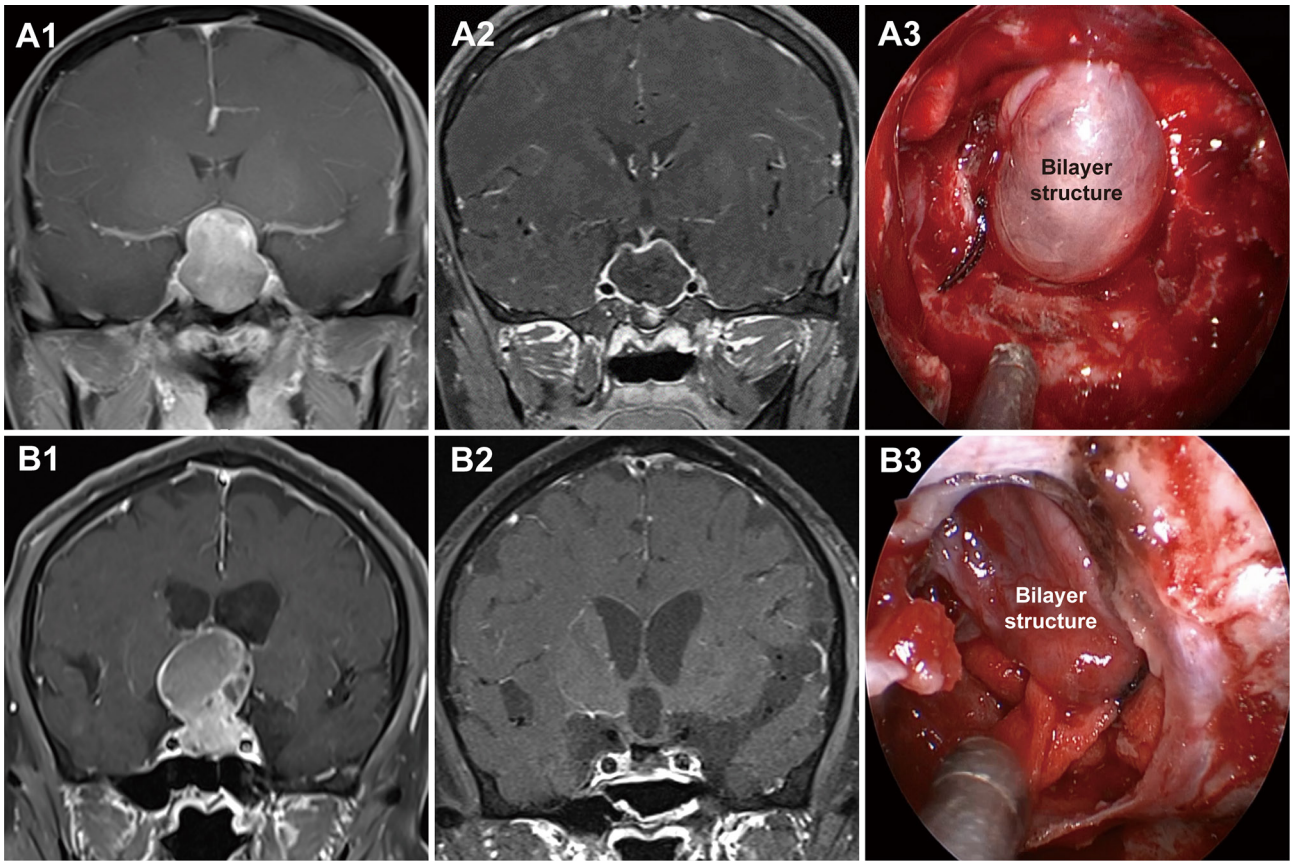

FIGURE 3 | Two cases with grade 1a pituitary adenomas (PAs). **(A1, B1)** Preoperative, coronal post-gadolinium magnetic resonance image (MRI) showing grade 1a tumor with a regular smooth shape and clear border. **(A2, B2)** Postoperative MRI showing gross total resection. **(A3, B3)** Endoscopic views showing an intact bilayer structure formed by the DS and DS-attached residual pituitary gland.

of weakness in the DS was relatively large, a wide-necked daughter tumor formed, while when the area was relatively small, a narrow-necked daughter tumor formed. Both single and multiple daughter tumors of varying sizes could be formed in the same patient. The daughter tumor could extend in the direction of the anterior cranial base, temporal lobe, and clivus (**Figures 4A1–C1**). Intraoperatively, a transparent and extremely thin wall of the daughter tumor could be observed inversely projecting into the tumor cavity forming a reverse daughter balloon after the tumor removal (**Figure 5F**), just as the DS descended into the sellar region after the tumor removal (**Figure 5**). The descending wall of reverse daughter balloon has no residual pituitary or only an extremely thin remnant pituitary attached that appears similar to the arachnoid membrane. Here, blood vessels were pushed by the tumor, and located at the tumor's edge. In some cases, blood vessels were located at the bifurcation of multiple lobulated daughter tumors, and the bifurcation covered the vessels, similar to blood vessel being encircled.

Grade 2 PAs broke through the DS or transgressed the diaphragmic opening to reach the intracranial cavity. Here, the lack of the bilayer barrier allowed the tumor to communicate directly with the cranial cavity, so this type of tumor was classified as an intradural subarachnoid tumor. Because of the lack of constraint by the bilayer, they lost their expansive growth characteristics and, like epidermoid cysts, spread along the subarachnoid space into the available space and encircled vital neurovascular structures such as the circle of Willis and its perforators, optic nerve, and optic chiasm (**Figure 6**). These tumors could even invade the floor of the third ventricle and enter the ventricular space. We have found that some PAs not extending very deep into the suprasellar cistern could also break through the DS into the intracranial cavity (**Figure 6A**). Notably, such tumors grew in grid-like structures formed by the perforating vessels (**Figure 6J**), posing a great challenge for tumor resection. These tumors could break though the Liliequist membrane and grow along the prepontine cistern into the clivus, characteristics unique to grade 2 PAs (characteristics of each grade show in **Table 3**).

Surgical approaches to resection were determined by tumor grade. Grade 1a PAs were located in the extradural/subdiaphragmatic space. The transsphenoidal approach is more appropriate for grade 1a PAs. However, we preferred EEA, owing to its advantages including wide-angle view and

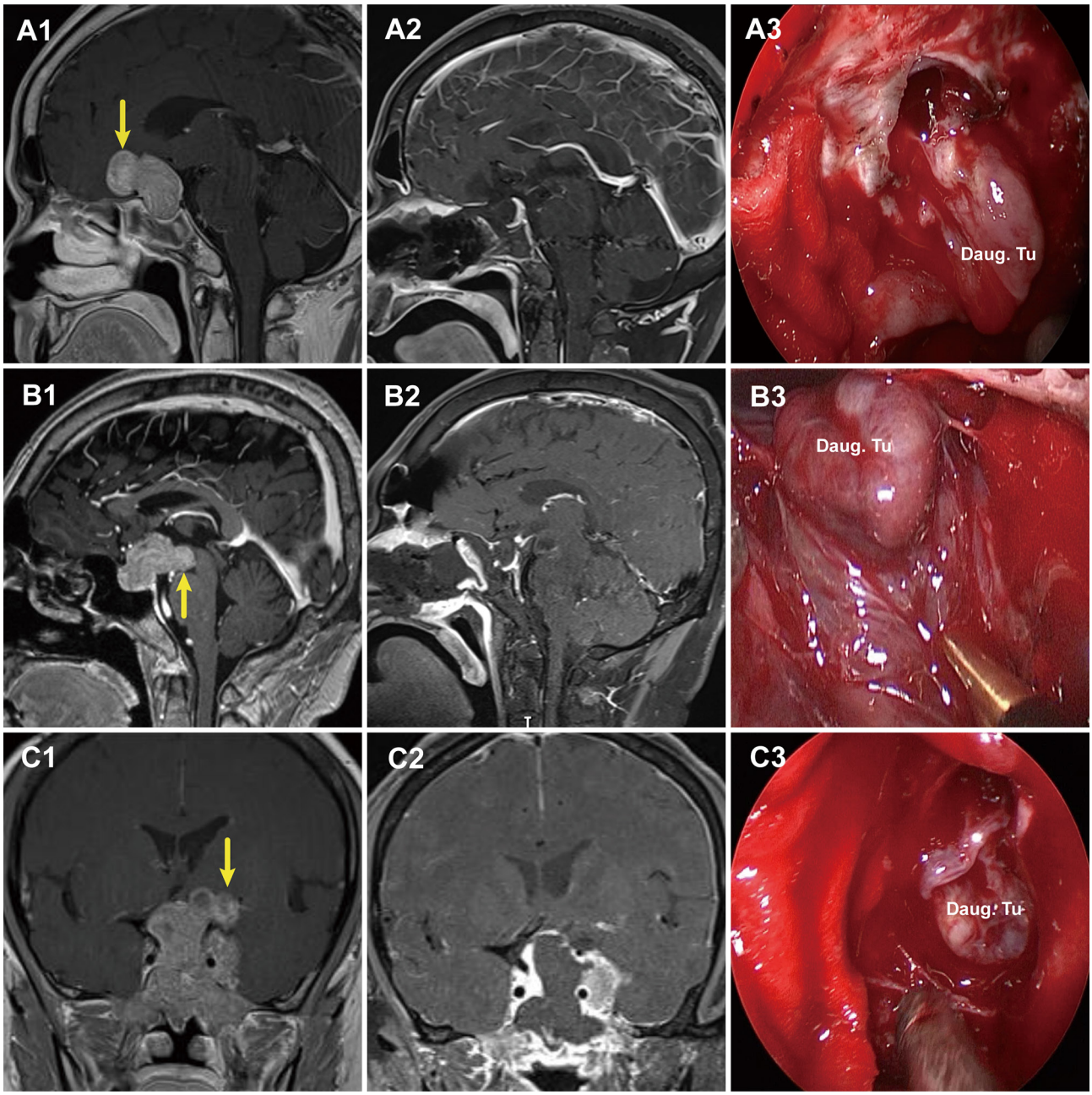

FIGURE 4 | Three cases with grade 1b PAs that underwent endoscopic endonasal surgery. **(A1, B1, C1)** Preoperative, sagittal post-gadolinium MRIs showing 3 grade 1b tumors with daughter tumor (yellow arrow) extending to the anterior skull base **(A1)**, the interpeduncular fossa **(B1)**, and the suprasellar lateral **(C1)**. **(A2, B2, C2)** Postoperative MRI demonstrating gross total resection of suprasellar part of tumor was achieved. **(A3, B3, C3)** Endoscopic views showing the intact wall of daughter tumor. Daug. Tu, daughter tumor; DS, diaphragm sellae.

elimination of brain retraction (12, 14, 29–31). Special attention should be given to protect the residual pituitary gland intraoperatively. When the residual pituitary is observed, the boundary of the tumor has been reached. If the tumor is removed and only a thin, transparent DS remains, the residual pituitary gland might have been excised. Thus, establishing the concept of a bilayer separating the cranial cavity from the tumor facilitates the protection of the residual pituitary gland. The transsphenoidal approach was also appropriate for grade 1b PAs, as they were also located in the extradural/subdiaphragmatic space. We utilized an EEA, which allowed closer visualization of the daughter tumor. Some tumor locations were difficult to reach with EEA (12, 13, 32, 33), requiring a transcranial route or transcranial combined transsphenoidal approach. For example, this approach was used

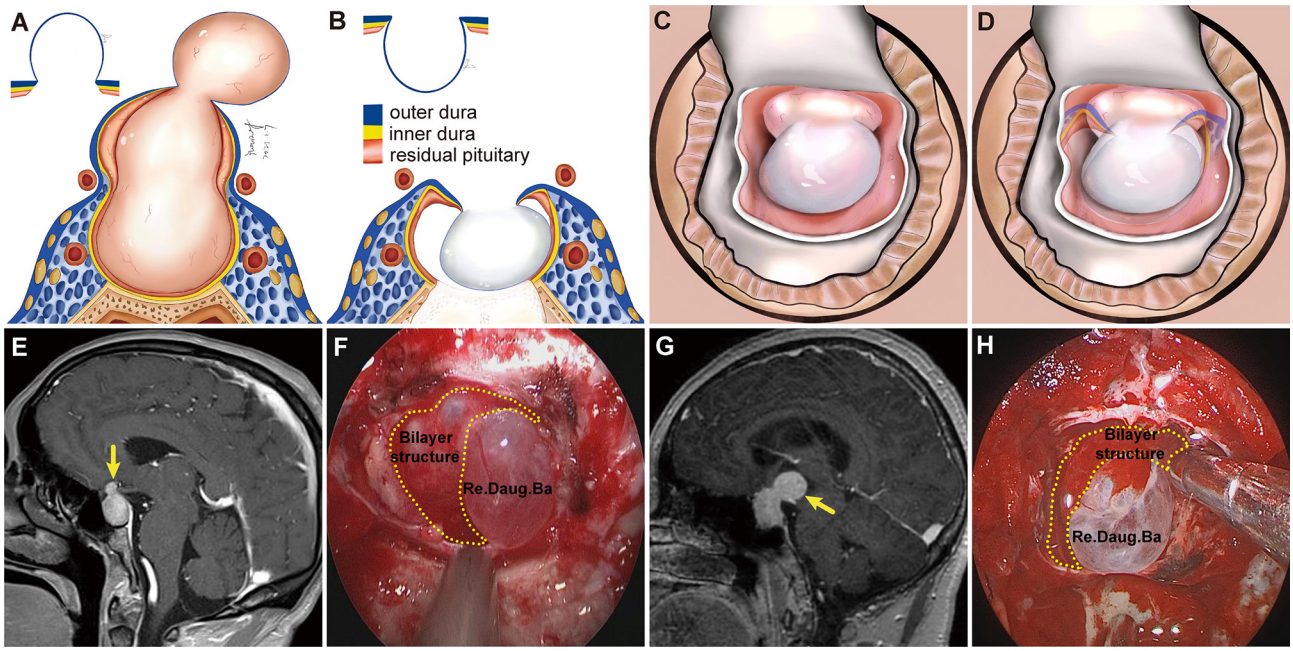

FIGURE 5 | Schemes, preoperative magnetic resonance images (MRI), and endoscopic views showing a daughter tumor and reverse daughter balloon. **(A)** Illustration of the formation of a daughter tumor. The thinning or even absence of the residual pituitary caused the bilayer to be weaker, leading to an inability to resist the intratumoral pressure. Thus, a daughter tumor formed, like a thinning tire creating a bulge. **(B, C)** Illustration of reverse daughter balloon. When the tumor was completely removed, due to the intracranial cerebrospinal fluid pressure, the thin dura on the surface of the daughter tumor inversely protruded into the tumor cavity, forming a reverse daughter balloon. Diagram **(D)** is a merge of diagrams **(B, C)**. **(E, G)** Preoperative, sagittal post-gadolinium MRI showing grade 1b tumor with a small daughter tumor extending into the suprasellar space. **(F, H)** Endoscopic view after tumor resection showing a reverse daughter balloon. Re. Daug. Ba, reverse daughter balloon.

when the daughter tumor extended from the retro-chiasmatic region to its superior anterior aspect, significantly lateral to the suprasellar cistern. Special attention should be paid to the treatment of daughter tumors intraoperatively. With EEA, when the neck of the daughter tumor was wide, the tumor could be resected along the natural corridor of the daughter tumor, using the opening of the daughter tumor as a starting point to remove the tumor within the daughter tumor. when the neck of the daughter tumor was small, the neck opening could be widened to remove the tumor within the daughter tumor. When the tumor within the daughter tumor was completely removed, because of the intracranial cerebrospinal fluid pressure, the thin dura on the surface of the daughter tumor could inversely protrude into the tumor cavity. Forming a reverse daughter balloon was a sign of complete removal of the daughter tumor.

The transsphenoidal and transcranial approaches were all very difficult for grade 2 PAs, as these tumors were located in the intradural space. These tumors grew in grid-like structures formed by the perforating vessels, and it was necessary to both remove the tumor and avoid damaging the perforators. In some patients, the third ventricle floor was compressed into a thin layer, and protection of the floor of the third ventricle is necessary to avoid damage to the hypothalamus. For these reasons, when such tumors are giant, the transcranial approach can also be an appropriate choice. When the tumor is coaxial with the transsphenoidal route, EEA may be preferred. If the tumor is giant or extends laterally to the temporal lobe with sphenoidal or cavernous sinus invasion, a combined transcranial and EEA approaches may be more appropriate.

We used the two-point-one-line method to predict the need for EEEA. Our data show that both SSE and H1 are effective predictors of the need for EEEA. The cut-off value of SSE was 17.4 mm, so Hardy's classification grades C and D may necessitate an EEEA. H1 can reflect the degree of tumor extension to the anterior skull base. We suggest that H1 is a more appropriate predictor of needing an EEEA. An EEEA is usually required for grade 1b, grade 2, and large or hard consistency grade 1a PAs.

The goal of the surgery was optic apparatus decompression and the safest possible tumor resection (32, 34). The GRT of suprasellar tumor in grade 1a PAs was higher than that of grade 1b and grade 2 tumors, due to the regular shape and the protection of the bilayer structure. Some residual tumor tended to remain in the daughter tumor, so the total resection rate was significantly lower than that of grade 1a PAs. Grade 2 tumors encircled vital blood vessels, making them more difficult to remove. Some grade 2 PAs were close to the hypothalamus, and care was taken to protect the hypothalamus and the floor of the third ventricle. These are among the reasons for incomplete resection in our series.

Severe postoperative complications, including postoperative hemorrhage, visual deterioration, cerebral infarction, and death occurred, though mostly in patients with grade 2 tumors. We

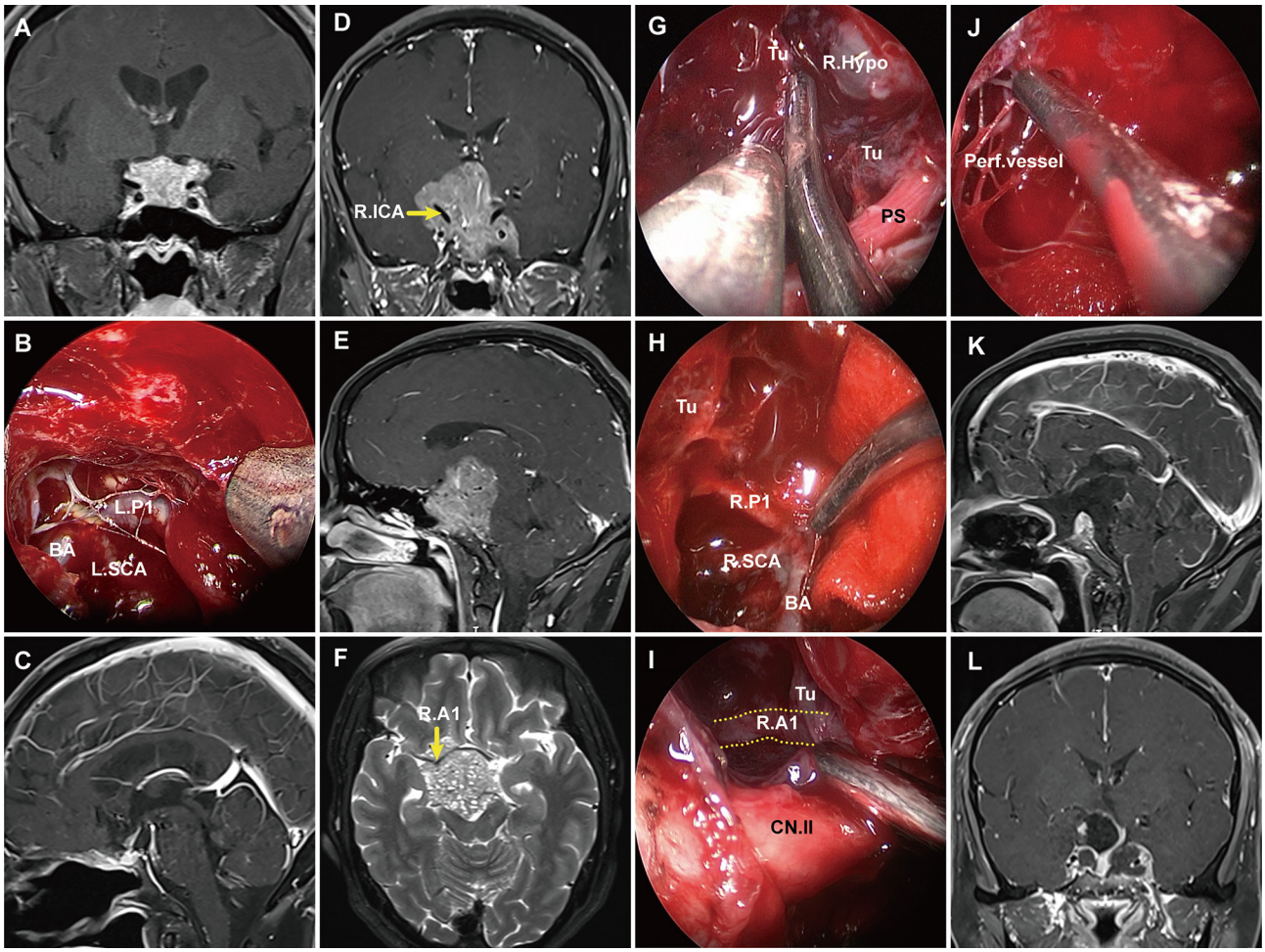

FIGURE 6 | Pre- and postoperative magnetic resonance imaging (MRI) demonstrating two cases of grade 2 pituitary adenoma. **(A)** A grade 2 PA that extended to the suprasellar region and grew along with the suprasellar cistern. **(B)** Endoscopic views showing the tumor entered into the arachnoid spaces and encased vital neurovascular structures. **(C)** postoperative MRI showing gross total resection. **(D–F)** Preoperative T1 contrast-enhanced images showing a grade 2 tumor significantly extended to the suprasellar and encircled vital neurovascular structures. **(G–J)** Endoscopic views showing the tumor entered into the suprasellar space and encased vital neurovascular structures. The tumor grew in grid-like structures formed by the perforating vessels **(J)**. **(K, L)** Postoperative T1 contrast-enhanced MRI demonstrating subtotal resection of the suprasellar component of adenoma. PS, pituitary stalk; PG, pituitary gland; Tu, tumor; R. A1, right A1 segment of anterior cerebral artery; R. P1, right P1 segment of posterior cerebral artery; SCA, superior cerebellar artery; BA, basilar artery; R. Ht, right hypothalamus.

believe that grade 2 tumors encircled vital neurovascular structures and were in close proximity to the hypothalamus, which greatly increased the chance of incidental damage during surgery. The tumors grew in the grids formed by the penetrating vessels, particularly in sites with abundant perforator vessels. Resection of tumors in these grids was prone to serious complications, such as postoperative stroke, due to damage to the perforator vessels.

The dura mater on the surface of daughter tumors was very thin and easily ruptured, potentially increasing the rate of CSF leakage. In our data, the rates of CSF leakage were higher in patients with grade 1b than grade 1a tumors, but not significantly. Since grade 2 PAs broke through the DS and extended into the subarachnoid space, the CSF leakage rate was significantly higher than that of patients with grade 1a PAs.

We suggest a possible pattern in which PAs extend into the suprasellar region. In grade 1 PAs, the tumor may originate in the lower part of the pituitary gland and push and stretch the pituitary gland and diaphragmatic dura upward into the suprasellar space. The possible patterns in which grade 2 PAs break through the DS into the suprasellar region include: (1) A grade 1b tumor further grows and traverses the extremely thin layer of the daughter tumor into the subarachnoid space. The distribution of the residual pituitary glands in grade 2 PAs formed this way are the same as that of grade 1b PAs. (2) In the early stages of PA growth, the tumor directly invades and penetrates the DS into the suprasellar region; (3) The tumor grows into the intracranial space through the loose diaphragmatic opening. For the latter two situations, the tumor may originate near the upper surface of the pituitary gland and

TABLE 3 | Characteristics and surgical strategies and outcomes of each grade.

Variable	Grade 1a	Grade 1b	Grade 2
Location	Located in extradural space	Still located in extradural space	Located in intradural space
Bilayer structure (the DS and the residual pituitary gland)	Intact	The DS was intact Thinning or absence of the residual pituitary gland in the area where the daughter tumor was formed	Lack of a bilayer structure, directly penetrate the DS or extend through the opening of DS into the suprasellar region
Location of the residual pituitary gland	The residual pituitary gland usually located on the superior and lateral surface of the tumor	The residual pituitary gland usually located on the superior and lateral surface of the tumor and was extremely thin or even absent at the site of the daughter tumor formation	The residual pituitary gland usually located on the bottom and lateral surface of the tumor
Relationship with vessels	Pushed the vessels and vessels located at the edge of the tumor and still outside the DS	Pushed the vessels and vessels located at the edge of the tumor and still outside the DS	Encircled the arteries of the circle of Willis, optic nerve, and optic chiasm
Growth pattern	"Inflatable ball" type of spherical expansion	spherical expansion, "Tire bulge"-like formation of large or small daughter balloons	Lost expansive growth characteristics and growth along with the arachnoid cistern
Morphology	A regular morphology with a smooth spherical surface	An irregularly lobulated appearance with clear border	An irregular shape, and matched the morphology of the suprasellar cistern
Surgical strategy	Preferred EEA	Preferred EEA If the daughter tumor extended from the retro-chiasmatic region to its superior anterior aspect, significantly lateral to the suprasellar cistern, a transcranial route or transcranial combined transsphenoidal approach might be required	When such tumors are giant, the transcranial approach can also be an appropriate choice. When the tumor is coaxial with the transsphenoidal route, the EEA may be preferred. If the tumor is giant or extends laterally to the temporal lobe with sphenoidal or cavernous sinus invasion, a combined transcranial and EEA approaches may be more appropriate.
Extent of resection	Higher rate of GTR relative to grade 1b and grade 2	Lower rate of GTR relative to grade 1a, residual tumors tended to remain in the daughter tumor	Lower rate of GTR relative to grade 1a
Complication	Lower	Medium, the dura mater on the surface of the daughter tumor is thin and prone to rupture leading to intraoperative CSF leakage	Higher, intraoperative CSF leak occurs 100% and is prone to serious complications such as neurovascular injury, cerebral hemorrhage, cerebral ischemia and hypothalamic injury

DS, diaphragm sellae; EEA, endoscopic endonasal approach; CSF, cerebrospinal fluid; GTR, Gross total removal.

easily transgress the DS or diaphragmatic opening. We have made these assumptions based on the location of the residual pituitary in these tumors. For example, the residual pituitary gland of grade 1 tumors tends to be located on the superior and lateral surface of the tumor. In contrast, the residual pituitary gland of grade 2 tumors (except those developed from grade 1b) tends to be located on the bottom and lateral surface of the tumor.

Goel et al. divided giant pituitary adenomas into 4 grades depending on their anatomical extensions and the nature of their meningeal coverings (28). In our classification, grade 1 PAs are beneath the DS, which is consistent with Goel's classification of grade I. However, we suggest that it is not only the DS that was elevated by the tumor but also the residual pituitary gland. The surfaces of these tumors were covered by an intact bilayer structure formed by the DS and the residual pituitary. We propose that the thinning or absence of the residual pituitary gland caused the double barrier (DS and residual pituitary) to become a weak barrier, which was the key to the formation of daughter tumors.

This study has some limitations. First, our classification focused on identifying whether PAs with SSEs are located in extradural or intradural spaces, but did not take into account the degree of the suprasellar and lateral tumor extensions. In the future, we hope to reconcile our study with Hardy's classification. In grade 1b and 2 tumors, for instance, if the tumor extends significantly lateral to the suprasellar region, a Hardy's classification grade D, a transcranial approach or a combined transsphenoidal approach may be more appropriate. Another limitation was that our proposed two-point-one-line method of predicting when an EEEA was required is only a prediction. As such, the need for an EEA may also be related to other factors, particularly the consistency of the tumor, revision surgery, and intraoperative CSF release.

CONCLUSION

The bilayer structure formed by the DS and the residual pituitary gland is the key to determining whether a PA is located in the

extradural or intradural space. The grade 1 PAs are located extradural which we further divided into 2 subtypes: grade 1a and grade 1b PAs. Grade 1a PAs push and stretch the bilayer structure up toward the suprasellar region. Grade 1b PAs demonstrate a thinning or absence of residual pituitary gland, leading to weakness of the bilayer structure and formation of a daughter tumor. Grade 2 PAs have a surface that is not surrounded by a bilayer structure and are located in the intradural space. GTR decreases with increasing grade, while the surgical risks and complications increase with increasing grade. Given the information provided by this classification scheme, surgeons can plan the most appropriate operative approach and extent of resection and can better predict the surgical outcomes.

DATA AVAILABILITY STATEMENT

The original contributions presented in the study are included in the article/supplementary material. Further inquiries can be directed to the corresponding authors.

ETHICS STATEMENT

The studies involving human participants were reviewed and approved by Institutional Ethics Committee of the First Affiliated Hospital of Nanchang University. Written informed consent to participate in this study was provided by the participants' legal guardian/next of kin. Written informed consent was obtained from the individual(s), and minor(s)' legal guardian/next of kin, for the publication of any potentially identifiable images or data included in this article.

AUTHOR CONTRIBUTIONS

TH and YY conceived of and directed the study. TH, YB, SX, and BT provided clinical information and analysis the data. XW, LY, and JW collected the data. SL and SZ made the tables and figures. TH, YY, YB, and SX reviewed the manuscript. All authors contributed to the article and approved the submitted version.

FUNDING

This study was supported by the National Natural Science Foundation of China (grant nos. 82060246 and 81460381), the Ganpo555 Engineering Excellence of Jiangxi Science and Technology Department (2013), and the Key Research and Invention Plan of Jiangxi Science and Technology Department (20192BBG70026).

ACKNOWLEDGMENTS

We express our sincere appreciation to Miss Jing Liu and Rong Yuan for the illustration.

REFERENCES

1. Melmed S. Pituitary-Tumor Endocrinopathies. *N Engl J Med* (2020) 382 (10):937–50. doi: 10.1056/NEJMra1810772
2. Pertichetti M, Serioli S, Belotti F, Mattavelli D, Schreiber A, Cappelli C, et al. Pituitary Adenomas and Neuropsychological Status: A Systematic Literature Review. *Neurosurg Rev* (2020) 43(4):1065–78. doi: 10.1007/s10143-019-01134-z
3. Zhang Y, Ko CC, Chen JH, Chang KT, Chen TY, Lim SW, et al. Radiomics Approach for Prediction of Recurrence in Non-Functioning Pituitary Macroadenomas. *Front Oncol* (2020) 10:590083. doi: 10.3389/fonc.2020.590083
4. Chatzellis E, Alexandraki KI, Androulakis II, Kaltsas G. Aggressive Pituitary Tumors. *Neuroendocrinology* (2015) 101(2):87–104. doi: 10.1159/000371806
5. Campero A, Martins C, Yasuda A, Rhoton AL Jr. Microsurgical Anatomy of the Diaphragma Sellae and its Role in Directing the Pattern of Growth of Pituitary Adenomas. *Neurosurgery* (2008) 62(3):717–23; discussion -23. doi: 10.1227/01.neu.0000317321.79106.37
6. Ishii K, Ikeda H, Takahashi S, Matsumoto K, Ishibashi T, Tazawa S. MR Imaging of Pituitary Adenomas With Sphenoid Sinus Invasion: Characteristic MR Findings Indicating Fibrosis. *Radiat Med* (1996) 14(4):173–8.
7. Sarkar S, Chacko AG, Chacko G. Clinicopathological Correlates of Extrasellar Growth Patterns in Pituitary Adenomas. *J Clin Neurosci: Off J Neurosurg Soc Australas* (2015) 22(7):1173–7. doi: 10.1016/j.jocn.2015.01.029
8. Singh H, Essayed WI, Cohen-Gadol A, Zada G, Schwartz TH. Resection of Pituitary Tumors: Endoscopic Versus Microscopic. *J Neurooncol* (2016) 130 (2):309–17. doi: 10.1007/s11060-016-2124-y
9. Meij BP, Lopes MB, Ellegala DB, Alden TD, Laws ER Jr. The Long-Term Significance of Microscopic Dural Invasion in 354 Patients With Pituitary Adenomas Treated With Transsphenoidal Surgery. *J Neurosurg* (2002) 96 (2):195–208. doi: 10.3171/jns.2002.96.2.0195
10. Jefferson G. Extrasellar Extensions of Pituitary Adenomas: (Section of Neurology). *Proc R Soc Med* (1940) 33(7):433–58. doi: 10.1177/003591574003300717
11. Cabuk B, Anik I, Kokturk S, Ceylan S, Ceylan S. Anatomic and Histologic Features of Diaphragma Sellae That Effects the Suprasellar Extension. *J Clin Neurosci: Off J Neurosurg Soc Australas* (2020) 71:234–44. doi: 10.1016/j.jocn.2019.11.014
12. de Divitiis E, Cavallo LM, Cappabianca P, Esposito F. Extended Endoscopic Endonasal Transsphenoidal Approach for the Removal of Suprasellar Tumors: Part 2. *Neurosurgery* (2007) 60(1):46–58; discussion -9. doi: 10.1227/01.Neu.0000249211.89096.25
13. Dehdashti AR, Ganna A, Witterick I, Gentili F. Expanded Endoscopic Endonasal Approach for Anterior Cranial Base and Suprasellar Lesions: Indications and Limitations. *Neurosurgery* (2009) 64(4):677–87. doi: 10.1227/01.Neu.0000339121.20101.85
14. Di Maio S, Cavallo LM, Esposito F, Stagno V, Corriero OV, Cappabianca P. Extended Endoscopic Endonasal Approach for Selected Pituitary Adenomas: Early Experience. *J Neurosurg* (2011) 114(2):345–53. doi: 10.3171/2010.9.JNS10262
15. Di Somma A, Torales J, Cavallo LM, Pineda J, Solari D, Gerardi RM, et al. Defining the Lateral Limits of the Endoscopic Endonasal Transtuberculum Transplanum Approach: Anatomical Study With Pertinent Quantitative Analysis. *J Neurosurg* (2018) 130(3):848–60. doi: 10.3171/2017.9.JNS171406
16. Kutlay M, Durmaz A, Ozer I, Kural C, Temiz C, Kaya S, et al. Extended Endoscopic Endonasal Approach to the Ventral Skull Base Lesions. *Clin Neurol Neurosurg* (2018) 167:129–40. doi: 10.1016/j.clineuro.2018.02.032
17. Mohr G, Hardy J, Comtois R, Beauregard H. Surgical Management of Giant Pituitary Adenomas. *Can J Neurol Sci* (1990) 17(1):62–6. doi: 10.1017/s0317167100030055
18. Thotakura AK, Patibandla MR, Panigrahi MK, Addagada GC. Predictors of Visual Outcome With Transsphenoidal Excision of Pituitary Adenomas Having Suprasellar Extension: A Prospective Series of 100 Cases and Brief

Review of the Literature. *Asian J Neurosur* (2017) 12(1):1–5. doi: 10.4103/1793-5482.149995
19. Dehdashti AR, Ganna A, Karabatsou K, Gentili F. Pure Endoscopic Endonasal Approach for Pituitary Adenomas: Early Surgical Results in 200 Patients and Comparison With Previous Microsurgical Series. *Neurosurgery* (2008) 62 (5):1006–15; discussion 15-7. doi: 10.1227/01.neu.0000325862.83961.12
20. Mortini P, Barzaghi R, Losa M, Boari N, Giovanelli M. Surgical Treatment of Giant Pituitary Adenomas: Strategies and Results in a Series of 95 Consecutive Patients. *Neurosurgery* (2007) 60(6):993–1002; discussion 3-4. doi: 10.1227/01.NEU.0000255459.14764.BA
21. Yang L, Xie SH, Fang C, Zeng EM, Tang B, Hong T. Preservation of Hypothalamic Function With Endoscopic Endonasal Resection of Hypothalamus-Invaded Craniopharyngiomas. *World Neurosurg* (2019) 132: e841–51. doi: 10.1016/j.wneu.2019.07.225
22. Wu X, Xie SH, Tang B, Yang YQ, Yang L, Ding H, et al. Pituitary Adenoma With Posterior Area Invasion of Cavernous Sinus: Surgical Anatomy, Approach, and Outcomes. *Neurosurg Rev* (2020) 1–9. doi: 10.1007/s10143-020-01404-1
23. Abdelmaksoud A, Fu P, Alwalid O, Elazab A, Zalloom A, Xiang W, et al. Degrees of Diaphragma Sellae Descent During Transsphenoidal Pituitary Adenoma Resection: Predictive Factors and Effect on Outcome. *Curr Med Sci* (2018) 38(5):888–93. doi: 10.1007/s11596-018-1958-2
24. Hadad G, Bassagasteguy L, Carrau RL, Mataza JC, Kassam A, Snyderman CH, et al. A Novel Reconstructive Technique After Endoscopic Expanded Endonasal Approaches: Vascular Pedicle Nasoseptal Flap. *Laryngoscope* (2006) 116(10):1882–6. doi: 10.1097/01.mlg.0000234933.37779.e4
25. Guinto Balanzar G, Abdo M, Mercado M, Guinto P, Nishimura E, Arechiga N. Diaphragma Sellae: A Surgical Reference for Transsphenoidal Resection of Pituitary Macroadenomas. *World Neurosurg* (2011) 75(2):286–93. doi: 10.1016/j.wneu.2010.08.002
26. Rhoton ALJr. The Sellar Region. *Neurosurgery* (2002) 51(4 Suppl):S335–74. doi: 10.1097/00006123-200210001-00009
27. Bergland RM, Ray BS, Torack RM. Anatomical Variations in the Pituitary Gland and Adjacent Structures in 225 Human Autopsy Cases. *J Neurosurg* (1968) 28(2):93–9. doi: 10.3171/jns.1968.28.2.0093
28. Goel A, Nadkarni T, Muzumdar D, Desai K, Phalke U, Sharma P. Giant Pituitary Tumors: A Study Based on Surgical Treatment of 118 Cases. *Surg Neurol* (2004) 61 (5):436–45; discussion 45-6. doi: 10.1016/j.surneu.2003.08.036
29. Laufer I, Anand VK, Schwartz TH. Endoscopic, Endonasal Extended Transsphenoidal, Transplanum Transtuberculum Approach for Resection of Suprasellar Lesions. *J Neurosurg* (2007) 106(3):400–6. doi: 10.3171/jns.2007.106.3.400
30. Khalafallah AM, Liang AL, Jimenez AE, Rowan NR, Oyesiku NM, Mamelak AN, et al. Trends in Endoscopic and Microscopic Transsphenoidal Surgery: A Survey of the International Society of Pituitary Surgeons Between 2010 and 2020. *Pituitary* (2020) 23(5):526–33. doi: 10.1007/s11102-020-01054-y
31. Van Gerven L, Qian Z, Starovoyt A, Jorissen M, Meulemans J, van Loon J, et al. Endoscopic, Endonasal Transsphenoidal Surgery for Tumors of the Sellar and Suprasellar Region: A Monocentric Historical Cohort Study of 369 Patients. *Front Oncol* (2021) 11:643550. doi: 10.3389/fonc.2021.643550
32. Koutourousiou M, Gardner PA, Fernandez-Miranda JC, Paluzzi A, Wang EW, Snyderman CH. Endoscopic Endonasal Surgery for Giant Pituitary Adenomas: Advantages and Limitations. *J Neurosurg* (2013) 118(3):621–31. doi: 10.3171/2012.11.Jns121190
33. Nishioka H, Hara T, Nagata Y, Fukuhara N, Yamaguchi-Okada M, Yamada S. Inherent Tumor Characteristics That Limit Effective and Safe Resection of Giant Nonfunctioning Pituitary Adenomas. *World Neurosurg* (2017) 106:645–52. doi: 10.1016/j.wneu.2017.07.043
34. Elshazly K, Kshettry VR, Farrell CJ, Nyquist G, Rosen M, Evans JJ. Clinical Outcomes After Endoscopic Endonasal Resection of Giant Pituitary Adenomas. *World Neurosurg* (2018) 114:e447–56. doi: 10.1016/j.wneu.2018.03.006

Conflict of Interest: The authors declare that the research was conducted in the absence of any commercial or financial relationships that could be construed as a potential conflict of interest.

frontiers in Oncology

ORIGINAL RESEARCH
published: 13 September 2021
doi: 10.3389/fonc.2021.739290

Clinical Relevance of New World Health Organization Classification System for Pituitary Adenomas: A Validation Study With 2-Year Experience

Seung Woo Hong[1], Se Hoon Kim[2,3], Seung Hoon Lim[1], Eun Jig Lee[3,4,5], Sun Ho Kim[1,6], Cheol Ryong Ku[3,4,5†] and Eui Hyun Kim[1,3,4†]*

[1] Department of Neurosurgery, Yonsei University College of Medicine, Seoul, South Korea, [2] Department of Pathology, Yonsei University College of Medicine, Seoul, South Korea, [3] Pituitary Tumor Center, Severance Hospital, Seoul, South Korea, [4] Yonsei Endocrine Research Institute, Yonsei University College of Medicine, Seoul, South Korea, [5] Division of Endocrinology and Metabolism, Department of Internal Medicine, Yonsei University College of Medicine, Seoul, South Korea, [6] Department of Neurosurgery, Ewha Woman's University College of Medicine, Seoul, South Korea

Background: The new World Health Organization (WHO) classification system proposed a cell lineage-based classification scheme for pituitary adenomas in which transcription factors (TFs) play a major role as key classifiers. We aimed to evaluate clinical relevance of the new classification system in a clinical setting.

Methods: TF staining was retrospectively performed for 153 clinically and histologically well characterized pituitary adenomas. Then, 484 pituitary adenomas were prospectively stained for TFs and then for relevant pituitary hormones. TF and hormone stain-based diagnoses were compared, and differences in clinical manifestations were evaluated.

Results: The accuracies of antibodies for three TFs were successfully validated and had an overall matching rate was 89.6%. We identified 50 (10.4%) cases with discrepancies between TF and pituitary hormone stains. Gonadotroph adenomas lacking follicle-stimulating hormone and luteinizing hormone stains account for most discrepancies. Null cell adenomas may be more prevalent than reported and may be clinically more aggressive than gonadotroph adenomas.

Conclusion: The new WHO classification is mostly well matched with the traditional classification. However, until the new classification is further validated and interpreted in the context of long-term clinical outcomes, routine histological examination should include full slate of immunostains for pituitary hormones as well as TFs.

Keywords: immunohistochemistry, pituitary adenoma, pituitary hormone, transcription factor, WHO classification

OPEN ACCESS

Edited by:
Zhixiong Liu,
Central South University, China

Reviewed by:
Alejandro Ibáñez-Costa,
Maimonides Biomedical Research Institute of Cordoba (IMIBIC), Spain
Anca Maria Cimpean,
Victor Babes University of Medicine and Pharmacy, Romania
Bing Xing,
Peking Union Medical College Hospital (CAMS), China

****Correspondence:***
Eui Hyun Kim
euihyunkim@yuhs.ac

†These authors have contributed equally to this work and share last authorship

Specialty section:
This article was submitted to Neuro-Oncology and Neurosurgical Oncology, a section of the journal Frontiers in Oncology

Received: *10 July 2021*
Accepted: *23 August 2021*
Published: *13 September 2021*

Citation:
Hong SW, Kim SH, Lim SH, Lee EJ, Kim SH, Ku CR and Kim EH (2021) Clinical Relevance of New World Health Organization Classification System for Pituitary Adenomas: A Validation Study With 2-Year Experience. Front. Oncol. 11:739290. doi: 10.3389/fonc.2021.739290

INTRODUCTION

Pituitary adenomas are neuroendocrine tumors in the anterior pituitary gland. They are traditionally classified based on their hormonal activity as non-functioning and endocrine-active tumors. Histopathological examination is important to confirm the diagnosis by validation of positive immunohistochemistry (IHC) for relevant pituitary hormones. The fourth edition of the World Health Organization (WHO) classification of endocrine tumors was published in 2017 (1). One of the major changes in the new scheme is the cell lineage-based classification of pituitary adenomas characterized by lineage-specific transcription factors (TFs). All pituitary adenomas are divided into the three following lineages: lactotroph, somatotroph, and thyrotroph belong to PIT-1 (pituitary-specific TF 1), corticotroph belongs to T-PIT (pituitary cell-restricted factor), and gonadotroph belongs to SF-1 (steroidogenic factor 1). Tumors negative for all three TFs are considered as true null cell adenomas.

In September 2018, we started to provide pathological diagnoses for all pituitary adenomas surgically removed in our institution based on the new WHO classification system. Based on our 2-year experience, we aimed to evaluate the clinical relevance of new classification system and discrepancies between pituitary hormone-based and TF-based diagnoses.

MATERIALS AND METHODS

This study was conducted in accordance with the Declaration of Helsinki and approved by the local Institutional Review Board. The IHC antibodies used for TFs and pituitary hormones are listed in **Table 1**. Every single sample was examined by two experienced neuropathologists. The hormone-positivity was described as focal/diffuse and weak/strong. For the stains for TFs, roughly 5% of cutoff was adopted. We considered cases with even very week stains for TFs in the nucleus as positive.

Retrospective Validation

Before September 2018, our routine pathological examination for pituitary adenomas included IHC for all anterior pituitary hormones: adrenocorticotropic hormone (ACTH), growth hormone (GH), prolactin (PRL), thyroid-stimulating hormone (TSH), luteinizing hormone (LH), and follicle-stimulating hormone (FSH). We retrospectively selected 49 non-functioning pituitary adenomas including 27 null cell tumors and 22 gonadotroph adenomas. None of these patients presented any symptoms suggesting hormonal excess. We then identified 104 endocrine-active pituitary adenomas: 36 GH-secreting adenomas, 28 prolactinomas, 21 TSH-secreting adenomas, and 19 ACTH-secreting adenomas. For all 104 patients with endocrine-active pituitary adenomas, their hormonal excess was well matched with laboratory tests and clinical symptoms. Acromegaly was defined when the nadir serum GH level after an 75g oral glucose tolerance test was less than 1.0 ng/mL with elevation of serum insulin-like growth factor-1 adjusted for age and sex. The diagnosis of Cushing's disease was established on the basis of clinical features and the results of biochemical tests including 24 h urinary free cortisol excretion, low- and/or high-dose dexamethasone suppression test. And bilateral inferior petrosal sinus sampling was performed in all cases. The diagnosis of TSH-secreting pituitary adenoma was made based on serum TSH, free thyroxine, triiodothyronine levels together with the radio of free alpha subunit and TSH, which was later confirmed by postoperative normalization of TSH. A T3

TABLE 1 | Antibodies used for immunohistochemistry for transcription factors and pituitary hormones.

	Company	Clone	Dilution factor	Machine	Expression pattern	Antigen retrieval	Antibody primary
	Transcription factors						
PIT-1	Novus Biologicals	NBP1-92273	1/500	Ventana, BenchMark XT	Nuclear	Conventional	BenchMark XT instrument, 32 minutes, 37°C
T-PIT	Atlas Antibodies	AMAb91409	1/1000	Dako, Omnis	Nuclear	Low pH, 30 minutes	Omnis instrument, 20 minutes, 32°C
SF-1	Perseus Proteomics Inc.	PP-N1665-0C	1/400	Dako, Omnis	Nuclear	Low pH, 30 minutes	Omnis instrument, 20 minutes, 32°C
	Pituitary hormones						
GH	DAKO, Agilent	A0570	1/400	Ventana, BenchMark XT	Cytoplasmic	Not required	BenchMark XT instrument, 32 minutes, 37°C
PRL	DAKO, Agilent	A0569	1/300	Ventana, BenchMark XT	Cytoplasmic	Not required	BenchMark XT instrument, 32 minutes, 37°C
TSH	DAKO, Agilent	M3503	1/50	Ventana, BenchMark XT	Cytoplasmic	Not required	BenchMark XT instrument, 32 minutes, 37°C
ACTH	DAKO, Agilent	M3501	1/200	Ventana, BenchMark XT	Cytoplasmic	Not required	BenchMark XT instrument, 32 minutes, 37°C
LH	DAKO, Agilent	M3502	1/50	Ventana, BenchMark XT	Cytoplasmic	Not required	BenchMark XT instrument, 32 minutes, 37°C
FSH	DAKO, Agilent	M3504	1/50	Ventana, BenchMark XT	Cytoplasmic	Not required	BenchMark XT instrument, 32 minutes, 37°C

ACTH, adrenocorticotropic hormone; FSH, follicle stimulating hormone; GH, growth hormone; LH, luteinizing hormone; PIT-1, pituitary specific transcription factor 1; PRL, prolactin; SF-1, steroidogenic factor 1; T-PIT, pituitary cell restricted factor; TSH, thyroid stimulating hormone.

suppression test was performed when it was unclear whether the patient had a TSH-secreting pituitary adenoma or a non-functioning pituitary adenoma in the presence of secondary hyperthyroidism. IHC of three TFs was then performed for cell-lineage classification. The classifications based on pituitary hormones and TFs were compared.

Prospective Validation

Since September 2018, the routine pathological examination protocol for pituitary adenomas was updated based on the new WHO classification (**Figure 1**). Informed consent was obtained from enrolled patients. We first performed IHC for three TFs: PIT-1, T-PIT, and SF-1. Then, IHC was performed for possibly associated hormones based on the result of TF stains: GH, PRL, and TSH for PIT-1 adenomas; only ACTH for T-PIT adenomas; and LH and FSH for SF-1 adenomas. When the hormone stain results were not matched to TF stains, the tests were repeated and IHC was performed for all pituitary hormones. For all discordant cases, IHC for TF stains and hormone stains were repeated to confirm the results. Cases with incomplete study and with pituitary apoplexy that prevented reliable IHC were excluded from this study. A total of 484 patients who underwent surgical resection for their pituitary adenomas by two neurosurgeons from September 2018 to August 2020 were included in this analysis. First, hormone and TF stains were compared to determine whether they were well matched. For patients with concordant results, histological and clinical diagnoses were compared with subgroup analysis of their tumor nature.

Statistical Analysis

We performed *t*-tests and chi-square tests to identify statistically significant differences. All analyses were performed using IBM SPSS Statistics (version 20.0; IBM, Armonk, NY, USA), and $P < 0.05$ was considered statistically significant.

RESULTS

Retrospective Validation

The results of our retrospective analysis are summarized in **Table 2**. For 153 cases of pituitary adenomas previously operated in our institution based on the traditional classification scheme, we performed IHC for three TFs and compared the findings. The results were consistent in 149 (97.4%) cases. We identified only five cases with discrepancies between hormonal and TF stains. One patient with overt Cushingoid features and positive ACTH stain was negative for all TFs. There were four endocrine-inactive pituitary adenomas with negative stains for all pituitary hormones; a positive stain for T-PIT was observed in one patient and SF-1 in three patients.

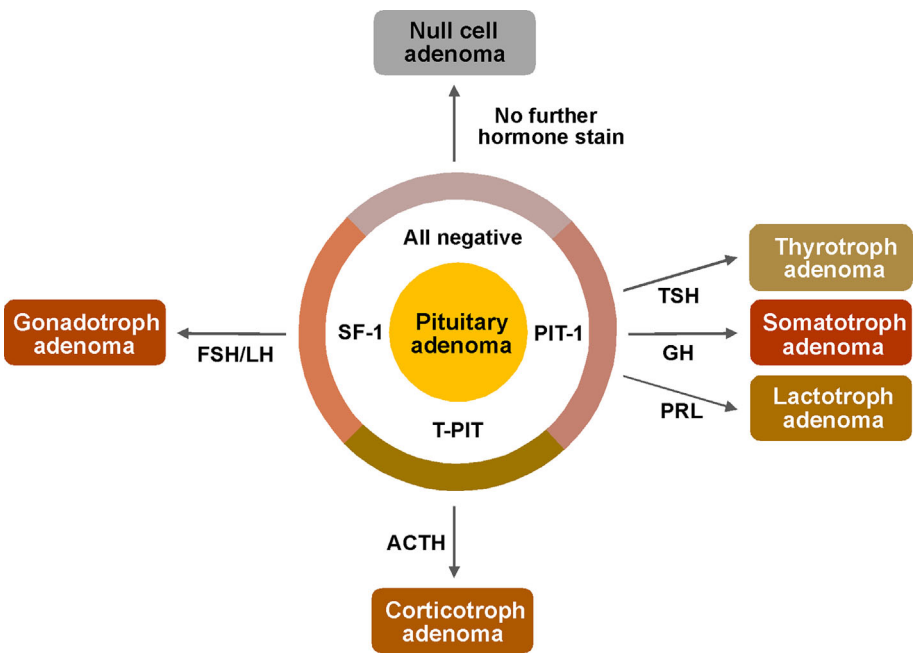

FIGURE 1 | Pathological examination protocol for pituitary adenomas based on the new WHO classification. First, immunostains of transcriptions factors (PIT-1, T-PIT and SF-1) were performed for determination of cell lineage. And then, following stains were performed only for possibly associated hormones based on the result of TF stains; GH, PRL and TSH for PIT-1 positive adenomas, only ACTH for T-PIT positive adenomas and LH, FSH for SF-1 positive adenomas. ACTH, adrenocorticotropic hormone; FSH, follicle stimulating hormone; GH, growth hormone; LH, luteinizing hormone; PIT-1, pituitary specific transcription factor 1; PRL, prolactin; SF-1, steroidogenic factor 1; T-PIT, pituitary cell restricted factor; TSH, thyroid stimulating hormone.

TABLE 2 | Retrospective comparison of immunohistochemistry between pituitary hormones and transcription factors.

Pituitary hormone stain	Number of cases examined	Number of cases with matched TFs	Details on mismatched cases
Single ACTH positive	19	18 (94.7%)	Negative for all TFs
Single PRL positive	28	28 (100%)	
Single GH positive	36	36 (100%)	
Single TSH positive	21	21 (100%)	
Positive for FSH and/or LH	22	22 (100%)	
All negative	27	23 (85.2%)	Positive for T-PIT in 1 and SF-1 in 3
Total	153	148 (96.7%)	

ACTH, adrenocorticotropic hormone; FSH, follicle stimulating hormone; GH, growth hormone; LH, luteinizing hormone; PRL, prolactin; SF-1, steroidogenic factor 1; TF, transcription factor; T-PIT, pituitary cell restricted factor; TSH, thyroid stimulating hormone.

Prospective Validation

The cohort included 303 endocrine-inactive tumors and 181 endocrine-active tumors including 86 GH-secreting pituitary adenomas, 57 prolactinomas, 36 ACTH-secreting pituitary adenomas, 2 TSH-secreting adenomas. While prolactinoma is known to be the most common type of pituitary adenomas, the prevalence of prolactinomas is possibly underestimated in our surgical series because majority of them were treated with dopamine agonists without pathological diagnosis. Also, compared to other series in the literature, much more patients with endocrine-inactive pituitary adenomas (62.6%) were enrolled to our study.

Comparison Between TF and Pituitary Hormone Stains

First, we identified three unusual tumors that could not be classified into any specific category. These tumors were positive for multiple TFs; one Cushing's disease patient had positive IHC for T-PIT, and SF-1, and two acromegalic patients had positive IHC for both PIT-1 and SF-1 (**Figure 2**). Complete resection was done in all three cases, but one acromegalic patient did not achieve endocrinological remission.

For the other 481 patients, we evaluated whether their TF stains were well matched with their pituitary hormone stains (**Figure 3** and **Table 3**). The most common subtype was PIT-1 positive adenoma, and the overall matching rate was 89.6%. We identified 50 (10.4%) patients with pituitary adenomas whose pathological examinations were discrepant between TF and pituitary hormone stains. The majority of mismatched cases were gonadotroph adenomas (43 patients, 86.0%) with stains positive for SF-1 but negative for both FSH and LH. The second-most common tumor type was null cell adenomas positive for ACTH stain (n=4). The most common subtype of gonadotroph adenoma was FSH positive, while LH-positive tumors were the least common. In 171 PIT-1 positive adenomas, the most prevalent subtype was GH-positive tumors followed by prolactinoma. Tumors with positive stains for two or more hormones were more prevalent than single hormone-positive tumors (53.2% *vs.* 46.8%). PRL, GH

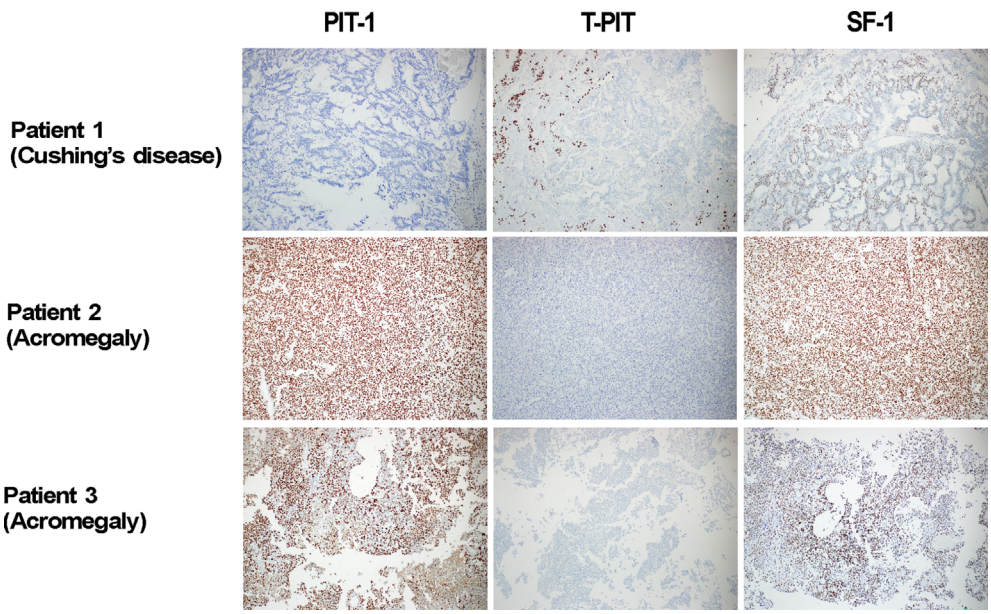

FIGURE 2 | Three tumor cases with positive IHC for multiple transcriptions factors. In our prospective investigation on 484 pituitary adenomas, three unusual cases were identified as their cell lineages were not clearly classified. They were 1 Cushing's disease patient with positive IHC for T-PIT, and SF-1, and two acromegalic patients with positive IHC for both PIT-1 and SF-1. In Patient 2, positive stains for PIT-1 and SF-1 were observed in the same cells. PIT-1, T-PIT and SF-1 X 100. IHC, immunohistochemistry; PIT-1, pituitary specific transcription factor 1; SF-1, steroidogenic factor 1; T-PIT, pituitary cell restricted factor.

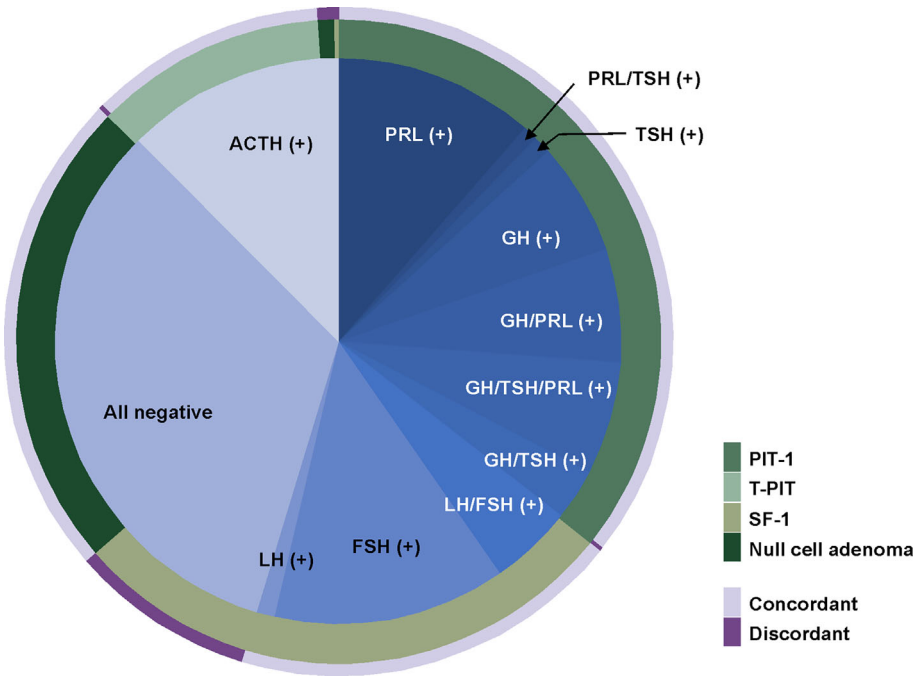

FIGURE 3 | Comparison between immunohistochemical stain for transcription factors and pituitary hormones. The most common subtype was PIT-1 positive adenomas. In 171 PIT-1 positive adenomas, the most prevalent subtype was a prolactinoma followed by GH-positive tumors. The most common subtype of gonadotroph adenomas was a FSH-positive tumor and LH-positive tumors were the least common. Overall, 10.4% of cases showed discordance between TF stains and pituitary hormone stains. The majority of mismatched cases were gonadotroph adenomas of which stains were positive for SF-1 but negative for both FSH and LH. FSH, follicle stimulating hormone; GH, growth hormone; LH, luteinizing hormone; PIT-1, pituitary specific transcription factor 1.

TABLE 3 | Comparison between immunohistochemical stain for TFs and pituitary hormones.

TF stain	Pituitary hormone stain				
	GH, PRL, TSH positive	ACTH positive	FSH, LH positive	All negative	Total
PIT-1 positive	171		1*		172 (35.8%)
T-PIT positive		55		1*	56 (11.6%)
SF-1 positive		1*	91	43*	135 (28.1%)
All negative		4*		114	118 (24.5%)
Total	171	60	92	158	481

**Cases with discrepancy between TF and pituitary hormone stains.*
ACTH, adrenocorticotropic hormone; FSH, follicle stimulating hormone; GH, growth hormone; LH, luteinizing hormone; PIT-1, pituitary specific transcription factor 1; PRL, prolactin; SF-1, steroidogenic factor 1; TF, transcription factor; T-PIT, pituitary cell restricted factor; TSH, thyroid stimulating hormone.

TABLE 4 | Comparison between clinical manifestations and histology for 431 patients with concordant immunohistochemical stains for TFs and pituitary hormones.

Clinical diagnosis	PIT-1 positive	T-PIT positive	SF-1 positive	All negative	Total
Cushing's disease	*1	32		*1	34
Acromegaly	84				84
Prolactinoma	55			*2	57
TSHoma	2				2
Non-functioning adenoma	*29	*23	91	111	254
Total	171	57	91	114	431

**Cases with discrepancy between clinical manifestations and histology.*
PIT-1, pituitary specific transcription factor 1; SF-1, steroidogenic factor 1; TF, transcription factor; T-PIT, pituitary cell restricted factor; TSH, thyroid stimulating hormone.

and TSH stain were positive in 121 (70.8%), 107 (62.6%) and 40 (23.4%) PIT-1 positive adenomas, respectively.

Comparison Between Histological Diagnosis and Clinical Diagnosis

For the 431 patients with concordant results between TF and pituitary hormone stains, comparative analysis was performed for their histological and clinical diagnoses (**Table 4**).

Among 177 endocrine-active tumors, 174 (98.3%) had concordant clinical and histological diagnoses. When we compared 32 patients with endocrine-active corticotroph adenoma (Cushing's disease) with its counterpart (23 silent corticotroph adenomas), we observed that tumors were much larger in silent corticotroph adenoma patients than in Cushing's disease patients (25.3 mm *vs.* 12.4 mm, $P<0.001$). However, there was no statistically significant difference between the incidence of cavernous sinus invasion and total tumor removal. In the comparison between patients with functioning PIT-1 adenomas (GH-secreting adenoma, prolactinoma, and thyrotropinoma) and silent PIT-1 adenoma patients, we failed to identify any of these.

A total of 254 endocrine-inactive tumors with no clinical or laboratory evidence of hormonal excess were further analyzed

(**Figure 4**). In this group, there were more patients with true null cell adenomas (n=111) that were not positive for TFs or pituitary hormones than gonadotroph adenoma patients (n=91), followed by 23 patients with silent corticotroph adenoma and 29 with silent PIT-1 adenomas. Although tumor size did not differ, null cell adenomas showed more frequent cavernous sinus invasion than gonadotroph adenomas (P=0.043), which led to a difference in the likelihood of total tumor removal (P=0.039). Tumors were the smallest in patients with silent PIT-1 adenomas (P<0.001 *vs.* null cell adenomas and gonadotroph adenomas, P=0.054 *vs.* silent corticotroph adenomas). The incidence of cavernous sinus invasion was highest for silent corticotroph adenoma (P=0.032 *vs.* gonadotroph adenomas), which is a well-known aggressive form of pituitary adenoma. Conversely, patients with gonadotroph adenomas were less likely to have cavernous sinus invasion. Among 29 patients with silent PIT-1 adenomas, 28 underwent total removal, which was a significantly higher percentage than patients with null cell adenomas or silent corticotroph adenomas.

DISCUSSION

In recent decades, several TFs have been found to regulate cellular differentiation of the adenohypophysis, and they are also essential for differentiation and maturation of the neuroendocrine cells from Rathke's pouch (2, 3). As TFs determine hormone-specific pituitary stem cell development, IHC for pituitary hormones and cell-specific TFs enables classification of differentiated pituitary adenomas based on pituitary cell lineage (4). Many studies have shown that TF staining can be a major ancillary diagnostic tool for more precise classification of pituitary adenomas (5–7). Considering that immunostain findings for pituitary hormones are often focal, very weak, or uncertain, TF staining may serve as a critical determinant for histological diagnoses in such instances. Based on these findings, the fourth edition of WHO classification system proposed a cell lineage-based classification scheme for pituitary adenomas, in which TFs such as PIT-1, T-PIT, and SF-1 serve as key classifiers. Many groups have adopted this new classification system and updated their guidelines for pathological diagnosis of pituitary adenomas (8). There have been several reports on early experiences with the new WHO classification system (9, 10). Before adopting a new classification system at our institution, we validated the reliability of antibodies for three TFs: PIT-1, T-PIT, and SF-1.

We created a cohort in which (1) patients' pituitary hormone stains were all negative or singly positive and (2) their clinical manifestation and endocrine laboratory tests were consistent with the pituitary hormone stain results. In this 153-patient cohort, tumor hormonal activity was clearly defined by serum hormone levels and IHC for pituitary hormones. We then performed TF stains and evaluated whether the results were well matched to the previously established diagnosis. In this well-refined cohort, the diagnoses based on the new WHO classification were concordant with the original diagnosis. There were only five cases with discordant results, including three positive for SF-1 even though all negative hormonal stains were the majority. Although there has been concern that reliable commercial antibodies for T-PIT are not yet available (1), our T-PIT antibody was successfully validated for its accuracy (94.7%).

Convinced by the successful retrospective validation results, we changed our diagnostic protocol of pathological pituitary adenoma examination (**Figure 1**). We first performed IHC for three different TFs: PIT-1, T-PIT, and SF-1. After tumor cell lineage was identified, IHC was only performed for the relevant hormones. When the TF and pituitary hormone staining results were discordant, IHC was carried out for the remaining pituitary hormones. We experienced 3 cases with positive stains for multiple TFs; 2 in acromegaly and 1 in Cushing's disease. We repeated IHC for both TFs and pituitary hormones and confirmed the same results. Moreover, these unusual cases have been reported by other groups (10–12). This should be further investigated as current WHO classification system does not provide how to classify theses unusual tumors. Recently, Neou et al.

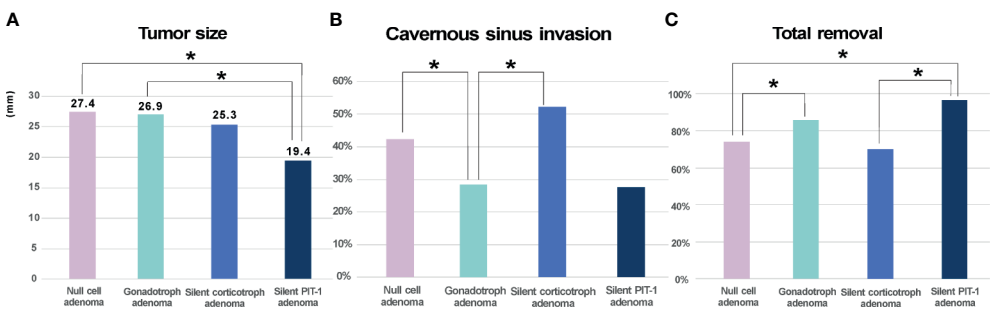

FIGURE 4 | Clinical characteristics of endocrine-inactive tumors. **(A)**. Null cell adenomas and gonadotroph adenomas did not differ in size whereas silent PIT-1 adenomas were the smallest. **(B, C)**. Null cell adenomas showed more frequent cavernous sinus invasion than gonadotroph adenomas, which makes total removal loss feasible in patient with null cell adenomas. The incidence of cavernous sinus invasion was the highest in silent corticotroph adenoma. On the contrary, patients with gonadotroph adenomas were less likely to have cavernous sinus invasion. Among 29 patients with silent PIT-1 adenomas, 28 patients underwent total removal, which was significantly higher than patients with null cell adenomas or silent corticotroph adenomas. *Cavernous sinus invasion was identified by preoperative magnetic resonance imaging and based on surgeon's inspection intraoperatively.* PIT-1, pituitary specific transcription factor 1; *P < 0.05.

demonstrated that unsupervised multi-panel genomic classification of pituitary adenomas generally well correlates with cell lineage classification, which is good agreement with the new WHO classification scheme (13). For the cases with discrepancies between TFs and pituitary hormones, transcriptome or methylome analysis may help to clarify their identities.

While a guideline or consensus on the threshold of hormone-positive tumor cells for immunohistochemical classification is not available, it has been our strategy that only one positive, unequivocally neoplastic cell is regarded as significant. In our clinical practice, we have often experienced cases in which the presence of single hormone-positive tumor cell was well matched with clinical diagnosis. However, low threshold of positive stain for pituitary hormones in our institution may possibly result in different observations from the literature. Indeed, we have more tumors with positive stains for two or more hormones than single hormone-positive tumors in PIT-1 positive adenomas, and low threshold of hormone-positivity may be the reason for this observation.

In our earlier series (14) when TF stains were not available, 66.3% of clinically endocrine-inactive pituitary adenomas were negative for any of pituitary hormone stains and thus classified as null cell adenomas. In our current study, among 254 endocrine-inactive tumors with no clinical or laboratory evidence of hormonal excess, we identified 111 tumors (43.7%) true null cell adenomas. Although the proportion of null cell adenomas were much lowered, this is still much higher proportion compared with other groups (1, 9, 15, 16). One of the possible explanation for the discrepancies in the incidence of null cell adenomas is that gonadotroph adenomas are possibly underdiagnosed in our study although we validated the reliability of SF-1 antibody in our retrospective investigation. Among 50 patients with pituitary adenomas whose pathological examinations were discrepant between transcription factor stains and pituitary hormone stains, the majority of mismatched cases were gonadotroph adenomas (43 patients, 86.0%) with stains positive for SF-1 but negative for both FSH and LH. Considering the threshold of hormone-positivity is very low in our study, we believe it should be further validated whether single SF-1immunostain is sufficient to characterize gonadotroph adenomas and whether current antibody for SF-1 is a reliable. Further investigation with IHC for GATA2, GATA3 and alpha subunit would help the differentiation between true null cell adenomas and gonadotroph adenomas and thus provide the true prevalence of null cell adenomas (17–19). Unlike other endocrine-active adenomas, most gonadotroph adenomas are clinically non-functioning tumors that lack hormone overproduction. Although their cell linages are apparently different, distinguishing between gonadotroph and null cell adenomas has always been difficult. Traditionally, null cell adenomas were considered a synonym of pituitary hormone-negative pituitary adenomas; however, the new WHO classification clearly defined null adenomas as tumors that do not exhibit immunoreactivity for pituitary hormones or TFs. Nishioka et al. demonstrated that up to 95% of pituitary adenomas negative for any pituitary hormones actually expressed lineage-specific TFs: SF-1 and/or estrogen receptor-α positive in 67%, T-PIT positive in 27% and PIT-1 positive in 2% (15). Thus, they suggested only 5% of tumors were true null cell adenomas. This observation was supported by Mete et al., who reported that the incidence of null cell tumors in their series was only 4.5% (20). We identified 111 null cell adenomas out of 158 adenomas with negative stains for any pituitary hormones, suggesting that its prevalence may be much higher than previously reported (**Table 3**).

In the subgroup analysis on 254 clinically endocrine-inactive tumors (**Table 4**), null cell adenomas were the majority, followed by gonadotroph adenomas. We also observed more silent PIT-1 adenomas (n=29) than silent corticotroph adenomas (n=23), which was different from a previous observation (15). We compared these four subtypes of endocrine-inactive tumors in terms of size, cavernous invasion probability, and likelihood of total resection. Unsurprisingly, silent corticotroph adenomas showed the highest incidence of cavernous sinus invasion and the lowest possibility of complete tumor removal. Null cell adenomas, gonadotroph adenomas, and silent corticotroph adenomas were similar in size. Null cell adenomas were more likely to invade the cavernous sinus compared with gonadotroph adenomas. Consequently, total resection was less likely for null cell adenomas. Although this finding should be further validated with long-term follow-up (21), null adenomas seem to be clinically more aggressive than gonadotroph adenomas, suggesting that this discrimination may be critical for patient management.

CONCLUSION

The new WHO classification scheme is mostly well matched with the traditional classification scheme. Gonadotroph adenomas lacking FSH and LH stains account for the majority of discrepancies in clinical settings, and further validation and characterization of this small subset of pituitary adenomas may be necessary. Null cell adenomas may be more prevalent than previously reported, which requires further verification. Until the new classification is further validated and interpreted with long-term clinical outcomes, routine histological examination should include a full slate of immunostains for both pituitary hormones and TFs.

DATA AVAILABILITY STATEMENT

The raw data supporting the conclusions of this article will be made available by the authors, without undue reservation.

ETHICS STATEMENT

The studies involving human participants were reviewed and approved by Institutional Review Board of Severance Hospital. Written informed consent for participation was not required for

this study in accordance with the national legislation and the institutional requirements.

AUTHOR CONTRIBUTIONS

Conceptualization, EK. Methodology, CK and EK. Software, EK. Validation, EK. Formal Analysis, SH, CK and EK. Investigation, SH, SeK, SL, EL, SuK, CK and EK. Resources, CK and EK. Data Curation, SH, CK and EK. Writing – Original Draft Preparation, SH. Writing – Review & Editing, EK. Visualization, EK. Supervision, EK. Project Administration, EK. Funding Acquisition, Not available. All authors contributed to the article and approved the submitted version.

FUNDING

This study was supported by a faculty research grant of Yonsei University College of Medicine (6-2020-0224).

ACKNOWLEDGMENTS

The authors thank Juyoon Park, RN, MPH, OCN, Min Kyeong Jang, PhD, RN, KOAPN, Sung Ja Kang, RN, Sujin Ryu, RN, Yong Jun Jang, RN for their tremendous effort in performing the endocrinological tests and data acquisition for such a long follow-up duration.

REFERENCES

1. Lopes MBS. The 2017 World Health Organization Classification of Tumors of the Pituitary Gland: A Summary. *Acta Neuropathol* (2017) 134(4):521–35. doi: 10.1007/s00401-017-1769-8
2. Scully KM, Rosenfeld MG. Pituitary Development: Regulatory Codes in Mammalian Organogenesis. *Science* (2002) 295(5563):2231–5. doi: 10.1126/science.1062736
3. Zhu X, Rosenfeld MG. Transcriptional Control of Precursor Proliferation in the Early Phases of Pituitary Development. *Curr Opin Genet Dev* (2004) 14 (5):567–74. doi: 10.1016/j.gde.2004.08.006
4. Ho K, Fleseriu M, Kaiser U, Salvatori R, Brue T, Lopes MB, et al. Pituitary Neoplasm Nomenclature Workshop: Does Adenoma Stand the Test of Time? *J Endocrine Soc* (2021) 5(3):bvaa205. doi: 10.1210/jendso/bvaa205
5. Asa S, Casar-Borota O, Chanson P, Delgrange E, Earls P, Ezzat S, et al. From Pituitary Adenoma to Pituitary Neuroendocrine Tumor (PitNET): An International Pituitary Pathology Club Proposal. *Endocrine-Related Cancer* (2017) 24(4):C5–8. doi: 10.1530/ERC-17-0004
6. Melmed S. Pituitary-Tumor Endocrinopathies. *N Engl J Med* (2020) 382 (10):937–50. doi: 10.1056/NEJMra1810772
7. Mete O, Asa SL. Structure, Function, and Morphology in the Classification of Pituitary Neuroendocrine Tumors: The Importance of Routine Analysis of Pituitary Transcription Factors. *Endocrine Pathol* (2020) 31(4):330–6. doi: 10.1007/s12022-020-09646-x
8. Villa C, Vasiljevic A, Jaffrain-Rea M, Ansorge O, Asioli S, Barresi V, et al. A Standardised Diagnostic Approach to Pituitary Neuroendocrine Tumours (PitNETs): A European Pituitary Pathology Group (EPPG) Proposal. *Virchows Archiv* (2019) 475(6):687–92. doi: 10.1007/s00428-019-02655-0
9. Liu J, He Y, Zhang X, Yan X, Huang Y. Clinicopathological Analysis of 250 Cases of Pituitary Adenoma Under the New WHO Classification. *Oncol Lett* (2020) 19(3):1890–8. doi: 10.3892/ol.2020.11263
10. Tamanini JVG, Dal Fabbro M, de Freitas LLL, Vassallo J, de Souza Queiroz L, Rogerio F. Digital Analysis of Hormonal Immunostaining in Pituitary Adenomas Classified According to WHO 2017 Criteria and Correlation With Preoperative Laboratory Findings. *Neurosurg Focus* (2020) 48(6):E12. doi: 10.3171/2020.3.FOCUS2039
11. Asa SL, Puy LA, Lew AM, Sundmark VC, Elsholtz HP. Cell Type-Specific Expression of the Pituitary Transcription Activator Pit-1 in the Human Pituitary and Pituitary Adenomas. *J Clin Endocrinol Metab* (1993) 77 (5):1275–80. doi: 10.1210/jcem.77.5.8077321
12. McDermott MT, Haugen BR, Gordon DF, Wood WM, Brown NS, Bauer CA, et al. Reverse Transcription Polymerase Chain Reaction Analysis of Pituitary Hormone, Pit-1 and Steroidogenic Factor-1 Messenger RNA Expression in Pituitary Tumors. *Pituitary* (1999) 2(3):217–24. doi: 10.1023/A:1009957411973
13. Neou M, Villa C, Armignacco R, Jouinot A, Raffin-Sanson M-L, Septier A, et al. Pangenomic Classification of Pituitary Neuroendocrine Tumors. *Cancer Cell* (2020) 37(1):123–34.e5. doi: 10.1016/j.ccell.2019.11.002
14. Kim J, Yoon SJ, Moon JH, Ku CR, Kim SH, Lee EJ, et al. Clinical Significance of Radical Surgery in the Treatment of Silent Corticotroph Adenoma. *J Korean Neurosurg Soc* (2019) 62(1):114. doi: 10.3340/jkns.2018.0027
15. Nishioka H, Inoshita N, Mete O, Asa SL, Hayashi K, Takeshita A, et al. The Complementary Role of Transcription Factors in the Accurate Diagnosis of Clinically Nonfunctioning Pituitary Adenomas. *Endocrine Pathol* (2015) 26 (4):349–55. doi: 10.1007/s12022-015-9398-z
16. Saeger W, Lüdecke DK, Buchfelder M, Fahlbusch R, Quabbe H-J, Petersenn S. Pathohistological Classification of Pituitary Tumors: 10 Years of Experience With the German Pituitary Tumor Registry. *Eur J Endocrinol* (2007) 156 (2):203–16. doi: 10.1530/eje.1.02326
17. Mete O, Kefeli M, Çalışkan S, Asa SL. GATA3 Immunoreactivity Expands the Transcription Factor Profile of Pituitary Neuroendocrine Tumors. *Modern Pathol* (2019) 32(4):484–9. doi: 10.1038/s41379-018-0167-7
18. Snyder PJ. *Gonadotroph Adenomas. The Pituitary*. Amsterdam: Elsevier (2011). p. 637–54.
19. Umeoka K, Sanno N, Osamura RY, Teramoto A. Expression of GATA-2 in Human Pituitary Adenomas. *Modern Pathol* (2002) 15(1):11–7. doi: 10.1038/modpathol.3880484
20. Mete O, Cintosun A, Pressman I, Asa SL. Epidemiology and Biomarker Profile of Pituitary Adenohypophysial Tumors. *Modern Pathol* (2018) 31(6):900–9. doi: 10.1038/s41379-018-0016-8
21. Ceccato F, Regazzo D, Barbot M, Denaro L, Emanuelli E, Borsetto D, et al. Early Recognition of Aggressive Pituitary Adenomas: A Single-Centre Experience. *Acta Neurochirurgica* (2018) 160(1):49–55. doi: 10.1007/s00701-017-3396-5

Conflict of Interest: The authors declare that the research was conducted in the absence of any commercial or financial relationships that could be construed as a potential conflict of interest.

Publisher's Note: All claims expressed in this article are solely those of the authors and do not necessarily represent those of their affiliated organizations, or those of the publisher, the editors and the reviewers. Any product that may be evaluated in this article, or claim that may be made by its manufacturer, is not guaranteed or endorsed by the publisher.

frontiers in Oncology

ORIGINAL RESEARCH
published: 13 October 2021
doi: 10.3389/fonc.2021.754882

Electronic Medical Records as Input to Predict Postoperative Immediate Remission of Cushing's Disease: Application of Word Embedding

Wentai Zhang[1†], Dongfang Li[2†], Ming Feng[1], Baotian Hu[2], Yanghua Fan[3], Qingcai Chen[2,4] and Renzhi Wang[1*]*

[1] Department of Neurosurgery, Chinese Academy of Medical Sciences and Peking Union Medical College, Peking Union Medical College Hospital, Beijing, China, [2] School of Computer Science, and Technology, Harbin Institute of Technology (Shenzhen), Shenzhen, China, [3] Department of Neurosurgery, Beijing Tiantan Hospital, Beijing Neurosurgical Institute, Capital Medical University, Beijing, China, [4] Peng Cheng Laboratory, Shenzhen, China

OPEN ACCESS

Edited by:
Qun Wu,
Zhejiang University, China

Reviewed by:
Qingfang Sun,
Shanghai Jiao Tong University, China
Anke Zhang,
Shanghai Jiao Tong University, China

****Correspondence:***
Renzhi Wang
wangrz@126.com
Qingcai Chen
qingcai.chen@hit.edu.cn

[†]These authors have contributed equally to this work and share first authorship

Specialty section:
This article was submitted to Neuro-Oncology and Neurosurgical Oncology, a section of the journal Frontiers in Oncology

Received: *07 August 2021*
Accepted: *20 September 2021*
Published: *13 October 2021*

Citation:
Zhang W, Li D, Feng M, Hu B, Fan Y, Chen Q and Wang R (2021) Electronic Medical Records as Input to Predict Postoperative Immediate Remission of Cushing's Disease: Application of Word Embedding. Front. Oncol. 11:754882. doi: 10.3389/fonc.2021.754882

Background: No existing machine learning (ML)-based models use free text from electronic medical records (EMR) as input to predict immediate remission (IR) of Cushing's disease (CD) after transsphenoidal surgery.

Purpose: The aim of the present study is to develop an ML-based model that uses EMR that include both structured features and free text as input to preoperatively predict IR after transsphenoidal surgery.

Methods: A total of 419 patients with CD from Peking Union Medical College Hospital were enrolled between January 2014 and August 2020. The EMR of the patients were embedded and transformed into low-dimensional dense vectors that can be included in four ML-based models together with structured features. The area under the curve (AUC) of receiver operating characteristic curves was used to evaluate the performance of the models.

Results: The overall remission rate of the 419 patients was 75.7%. From the results of logistic multivariate analysis, operation ($p < 0.001$), invasion of cavernous sinus from MRI ($p = 0.046$), and ACTH ($p = 0.024$) were strongly correlated with IR. The AUC values for the four ML-based models ranged from 0.686 to 0.793. The highest AUC value (0.793) was for logistic regression when 11 structured features and "individual conclusions of the case by doctor" were included.

Conclusion: An ML-based model was developed using both structured and unstructured features (after being processed using a word embedding method) as input to preoperatively predict postoperative IR.

Keywords: natural language processing, Cushing's disease, immediate remission, preoperative prediction, machine learning

INTRODUCTION

Pituitary corticotroph adenoma is also called Cushing's disease (CD). It accounts for the majority of Cushing's syndrome cases (1, 2). Cushing's syndrome causes various types of symptoms and signs, such as central obesity, supraclavicular fat accumulation, thinned skin, purple striae, proximal muscle weakness, fatigue, high blood pressure, glucose intolerance, acne, hirsutism, and neurological deficits (3). The first-line treatment method is transsphenoidal surgery (TSS) according to a consensus statement (4). Thus, immediate remission (IR) is important for both patients and surgeons. A previous systemic review showed that the overall IR rate was 77% (52.1%–96.6%) (5).

Several studies have been conducted to investigate perioperative risk factors for the prediction of postoperative prognosis using both traditional biostatistical and machine learning (ML) methods (6–9). ML is a computer-based method for data analysis based on the theory that there are patterns hidden in data, and it helps to predict the prognosis of diseases (10). ML enables a computer to construct models by iteratively learning from the patterns in the dataset. Therefore, an ML-based model is formed based on learning from real-world data rather than learning from doctors' experience, which may be limited (11). In recent years, there have been an increasing number of ML-related studies on pituitary adenoma. For example, Liu et al. used seven ML-based models that incorporated 17 clinical variables to preoperatively predict the recurrence of CD. The model that performed the best was random forest (RF) with an AUC value of 0.781 (8). Fan et al. used six ML-based models that incorporated 12 clinical variables to predict the TSS response. The final model with the highest AUC value of 0.8555 was the GBDT model.

Features including the preoperative and postoperative serum adrenocorticotropic hormone (ACTH) level, postoperative serum cortisol level, age, and preoperative cavernous sinus invasion on MRI (IOMRI) have been shown to be related to postoperative prognosis (8). All risk factors initially considered in previous studies were selected by clinicians according to their clinical experience and related literature. No existing models use electronic medical records (EMR) as input to predict postoperative IR of patients with CD, even though they may contain a great deal of information that is useful for the prediction of IR. In the present study, EMR is included in the model for the preoperative prediction of postoperative IR of CD.

In recent years, EMR has facilitated data accessibility. There are different types of manifestations in patients with CD because of hypercortisolism that may contain information related to the severity of CD. However, the analysis of diverse and massive EMR data remains challenging because of the complex nature of clinical language and the interpretation process. To address these challenges, in this study, natural language processing techniques are used, specifically contextualized word embeddings, to help humans to access this information in free text to improve predictions. Word embedding is a typical type of natural language processing technique, and it is a suitable method for vectorizing free text so that it can be processed by downstream learning models. Although there has been exponential growth in the number of studies involving radiomics methods, the application of word embedding techniques is still limited (12, 13). In those studies, the text part of EMR was incorporated into the ML model as input, which increased the modal and made the input data closer to real-world data (14, 15).

Postoperative IR is important for clinician–patient communication, and it may influence the treatment strategy. The objective of the present study is to develop an ML model to preoperatively predict postoperative IR using both free text from EMR (after being processed by a word embedding technique) and structured features as input.

Abbreviations: ML, machine learning; TSS, transsphenoidal surgery; CD, Cushing's disease; ROC, receiver operating characteristic curve; AUC, area under the curve; UFC, urine free cortisol; LDDST, low-dose dexamethasone suppression test; HDDST, high-dose dexamethasone suppression test; MRI, magnetic resonance imaging; BIPSS, bilateral inferior petrosal sinus sampling; IOMRI, invasion of cavernous sinus from MRI; LR, logistic regression; RF, random forest; MLP, Multiparametric Linear Programming; SVM, support vector machine.

MATERIALS AND METHODS

Study Population

The present study was approved by the ethical review committee of Peking Union Medical College Hospital (PUMCH). A total of 419 patients with CD were enrolled between January 2014 and August 2020. All surgery was performed by MF.

The inclusion criteria were as follows: (1) manifestations of Cushing's syndrome; (2) positive result on MRI or negative result on MRI, but CD was strongly suspected according to manifestations; (3) ruling out the possibility of ectopic ACTH syndrome; and (4) plasma cortisol level (8:00 a.m.) > 22.3 μg/dl or 24-h UFC level > 103.5 μg.

Diagnosis of Cushing's Disease

All patients had T1-weighted, T2-weighted, and T1-weighted gadolinium-enhanced MRI. Patients whose T1-weighted gadolinium-enhanced MRI showed the negative result of a pituitary tumor had T1-weighted dynamic gadolinium-enhanced MRI. A hypointense region in T1-weighted MRI within the pituitary gland indicated the positive result of a pituitary adenoma. In cases in which the profiles of the potential tumors were inconspicuous, T1-weighted gadolinium-enhanced MRI was required to outline the tumor. A microadenoma was defined as a tumor whose largest diameter was less than 10 mm and a macroadenoma was defined as a tumor whose largest diameter was ≥10 mm. A total of 392/419 participants had histological confirmation of CD, and the diagnosis of CD was based on synthesized evidence that included MRI results, clinical manifestations, results of the low-dose dexamethasone suppression test (LDDST) and high-dose dexamethasone suppression test (HDDST), and pathological results.

All patients underwent a routine combined LDDST and HDDST to verify hypercortisolism and the location of the tumor. In the LDDST, 0.5 mg of dexamethasone was given to

the patient every 6 h for 2 days. The LDDST was considered to be suppressed if 24-h UFC was lower than 12.3 μg/24 h on the second day or plasma cortisol was lower than 1.8 μg/dl in the morning of the third day. In the HDDST, 2 mg of dexamethasone was given to the patient every 6 h for 2 days. HDDST was considered to be suppressed if 24-h UFC on the second day or plasma cortisol in the morning of the third day was >50% lower than the original level. The failure of suppression of the LDDST together with successful suppression of the HDDST indicated CD.

In cases in which there was no evidence of a tumor in preoperative MRI, bilateral inferior petrosal sinus sampling with a desmopressin stimulation test was implemented to confirm the location of the tumor. During the desmopressin test process, 10 mg of desmopressin was given to the patient to stimulate the secretion of ACTH. A ratio of ACTH concentration in the inferior petrosal sinus to peripheral concentration that was larger than 2 in the basal state or larger than 3 after desmopressin stimulation indicated a diagnosis of CD.

The diagnosis of CD was based on the combination of compositive evidence, including MRI results, clinical manifestations, results of LDDST and HDDST, and pathological results.

All TSS was performed by one experienced surgeon (MF). The details of the TSS were discussed previously (16). No medical therapy was administered to patients because of a lack of medicine in China.

The resected tissues were examined for pathology and immunohistochemical analysis for ACTH, growth hormone, thyroid-stimulating hormone, luteinizing hormone, follicle-stimulating hormone, prolactin, Ki-67, and P-53.

Postoperative Management and Immediate Remission

In the first 3 days after TSS (7 days if IR was not achieved), the plasma cortisol level was tested each day. If the cortisol level was lower than 5 μg/dl, glucocorticoid replacement therapy was started. Glucocorticoid replacement therapy started with 100 mg of hydrocortisone twice a day for 3 days following 30 mg of hydrocortisone orally once a day. After being discharged from hospital, patients decreased the dose by 2.5 mg per week until it reached 2.5–5 mg per day. The cessation of the drug was decided by clinicians according to the evaluation of the pituitary function.

IR was defined as a plasma cortisol level (8:00 a.m.) lower than 5 μg/dl or 24-h UFC lower than 20 μg/24 h within 7 days after surgery (17).

Study Design

The data included 11 structured clinical features and 10 unstructured features. Missing values were replaced by average values. The structured data included gender, age, first operation or not, largest tumor diameter, invasion of cavernous sinus on MRI (IOMRI), sellar floor changes (SFC), disease duration, BMI, 24-h UFC, plasma cortisol (8:00 a.m.), and plasma ACTH (8:00 a.m.). The unstructured data included the chief complaint, history of present illness (HPI), past medical history, record of first ward round by superior surgeon, cautions, transferred-out record (from the endocrinology department), transferred-in record (to the neurosurgery department), characteristics of the case, discussions about cases, and individual conclusions of the case by doctor. The 10 unstructured features were routine features of EMR in PUMCH. "Characteristics of the case" were the records of the unique characteristics of an individual patient. "Discussions about cases" were the meeting summaries about all patients' conditions by all surgeons in the neurosurgery department of PUMCH. "Individual conclusions of the case by doctor" were the records of the summary of patients' characteristics provided by MF. "Cautions" were the main points that needed to be noticed about treating patients provided by MF. Transferred-out records were the main points that needed to be noticed about treating patients and basic conditions of the patient provided by the endocrinologist. Transferred-in records were the main points that needed to be noticed about treating patients and basic conditions of the patient provided by the neurosurgeon. The EMR of unstructured features was vectorized using a word embedding method, and could then can be analyzed in a similar manner to structured features.

The *F*-test was used to rank the structured data. The 10 structured features were sequentially included into each model. Then, each model outputs AUC values for different numbers of features. The min–max normalization method was used on the data. The highest AUC values of the four algorithms were used as their baseline values. Ten features of the unstructured data were introduced into each model individually, and the importance of each unstructured feature was ranked according to the change of AUC.

ML Algorithms

Four ML algorithms were applied: support vector machine (SVM), logistic regression (LR), RF, and multilayer perceptron (MLP). In each ML algorithm, structured data were sequentially introduced into the algorithm according to their rank in the training dataset. Then, in the test dataset, the same process was conducted. In both the training and test datasets, 10-fold cross-validation was performed. Then, a grid search was used to select the best hyperparameters, as discussed elsewhere (7).

Statistical Analysis

Statistical analysis was performed using RStudio software (1.2.5042), IBM SPSS Statistics 23 (IBM Corporation), and Python. The Shapiro–Wilk test was used to evaluate the normality of continuous variables. Normally distributed variables were displayed as mean ± standard deviation. Non-normally distributed variables were displayed as the interquartile range. The Wilcoxon test was used to compare non-normal distributed continuous variables in the training dataset and test dataset. Categorical variables were analyzed using a chi-squared test or Fisher's exact test.

Occlusion Tests

"Occlusion tests" were performed to determine the contributions that the symptomatic entities made to the ML-based models.

In the "occlusion tests", CMeKG (http://cmekg.pcl.ac.cn/) was used to select and delete the symptomatic entities to build a new HPI without symptomatic descriptions of CD. Then, the two HPIs were vectorized and merged into LR together with the structured features. The result demonstrated that the model with the input of the original HPI was conspicuously superior to that with the input of the newly built HPI.

RESULTS

Patients' Characteristics

A total of 419 patients were included in the study between January 2014 and August 2020. Eleven traditionally used predictors were selected in the study: age, gender, first operation (or not), SFC, IOMRI, tumor diameter (microadenoma or macroadenoma), disease duration, BMI, 24-h UFC, morning plasma cortisol level, and morning plasma ACTH level. All the predictors are presented in **Table 1**. The characteristics of the remission and non-remission groups are presented in **Table 2**. From the results of logistic univariate analysis, the first operation ($p < 0.001$), IOMRI ($p = 0.010$), SFC ($p = 0.011$), and ACTH ($p = 0.009$) were strongly correlated with IR. From the results of logistic univariate analysis, the first operation ($p < 0.001$), IOMRI ($p = 0.046$), and ACTH ($p = 0.024$) were strongly correlated with IR (**Table 3**).

Predictive Performance of Models

Four ML-based algorithms were used: MLP, SVM, RF, and LR. The performance of each model with different numbers of structured features is shown in **Figure 1**. The highest AUC values for MLP, SVM, RF, and LR were 0.759, 0.733, 0.678, and 0.699, respectively (**Figure 2**). Each unstructured feature was sequentially introduced into the model, which had all structured features included. Then, each model outputs an AUC value (**Table 4**). The chief complaint and individual conclusions of the case by doctor, HPI and individual conclusions of the case by doctor, together with chief complaint and HPI were then introduced into each model; however, the AUC values were not higher than when only one unstructured feature was introduced into the model. The highest AUC value (0.793) was achieved by LR when 11 structured features and individual conclusions of the case by doctor were introduced.

Unstructured features contain too much redundant information; hence, three or more unstructured features were not combined in this study to extract valid information.

Variable Importance

F-test univariate analysis was used to rank the importance of the 11 variables. Their rank was as follows: first operation, SFC, morning ACTH, IOMRI, 24-h UFC, disease duration, BMI, tumor diameter, gender, plasma cortisol, and age. The rank of the features of unstructured data was evaluated using the change in AUC value after adding a single unstructured feature into the model based only on the structured features. For LR, "individual conclusions of the case by doctor" was ranked first.

Occlusion Tests

The performance of the model with the input of the original HPI was conspicuously better than that with the input of the HPI without symptomatic entities (**Table 5**). The red Chinese characters indicate the deleted symptomatic entities.

DISCUSSION

TSS is the first-line treatment method for CD. IR rates are typically between 59% and 96.6% (18). In the present study,

TABLE 1 | Participants' characteristics in trainning and test datasets.

Characteristic	Total	Training dataset	Test dataset	*p*-value
Gender	419	335	84	0.991
Male	80 (19.09)	64 (19.10)	16 (19.05)	
Female	339 (80.91)	271 (80.90)	68 (80.95)	
Age (years)	37.86 ± 13.06	37.94 ± 13.04	37.55 ± 13.06	0.808
First Operation				0.492
Yes	359 (85.68)	289 (86.27)	70 (83.33)	
No	60 (14.32)	46 (13.73)	14 (16.67)	
Diameter				0.684
Macroadenoma	40 (9.55)	31 (9.25)	9 (10.71)	
Microadenoma	379 (90.45)	304 (90.75)	75 (89.29)	
IOMRI				0.098
Invasion	26 (6.21)	19 (5.67)	9 (10.71)	
Non-invasion	393 (93.79)	316 (94.33)	75 (89.29)	
Sellar Floor				0.700
Infiltrated	45 (10.74)	35 (10.45)	10 (11.90)	
Normal	374 (89.26)	300 (89.55)	74 (88.10)	
Disease Duration (months)	36 (18–72)	36 (18–72)	43.5 (24–84)	0.121
BMI	26.14 (24.04–28.93)	26.15 (24.12–29.03)	26.13 (23.51–28.21)	0.476
24-h UFC (μg)	426.40 (268.65–716.40)	441.80 (270.63–745.66)	411.68 (243.58–586.41)	0.139
Cortisol (μg/dl)	27.15 (22.39–33.01)	27.02 (22.48–32.49)	27.89 (21.59–33.67)	0.715
ACTH (pg/ml)	72.6 (49.6–105)	72.9 (50.7–106.5)	66.3 (44.23–95.75)	0.446

TABLE 2 | Patients' characteristics in remission and non-remission groups.

Characteristic	Remission	Non-remission	*p*
Gender	317	102	
Male	65 (20.50)	15 (14.71)	0.195
Female	252 (79.50)	87 (85.29)	
Age (years)	37.74 ± 13.01	38.25 ± 13.25	0.730
First Operation			
Yes	287 (90.54)	72 (70.59)	**0.005**
No	30 (9.46)	30 (29.41)	
Diameter			
Macroadenoma	27 (8.52)	13 (12.75)	0.206
Microadenoma	290 (91.48)	89 (87.25)	
IOMRI			
Invasion	14 (4.42)	12 (11.76)	**0.007**
Non-invasion	303 (95.58)	90 (88.24)	
Sellar Floor Changes			
Infiltrated	27 (8.52)	18 (17.65)	**0.010**
Normal	290 (91.48)	84 (82.35)	
Disease Duration (months)	36 (18–72)	48 (20.25–84)	0.256
BMI	26 (24.03–28.87)	26.56 (24.30–29.27)	0.448
24-h UFC (μg)	412.56 (266.7–675.24)	452.22 (283.92–821.78)	0.337
Cortisol (μg/dl)	27.5 (22.03–32.61)	26.72 (23.03–33.87)	0.954
ACTH (pg/ml)	68.3 (45.3–104)	86.45 (55.40–114.50)	**0.004**

Bold values in this table represent statistical significance (P < 0.05).

the IR rate was 75.7% (317/419), which is almost the same as the result of 76% from a previous study (19). IR may be a strong predictor of long-term remission (20). IR is also important for doctor–patient communication because patients are always concerned about whether clinical manifestations can be eliminated immediately. Thus, it is of great importance to develop an ML-based model for the preoperative prediction of IR.

Various types of manifestations exist in patients with CD because of hypercortisolism, such as abnormal fat distribution, weight gain, osteoporosis, diabetes mellitus ecchymosis, and hypokalemia. According to our limited experience, the symptoms and signs a patient has are strongly correlated with the patient's prognosis. Therefore, we speculate that the unstructured data of patients with CD contributes to the ML-based model for the preoperative prediction of IR. The manifestations of patients with CD may be recorded in EMR, which has been ignored by clinicians in quantitative analysis because natural language could not be processed in the past. However, natural language processing techniques can now deal with EMR as the input of ML-based models, which facilitates the full use of multimodal data (structured data and unstructured data in EMR). In the present study, we performed occlusion tests on HPI and the results demonstrated that the performance of the model with the input of the original HPI was better than that with the input of HPI without symptomatic entities. Therefore, we speculated from the occlusion test and our limited experience that symptomatic entities in HPI were strongly related to IR and conducive to the prediction of IR.

In our previous study, we used several ML algorithms to build ML-based models to preoperatively predict IR (7). In that study, we only included structured data in the ML-based model, whereas in the present study, we introduced not only structured data into the models but also unstructured data. Unstructured data may contain information related to the severity of CD in addition to the 11 features of structured data

TABLE 3 | Logistic univariate and multivariate analysis of the relationship between risk factors and IR.

Characteristics	Univariate analysis			Multivariate analysis		
	OR	95% CI	*p*-value	OR	95% CI	*p*-value
Gender	1.496	0.811–2.759	0.197			
Age (years)	0.997	0.980–1.014	0.726			
First Operation	3.986	2.258–7.036	**<0.001**	3.641	1.996–6.641	**<0.001**
Diameter	0.637	0.316–1.687	0.209			
IOMRI	0.347	0.155–0.776	**0.010**	0.413	0.17.–0.985	**0.046**
Sellar Floor Changes	0.434	0.228–0.827	**0.011**	0.818	0.393–1.703	0.591
Disease Duration (months)	0.998	0.994–1.002	0.436			
BMI	0.970	0.923–1.021	0.246			
24-h UFC (μg)	1.000	1.000–1.000	0.166			
Cortisol (μg/dl)	1.001	0.980–1.023	0.898			
ACTH (pg/ml)	0.994	0.990–0.999	**0.009**	0.995	0.991–0.999	**0.024**

Bold values in this table represent statistical significance (P < 0.05).

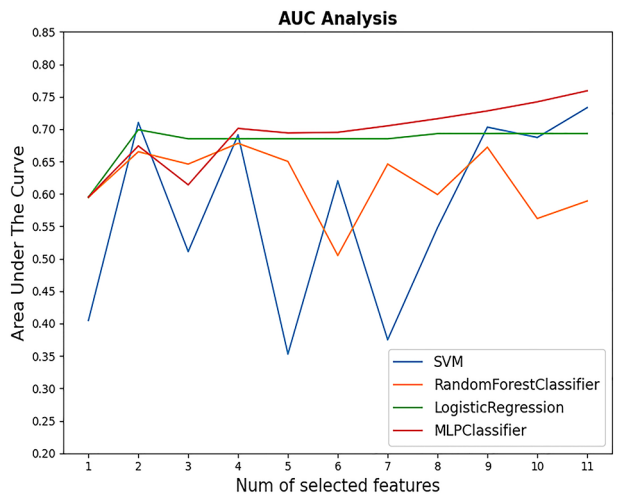

FIGURE 1 | AUC values of four models with different numbers of structured features selected. The highest AUC value appeared when MLP with 11 variables came into use (AUC = 0.759).

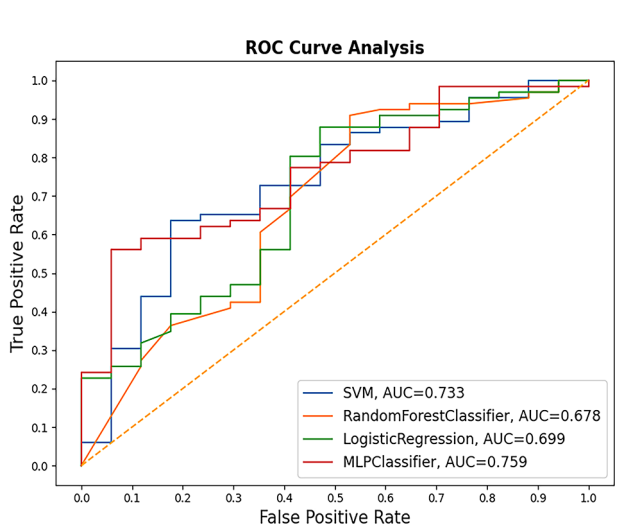

FIGURE 2 | Performances of models with optimal number of structured features. MLP performed the best.

that were summarized by clinicians according to their personal experience. The features included in the final model with the highest AUC (0.743) in our previous study were IOMRI, tumor size, whether it is the first operation, and ACTH level (8:00 a.m.), whereas in the present study, the model with the highest AUC (0.793) was constructed using LR with 11 structured features and "individual conclusions of the case by doctor." The model performance in the present study was superior to that in the previous study.

The importance of the features of structured data was ranked using the *F*-test, whereas the importance of the features of unstructured data was evaluated using the change in AUC value after adding a single unstructured feature into the model based only on the structured features. Information such as image and voice, itself has the characteristics of vectorization, continuity. Natural language (EMR) is different. It is the expression and abstract summary of objective things. This is the advantage of human thought; however, it restricts computers to the identification of natural language because it lacks a strong correlation between specific sensory information and natural language. In the past, computers could only perform statistical and logical reasoning through the relationship between symbols, which made it difficult to express the continuity of language. In 2013, Mikolov et al. (21) enabled vocabulary to form the deep model input of continuous real number space in the same manner as images and audio, and the learning efficiency of the model was much higher than that of previous models. Thus, we used a word embedding method in the present study to vectorize EMR. "Individual conclusions of the case by doctor" are routine records in EMR at PUMCH. They are the conclusions of clinicians according to the clinical characteristics of patients, and they may reflect the subjective perception of doctors about the severity of the disease. Therefore, we speculated that key information related to the severity of the disease may be hidden in free text and could contribute to the ML-based model.

Table 4 shows that the AUC values of MLP and SVM did not increase after unstructured features were introduced into the model, whereas, simultaneously, the AUC values increased significantly after "individual conclusions of the case by doctor" was introduced into the model. These two contrasting results are mainly caused by several factors, as we speculated. First, unstructured data text is generally long, with a great deal of useless information, and can easily be overfitted in MLP, which can lead to the decline of AUC values. Similarly, SVM looks for a hyperplane to separate data points, which makes it difficult to determine an appropriate hyperplane to separate them in the case of complex data features. Therefore, the performance of SVM decreases after unstructured data that contain a great deal of redundant information are introduced into the model. The linear model structure of LR enables it to capture quasi-linear characteristics and ignore high-dimensional redundant information; hence, it can capture key information in the unstructured text to obtain a high-grade classification capacity. To summarize, MLP and SVM are more complex than LR, which made the latter even more effective in the present study.

To the best of our knowledge, the present study is the first to use unstructured data from the EMR of patients with CD as the input of ML-based models. In this process, we embedded these unstructured features, and transformed them into relatively low-dimensional dense vectors to facilitate the model construction of ML (22, 23). In previous studies on the ML model construction process, one-hot encoding on discrete characteristics was typically feasible for clinically used binary structured data (e.g., gender). However, features with one-hot encoding may be too high-dimensional and sparse for EMR data, which is not conducive to model training. CD is a type of neuroendocrine tumor that causes not only a mass effect but also various types of

TABLE 4 | AUC values and 95 confidence interval of different models with different features.

	MLP	SVM	RF	LR
Structured data	**0.759**	**0.733**	0.678	0.699
	[0.633, 0.885]	**[0.612, 0.845]**	[0.544,0.812]	[0.594,0.803]
Chief complaint	0.729	0.661	**0.686**	0.777
	[0.606, 0.852]	[0.583,0.739]	**[0.610,0.756]**	[0.709, 0.845]
HPI	0.670	0.652	0.642	0.737
	[0.552, 0.788]	[0.570, 0.734]	[0.549, 0.735]	[0.624, 0.850]
Past medical history	0.606	0.610	0.556	0.577
	[0.515, 0.697]	[0.515, 0.705]	[0.491,0.621]	[0.474,0.640]
RFWR	0.506	0.692	0.533	0.573
	[0.413,0.599]	[0.572, 0.811]	[0.425,0.641]	[0.455,0.690]
Cautions	0.619	0.718	0.468	0.674
	[0.494, 0.744]	[0.608, 0.830]	[0.317,0.619]	[0.530, 0.818]
Transferred-out record	0.473	0.614	0.613	0.556
	[0.334,0.611]	[0.494, 0.734]	[0.503, 0.723]	[0.421,0.691]
Transferred-in record	0.656	0.625	0.602	0.679
	[0.521, 0.791]	[0.492, 0.758]	[0.479, 0.725]	[0.562, 0.796]
Characteristics of the case	0.571	0.575	0.474	0.676
	[0.484, 0.657]	[0.432,0.717]	[0.317,0.630]	[0.566,0.786]
Discussions about cases	0.582	0.628	0.505	0.622
	[0.445,0.718]	[0.556, 0.696]	[0.430, 0.580]	[0.505, 0.739]
Individual conclusions of the case by doctor	0.723	0.682	**0.686**	**0.793**
	[0.622, 0.824]	[0.584,0.780]	**[0.623,0.743]**	**[0.689, 0.897]**
Chief complaint and individual conclusions of the case by doctor	0.669	0.722	0.442	0.678
	[0.585,0.753]	[0.628, 0.816]	[0.252, 0.632]	[0.582,0.744]
HPI and individual conclusions of the case by doctor	0.737	0.691	0.499	0.678
	[0.677, 0.796]	[0.596, 0.785]	[0.359, 0.639]	[0.603,0.753]
Chief complaint and HPI	0.680	0.669	0.429	0.721
	[0.589,0.771]	[0.752,0.766]	[0.295,0.073]	[0.635, 0.806]

Bold values in this table represent highest AUC value in each ML based model.

TABLE 5 | Example of Occlusion Test Results.

	Original HPI	HPI after Deletion of Symptomatic Entities by CMeKG
Symptoms	患者诉于2年前无明显诱因出现双下肢水肿，乏力，无皮肤菲薄、紫纹。 (The patient complained that edema and weakness in lower limbs appeared 2 years ago without obvious causes. There was no thin skin or purple striae.)	患者诉于2年前无明显诱因出现，无皮肤菲薄、紫纹。 (The patient complained that appeared 2 years ago without obvious causes. There was no thin skin or purple striae.)
AUC	0.737	0.629

endocrine symptoms recorded in EMR that can be fully used by an ML-based model after embedding.

In the present study, the final model with the highest AUC included all structured features; however, according to the *F*-test, four structured features were correlated with IR. Their rank is as follows: first operation or not, SFC, ACTH, and IOMRI. If a patient has already undergone at least one operation, there is a higher chance that the tumor is more invasive and aggressive, which may cause postoperative residual (24). SFC was the second-most important predictor of IR in the present study. If the sellar floor of a patient is infiltrated on preoperative MRI, it is likely that the tumor has higher invasiveness that makes it invade the mucosa and bone in the sellar region. In this circumstance, there is a relatively great possibility of postoperative residual. Preoperative ACTH level was the third-most important predictor of IR, which is consistent with our previous study (9). IOMRI was the fourth-most important predictor, which is also consistent with our previous study (9). An intriguing observation is that tumor size was not a predictor of IR, which is inconsistent with previous studies (9, 19, 25, 26). In our previous study (7), tumor size was strongly correlated with IR when two surgeons performed operations over several decades. However, in the present study, only MF performed the operation. We can speculate from the result that with the evolution of surgical skills and personal experience, tumor size is no longer a major predictor of IR.

STRENGTHS AND LIMITATIONS

The present study has two strengths. First, this is the first study that used deep learning techniques to deal with EMR of patients with CD as input of an ML-based model that improved model performance. EMR contains sufficient information about the patient to reflect real-world information. Second, a relatively large CD cohort was considered. There are also two limitations. First, this was a single-center study. Second, the performance of the ML-based model depended on the quality of EMR.

CONCLUSIONS

EMR of patients with CD can be used as input to an ML-based model after being processed to preoperatively predict IR. The model with structured features together with unstructured features conspicuously enhanced the performance of the model compared with the model that used only structured features as input. First operation or not, SFC, ACTH, and IOMRI were the most important predictors of IR of CD.

DATA AVAILABILITY STATEMENT

The raw data supporting the conclusions of this article will be made available by the authors, without undue reservation.

ETHICS STATEMENT

The studies involving human participants were reviewed and approved by the ethical review committee of Peking Union Medical College Hospital. Written informed consent to participate in this study was provided by the participants' legal guardian/next of kin.

AUTHOR CONTRIBUTIONS

WZ and DL contributed equally to the present study. Each author contributes to the article in data collecting and analysis. RW and QC take final responsibility for this article. All authors contributed to the article and approved the submitted version.

FUNDING

This work was supported by the CAMS Innovation Fund for Medical Sciences (CIFMS) (2020-I2M-C&T-B-031), the Natural Science Foundation of China (Grant Nos. 61872113 and 62006061), and the Shenzhen Foundational Research Funding (JCYJ20200109113441941).

ACKNOWLEDGMENTS

We thank Maxine Garcia, PhD, from Liwen Bianji (Edanz) (www.liwenbianji.cn/) for editing the English text of a draft of this manuscript.

REFERENCES

1. Steffensen C, Bak AM, Rubeck KZ, Jorgensen JO. Epidemiology of Cushing's Syndrome. *Neuroendocrinology* (2010) 92(Suppl 1):1–5. doi: 10.1159/000314297
2. Pivonello R, De Leo M, Cozzolino A, Colao A. The Treatment of Cushing's Disease. *Endocr Rev* (2015) 36(4):385–486. doi: 10.1210/er.2013-1048
3. Arnaldi G, Angeli A, Atkinson AB, Bertagna X, Cavagnini F, Chrousos GP, et al. Diagnosis and Complications of Cushing's Syndrome: A Consensus Statement. *J Clin Endocrinol Metab* (2003) 88(12):5593–602. doi: 10.1210/jc.2003-030871
4. Biller BMK, Grossman AB, Stewart PM, Melmed S, Bertagna X, Bertherat J, et al. Treatment of Adrenocorticotropin-Dependent Cushing's Syndrome: A Consensus Statement. *J Clin Endocrinol Metab* (2008) 93(7):2454–62. doi: 10.1210/jc.2007-2734
5. Petersenn S, Beckers A, Ferone D, van der Lely A, Bollerslev J, Boscaro M, et al. Therapy of Endocrine Disease: Outcomes in Patients With Cushing's Disease Undergoing Transsphenoidal Surgery: Systematic Review Assessing Criteria Used to Define Remission and Recurrence. *Eur J Endocrinol* (2015) 172(6):R227–39. doi: 10.1530/EJE-14-0883
6. Zoli M, Staartjes VE, Guaraldi F, Friso F, Rustici A, Asioli S, et al. Machine Learning-Based Prediction of Outcomes of the Endoscopic Endonasal Approach in Cushing Disease: Is the Future Coming? *Neurosurg Focus* (2020) 48(6):E5. doi: 10.3171/2020.3.FOCUS2060
7. Zhang W, Sun M, Fan Y, Wang H, Feng M, Zhou S, et al. Machine Learning in Preoperative Prediction of Postoperative Immediate Remission of Histology-Positive Cushing's Disease. *Front Endocrinol* (2021) 12:635795. doi: 10.3389/fendo.2021.635795
8. Liu Y, Liu X, Hong X, Liu P, Bao X, Yao Y, et al. Prediction of Recurrence After Transsphenoidal Surgery for Cushing's Disease: The Use of Machine Learning Algorithms. *Neuroendocrinology* (2019) 108(3):201–10. doi: 10.1159/000496753
9. Dai C, Fan Y, Liu X, Bao X, Yao Y, Wang R, et al. Predictors of Immediate Remission After Surgery in Cushing's Disease Patients: A Large Retrospective Study From a Single Center. *Neuroendocrinology* (2020). doi: 10.1159/000509221
10. Cleophas TJ. Machine Learning in Therapeutic Research: The Hard Work of Outlier Detection in Large Data. *Am J Ther* (2016) 23(3):e837–43. doi: 10.1097/MJT.0b013e31827ab4a0
11. Rajkomar A, Dean J, Kohane I. Machine Learning in Medicine. *Reply N Engl J Med* (2019) 380(26):2589–90. doi: 10.1056/NEJMra1814259
12. José Antonio Miñarro-Giménez OM-A. Matthias, Samwald. Exploring the Application of Deep Learning Techniques on Medical Text Corpora. *Stud Health Technol Informatics* (2014) 205:584–8. doi: 10.3233/978-1-61499-432-9-584
13. Rajkomar A, Oren E, Chen K, Dai AM, Hajaj N, Hardt M, et al. Scalable and Accurate Deep Learning With Electronic Health Records. *NPJ Digital Med* (2018) 1.1:1–10. doi: 10.1038/s41746-018-0029-1
14. Esteva A, Robicquet A, Ramsundar B, Kuleshov V, DePristo M, Chou K, et al. A Guide to Deep Learning in Healthcare. *Nat Med* (2019) 25(1):24–9. doi: 10.1038/s41591-018-0316-z
15. Xiao C, Choi E, Sun J. Opportunities and Challenges in Developing Deep Learning Models Using Electronic Health Records Data: A Systematic Review. *J Am Med Inf Assoc* (2018) 25(10):1419–28. doi: 10.1093/jamia/ocy068
16. Feng M, Liu Z, Liu X, Bao X, Yao Y, Deng K, et al. Diagnosis and Outcomes of 341 Patients With Cushing's Disease Following Transsphenoid Surgery: A Single-Center Experience. *World Neurosurg* (2018) 109:e75–80. doi: 10.1016/j.wneu.2017.09.105
17. Nieman LK, Biller BMK, Findling JW, Murad MH, Newell-Price J, Savage MO, et al. Treatment of Cushing's Syndrome: An Endocrine Society Clinical Practice Guideline. *J Clin Endocrinol Metab* (2015) 100(8):2807–31. doi: 10.1210/jc.2015-1818
18. Ioachimescu AG. Prognostic Factors of Long-Term Remission After Surgical Treatment of Cushing's Disease. *Endocrinol Metab Clinics North America* (2018) 47(2):335–47. doi: 10.1016/j.ecl.2018.02.002
19. Abu Dabrh AMA, Singh Ospina NM, Al Nofal A, Farah WH, Barrionuevo P, Sarigianni M, et al. Predictors of Biochemical Remission and Recurrence After Surgical and Radiation Treatments of Cushing Disease: A Systematic Review and Meta-Analysis. *Endocr Pract: Off J Am Coll Endocrinol Am Assoc Clin Endocrinologists* (2016) 22(4):466–75. doi: 10.4158/EP15922.RA
20. Ironside N, Chatain G, Asuzu D, Benzo S, Lodish M, Sharma S, et al. Earlier Post-Operative Hypocortisolemia may Predict Durable Remission From Cushing's Disease. *Eur J Endocrinol* (2018) 178(3):255–63. doi: 10.1530/EJE-17-0873

21. Tomas Mikolov KC, Corrado G, Dean J. Efficient Estimation of Word Representation in Vector Space. *ICLR (workshop poster)* (2013).
22. Tomas Mikolov IS, Chen K, Corrado GS, Dean J. Distributed Representations of Words and Phrases and Their Compositionality. *Advances in Neural Information Processing System 26: 27th Annual Conference on Neural Information Processing System 2013. Proceeding of a meeting held December 5-8*. Lake Tahoe, Nevada, USA (2013) 26:3111–19. doi: 10.5555/2999792.2999959
23. Yan Song SS, Li J, Zhang H. Directional Skip-Gram: Explicitly Distinguishing Left and Right Context for Word Embeddings. *Proceeding of the 2018 Conference of the North American Chapter of the Association for Computational Linguistics: Human Laguage Technologies*. New Orleans, Louisiana, USA: NAACL-HLT (2018) 2:175–80. doi: 10.18653/v1/N18-2028
24. Starke RM, Reames DL, Chen C-J, Laws ER, Jane JA. Endoscopic Transsphenoidal Surgery for Cushing Disease: Techniques, Outcomes, and Predictors of Remission. *Neurosurgery* (2013) 72(2):240–7. doi: 10.1227/NEU.0b013e31827b966a
25. Blevins LS, Christy JH, Khajavi M, Tindall GT. Outcomes of Therapy for Cushing's Disease Due to Adrenocorticotropin-Secreting Pituitary Macroadenomas. *J Clin Endocrinol Metab* (1998) 83(1):63–7. doi: 10.1210/JCEM.83.1.4525
26. Chandler WF, Barkan AL, Hollon T, Sakharova A, Sack J, Brahma B, et al. Outcome of Transsphenoidal Surgery for Cushing Disease: A Single-Center Experience Over 32 Years. *Neurosurgery* (2016) 78(2):216–23. doi: 10.1227/NEU.0000000000001011

Conflict of Interest: The authors declare that the research was conducted in the absence of any commercial or financial relationships that could be construed as a potential conflict of interest.

Publisher's Note: All claims expressed in this article are solely those of the authors and do not necessarily represent those of their affiliated organizations, or those of the publisher, the editors and the reviewers. Any product that may be evaluated in this article, or claim that may be made by its manufacturer, is not guaranteed or endorsed by the publisher.

frontiers in Oncology

REVIEW
published: 17 November 2021
doi: 10.3389/fonc.2021.773905

Anti-VEGF Therapy in Refractory Pituitary Adenomas and Pituitary Carcinomas: A Review

Congxin Dai[1†], Siyu Liang[2†], Bowen Sun[1], Yong Li[1] and Jun Kang[1]*

[1] Department of Neurosurgery, Beijing Tongren Hospital, Capital Medical University, Beijing, China, [2] Eight-Year Program of Clinical Medicine, Peking Union Medical College Hospital (PUMCH), Chinese Academe of Medical Sciences & Peking Union Medical College (CAMS & PUMC), Beijing, China

Most pituitary tumors are considered benign adenomas, and only 0.1%–0.2% of them present metastasis and are defined as pituitary carcinomas (PCs). Refractory pituitary adenomas (PAs) lie between benign adenomas and true malignant PCs and are defined as aggressive-invasive PAs, characterized by a high Ki-67 index, rapid growth, frequent recurrence, and resistance to conventional treatments. Refractory PAs and PCs are notoriously difficult to manage because of limited therapeutic options. Vascular endothelial growth factor (VEGF) plays a crucial role in angiogenesis not only during development but also during pathological processes in pituitary tumors. Recently, increasing numbers of preclinical studies and clinical research have demonstrated that anti-VEGF therapy plays an important role in pituitary tumors. The purpose of this review is to report the role of VEGF in the development and pathology of pituitary tumors and the progress of anti-VEGF therapy in pituitary tumors, including refractory PAs and PCs. Previous preclinical studies indicated that cyclin-dependent kinase 5 (CDK5)-mediated VEGF expression might play a crucial role in the development of PAs. Vascular endothelial growth inhibitors have been reported as independent predictors of invasion in human PAs and have been indicated as markers for poor outcome. Furthermore, several studies have reported that angiogenesis decreases tumor sizes in experimental animal models of pituitary tumors. The expression of VEGF is relatively high in PAs; therefore, anti-VEGF therapy has been used in some refractory PAs and PCs. To date, anti-VEGF has been reported as monotherapy, in combination with temozolomide (TMZ), TMZ and radiotherapy, and with pasireotide, which might be a promising alternative therapy for refractory PAs and PCs resistant to conventional treatments. However, the role of anti-VEGF therapy in pituitary tumors is still controversial due to a lack of large-scale clinical trials. In summary, the results from preclinical studies and clinical trials indicated that anti-VEGF therapy monotherapy or in combination with other treatments may be a promising alternative therapy for refractory PAs and PCs resistant to conventional treatments. More preclinical studies and clinical trials are needed to further evaluate the exact efficacy of anti-VEGF in refractory PAs and PCs.

Keywords: refractory pituitary adenomas, pituitary carcinomas, VEGF, anti-VEGF, vascular endothelial growth inhibitor

OPEN ACCESS

Edited by:
Qun Wu,
Zhejiang University, China

Reviewed by:
Yubo Wang,
First Affiliated Hospital of Jilin University, China
Run Yu,
UCLA David Geffen School of Medicine, United States

****Correspondence:***
Jun Kang
junkang2015@163.com

[†]These authors have contributed equally to this work

Specialty section:
This article was submitted to Neuro-Oncology and Neurosurgical Oncology, a section of the journal Frontiers in Oncology

Received: *10 September 2021*
Accepted: *27 October 2021*
Published: *17 November 2021*

Citation:
Dai C, Liang S, Sun B, Li Y and Kang J (2021) Anti-VEGF Therapy in Refractory Pituitary Adenomas and Pituitary Carcinomas: A Review. Front. Oncol. 11:773905. doi: 10.3389/fonc.2021.773905

INTRODUCTION

Pituitary adenomas (PAs) are common tumors arising in the anterior pituitary gland with the second highest incidence, representing approximately 10%–15% of intracranial primary tumors (1–3). Most PAs are considered benign tumors that can be cured by surgery and medication. However, a subset of invasive PAs with a high Ki-67, rapid growth, and early recurrences is refractory to conventional treatments such as surgery, medication, and radiotherapy and are referred to as refractory PAs (4). Rarely, 0.1%–0.2% of pituitary tumors can present with either craniospinal dissemination or systemic metastases, which are true malignant tumors and defined as pituitary carcinomas (PCs) (5). Refractory PAs and PCs are notoriously difficult to manage because of limited availability of therapeutic approaches. Recently, temozolomide (TMZ) has been recommended as a first-line treatment for refractory PAs and PCs by the European Society of Endocrinology due to its promising efficacy. However, only approximately 60% of patients show a response to TMZ, and some patients develop resistance during treatment (6, 7). Therefore, the discovery of new therapeutic targets is of particular importance for the management of refractory PAs and PCs. Recent studies have shown that vascular endothelial growth factor (VEGF) and its receptor (VEGFR) play crucial roles in angiogenesis not only in its development but also during pathological processes in pituitary tumors (8). Moreover, an increasing number of clinical case reports have demonstrated that anti-VEGF therapy is beneficial in treating refractory PAs and PCs. Here, this review presents the role of the VEGF/VEGFR pathway in angiogenesis of pituitary tumors and the progress of anti-VEGF therapy in pituitary tumors, including refractory PAs and PCs.

ANGIOGENESIS IN PITUITARY TUMORS

Angiogenesis, the process of blood vessel growth, is essential for tumor progression and metastasis (9). During angiogenesis, an organized vascular network develops from a primitive vascular network (10). Angiogenesis correlates with the development of metastasis (11–13), recurrence (14), and poor prognosis (15, 16) in many human tumors, including breast, bladder, prostate, and stomach tumors. Contrary to most solid tumors, PA tissue contains fewer blood vessels than normal pituitary glands (17). In particular, not only was the number of vessels much lower but also the size of each vessel was much smaller in PAs than in normal pituitary glands (17–22). The angiogenesis between different PA subtypes is divergent among studies. Jugenburg et al. (22) reported that PAs have significantly lower vascular densities than non-tumorous adenohypophyses. Pituitary prolactin (PRL)-secreting adenomas have the highest vascular densities, and growth hormone (GH)-producing adenomas have the lowest vascular densities. However, no differences were observed between noninvasive and invasive PAs. Primary PCs show no significant increase in vascular densities, but some metastatic tumors exhibit high vascularity. These results indicated that PAs have a limited capacity to induce angiogenesis. Another study demonstrated that the highest counts of immunopositive vascular profiles were noted in follicle-stimulating hormone (FSH)-expressing adenomas, whereas the lowest vascular density was observed in GH-expressing tumors (22, 23). Angiogenesis has been shown to be related to clinical behavior, prognosis, and response to treatment in many different types of PAs. Turner et al. (17, 24) reported that invasive macroprolactinomas were significantly more vascular than noninvasive tumors; however, medical therapy with metyrapone or bromocriptine did not influence angiogenesis in adenomas. Vidal et al. (25) also reported a tendency of invasive PAs to be more highly vascularized than noninvasive PAs; the highest level of microvessel density was found in PCs, while the lowest was found in GH-producing adenomas. Moreover, they demonstrated that the microvessel density of macroadenomas in older patients was significantly higher than that in patients younger than 40 years (25). In summary, PAs are usually less vascularized than normal pituitary glands, while PCs are more vascular than PAs. Although the vascular densities may be related to tumor size, proliferation, hemorrhage, and the treatment response of PAs (19–22, 25), it is still unclear what specific role they play in the tumorigenesis and progression of PAs.

VASCULAR ENDOTHELIAL GROWTH FACTOR EXPRESSION IN PITUITARY TUMORS

VEGFs are key mediators of endothelial cell proliferation, angiogenesis, and vascular permeability. VEGFs are a family of angiogenic and lymphangiogenic growth factors. VEGF pathways comprise multiple VEGF glycoproteins (VEGFA, VEGFB, VEGFC, VEGFD, and VEGFE) and multiple transmembrane receptors (VEGFR1, VEGFR2, and VEGFR3) (26). VEGFA, commonly referred to as VEGF, has multiple isoforms as a result of alternative exon splicing (27). Although they have various affinities, these isoforms are all capable of binding to VEGFR1 or VEGFR2. VEGFR has intracellular tyrosine kinase activity, which is considered to be the major mediator of the angiogenic properties of VEGF. VEGF binds to the external membrane domain of VEGFR and causes intracellular signaling in endothelial cells, resulting in proliferation and migration (28). VEGF and VEGFR contribute to a potential therapeutic target in a variety of tumors (29–31). VEGF and its receptors are regularly overexpressed in a wide variety of human cancers, including PAs and PCs. Although the concordance of VEGF expression between studies may be poor, in general, VEGF immunoreactivity is moderate to strong in most cases (32). Lloyd et al. (33) analyzed VEGF expression in 148 cases and found positive staining in all subtypes, with a mild to moderate degree in 92.3% (131/142) of PAs and a strong degree in 100% (6/6) of PCs. Fukui et al. (34) also found that VEGF expression was weak in 12.5% (6/48), moderate in 54.2% (26/48), and strong in 33.3% (16/48) in a total of 48 PAs. Wang

et al. (35) reported that 58.9% of 197 PAs had strong VEGF expression. VEGF mRNA was detected in more than 85% of PAs and had a significant correlation with VEGF protein expression (32, 36). VEGF expression varies in different subtypes of PAs (33, 35, 37). High VEGF expression was found in nonfunctioning (19, 21, 33, 35, 38) and pituitary adrenocorticotropic hormone (ACTH) (19, 33, 35)-, GH (19, 33, 38)-, PRL (35, 37, 38)-, and FSH (35, 37)-secreting PAs. In tumor tissues, pituitary GH- and PRL-secreting adenomas had diffuse VEGF distribution, while ACTH-, TSH-, and luteinizing hormone (LH)-secreting adenomas showed focal VEGF expression (32, 36, 39). In addition to tumor cells, VEGF mRNA and VEGF expression were mainly present in endothelial cells and folliculostellate cells (36, 40, 41). PCs had significantly higher VEGF mRNA amplification and stronger VEGF immunostaining than those of PAs (33). Therefore, different subtypes of PAs have different levels of VEGF, indicating that anti-VEGF therapy has distinct therapeutic effects on different subtypes of PAs.

VEGF has significant roles in the development of tumor neovascularity and peritumoral edema. Anti-VEGF antibodies removed 75%–99% of the permeability activity (42). Evidence has shown that VEGF is correlated with the pathogenesis of cystic formation in PAs (34). Other features affected by VEGF expression remain controversial. Overexpression of VEGF was associated with intratumoral hemorrhage (43), extrasellar invasion (37, 44), and rapid recurrence (37), although these findings were not significant in other studies (19, 21, 34, 35, 37, 38, 45, 46). Moreover, as shown in several studies, VEGF expression had no relation with tumor size (19, 34, 35, 45) or Ki-67 index (21, 38, 43). Moreover, no clear association was found between microvessel density and VEGF expression (19, 21). The low microvessel density despite VEGF overexpression has caused researchers to ask if inhibitory factors related to VEGF exist in PAs (36). The role of VEGF in the development and progression of PAs is still controversial; however, the expression of VEGF has not yet been used as a conclusive marker of the aggressive behavior of PAs. Current studies indicate that VEGF might play a role in tumoral vascular growth, not by increasing the number of vessels, but by other mechanisms, such as an increase in vascular permeability that favors the abundant diffusion of nutrients.

PRECLINICAL STUDIES OF ANGIOGENESIS IN PITUITARY TUMORS

Preclinical data indicated that VEGF is a potential therapeutic target in PAs. A previous study demonstrated that VEGF plays a crucial role in tumor angiogenesis during the development of a rat prolactinoma animal model (40). Estrogen-induced prolactinoma expresses a high level of VEGF associated with marked angiogenesis (47). Anti-VEGF resulted in a significant shrinkage in tumor volume, a decrease in the Ki-67 index, and the repair of pituitary vessels (48). Additionally, the characteristic "blood lakes" in prolactinoma were replaced by repaired microvascular structures on three-dimensional (3D) observation under a confocal laser scanning microscope. The current first-line therapy for prolactinomas is dopamine (DA) agonists (Das). Dopamine D2 receptors (D2Rs), which are widely localized in the anterior and intermediate lobes of pituitary glands, can combine with DA to activate signaling cascades (49). DA therapy targeting D2R yields an excellent response in prolactinomas and some clinical benefits in non-prolactinoma pituitary tumors (50). The decrease in D2R expression may explain the resistance to DA. Previous studies have identified the association between VEGF and D2R. In D2R knockout mice, Cristina et al. (51) reported increases in VEGF mRNA transcription, VEGF expression, and highly vascular adenomas. When treating D2R-deficient mice with anti-VEGF, Luque et al. (52, 53) noticed a substantial decrease in serum prolactin, a reduction in tumor size, and a significant decrease in vascularity. Furthermore, anti-VEGF might have additive effects in combination with drugs targeting complementary pathways related to angiogenesis. In mice with hemorrhagic prolactinoma, monotherapy with anti-VEGF or DA can restrain tumor growth and improve vascular remodeling. Only the combination of anti-VEGF and DA can suppress intratumoral hemorrhage (54). In concurrence, prolonged DA treatment enhanced pituitary VEGF expression in wild-type mice (51). These findings provide a provocative possibility of combination therapy with anti-VEGF and DA.

THERAPEUTIC TARGETING OF VASCULAR ENDOTHELIAL GROWTH FACTORS IN PITUITARY TUMORS

Bevacizumab

PAs and PCs highly express VEGF, which is one of the justifications for targeting VEGF and its receptors in this disease. Anti-VEGF has demonstrated significant activity as a single agent in murine studies. The recombinant humanized monoclonal antibody bevacizumab is the first approved agent directed against VEGF (**Figure 1** and **Table 1**). The common side effects of bevacizumab are fatigue, hoarseness, and hypertension. The rare side effects of this agent include clotting, hemorrhage, wound-healing disorders, gastrointestinal perforation, reversible posterior leukoencephalopathy syndrome, and proteinuria (55). Bevacizumab needs to be administered only every 2 or 3 weeks due to its prolonged half-life. This agent can be readily combined with chemotherapy agents, and preclinical evidence indicates synergy for some combinations of chemotherapeutic compounds when used alongside bevacizumab. Bevacizumab has thus far been the drug most tried for targeting the VEGF pathway in pituitary tumors.

The published clinical cases (7, 56–68) are presented in **Table 2**. In this review, we used the same criteria used in the recent European Society of Endocrinology survey (7). A complete radiological response was defined as no visible tumor, partial response (PR) as at least 30% tumor regression, stable disease (SD) as less than 30% regression but no more than a 10% increase, and progressive disease (PD) as more than a 10% increase in

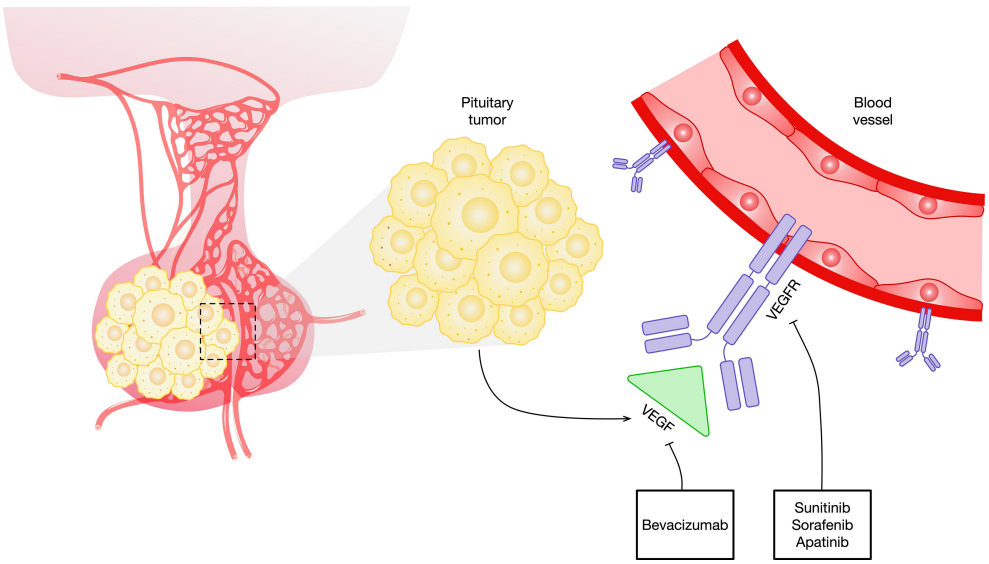

FIGURE 1 | Schematic representation of antiangiogenic agents that target the VEGF and VEGF signaling pathways in pituitary tumors. VEGF, vascular endothelial growth factor; VEGFR, vascular endothelial growth factor receptor.

tumor size or presentation of new metastasis. For functioning tumors, complete biochemical response was defined as normalization of hormone concentration, PR as more than a 20% reduction in hormone, SD as less than but no more than a 20% change in hormone, and PD as more than a 20% increase in hormone levels. To date, 19 cases treated with bevacizumab have been reported. Among these cases, eight are corticotroph tumors. Three were other subtypes (one somatotroph, one lactotroph, and one null cell), and the subtypes of other cases were not available. The majority of the PAs (8/11) were clinically functioning when the cases were reported; five in 12 cases presented with extracranial metastases, and seven in 12 were diagnosed with PC at the time of data collection. Most of the patients (9/12) underwent more than two surgeries in the sella. All patients received radiotherapy. One hundred percent (10/10) of tumors showed a Ki-67 index ≥10% at the last pathological examination.

Of the 12 patients to whom TMZ was administered prior to bevacizumab, all yielded PD. A second course of TMZ was administered to two patients (one on monotherapy, one on TMZ combined with cabergoline), which resulted in further progress. Notably, O^6-methylguanine-DNA methyltransferase (MGMT) immunohistochemistry was observed to be low in two and high in two. None of the four cases responded to TMZ. Bevacizumab was chosen as the second- or third-line therapy after TMZ failed. Six patients achieved SD [five on monotherapy, one on somatostatin analog (SSA) + bevacizumab], and four had disease progression. Ortiz et al. (56) reported an aggressive silent corticotroph cell PA that progressed to carcinoma despite TMZ administration and was subsequently treated with bevacizumab, achieving 26 months of SD, as documented on serial MRI and positron emission tomography scans. Bevacizumab therapy resulted in severe cell injury, vascular abnormalities, and fibrosis in tumors. This case first revealed the effectiveness of targeting VEGF in blocking angiogenesis, thus inhibiting tumor growth. VEGF immunoreactivity was positive in this case. However, VEGF/VEGFR immunoreactivity may not directly demonstrate efficacy. In another three patients with VEGFR expression in PC, two showed poor responses to bevacizumab (67).

In the other seven cases, bevacizumab was administered in parallel with TMZ as the first-line therapy. Although the outcomes were not available in two cases, PR or SD was reported in five patients, including one who failed to receive TMZ as a first-line therapy. Preclinical studies showed that most

TABLE 1 | Targets and sites of action of the VEGF angiogenesis receptor and ligand in pituitary tumors.

Target	Agent	Drug class	Site(s) of action
VEGF	Bevacizumab	Monoclonal antibody	VEGF
VEGF receptor	Sunitinib	TKI	VEGFR1, VEGFR2, PDGFR, KIT, FLT3, and CSF1R
	Sorafenib	TKI	VEGFR2, FLT3, PDGFR, KIT, FLT3, and FGFR1
	Apatinib	TKI	VEGFR2

CSF1R, colony-stimulating factor receptor type 1; FGFR1, fibroblast growth factor receptor 1; FLT3, fms-like tyrosine kinase 3; KIT, stem cell factor receptor; PDGFR, platelet-derived growth factor receptor; TKI, tyrosine kinase inhibitor; VEGF, vascular endothelial growth factor; VEGFR1, vascular endothelial growth factor receptor 1; VEGFR2, vascular endothelial growth factor receptor 2.

PAs exhibited low expression of MGMT and high expression of VEGF, while the expression of VEGF was positively associated with MGMT (35). TMZ and bevacizumab might be considered a combination therapy under the premise of indications. Touma et al. (62) reported a patient with ACTH-secreting PC who received adenomectomy in combination with radiation, TMZ, and bevacizumab and was kept in remission over 5 years of follow-up after therapy. Rotman et al. (64) reported a comparable result in another case with a corticotroph PC. The patient underwent surgery and radiotherapy for metastasis, followed by combined, overlapping chemotherapy with TMZ and bevacizumab, leading to a progression-free survival of 8 years. In the ESE survey (7) on 166 patients with aggressive PAs or PCs, seven were administered bevacizumab once, as shown in **Table 2**. Three patients were treated with bevacizumab monotherapy, resulting in SD in one patient and PD in one patient. Four patients took bevacizumab combined with TMZ, and 50% (2/2) had PR. These observations are consistent with other studies that have shown complementary effects of anti-VEGF combined with drugs targeting alternative pathways implicated in angiogenesis and further underline the importance of combination therapies when choosing bevacizumab.

Importantly, bevacizumab is a new option in the treatment of aryl hydrocarbon receptor-interacting protein (AIP)-related PA. Inactivating germline mutations in the AIP gene are linked to PA predisposition. Korbonits et al. (60) and Dutta et al. (61) treated a 4-year-old child diagnosed with AIP-mutated somatotroph PA with combination therapy of TMZ and bevacizumab concomitantly with radiation and pegvisomant, which stabilized tumor growth and hormone secretion over 4 years. This case revealed that bevacizumab could play a role in controlling genetically driven refractory PAs.

Tyrosine Kinase Inhibitors

Although bevacizumab has been the most studied VEGF inhibitor in pituitary tumors, various other agents are in development (**Table 1**). The majority of these agents are tyrosine kinase (TK) inhibitors. Sunitinib and sorafenib are small molecules that inhibit multiple TK receptors, some of which are implicated in angiogenesis, tumor growth, and metastatic progression (**Figure 1**) (69–71). Sunitinib and sorafenib have been approved in different clinical scenarios such as advanced renal cell carcinoma (72) and local or metastatic thyroid carcinoma refractory to radioactive iodine treatment (73) and hence are used in the treatment of pituitary metastasis from renal cell carcinoma (74–81) and thyroid carcinoma (82, 83). Apatinib, also known as rivoceranib, is a TK inhibitor that selectively targets VEGFR (**Figure 1**) (84). The toxicity and side-effect profile of TK inhibitors varies as a function of their target TKs, including hematological events (anemia, neutropenia, and thrombocytopenia), diarrhea, nausea, fatigue, hypertension, skin rash, elevation of liver enzymes, and proteinuria.

Sunitinib has been reported in the treatment of PAs and PC in two cases thus far. Both cases had observed PD (**Table 2**). Apatinib was administered in a 41-year-old female in combination with TMZ as a second-line treatment (68). This patient was diagnosed with GH-secreting recurrent PA that resisted surgeries, radiation, and

TABLE 2 | Cases of pituitary carcinomas and aggressive pituitary tumors treated with anti-VEGF.

Ref	ID	Age/ Sex	Tumor subtypes	Extent of disease beyond sellar region	Prior surgeries	Prior radiation	Medical treatments	Gene, molecular data	Response to anti-VEGF	PFS after first dose of anti-VEGF (mo)/ Outcome
Anti-VEGF										
(56)	1	44/ M	Corticotroph tumor, nonfunctioning	Intracranial: suprasellar, cavernous sinus, optic chiasm Extracranial: spine	7 CNS surgeries Spine surgery Sellar lesion biopsy	1. Sellar region 2. Vertebral metastases	1. TMZ×8 cycles (PD) 2. TMZ×16 cycles (PD) 3. TMZ×8 cycles (PD) 4. BEV×26 cycles (SD)	VEGF pos MGMT high Pathology after BEV: cell injury, vascular abnormalities, and fibrosis	R: SD	26/Survival
(57)	2	25/F	Corticotroph tumor, functioning	Extracranial: bone	3 CNS surgeries Bilateral adrenalectomy	1. Pituitary fossa	1. SSA (PD) 2. TMZ (PD) 3. BEV and SSA×6 cycles (SD)	NA	R: SD B: PR, plasma ACTH decreased from >200,000 to 113,000 pg/ ml	6/Survival
(58, 59)	3	56/F	Corticotroph tumor, functioning	Intracranial: suprasellar, cavernous sinus, optic chiasm, sphenoid sinus	6 CNS surgeries Bilateral adrenalectomy	1. Sellar region	1. SSA×1 mo (PD) 2. CAB×2 mo (PD) 3. TMZ×9 cycles (PD, after withdrawal) 4. BEV (SD)	Ki-67 40% MGMT low	R: SD	NA/Death (postoperative complication)

(Continued)

TABLE 2 | Continued

Ref	ID	Age/ Sex	Tumor subtypes	Extent of disease beyond sellar region	Prior surgeries	Prior radiation	Medical treatments	Gene, molecular data	Response to anti-VEGF	PFS after first dose of anti-VEGF (mo)/ Outcome
(60, 61)	4	4/M	Somatotroph tumor, functioning	Intracranial: suprasellar, cavernous sinus, optic chiasm	1 CNS surgeries	1. Sellar region	1. TMZ×3 cycles, TMZ and BEV×35 cycles, PEG (PR, concurrent with surgery and radiotherapy, stopped due to potential gonadal toxicity) 2. PEG and SSA (PR)	Nonsense AIP mutation VEGF pos Ki-67 12% P53 neg MGMT low	R: PR, reduction in pituitary tumor volume B: SD	48/Survival
(62)	5	63/ M	Corticotroph tumor, functioning	Intracranial: suprasellar, cavernous sinus, optic chiasm, sphenoid sinus Extracranial: lung	1 CNS surgery	1. Sellar region and/ or lung metastasis	1. BEV and TMZ×2 cycles, TMZ×12 cycles (PR, concurrent with surgery and radiotherapy)	Ki-67 50%	R: PR, reduction in lung metastasis volume B: SD	60/Survival
(7)	6	NA	NA	NA	NA	NA	1. TMZ and BEV (PR)	NA	PR	NA
(7)	7	NA	NA	NA	NA	NA	1. TMZ (PD) 2. TMZ and BEV (PR)	NA	PR	NA
(7)	8	NA	NA	NA	NA	NA	1. TMZ (PD) 2. TMZ and BEV (NA)	NA	NA	NA
(7)	9	NA	NA	NA	NA	NA	1. TMZ (PD) 2. TMZ and BEV (NA)	NA	NA	NA
(7)	10	NA	NA	NA	NA	NA	1. TMZ (PD) 2. BEV (SD)	NA	SD	NA
(7)	11	NA	NA	NA	NA	NA	1. TMZ (PD) 2. BEV (PD)	NA	PD	NA
(7)	12	NA	NA	NA	NA	NA	1. TMZ (PD) 2. BEV (NA)	NA	NA	NA
(63)	13	49/F	Corticotroph tumor, functioning	Intracranial: cerebrum Extracranial: bone, liver	3 CNS surgeries Bilateral adrenalectomy	1. Sellar region	1. TMZ (PD) 2. EVE (PD) 3. SUN (PD) 4. BEV (PD)	Ki-67 10%	R: PD B: PD	NA/Death
(64)	14	51/ M	Corticotroph tumor, functioning	Intracranial: right temporal lobe, cervico-medullary junction, dural based	2 CNS surgeries	1. Sellar region 2. Cervico-medullary metastasis	1. TMZ×12 cycles and BEV×26 cycles (SD, concurrent with surgery and radiotherapy)	Ki-67 15%	R: SD B: SD	96/Survival
(65)	15	72/F	Lactotroph tumor, nonfunctioning	Intracranial: dura Extracranial: spine	3 CNS surgeries Spine surgery	1. Sellar region 2. Spinal metastasis	1. TMZ×3 cycles (PD) 2. IPI and NIV×2 cycles (SD, stopped due to nephritis) 3. NIV×17 cycles (PD) 4. IPI and NIV×4 cycles (PD, with nephritis and hepatitis) 5. BEV×3 cycles (SD, stopped due to nephritis)	Ki-67 20% MGMT high PD-L1 neg TMB low Mismatch repair deficient neg	R: SD	9/Survival
(66)	16	55/ M	NA	Intracranial: suprasellar, cavernous sinus, optic chiasm, left frontotemporal dura, middle cranial fossa	3 CNS surgeries Thyroidectomy	1. Sellar region	1. TMZ×7 cycles (PD, after withdrawal) 2. CCNU×2 cycles (SD, stopped due to poor tolerance) 3. BEV (NA)	Ki-67 13-25.5% P53 neg MGMT low	NA	NA/Death
(67)	17	NA	Corticotroph tumor, functioning	Intracranial: cavernous sinus	5 CNS surgeries Bilateral adrenalectomy	1. Sellar region	1. SSA (SD, stopped due to poor tolerance) 2. CAB (PD) 3. TMZ×7 cycles (PD, after withdrawal) 4. BEV×2 cycles (PD)	VEGFR pos Ki-67 8-20% P53 pos	R: PD B: PD	1/Death

(Continued)

TABLE 2 | Continued

Ref	ID	Age/ Sex	Tumor subtypes	Extent of disease beyond sellar region	Prior surgeries	Prior radiation	Medical treatments	Gene, molecular data	Response to anti-VEGF	PFS after first dose of anti-VEGF (mo)/ Outcome
(67)	18	NA	Corticotroph tumor, functioning	Intracranial: cavernous sinus, clivus	5 CNS surgeries Bilateral adrenalectomy	1. Sellar region	1. SSA (PD) 2. TMZ×3 cycles (PD) 3. CAB and TMZ×3 cycles (PD) 4. BEV×1 cycles (PD)	VEGFR pos Ki-67 5-10% P53 pos	R: PD B: PD	1/Death
(67)	19	NA	Null cell tumor	Intracranial: cavernous sinus	5 CNS surgeries	1. Sellar region	1. TMZ×6 cycles (PD) 2. BEV×6 cycles (SD)	VEGFR pos Ki-67 5-10% P53 neg	R: SD B: SD	18/Death (postoperative complication)
Anti-VEGFR										
(7)	20	NA	NA	NA	NA	NA	1. TMZ (PD) 2. SUN (PD)	NA	PD	NA
(68)	21	41/F	Somatotroph tumor, functioning	Intracranial: suprasellar, cavernous sinus, optic chiasm, clivus	4 CNS surgeries	1. Sellar region	1. SSA×2 mo (PD) 2. TMZ and APA×12 cycles (SD, concurrent with surgery)	VEGFR pos Ki-67 5-10%	R: SD B: PR, plasma GH decreased from 10 to 1.5 ng/ml	31.5/Survival

AIP, aryl hydrocarbon receptor-interacting protein; APA, apatinib; B, biochemical criteria; BEV, bevacizumab; CAB, cabergoline; CCNU, 1-(2-chlorethyl)-3-cyclohexyl-1-nitrosurea; CNS, central nervous system; EVE, everolimus; F, female; IPI, ipilimumab; IHC, immunohistochemistry; M, male; MGMT, O^6-methylguanine-DNA methyltransferase; mo, months; NA, not available; neg, negative; NIV, nivolumab; PD, progressive disease; PD-L1, programmed death-ligand 1; PEG, pegvisomant; PFS, progression-free survival; pos, positive; PR, partial response; R, radiological criteria; Ref, reference; SD, stable disease; SSA, somatostatin analogs; SUN, sunitinib; TMB, tumor mutational burden; TMZ, temozolomide; VEGF, vascular endothelial growth factor; VEGFR, vascular endothelial growth factor receptor.

SSA. As VEGFR was expressed in the tumor, apatinib and TMZ were recommended. She achieved stabilization in the tumor and a decrease in serum GH levels over a period of 31.5 months of follow-up.

TK inhibitors might represent a therapeutic target in PAs associated with somatic genetic defects. Multiple endocrine neoplasia type 1 (MEN1) is an autosomal dominant disorder characterized by tumors of the pituitary gland, parathyroid gland, endocrine-gastrointestinal tract, and pancreas. In patients with MEN1, PAs are usually diagnosed at an earlier age, have higher degrees of aggressiveness and invasiveness, are more often resistant to treatment, and have higher risks of recurrence than sporadic PAs (85). Murine studies support that targeted angiogenesis in MEN1 leads to an obvious inhibition of pituitary tumor growth and hormone secretion and a significantly increased tumor-free survival time. Additionally, the vascular density in pancreatic islet tumors was significantly reduced by the treatment (86). Sunitinib was approved to treat locally advanced or metastatic pancreatic neuroendocrine tumors and refractory gastrointestinal stromal tumors (87, 88). Sunitinib has also been studied in MEN1 syndrome (89–92). However, data are still limited to drive any conclusion on the treatment of MEN1-related PAs.

To date, although attempts at bevacizumab and TK inhibitors in pituitary tumors have not gone beyond case studies, the anti-VEGF/VEGFR pathway has shown promise as an alternative therapy for patients with refractory PAs and PCs resistant to conventional treatments. Furthermore, the anti-VEGF/VEGFR pathway in combination with TMZ, TMZ and/or radiotherapy with SSA might have a synergistic therapeutic effect. However, the specific efficacy of the anti-VEGF/VEGFR pathway in patients with refractory PAs and PCs still needs further large-scale prospective clinical trials for confirmation.

CONCLUSION

In summary, the results from preclinical studies and clinical trials indicated that anti-VEGF monotherapy or in combination with other treatments may be promising alternative therapies for patients with refractory PAs and PCs resistant to conventional treatments. However, more preclinical studies and large-scale prospective clinical trials are needed to further evaluate the exact efficacy of anti-VEGF in pituitary tumors.

AUTHOR CONTRIBUTIONS

All authors listed have made substantial, direct, and intellectual contribution to the work and approved it for publication.

FUNDING

Financial support for this study was provided by the Scientific Research Project of Capital Health Development in 2018 (grant number: 2018-4-4018), the CAMS Innovation fund for Medical Science (grant number: CIFMS, 2017-12M-2-005), and the Beijing Natural Science Foundation (grant number: 7182137). The funding institutions had no role in the design of the study, data collection and analysis, the decision to publish, or the preparation of the article.

REFERENCES

1. Aflorei ED, Korbonits M. Epidemiology and Etiopathogenesis of Pituitary Adenomas. *J Neurooncol* (2014) 117(3):379–94. doi: 10.1007/s11060-013-1354-5
2. Melmed S. Pathogenesis of Pituitary Tumors. *Nat Rev Endocrinol* (2011) 7 (5):257–66. doi: 10.1038/nrendo.2011.40
3. Ezzat S, Asa SL, Couldwell WT, Barr CE, Dodge WE, Vance ML, et al. The Prevalence of Pituitary Adenomas: A Systematic Review. *Cancer* (2004) 101 (3):613–9. doi: 10.1002/cncr.20412
4. Dai C, Liu X, Ma W, Wang R. The Treatment of Refractory Pituitary Adenomas. *Front Endocrinol (Lausanne)* (2019) 10:334. doi: 10.3389/fendo.2019.00334
5. Lloyd RV, Osamura RY, Klöppel G, Rosai J. *WHO Classification of Tumours of Endocrine Organs. 4th Edition Ed*. Lyons: IARC (2017).
6. Elbelt U, Schlaffer SM, Buchfelder M, Knappe UJ, Vila G, Micko A, et al. Efficacy of Temozolomide Therapy in Patients With Aggressive Pituitary Adenomas and Carcinomas-a German Survey. *J Clin Endocrinol Metab* (2020) 105(3):e660–75. doi: 10.1210/clinem/dgz211
7. McCormack A, Dekkers OM, Petersenn S, Popovic V, Trouillas J, Raverot G, et al. Treatment of Aggressive Pituitary Tumours and Carcinomas: Results of a European Society of Endocrinology (ESE) Survey 2016. *Eur J Endocrinol* (2018) 178(3):265–76. doi: 10.1530/eje-17-0933
8. Yang Q, Li X. Molecular Network Basis of Invasive Pituitary Adenoma: A Review. *Front Endocrinol (Lausanne)* (2019) 10:7. doi: 10.3389/fendo.2019.00007
9. Kerbel RS. Tumor Angiogenesis. *N Engl J Med* (2008) 358(19):2039–49. doi: 10.1056/NEJMra0706596
10. Carmeliet P. Angiogenesis in Life, Disease and Medicine. *Nature* (2005) 438 (7070):932–6. doi: 10.1038/nature04478
11. Weidner N, Semple JP, Welch WR, Folkman J. Tumor Angiogenesis and Metastasis–Correlation in Invasive Breast Carcinoma. *N Engl J Med* (1991) 324(1):1–8. doi: 10.1056/NEJM199101033240101
12. Weidner N, Carroll PR, Flax J, Blumenfeld W, Folkman J. Tumor Angiogenesis Correlates With Metastasis in Invasive Prostate Carcinoma. *Am J Pathol* (1993) 143(2):401–9.
13. Folkman J. Role of Angiogenesis in Tumor Growth and Metastasis. *Semin Oncol* (2002) 29(6 Suppl 16):15–8. doi: 10.1053/sonc.2002.37263
14. Maeda K, Chung YS, Takatsuka S, Ogawa Y, Sawada T, Yamashita Y, et al. Tumor Angiogenesis as a Predictor of Recurrence in Gastric Carcinoma. *J Clin Oncol* (1995) 13(2):477–81. doi: 10.1200/JCO.1995.13.2.477
15. Weidner N, Folkman J, Pozza F, Bevilacqua P, Allred EN, Moore DH, et al. Tumor Angiogenesis: A New Significant and Independent Prognostic Indicator in Early-Stage Breast Carcinoma. *J Natl Cancer Inst* (1992) 84 (24):1875–87. doi: 10.1093/jnci/84.24.1875
16. Bochner BH, Cote RJ, Weidner N, Groshen S, Chen SC, Skinner DG, et al. Angiogenesis in Bladder Cancer: Relationship Between Microvessel Density and Tumor Prognosis. *J Natl Cancer Inst* (1995) 87(21):1603–12. doi: 10.1093/jnci/87.21.1603
17. Turner HE, Nagy Z, Gatter KC, Esiri MM, Harris AL, Wass JA. Angiogenesis in Pituitary Adenomas and the Normal Pituitary Gland. *J Clin Endocrinol Metab* (2000) 85(3):1159–62. doi: 10.1210/jcem.85.3.6485
18. Schechter J. Ultrastructural Changes in the Capillary Bed of Human Pituitary Tumors. *Am J Pathol* (1972) 67(1):109–26.
19. Viacava P, Gasperi M, Acerbi G, Manetti L, Cecconi E, Bonadio AG, et al. Microvascular Density and Vascular Endothelial Growth Factor Expression in Normal Pituitary Tissue and Pituitary Adenomas. *J Endocrinol Invest* (2003) 26(1):23–8. doi: 10.1007/BF03345118
20. Takada K, Yamada S, Teramoto A. Correlation Between Tumor Vascularity and Clinical Findings in Patients With Pituitary Adenomas. *Endocr Pathol* (2004) 15(2):131–9. doi: 10.1385/ep:15:2:131
21. Niveiro M, Aranda FI, Peiro G, Alenda C, Pico A. Immunohistochemical Analysis of Tumor Angiogenic Factors in Human Pituitary Adenomas. *Hum Pathol* (2005) 36(10):1090–5. doi: 10.1016/j.humpath.2005.07.015
22. Jugenburg M, Kovacs K, Stefaneanu L, Scheithauer BW. Vasculature in Nontumorous Hypophyses, Pituitary Adenomas, and Carcinomas: A Quantitative Morphologic Study. *Endocr Pathol* (1995) 6(2):115–24. doi: 10.1007/BF02739874
23. Pawlikowski M, Pisarek H, Jaranowska M. Immunocytochemical Investigations on the Vascularization of Pituitary Adenomas. *Endocr Pathol* (1997) 8(3):189–93. doi: 10.1007/BF02738785
24. Turner HE, Nagy Z, Gatter KC, Esiri MM, Harris AL, Wass JA. Angiogenesis in Pituitary Adenomas - Relationship to Endocrine Function, Treatment and Outcome. *J Endocrinol* (2000) 165(2):475–81. doi: 10.1677/joe.0.1650475
25. Vidal S, Kovacs K, Horvath E, Scheithauer BW, Kuroki T, Lloyd RV. Microvessel Density in Pituitary Adenomas and Carcinomas. *Virchows Arch* (2001) 438(6):595–602. doi: 10.1007/s004280000373
26. Ferrara N, Gerber HP, LeCouter J. The Biology of VEGF and Its Receptors. *Nat Med* (2003) 9(6):669–76. doi: 10.1038/nm0603-669
27. Harper SJ, Bates DO. VEGF-a Splicing: The Key to Anti-Angiogenic Therapeutics? *Nat Rev Cancer* (2008) 8(11):880–7. doi: 10.1038/nrc2505
28. Claesson-Welsh L, Welsh M. VEGFA and Tumour Angiogenesis. *J Intern Med* (2013) 273(2):114–27. doi: 10.1111/joim.12019
29. Frezzetti D, Gallo M, Maiello MR, D'Alessio A, Esposito C, Chicchinelli N, et al. VEGF as a Potential Target in Lung Cancer. *Expert Opin Ther Targets* (2017) 21(10):959–66. doi: 10.1080/14728222.2017.1371137
30. Schneider BP, Sledge GWJr. Drug Insight: VEGF as a Therapeutic Target for Breast Cancer. *Nat Clin Pract Oncol* (2007) 4(3):181–9. doi: 10.1038/ncponc0740
31. Choueiri TK, Kaelin WGJr. Targeting the HIF2-VEGF Axis in Renal Cell Carcinoma. *Nat Med* (2020) 26(10):1519–30. doi: 10.1038/s41591-020-1093-z
32. Melnic E, Cimpean AM, Gaje PN, Raica M. Influence of Hormone Profile on Vascular Endothelial Growth Factor (VEGF a) Expression in Human Pituitary Adenomas. *Anticancer Res* (2014) 34(10):5867.
33. Lloyd RV, Scheithauer BW, Kuroki T, Vidal S, Kovacs K, Stefaneanu L. Vascular Endothelial Growth Factor (VEGF) Expression in Human Pituitary Adenomas and Carcinomas. *Endocr Pathol* (1999) 10(3):229–35. doi: 10.1007/BF02738884
34. Fukui S, Nawashiro H, Otani N, Ooigawa H, Yano A, Nomura N, et al. Vascular Endothelial Growth Factor Expression in Pituitary Adenomas. *Acta Neurochir Suppl* (2003) 86:519–21. doi: 10.1007/978-3-7091-0651-8_106
35. Wang Y, Li J, Tohti M, Hu Y, Wang S, Li W, et al. The Expression Profile of Dopamine D2 Receptor, MGMT and VEGF in Different Histological Subtypes of Pituitary Adenomas: A Study of 197 Cases and Indications for the Medical Therapy. *J Exp Clin Cancer Res* (2014) 33(1):56. doi: 10.1186/s13046-014-0056-y
36. Corlan AS, Cimpean AM, Melnic E, Raica M, Sarb S. VEGF, VEGF165b and EG-VEGF Expression Is Specifically Related With Hormone Profile in Pituitary Adenomas. *Eur J Histochem* (2019) 63(1):3010. doi: 10.4081/ejh.2019.3010
37. Sanchez-Ortiga R, Sanchez-Tejada L, Moreno-Perez O, Riesgo P, Niveiro M, Pico Alfonso AM. Over-Expression of Vascular Endothelial Growth Factor in Pituitary Adenomas is Associated With Extrasellar Growth and Recurrence. *Pituitary* (2013) 16(3):370–7. doi: 10.1007/s11102-012-0434-4
38. Cristina C, Perez-Millan MI, Luque G, Dulce RA, Sevlever G, Berner SI, et al. VEGF and CD31 Association in Pituitary Adenomas. *Endocr Pathol* (2010) 21 (3):154–60. doi: 10.1007/s12022-010-9119-6
39. Kurosaki M, Saegert W, Abe T, Ludecke DK. Expression of Vascular Endothelial Growth Factor in Growth Hormone-Secreting Pituitary Adenomas: Special Reference to the Octreotide Treatment. *Neurol Res* (2008) 30(5):518–22. doi: 10.1179/174313208X289499
40. Banerjee SK, Zoubine MN, Tran TM, Weston AP, Campbell DR. Overexpression of Vascular Endothelial Growth Factor164 and its Co-Receptor Neuropilin-1 in Estrogen-Induced Rat Pituitary Tumors and GH3 Rat Pituitary Tumor Cells. *Int J Oncol* (2000) 16(2):253–60. doi: 10.3892/ijo.16.2.253
41. Alfer J, Neulen J, Gaumann A. Lactotrophs: The New and Major Source for VEGF Secretion and the Influence of ECM on Rat Pituitary Function *In Vitro*. *Oncol Rep* (2015) 33(5):2129–34. doi: 10.3892/or.2015.3851
42. Berkman RA, Merrill MJ, Reinhold WC, Monacci WT, Saxena A, Clark WC, et al. Expression of the Vascular Permeability Factor/Vascular Endothelial Growth Factor Gene in Central Nervous System Neoplasms. *J Clin Invest* (1993) 91(1):153–9. doi: 10.1172/jci116165
43. Arita K, Kurisu K, Tominaga A, Sugiyama K, Eguchi K, Hama S, et al. Relationship Between Intratumoral Hemorrhage and Overexpression of Vascular Endothelial Growth Factor (VEGF) in Pituitary Adenoma. *Hiroshima J Med Sci* (2004) 53(2):23–7.
44. Yarman S, Kurtulmus N, Canbolat A, Bayindir C, Bilgic B, Ince N. Expression of Ki-67, P53 and Vascular Endothelial Growth Factor (VEGF) Concomitantly in Growth Hormone-Secreting Pituitary Adenomas; Which One has a Role in Tumor Behavior? *Neuro Endocrinol Lett* (2010) 31 (6):823–8.

45. Iuchi T, Saeki N, Osato K, Yamaura A. Proliferation, Vascular Endothelial Growth Factor Expression and Cavernous Sinus Invasion in Growth Hormone Secreting Pituitary Adenomas. *Acta Neurochir (Wien)* (2000) 142 (12):1345–51. doi: 10.1007/s007010070003
46. Borg SA, Kerry KE, Royds JA, Battersby RD, Jones TH. Correlation of VEGF Production With IL1 Alpha and IL6 Secretion by Human Pituitary Adenoma Cells. *Eur J Endocrinol* (2005) 152(2):293–300. doi: 10.1530/eje.1.01843
47. Banerjee SK, Sarkar DK, Weston AP, De A, Campbell DR. Over Expression of Vascular Endothelial Growth Factor and its Receptor During the Development of Estrogen-Induced Rat Pituitary Tumors may Mediate Estrogen-Initiated Tumor Angiogenesis. *Carcinogenesis* (1997) 18(6):1155–61. doi: 10.1093/carcin/18.6.1155
48. Miyajima K, Takekoshi S, Itoh J, Kakimoto K, Miyakoshi T, Osamura RY. Inhibitory Effects of Anti-VEGF Antibody on the Growth and Angiogenesis of Estrogen-Induced Pituitary Prolactinoma in Fischer 344 Rats: Animal Model of VEGF-Targeted Therapy for Human Endocrine Tumors. *Acta Histochem Cytochem* (2010) 43(2):33–44. doi: 10.1267/ahc.09034
49. Liu X, Tang C, Wen G, Zhong C, Yang J, Zhu J, et al. The Mechanism and Pathways of Dopamine and Dopamine Agonists in Prolactinomas. *Front Endocrinol (Lausanne)* (2018) 9:768. doi: 10.3389/fendo.2018.00768
50. Cooper O, Greenman Y. Dopamine Agonists for Pituitary Adenomas. *Front Endocrinol (Lausanne)* (2018) 9:469. doi: 10.3389/fendo.2018.00469
51. Cristina C, Díaz-Torga G, Baldi A, Góngora A, Rubinstein M, Low MJ, et al. Increased Pituitary Vascular Endothelial Growth Factor-a in Dopaminergic D2 Receptor Knockout Female Mice. *Endocrinology* (2005) 146(7):2952–62. doi: 10.1210/en.2004-1445
52. Luque GM, Perez-Millan MI, Ornstein AM, Cristina C, Becu-Villalobos D. Inhibitory Effects of Anti-VEGF Strategies in Experimental Dopamine-Resistant Prolactinomas. *J Pharmacol Exp Ther* (2011) 337(3):766–74. doi: 10.1124/jpet.110.177790
53. Luque GM, Perez-Millán MI, Ornstein AM, Cristina C, Becu-Villalobos D. Inhibitory Effects of Antivascular Endothelial Growth Factor Strategies in Experimental Dopamine-Resistant Prolactinomas. *J Pharmacol Exp Ther* (2011) 337(3):766–74. doi: 10.1124/jpet.110.177790
54. Chauvet N, Romanò N, Lafont C, Guillou A, Galibert E, Bonnefont X, et al. Complementary Actions of Dopamine D2 Receptor Agonist and Anti-VEGF Therapy on Tumoral Vessel Normalization in a Transgenic Mouse Model. *Int J Cancer* (2017) 140(9):2150–61. doi: 10.1002/ijc.30628
55. Kamba T, McDonald DM. Mechanisms of Adverse Effects of Anti-VEGF Therapy for Cancer. *Br J Cancer* (2007) 96(12):1788–95. doi: 10.1038/sj.bjc.6603813
56. Ortiz LD, Syro LV, Scheithauer BW, Ersen A, Uribe H, Fadul CE, et al. Anti-VEGF Therapy in Pituitary Carcinoma. *Pituitary* (2012) 15(3):445–9. doi: 10.1007/s11102-011-0346-8
57. O'Riordan LM, Greally M, Coleman N, Breathnach OS, Hennessy B, Thompson CJ, et al. Metastatic ACTH-Producing Pituitary Carcinoma Managed With Combination Pasireotide and Bevacizumab Following Failure of Temozolamide Therapy: A Case Report. *J Clin Oncol* (2013) 31 (15):e13022. doi: 10.1200/jco.2013.31.15_suppl.e13022
58. Kurowska M, Malicka J, Tarach JS. Are the "Classic" and the "Modern" Forms of Nelson's Syndrome the Same or Different Disorders? *Endokrynologia Polska* (2014) 65(5):425–6.
59. Kurowska M, Nowakowski A, Zielinski G, Malicka J, Tarach JS, Maksymowicz M, et al. Temozolomide-Induced Shrinkage of Invasive Pituitary Adenoma in Patient With Nelson's Syndrome: A Case Report and Review of the Literature. *Case Rep Endocrinol* (2015) 2015:623092. doi: 10.1155/2015/623092
60. Korbonits M, Dutta P, Reddy KS, Bhansali A, Gupta P, Rai A, et al. Exome Sequencing Reveals Double Hit by AIP Gene Mutation and Copy Loss of Chromosome 11 But Negative Xlag in a Pituitary Adenoma of a 4 Yrs Child With Gigantism Treated With Multimodal Therapy. *98th Annual Meeting and Expo of the Endocrine Society*, Boston, MA, United States. (2016).
61. Dutta P, Reddy KS, Rai A, Madugundu AK, Solanki HS, Bhansali A, et al. Surgery, Octreotide, Temozolomide, Bevacizumab, Radiotherapy, and Pegvisomant Treatment of an AIP Mutation-Positive Child. *J Clin Endocrinol Metab* (2019) 104(8):3539–44. doi: 10.1210/jc.2019-00432
62. Touma W, Hoostal S, Peterson RA, Wiernik A, SantaCruz KS, Lou E. Successful Treatment of Pituitary Carcinoma With Concurrent Radiation, Temozolomide, and Bevacizumab After Resection. *J Clin Neurosci* (2017) 41:75–7. doi: 10.1016/j.jocn.2017.02.052
63. Alshaikh OM, Asa SL, Mete O, Ezzat S. An Institutional Experience of Tumor Progression to Pituitary Carcinoma in a 15-Year Cohort of 1055 Consecutive Pituitary Neuroendocrine Tumors. *Endocrine Pathol* (2019) 30(2):118–27. doi: 10.1007/s12022-019-9568-5
64. Rotman LE, Vaughan TB, Hackney JR, Riley KO. Long-Term Survival After Transformation of an Adrenocorticotropic Hormone–Secreting Pituitary Macroadenoma to a Silent Corticotroph Pituitary Carcinoma. *World Neurosurg* (2019) 122:417–23. doi: 10.1016/j.wneu.2018.11.011
65. Lamb LS, Sim HW, McCormack AI. Case Report: A Case of Pituitary Carcinoma Treated With Sequential Dual Immunotherapy and Vascular Endothelial Growth Factor Inhibition Therapy. *Front Endocrinol (Lausanne)* (2020) 11:576027. doi: 10.3389/fendo.2020.576027
66. Xu L, Khaddour K, Chen J, Rich KM, Perrin RJ, Campian JL. Pituitary Carcinoma: Two Case Reports and Review of Literature. *World J Clin Oncol* (2020) 11(2):91–102. doi: 10.5306/wjco.v11.i2.91
67. Osterhage K, Rotermund R, Droste M, Dierlamm J, Saeger W, Petersenn S, et al. Bevacizumab in Aggressive Pituitary Adenomas - Experience With 3 Patients. *Exp Clin Endocrinol Diabetes* (2021) 129(3):178–85. doi: 10.1055/a-1260-3975
68. Wang Y, He Q, Meng X, Zhou S, Zhu Y, Xu J, et al. Apatinib (YN968D1) and Temozolomide in Recurrent Invasive Pituitary Adenoma: Case Report and Literature Review. *World Neurosurg* (2019) 124:319–22. doi: 10.1016/j.wneu.2018.12.174
69. Chow LQ, Eckhardt SG. Sunitinib: From Rational Design to Clinical Efficacy. *J Clin Oncol* (2007) 25(7):884–96. doi: 10.1200/JCO.2006.06.3602
70. Wilhelm SM, Adnane L, Newell P, Villanueva A, Llovet JM, Lynch M. Preclinical Overview of Sorafenib, a Multikinase Inhibitor That Targets Both Raf and VEGF and PDGF Receptor Tyrosine Kinase Signaling. *Mol Cancer Ther* (2008) 7(10):3129–40. doi: 10.1158/1535-7163.MCT-08-0013
71. Christensen JG. A Preclinical Review of Sunitinib, a Multitargeted Receptor Tyrosine Kinase Inhibitor With Anti-Angiogenic and Antitumour Activities. *Ann Oncol* (2007) 18(Suppl 10):x3–10. doi: 10.1093/annonc/mdm408
72. Motzer RJ, Hutson TE, Tomczak P, Michaelson MD, Bukowski RM, Rixe O, et al. Sunitinib Versus Interferon Alfa in Metastatic Renal-Cell Carcinoma. *N Engl J Med* (2007) 356(2):115–24. doi: 10.1056/NEJMoa065044
73. Schneider TC, Abdulrahman RM, Corssmit EP, Morreau H, Smit JW, Kapiteijn E. Long-Term Analysis of the Efficacy and Tolerability of Sorafenib in Advanced Radio-Iodine Refractory Differentiated Thyroid Carcinoma: Final Results of a Phase II Trial. *Eur J Endocrinol* (2012) 167 (5):643–50. doi: 10.1530/EJE-12-0405
74. Srikugan L, Powrie J. Effects of Sunitinib, a Protein Tyrosine Kinase Inhibitor, on a Pituitary Lesion in a Patient With Renal Carcinoma. *93rd Annual Meeting and Expo of the Endocrine Society*, Boston, MA, United States. (2011). Available at: https://endo.confex.com/endo/2016endo/webprogram/Paper28082.html.
75. Yang L, Yu SY, Hu GY. Pituitary Metastasis From a Renal Cell Carcinoma Progressed After Sorafenib Treatment. *Chin J Cancer* (2013) 32(6):353–6. doi: 10.5732/cjc.012.10184
76. Upton TJ, Hunt PJ. Renal Cell Pituitary Metastasis Masquerading as a Prolactinoma. *96th Annual Meeting and Expo of the Endocrine Society*, Chicago, IL, United States. (2014).
77. Payandeh M, Sadeghi M, Sadeghi E. The Complete Response to Targeted Drugs Without Surgery or Radiotherapy: A Case of Pituitary Metastasis From Renal Cell Carcinoma. *Acta Med Iranica* (2016) 54(9):617–9.
78. Wendel C, Campitiello M, Plastino F, Eid N, Hennequin L, Quétin P, et al. Pituitary Metastasis From Renal Cell Carcinoma: Description of a Case Report. *Am J Case Rep* (2017) 18:7–11. doi: 10.12659/ajcr.901032
79. Liu W, Varlamov E, Woltjer R, Cetas J, Fleseriu M. Metastatic Renal Cell Carcinoma to the Pituitary-a Clinical Conundrum. *100th Annual Meeting of the Endocrine Society, Chicago, IL, United States*. (2018).
80. Selby LD, Stiefel HC, Skalet AH, Cardenal MS, Bhavsar KV, Winges KM. Vision Loss From Choroidal and Pituitary Metastases Secondary to Renal Cell Carcinoma: A Case Report. *Neuro-Ophthalmology* (2018) 42(6):391–8. doi: 10.1080/01658107.2018.1454479
81. Di Nunno V, Mollica V, Corcioni B, Fiorentino M, Nobili E, Schiavina R, et al. Clinical Management of a Pituitary Gland Metastasis From Clear Cell Renal Cell Carcinoma. *Anti-Cancer Drugs* (2018) 29(7):710–5. doi: 10.1097/CAD.0000000000000644
82. Hammami MM, Duaiji N, Mutairi G, Aklabi S, Qattan N, Abouzied Mel D, et al. Case Report of Severe Cushing's Syndrome in Medullary Thyroid Cancer

Complicated by Functional Diabetes Insipidus, Aortic Dissection, Jejunal Intussusception, and Paraneoplastic Dysautonomia: Remission With Sorafenib Without Reduction in Cortisol Concentration. *BMC Cancer* (2015) 15:624. doi: 10.1186/s12885-015-1620-3
83. Souza Mota J, Caldas AS, Nascimento AGPAC, Faria MS, Sobral CSP. Pituitary Metastasis of Thyroid Carcinoma: A Case Report. *Am J Case Rep* (2018) 19:896–902. doi: 10.12659/AJCR.909523
84. Scott LJ. Apatinib: A Review in Advanced Gastric Cancer and Other Advanced Cancers. *Drugs* (2018) 78(7):747–58. doi: 10.1007/s40265-018-0903-9
85. Syro LV, Scheithauer BW, Kovacs K, Toledo RA, Londono FJ, Ortiz LD, et al. Pituitary Tumors in Patients With MEN1 Syndrome. *Clinics (Sao Paulo)* (2012) 67 Suppl 1:43–8. doi: 10.6061/clinics/2012(sup01)09
86. Korsisaari N, Ross J, Wu X, Kowanetz M, Pal N, Hall L, et al. Blocking Vascular Endothelial Growth Factor-a Inhibits the Growth of Pituitary Adenomas and Lowers Serum Prolactin Level in a Mouse Model of Multiple Endocrine Neoplasia Type 1. *Clin Cancer Res* (2008) 14(1):249–58. doi: 10.1158/1078-0432.CCR-07-1552
87. Demetri GD, van Oosterom AT, Garrett CR, Blackstein ME, Shah MH, Verweij J, et al. Efficacy and Safety of Sunitinib in Patients With Advanced Gastrointestinal Stromal Tumour After Failure of Imatinib: A Randomised Controlled Trial. *Lancet* (2006) 368(9544):1329–38. doi: 10.1016/S0140-6736(06)69446-4
88. Raymond E, Dahan L, Raoul JL, Bang YJ, Borbath I, Lombard-Bohas C, et al. Sunitinib Malate for the Treatment of Pancreatic Neuroendocrine Tumors. *N Engl J Med* (2011) 364(6):501–13. doi: 10.1056/NEJMoa1003825
89. Palmieri G, Buonerba C, Formisano L, Damiano V, Nappi L, Federico P, et al. Sunitinib in a Men-1 Patient With Small Cell Neuroendocrine Tumor of the Thymus. *Neuroendocrinology* (2012) 96:11–2. doi: 10.1159/000340053
90. Li Y, Su X, Tan H. Type 2 Gastric Neuroendocrine Tumor: Report of One Case. *Trans Gastroenterol Hepatol* (2016) 30(1):88. doi: 10.21037/tgh.2016.11.05
91. Shell J, Patel D, Powers A, Quezado M, Killian K, Meltzer P, et al. Somatic VHL Mutation in a Patient With MEN1-Associated Metastatic Pancreatic Neuroendocrine Tumor Responding to Sunitinib Treatment: A Case Report. *J Endocr Soc* (2017) 1(9):1124–34. doi: 10.1210/js.2017-00156
92. Nunez JE, Donadio M, Filho DR, Rego JF, Barros M, Formiga MN, et al. The Efficacy of Everolimus and Sunitinib in Patients With Sporadic or Germline Mutated Metastatic Pancreatic Neuroendocrine Tumors. *J Gastrointest Oncol* (2019) 10(4):645–51. doi: 10.21037/jgo.2019.01.33

Conflict of Interest: The authors declare that the research was conducted in the absence of any commercial or financial relationships that could be construed as a potential conflict of interest.

Publisher's Note: All claims expressed in this article are solely those of the authors and do not necessarily represent those of their affiliated organizations, or those of the publisher, the editors and the reviewers. Any product that may be evaluated in this article, or claim that may be made by its manufacturer, is not guaranteed or endorsed by the publisher.

frontiers in Oncology

ORIGINAL RESEARCH
published: 10 December 2021
doi: 10.3389/fonc.2021.778824

Cyst Type Differentiates Rathke Cleft Cysts From Cystic Pituitary Adenomas

Sherwin Tavakol[1,2], Michael P. Catalino[3], David J. Cote[1,4], Xian Boles[1], Edward R. Laws Jr[1†] and Wenya Linda Bi[1*†]*

[1] Department of Neurosurgery, Brigham and Women's Hospital, Harvard Medical School, Boston, MA, United States, [2] Department of Neurosurgery, University of Oklahoma Health Sciences Center, Oklahoma City, OK, United States, [3] Department of Neurosurgery, University of North Carolina Hospitals, Chapel Hill, NC, United States, [4] Department of Neurosurgery, Keck School of Medicine of USC, Los Angeles, CA, United States

OPEN ACCESS

Edited by:
Zhixiong Liu,
Central South University, China

Reviewed by:
Min Guo,
Fudan University, China
Xiaohai Liu,
Capital Medical University, China
Zhaohui He,
Chongqing Medical University, China

***Correspondence:**
Edward R. Laws Jr
elaws@bwh.harvard.edu
Wenya Linda Bi
wbi@bwh.harvard.edu

†These authors share senior authorship

Specialty section:
This article was submitted to Neuro-Oncology and Neurosurgical Oncology, a section of the journal Frontiers in Oncology

Received: 17 September 2021
Accepted: 19 November 2021
Published: 10 December 2021

Citation:
Tavakol S, Catalino MP, Cote DJ, Boles X, Laws ER Jr and Bi WL (2021) Cyst Type Differentiates Rathke Cleft Cysts From Cystic Pituitary Adenomas. Front. Oncol. 11:778824. doi: 10.3389/fonc.2021.778824

Purpose: A classification system for cystic sellar lesions does not exist. We propose a novel classification scheme for these lesions based on the heterogeneity of the cyst wall/contents and the presence of a solid component on imaging.

Methods: We retrospectively reviewed 205 patients' medical records (2008–2020) who underwent primary surgery for a cystic sellar lesion. Cysts were classified *a priori* into 1 of 4 cyst types based on the heterogeneity of the cyst wall/contents and the presence of a solid component imaging. There was high interrater reliability. Univariable and multivariable models were used to estimate the ability of cyst type to predict the two most common diagnoses: Rathke cleft cyst (RCC) and cystic pituitary adenoma.

Results: The frequencies of RCC and cystic pituitary adenoma in our cohort were 45.4% and 36.4%, respectively. Non-neoplastic lesions (e.g., arachnoid cysts and RCC) were more likely to be Type 1 or 2, whereas cystic neoplasms (e.g., pituitary adenomas and craniopharyngiomas) were more likely to be Type 3 or 4 ($p<0.0001$). Higher cyst types, compared to Type 1, had higher odds of being cystic pituitary adenomas compared to RCCs (OR: 23.7, $p=0.033$, and 342.6, $p<0.0001$, for Types 2 and 4, respectively). Lesions with a fluid-fluid level on preoperative MRI also had higher odds of being pituitary adenomas (OR: 12.7; $p=0.023$). Cystic pituitary adenomas were more common in patients with obesity (OR: 5.0, $p=0.003$) or symptomatic hyperprolactinemia (OR: 11.5; $p<0.001$, respectively). The multivariable model had a positive predictive value of 82.2% and negative predictive value of 86.4%.

Conclusion: When applied to the diagnosis of RCC versus cystic pituitary adenoma, higher cystic lesion types (Type 2 & 4), presence of fluid-fluid level, symptomatic hyperprolactinemia, and obesity were predictors of cystic pituitary adenoma. Further validation is needed, but this classification scheme may prove to be a useful tool for the management of patients with common sellar pathology.

Keywords: cystic sellar lesion, pituitary adenoma, pituitary cyst, pituitary tumor, Rathke cleft cyst, craniopharyngioma

INTRODUCTION

Cystic lesions in the sellar region encompass a broad gamut of pathologies, which can be challenging to distinguish on imaging, given their variability in clinical presentation and heterogeneity of cyst appearance. The presence of a sellar cyst generates a range of presumptive diagnoses — with pathologies including cystic pituitary adenomas, craniopharyngiomas, Rathke cleft cysts (RCC), arachnoid cysts, epidermoid cysts, dermoid cysts, and xanthogranulomas, among others (1, 2). Although some cystic lesions are benign, incidentally found lesions, others can lead to significant morbidity through disruption of hormonal axes or associated mass effect. Incidentally found lesions such as small pituitary adenoma or RCC may be observed, while surgical resection is indicated for symptomatic lesions or those requiring tissue diagnosis. Clinical and imaging factors are often used to generate a preliminary diagnosis and guide management. This variation in treatment pathways necessitates further study into the features that distinguish these various cystic pathologies, especially the two most common pathologies: RCC and cystic pituitary adenoma. No validated classification system of cystic sellar lesions exists. The localization of the lesion within the sella has been classically used to differentiate lesions originating from the pars intermedia (e.g., RCC) from those originating from the pars distalis (e.g., classic adenomas). Anterior lesions from the pars distalis often exhibit posterior displacement of the infundibulum, and posterior lesions from the pars intermedia often displace the infundibulum anteriorly. For large lesions extending into the suprasellar cisterns, the infundibulum is often hard to identify, and, therefore, this method cannot reliably predict the origin of the lesion. In this study, the classification scheme can be applied to every lesion, regardless of size using the heterogeneity of the cyst wall/contents and presence of a solid component on preoperative magnetic resonance imaging (MRI). We used this *a priori* classification scheme and applied it to a retrospective cohort of patients.

MATERIALS AND METHODS

We retrospectively queried an institutional neurosurgical database from April 2008 to January 2020 for cases with the keywords "cyst" and "cystic" in preoperative radiology reports. Only patients with a final tissue diagnosis after surgical excision and/or cyst drainage were included in the study. Patients with non-sellar cysts, such as pineal cyst or epidermal inclusion cyst, were excluded. This study was approved by our institutional review board for ethical conduct of research and protection of human subjects. Patient consent was not required since no identifying information was used in this article.

Our primary aim was to apply an *a priori* cyst classification scheme and compare cystic lesion type with final pathologic diagnosis. Pre-operative thin-slice MRI (1.5T or 3T) and clinical and biochemical data were reviewed for each case. T1 pre- and post-gadolinium contrast images were reviewed along with T2-weighted images. The cyst classification scheme was developed based on focused discussions amongst the authors prior to its application to cyst classification in a retrospective fashion. Classification was independently performed by three authors (ST, MPC, and DJC) who were blinded from the final cyst pathology. Agreement by two or more authors was required for final cyst classification. Inter-rater reliability was assessed using Fleiss' kappa (κ). Confirmed lesion identity was extracted from pathology reports. Fisher's exact test was used to evaluate the relationship between cystic lesion type and lesion pathology.

The primary objective of the study was to estimate the association between cyst type and pathology, especially as it helped distinguish RCC from cystic pituitary adenomas. Cystic lesions were classified by the heterogeneity of the cyst wall/contents and the presence of a solid component on preoperative MRI (**Figure 1**). Type 1 cystic lesions were defined by a well-circumscribed regular border and homogeneous contents with no solid component (i.e. containing cyst contents and cyst wall only). Type 2 cystic lesions were defined by a well-circumscribed but irregular border with heterogenous content/septations and a subtle solid, non-cystic component. Type 3 lesions were defined by a well-circumscribed regular boarder and homogenous contents (like Type 1), but with an obvious solid component. Type 4 lesions were defined by irregular borders with heterogenous contents/septations (like Type 2) with multiple cysts, was predominately solid, and sometimes not well-circumscribed (**Figure 2**). The radiographic classification scheme was consistent and easy to apply. There was unanimous consensus on cyst type for 91% of cases, and 100% agreement between at least 2 of the 3 reviewers (κ=0.86).

Data Analysis

Student's t-test, Wilcoxon rank sum tests, Chi-square tests, and Fisher's exact tests were used for the comparison of continuous and categorical covariates of interest. A purposeful selection approach was used to create a multivariable logistic model. Odds ratios (OR), 95% confidence intervals, and p-values are reported, in addition to receiver operating characteristics (ROC) analysis. All analyses were performed using the SAS/STAT software (Version 9.4, 2013; Cary, NC). Statistical significance was defined as $p < 0.05$.

RESULTS

We originally queried an institutional database of 1083 transsphenoidal operations in 982 patients for sellar pathology (757 operations for pituitary adenoma) performed by one of the senior authors (ERL) from April 2008 to January 2020. In total, 205 patients were found to have undergone transsphenoidal surgery for cystic sellar pathology. We classified the lesions of these patients (mean age 42 years, range 16-90 years; 68% women) into the four cyst types (**Table 1**). Type 1 and 2 cysts were the most prevalent (33% and 35%, respectively), with 5% of lesions being classified as Type 3, and 27% as Type 4. In our cohort, RCC and cystic pituitary adenomas comprised the vast

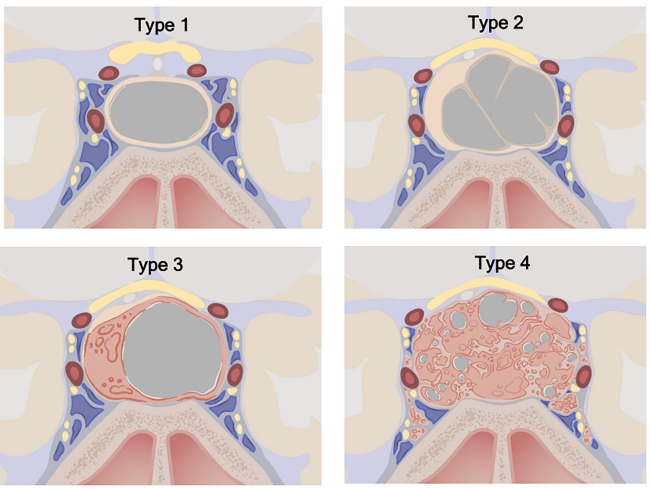

FIGURE 1 | Cystic sellar lesion classification scheme. Type 1: No solid component; well-circumscribed, homogenous cyst. Type 2: Little or no solid component; irregular cyst, with septations or abnormal walls. Type 3: Obvious solid component; well-circumscribed homogenous cyst. Type 4: Obvious solid component present; irregular cyst(s) with septations or abnormal walls. Type 1: n=68 (33.2%), Type 2: n=72 (35.1%), Type 3: n=10 (4.9%), Type 4: n=55 (26.8%). ©2020 Xian Boles, Used by permission.

majority of cystic lesions (36% and 45%, respectively). Arachnoid cysts (7%) and craniopharyngiomas (6%) were the next most common, with only one patient each having a pathologic diagnosis of chordoma, apoplexy without evident tumor, epidermoid cyst, and colloid cyst. There was a significant association between cyst type and histopathologic diagnosis ($p<0.0001$; **Table 2**).

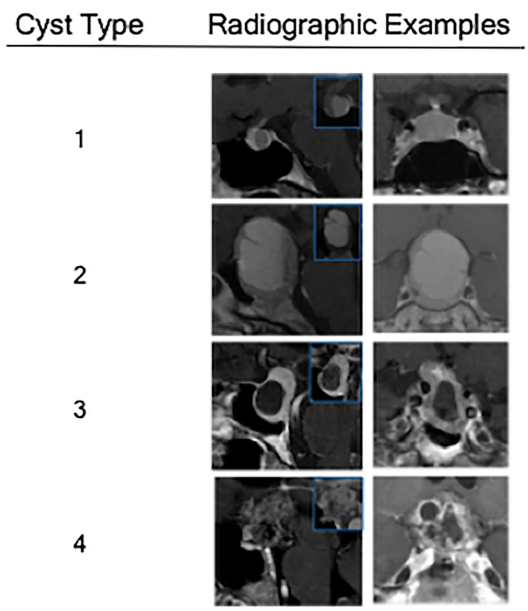

FIGURE 2 | Radiographic examples of each class of cystic sellar masses, with illustrative sagittal post-contrast T1-weighted MRI (left), sagittal pre-contrast T1-weighted MRI (small box), and coronal post-contrast T1-weighted MRI (right).

The majority of the cystic pituitary adenomas were non-staining tumors (38.7% of adenomas), with prolactin- (31.2%) and ACTH-staining (11.8%) tumors following in prevalence. Approximately 46.2% of pituitary adenomas exhibited evidence of hormone secretion, and the remainder were non-functioning. Among the functioning tumors, 67.4% were prolactinomas, 18.6% presented with Cushing disease and 9.3% were associated with acromegaly. Roughly 30% of patients presented with symptomatic hypopituitarism, and roughly 25% of patients exhibited clinical signs of hyperprolactinemia (**Table 1**).

Cyst Type and Pathology

Cyst Type 1 lesions (n=68, 33.2% of total) were largely comprised of RCCs (n=44, 65%), followed by cystic pituitary adenomas (n=14, 21%) and arachnoid cysts (n=8, 12%). They were nearly twice as likely to be located posteriorly, and were also, on average, smaller than other cystic lesion types - only 60% had a maximal diameter larger than 1 cm. Type 1 lesions rarely showed radiographic evidence of cavernous sinus invasion (3%). Additionally, clinical evidence of a headache was a common symptom seen in 78% of patients. Finally, patients with Type 1 lesions were younger and more likely to be female (mean age: 37 years; 84% female).

Cyst Type 2 lesions (n=72, 35.1% of total) were primarily either an RCC (n=29, 43%) or a cystic pituitary adenoma (n=28, 41%). These lesions, unlike Type 1 lesions, were located anteriorly in 65% of cases. The higher proportion of cystic pituitary adenomas among this cyst type is in agreement with the anterior predominance. Furthermore, as expected, all adenomas in our cohort, regardless of cyst type, were more

TABLE 1 | Preoperative patient/lesion characteristics, including patient demographic data, tumor symptoms, serum hormone levels, and radiographic features.

	N (%)
Age, mean (range)	41.7 (16–90)
Sex	
Male	66 (32.2)
Female	139 (67.8)
Obesity	
Yes	70 (34.1)
No	135 (65.9)
History of Other Cysts	
Ovarian, n (% of women)	21 (15.1)
Renal	10 (4.9)
Hepatic	2 (1.0)
Adrenal	0
Pineal Gland	2 (1.0)
PCOS, n (% of women)	5 (3.6)
Inclusion	
Cyst mentioned on radiology report	166 (81.4)
Cyst not mentioned, but seen on T2 image	38 (18.6)
Clinical Presentation	
Headache	132 (64.4)
Visual abnormalities	71 (34.8)
Symptomatic hypopituitarism	69 (33.7)
Symptomatic hyperprolactinemia	51 (25.0)
Apoplexy	4 (1.9)
Hormonal abnormalities	
Hyperprolactinemia	97 (47.3)
GH deficient	13 (6.3)
Acromegaly	4 (2.0)
Cortisol deficient	28 (13.7)
Cushing disease	8 (3.9)
Gonadotropin deficient	42 (20.5)
Thyroid deficient	39 (19.0)
Thyroid excess	2 (1.0)
Pre-operative ADH deficient	10 (4.9)
Cyst Category	
Type 1	68 (33.2)
Type 2	72 (35.1)
Type 3	10 (4.9)
Type 4	55 (26.8)
Lesion Location	
Anterior	125 (61.0)
Posterior	80 (39.0)
Maximum diameter (cm)	
≥ 10mm	151 (73.7)
< 10mm	54 (26.3)
Knosp Score	
0-2	183 (88.8)
3-4	23 (11.2)
Fluid-Fluid level	27 (13.2)

likely than RCCs to be anteriorly located (p=0.029). Finally, although 72% of Type 2 cysts were larger than 1 cm in diameter, these cysts rarely exhibited cavernous sinus invasion (1%).

Cyst Type 3 lesions (n=10, 4.9% of total) represented the least prevalent cyst type, and only consisted of RCCs (n=3, 30%) and cystic pituitary adenomas (n=7, 70%). Six of the seven (86%) cystic pituitary adenomas were located anteriorly, and all RCCs were posterior lesions. All Type 3 cysts had a maximal diameter greater than 1 cm, with a mean maximal diameter of 1.9 cm.

Cyst Type 4 lesions (n=55, 26.8% of total) were mostly cystic pituitary adenomas (n=45, 83%). Only 15% of Type 4 cystic lesions were craniopharyngiomas, although, the majority of craniopharyngiomas (62%) fell into this category. These lesions were located anteriorly 82% of the time, and Type 4 lesions were, on average, larger than other cyst types; 87% of Type 4 lesions were larger than 1 cm in diameter. Type 4 lesions were the most likely to show evidence of cavernous sinus invasion on preoperative MRI (35%). They were also most likely to have evidence of pre-operative visual abnormalities (62%). Finally, patients with these complex cysts were, on average, older than other patients, with a mean age of 50 years.

Differentiating Rathke Cleft Cysts and Cystic Pituitary Adenoma

Type 2 and 4 lesions were significantly more likely to be diagnosed as cystic pituitary adenomas compared to Type 1 lesions (OR: 23.7, 342.6; p=0.033, p<0.0001, respectively; **Table 3**). Those with Type 3 lesions had over a 5-fold increase in odds of being diagnosed as cystic pituitary adenomas as compared with RCC but this did not reach statistical significance, likely due to low power. A fluid-fluid level on preoperative MRI was significantly associated with a cystic pituitary adenoma (OR: 12.7; p=0.023). Obesity (OR: 5.0, p=0.003) and symptomatic hyperprolactinemia (OR: 11.5, p<0.001) were also significantly associated with cystic pituitary adenomas. Interestingly, although lesion relationship to the infundibulum (anterior versus posterior) was significant on univariable analysis, this was not statistically significant in the multivariable model. Additionally, we investigated whether the presence of Cushing disease or elevated serum cortisol level was driving the association between obesity and presence of a pituitary adenoma, however, these confounders were not found to be significant, and obesity was thus shown to be a true independent predictor of adenoma. Similarly, confounding of

TABLE 2 | Cyst category by pathologic diagnosis.

		Pathology*, n (%)			
		Arachnoid Cyst	**RCC**	**Pituitary Adenoma**	**Craniopharyngioma**
Cyst Category	Type 1	8 (11.8)	44 (64.7)	14 (20.6)	1 (1.5)
	Type 2	7 (9.7)	31 (43.1)	29 (40.3)	4 (5.6)
	Type 3	–	3 (30.0)	7 (70.0)	–
	Type 4	–	1 (1.9)	45 (83.3)	8 (14.8)

*$p < 0.001$.

The distribution of the four main pathologies represented by each of the cyst types in our cohort is presented. One colloid cyst (Type 1), one epidermoid cyst (Type 2), and one chordoma (Type 4) are not represented in this table.

TABLE 3 | Adjusted predictors of cystic pituitary adenomas versus Rathke cleft cysts.

	Odds Ratio	95% Confidence Interval	P-value
Cyst Type 1	REF	REF	REF
Cyst Type 2	23.7	1.3-10.6	**0.033**
Cyst Type 3	5.3	0.9-31.9	0.430
Cyst Type 4	342.6	36.2-999.9	**<0.0001**
Fluid-Fluid Level	12.7	1.4-111.9	**0.023**
Symptomatic Hyperprolactinemia	11.5	3.6-37.1	**<0.0001**
Obese	5.0	1.8-14.2	**0.003**

Odds ratios (OR), 95% confidence intervals (CI), and p-values for predictors of cystic pituitary adenoma compared to Rathke cleft cyst (RCC) in our cohort are presented. Bolded P-values indicate statistical significance.

symptomatic hyperprolactinemia by lesion size was also assessed, but not determined to be significant, and thus, only symptomatic hyperprolactinemia was included in the final model. Our multivariable clinical and radiographic model correctly predicted pathology 83.8% of the time (AUC 0.922; sensitivity 90.2%, specificity 76.0%, positive predictive value 82.2%, negative predictive value 86.4%; **Table 3**).

DISCUSSION

Differentiating cystic sellar lesions can be challenging given the heterogeneity of cyst appearance on preoperative imaging and the wide array of cystic pathologies that can present in this region. The initial differential strongly impacts the recommended management, especially in incidentally found lesions. Our proposed classification system is transparent and simple to use with a high interrater reliability. It summarizes key imaging features and may be most helpful when used alongside clinical and biochemical findings to steer management and treatment.

Differentiating Cystic Sellar Lesions

Key differentiating features among cystic lesions include heterogeneity of cyst contents, thickness of the cyst wall, cyst location (anterior versus posterior and midline versus lateral location), globular versus eccentric shape, size, degree of invasiveness, presence of solid component, and presence of intracystic nodule (3–19). We distilled these radiographic characteristics to two main factors: heterogeneity of cyst wall/contents and the presence of solid component. Overall, cyst type was found to be significantly associated with lesion pathology ($p<0.0001$), with non-neoplastic pathologies (e.g., arachnoid cysts and RCC) falling within Types 1 and 2, and neoplastic lesions (e.g., pituitary adenomas and craniopharyngiomas) categorized more frequently as Types 3 and 4. Interestingly, although the vast majority of Type 2 lesions were larger than 1 cm (72%), these cysts rarely exhibited cavernous sinus invasion (1%). This finding suggest that Type 2 cysts are associated with less invasive pituitary adenomas, which represented 41% (n=28) of type 2 cystic lesions.

Predictors of Cystic Pituitary Adenoma

This classification scheme has predictive value in a multivariable model differentiating between RCC and cystic pituitary adenoma in the pre-operative setting, correctly predicting the pathology 83.8% of the time. Radiographic features (e.g., cyst Type 2-4 and the presence of fluid-fluid level on MRI) and clinical/biochemical features (e.g., obesity and symptomatic hyperprolactinemia) were significant predictors of cystic adenomas. Our goal was to create a simple and effective tool for the clinician. Further in-depth analysis of multiple MRI and computed tomography sequences should also be employed to further aid in the differentiation of rare, but often misdiagnosed, cystic lesions, like hemorrhagic cystic pituitary adenomas (**Table 4**). Analogous to other reports, we observed that the presence of a fluid-fluid level on preoperative MRI is also predictive of cystic pituitary adenoma as compared with RCC (21, 28). We posit that the prevalence of fluid-fluid level among adenomas may be the result of intracystic hemorrhage from the abnormal vasculature architecture of these cystic lesions. We also redemonstrated that obesity is an independent predictor of pituitary adenoma (29, 30). Body mass index and waist circumference throughout early adulthood have been recently associated with higher risk of pituitary adenoma (31).

Surgical Implications for Cystic Prolactinomas

Indications for surgical resection of a pituitary mass include large lesions with mass effect and biochemically active tumors causing clinical hyperpituitarism (2, 32). Symptomatic hyperprolactinemia is the most common form of clinical hyperpituitarism and can be caused by a functional lactotroph tumor (prolactinoma) or stalk effect. Large cysts can produce stalk effect through compression of the infundibulum and suppression of dopaminergic negative feedback to the anterior pituitary gland. Prolactinomas directly secrete prolactin, which can be measured in the serum and used

TABLE 4 | Key preoperative radiographic findings for various cystic sellar pathology.

Cyst Pathology	Key Radiographic Features
Rathke cleft cyst (6, 12, 14, 15, 20)	- T2-hyperintense- Homogenously T2-hypointense/T1-hyperintense with high intrinsic protein content
Hemorrhagic cystic pituitary adenoma (20–24)	- T2-hypointense/T1-hyperintense (can mimic RCC when solid component is lacking)
Arachnoid cyst (6)	- Parallels CSF signal intensity on all MRI sequences
Dermoid cyst (16, 17)	- Follows fat signal intensity on all MRI sequences
Epidermoid cyst (16, 19, 25)	- Follows CSF intensity on T1 and T2, but bright on diffusion-weighted images (DWI)
Craniopharyngiomas (24, 26, 27)	- Contrast enhancement of solid portions on MRI- Intensity of cystic component can be variable depending on proportion of protein, cholesterol, and blood- 90% exhibit calcification on CT

in conjunction with tumor volume to diagnose a prolactinoma with high predictive value (33, 34). Cystic prolactinomas with minimal cellular/solid component, however, may not exhibit marked hyperprolactinemia, thereby mimicking hyperprolactinemia caused by stalk effect. This can lead to misclassification by conventional methods due to the mismatch between size and prolactin level, and, therefore, mimicking stalk effect. In our cohort, we found that the presence of clinical symptoms of hyperprolactinemia was one of the most predictive factors in diagnosing a cystic pituitary adenoma compared to an RCC, independent of serum prolactin level and lesion size. This important finding implies that careful distinction should be made between Type 1 and Type 2 lesions in the presence of a mild elevation of prolactin that may otherwise be attributable to stalk effect.

CONCLUSION

This study presents a novel cyst classification scheme for categorizing cystic sellar lesions based on the heterogeneity of the cyst wall/contents and the presence of a solid component on pre-operative MRI. We suggest that cyst type can be used in conjunction with other pre-operative factors to aid in the differentiating RCC from cystic pituitary adenomas, including cystic prolactinomas.

DATA AVAILABILITY STATEMENT

The raw data supporting the conclusions of this article will be made available by the authors, without undue reservation.

AUTHOR CONTRIBUTIONS

ST, MC, and DC were involved in data collection, data analysis, and manuscript writing. XB created figures and provided image formatting. EL provided the idea for the study and the cohort of cases from which the data was derived. All authors were heavily involved in manuscript editing. All authors contributed to the article and approved the submitted version.

REFERENCES

1. Cavallo LM, Prevedello D, Esposito F, Laws ER, Dusick JR, Messina A, et al. The Role of the Endoscope in the Transsphenoidal Management of Cystic Lesions of the Sellar Region. *Neurosurg Rev* (2008) 31(1):55–64. doi: 10.1007/s10143-007-0098-0
2. Laws ER. Endoscopic Surgery for Cystic Lesions of the Pituitary Region. *Nat Clin Pract Endocrinol Metab* (2008) 4(12):662–3. doi: 10.1038/ncpendmet0975
3. Park M, Lee SK, Choi J, Kim S-H, Kim SH, Shin N-Y, et al. Differentiation Between Cystic Pituitary Adenomas and Rathke Cleft Cysts: A Diagnostic Model Using MRI. *AJNR Am J Neuroradiol* (2015) 36(10):1866–73. doi: 10.3174/ajnr.A4387
4. Poussaint TY, Barnes PD, Anthony DC, Spack N, Scott RM, Tarbell NJ. Hemorrhagic Pituitary Adenomas of Adolescence. *AJNR Am J Neuroradiol* (1996) 17(10):1907–12.
5. Chabot JD, Chakraborty S, Imbarrato G, Dehdashti AR. Evaluation of Outcomes After Endoscopic Endonasal Surgery for Large and Giant Pituitary Macroadenoma: A Retrospective Review of 39 Consecutive Patients. *World Neurosurg* (2015) 84(4):978–88. doi: 10.1016/j.wneu.2015.06.007
6. Zamora C, Castillo M. Sellar and Parasellar Imaging. *Neurosurg* (2017) 80(1):17–38. doi: 10.1093/neuros/nyw013
7. Bonneville JF, Bonneville F, Cattin F. Magnetic Resonance Imaging of Pituitary Adenomas. *Eur Radiol* (2005) 15(3):543–8. doi: 10.1007/s00330-004-2531-x
8. Shatri J, Ahmetgjekaj I. Rathke's Cleft Cyst or Pituitary Apoplexy: A Case Report and Literature Review. *Open Access Maced J Med Sci* (2018) 6(3):544–7. doi: 10.3889/oamjms.2018.115
9. Gittleman H, Ostrom QT, Farah PD, Ondracek A, Chen Y, Wolinsky Y, et al. Descriptive Epidemiology of Pituitary Tumors in the United States, 2004-2009. *J Neurosurg* (2014) 121(3):527–35. doi: 10.3171/2014.5.JNS131819
10. Graziani N, Dufour H, Figarella-Branger D, Donnet A, Bouillot P, Grisoli F. Do the Suprasellar Neurenteric Cyst, the Rathke Cleft Cyst and the Colloid Cyst Constitute a Same Entity? *Acta Neurochir (Wien)* (1995) 133(3-4):174–80. doi: 10.1007/BF01420070
11. Hama S, Arita K, Nishisaka T, Fukuhara T, Tominaga A, Sugiyama K, et al. Changes in the Epithelium of Rathke Cleft Cyst Associated With Inflammation. *J Neurosurg* (2002) 96(2):209–16. doi: 10.3171/jns.2002.96.2.0209
12. Kunii N, Abe T, Kawamo M, et al. Rathke's Cleft Cysts: Differentiation From Other Cystic Lesions in the Pituitary Fossa by Use of Single-Shot Fast Spin-Echo Diffusion-Weighted MR Imaging. *Acta Neurochir (Wien)* (2007) 149(8):759–69. doi: 10.1007/s00701-007-1234-x
13. Laws ER, Kanter AS. Rathke Cleft Cysts. *J Neurosurg* (2004) 101(4):571–2. doi: 10.3171/jns.2004.101.4.0571
14. Nishioka H, Haraoka J, Izawa H, Ikeda Y. Magnetic Resonance Imaging, Clinical Manifestations, and Management of Rathke's Cleft Cyst. *Clin Endocrinol (Oxf)* (2006) 64(2):184–8. doi: 10.1111/j.1365-2265.2006.02446.x
15. Binning MJ, Gottfried ON, Osborn AG, Couldwell WT. Rathke Cleft Cyst Intracystic Nodule: A Characteristic Magnetic Resonance Imaging Finding. *J Neurosurg* (2005) 103(5):837–40. doi: 10.3171/jns.2005.103.5.0837
16. Caldarelli M, Massimi L, Kondageski C, Di Rocco C. Intracranial Midline Dermoid and Epidermoid Cysts in Children. *J Neurosurg* (2004) 100(5):473–80. doi: 10.3171/ped.2004.100.5.0473
17. Orakcioglu B, Halatsch ME, Fortunati M, Unterberg A, Yonekawa Y. Intracranial Dermoid Cysts: Variations of Radiological and Clinical Features. *Acta Neurochir (Wien)* (2008) 150(12):1227–34. doi: 10.1007/s00701-008-0152-x
18. Tatagiba M, Iaconetta G, Samii M. Epidermoid Cyst of the Cavernous Sinus: Clinical Features, Pathogenesis and Treatment. *Br J Neurosurg* (2000) 14(6):571–5. doi: 10.1080/02688690050206747
19. Tsuruda JS, Chew WM, Moseley ME, Norman D. Diffusion-Weighted MR Imaging of the Brain: Value of Differentiating Between Extraaxial Cysts and Epidermoid Tumors. *AJR Am J Roentgenol* (1990) 155(5):1059–65. doi: 10.2214/ajr.155.5.2120936
20. Choi SH, Kwon BJ, Na DG, Kim JK, Han MH, Chang KH. Pituitary Adenoma, Craniopharyngioma, and Rathke Cleft Cyst Involving Both Intrasellar and Suprasellar Regions: Differentiation Using MRI. *Clin Radiol* (2007) 62(5):453–62. doi: 10.1016/j.crad.2006.12.001
21. Xiao D, Wang S, Zhao L, Zhong Q, Huang Y, Ding C. Fluid-Fluid Level on Magnetic Resonance Images may Predict the Occurrence of Pituitary Adenomas in Cystic Sellar-Suprasellar Masses. *Exp Ther Med* (2017) 13(6):3123–9. doi: 10.3892/etm.2017.4299
22. Mohr G, Hardy J. Hemorrhage, Necrosis, and Apoplexy in Pituitary Adenomas. *Surg Neurol* (1982) 18(3):181–9. doi: 10.1016/0090-3019(82)90388-3
23. Tosaka M, Sato N, Hirato J, Fujimaki H, Yamiguchi R, Kohga H, et al. Assessment of Hemorrhage in Pituitary Macroadenoma by T2*-Weighted Gradient-Echo MR Imaging. *AJNR Am J Neuroradiol* (2007) 28:2023–29. doi: 10.3174/ajnr.A0692
24. Shin JL, Asa SL, Woodhouse LJ, Smyth HS, Ezzat S. Cystic Lesions of the Pituitary: Clinicopathological Features Distinguishing Craniopharyngioma,

Rathke's Cleft Cyst, and Arachnoid Cyst. *J Clin Endocrinol Metab* (1999) 84 (11):3972–82. doi: 10.1210/jcem.84.11.6114
25. Harrison MJ, Morgello S, Post KD. Epithelial Cystic Lesions of the Sellar and Parasellar Region: A Continuum of Ectodermal Derivatives? *J Neurosurg* (1994) 80(6):1018–25. doi: 10.3171/jns.1994.80.6.1018
26. Bunin GR, Surawicz TS, Witman PA, Preston-Martin S, Davis F, Bruner JM. The Descriptive Epidemiology of Craniopharyngioma. *J Neurosurg* (1998) 89 (4):547–51. doi: 10.3171/jns.1998.89.4.0547
27. Prabhu VC, Brown HG. The Pathogenesis of Craniopharyngiomas. *Childs Nerv Syst* (2005) 21(8-9):622–7. doi: 10.1007/s00381-005-1190-9
28. Goel A, Shah A, Jhawar SS, Goel NK. Fluid-Fluid Level in Pituitary Tumors: Analysis of Management of 106 Cases. *J Neurosurg* (2010) 112(6):1341–6. doi: 10.3171/2009.11.JNS091083
29. Hayashi M, Tachibana O, Muramatsu N, Tsuchiya H, Tada M, Arakawa Y, et al. Rathke Cleft Cyst: MR and Biomedical Analysis of Cyst Content. *J Comput Assist Tomogr* (1999) 23(1):34–8. doi: 10.1097/00004728-199901000-00008
30. Zada G. Rathke Cleft Cysts: A Review of Clinical and Surgical Management. *Neurosurg Focus* (2011) 31(1):E1. doi: 10.3171/2011.5.FOCUS1183
31. Cote DJ, Smith TR, Kaiser UB, Laws ER, Stampfer MJ. Body Habitus Across the Lifespan and Risk of Pituitary Adenoma. *J Clin Endocrinol Metab* (2021) 106(4):e1591–602. doi: 10.1210/clinem/dgaa987
32. Zada G, Lin N, Ojerholm E, Ramkissoon S, Laws ER. Craniopharyngioma and Other Cystic Epithelial Lesions of the Sellar Region: A Review of Clinical, Imaging, and Histopathological Relationships. *Neurosurg Focus* (2010) 28 (4):4–5. doi: 10.3171/2010.2.FOCUS09318
33. Burke WT, Penn DL, Castlen JP, Donoho DA, Repetti CS, Luliano S, et al. Prolactinomas and Nonfunctioning Adenomas: Preoperative Diagnosis of Tumor Type Using Serum Prolactin and Tumor Size. *J Neurosurg* (2019) 133:321–8. doi: 10.3171/2019.3.JNS19121
34. Hamilton DK, Vance ML, Boulos PT, Laws ER. Surgical Outcomes in Hyporesponsive Prolactinomas: Analysis of Patients With Resistance or Intolerance to Dopamine Agonists. *Pituitary* (2005) 8(1):53–60. doi: 10.1007/s11102-005-5086-1

Conflict of Interest: The authors declare that the research was conducted in the absence of any commercial or financial relationships that could be construed as a potential conflict of interest.

frontiers in Oncology

REVIEW
published: 23 December 2021
doi: 10.3389/fonc.2021.784819

The Application of Artificial Intelligence and Machine Learning in Pituitary Adenomas

Congxin Dai[1†], *Bowen Sun*[1†], *Renzhi Wang*[2*] *and Jun Kang*[1*]

[1] *Department of Neurosurgery, Beijing Tongren Hospital, Capital Medical University, Beijing, China,* [2] *Department of Neurosurgery, Peking Union Medical College Hospital, Chinese Academy of Medical Sciences and Peking Union Medical College, Beijing, China*

Pituitary adenomas (PAs) are a group of tumors with complex and heterogeneous clinical manifestations. Early accurate diagnosis, individualized management, and precise prediction of the treatment response and prognosis of patients with PA are urgently needed. Artificial intelligence (AI) and machine learning (ML) have garnered increasing attention to quantitatively analyze complex medical data to improve individualized care for patients with PAs. Therefore, we critically examined the current use of AI and ML in the management of patients with PAs, and we propose improvements for future uses of AI and ML in patients with PAs. AI and ML can automatically extract many quantitative features based on massive medical data; moreover, related diagnosis and prediction models can be developed through quantitative analysis. Previous studies have suggested that AI and ML have wide applications in early accurate diagnosis; individualized treatment; predicting the response to treatments, including surgery, medications, and radiotherapy; and predicting the outcomes of patients with PAs. In addition, facial imaging-based AI and ML, pathological picture-based AI and ML, and surgical microscopic video-based AI and ML have also been reported to be useful in assisting the management of patients with PAs. In conclusion, the current use of AI and ML models has the potential to assist doctors and patients in making crucial surgical decisions by providing an accurate diagnosis, response to treatment, and prognosis of PAs. These AI and ML models can improve the quality and safety of medical services for patients with PAs and reduce the complication rates of neurosurgery. Further work is needed to obtain more reliable algorithms with high accuracy, sensitivity, and specificity for the management of PA patients.

Keywords: pituitary adenomas, artificial intelligence, machine learning, radiomics, individualized treatment

OPEN ACCESS

Edited by:
Qun Wu,
Zhejiang University, China

Reviewed by:
Zihang Chen,
Shandong University, China
Xun Zhang,
Massachusetts General Hospital and Harvard Medical School, United States

***Correspondence:**
Jun Kang
junkang2015@163.com
Renzhi Wang
Wangrz@126.com

[†]These authors have contributed equally to this work

Specialty section:
This article was submitted to Neuro-Oncology and Neurosurgical Oncology, a section of the journal Frontiers in Oncology

Received: *28 September 2021*
Accepted: *02 December 2021*
Published: *23 December 2021*

Citation:
Dai C, Sun B, Wang R and Kang J (2021) The Application of Artificial Intelligence and Machine Learning in Pituitary Adenomas. Front. Oncol. 11:784819. doi: 10.3389/fonc.2021.784819

INTRODUCTION

Pituitary adenomas (PAs) account for approximately 10%–15% of all intracranial neoplasms and are the second most common primary brain tumors (1). PAs are a group of tumors with complex and heterogeneous clinical manifestations that can be classified based on hormone secretion status, clinical features, and radiologic and pathological results. Some PAs are microadenomas (<10 mm)

but secrete excess hormones, whereas others are invasive giant PAs (≥40 mm), leading to mass effects but without excessive hormone secretion. Some PAs are asymptomatic and remain stable with long-term follow-up, but others have obvious clinical symptoms at initial diagnosis and need to be treated in a timely manner (2). A subset of PAs is responsive to surgery, medical therapy, and radiotherapy, while others do not respond to these treatments. After standard treatment, some benign PAs achieve long-term remission, whereas other aggressive PAs are refractory to conventional treatments and recur (3). Therefore, it is essential to accurately diagnose PAs early, individually manage PAs, precisely predict the response to treatments, and predict the outcomes of patients with PAs. However, there currently exist no clinical models that can accurately predict the early diagnosis, therapeutic response, and outcomes of patients with PAs.

ARTIFICIAL INTELLIGENCE AND MACHINE LEARNING

Artificial intelligence (AI) is a methodology of computer systems that uses algorithms to tirelessly process data, automatically learn and understand its meaning, generate computer models, and identify the best predictive features present in training data (4). As a domain of AI, machine learning (ML) is defined as performing automated learning from the input or data (experience) that it has been presented, and it converts these data to expertise or knowledge. ML can be used to design and train software algorithms to learn from and act on data (5). ML has gained wide applicability to develop sophisticated tools in various areas of data processing, such as images, natural language processing, data mining, gaming, robotics, and big data in general (6). In the past few years, the applications of AI and ML in the healthcare sector have shown ever-increasing growth owing to the rapid progress made possible by deep ML (7).

APPLICATIONS OF AI AND ML IN PAs

With the rapid advancement of computer technology, AI and ML have more widely been used in the diagnosis and management of patients with PAs. AI and ML have seen a resurgence with specific application areas in PAs, which involve radiomics, facial imaging, pathological images, electronic medical records including texts, and medical image analyses (6).

MAGNETIC RESONANCE IMAGING-BASED RADIOMICS AND ML IN PAs

As one of the standard examination methods, magnetic resonance imaging (MRI) has been considered one of the most useful tools for detecting PAs. MRI-based radiomics and ML have been used for early screening, differential diagnosis, grading and staging of tumors, clinical decision-making, predicting outcomes, and identifying pathological subtypes (8, 9). The details of the reviewed studies are summarized in **Table 1**. Acromegaly is usually caused by a pituitary growth hormone (GH)-secreting adenoma. Transsphenoidal surgery (TSS) is the first-choice treatment for acromegaly, and tumor consistency is one of the important factors that affect the surgical resection rate. Therefore, it is pivotal to predict the tumor consistency before surgery and to identify individualized surgical strategies for patients with acromegaly. Fan and colleagues (10) enrolled 158 patients with acromegaly and randomly divided them into primary cohort (n = 100) and validation cohort (n = 58). The preoperative clinical characteristics were collected, and the consistency of the tumor was classified as soft or firm according to the neurosurgeon's evaluation. The most valuable clinical characteristics were then selected based on the multivariable logistic regression analysis. The critical radiomics features were determined using the elastic net feature selection algorithm, and the radiomics signature was established based on the radiomics features selected from the primary cohort through the support vector machine method. Furthermore, differences in the signature distribution between soft and firm tumors were compared using a violin plot. The radiomics model was then obtained to precisely predict tumor consistency, and the AUC was 0.83 (95% confidence interval, 0.81–0.85) and 0.81 (95% confidence interval, 0.78–0.83) in the primary and validation cohorts, respectively. The authors found that radiomics model is more effective in the prediction of the tumor consistency comparing with the clinical characteristics. Zeynalova and colleagues (11) also enrolled 55 patients with 13 hard and 42 soft pituitary macroadenomas and used an open-source Python package named PyRadiomics for texture feature extraction from coronal T2-weighted original. They reduced the high dimensionality of the histogram texture features with reproducibility analysis, collinearity analysis, and feature selection. Reference standard (hard versus soft) for the classifications of macroadenomas was based on surgical and histopathological findings. The artificial neural network using multilayer perceptron algorithm was utilized for classifications. The authors found that using the ML-based histogram analysis, about three-fourths of pituitary macroadenomas can be correctly classified in term of tumor consistency with an AUC value of 0.710. Furthermore, the ML-based histogram analysis performed better than the signal intensity ratio (SIR) evaluation with an AUC value of 0.551. They indicated that ML-based T2-weighted MRI histogram analysis might be a better technique in predicting the consistency of pituitary macroadenomas than that of conventional SIR evaluation.

Zhu and colleagues (12) also used 152 patient data with labels (including 112 T1 MRI spatial sequences and 40 T2 MRI spatial sequences) and presented an automatic method for accurately determining the softness level of pituitary tumors preoperatively. Because their pituitary tumor MRI image dataset where T1 and T2 sequence data are unbalanced (due to data missing) and undersampled. They first obtained fully sampled MRI spatial sequence by using a CycleConsistent Adversarial Networks (CycleGAN) model. They then used a Densely Connected

TABLE 1 | Summary of recent studies related to artificial intelligence and machine learning applications in the pituitary adenomas.

Author and ref.	Tumor subtypes	Sample size	Task	Models (parameters)	Prediction performance (AUC)
Fan et al. (10)	Acromegaly	Training (*n* = 100) Test datasets (*n* = 58)	Predicting consistency	Elastic net feature selection algorithm	0.83
Zeynalova et al. (11)	Pituitary macroadenoma	*N* = 55	Predicting consistency	Artificial neural network	0.710
Zhu et al. (12)	PAs	*N* = 152	Determining the softness	CRNN (DenseNet+ResNet)	0.9178
Niu et al. (13)	PAs	Training set (*n* = 97) Test set (*n* = 97)	Predicting CSI	Linear support vector machine and nomogram	Training (0.899) Test (0.871)
Fan et al. (14)	Invasive functional PAs	Primary (*n* = 108) Validation (*n* = 55)	Predicting treatment response	Support vector machine	Training (0.832) Validation (0.811)
Staartjes et al. (15)	PAs	*N* = 140	Predicting gross-total resection	Deep neural network	0.96
Fan et al. (16)	Acromegaly	Training (*n* = 534) Test datasets (*n* = 134)	Predicting TSS response	Forward search algorithm	Training (0.8555) Validation (0.8178)
Qiao et al. (17)	Acromegaly	Training (*n* = 833)	Test datasets (*n* = 99) Predicting early remission of TSS	Partial model, full model	Partial model / Full model
				Penalized logistic regression	0.781 / 0.867
				Gradient boost machine	0.752 / 0.789
				Support vector machine	0.759 / 0.850
				Neural network	0.790 / 0.787
				Ensemble algorithm	0.775 / 0.853
				Validation cohort	0.759 / 0.897
Hollon et al. (18)	PAs	Training (*n* = 300) Test datasets (*n* = 100)	Predicting early outcomes	Naive Bayes	0.795
				Support vector machines	0.826
				Random forest	0.848
				LR-EN regularization	0.827
Dai et al. (19)	Acromegaly	Training (*n* = 244) Test dataset (*n* = 62)	Predicting delayed remission	Logistic regression	0.7945
				Adaptive boosting	0.7013
				GBDT	0.8061
				Extreme gradient boost	0.8260
				Categorical boosting	0.8239
				Random forest	0.7338
Fan et al. (20)	Acromegaly	*N* = 57	Predicting radiotherapeutic response	Support vector machine	0.96
Kocak et al. (21)	Acromegaly	*N* = 47	Predicting response to SA	Wrapper-based algorithm	0.847
Park et al. (22)	Prolactinoma	Training (*n* = 141) Test dataset (*n* = 36)	Predicting the DA response	Random forest	0.78 (0.63–0.94)
				Extra-trees	0.79 (0.63–0.95)
				Light GBM	0.74 (0.57–0.93)
				QDA	0.66 (0.48–0.84)
				LDA	0.66 (0.46–0.86)
				Soft voting ensemble	0.81 (0.67–0.96)
Zoli et al. (23)	Cushing disease	Training (*n* = 121) Test dataset (*n* = 30)	Predicting outcomes of TSS		Training and test
				Support vector machine	0.681 and 1.00
				GBM	0.719 and 0.783
				K-nearest neighbor	0.993 and 0.988
Zhang et al. (24)	Cushing disease	Training (*n* = 836) Test dataset (*n* = 209)	Predicting postoperative immediate remission	Extreme gradient boost	0.712
				GBDT	0.734
				Random forest	0.726
				Adaptive boost	0.699
				Naïve Bayes	0.681
				Logistic regression	0.701
				Decision tree	0.664
				Multilayer perceptron	0.700
				Stacking	0.743
Fan et al. (25)	Cushing disease	Training (*n* = 836) Test dataset (*n* = 209)	Predicting Postoperative Delayed remission	Logistic regression	0.7262
				Adaptive boosting	0.7619
				GBDT	0.7262
				XGboost	0.7262
				Catboost	0.7

(Continued)

TABLE 1 | Continued

Author and ref.	Tumor subtypes	Sample size	Task	Models (parameters)	Prediction performance (AUC)	
Liu et al. (26)	Cushing disease	Training (n = 283) Test dataset (n = 71)	Predicting recurrence after TSS	Decision tree	0.629	
				Random forest	0.779	
				Logistic regression	0.684	
				Naïve Bayes	0.608	
				GBDT	0.694	
				Adaptive boost	0.716	
				Extreme gradient boost	0.735	
Voglis et al. (27)	PAs	N = 207	Predicting postoperative hyponatremia	Random forest	0.637	
				Naïve Bayes	0.646	
				Boosted GLMs	0.671	
				GLMs	0.595	
Machado et al. (28)	NFP macroadenomas	N = 27	Predicting recurrence after the first surgery		2D radiomics	3D radiomics
				Multilayer perceptron	0.92.9	0.962
				Random forest	0.877	0.962
				Support vector machine	0.860	0.946
				Logistic regression (LR)	0.929	0.946
				K-nearest neighbor	0.979	0.945
Meng et al. (29)	Acromegaly	62 patients with acromegaly and 62 matched controls	Identifying facial features and predicting patients of acromegaly	Linear discriminant analysis	0.9286	
Wei et al. (30)	Acromegaly and Cushing disease	642 Cushing disease, 896 acromegaly, and 11,447 normal images	Identifying facial anomalies	Convolutional neural networks	Cushing disease	0.9647
					Acromegaly	0.9556
					Normal	0.9393
Peng et al. (31)	PAs	235 patients with pathologically diagnosed PAs	Immunohistochemically classify PAs subtypes	Support vector machine	0.9549	
				K-nearest neighbor	0.9266	
				Naïve Bayes	0.932	
Ugga et al. (32)	PAs	89 patients with available Ki-67 labeling index	Predicting of high proliferative index	K-nearest neighbors	0.87	

Convolutional Networks (DenseNet)-Deep Residual Networks (ResNet)-based Autoencoder framework to optimize the feature extraction process for pituitary tumor image data. Finally, they used a Convolutional Recurrent Neural Network (CRNN) model to classify pituitary tumors based on their predicted softness levels. They found that this semisupervised deep neural network model can accurately determine the softness level of pituitary tumors with high accuracy (91.78%).

Although these ML-based radiomics have been shown a very high accuracy in predicting consistency of the pituitary tumors, each approach has its own pros and cons. Firstly, all the studies were a retrospective analysis with a relatively small number of patients, which would lead to bias in ML-based classifications. Secondly, Zeynalova and colleagues (11) only used histogram analysis with few texture features, two dimensional segmentations, and conventional T2-weighted MRI, which were not comprehensive. More ML and feature selection algorithms and more comprehensive MRI data including contrast-enhanced MRI scans may have a potential for developing better ML-based models. Thirdly, the data samples used in Zhu's (12) study were unbalanced sequence image data and insufficient; it is easy to produce the overfitting phenomenon. Although the loss of feature extraction model training was low and convergence was achieved, the accuracy was still not high enough. Taken together, these ML-based radiomics models performed better than conventional methods in predicting the consistency of the pituitary tumors; further large-scale and more comprehensive studies are needed to confirm and improve these approaches.

Invasive PAs are complicated and difficult to treat; therefore, it is critical to predict cavernous sinus (CS) invasion and treatment response for these patients preoperatively. Niu and colleagues (13) predicted CS invasion preoperatively for patients with Knosp grades II and III PAs using a radiomics method based on MR, which might contribute to designing surgical strategies. Fan and colleagues (14) developed and validated a radiomic model incorporating an MRI-based radiomic signature using a support vector machine, which predicts the treatment response and help doctors determine individual treatment strategies for these patients with invasive functional PAs. Gross-total resection is often the primary surgical goal in TSS for PAs. Staartjes and colleagues (15) demonstrated that a deep ML model could be used to preoperatively predict the likelihood of GTR with excellent performance, which would be a valuable addition to risk stratification and surgical decision-making. Accurate prediction of postoperative remission may be helpful for decision-making and prognosis regarding treatment strategies for patients with acromegaly. Fan and colleagues (16) enrolled 668 patients with acromegaly and divided them into a training set of 534 cases and a test set of 134 cases. The author used six machine learning methods in Python, including random forest, logistic regression, logistic GAMs, gradient boosting decision tree (GBDT), adaptive boosting, and extreme gradient boost, to construct a predictive model for postoperative

remission. By comparing the six models, the GBDT model has the best predictive performance, can obtain quantitative predictive value, has a higher accuracy rate than clinicians, and can better assist the preoperative clinical diagnosis and treatment decision-making of patients with acromegaly. Qiao (17) included 833 patients with GH-secreting PAs as a training cohort and trained a partial model (using only preoperative variables) and a full model (using all variables) to predict off-medication endocrine remission at the 6-month follow-up after TSS using multiple ML algorithms. These models have been validated to accurately predict early endocrine remission after TSS in patients with GH-secreting PAs. The prediction accuracy of the ML-trained models was better than those using single variables. Hollon (18) also demonstrated that early surgical outcomes of PAs can be predicted with 87% accuracy using a machine learning approach.

For patients with acromegaly who do not reach immediate remission after surgery, a subset of them achieves delayed remission during long-term follow-up without further postoperative therapy. Therefore, it is necessary to predict the delayed remission of acromegaly after surgery (33). We used the recursive feature elimination algorithm to select features and applied six ML algorithms to establish an ML model for predicting delayed remission of acromegaly. As an effective noninvasive approach, ML-based models can predict delayed remission and aid in determining individual treatment and follow-up strategies for patients with acromegaly who have not achieved remission within 6 months of surgery (19).

For acromegaly patients who do not achieve remission after TSS, radiotherapy is a third-line treatment. Fan and colleagues developed a radiomics model using preradiotherapy clinical and MRI data to noninvasively predict the radiotherapeutic response of acromegaly, which may help doctors identify acromegaly patients who will benefit from radiotherapy (20). Somatostatin analogs (SAs) are widely used in the medical treatment of patients with acromegaly, and it is necessary to predict the response to SA for these patients. Kocak (21) demonstrated that ML-based high-dimensional quantitative texture analysis on T2-weighted MRI has the potential to predict the response to SAs in patients with acromegaly, and it performs better than quantitative and qualitative T2-weighted relative signal intensity or immunohistochemical granulation pattern evaluation.

For prolactinomas, medical treatment with dopamine agonists (DAs) is the first-line therapy. However, approximately 10%–30% of patients with prolactinomas show resistance to DA (34). Therefore, it is crucial to identify DA-resistant prolactinomas early because then the patients would not have to endure a prolonged therapeutic trial. Park (22) developed a radiomics model using an ensemble machine learning classifier with conventional MRIs and demonstrated that radiomics features might be useful biomarkers to predict the DA response in patients with prolactinoma.

Cushing disease (CD) is a devastating condition that is usually caused by excessive secretions arising from pituitary corticotroph adenomas (35). It remains challenging to accurately diagnose and individually manage CD due to the disease complexity and heterogeneity (36). It is especially important to preoperatively predict the treatment outcomes of these patients due to variable rates of remission and a high risk of recurrence (37). In recent years, AI and ML have been increasingly reported in the diagnosis and management of CD (38). TSS is the first-line treatment for patients with CD; however, surgical outcomes are usually the most difficult to predict preoperatively. Zoli and colleagues (23) trained and internally validated robust models using ML algorithms to make accurate preoperative surgical outcome predictions for CD patients. Zhang (24) also developed a readily available ML-based model for the preoperative prediction of immediate remission in patients with histology-positive CD. After TSS, a subset of patients with CD do not achieve immediate remission but achieve remission without further postoperative therapy during long-term follow-up, which is defined as postoperative delayed remission (39). Among these patients with persistent hypercortisolism after TSS, some patients will achieve delayed remission without the need for further treatment. To identify patients who have the potential to achieve delayed remission, Fan (25) developed ML-based models to predict delayed remission or persistent active disease in patients with CD whose remission status is uncertain. Use of this model could help doctors judge the surgical response and determine whether the patient needs postoperative adjuvant therapy, thus avoiding unnecessary additional treatments. According to previous studies, recurrence after TSS for CD ranges from 15% to 66% (40), whereas no valid predictor for recurrence has been developed. Liu (26) reported that using ML-based models was feasible for predicting CD recurrence after initial TSS, which was significantly better than that of some conventional models.

After TSS, postoperative hyponatremia is one of the common procedural complications in patients with PAs. Voglis (27) demonstrated that a trained ML model was able to learn complex risk factor interactions and could predict postoperative hyponatremia, thus potentially reducing morbidity and improving patient safety.

After the first surgery, 12% to 66% of patients with clinically nonfunctioning pituitary adenoma (NFPA) experience a tumor recurrence. Nevertheless, there is still no factor that could concisely predict the recurrence of NFPA. Machado (28) reported that a combination of radiomics with machine-learning algorithms could offer computational models capable of noninvasive, unbiased, and quick assessment that might improve the prediction of NFPA recurrence.

Taken together, these ML-based and MRI-based radiomics analytical methods are playing an increasingly important role in early accurate diagnosis, individualized treatment, predicting the response to treatments, including surgery, medications and radiotherapy, and the prognosis of patients with PAs. However, there is significant variability in the applied ML paradigms and prediction performance (AUC) at different studies (**Table 1**). The main reasons for that include variation in data extraction and lack of consistency among the statistical methodologies and ML algorithms used in the varied studies. In the future, ML-based and MRI-based radiomics will have great

promise for potentially improving patients' individualized treatment and prognosis.

FACIAL IMAGING-BASED AI AND ML IN PAs

Facial changes are common among nearly all patients with acromegaly and CD. It is difficult to notice such facial changes early because they are a slow and gradual process. The diagnosis and treatment of these diseases are often delayed until these clinical symptoms become obvious. Meng (29) demonstrated that combining 3D imaging and ML techniques could accurately identify and predict early facial changes in patients with acromegaly, which might be beneficial for the early detection of acromegalic patients, enabling immediate treatment. Wei (30) also developed a deep-learning model to recognize facial anomalies with underlying endocrine disorders, and its performance was comparable with that of professional medical practitioners. These models have the potential to assist in the diagnosis and follow-up of these patients with hypersecretion statuses, which may be helpful for the early detection of the disease.

PATHOLOGICAL PICTURES-BASED AI AND ML IN PAs

The type of PA cannot be clearly recognized by preoperative MRI but can be classified by immunohistochemical staining of resected tumor samples after surgery. Recently, PAs have been classified based on a combination of tumor hormonal content and pituitary transcription factors. The correct PA classification before surgery can help doctors decide on the right treatment strategy. Peng (31) developed a classification model using ML-based radiomics, which can potentially precisely immunohistochemically classify PA subtypes. This model exhibited good performance and might offer potential guidance to doctors in clinical decision-making before surgery. The Ki-67 labeling index, representing a proliferative marker, has been reported as a marker of aggressiveness in PAs (41), and it is crucial to identify the Ki-67 labeling index early to allow timely diagnosis and treatment. Ugga and colleagues (32) proved that ML analysis of texture-derived parameters from preoperative T2 MRI could effectively predict the Ki-67 proliferation index class in pituitary macroadenomas. This might provide a more accurate preoperative lesion classification for doctors before surgery and help neurosurgeons develop surgical strategies.

SURGICAL MICROSCOPIC VIDEO-BASED AI AND ML IN PAs

In pituitary surgery, segmentation of the surgical workflow might be helpful for providing context-sensitive user interfaces or generating automatic reports. Moreover, neurosurgeons must deal with intraoperative adverse events, which come from not only the patients but also surgical management. It is very important to be aware of these difficulties quickly and efficiently, to better handle risky situations and to relieve the neurosurgeons' responsibilities. It is necessary to assist neurosurgeries through the understanding of operating room activities, increase medical safety, and support decision-making. Lalys (42) recognized surgical phases of every unknown image by computing their signatures and then simulating them with machine learning techniques and validated this methodology with a specific type of neurosurgery. Currently, this methodology could be used for postoperative video indexation as an aid to surgeons, which contains relevant surgical phases of each procedure for easy browsing.

TOTAL CHARGES AND DRIVERS OF COST IN PAs

The effective allocation of resources in the healthcare system enables providers to care for an increasing number of needier patients. It is necessary to identify drivers of total charges for TSS for PAs, which may help neurosurgeons reduce waste and provide higher-quality care for patients. Muhlestein and colleagues (43) used a large, national database to develop ML ensembles that directly predict total charges for PA patients with good fidelity. They identified extended length of stay, postoperative complications, private investor hospital ownership, etc. as drivers of total charges and potential targets for cost-lowering interventions. Minimizing the effects of these variables may improve efficiency in the resource-limited healthcare system and lead to higher-quality care and improved outcomes for more patients.

FUTURE PERSPECTIVES OF AI AND ML IN PAs

To date, AI and ML are promising in the diagnosis, prediction of therapy response, and prognosis, as well as the pathological classification of PAs. AI-based radiomics has especially made the greatest contributions to bridging the gap of AI-assisted diagnostics and prognostics to individualized treatment. However, the sample sizes included in the previous studies were relatively small, and the accuracy of the algorithms is not yet very high. Therefore, future studies including larger sample sizes may obtain more reliable algorithms with high accuracy, sensitivity, and specificity. Currently, there is a lack of consistency among the statistical methodologies and ML algorithms incorporated by the studies described. The wide variety of methodologies and ML models always leads to inconsistent conclusions. Given this lack of standardization, a consensus is required to standardize the extrapolation of data and model development. Moreover, it appears that there are many aspects for future researchers to include contributions of AI and ML in PAs. First, it is important to accurately predict the

disability and mortality risks among patients with PAs using ML algorithms. Accurately predicting these risks, such as heart failure risk in patients with acromegaly and fracture risk in patients with CD, enables an individualized approach to prevention, monitoring, and therapy strategies. Second, there is currently a lack of healthcare policy generated by AI technologies on PAs. Making appropriate medical policies by analyzing big data from public healthcare using AI technologies would be helpful to improve the accuracy and personalized medical care of the entire medical community. Third, more interdisciplinary studies are necessary to strengthen AI links with medical big data management and enable the creation of publicly available datasets for neuroimaging- and visual imaging-guided diagnosis and treatment of PAs.

CONCLUSIONS

As an emerging field, AI and ML method research has displayed great prospects in patients with PAs. The current use of AI and ML models has the potential to assist doctors and patients in making crucial surgical decisions by providing an accurate diagnosis and predicting the response to treatment and the outcomes of PAs. These AI and ML models have more individual specificity and accuracy than traditionally used models, and AI-based clinical decision support systems are likely to improve further the quality and safety of medical services for patients with PAs and reduce the complication rates of neurosurgery. Additional work is necessary to obtain more reliable algorithms with high accuracy, sensitivity, and specificity for the management of PA patients.

AUTHOR CONTRIBUTIONS

CD and BS revised the manuscript. RW and JK take final responsibility for this article. All authors listed have made substantial, direct, and intellectual contribution to the work and approved it for publication.

FUNDING

Financial support for this study was provided by the Beijing Municipal Administration of Hospitals Incubating Program, (grant number: PX2022004). The funding institutions had no role in the design of the study, data collection and analysis, decision to publish, or preparation of the manuscript.

REFERENCES

1. Araujo-Castro M, Berrocal VR, Pascual-Corrales E. Pituitary Tumors: Epidemiology and Clinical Presentation Spectrum. *Hormones (Athens)* (2020) 19(2):145–55. doi: 10.1007/s42000-019-00168-8
2. Dai C, Kang J, Liu X, Yao Y, Wang H, Wang R. How to Classify and Define Pituitary Tumors: Recent Advances and Current Controversies. *Front Endocrinol (Lausanne)* (2021) 12:604644. doi: 10.3389/fendo.2021.604644
3. Dai C, Liu X, Ma W, Wang R. The Treatment of Refractory Pituitary Adenomas. *Front Endocrinol* (2019) 10:334. doi: 10.3389/fendo.2019.00334
4. Gurgitano M, Angileri SA, Roda GM, Liguori A, Pandolfi M, Ierardi AM, et al. Interventional Radiology Ex-Machina: Impact of Artificial Intelligence on Practice. *Radiol Med* (2021) 126(7):998–1006. doi: 10.1007/s11547-021-01351-x
5. Hong N, Park H, Rhee Y. Machine Learning Applications in Endocrinology and Metabolism Research: An Overview. *Endocrinol Metab (Seoul)* (2020) 35 (1):71–84. doi: 10.3803/EnM.2020.35.1.71
6. Saha A, Tso S, Rabski J, Sadeghian A, Cusimano MD. Machine Learning Applications in Imaging Analysis for Patients With Pituitary Tumors: A Review of the Current Literature and Future Directions. *Pituitary* (2020) 23 (3):273–93. doi: 10.1007/s11102-019-01026-x
7. Secinaro S, Calandra D, Secinaro A, Muthurangu V, Biancone P. The Role of Artificial Intelligence in Healthcare: A Structured Literature Review. *BMC Med Inform Decis Mak* (2021) 21(1):125. doi: 10.1186/s12911-021-01488-9
8. Fan Y, Feng M, Wang R. Application of Radiomics in Central Nervous System Diseases: A Systematic Literature Review. *Clin Neurol Neurosurg* (2019) 187:105565. doi: 10.1016/j.clineuro.2019.105565
9. Soldozy S, Farzad F, Young S, Yagmurlu K, Norat P, Sokolowski J, et al. Pituitary Tumors in the Computational Era, Exploring Novel Approaches to Diagnosis, and Outcome Prediction With Machine Learning. *World Neurosurg* (2021) 146:315–21.e1. doi: 10.1016/j.wneu.2020.07.104
10. Fan Y, Hua M, Mou A, Wu M, Liu X, Bao X, et al. Preoperative Noninvasive Radiomics Approach Predicts Tumor Consistency in Patients With Acromegaly: Development and Multicenter Prospective Validation. *Front Endocrinol (Lausanne)* (2019) 10:403. doi: 10.3389/fendo.2019.00403
11. Zeynalova A, Kocak B, Durmaz ES, Comunoglu N, Ozcan K, Ozcan G, et al. Preoperative Evaluation of Tumour Consistency in Pituitary Macroadenomas: A Machine Learning-Based Histogram Analysis on Conventional T2-Weighted MRI. *Neuroradiology* (2019) 61(7):767–74. doi: 10.1007/s00234-019-02211-2
12. Zhu H, Fang Q, Huang Y, Xu K. Semi-Supervised Method for Image Texture Classification of Pituitary Tumors *via* CycleGAN and Optimized Feature Extraction. *BMC Med Inform Decis Mak* (2020) 20(1):215. doi: 10.1186/s12911-020-01230-x
13. Niu J, Zhang S, Ma S, Diao J, Zhou W, Tian J, et al. Preoperative Prediction of Cavernous Sinus Invasion by Pituitary Adenomas Using a Radiomics Method Based on Magnetic Resonance Images. *Eur Radiol* (2019) 29(3):1625–34. doi: 10.1007/s00330-018-5725-3
14. Fan Y, Liu Z, Hou B, Li L, Liu X, Liu Z, et al. Development and Validation of an MRI-Based Radiomic Signature for the Preoperative Prediction of Treatment Response in Patients With Invasive Functional Pituitary Adenoma. *Eur J Radiol* (2019) 121:108647. doi: 10.1016/j.ejrad.2019.108647
15. Staartjes VE, Serra C, Muscas G, Maldaner N, Akeret K, van Niftrik C, et al. Utility of Deep Neural Networks in Predicting Gross-Total Resection After Transsphenoidal Surgery for Pituitary Adenoma: A Pilot Study. *Neurosurg Focus* (2018) 45(5):E12. doi: 10.3171/2018.8.FOCUS18243
16. Fan Y, Li Y, Li Y, Feng S, Bao X, Feng M, et al. Development and Assessment of Machine Learning Algorithms for Predicting Remission After Transsphenoidal Surgery Among Patients With Acromegaly. *Endocrine* (2020) 67(2):412–22. doi: 10.1007/s12020-019-02121-6
17. Qiao N, Shen M, He W, He M, Zhang Z, Ye H, et al. Machine Learning in Predicting Early Remission in Patients After Surgical Treatment of Acromegaly: A Multicenter Study. *Pituitary* (2021) 24(1):53–61. doi: 10.1007/s11102-020-01086-4
18. Hollon TC, Parikh A, Pandian B, Tarpeh J, Orringer DA, Barkan AL, et al. A Machine Learning Approach to Predict Early Outcomes After Pituitary Adenoma Surgery. *Neurosurg Focus* (2018) 45(5):E8. doi: 10.3171/2018.8.FOCUS18268
19. Dai C, Fan Y, Li Y, Bao X, Li Y, Su M, et al. Development and Interpretation of Multiple Machine Learning Models for Predicting Postoperative Delayed Remission of Acromegaly Patients During Long-Term Follow-Up. *Front Endocrinol (Lausanne)* (2020) 11:643. doi: 10.3389/fendo.2020.00643

20. Fan Y, Jiang S, Hua M, Feng S, Feng M, Wang R. Machine Learning-Based Radiomics Predicts Radiotherapeutic Response in Patients With Acromegaly. *Front Endocrinol (Lausanne)* (2019) 10:588. doi: 10.3389/fendo.2019.00588
21. Kocak B, Durmaz ES, Kadioglu P, Polat KO, Comunoglu N, Tanriover N, et al. Predicting Response to Somatostatin Analogues in Acromegaly: Machine Learning-Based High-Dimensional Quantitative Texture Analysis on T2-Weighted MRI. *Eur Radiol* (2019) 29(6):2731–9. doi: 10.1007/s00330-018-5876-2
22. Park YW, Eom J, Kim S, Kim H, Ahn SS, Ku CR, et al. Radiomics With Ensemble Machine Learning Predicts Dopamine Agonist Response in Patients With Prolactinoma. *J Clin Endocrinol Metab* (2021) 106(8):e3069–77. doi: 10.1210/clinem/dgab159
23. Zoli M, Staartjes VE, Guaraldi F, Friso F, Rustici A, Asioli S, et al. Machine Learning-Based Prediction of Outcomes of the Endoscopic Endonasal Approach in Cushing Disease: Is the Future Coming? *Neurosurg Focus* (2020) 48(6):E5. doi: 10.3171/2020.3.FOCUS2060
24. Zhang W, Sun M, Fan Y, Wang H, Feng M, Zhou S, et al. Machine Learning in Preoperative Prediction of Postoperative Immediate Remission of Histology-Positive Cushing's Disease. *Front Endocrinol (Lausanne)* (2021) 12:635795. doi: 10.3389/fendo.2021.635795
25. Fan Y, Li Y, Bao X, Zhu H, Lu L, Yao Y, et al. Development of Machine Learning Models for Predicting Postoperative Delayed Remission in Patients With Cushing's Disease. *J Clin Endocrinol Metab* (2021) 106(1):e217–31. doi: 10.1210/clinem/dgaa698
26. Liu Y, Liu X, Hong X, Liu P, Bao X, Yao Y, et al. Prediction of Recurrence After Transsphenoidal Surgery for Cushing's Disease: The Use of Machine Learning Algorithms. *Neuroendocrinology* (2019) 108(3):201–10. doi: 10.1159/000496753
27. Voglis S, van Niftrik C, Staartjes VE, Brandi G, Tschopp O, Regli L, et al. Feasibility of Machine Learning Based Predictive Modelling of Postoperative Hyponatremia After Pituitary Surgery. *Pituitary* (2020) 23(5):543–51. doi: 10.1007/s11102-020-01056-w
28. Machado LF, Elias P, Moreira AC, Dos SA, Murta JL. MRI Radiomics for the Prediction of Recurrence in Patients With Clinically Non-Functioning Pituitary Macroadenomas. *Comput Biol Med* (2020) 124:103966. doi: 10.1016/j.compbiomed.2020.103966
29. Meng T, Guo X, Lian W, Deng K, Gao L, Wang Z, et al. Identifying Facial Features and Predicting Patients of Acromegaly Using Three-Dimensional Imaging Techniques and Machine Learning. *Front Endocrinol (Lausanne)* (2020) 11:492. doi: 10.3389/fendo.2020.00492
30. Wei R, Jiang C, Gao J, Xu P, Zhang D, Sun Z, et al. Deep-Learning Approach to Automatic Identification of Facial Anomalies in Endocrine Disorders. *Neuroendocrinology* (2020) 110(5):328–37. doi: 10.1159/000502211
31. Peng A, Dai H, Duan H, Chen Y, Huang J, Zhou L, et al. A Machine Learning Model to Precisely Immunohistochemically Classify Pituitary Adenoma Subtypes With Radiomics Based on Preoperative Magnetic Resonance Imaging. *Eur J Radiol* (2020) 125:108892. doi: 10.1016/j.ejrad.2020.108892
32. Ugga L, Cuocolo R, Solari D, Guadagno E, D'Amico A, Somma T, et al. Prediction of High Proliferative Index in Pituitary Macroadenomas Using MRI-Based Radiomics and Machine Learning. *Neuroradiology* (2019) 61 (12):1365–73. doi: 10.1007/s00234-019-02266-1
33. Wang Z, Guo X, Gao L, Feng C, Lian W, Deng K, et al. Delayed Remission of Growth Hormone-Secreting Pituitary Adenoma After Transsphenoidal Adenectomy. *World Neurosurg* (2019) 122:e1137–45. doi: 10.1016/j.wneu.2018.11.004
34. Maiter D. Management of Dopamine Agonist-Resistant Prolactinoma. *Neuroendocrinology* (2019) 109(1):42–50. doi: 10.1159/000495775
35. Nishioka H, Yamada S. Cushing's Disease. *J Clin Med* (2019) 8(11):1951. doi: 10.3390/jcm8111951
36. Serban AL, Del SG, Sala E, Carosi G, Indirli R, Rodari G, et al. Determinants of Outcome of Transsphenoidal Surgery for Cushing Disease in a Single-Centre Series. *J Endocrinol Invest* (2020) 43(5):631–9. doi: 10.1007/s40618-019-01151-1
37. Braun LT, Rubinstein G, Zopp S, Vogel F, Schmid-Tannwald C, Escudero MP, et al. Recurrence After Pituitary Surgery in Adult Cushing's Disease: A Systematic Review on Diagnosis and Treatment. *Endocrine* (2020) 70 (2):218–31. doi: 10.1007/s12020-020-02432-z
38. Laws ER, Catalino MP. Editorial. Machine Learning and Artificial Intelligence Applied to the Diagnosis and Management of Cushing Disease. *Neurosurg Focus* (2020) 48(6):E6. doi: 10.3171/2020.3.FOCUS20213
39. Hinojosa-Amaya JM, Cuevas-Ramos D. The Definition of Remission and Recurrence of Cushing's Disease. *Best Pract Res Clin Endocrinol Metab* (2021) 35(1):101485. doi: 10.1016/j.beem.2021.101485
40. Nieman LK, Biller BM, Findling JW, Murad MH, Newell-Price J, Savage MO, et al. Treatment of Cushing's Syndrome: An Endocrine Society Clinical Practice Guideline. *J Clin Endocrinol Metab* (2015) 100(8):2807–31. doi: 10.1210/jc.2015-1818
41. Liu X, Dai C, Feng M, Li M, Chen G, Wang R. Diagnosis and Treatment of Refractory Pituitary Adenomas: A Narrative Review. *Gland Surg* (2021) 10 (4):1499–507. doi: 10.21037/gs-20-873
42. Lalys F, Riffaud L, Morandi X, Jannin P. Automatic Phases Recognition in Pituitary Surgeries by Microscope Images Classification. In: *IPCAI 2010: Information Processing in Computer-Assisted Interventions, First International Conference; 2010 June 23*. Geneva, Switzerland. Berlin: Springer (2010). p. 34–44. doi: 10.1007/978-3-642-13711-2_4
43. Muhlestein WE, Akagi DS, McManus AR, Chambless LB. Machine Learning Ensemble Models Predict Total Charges and Drivers of Cost for Transsphenoidal Surgery for Pituitary Tumor. *J Neurosurg* (2018) 131 (2):507–16. doi: 10.3171/2018.4.JNS18306

Conflict of Interest: The authors declare that the research was conducted in the absence of any commercial or financial relationships that could be construed as a potential conflict of interest.

frontiers in Neurology

ORIGINAL RESEARCH
published: 05 January 2022
doi: 10.3389/fneur.2021.780628

A Preoperative MRI-Based Radiomics-Clinicopathological Classifier to Predict the Recurrence of Pituitary Macroadenoma Within 5 Years

Yu Zhang[1], *Yuqi Luo*[1], *Xin Kong*[1], *Tao Wan*[2], *Yunling Long*[3,4] *and Jun Ma*[1]*

[1] *Department of Radiology, Beijing Tiantan Hospital, Capital Medical University, Beijing, China,* [2] *School of Biomedical Science and Medical Engineering, Beijing Advanced Innovation Centre for Biomedical Engineering, Beihang University, Beijing, China,* [3] *Department of Biomedical Engineering, School of Biomedical Engineering, Capital Medical University, Beijing, China,* [4] *Beijing Neurosurgical Institute, Beijing Tiantan Hospital, Beijing, China*

OPEN ACCESS

Edited by:
Zhixiong Liu,
Central South University, China

Reviewed by:
S. Ottavio Tomasi,
Paracelsus Medical University, Austria
Antonino F. Germano,
University of Messina, Italy
Teresa Somma,
Federico II University Hospital, Italy

***Correspondence:**
Jun Ma
dr.junma@foxmail.com

Specialty section:
This article was submitted to Neuro-Oncology and Neurosurgical Oncology, a section of the journal Frontiers in Neurology

Received: *14 October 2021*
Accepted: *02 December 2021*
Published: *05 January 2022*

Citation:
Zhang Y, Luo Y, Kong X, Wan T, Long Y and Ma J (2022) A Preoperative MRI-Based Radiomics-Clinicopathological Classifier to Predict the Recurrence of Pituitary Macroadenoma Within 5 Years. Front. Neurol. 12:780628. doi: 10.3389/fneur.2021.780628

Objective: To investigate the ability of a MRI-based radiomics-clinicopathological model to predict pituitary macroadenoma (PMA) recurrence within 5 years.

Materials and Methods: We recruited 74 recurrent and 94 non-recurrent subjects, following first surgery with 5-year follow-up data. Univariate and multivariate analyses were conducted to identify independent clinicopathological risk factors. Two independent and blinded neuroradiologists used 3D-Slicer software to manually delineate whole tumors using preoperative axial contrast-enhanced T1WI (CE-T1WI) images. 3D-Slicer was then used to extract radiomics features from segmented tumors. Dimensionality reduction was carried out by the least absolute shrinkage and selection operator (LASSO). Two multilayer perceptron (MLP) models were established, including independent clinicopathological risk factors (Model 1) and a combination of screened radiomics features and independent clinicopathological markers (Model 2). The predictive performance of these models was evaluated by receiver operator characteristic (ROC) curve analysis.

Results: In total, 1,130 features were identified, and 4 of these were selected by LASSO. In the test set, the area under the curve (AUC) of Model 2 was superior to Model 1 {0.783, [95% confidence interval (CI): 0.718—.860] vs. 0.739, (95% CI: 0.665–0.818)}. Model 2 also yielded the higher accuracy (0.808 vs. 0.692), sensitivity (0.826 vs. 0.652), and specificity (0.793 vs. 0.724) than Model 1.

Conclusions: The integrated classifier was superior to a clinical classifier and may facilitate the prediction of individualized prognosis and therapy.

Keywords: pituitary macroadenoma, recurrence, predictive model, deep learning, multilayer perceptron

INTRODUCTION

Pituitary adenoma is one of the most prevalent intracranial masses that can affect adults (1, 2). The varied clinical manifestations usually result from the endocrine activity, or volume of tumors. The classification of PA is based on different criteria, such as size, immunohistochemistry (IHC), invasion, hormone secretion, and clinical manifestation (1, 3). PAs are classified into micro, macro, and giant adenomas by the MRI size. The IHC subtypes of PAs are composed of growth hormone (GH), prolactin (PRL), adrenocorticotropic hormone (ACTH), thyroid-stimulating hormone (TSH), and follicle-stimulating hormone-luteinising hormone (FSH-LH), including the monohormonal and plurihormonal adenomas. Although benign in terms of their biological behavior, 30–45% of tumors invade the cavernous or sphenoid sinus, which can be categorized into invasive and non-invasive adenomas (1, 3, 4). According to the clinical classification, PAs consist of functioning and non-functioning types (1).

The treatment strategy for most tumors is operation. The postsurgical recurrence rate of pituitary macroadenoma (PMA) within 5 years is considerably high (5). The tendency to relapse has been related to many factors, including different histotypes, tumor remnants, or the extent of invasion into adjacent anatomical structures (6). Previous research has demonstrated that many clinicopathological prognostic tools have potential to predict the recurrence of PMA, consisting of IHC characteristics, invasion of tumors, genetic expression, and markers of proliferation (7–11). However, very few attempts have been made to integrate these risk factors with a machine-learning approach.

Radiomics is a form of analysis that quantitatively extracts imaging features from medical data (12). Thus far, radiomics studies of PA have predominantly focused on two aspects: presurgical evaluation and subtype classification (13–17). Some researchers have used radiomics to explore the potential for relapse in PA. However, these previous models have been associated with small sample sizes and only cases involving non-functioning tumors (18, 19).

In the present study, we aimed to establish a comprehensive classification model that combined independent clinicopathological risk factors with preoperative radiomics signatures for the prediction of PMA recurrence within 5 years of surgery. Our goal was to provide an efficient tool for guiding clinical management and predicting prognosis.

MATERIALS AND METHODS

Ethics Statement

This retrospective study involved human subjects and was approved by the Ethics Committee of Beijing Tiantan Hospital. The requirement for written informed consent was waived.

Subjects

The recurrence of adenomas was defined as incidence of enlarged remnant tumors in non-functioning PMAs, and/or endocrine biochemical recurrence in functioning PMAs (20, 21).

PMAs referred to adenomas with preoperative size > 10 mm by MRI in our study, based on Asioli et al. (20). PMAs were classified into immunonegative, monohormonal-including GH-positive, PRL-positive, ACTH-positive, FSH-LH-positive, TSH-positive, and plurihormonal by the results of IHC staining (22). The radiological signs of aggressive tumors were determined according to Knosp and Hardy—Wilson classifications on preoperative MRI by a blinded and experienced neuroradiologist. The Knosp and Hardy—Wilson criteria were used to evaluate the degree of invasion of cavernous sinus (CS) and suprasella, respectively. Knosp Scores 3 and 4 were described as adenomas extending beyond the lateral tangents of the cavernous segment of internal carotid artery (ICA) on coronal MRI and completely involving CS and ICA. Hardy—Wilson Grades 3 and 4 were represented as local and extensive invasion of the sellar floor; Stages C and D and E were characterized as total replacement of the third ventricle, intracranial adenomas, and invasion of CS (**Supplementary Material 1**) (5, 23). The aggressive PMAs were defined as grade of Knosp 3 or 4, and/or Hardy—Wilson Grades 3 or 4 (and/or Hardy—Wilson Stage C or D or E), and/or histological evidence of invasion of cavernous or sphenoid sinus (1). The patients who experienced subtotal resection were recognized as cases with residual tumor, and the subjects who underwent gross- or near-total resection were regarded as cases without remnants (24, 25).

A total of 168 consecutive postoperative subjects with a confirmed pathological diagnosis of PMA were acquired from our institutional medical database between January 2010 and December 2015. Analysis of medical records showed that 74 of these patients reported recurrent attacks (39 men/35 women); and 94 patients had not experienced recurrence (43 men/51 women). All the patients completed the 5-year follow-up period. The inclusion criteria were as follows: (1) available investigation for medical data; (2) underwent surgery; (3) had preoperative MRI; and (4) followed-up for duration of 5 years since first surgery. The exclusion criteria included (1) underwent other treatments for PMA before the first surgery or during the follow-up period; (2) pituitary apoplexy; (3) multiple intracranial lesions; and (4) poor-quality image or lack of contrast-enhancement MRI.

MRI Acquisition and the Segmentation of Tumors

All enrolled subjects underwent MRI of the head prior to surgery, including several different acquisition protocols [axial T1WI and T2WI, axial, coronal, and sagittal contrast-enhanced T1WI (CE-T1WI)]. The contrast agent, dimeglumine gadopentetate, was injected at a dose of.2 ml/kg, following pre-contrast T1 scanning. MRI images were obtained from four different MRI scanners with 3 T (GE Discovery MR 750, $n = 59$; Siemens MAGNETOM Trio TimSystem, $n = 43$; Siemens MAGNETOM Verio, $n = 22$; Philips Ingenia, $n = 9$), and a 1.5 T scanner (GE Medical System Genesis Signa, $n = 35$). **Supplementary Material 2** shows the

type of the contrast medium and the parameters used for axial CE-T1WI for five MRI modalities.

Whole tumors, based on preoperative axial CE-T1WI images, were identified as the region of interest (ROI). The manual delineation of each ROI was conducted by a neuroradiologist with 5 years of experience, using 3D-Slicer software (version 4.10.2 r28257, National Institutes of Health). Prior to segmentation, we applied three steps to standardize different MRI images: N4ITK bias correction, resampling with resampled voxel sizes of 1, 1, and 1, and Laplacian of Gaussian (LOG) with LOG kernel sizes being 1.5, 2, and 2.5 by 3D-Slicer.

Assessments of Intra- and Interobserver Reproducibility

Neuroradiologist 1 segmented the ROIs of 60 randomly selected cases on two occasions separated by an interval of 2 weeks. Neuroradiologist 2 with 5 years of experience independently performed the same analyses on one occasion. Intraclass correlation coefficient (ICC) was then calculated by R (version 4.0.2, http://www.R-project.org) to compare intra- and inter-observer reproducibility. The high reproducibility of these radiomics features was recognized as the ICC score for Radiologist 1 (on two occasions) or between Radiologists 1 and 2 >.75.

The Extraction of Features and Dimension Reduction

In total, 1,130 features were extracted from the segmented ROIs by 3D-Slicer software. These features encompassed eight types: first-order, shape, gray-level dependence matrix (GLDM), gray-level co-occurrence matrix (GLCM), gray-level run length matrix (GLRLM), gray-level size zone matrix (GLSZM), neighboring gray tone difference matrix (NGTDM), and wavelet-based features, which were four distinct categories: intensity histogram, texture, shape, and wavelet. The detailed information for all features is shown in **Supplementary Material 3**.

The features with ICC score <0.75 were excluded in the first stage, because of the poor reproducibility. Then, we performed the least absolute shrinkage and selection operator (LASSO) in the R environment to carry out dimensionality reduction in the training set. The corresponding regularization coefficient (λ) was obtained by 10-fold cross-validation in LASSO regression based on the 1-standard error of the minimum criteria (1-SE criteria).

The Establishment and Validation of a Radiomics-Clinicopathological Model

The z-score was used to normalize all features onto a similar scale. We randomly separated these subjects into a training set (including 51 recurrence and 65 non-recurrence subjects) and a test set (23 cases with relapse and 29 without relapse; based on a data-partition ratio of 7:3).

Two multilayer perceptron (MLP) classifiers were built by python (version 3.8.2, http://www.python.org) for the prediction of recurrence in PMA, including independent clinicopathological risk factors (Model 1—clinical model) and a combination of screened radiomics features and independent clinicopathological markers (Model 2—integrated model). Receiver operator characteristic (ROC) curves were performed and used to estimate the predictive performance of the two models by area under curve (AUC) analysis. This analysis allowed us to determine the accuracy, specificity, and sensitivity of each model.

MLP was composed of an input layer, a hidden layer, and an output layer. In the process of forward propagation, a series of algorithms were performed to obtain the output of each layer, which was used to be the input of the next layer. The equation was as follows:

$$y = f(wx + b)$$

where y represents the outcome of output, x represents the input vector, w represents the weight, b represents the bias, and f represents the activation function. Our classifiers included three hidden layers, for which the numbers of neurons were 64, 512, and 64, respectively. The dropout layer was conducted to lose 20% of neurons to reduce overfitting. We applied Rectified Linear Unit (ReLU) and Sigmoid to be activation functions for the hidden and output layers. The binary cross entropy was calculated for use as loss function. The weights were tuned by the back propagation method based on the derivation of the chain rule. In our study, the training epochs were set to 500. Before model establishment, the training cohort was shuffled. The monitoring indicators were accuracy, sensitivity, specificity, and AUC in the training set. Stochastic gradient descent (SGD) was used as the optimizer, with an initial learning rate of.1. The learning rate decay strategy was set to the reduction of 70% if the accuracy of training cohort did not improve for consecutive 100 epochs. Optimized class weights were obtained according to the numbers of recurrent and non-recurrent patients in the training set, and the batch size was default value of 32. The predictive performance of each model was validated in the test cohort and evaluated by 5-fold cross-validation. **Figure 1** shows the process used for the analysis of radiomics.

Statistical Analysis

The normality test of the data was performed by Shapiro—Wilk. Two-sided independent sample *t*-test and Mann—Whitney *U*-test were conducted to compare the differences in continuous variates, and Pearson's χ^2 test and Fisher's precision probability test were used to investigate the differences in categorical variates in the training and test sets. Univariate and multivariable logistic regression were used to identify independent clinicopathological risk factors for the recurrence of PMA in the training set. The differences of extracted radiomics features between groups of recurrence and non-recurrence in the training set were determined by Mann—Whitney *U*-test; these analyses were carried out with SPSS (version 23.0, IBM), and a p of < 0.05 was considered to be statistically significant.

RESULTS

Clinical Characteristics of the Study Cohort

The baseline investigation of the study patients is shown in **Table 1**. The differences with regard to clinical

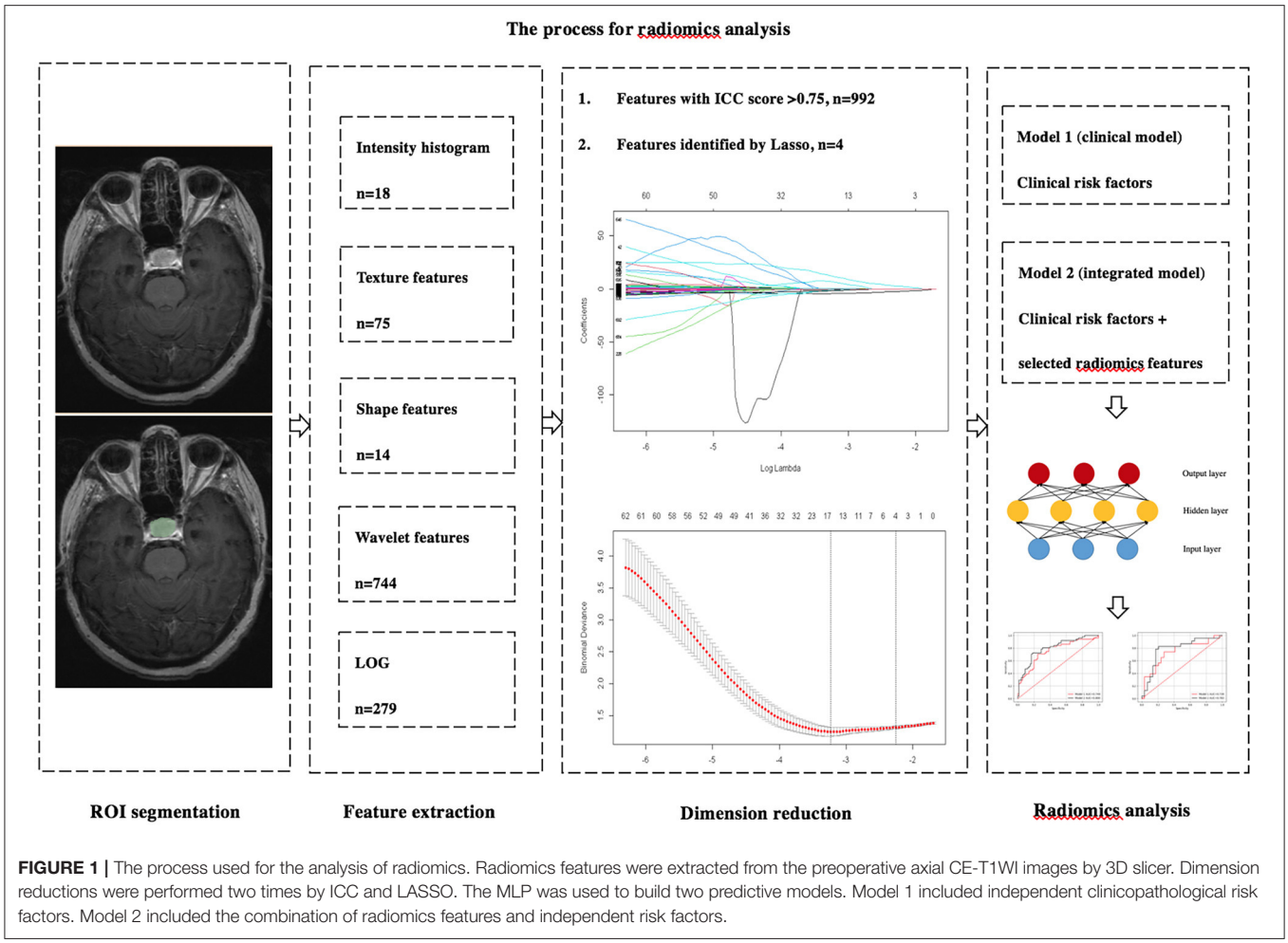

FIGURE 1 | The process used for the analysis of radiomics. Radiomics features were extracted from the preoperative axial CE-T1WI images by 3D slicer. Dimension reductions were performed two times by ICC and LASSO. The MLP was used to build two predictive models. Model 1 included independent clinicopathological risk factors. Model 2 included the combination of radiomics features and independent risk factors.

characteristics between training and test cohorts were not statistically significant.

Univariate analysis demonstrated that age {$p = 0.034$; OR, 0.967 [95% confidence interval (CI), 0.937–0.997]}, height [$p = 0.007$; OR, 1.068 (95% CI, 1.018–1.120)], residual tumor [$p = 0.009$; OR, 2.963 (95% CI, 1.319–6.659)], and invasion [$p = 0.009$; OR, 3.359 (95% CI, 1.359–8.305)] were significant risk factors for relapse. Multivariate analysis identified two independent risk factors for the recurrence of PMA: age [$p = 0.035$; OR, 0.963 (95% CI, 0.930–0.997)] and residual tumor [$p = 0.047$; OR, 2.393 (95% CI, 1.011–5.667)] (**Table 2**). Our study included four clinicopathological features: age, height, residual tumor, and invasion in Models 1 and 2 based on univariate and multivariate analyses.

Intra- and Interobserver Analyses

The mean ICC scores for intra- (Neuroradiologist 1 on two occasions) and interobserver (Neuroradiologists 1 and 2) agreements were 0.913 ± 0.129 and 0.903 ± 0.127, respectively, for all selected patients, which showed the high agreement of these features.

Comparing the Predictive Performance of the Two Models

Of the 1,130 features, 138 with unsatisfactory agreement were excluded by the first round, and four of these radiomics features were then identified by LASSO regression, consisting of one shape feature, one LOG, and two wavelet features. All of four selected signatures showed statistically significant differences ($p < 0.05$) in the training set (**Figure 2**).

The ROC curves in the training and test sets are shown in **Figure 3**; the AUCs, accuracy, sensitivity, and specificity of the two models are presented in **Table 3**. In the test set, the AUC of Model 2 was superior to Model 1 [0.783, (95% CI: 0.718–0860) vs. 0.739, (95% CI: 0.665–0.818)]. Model 2 also yielded the higher accuracy (0.808 vs. 0.692), sensitivity (0.826 vs. 0.652), and specificity (0.793 vs. 0.724) than Model 1.

DISCUSSION

In this study, we constructed a diagnostic classification strategy based on the presurgical MRI to predict the recurrence risk of PMA within 5 years. This comprehensive classifier incorporates

TABLE 1 | Clinical characteristics of PMA subjects in the training and test sets.

	Training set (n = 116)	Test set (n = 52)	Whole set (n = 168)	p
Age, mean (SD), y	45.59 (12.38)	44.96 (11.63)	45.39 (12.12)	0.758†
Sex, No. (%)				0.899§
Male	57 (49.14)	25 (48.08)	82 (48.81)	
Female	59 (50.86)	27 (51.92)	86 (51.19)	
Endocrine level, No. (%)				0.214§
Non-functioning	71 (61.21)	37 (71.15)	108 (64.29)	
Functioning	45 (38.79)	15 (28.85)	60 (35.71)	
Height, median (IQR), mm	30.73 (20.42-41.04)	31.82 (19.21-44.43)	30.96 (25.81-36.93)	0.284‡
Residual tumor, No. (%)				0.584§
Without	43 (37.07)	17 (32.69)	60 (35.71)	
With	73 (62.93)	35 (67.31)	108 (64.29)	
Invasion, No. (%)				0.578§
No	33 (28.45)	17 (32.69)	50 (29.76)	
Yes	83 (71.55)	35 (67.31)	118 (70.24)	
Surgical methods, No. (%)				0.686§
Craniotomy	29 (25.00)	12 (23.08)	41 (24.40)	
Trans-sphenoidal	59 (50.86)	30 (57.69)	89 (52.98)	
Endoscopic	28 (24.14)	10 (19.23)	38 (22.62)	
The IHC subtypes, No. (%)				0.906&
Immunonegative	48 (41.38)	25 (48.08)	73 (43.45)	
GH-positive	6 (5.17)	1 (1.92)	7 (4.17)	
PRL-positive	5 (4.31)	3 (5.77)	8 (4.76)	
ACTH-positive	11 (9.48)	3 (5.77)	14 (8.33)	
FSH-LH-positive	22 (18.97)	8 (15.38)	30 (17.86)	
TSH-positive	2 (1.72)	1 (1.92)	3 (1.79)	
Plurihormonal	22 (18.97)	11 (21.15)	33 (19.64)	

ACTH, adrenocorticotropic hormone; FSH, follicle-stimulating hormone; GH, growth hormone; IHC, immunohistochemistry; IQR, interquartile range; LH, luteinizing hormone; No, number; PRL, prolactin; SD, standard deviation; TSH, thyroid-stimulating hormone.

†*Two-sided independent sample t-test.*

‡*Mann—Whitney U-test.*

§*Pearson's* χ^2 *test.*

&*Fisher's precision probability test.*

clinicopathological and radiomics features and can accurately predict the recurrence of PMA.

Various factors are known to be associated with a higher risk of PMA recurrence, which remains a significant problem for both clinicians and patients. Very few previous reports have attempted to combine clinicopathology analysis with radiomics for the prediction of PMA. MRI radiomics approaches have been described in previous literature. For example, Zhang et al. (18) and Machado et al. (19) used this method to explore the recurrence of non-functioning PA. Compared with these previous results, the Model 2 in our study presented with relative low diagnostic accuracy. This is probably because we built the test set using an independent set of subjects rather than the training group. Moreover, our study simultaneously included functioning and non-functioning PMAs. The study cohorts and enrollment criteria may lead to the different predictive performances. However, our Model 2, which had a relatively large sample size and incorporated comprehensive markers, showed a better level of classification performance than Model 1. This improved predictive efficiency demonstrates that the combination of clinicopathological data and imaging may provide more practical information and guidance for developing a treatment and prognosis strategy than clinical analysis alone.

MLP model is a feed-forward artificial neural network (ANN) model that is applicable to a non-linear inseparable issue; Almubark et al. demonstrated the predictive value of this approach in their previous study (26). The generalization and efficacy of this method have been widely confirmed in several papers (27–29). Given these characteristics, we also established an MLP classifier for the recurrence of PMA and achieved satisfactory levels of predictive performance in a test cohort. These data indicate that this deep learning algorithm is a reproducible and robust technique for classification.

Many risk factors are associated with the recurrence of PMA. In the present study, we incorporated some of the primary predictors that have been described in previous literature (30). Four clinicopathological risk factors—age, height, invasion, and residual tumor—were finally included in our comprehensive model; these factors were identified by a combination of univariate and multivariate analyses. We found that the patients

TABLE 2 | Univariate and multivariate analysis of clinical characteristics to identify risk factors in the recurrence of PMA in the training set.

	Univariate analysis		Multivariate analysis	
	OR (95%CI)	***p***	**OR (95%CI)**	***p***
Age, y	0.967 (0.937–0.997)	0.034*	0.963 (0.930–0.997)	0.035*
Sex				
Male (ref.)	1			
Female	1.008 (0.484–2.100)	0.982		
Endocrine level				
Non-functioning (ref.)	1			
Functioning	1.196 (0.564–2.535)	0.641		
Height, mm	1.068 (1.018–1.120)	0.007*	1.045 (0.992–1.100)	0.097
Residual tumor				
Without (ref.)	1			
With	2.963 (1.319–6.659)	0.009*	2.393 (1.011–5.667)	0.047*
Invasion				
No (ref.)	1			
Yes	3.359 (1.359–8.305)	0.009*	2.746 (0.994–7.585)	0.051
Surgical methods				
Transcranial (ref.)	1			
Trans-sphenoidal	0.904 (0.371–2.202)	0.824		
Endoscopic	0.595 (0.206–1.722)	0.338		
The IHC subtypes				
Immunonegative (ref.)	1			
Monohormonal	0.821 (0.358–1.881)	0.640		
Plurihormonal	2.450 (0.865–6.939)	0.092		

CI, confidence interval; IHC, immunohistochemistry; OR, odds ratio.
*$p < 0.05$.

in the recurrence group tended to be younger. We believe that this is because there is a greater risk of gene disorders in younger age groups (31). In a previous study, Trott concluded that young patients express elevated levels of ki-67 in non-functioning pituitary adenoma, and that this is strongly associated with relapse (32). Moreover, some ultrastructural types of PMA resulted in regrowth, such as sparsely granulated somatotroph adenoma, and are more likely to affect younger patients. The aggressive growth pattern of PMA is one of the main reasons concerned with the prognosis (33). The invasive tumors usually exhibit more rapid growth, a higher proliferative index, and larger size. Thus, the severe erosion of surrounding structures (e.g., cavernous sinus and sellar floor) and great extension of the supra- and para-sellar lead to increased rates of recurrence (34). Similar results in the present literature provide support to our conclusion that tumor remnant is also known to be significantly correlated with PMA behavior, especially the higher incidence of larger extra-sellar residuals (5, 6, 34). Height is another recognized predictive candidate. It is evident that the tumors with higher height may result in incomplete resection and invasive behavior, which consequently raise the likelihood of regrowth. These findings are consistent with previous reports (5, 6, 35). This suggests that the clinical characteristics described above are useful and reliable tools for predicting the prognosis of patients with PMA.

The tumor classification involving the transcription factor or ultrastructure showed that the presence of giant lactotroph, sparsely granulated somatotroph, crooke's cell, or silent corticotroph adenomas tends to present the recurrence nature (5, 36, 37). Our study focused on the proposed IHC subtypes that are also important and potential indicators related to the progression. The study reported by Asioli et al. showed that PRL, ACHT, and FSH-LH subunits had relapse risk with high probability (20). These indices were not statistically significant when compared between the two groups in our study; it is possible that this was owing to the small sample size compared with the previous study. Although the rate of TSH adenoma was the lowest among all cases, the trend of incidence is in line with tangible clinical practice. The morbidity of this type is low based on the demographic investigation, comprising <3% of all tumors (38). We included the plurihormonal adenoma in our study. The most common type is the co-secretion of GH and PRL (39). But the combination of different hormones tends to be more complicated. Little is known with regard to the correlation between recurrence and plurihormonal tumors.

The trans-sphenoidal and endoscopic surgical methods are extensively applied to dealing with PMA (40–42). Our study did not show the correlation between operative approaches and recurrence. According to current studies, tumor size and invasive extension were decisive factors in extent of resection.

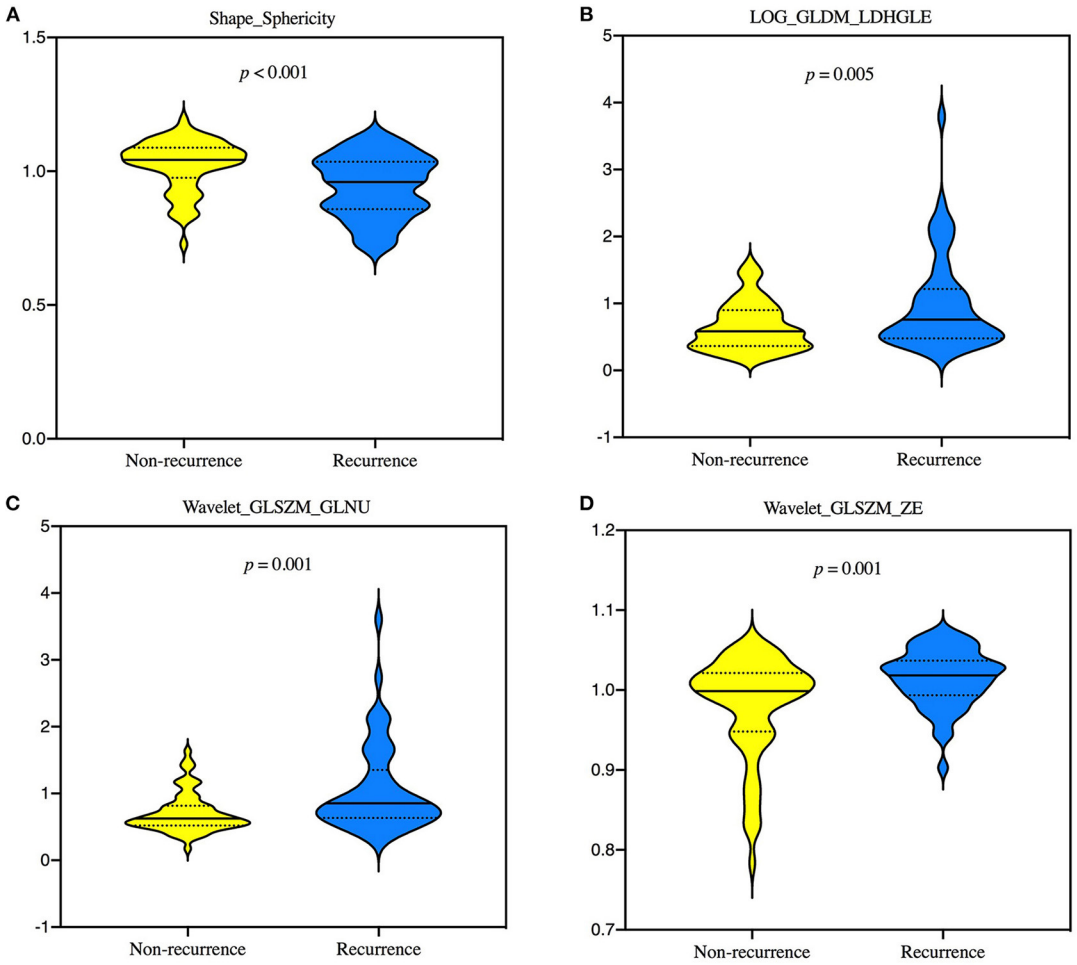

FIGURE 2 | Violin plots showing the differences of 4 selected radiomics features, Shape_Sphericity **(A)**, LOG_GLDM_LDHGLE **(B)**, Wavelet_GLSZM_GLNU **(C)**, and Wavelet_GLSZM_ZE **(D)** between groups of recurrence and non-recurrence in the training set by Mann—Whitney *U*-test. GLDM, gray-level dependence matrix; GLNU, gray-level non-uniformity; GLSZM, gray-level size zone matrix; LDHGLE, large dependence high-gray-level emphasis; LOG, laplacian of gaussian; ZE, zone entropy.

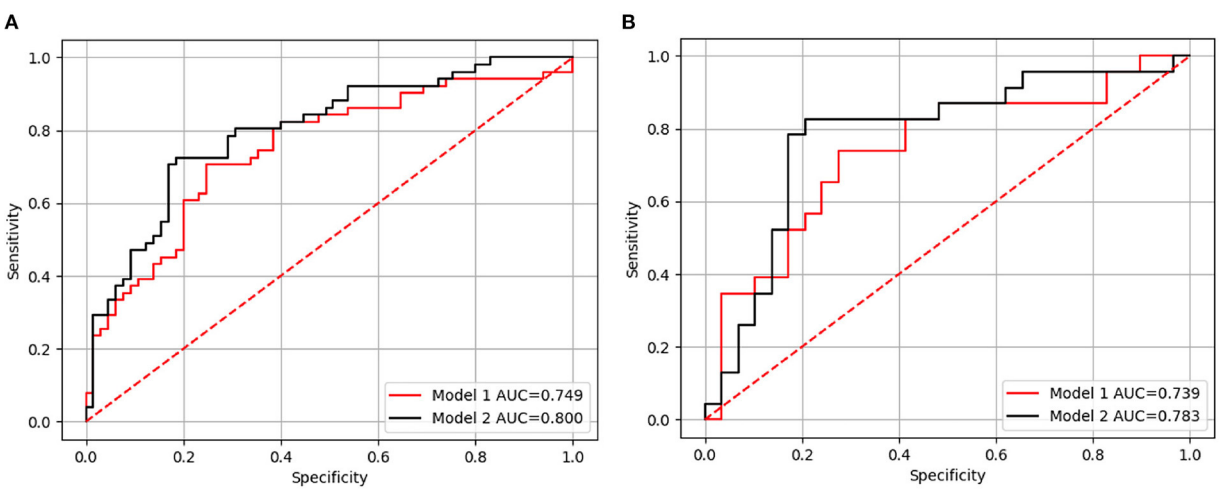

FIGURE 3 | The receiver-operating characteristic (ROC) curve for Models 1 and 2 in the training **(A)** and test sets **(B)**, respectively. Model 1 included independent clinicopathological risk factors and Model 2 included both radiomics features and independent clinicopathological risk factors.

TABLE 3 | Predictive performance of Models 1 and 2 in the training and test set.

	Training set ($n = 116$)				Test set ($n = 52$)			
	AUC (95% CI)	ACC	SEN	SPE	AUC (95% CI)	ACC	SEN	SPE
Model 1	0.749 (0.702–0.804)	0.724	0.706	0.738	0.739 (0.665–0.818)	0.692	0.652	0.724
Model 2	0.800 (0.759–0.845)	0.776	0.725	0.815	0.783 (0.718–0.860)	0.808	0.826	0.793

Model 1 included independent clinicopathological markers and Model 2 included both radiomic features and clinicopathological markers.
AUC, area under the curve; ACC, accuracy; CI, confidence interval; SEN, sensitivity; SPE, specificity.

The macro or giant adenomas and extensive invasion tended to be difficult to achieve grossly complete resection, although the trans-sphenoidal or endoscopic resection was used (43–45). The residual tumor is likely to be the crucial factor that affects the prognosis, suggesting that the surgical resection may be more likely to associate with intrinsic biological characteristics of tumors, compared with an operative procedure. Patients who received total resection still have the possibility of relapse (5). This indicates that surgery alone may not enable to decrease the recurrence rate. It is also important and beneficial to combine radiotherapy or other methods (46).

The consistency of adenomas probably influences the prognostic outcomes. A study showed that texture was correlated with tumor profiles, complications, and surgical resection. The hard adenomas were at higher risk of large and aggressive behavior and subtotal removal (47). This suggests that consistency is potential to predict the recurrence of PMAs. Rui et al. confirmed the utility of the radiomics method for determining the texture of PMAs (13). Future PA studies may pay more attention to the relationship between the stiffness and recurrence by radiomics.

The proliferative biomarkers of ki-67, p53, and mitosis play an important role in tumor prognosis. Although there remains the controversy of arguments, the changes of these proliferation indices are often associated with aggressive PAs. The prognoses of the patients tended to be recurrent or poorer in the presence of ki-67 $\geq$3, mitoses $>$2, and p53 overexpression based on the study by Raverot and European Society of Endocrinology (48). Above all, the most effective and useful predictive strategies are incorporating the predictors of different fields, such as clinical, imaging, and immunohistochemical examination.

LIMITATIONS

First, the proliferations, transcription factors, ultrastructural subtypes, along with expression profiles of certain genes, were not considered in this study but may improve the performance of our classifier. Second, the pituitary scanning sequence with smaller slice thickness and interval was not applied in the study, because the protocol is not clinical routine examination; it may be considered in future studies. Third, microadenoma is another common subgroup of pituitary tumor; radiomic studies of this form of tumor are very rare. We did not include this type of tumor in the present study due to a limited sample size. Finally, this study was based in a single center and lacks external validation in multiple centers.

CONCLUSION

The combination of clinicopathological characteristics and imaging is useful for predicting the recurrence of PMA within 5 years. The integrated classifier was superior to a clinical classifier and may facilitate the prediction of individualized prognosis and therapy.

DATA AVAILABILITY STATEMENT

The original contributions presented in the study are included in the article/**Supplementary Material**, further inquiries can be directed to the corresponding author/s.

ETHICS STATEMENT

The studies involving human participants were reviewed and approved by the Ethics Committee of Beijing Tiantan Hospital. The Ethics Committee obtained written informed consent from the participants.

AUTHOR CONTRIBUTIONS

JM designed the original research. YZ conducted the research and wrote the manuscript. YZ, YLu, and XK analyzed the data. JM, TW, and YLo revised the paper. All authors contributed to the article and approved the submitted version.

FUNDING

This research project was funded by National Natural Science Foundation of China (No. 61771325).

SUPPLEMENTARY MATERIAL

The Supplementary Material for this article can be found online at: https://www.frontiersin.org/articles/10.3389/fneur.2021.780628/full#supplementary-material

REFERENCES

1. Raverot G, Jouanneau E, Trouillas J. Management of endocrine disease: clinicopathological classification and molecular markers of pituitary tumours for personalized therapeutic strategies. *Eur J Endocrinol.* (2014) 170:R121–32. doi: 10.1530/EJE-13-1031
2. Bi WL, Greenwald NF, Ramkissoon SH, Abedalthagafi M, Coy SM, Ligon KL, et al. Clinical identification of oncogenic drivers and copy-number alterations in pituitary tumors. *Endocrinology.* (2017) 158:2284–91. doi: 10.1210/en.2016-1967
3. Trouillas J. In search of a prognostic classification of endocrine pituitary tumors. *Endocr Pathol.* (2014)25:124–32. doi: 10.1007/s12022-014-9322-y
4. Raverot G, Vasiljevic A, Jouanneau E, Trouillas J. A prognostic clinicopathologic classification of pituitary endocrine tumors. *Endocrinol Metab Clin North Am.* (2015) 44:11–8. doi: 10.1016/j.ecl.2014.10.001
5. Hayhurst C, Taylor PN, Lansdown AJ, Palaniappan N, Rees DA, Davies JS. Current perspectives on recurrent pituitary adenoma: the role and timing of surgery vs. adjuvant treatment. *Clin Endocrinol.* (2020) 92:89–97. doi: 10.1111/cen.14127
6. Raverot G, Vasiljevic A, Jouanneau E. Prognostic factors of regrowth in nonfunctioning pituitary tumors. *Pituitary.* (2018) 21:176–82. doi: 10.1007/s11102-017-0861-3
7. Das C, Mondal P, Mukhopadhyay M, Mukhopadhyay S, Ghosh I, Handral A. Evaluation of prognostic utility of Ki-67, P53, and O-6-methylguanine-DNA methyltransferase expression in pituitary tumors. *J Lab Phys.* (2019) 11:323–9. doi: 10.4103/JLP.JLP_76_19
8. Pappy AL II, Savinkina A, Bicknese C, Neill S, Oyesiku NM, Ioachimescu AG. Predictive modeling for pituitary adenomas: single center experience in 501 consecutive patients. *Pituitary.* (2019) 22:520–31. doi: 10.1007/s11102-019-00982-8
9. Ko CC, Chen TY, Lim SW, Kuo YT, Wu TC, Chen JH. Prediction of recurrence in solid nonfunctioning pituitary macroadenomas: additional benefits of diffusion-weighted MR imaging. *J Neurosurg.* (2019) 132:351–9. doi: 10.3171/2018.10.JNS181783
10. Kim JS, Lee YS, Jung MJ, Hong YK. The predictive value of pathologic features in pituitary adenoma and correlation with pituitary adenoma recurrence. *J Pathol Transl Med.* (2016) 50:419–25. doi: 10.4132/jptm.2016.06.30
11. Turner HE, Nagy Z, Gatter KC, Esiri MM, Wass JA, Harris AL. Proliferation, bcl-2 expression and angiogenesis in pituitary adenomas: relationship to tumour behaviour. *Br J Cancer.* (2000) 82:1441–5. doi: 10.1054/bjoc.1999.1074
12. Lambin P, Rios-Velazquez E, Leijenaar R, Carvalho S, van Stiphout RG, Granton P, et al. Radiomics: extracting more information from medical images using advanced feature analysis. *Eur J Cancer.* (2012) 48:441–6. doi: 10.1016/j.ejca.2011.11.036
13. Rui W, Wu Y, Ma Z, Wang Y, Wang Y, Xu X, et al. MR textural analysis on contrast enhanced 3D-SPACE images in assessment of consistency of pituitary macroadenoma. *Eur J Radiol.* (2019) 110:219–24. doi: 10.1016/j.ejrad.2018.12.002
14. Fan Y, Liu Z, Hou B, Li L, Liu X, Liu Z, et al. Development and validation of an MRI-based radiomic signature for the preoperative prediction of treatment response in patients with invasive functional pituitary adenoma. *Eur J Radiol.* (2019) 121:108647. doi: 10.1016/j.ejrad.2019.108647
15. Peng A, Dai H, Duan H, Chen Y, Huang J, Zhou L, et al. A machine learning model to precisely immunohistochemically classify pituitary adenoma subtypes with radiomics based on preoperative magnetic resonance imaging. *Eur J Radiol.* (2020) 125:108892. doi: 10.1016/j.ejrad.2020.108892
16. Niu J, Zhang S, Ma S, Diao J, Zhou W, Tian J, et al. Preoperative prediction of cavernous sinus invasion by pituitary adenomas using a radiomics method based on magnetic resonance images. *Eur Radiol.* (2019) 29:1625–34. doi: 10.1007/s00330-018-5725-3
17. Ugga L, Cuocolo R, Solari D, Guadagno E, D'Amico A, Somma T, et al. Prediction of high proliferative index in pituitary macroadenomas using MRI-based radiomics and machine learning. *Neuroradiology.* (2019) 61:1365–73. doi: 10.1007/s00234-019-02266-1
18. Zhang Y, Ko CC, Chen JH, Chang KT, Chen TY, Lim SW, et al. Radiomics approach for prediction of recurrence in non-functioning pituitary macroadenomas. *Front Oncol.* (2020) 10:590083. doi: 10.3389/fonc.2020.590083
19. Machado LF, Elias PCL, Moreira AC, Dos Santos AC, Murta Junior LO. MRI radiomics for the prediction of recurrence in patients with clinically non-functioning pituitary macroadenomas. *Comput Biol Med.* (2020) 124:103966. doi: 10.1016/j.compbiomed.2020.103966
20. Asioli S, Righi A, Iommi M, Baldovini C, Ambrosi F, Guaraldi F, et al. Validation of a clinicopathological score for the prediction of post-surgical evolution of pituitary adenoma: retrospective analysis on 566 patients from a tertiary care centre. *Eur J Endocrinol.* (2019) 180:127–34. doi: 10.1530/EJE-18-0749
21. Almeida JP, Tabasinejad R, Kalyvas A, Takami H, Mohan N, O'Halloran PJ, et al. The importance of long term follow up after endoscopic pituitary surgery: durability of results and tumor recurrence. *Neurol India.* (2020) 68(Suppl.):S92–100. doi: 10.1055/s-0040-1702474
22. Trouillas J, Jaffrain-Rea ML, Vasiljevic A, Raverot G, Roncaroli F, Villa C. How to classify the pituitary neuroendocrine tumors (PitNET)s in 2020. *Cancers.* (2020) 12:514. doi: 10.3390/cancers12020514
23. Shin SS, Tormenti MJ, Paluzzi A, Rothfus WE, Chang YF, Zainah H, et al. Endoscopic endonasal approach for growth hormone secreting pituitary adenomas: outcomes in 53 patients using 2010 consensus criteria for remission. *Pituitary.* (2013) 16:435–44. doi: 10.1007/s11102-012-0440-6
24. Juthani RG, Reiner AS, Patel AR, Cowan A, Roguski M, Panageas KS, et al. Radiographic and clinical outcomes using intraoperative magnetic resonance imaging for transsphenoidal resection of pituitary adenomas. *J Neurosurg.* (2020) 134:1824–35. doi: 10.3171/2020.4.JNS20178
25. Lee CC, Yang HC, Chen CJ, Lin CJ, Wu HM, Chung WY, et al. Empirical versus progression-guided stereotactic radiosurgery for non-functional pituitary macroadenomas after subtotal resection. *J Neurooncol.* (2019) 142:291–7. doi: 10.1007/s11060-019-03095-1
26. Almubark I, Chang LC, Shattuck KF, Nguyen T, Turner RS, Jiang X, et al. 5-min cognitive task with deep learning accurately detects early Alzheimer's disease. *Front Aging Neurosci.* (2020) 12:603179. doi: 10.3389/fnagi.2020.603179
27. Shehata M, Alksas A, Abouelkheir RT, Elmahdy A, Shaffie A, Soliman A, et al. A comprehensive computer-assisted diagnosis system for early assessment of renal cancer tumors. *Sensors.* (2021) 21:4928. doi: 10.3390/s21144928
28. Heise D, Schulze-Hagen M, Bednarsch J, Eickhoff R, Kroh A, Bruners P, et al. CT-based prediction of liver function and post-PVE hypertrophy using an artificial neural network. *J Clin Med.* (2021) 10:3079. doi: 10.3390/jcm10143079
29. Detmer FJ, Lückehe D, Mut F, Slawski M, Hirsch S, Bijlenga P, et al. Comparison of statistical learning approaches for cerebral aneurysm rupture assessment. *Int J Comput Assist Radiol Surg.* (2020) 15:141–50. doi: 10.1007/s11548-019-02065-2
30. Lv L, Yin S, Zhou P, Hu Y, Chen C, Ma W, et al. Clinical and pathologic characteristics predicted the postoperative recurrence and progression of pituitary adenoma: a retrospective study with 10 years follow-up. *World Neurosurg.* (2018) 118:e428–35. doi: 10.1016/j.wneu.2018.06.210
31. Tatsi C, Stratakis CA. Aggressive pituitary tumors in the young and elderly. *Rev Endocr Metab Disord.* (2020) 21:213–23. doi: 10.1007/s11154-019-09534-8
32. Trott G, Ongaratti BR, de Oliveira Silva CB, Abech GD, Haag T, Rech CGSL, et al. PTTG overexpression in non-functioning pituitary adenomas: Correlation with invasiveness, female gender and younger age. *Ann Diagn Pathol.* (2019) 41:83–9. doi: 10.1016/j.anndiagpath.2019.04.016
33. Miller BA, Rutledge WC, Ioachimescu AG, Oyesiku NM. Management of large aggressive nonfunctional pituitary tumors: experimental medical options when surgery and radiation fail. *Neurosurg Clin N Am.* (2012) 23:587–94. doi: 10.1016/j.nec.2012.06.013
34. Li C, Zhu H, Zong X, Wang X, Gui S, Zhao P, et al. Experience of transnasal endoscopic surgery for pituitary tumors in a single center in China: Surgical results in a cohort of 2032 patients, operated between 2006 and 2018. *Clin Neurol Neurosurg.* (2020) 197:106176. doi: 10.1016/j.clineuro.2020.106176
35. Monsalves E, Larjani S, Loyola Godoy B, Juraschka K, Carvalho F, Kucharczyk W, et al. Growth patterns of pituitary adenomas and histopathological correlates. *J Clin Endocrinol Metab.* (2014) 99:1330–8. doi: 10.1210/jc.2013-3054
36. Farrell CJ, Garzon-Muvdi T, Fastenberg JH, Nyquist GG, Rabinowitz MR, Rosen MR, et al. Management of nonfunctioning

recurrent pituitary adenomas. *Neurosurg Clin N Am.* (2019) 30:473–82. doi: 10.1016/j.nec.2019.05.006
37. Walsh MT, Couldwell WT. Symptomatic cystic degeneration of a clinically silent corticotroph tumor of the pituitary gland. *Skull Base.* (2010) 20:367–70. doi: 10.1055/s-0030-1253579
38. Luo P, Zhang L, Yang L, An Z, Tan H. Progress in the pathogenesis, diagnosis, and treatment of tsh-secreting pituitary neuroendocrine tumor. *Front Endocrinol.* (2020) 11:580264. doi: 10.3389/fendo.2020.580264
39. Rasul FT, Jaunmuktane Z, Khan AA, Phadke R, Powell M. Plurihormonal pituitary adenoma with concomitant adrenocorticotropic hormone (ACTH) and growth hormone (GH) secretion: a report of two cases and review of the literature. *Acta Neurochir.* (2014) 156:141–6. doi: 10.1007/s00701-013-1890-y
40. Miller BA, Ioachimescu AG, Oyesiku NM. Contemporary indications for transsphenoidal pituitary surgery. *World Neurosurg.* (2014) 82(6 Suppl.):S147–51. doi: 10.1016/j.wneu.2014.07.037
41. Vasudevan K, Saad H, Oyesiku NM. The role of three-dimensional endoscopy in pituitary adenoma surgery. *Neurosurg Clin N Am.* (2019) 30:421–32. doi: 10.1016/j.nec.2019.05.012
42. Khalafallah AM, Liang AL, Jimenez AE, Rowan NR, Oyesiku NM, Mamelak AN, et al. Trends in endoscopic and microscopic transsphenoidal surgery: a survey of the international society of pituitary surgeons between 2010 and 2020. *Pituitary.* (2020) 23:526–33. doi: 10.1007/s11102-020-01054-y
43. Hoang N, Tran DK, Herde R, Couldwell GC, Osborn AG, Couldwell WT. Pituitary macroadenomas with oculomotor cistern extension and tracking: implications for surgical management. *J Neurosurg.* (2016) 125:315–22. doi: 10.3171/2015.5.JNS15107
44. Dallapiazza RF, Grober Y, Starke RM, Laws ER Jr, Jane JA Jr. Long-term results of endonasal endoscopic transsphenoidal resection of nonfunctioning pituitary macroadenomas. *Neurosurgery.* (2015) 76:42–52. doi: 10.1227/NEU.0000000000000563
45. Schult D, Hölsken A, Siegel S, Buchfelder M, Fahlbusch R, Kreitschmann-Andermahr I, et al. EZH2 is highly expressed in pituitary adenomas and associated with proliferation. *Sci Rep.* (2015) 5:16965. doi: 10.1038/srep16965
46. Taussky P, Kalra R, Coppens J, Mohebali J, Jensen R, Couldwell WT. Endocrinological outcome after pituitary transposition (hypophysopexy) and adjuvant radiotherapy for tumors involving the cavernous sinus. *J Neurosurg.* (2011) 115:55–62. doi: 10.3171/2011.2.JNS10566
47. Rutkowski MJ, Chang KE, Cardinal T, Du R, Tafreshi AR, Donoho DA, et al. Development and clinical validation of a grading system for pituitary adenoma consistency. *J Neurosurg.* (2020) 134:1800–7. doi: 10.3171/2020.4.JNS193288
48. Raverot G, Burman P, McCormack A, Heaney A, Petersenn S, Popovic V, et al. European Society of endocrinology clinical practice guidelines for the management of aggressive pituitary tumours and carcinomas. *Eur J Endocrinol.* (2018) 178:G1–24. doi: 10.1530/EJE-17-0796

Conflict of Interest: The authors declare that the research was conducted in the absence of any commercial or financial relationships that could be construed as a potential conflict of interest.

Publisher's Note: All claims expressed in this article are solely those of the authors and do not necessarily represent those of their affiliated organizations, or those of the publisher, the editors and the reviewers. Any product that may be evaluated in this article, or claim that may be made by its manufacturer, is not guaranteed or endorsed by the publisher.

frontiers in Oncology

ORIGINAL RESEARCH
published: 17 January 2022
doi: 10.3389/fonc.2021.812468

Pseudocapsule-Based Resection for Pituitary Adenomas *via* the Endoscopic Endonasal Approach

Yuefei Zhou[1†], Jialiang Wei[1†], Feng Feng[2†], Jianguo Wang[3], Pengfei Jia[1], Shuangwu Yang[1] and Dakuan Gao[1]*

[1] Department of Neurosurgery, Xijing Hospital, Fourth Military Medical University, Xi'an, China, [2] Department of Rehabilitation Medicine, Xijing Hospital, Fourth Military Medical University, Xi'an, China, [3] Department of Neurosurgery, Shenmu County Hospital, Yulin, China

Introduction: The endoscopic endonasal approach (EEA) is a safe and effective treatment for pituitary adenomas (PAs). Since extracapsular resection (ER) of PAs improves tumor resection and endocrine remission rates, the interface between the pseudocapsule and gland draws increasing attention. However, it is difficult to precisely dissect the tumor along the exact boundary, and complete removal of the tumor increases the risks of normal tissue damage and cerebrospinal fluid (CSF) leakage. In this study, we investigated the extracapsular resection as well as the pseudocapsule histology to evaluate the effectiveness and safety of pseudocapsule-related surgical interventions.

Methods: From December 2017 to December 2019, 189 patients of PAs *via* EEA in our single center were analyzed retrospectively. The images, operative details, and clinical follow-up of patients were collected. Sixty-four patients underwent pseudocapsule-based ER, and 125 patients also underwent traditional intracapsular resection (IR) with or without intensive excision for FPAs. The clinical characteristics, tumor resection, endocrinological outcomes, and postoperative morbidities of the two groups were compared. Informed consent for publication of our article was obtained from each patient. Histological examination of pseudocapsule was performed using hematoxylin and eosin and reticulin staining.

Results: The gross total recession was 62 (96.9%) in the ER group and 107 (85.6%) cases in the IR group, whereas the endocrine remission rate was 29/31 (93.5%) and 40/53 (75.5%) cases, respectively. Anterior pituitary functions were not aggravated postoperatively in any patient, but transient diabetes insipidus (DI) occurred more in the IR group (64.0%) than in ER (48.4%). Pseudocapsule specimens were obtained in 93 patients, and clusters of small cell aggregation were detected in 11 pseudocapsule specimens (11.8%) whereas other patients showed no remarkable developed pseudocapsule. Intraoperative CSF leak occurred more in the ER group (28.1%) than in the IR group (13.6%), but no difference was seen between two groups postoperatively. No case of intracranial hematoma or pituitary crisis occurred in both groups. After a mean follow-up of 22.8 months, tumor recurrence was observed in 4 (2.1%) cases.

OPEN ACCESS

Edited by:
Qun Wu,
Zhejiang University, China

Reviewed by:
Nguyen Minh Duc,
Pham Ngoc Thach University of Medicine, Vietnam
Mohammed A. Azab,
Boise State University, United States

****Correspondence:***
Dakuan Gao
gaodakuan1975@163.com

[†]These authors have contributed equally to this work and share first authorship

Specialty section:
This article was submitted to Neuro-Oncology and Neurosurgical Oncology, a section of the journal Frontiers in Oncology

Received: *10 November 2021*
Accepted: *22 December 2021*
Published: *17 January 2022*

Citation:
Zhou Y, Wei J, Feng F, Wang J, Jia P, Yang S and Gao D (2022) Pseudocapsule-Based Resection for Pituitary Adenomas via the Endoscopic Endonasal Approach. Front. Oncol. 11:812468. doi: 10.3389/fonc.2021.812468

Conclusion: Pseudocapsule-based extracapsular resection of PAs *via* EEA is an effective and safe procedure to achieve complete resection with high and sustained endocrine remission and without deteriorating pituitary function.

Keywords: endoscopic endonasal approach, pituitary adenoma, pseudocapsule, extracapsular resection, skull base reconstruction, cerebrospinal fluid leakage

INTRODUCTION

Over the last two decades, the endoscopic endonasal approach (EEA) has been extensively developed and refined for the resection of pituitary adenomas (PAs). The endoscopic panoramic view is superior in terms of efficacy and safety for sellar surgery, and studies have reported that PAs can be effectively resected by EEA with minimal postoperative morbidity (1). A pseudocapsule between PA and normal adenohypophysis was initially observed by Costello in 1936 (2). Oldfield and colleagues used the phrase "surgical capsule of adenoma" to describe this histologically confirmed pseudocapsule in 2006 which was found in about 50% of patients and tends to be more frequent in larger tumors (3). The studies elaborated procedure along the outer face of the pseudocapsule between the adenoma and surrounding normal gland tissue achieved radical removal of the tumor while preserving normal pituitary function (4–6). Thus, in recent years, extracapsular resection (ER), which emphasized the importance of pseudocapsule as a surgical plane, was adopted for more radical resection of the tumor (7).

Although PAs were frequently present within the pseudocapsule and complete tumor resection using the ER technique has been reported to maximize the effectiveness for PAs with pseudocapsules (4, 8), many authors believe that resection without compromising pituitary function is imperative to improving the ultimate health outcome of patients. In some selective cases, an incomplete adenoma resection is advised because it is expected that this is best for the patients, through lower complication rates and preserving pituitary function. The actual effects of ER-based complete resection of PA are still under debate.

To explore the effectiveness and safety of the operative management of the pseudocapsule, we grouped our patients based on the resection techniques we adopted. The surgical and endocrinological outcomes and complications were also collected and analyzed to evaluate the potential benefits or flaws of ER surgery. This current manuscript reports our preliminary experience about pseudocapsule-based resection procedure with different strategies in a series.

MATERIALS AND METHODS

General Data and Clinical Manifestations

In this retrospective study, we reviewed patients in our single institution (Department of Neurosurgery, Xijing Hospital, Fourth Military Medical University, Xi'an, China) who underwent EEA for PAs from December 2017 to December 2019. The information collected from patients' electronic medical records included presenting symptoms, operative notes, postoperative course, histopathological diagnosis, laboratory data, and image files. Informed consent was obtained from all patients.

In the current study, patients with other primary endocrine diseases, with obviously suprasellar and parasellar extensions or with cavernous sinus invasion (Knosp 4), were excluded from this study. The average age and disease history were 48.2 years and 16.5 months, respectively. All cases were given initial surgical treatment, and tumor recurrence postoperatively was removed from the groups.

Endocrinological Evaluations

All patients underwent a baseline preoperative pituitary hormone examination including serum cortisol, free thyroxine, thyroid stimulation hormone (TSH), adrenocorticotropic hormone (ACTH), growth hormone (GH) and insulin-like growth factor-1 (IGF-1), prolactin (PRL), luteinizing hormone (LH) and follicle-stimulating hormone (FSH), testosterone (in males), and estradiol (in females). Postoperative biochemical remission was defined as a nadir serum GH level of <0.4 ng/ml after an oral glucose load and/or a subsequently normal IGF-1 level adjusted for gender and age for acromegaly; morning serum cortisol level that was <5 μg/dl within 1 week postoperatively and thereafter, indicating no evidence of hypercortisolism for Cushing disease; normalized morning serum TSH, free triiodothyronine (FT3), and FT4 levels for thyrotroph adenoma; and serum PRL level of <15 ng/ml for prolactinoma. Diabetes insipidus (DI) was diagnosed when hypotonic polyuria was >3,000 ml/day. Hormonal status was evaluated at 1 week and 3 months after surgery and twice per year thereafter to evaluate anterior pituitary functions.

Imaging Analysis

The imaging and volumetric assessment and analysis were independently performed by an experienced neuroradiologist with access to all imaging sequences. Computed tomography is useful for demonstrating the degree of pneumatization and locations of septations in the sphenoid sinus. The magnetic resonance imaging (MRI) scanning was performed before surgery to provide excellent details about the tumor's size and texture and the location of normal adenohypophysis and pseudocapsule. The distribution and density of the pituitary gland could be seen on T1-weighted MR images (**Figure 1**). The position of the anterior communicating artery and internal carotid artery could be seen on T2-weighted images, also enabling us to reduce the surgical risks. The degree of resection was calculated by measuring the residual tumor volume using MRI data.

Surgical Procedure and Technique

Under general anesthesia by endotracheal intubation, patients were in a supine position with the head rotated to the right side. A fascia

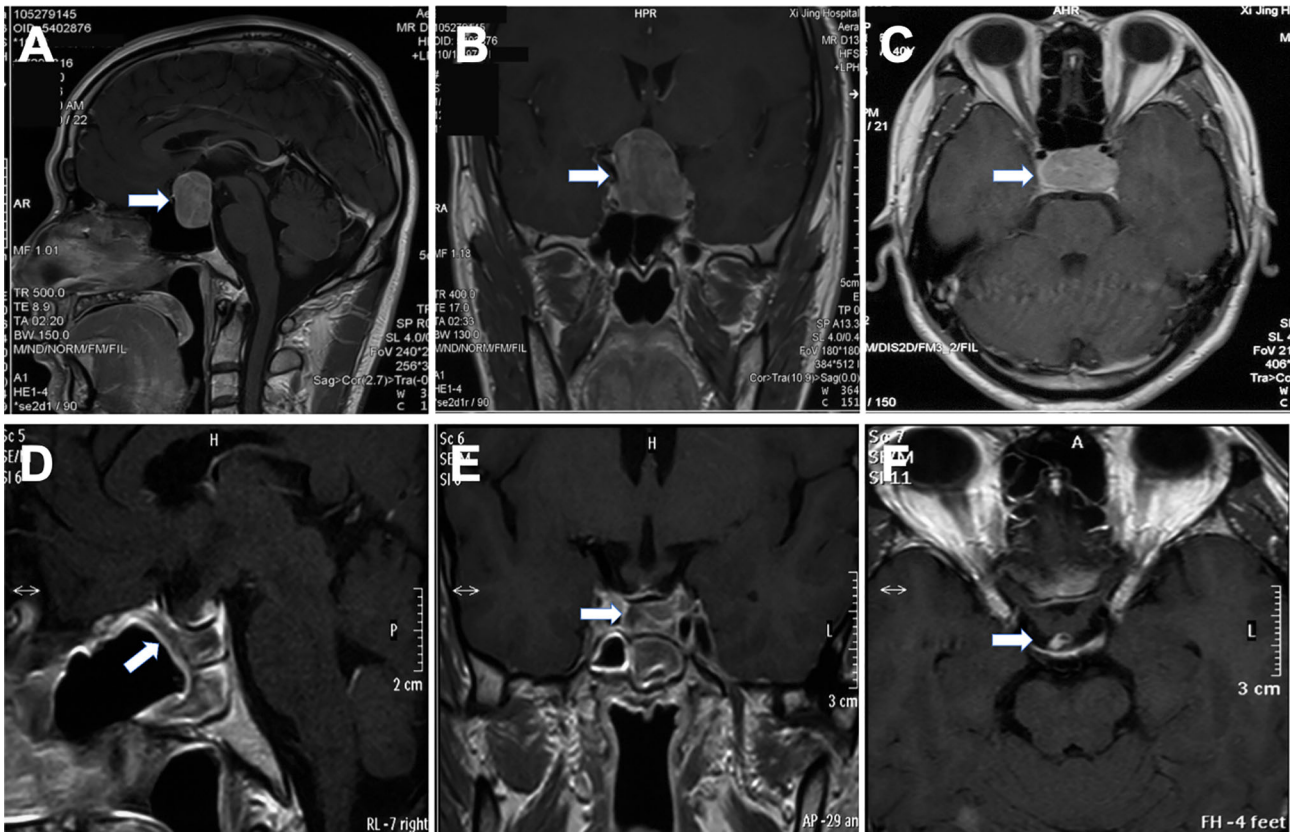

FIGURE 1 | Preoperative and postoperative magnetic resonance images of pituitary adenoma. The lesion was seen in the sellar region **(A, B),** and the normal pituitary gland was squeezed to the right side (arrow) **(C)**. The tumor was excised completely by EEA, mucosal flap was in good condition **(D)**. Optic chiasm and pituitary stalk were in normal position **(E, F)**.

lata donor site is also prepared to harvest autologous fascia for skull base reconstruction, in case of nasoseptal flap deficit. The operation proceeds with a binostril technique: one surgeon works bimanually while another one drives the endoscope to facilitate 3D perception of the surgical field. The middle turbinate was pushed laterally to enhance visibility, and a needle electrode was used to make a pedicled nasoseptal flap. A wide sphenoidotomy is important as it allows more degrees of freedom for instrument manipulation in the tumor cavity. It is also important to ensure meticulous hemostasis when operating in the nasal cavity, as it may be a constant source of blood rundown into the surgical field. Furthermore, the septations were drilled away carefully by not damaging the internal carotid artery, and the mucosa over the sella was opened in a curtain-like manner or fully removed to allow for optimal bony anatomy identification. Navigation can be used to compensate the under-pneumatized sinus for safety. To benefit from the panoramic view the endoscope offers, a larger bone window of the sellar floor is preferred and was further tailored according to preoperative MRI findings to protect the healthy pituitary gland, prevent any new endocrine deficit, and reduce the difficulty of skull base reconstruction. The bone over the carotid arteries and sellar floor was drilled with copious irrigation to avoid thermal injury to the underlying neurovascular tissues, and an eggshell bone could be made to facilitate bone resection. A rongeur is used, if necessary, to satisfactory extend the bone window, and Doppler is used to ensure security. Venous bleeding was usually easily controlled with SURGIFLO (Ethicon, America) and gentle pressure.

The dura incision can be flexibly adjusted to meet the need of surgical procedures. Depending on different tumor sizes and pseudocapsule development, we adopted different resection strategies. 1) In microadenoma, the exposed surface of the pituitary gland looks completely normal; a small cut was made in the gland at the location where the adenoma is expected according to preoperative imaging. The right dissector was used to separate the tumor and to preserve the integrity of the pseudocapsule, and achieved total extracapsular resection. Usually, the microadenoma texture is soft, limiting the option of extracapsular dissection. With small ring curettes, the tumor is removed and the tumor cavity was explored meticulously. 2) For macroadenomas, no attempt is made to remove the entire tumor or pull it forward during the initial phases of the dissection. After the intracapsular tumor is debulked and partially removed followed by a median-lateral or basal-superior order (**Figures 2A–C**), the residual tumor was separated carefully along the pseudocapsular interface. 3) If the pseudocapsule was not

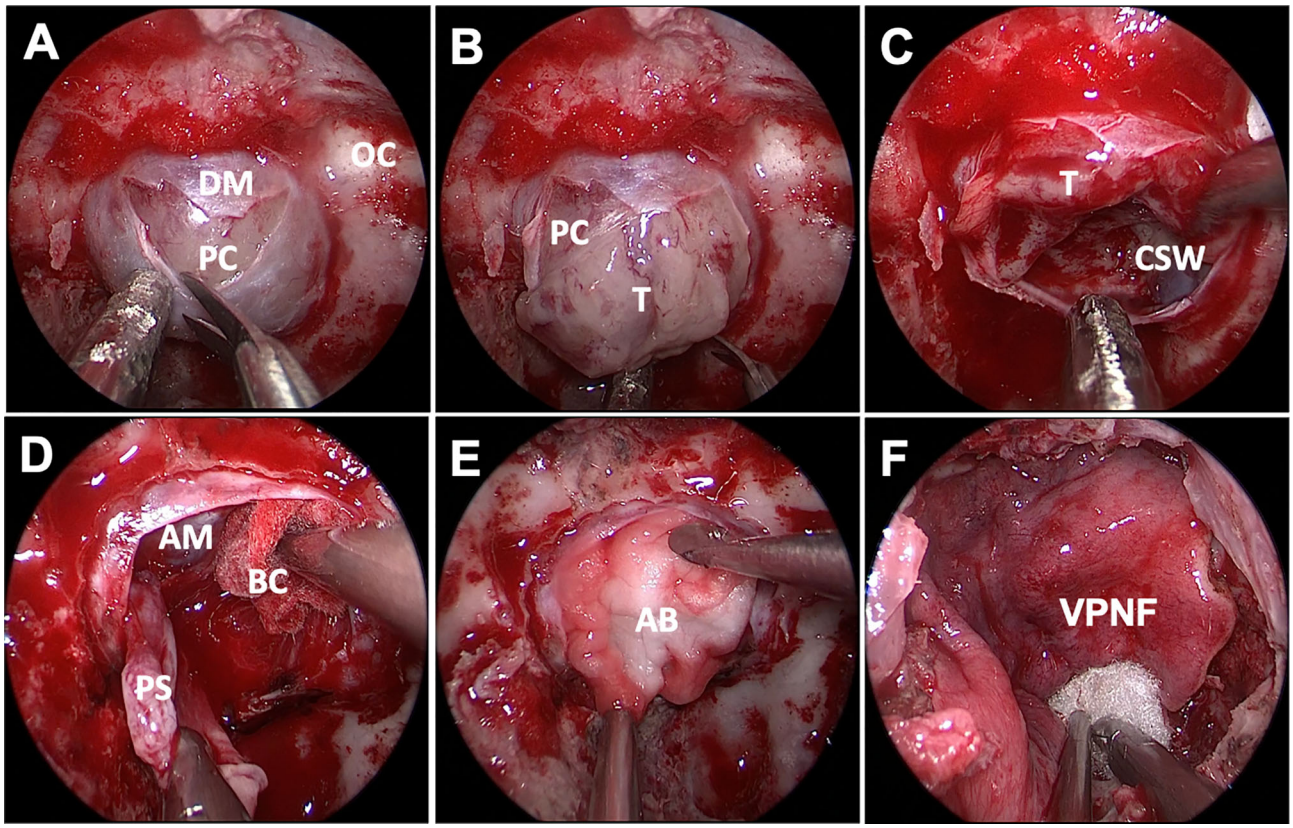

FIGURE 2 | Endoscopic endonasal approach of PA surgery. The soft and gray tumor was visualized after sellar floor opening and dura incision, but no obvious pseudocapsule was found **(A, B)**. The inferior and lateral were removed to expose the cavernous sinus wall **(C).** After adequate intracapsular debulking, the pseudocapsule was carefully separated under the protection of brain cotton without hurting the arachnoid membrane of suprasellar cistern **(D)**.An absorbable artificial biomembrane was placed firstly **(E)** before the vascularized pedicled nasoseptal flap **(F)** to reconstruct the skull base. DM, dura mater; OC, optic canal; PC, pituitary capsule; T, tumor; CSW, cavernous sinus wall; AM, arachnoid membrane; BC, brain cotton; AB, artificial biomembrane; VPNF, vascularized pedicled nasoseptal flap.

visible in the first stage, we used conventional conservative intracapsular resection. Internal debulking was continued until visualization of the pseudocapsule or cavernous sinus wall was achieved (**Figure 2D**). Extrapseudocapsulary dissection was continued along the plane, preserving as much integrity of the pseudocapsule as possible. 4) After internal debulking, if the pseudocapsule was still unidentifiable, the adenoma was excised piecemeal progressively. Noteworthily, we adopted intensive excision and meticulous sweeping to remove small remnants that are hidden behind the fibrin membranes for PA. The surface of the pituitary gland was peeled off as thin a slice as possible, and the tumor bed was circumferentially resected to remove any small tumor remnant in Cushing disease or acromegaly patients. 5) To minimize the impact on pituitary functions, the suspicious tissue was sent to the pathology department for histopathology intraoperatively. A residual fragmental pseudocapsule may be beneficial if further dissection increases the risk of unacceptable neurological morbidity or obvious cerebrospinal fluid (CSF) leakage.

After tumor resection, the surgical areas were repeatedly irrigated with warm saline to reduce potential inflammation and to achieve hemostasis. It can be useful to fill the resection cavity with saline and dive into the cavity with the endoscope, rinsing continuously for detailed inspection. Depending on the presence or absence of CSF leakage during surgery, we also adopted different strategies for skull base reconstruction. 1) If no CSF leak was observed intraoperatively, the reconstruction is simple and standardized. The sphenoidal mucosa is also draped over the sella to promote remucosalization for microadenoma. The nasoseptal flap can also be restored and located in its original position. 2) The arachnoidal tear was closed by placing a small piece of abdominal fat or gelatin sponge, and overpack should be avoided. The free nasoseptal graft that was harvested at the beginning of the surgery is placed on the sellar floor. 3) In patients with bigger CSF leakage, an absorbable artificial biomembrane supported with fat or gelatin sponge was vital to preventing CSF leaks. Furthermore, pedicled nasoseptal flap was covered on the sellar floor for further reinforcement (**Figures 2E, F**). Surgicel and gelatin sponges were stuffed around to further enhance the flap in case of displacement or migration, and to accelerate healing. 4) The anterior sellar dura could also be reconstructed by dural suturing. 5) If the mucosal flap is defective, the fascia lata can further strengthen the skull base. Lumbar drainage was not used as a preventive maneuver postoperatively.

Pathological Examinations

All resected tumor tissues were evaluated by routine pathological and immunohistochemical examination. The composition of complete and fragmentary pseudocapsules was pathologically examined. All tissues obtained in the study were paraformaldehyde fixed and paraffin embedded. The sections were stained using hematoxylin and eosin staining or Masson's trichrome staining.

Statistical Analysis

Statistical analyses were conducted by blinded researchers. All values of each group were presented as means ± SD. Statistical difference was analyzed, according to different comparison situations, by the chi-square test with Fisher's exact test. $p < 0.05$ was considered statistically significant.

RESULTS

Sixty-four patients received ER surgery, and 125 patients received IR surgery. The follow-up was conducted 1 and 6 months postoperatively and annually thereafter. The overall mean follow-up period was 6∼42 months (average 22.8 months). According to preoperative MRI findings, the tumors consisted of 56 microadenomas (<10 mm) and 133 macroadenomas (≥10 mm); the overall mean value of the tumor diameter was 22.4 mm. There were statistically significant differences in age ($p = 0.0228$) and maximum tumor diameter ($p = 0.0007$) between the two groups, respectively (**Table 1**).

Tumor Removal

Postoperative MRI showed gross total resection achieved in 62 (96.9%) in the ER group and 107 (85.6%) cases in the IR group. There was no statistical difference in the incidence of recurrence between two groups ($p = 0.900$) (**Table 2**). Among 64 patients in the ER group, the pseudocapsule was apparent and complete enough to be used as a surgical plane initially in only 27 patients; for the remaining 37 patients, the pseudocapsule was identified at the outer margin of the tumor after internal debulking. The tumors were removed in a piecemeal fashion in 125 patients (66.1%) whose pseudocapsule was not well-demarcated and fragmentized (**Figure 3**).

Pseudocapsules were identified in 48.4% of functioning pituitary tumors and in 51.6% of non-functioning ones. Considering the postoperative risk of CSF leak, we fragmentalized the pseudocapsule and reserved part of the pseudocapsule that is adjacent to the suprasellar cistern arachnoid in 23/125 (18.4%) patients. Excessive resection of the cavernous sinus wall resulted in abducens nerve palsy in 1 case, which returned to normal after a 2-month treatment. A larger portion of microadenoma patients received ER surgery, compared with the IR group ($p < 0.0001$) (**Table 2**).

Endocrine Outcome

Pituitary function was tested 3 months postoperatively and at regular intervals on an individual basis depending on the patient's clinical status. Overall, the remission rate was higher in the ER group (93.5%, 29/31) than in the IR group (75.5%, 40/53) ($p = 0.042$). In addition, anterior pituitary functions were not aggravated in any patient postoperatively. Transient DI was a more common symptom in the IR group (80 in IR vs. 31 in ER, $p = 0.044$). One acromegalic patient in the ER group, who had achieved early biochemical remission by EEA alone, showed elevated serum IGF-1 levels at 1 year postoperatively. The patient received octreotide acetate microspheres (20 mg) for injection and achieved endocrinological relief after 3 months (**Table 2**).

Histopathology Features

Surgically resected specimens were examined histologically. All preoperative clinical diagnoses were confirmed by pathological examination. The classification of PAs according to hormonal activity was verified from the postoperative immunohistochemistry of the tumor tissue. Endocrine-active tumors were observed in 84 patients (44.4%); PRL, GH, ACTH, and TSH-secreting tumors were observed in 45, 31, 5, and 3, respectively, and non-functioning tumors were confirmed in 105 patients (55.6%). There was no difference between groups ($p = 0.444$).

Pseudocapsular specimens were histologically examined using hematoxylin and eosin and reticulin staining in 93

TABLE 1 | Preoperative characteristics of patients.

Symptoms preoperative (%)	Total (n = 189)	Extracapsular resection (n = 64)	Intracapsular resection (n = 125)	p value
Male	90 (47.6%)	31 (48.4%)	59 (47.2%)	0.8719[b]
Age	48.2 ± 11.0	51.7 ± 12.9	47.1 ± 13.1	0.0228[a]
Visual impairment	86 (45.5%)	28 (43.8%)	58 (46.4%)	0.7292[b]
Functional adenoma	84 (44.4%)	31 (48.4%)	53 (42.4%)	0.4292[b]
Acromegaly	31 (16.4%)	14 (21.9%)	17 (13.6%)	0.1460[b]
Prolactinoma	45 (23.8%)	13 (20.3%)	32 (25.6%)	0.4193[b]
Cushing disease	5 (2.6%)	2 (3.1%)	3 (2.4%)	0.7688[b]
Thyroid dysfunction	3 (1.6%)	2 (3.1%)	1 (0.8%)	0.2262[b]
Maximum tumor diameter (mm)	22.4 ± 7.9	20.3 ± 6.2	24.5 ± 8.7	0.0007[a]
Tumor size				
Microadenoma (<10 mm)	56 (53.1%)	34 (53.1%)	22 (17.6%)	<0.0001[b]
Macroadenoma (≥10 mm)	133 (23.8%)	30 (46.8%)	103 (82.4%)	<0.0001[b]

[a]*The Student t test was used for statistic analysis.*
[b]*The chi-square test was used for statistic analysis.*

TABLE 2 | Postoperative characteristics of patients.

Symptoms postoperative	Total (n = 189)	Extracapsular resection (n = 64)	Intracapsular resection (n = 125)	p value
Gross total resection	169 (89.4%)	62 (96.9%)	107 (85.6%)	**0.0171**
Tumor recurrence	4 (2.1%)	1 (1.6%)	3 (2.4%)	0.7050
Intraoperative CSF leakage	35 (18.5%)	18 (28.1%)	17 (13.6%)	**0.0150**
postoperative CSF rhinorrhea	1 (1.6%)	0	1 (1.6%)	0.4731
Transient diabetes insipidus[b]	111 (58.7%)	31 (48.4%)	80 (64.0%)	**0.0397**
Endocrinological remission [n (%)][a]	69/84 (82.1%)	29/31 (93.5%)	40/53 (75.5%)	**0.0369**

[a]Postoperative endocrinological remission was defined as: a nadir serum GH level of < 0.4 ng/ml after an oral glucose load and/or a subsequently normal IGF-1 level adjusted for gender and age for acromegaly; morning serum cortisol level that was >5 μg/dl within 1 week postoperatively for Cushing disease; normalized morning serum TSH, free triiodothyronine (FT3) and FT4 levels for thyrotroph adenoma, and serum PRL level of <15 ng/ml for prolactinoma.

[b]Diabetes insipidus (DI) was diagnosed as hypotonic polyuria > 3,000 ml/day.

The chi-square test was used for statistic analysis.

Bold formation means the differences that reached the statistically significance.

(49.2%) samples. The results revealed that the pseudocapsules were composed of fibroblasts, collagen fibers, and condensations of small cells on the background of myxoid materials (**Figure 4**). Reticulin staining demonstrated that the pseudocapsule existed in the adjacent pituitary even in patients without visible pseudocapsule intraoperatively (**Figure 5**).

Cerebrospinal Fluid Leak and Efficiency of Skull Base Construction

Intraoperative CSF leakage rates of the ER and IR groups were 28.1% (18/64) and 13.6% (17/125), respectively (p = 0.018). However, no difference was seen in postoperative CSF leakage of two groups (p = 0.773). One case in the ER group developed

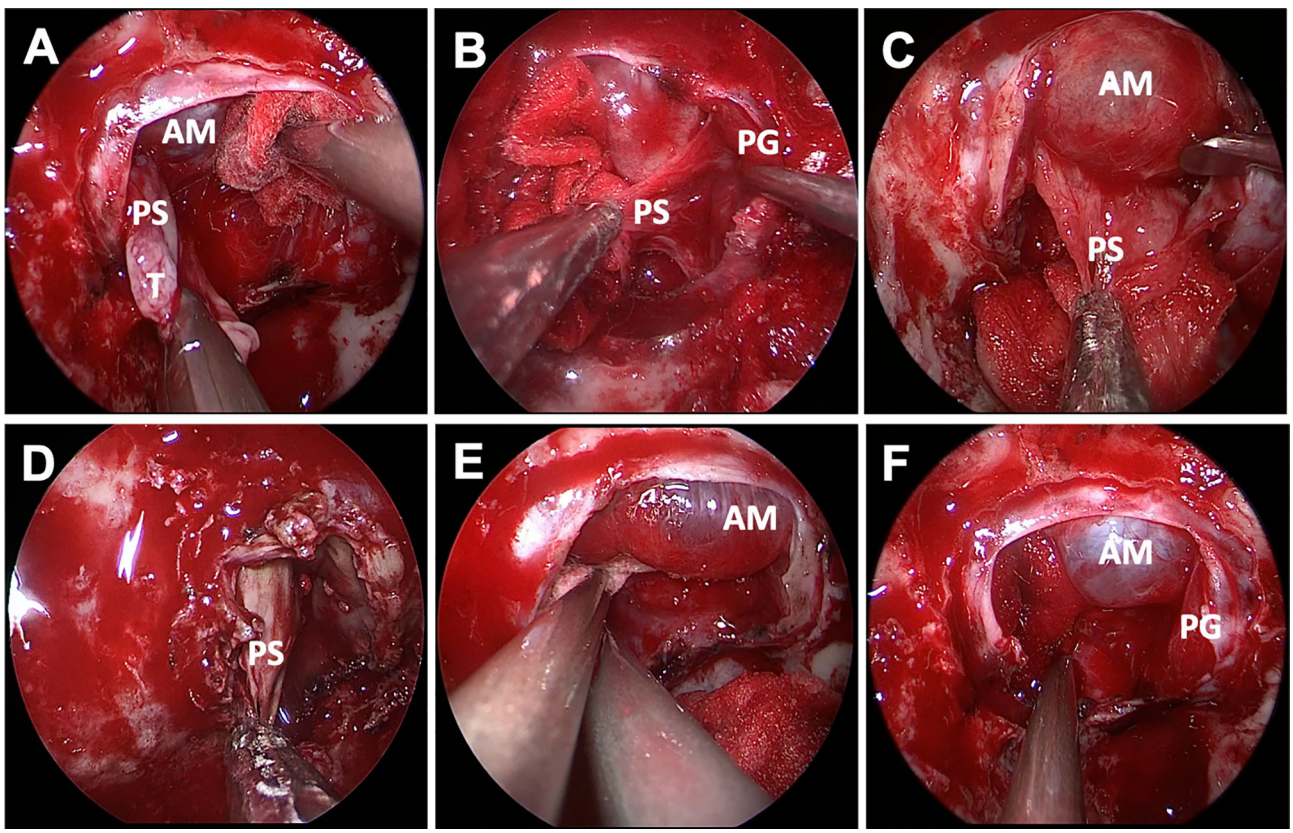

FIGURE 3 | Endoscopic endonasal view of pseudocapsular excision. The distinct pseudocapsule during surgery was exposed **(A)**. Relative interface between the pituitary adenoma and the normal pituitary gland was observed after adequate intracapsular debulking, and only degenerated pituitary tissue or fibers were detected by pathological examination **(B)**. The pseudocapsule adhered tightly to the arachnoid membrane and was separated using a dissector **(C)**. The pseudocapsule was firm and dissected piece by piece **(D)**. Bleeding from the cavernous sinus was packed with gelatin sponge, and the normal pituitary gland can be seen without arachnoid membrane injury after tumor resection **(E, F)**. AM, arachnoid membrane; PS, pseudocapsule; PG, pituitary gland; PP, posterior pituitary; GS, gelatin sponge.

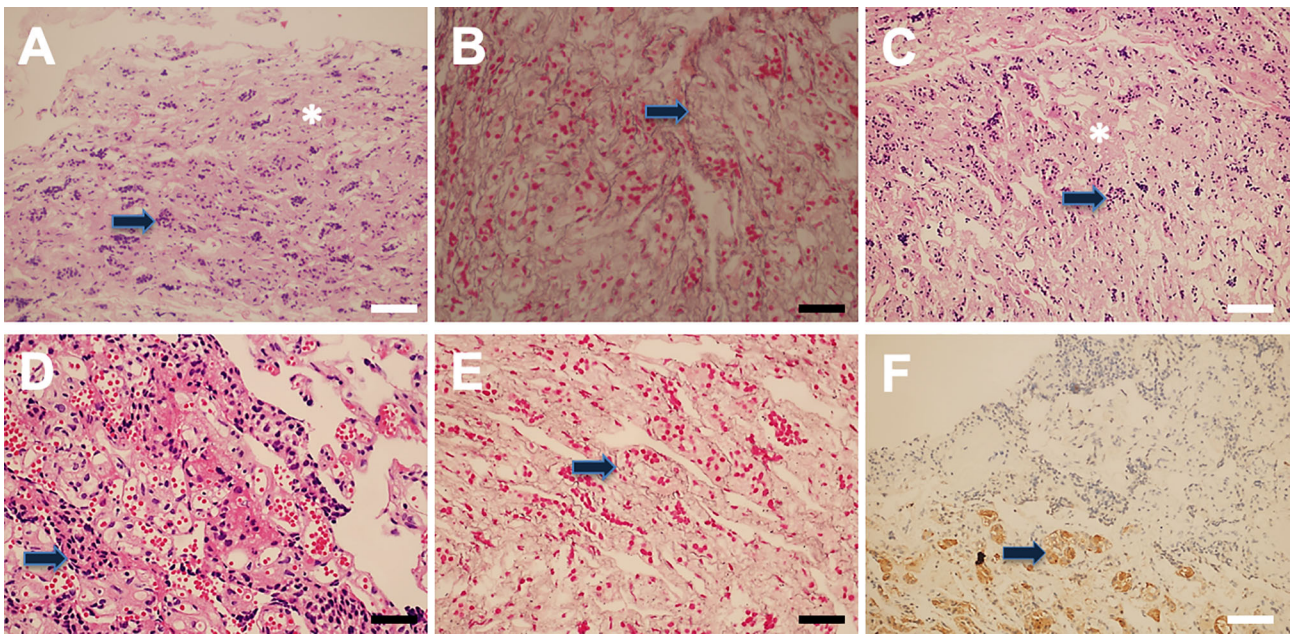

FIGURE 4 | Pseudocapsule histopathology. The pituitary-like tissue (arrow) and interfibrillar substance (asterisk) were found **(A)**. Reticulin staining results showed normal pituitary tissue(arrow) **(B)**. Hematoxylin and eosin (H&E) staining showed normal adenohypophyseal components in the fibrous capsule, which exhibited acinar-like morphology **(C, D).** Reticulin staining showed an intact mesh structure inside the fibrous capsule **(E),** and PRL immune-reactivity was also detected **(F)**. White bar = 100 μm, black bar = 50 μm.

CSF rhinorrhea with pulmonary infection postoperatively and was cured after reoperation (**Table 2**).

DISCUSSION

The pseudocapsule was first described in the early 1900s, which was formed by the compression between the tumor and normal gland (3). Adenoma growth leads to compression of the acinar structure of the adjacent normal gland, resulting in a reticulin-rich pseudocapsule that encases the entire adenoma in. Since Oldfield and Vortmeyer firstly dissected the pseudocapsule around microadenomas instead of internal piecemeal removal (3, 6), the understanding of pseudocapsule formation and clinical significance has been developed. Early identification of the adenoma edges is crucial to limiting the risk of damage to the pituitary gland and tearing of the arachnoid at the level of the diaphragm sellae; thus, using the pseudocapsule as a surgical plane could be effective for surgeons to better confine the resection area (9).

Studies have demonstrated that the possession rate of a pseudocapsule varies depending on the characteristics of the PA, including the pathological type and tumor size (4). Whether the resection is performed outside or inside the pseudocapsule largely depends on the consistency of the tumor and the degree of pseudocapsule development. Thus, different surgical techniques should be adopted according to the presence of the resectable pseudocapsule. When a tumor has a fibrous and thick pseudocapsule or when a tumor is very hard or fibrous, dissection should be performed completely outside the pseudocapsule. Kawamata (10) suggested that, in smaller tumors, the pseudocapsule tended to exist more prominently and to cover the whole tumor, whereas in larger tumors the pseudocapsule tended to be discontinuous or disrupted. Similarly, in the present study, we found that ER was more performed in microadenomas, whereas IR was more adopted in macroadenomas. Furthermore, in some macroadenomas, the pseudocapsule could not be seen until proper intracapsular debulking. By contrast, some PAs exhibited no or undefinable pseudocapsule; during the entire procedure, the adenoma was excised piecemeal progressively with a dissector, blunt ring curette, and aspirator.

Previous studies showed that the ER helps in achieving complete tumor resection (7, 11, 12). Similarly, in the present study, patients who received ER surgery achieved a higher rate of total adenoma resection, which indicated the beneficial role of ER surgery. Studies revealed heterogeneous conclusions that there still existed a discrepancy of whether ER brings a higher chance of damage than traditional ones. Some believed that ER methods could also increase the chance of pituitary gland damage, which leads to pituitary dysfunction. Others, on the contrary, summarized optimistic results (13). Typically, since repeated PA surgery has been proved safe for the experienced doctors and well tolerated by patients, intact pituitary gland function is deemed more important than adenoma total removal (14), Theoretically, it is hard for surgeons to extirpate only tumor cells completely during surgery without removing any normal pituitary gland tissue because in most cases the adenoma directly contacts with the normal pituitary gland. Thus, although we might resect a thin layer of anterior pituitary gland when resecting the tumor using the ER method, a meticulous

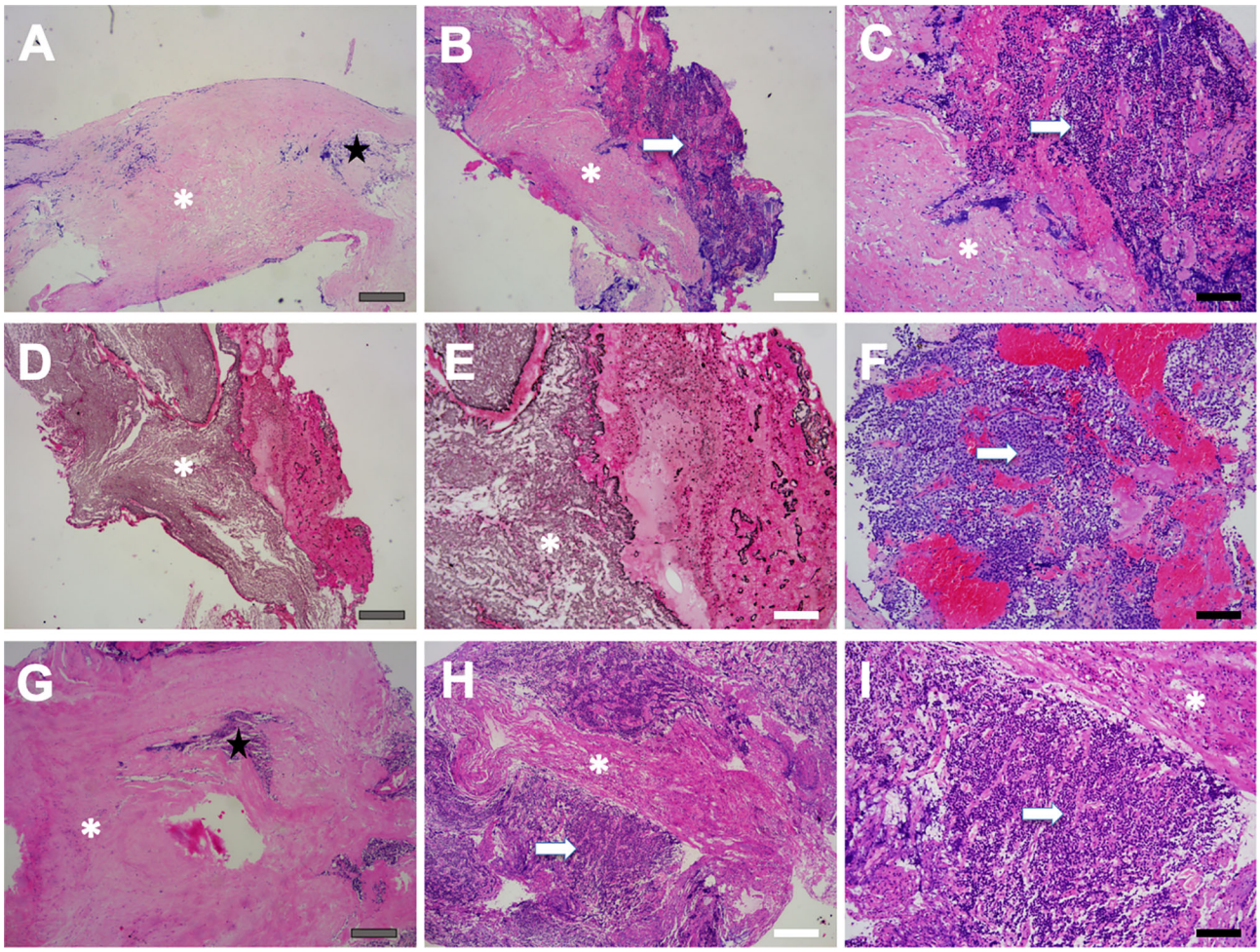

FIGURE 5 | Pseudocapsule specimen histopathology. Patchy fibrous tissue (asterisk) as well as a few pituitary-like cells (star) were found **(A)**, and the fibrous tissue was surrounded by pituitary-like cells **(B, C)**. Reticulin staining showed destruction and disorder of adenoid structure of hyperplastic pituitary-like cells, suggesting the pituitary adenoma **(D, E)**. Tumor cells were exhibited as small cell aggregation, which was found in pseudocapsule specimen (arrow) **(F)**. The pseudocapsule contained normal pituitary tissue (star) **(G)**. Pituitary adenoma (arrow) featured with homo-size tumor cells as well as vascularized structure, and fibrous hyperplasia was also observed (asterisk) **(H, I)**. Gray bar = 200 μm, white bar = 100 μm, black bar = 50 μm.

operation could avoid extra collateral damage of the pituitary gland and do no more harm than the traditional IR way. Besides, intracapsular resection sometimes requires more aggressive resection that could injure the remaining pituitary gland, which consequently increases the risk of worsening of pituitary function and increases the possibility of complications (15). This may be the reason why patients who received ER operation in our study showed less incidence of DI and better endocrinological remission rate after surgery, indicating that ER could cause less pituitary gland damage, compared with IR methods.

Some scholars found that the capsule itself contains tumor cells and may be a main cause of persistent hypersecretion of the hormone and possibly the source of recurrence (16). In addition, some studies found that the pseudocapsule is disrupted by tumor invasion so that the extracapsular removal and management of tumor invasion outside of the pseudocapsule are crucial to accomplishing complete PA removal (17, 18). Noteworthily, in our study, the histological staining revealed that the tumor was partially infiltrated in the pseudocapsule. Hence, if necessary, we applied intensive excision to remove all the confinable pseudocapsule and small remnants that are hidden behind the membranes to reach complete resection. New classification recognizes some subtypes of PAs as high-risk PAs, which include sparsely granulated somatotroph adenoma, lactotroph adenoma in men, silent corticotroph adenoma, and plurihormonal Pit-1-positive adenoma (19). For these refractory pituitary adenomas, we recommend aggressive resection, especially in IR resection cases. Partial gland resection or resection of the cavernous sinus medial wall is necessary in some cases since studies showed that it could help improve biochemical remission for the pituitary gland (20, 21).

Postoperative CSF leaks represent one of dreaded surgical complications encountered after EEA and have been reported to occur in approximately 3% at high-volume institutions (22). After the pedicled nasoseptal flap development by Haddad, there is a striking decrease of CSF leak rates in endonasal approaches series.

The pseudocapsule resection might violate and tear the arachnoid membrane in cases that the pseudocapsule was very adhesive to the arachnoid membrane, and sometimes CSF leakage is encountered. There are many techniques to avoid CSF leaks (23); focuses on limiting trauma to the diaphragm arachnoid membrane may be the most critical factor. According to the severity of intraoperative cerebrospinal fluid leak, proper closure techniques were used. In our present study, there was just one case in CSF rhinorrhea postoperatively in the ER group due to the defective nasoseptal and adopted reoperation and revision using autologous fascia grafts. The results indicated that our skull base reconstruction is also effective for patients receiving ER surgery. Considering the heterogeneity of PA patients, we suggested personalized decision in complicated cases, and pseudocapsule remnant is acceptable if the complete removal could cause refractory CSF leak.

Study Limitations

There is great heterogeneity in the operative procedure of PA across different institutions, with limited evidence regarding the comparative surgical tips and complications. There is a striking variance between centers for Pas (32862300), depending on local experience, alternative strategies, and so forth. There are also some differences in distinguishing the histology of pseudocapsule samples. More detection methods will be used to further observe the characteristic of the pseudocapsule. Future transmission electron microscopy is needed to further inquire the histological features of the pseudocapsule. Further data including long-term pituitary function in different groups are needed to justify the proposed techniques.

CONCLUSION

Extra-pseudocapsular resection is an effective technique that maximizes the extent of resection, improves endocrinological remission, and reduces certain complication incidences.

DATA AVAILABILITY STATEMENT

The original contributions presented in the study are included in the article/supplementary material. Further inquiries can be directed to the corresponding author.

ETHICS STATEMENT

The studies involving human participants were reviewed and approved by the Ethics Committee of Fourth Military Medical University. The patients/participants provided their written informed consent to participate in this study.

AUTHOR CONTRIBUTIONS

YZ and DG conceived and designed the analysis. YZ, JW, and FF wrote the manuscript. JLW analyzed the relevant data. JGW, PJ, and SY collected the MR images. All authors contributed to the article and approved the submitted version. All authors contributed to the article and approved the submitted version.

FUNDING

This research was supported by the National Natural Science Foundation of China, No.81971227 and Key Project of Social Development of Shaanxi Province, No.2018ZDXM-SF-086.

REFERENCES

1. Nagata Y, Inoshita N, Fukuhara N, Yamaguchi-Okada M, Nishioka H, Iwata T, et al. Growth Hormone-Producing Pituitary Adenomas in Childhood and Young Adulthood: Clinical Features and Outcomes. *Pituitary* (2018) 21(1):1–9. doi: 10.1007/s11102-017-0836-4
2. Costello RT. Subclinical Adenoma of the Pituitary Gland. *Am J Pathol* (1936) 12(2):205–16 1. doi: 10.1121/1.1915843
3. Oldfield EH, Vortmeyer AO. Development of a Histological Pseudocapsule and Its Use as a Surgical Capsule in the Excision of Pituitary Tumors. *J Neurosurg* (2006) 104(1):7–19. doi: 10.3171/jns.2006.104.1.7
4. Lee EJ, Ahn JY, Noh T, Kim SH, Kim TS, Kim SH. Tumor Tissue Identification in the Pseudocapsule of Pituitary Adenoma: Should the Pseudocapsule be Removed for Total Resection of Pituitary Adenoma? *Neurosurgery* (2009) 64(3Suppl):ons62–9; discussion ons9-70. doi: 10.1227/01.NEU.0000330406.73157.49
5. Qu X, Xu G, Qu Y, Song T. The Pseudocapsule Surrounding a Pituitary Adenoma and Its Clinical Significance. *J Neurooncol* (2011) 101(2):171–8. doi: 10.1007/s11060-010-0247-0
6. Monteith SJ, Starke RM, Jane JA Jr, Oldfield EH. Use of the Histological Pseudocapsule in Surgery for Cushing Disease: Rapid Postoperative Cortisol Decline Predicting Complete Tumor Resection. *J Neurosurg* (2012) 116 (4):721–7. doi: 10.3171/2011.12.JNS11886
7. Ceylan S, Cabuk B, Koc K, Anik I, Vural C. Endoscopic Distinction Between Capsule and Pseudocapsule of Pituitary Adenomas. *Acta Neurochir (Wien)* (2013) 155(9):1611–9; discussion 9. doi: 10.1007/s00701-013-1754-5
8. Kim EH, Ku CR, Lee EJ, Kim SH. Extracapsular En Bloc Resection in Pituitary Adenoma Surgery. *Pituitary* (2015) 18(3):397–404. doi: 10.1007/s11102-014-0587-4
9. Campero A, Martins C, Yasuda A, Rhoton AL Jr. Microsurgical Anatomy of the Diaphragma Sellae and Its Role in Directing the Pattern of Growth of Pituitary Adenomas. *Neurosurgery* (2008) 62(3):717–23; discussion -23. doi: 10.1227/01.neu.0000317321.79106.37
10. Kawamata T, Kubo O, Hori T. Surgical Removal of Growth Hormone-Secreting Pituitary Adenomas With Intensive Microsurgical Pseudocapsule Resection Results in Complete Remission of Acromegaly. *Neurosurg Rev* (2005) 28(3):201–8. doi: 10.1007/s10143-005-0384-7
11. Kinoshita Y, Tominaga A, Usui S, Arita K, Sakoguchi T, Sugiyama K, et al. The Surgical Side Effects of Pseudocapsular Resection in Nonfunctioning Pituitary Adenomas. *World Neurosurg* (2016) 93:430–5.e1. doi: 10.1016/j.wneu.2016.07.036
12. Ku CR, Kim EH, Oh MC, Lee EJ, Kim SH. Surgical and Endocrinological Outcomes in the Treatment of Growth Hormone-Secreting Pituitary Adenomas According to the Shift of Surgical Paradigm. *Neurosurgery* (2012) 71(2Suppl Operative):ons192–203; discussion ons. doi: 10.1227/NEU.0b013e318265a288
13. Chacko AG, Chacko G, Seshadri MS, Chandy MJ. The 'Capsule' of Pituitary Macroadenomas Represents Normal Pituitary Gland: A Histopathological

Study. *Br J Neurosurg* (2003) 17(3):213–8. doi: 10.1080/0268869031000153099
14. van Furth WR, de Vries F, Lobatto DJ, Kleijwegt MC, Schutte PJ, Pereira AM, et al. Endoscopic Surgery for Pituitary Tumors. *Endocrinol Metab Clin North Am* (2020) 49(3):487–503. doi: 10.1016/j.ecl.2020.05.011
15. Molitch ME. Diagnosis and Treatment of Pituitary Adenomas: A Review. *JAMA* (2017) 317(5):516–24. doi: 10.1001/jama.2016.19699
16. Oldfield EH. Cushing's Disease: Lessons Learned From 1500 Cases. *Neurosurgery* (2017) 64(CN_suppl_1):27–36. doi: 10.1093/neuros/nyx378
17. Nagata Y, Takeuchi K, Yamamoto T, Ishikawa T, Kawabata T, Shimoyama Y, et al. Peel-Off Resection of the Pituitary Gland for Functional Pituitary Adenomas: Pathological Significance and Impact on Pituitary Function. *Pituitary* (2019) 22(5):507–13. doi: 10.1007/s11102-019-00980-w
18. Nagata Y, Takeuchi K, Yamamoto T, Ishikawa T, Kawabata T, Shimoyama Y, et al. Removal of the Medial Wall of the Cavernous Sinus for Functional Pituitary Adenomas: A Technical Report and Pathologic Significance. *World Neurosurg* (2019) 126:53–8. doi: 10.1016/j.wneu.2019.02.134
19. Mete O, Lopes MB. Overview of the 2017 WHO Classification of Pituitary Tumors. *Endocr Pathol* (2017) 28(3):228–43. doi: 10.1007/s12022-017-9498-z
20. Anik I, Cabuk B, Gokbel A, Selek A, Cetinarslan B, Anik Y, et al. Endoscopic Transsphenoidal Approach for Acromegaly With Remission Rates in 401 Patients: 2010 Consensus Criteria. *World Neurosurg* (2017) 108:278–90. doi: 10.1016/j.wneu.2017.08.182
21. Barkhoudarian G, Cutler AR, Yost S, Lobo B, Eisenberg A, Kelly DF. Impact of Selective Pituitary Gland Incision or Resection on Hormonal Function After Adenoma or Cyst Resection. *Pituitary* (2015) 18(6):868–75. doi: 10.1007/s11102-015-0664-3
22. Strickland BA, Lucas J, Harris B, Kulubya E, Bakhsheshian J, Liu C, et al. Identification and Repair of Intraoperative Cerebrospinal Fluid Leaks in Endonasal Transsphenoidal Pituitary Surgery: Surgical Experience in a Series of 1002 Patients. *J Neurosurg* (2018) 129(2):425–9. doi: 10.3171/2017.4.JNS162451
23. Liu JK, Schmidt RF, Choudhry OJ, Shukla PA, Eloy JA. Surgical Nuances for Nasoseptal Flap Reconstruction of Cranial Base Defects With High-Flow Cerebrospinal Fluid Leaks After Endoscopic Skull Base Surgery. *Neurosurg Focus* (2012) 32(6):E7. doi: 10.3171/2012.5.FOCUS1255

Conflict of Interest: The authors declare that the research was conducted in the absence of any commercial or financial relationships that could be construed as a potential conflict of interest.

Publisher's Note: All claims expressed in this article are solely those of the authors and do not necessarily represent those of their affiliated organizations, or those of the publisher, the editors and the reviewers. Any product that may be evaluated in this article, or claim that may be made by its manufacturer, is not guaranteed or endorsed by the publisher.

frontiers in Oncology

ORIGINAL RESEARCH
published: 20 January 2022
doi: 10.3389/fonc.2021.735778

Diagnostic Value of Non-Contrast CT in Cerebrospinal Fluid Leakage After Endoscopic Transnasal Surgery for Sellar and Suprasellar Tumors

Wei Gao[1,2†], *Xiaoyu Wang*[1†], *Yuanjian Fang*[1], *Yuan Hong*[1], *Wei Yan*[1], *Sheng Zhang*[3*] *and Chenguang Li*[1*]

[1] *Department of Neurosurgery, The Second Affiliated Hospital of Zhejiang University, Hangzhou, China,* [2] *Department of Neurosurgery, Changxing People's Hospital, Changxing, China,* [3] *Department of Neurology, Zhejiang Provincial People's Hospital, People's Hospital of Hangzhou Medical College, Hangzhou, China*

We aimed to study the relationship between pneumocephalus on non-contrast CT (NCCT) and post-operative cerebrospinal fluid leakage (p-CFL) after endoscopic transsphenoidal sellar and suprasellar tumor surgeries. Data from patients who underwent endoscopic treatment for sellar or suprasellar tumors from January 2018 to March 2020 were consecutively collected and reviewed. The NCCT pneumocephalus (NP) was measured the first day after operation and the first day after the expansive sponge was extracted. p-CFL was determined according to post-operative clinical symptoms, high resolution CT and glucose test, and expert consensus. Of the 253 patients enrolled in this study, 32 (12.6%) had p-CFL. Compared with patients without p-CFL, patients with p-CFL had a higher occurrence of intra-operative CFL, a longer operation time, a higher rate of pneumocephalus on first-day NCCT after operation (i.e., first-day NP), and a higher rate of NP volume change between two NCCT measurements (referred to as the NP change) (all $p < 0.05$). In multivariate regression analysis, first-day NP was independently associated with p-CFL occurrence [odds ratio (OR)=6.395, 95% confidence interval (CI)=2.236-18.290, p=0.001). After adding the NP change into the regression model, first-day NP was no longer independently associated with p-CFL, and NP change (OR = 19.457, 95% CI = 6.095–62.107, p<0.001) was independently associated with p-CFL. The receiver operating characteristic curve comparison analysis showed that NP change had a significantly better predicting value than first-day NP (area under the curve: 0.988 vs. 0.642, Z=6.451, p=0.001). NP is an effective imaging marker for predicting p-CFL after endoscopic sellar and suprasellar tumors operation, and the NP change has a better predicting value.

Keywords: cerebrospinal fluid leakage, endoscopic transnasal surgery, head CT, pneumocephalus, diagnosis

OPEN ACCESS

Edited by:
Zhixiong Liu,
Central South University, China

Reviewed by:
Mohammed A. Azab,
Boise State University, United States
Min Guo,
Fudan University, China

****Correspondence:***
Sheng Zhang
xiaoxiaoqing_23@hotmail.com
Chenguang Li
2315084@zju.edu.cn

†These authors have contributed equally to this work

Specialty section:
This article was submitted to Neuro-Oncology and Neurosurgical Oncology, a section of the journal Frontiers in Oncology

Received: *03 July 2021*
Accepted: *13 December 2021*
Published: *20 January 2022*

Citation:
Gao W, Wang X, Fang Y, Hong Y, Yan W, Zhang S and Li C (2022) Diagnostic Value of Non-Contrast CT in Cerebrospinal Fluid Leakage After Endoscopic Transnasal Surgery for Sellar and Suprasellar Tumors. Front. Oncol. 11:735778. doi: 10.3389/fonc.2021.735778

INTRODUCTION

Endoscopic transsphenoidal surgery is increasingly performed by neurosurgeons to treat skull base lesions, but cerebrospinal fluid (CSF) leakage (CFL) is a difficult-to-avoid complication, with an incidence as high as 11% (1). The most common sites of surgical traumatic CFL are the ethmoid roof and sphenoid sinus (2). In one study, pituitary tumor resections accounted for nearly half of the cases of confirmed CFL following tumor removal (3). CFL can cause symptoms of low intracranial pressure, pneumocephalus, and life-threatening intracranial infection, all of which seriously affect patient prognosis (4, 5). Although there are many ways to repair CFL, such as lumbar cistern drainage and multilayered techniques including fat tamponade, fascia lata, artificial dura, pediculate nasoseptal flap, and balloon compression (6–10), leakage is still difficult to repair. Moreover, post-operative CFL is difficult to detect and easily neglected by clinicians.

Early detection of CFL is quite important. Methods reported to diagnose CFL include β2-transferrin testing, glucose rhinorrhea content analysis, high-resolution computed tomography (HRCT), magnetic resonance imaging (MRI), and cisternography (11–13). However, these methods are inconvenient and carry a certain risk of misdiagnosis (14, 15). Pneumocephalus is a common clinical manifestation of CFL (16). In cases of low intracranial pressure, air can enter the brain and cause pneumocephalus (17, 18). Non-contrast CT (NCCT) can clearly show pneumocephalus after transsphenoidal surgery. However, since no study has assessed the relationship between pneumocephalus on NCCT and CFL after transnasal surgery, the diagnostic value of post-operative NCCT for CFL is uncertain.

Here, we analyzed surgical cases of endoscopic transsphenoidal sellar and suprasellar tumors, focusing on the relationship between CFL and the occurrence and volume change of NCCT pneumocephalus (NP) to identify a new method of CFL diagnosis.

METHODS

Ethics Statement

Each subject or an appropriate family member provided written informed consent prior to the study, and the protocols were approved by the local ethics committee. All clinical investigations were conducted according to the principles expressed in the Declaration of Helsinki.

Study Subjects

The retrospective study included consecutively collected patients who underwent endoscopic treatment for sellar or suprasellar tumors from January 2018 to March 2020. Patients' demographics, medical histories, pathological findings, and repair outcomes were recorded. Pre- and post-operative imaging, operative reports, medical records, and operative videos were reviewed. We excluded cases if (i) post-operative pathology did not show evidence of a tumor or (ii) they were missing imaging and clinical data (**Figure 1**).

Operation Procedure

Endoscopic resection of sellar or suprasellar tumors was performed routinely. Most operations were performed through the right nostril. If sellar septum injury or CFL was noticed during the operation, a repair was performed *via* lumbar cistern drainage; artificial dura repair; balloon compression; or autologous tissue like fat tamponade, fascia lata, or a pediculate nasoseptal flap (**Figure 2**). Depending on the intra-operative conditions, the surgeon might choose some or all of these methods for skull base reconstruction. Regardless of the occurrence of CFL during surgery, we routinely filled the nasal cavity with an expansive sponge, which was extracted on the third day after operation. The initial head NCCT scan was performed on the first day after surgery, and the second scan was performed the first day after expansive sponge extraction.

Calculation of NP Volume

The presence of NCCT pneumocephalus (NP) was measured on the first day after operation, and NP volume was estimated the first day after expansive sponge extraction. NP change was defined as the volume change in NP between the first day after operation and 24 h after sponge extraction, and it was divided into four categories: no NP in both NCCT measurements, NP volume decreased, NP volume remained and NP volume increased, which were abbreviated as no NP, decreased NP, unchanged NP and increased NP, respectively. The latter three categories were ascribed as NP change. NP delineation and volumetric analysis were conducted using MRIcron software (http://www.mccauslandcenter.sc.edu/mricro/mricron). The NP

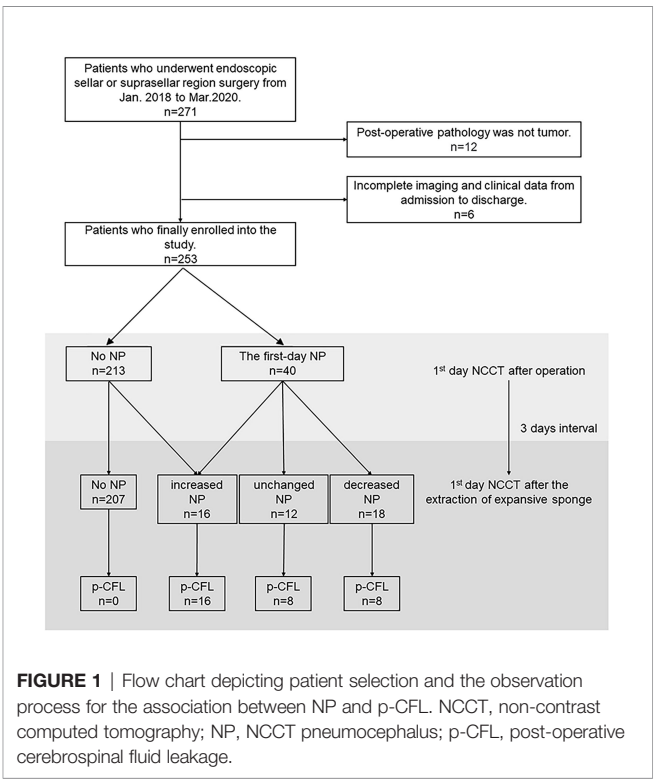

FIGURE 1 | Flow chart depicting patient selection and the observation process for the association between NP and p-CFL. NCCT, non-contrast computed tomography; NP, NCCT pneumocephalus; p-CFL, post-operative cerebrospinal fluid leakage.

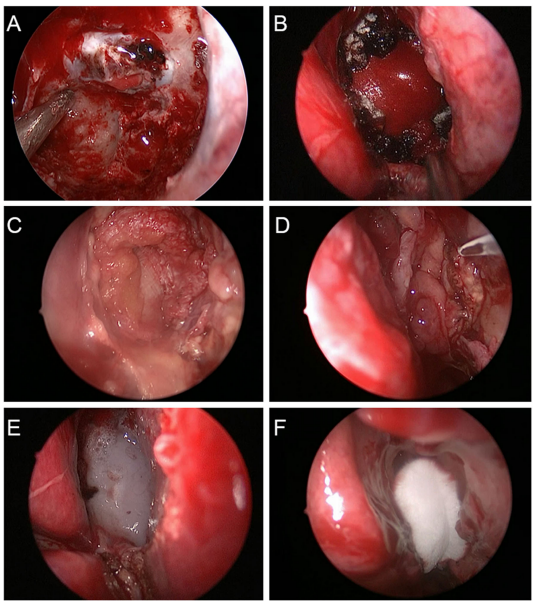

FIGURE 2 | Multilayered repair procedure for cerebrospinal fluid leakage in endoscopic transsphenoidal surgery. **(A)** A piece of artificial dura mater was inserted into the subdural space. **(B)** Another piece of artificial dura mater was place in the epidural space. **(C)** Autogenous fascia lata was placed on the sellar floor for further repair. **(D)** The pediculate nasoseptal flap was used to reconstruct skull base defects. **(E)** Fibrin sealant was used for reinforcement of skull base defect repair. **(F)** The nasal cavity was filled with Nasopore dressing to strengthen the repair of skull base defects.

volume measurement method is shown in **Supplementary Figure S1**.

Post-Operative Diagnosis of CFL

The diagnostic flow chart is shown in **Figure 3**.

Post-operative CFL (p-CFL) was diagnosed if patients had

①Persistent post-operative nasal discharge regardless of the occurrence of intra-operative CFL;

②Neither intra-operative CFL nor persistent post-operative nasal discharge but positive HRCT finding (CSF leak through a defect);

③Non-persistent nasal discharge after surgery, negative HRCT, but positive glucose test (glucose rhinorrhea content ≥1.7 mmol/L). In that case, glucose was repetitively tested, and the p-CFL diagnosis was determined by two experienced neurosurgeons (YH and WY, 5+ years' experience in endoscopic surgery). When there were different diagnostic opinions, the neurosurgeons reached consensus after discussion.

Patients without post-operative nasal discharge and negative CSF tests were defined as non-p-CFL.

Statistical Analysis

The characteristics of patients with and without p-CFL (i.e., p-CFL vs. non-p-CFL) are presented as mean and standard deviation (SD) for normally distributed continuous data, non-normally distributed variables are described as quartiles, and categorical variables are given as counts and percentages. Between-group differences were evaluated using Student's t-

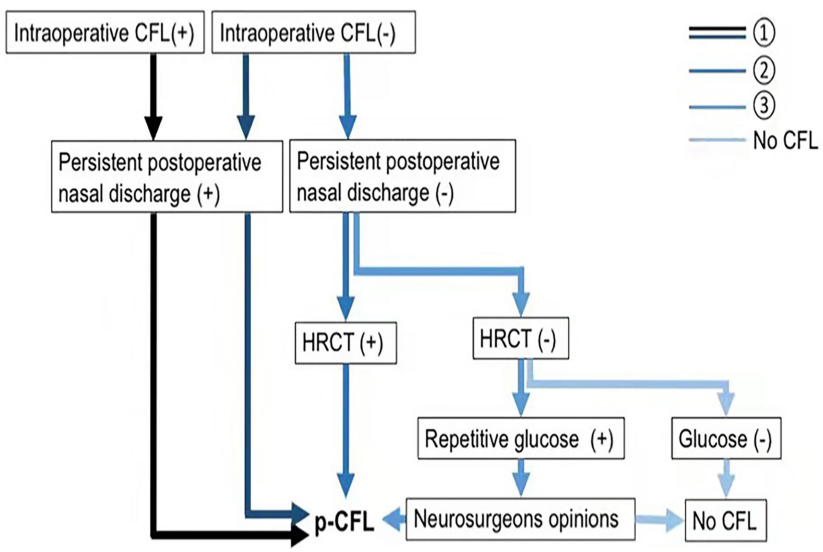

FIGURE 3 | Flow chart of p-CFL diagnosis. p-CFL can be diagnosed if any of the following are met: ①②③. HRCT (+) indicates a positive finding on HRCT that cerebrospinal fluid leaks through a defect, and HRCT (–) means no positive findings on HRCT. Glucose (+) indicates that glucose rhinorrhea content ≥1.7 mmol/L, and glucose (–) means that glucose rhinorrhea content <1.7 mmol/L. CFL, cerebrospinal fluid leakage; HRCT, high-resolution computer tomography; p-CFL, post-operative cerebrospinal fluid leakage.

tests or Mann–Whitney U-tests for continuous data and chi-square tests or Fisher's exact tests for categorical variables.

Variables that were significant on univariate analysis ($p < 0.05$) were included in the binary logistic regression model. Adjusted odds ratios (ORs) with 95% confidence intervals (CIs) were calculated, and $p < 0.05$ was considered significant. Receiver operative curve (ROC) analysis was performed to test the predictive power of independent variables for the dependent variable; we calculated the areas under the ROC curve (AUC), sensitivity, and specificity. All analyses were performed after blinding the participants' identifying information. Statistical analysis was performed using SPSS 19 (SPSS Inc., Armonk, NY, USA). ROC curve comparison analyses were conducted by MedCalc statistical software version 15 (MedCalc Software, Mariakerke, Belgium).

RESULTS

Patient Characteristics

A total of 271 patients were reviewed, and we identified 253 patients who met the study criteria after excluding 18 patients for the following: (i) post-operative pathology did not show evidence of a tumor (n = 12), and (ii) incomplete imaging and clinical data from admission to discharge (n = 6). Of the 253 patients, 49.6% were female, and the median patient age was 50 years (IQR, 40–60 years).

Of all the 253 patients, 40 (15.8%) showed first-day NP after operation. After the extraction of the expansive sponge, 46 patients (18.2%) showed NP change, and 32 (12.6%) were finally confirmed with p-CFL. The median test time for p-CFL was 2 days (IQR, 1–5 days) after the removal of the expansive sponge, and 62.5% of p-CFL patients were tested beyond 2 days after the removal of the expansive sponge.

Compared with non-p-CFL group, the p-CFL group showed a significantly longer duration of hospitalization and a higher rate of post-operative infection (62.5% vs. 11.8%, $\chi^2 = 48.090$, $p < 0.001$) (**Supplementary Table S1**). Ten patients received the repairment operation once or more, but still two of them died because of severe intracranial infection during hospitalization.

Factors Influencing the Occurrence of p-CFL

Compared to the non-p-CFL group, patients with p-CFL had a higher rate of intraoperative CFL, a higher use of free fat interpositional graft, lumbar cistern drainage, balloon compression, artificial dura mater implantation, and a longer duration time of operation (all $p < 0.05$). After resecting tumors, patients with p-CFL showed a higher rate of first-day NP and NP change during hospitalization, a higher occurrence of high fever and infection, and a longer duration of hospitalization (all $p < 0.05$) (**Supplementary Table S1**).

Among patients with no NP (N=207), none was found of p-CFL in both NCCT measurements. Among patients with an NP change (n = 46), 10 were in the decreased-NP subgroup who initially showed first-day NP but not on follow-up NCCT and were determined not to have p-CFL. Sixteen patients who showed increased NP between both NCCT measurements were confirmed to have p-CFL, including six patients without NP on first-day NCCT but with NP on follow-up NCCT after sponge extraction (**Figure 1**). Factors associating with NP change were tested and shown in **Supplemental Table S2**.

When adding first-day NP into the multivariate regression model, both the first-day NP (OR = 6.395, 95% CI = 2.236–18.290, p=0.001) and operative duration time (OR = 1.027, 95% CI=1.018–1.036, p<0.001) were independently associated with the occurrence of p-CFL after adjusting for pathology type (Model 1, **Supplementary Table S3**).

After adding NP change into the regression model, first-day NP was no longer independently associated with the occurrence of p-CFL. However, NP change (OR = 19.457, 95% CI = 6.292-71.373, p<0.001) and operative duration time (OR = 1.019, 95% CI=1.004-1.034, p=0.015) were independently associated with p-CFL (Model 2, **Supplementary Table S3**). In patients with NP change, decreased NP (OR = 0.133, 95%CI = 0.033-0.545, p=0.005) was significantly associated with a lower risk for having p-CFL in comparison of unchanged and increased NP.

Comparison of p-CFL Predictive Power Between Presence of First-Day NP and NP Change

ROC analysis showed that the AUC of first-day NP for predicting p-CFL was 0.642 (95% CI = 0.529–0.755, p=0.009), with sensitivity of 68.6% and specificity of 87.8%. The AUC of NP change for predicting p-CFL was 0.988 (95% CI = 0.977–0.998, p<0.001), with sensitivity of 100% and specificity of 93.7%. The ROC comparison showed that NP change had a significantly better predicting value than first-day NP (Z=6.451, p=0.001).

DISCUSSION

Diagnosis and management of p-CFL can be challenging, even for the most experienced neurosurgeons (13). Clear rhinorrhea and/or headache is common in many conditions. Those that should be considered to have CFL exhibit allergic rhinitis, common cold, vasomotor rhinitis, spontaneous intracranial hypotension, subarachnoid hemorrhage, and meningitis (18, 19). CFL can pose a serious hazard and is associated with delayed wound healing, meningitis, epidural infections, and pneumocephalus (20, 21). These complications often lead to prolonged hospitalization, reoperation, and increased healthcare costs (22–25). The most serious potential complication of CFL is meningitis (16, 26). Two patients in our study contracted *Klebsiella pneumoniae* infection and died. Thus, it is vital to find early signs that can be used to diagnose CFL. We found that both first-day post-operative NP and its volume change over time could predict p-CFL, and the latter had a higher predictive value. Compared with patients who had no NP, those with no change and increased NP had a higher risk of having p-CFL, and 100% of increased-NP patients (n = 16) were confirmed to have p-CFL.

There are two possible pathophysiologic explanations for the correlation between the presence of NP and p-CFL: the inverted bottle mechanism and the ball-valve mechanism (18, 27, 28). In the

first, it is postulated that as CSF flows out of the subarachnoid space through a dural-arachnoid tear, it creates negative pressure within the subarachnoid space. The negative pressure prevents the leakage of more CSF until air enters to take its place and equilibrates the pressure differential. The ball-valve mechanism hypothesizes that air enters through a fracture next to an air-containing space (18, 27, 28). Use of a vacuum drainage system predisposes patients to pneumocephalus in the presence of CFL (18, 29, 30).

We found that the NP change after expansive sponge extraction could better predict p-CFL than the first-day NP. Previous studies considered post-operative NP as an epiphenomenon of intra-operative CSF leak which would correlate with a higher risk of p-CFL (31, 32). Head NCCT examination was routinely performed on the first day after operation when the patient's bilateral nasal cavity was filled with an expansive sponge, and they were in a continuous supine position. Even if there was CSF leakage, it could not easily flow out of the nasal cavity. This situation also made it difficult for air to enter the brain. Therefore, if CFL is slight during and after operation, pneumocephalus is not always evident on early post-operative CT. A second CT scan was performed after sponge extraction and off-bed training for 1 day. If CFL existed at that time, CSF would be more likely to flow out than before. The reduced intracranial pressure means that air is more likely to enter the brain and causes pneumocephalus. Therefore, detecting NP volume changes can more effectively predict p-CFL than observing the NP on the first CT. However, most of the patients were discharged within 5 days of the operation, which precluded further CT dynamic observation.

In patients with first-day NP after tumor resection, the occurrence of p-CFL was lower among those with reduced NP volume compared with those with increased or unchanged NP volume. The probable cause is that pneumocephalus was gradually absorbed after the CFL resolved. Intra-operative CFL and the loss of a large amount of CSF initially leads to pneumocephalus. However, when the CFL was properly repaired with skull base reconstruction, the post-operative pneumocephalus gradually absorbed. In contrast, no change or an increase in CT pneumocephalus suggested persistent CFL. If the CFL is completely solved, the pneumocephalus will be gradually absorbed, and CT re-examination after 3 days is sufficient to observe the pneumocephalus reduction. If there is no change or there is an increase in pneumocephalus volume post-operatively, it indicates that intracranial pressure continues to decrease and a leak still exists, so the incidence of p-CFL increases.

In this study, p-CFL developed in two patients who had no pneumocephalus on the first day after the operation. Pneumocephalus was found on imaging on the fourth day after the operation, suggesting that dynamic review of head NCCT has supplementary significance for CFL evaluation. Although there was an increase in pneumocephalus volume after operation in one case, there was no CSF leakage, possibly due to excessive drainage of CSF *via* lumbar cistern drainage.

Our study was limited by the small number of patients and single-center retrospective design, so multicenter studies with larger samples sizes are needed to confirm our findings. In addition, we did not use beta-2 transferrin or beta trace protein testing to diagnose CFL because our hospital does not routinely perform these analyses. Nevertheless, glucose rhinorrhea content testing is fast, simple, inexpensive, and can be carried out in most hospitals, which could promote the wide application of our findings. An evidence-based review also pointed out that the guidance level for glucose testing was not inferior to that of beta-2 transferrin or beta trace protein testing in identifying CFL (14). Finally, the short observation time of our study was limited to the hospitalization duration, and future investigations should perform longer follow-ups.

CONCLUSION

Our results show that NP change is a more convenient and effective imaging marker than first-day NP for predicting p-CFL after endoscopic sellar and suprasellar tumor resection. During dynamic NCCT observation, attention should be paid to the risk of p-CFL in patients with no change or increased NP.

DATA AVAILABILITY STATEMENT

The original contributions presented in the study are included in the article/**Supplementary Material**, further inquiries can be directed to the corresponding authors.

ETHICS STATEMENT

This study was approved by the ethics committee of The second Affiliated Hospital of Zhejiang University, School of Medicine. The patients/participants provided their written informed consent to participate in this study.

AUTHOR CONTRIBUTIONS

WG, XW and SZ: drafted the manuscript. YF: acquisition of data. SZ: analysis or interpretation of data. CL, YH and WY: study concept and design. SZ and CL: help to revise the whole framework and polish the language.

FUNDING

This work was supported by the National Natural Science Foundation of China (grant number 81801162), the Zhejiang Provincial Natural Science Foundation of China (grant number LGF22H090020) and the Medical Health Science and Technology Project of Zhejiang Provincial Health Commission (grant number 2022KY600).

SUPPLEMENTARY MATERIAL

The Supplementary Material for this article can be found online at: https://www.frontiersin.org/articles/10.3389/fonc.2021.735778/full#supplementary-material

Supplementary Figure S1 | NP volume measurement on the first day and the fourth day after endoscopic transsphenoidal surgery. This is a case of 45-year-old male diagnosed with tuberculum sellae meningioma. **(A)** On the first day after operation, a small amount of CT pneumocephalus was found, which was 2.1ml. **(B)** On the fourth day after operation, CT scan showed increased pneumocephalus volume, which was 23.7ml. Cerebrospinal fluid rhinorrhea was confirmed on the sixth day after operation. The red area represents the pneumocephalus.

REFERENCES

1. Ivan ME, Iorgulescu JB, El-Sayed I, McDermott MW, Parsa AT, Pletcher SD, et al. Risk Factors for Postoperative Cerebrospinal Fluid Leak and Meningitis After Expanded Endoscopic Endonasal Surgery. *J Clin Neurosci* (2015) 22 (1):48–54. doi: 10.1016/j.jocn.2014.08.009
2. Psaltis AJ, Schlosser RJ, Banks CA, Yawn J, Soler ZM. A Systematic Review of the Endoscopic Repair of Cerebrospinal Fluid Leaks. *Otolaryngol Head Neck Surg* (2012) 147(2):196–203. doi: 10.1177/0194599812451090
3. Banks CA, Palmer JN, Chiu AG, O'Malley BW Jr, Woodworth BA, Kennedy DW. Endoscopic Closure of CSF Rhinorrhea: 193 Cases Over 21 Years. *Otolaryngol Head Neck Surg* (2009) 140(6):826–33. doi: 10.1016/j.otohns.2008.12.060
4. Li M, Mao S, Tang R, Lin H, Li D, Ye H, et al. Delayed Diagnosis and Treatment of Cerebrospinal Fluid Leakage in Current Practice. *J Craniofac Surg* (2019) 30(6):1657–61. doi: 10.1097/SCS.0000000000005402
5. Majhi S, Sharma A. Outcome of Endoscopic Cerebrospinal Fluid Rhinorrhoea Repair: An Institutional Study. *Indian J Otolaryngol Head Neck Surg* (2019) 71 (1):76–80. doi: 10.1007/s12070-018-1485-2
6. Illing E, Chaaban MR, Riley KO, Woodworth BA. Porcine Small Intestine Submucosal Graft for Endoscopic Skull Base Reconstruction. *Int Forum Allergy Rhinol* (2013) 3(11):928–32. doi: 10.1002/alr.21206
7. Ismail AS, Costantino PD, Sen C. Transnasal Transsphenoidal Endoscopic Repair of CSF Leakage Using Multilayer Acellular Dermis. *Skull Base* (2007) 17(2):125–32. doi: 10.1055/s-2007-970556
8. McCormack B, Cooper PR, Persky M, Rothstein S. Extracranial Repair of Cerebrospinal Fluid Fistulas: Technique and Results in 37 Patients. *Neurosurgery* (1990) 27(3):412–7. doi: 10.1097/00006123-199009000-00012
9. Saafan ME, Albirmawy OA, Tomoum MO. Sandwich Grafting Technique for Endoscopic Endonasal Repair of Cerebrospinal Fluid Rhinorrhoea. *Eur Arch Otorhinolaryngol* (2014) 271(5):1073–9. doi: 10.1007/s00405-013-2674-y
10. Sinha P, Desai SC, Ha DH, Chicoine MR, Haughey BH. Extracranial Radial Forearm Free Flap Closure of Refractory Cerebrospinal Fluid Leaks: A Novel Hybrid Transantral-Endoscopic Approach. *Neurosurgery* (2012) 71(2 Suppl Operative):ons219–25; discussion ons225–6. doi: 10.1227/NEU.0b013e3182684ac8
11. Shelesko EV, Kravchuk AD, Kapitanov DN, Chernikova NA, Zinkevich DN. Sovremennyĭ Podkhod K Diagnostike Nazal'noĭ Likvorei A Modern Approach to the Diagnosis of Nasal Liquorrhea. *Zh Vopr Neirokhir Im N N Burdenko* (2018) 82(3):103–11. doi: 10.17116/neiro2018823103
12. Zapalac JS, Marple BF, Schwade ND. Skull Base Cerebrospinal Fluid Fistulas: A Comprehensive Diagnostic Algorithm. *Otolaryngol Head Neck Surg* (2002) 126(6):669–76. doi: 10.1067/mhn.2002.125755
13. Meco C, Oberascher G. Comprehensive Algorithm for Skull Base Dural Lesion and Cerebrospinal Fluid Fistula Diagnosis. *Laryngoscope* (2004) 114 (6):991–9. doi: 10.1097/00005537-200406000-00007
14. Oakley GM, Alt JA, Schlosser RJ, Harvey RJ, Orlandi RR. Diagnosis of Cerebrospinal Fluid Rhinorrhea: An Evidence-Based Review With Recommendations. *Int Forum Allergy Rhinol* (2016) 6(1):8–16. doi: 10.1002/alr.21637
15. Mantur M, Łukaszewicz-Zając M, Mroczko B, Kułakowska A, Ganslandt O, Kemona H, et al. Cerebrospinal Fluid Leakage-Reliable Diagnostic Methods. *Clin Chim Acta* (2011) 412(11–12):837–40. doi: 10.1016/j.cca.2011.02.017
16. Lai LT, Trooboff S, Morgan MK, Harvey RJ. The Risk of Meningitis Following Expanded Endoscopic Endonasal Skull Base Surgery: A Systematic Review. *J Neurol Surg B Skull Base* (2014) 75(1):18–26. doi: 10.1055/s-0033-1353365
17. Karavelioglu E, Eser O, Haktanir A. Pneumocephalus and Pneumorrhachis After Spinal Surgery: Case Report and Review of the Literature. *Neurol Med Chir (Tokyo)* (2014) 54(5):405–7. doi: 10.2176/nmc.cr2013-0118
18. Ozturk E, Kantarci M, Karaman K, Basekim CC, Kizilkaya E. Diffuse Pneumocephalus Associated With Infratentorial and Supratentorial Hemorrhages as a Complication of Spinal Surgery. *Acta Radiol* (2006) 47 (5):497–500. doi: 10.1080/02841850600644766
19. Daele JJ, Goffart Y, Machiels S. Traumatic, Iatrogenic, and Spontaneous Cerebrospinal Fluid (CSF) Leak: Endoscopic Repair. *B-ENT* (2011) 7(Suppl 17):47–60.
20. Guo K, Heng L, Zhang H, Ma L, Zhang H, Jia D. Risk Factors for Postoperative Intracranial Infections in Patients With Pituitary Adenoma After Endoscopic Endonasal Transsphenoidal Surgery: Pneumocephalus Deserves Further Study. *Neurosurg Focus* (2019) 47(2):E5. doi: 10.3171/2019.5
21. Strickland BA, Lucas J, Harris B, Kulubya E, Bakhsheshian J, Liu C, et al. Identification and Repair of Intraoperative Cerebrospinal Fluid Leaks in Endonasal Transsphenoidal Pituitary Surgery: Surgical Experience in a Series of 1002 Patients. *J Neurosurg* (2018) 129(2):425–9. doi: 10.3171/2017.4.JNS162451
22. Horowitz G, Fliss DM, Margalit N, Wasserzug O, Gil Z. Association Between Cerebrospinal Fluid Leak and Meningitis After Skull Base Surgery. *Otolaryngol Head Neck Surg* (2011) 145(4):689–93. doi: 10.1177/0194599811411534
23. Grotenhuis JA. Costs of Postoperative Cerebrospinal Fluid Leakage: 1-Year, Retrospective Analysis of 412 Consecutive Nontrauma Cases. *Surg Neurol* (2005) 64(6):490–3, discussion 493–4. doi: 10.1016/j.surneu.2005.03.041
24. Giovanni S, Della Pepa GM, La Rocca G, Lofrese G, Albanese A, Maria G, et al. Galea-Pericranium Dural Closure: Can We Safely Avoid Sealants? *Clin Neurol Neurosurg* (2014) 123:50–4. doi: 10.1016/j.clineuro.2014.05.005
25. Green AL, Arnaud A, Batiller J, Eljamel S, Gauld J, Jones P, et al. A Multicentre, Prospective, Randomized, Controlled Study to Evaluate the Use of a Fibrin Sealant as an Adjunct to Sutured Dural Repair. *Br J Neurosurg* (2015) 29(1):11–7. doi: 10.3109/02688697.2014.948808
26. Bernal-Sprekelsen M, Alobid I, Mullol J, Trobat F, Tomás-Barberán M. Closure of Cerebrospinal Fluid Leaks Prevents Ascending Bacterial Meningitis. *Rhinology* (2005) 43(4):277–81.
27. Lunsford LD, Maroon JC, Sheptak PE, Albin MS. Subdural Tension Pneumocephalus. Report of Two Cases. *J Neurosurg* (1979) 50(4):525–7. doi: 10.3171/jns.1979.50.4.0525
28. Biju RD, Wu J, Hussain Z. Tension Pneumocephalus After Skull Base Surgery. A Case Report and Review of Literature. *J Clin Neurosci* (2020) 75:218–20. doi: 10.1016/j.jocn.2020.03.041
29. Turgut M, Akyüz O. Symptomatic Tension Pneumocephalus: An Unusual Post-Operative Complication of Posterior Spinal Surgery. *J Clin Neurosci* (2007) 14(7):666–8. doi: 10.1016/j.jocn.2006.02.021
30. Guo X, Zhu Y, Hong Y. Efficacy and Safety of Intraoperative Lumbar Drain in Endoscopic Skull Base Tumor Resection: A Meta-Analysis. *Front Oncol* (2020) 10:606. doi: 10.3389/fonc.2020.00606
31. Van Gerven L, Qian Z, Starovoyt A, Jorissen M, Meulemans J, van Loon J, et al. Endoscopic, Endonasal Transsphenoidal Surgery for Tumors of the Sellar and Suprasellar Region: A Monocentric Historical Cohort Study of 369 Patients. *Front Oncol* (2021) 11:643550. doi: 10.3389/fonc.2021.643550
32. Schievink WI, Meyer FB, Atkinson JL, Mokri B. Spontaneous Spinal Cerebrospinal Fluid Leaks and Intracranial Hypotension. *J Neurosurg* (1996) 84(4):598–605. doi: 10.3171/jns.1996.84.4.0598

Conflict of Interest: The authors declare that the research was conducted in the absence of any commercial or financial relationships that could be construed as a potential conflict of interest.

frontiers in Oncology

ORIGINAL RESEARCH
published: 20 January 2022
doi: 10.3389/fonc.2021.807040

Radiological Knosp, Revised-Knosp, and Hardy–Wilson Classifications for the Prediction of Surgical Outcomes in the Endoscopic Endonasal Surgery of Pituitary Adenomas: Study of 228 Cases

Marta Araujo-Castro[1,2], Alberto Acitores Cancela[3], Carlos Vior[3], Eider Pascual-Corrales[1] and Víctor Rodríguez Berrocal[3,4]*

[1] Neuroendocrinology Unit, Department of Endocrinology & Nutrition, Hospital Universitario Ramón y Cajal & Instituto de Investigación Biomédica Ramón y Cajal (IRYCIS), Madrid, Spain, [2] Department of Medicine, Universidad de Alcalá de Henares, Madrid, Spain, [3] Department of Neurosurgery, Hospital Universitario Ramón y Cajal, Madrid, Spain, [4] Department of Neurosurgery, Hospital HM Puerta del Sur, Madrid, Spain

Purpose: To evaluate which radiological classification, Knosp, revised-Knosp, or Hardy–Wilson classification, is better for the prediction of surgical outcomes in the endoscopic endonasal transsphenoidal (EET) surgery of pituitary adenomas (PAs).

Methods: This is a retrospective study of patients with PAs who underwent EET PA resection for the first time between January 2009 and December 2020. Radiological cavernous sinus invasiveness was defined as a Knosp or revised-Knosp grade >2 or a grade E in the Hardy–Wilson classification.

Results: A total of 228 patients with PAs were included. Cavernous sinus invasion was evident in 35.1% and suprasellar extension was evident in 74.6%. Overall, surgical cure was achieved in 64.3% of patients. Surgical cure was lower in invasive PAs than in non-invasive PAs (28.8% vs. 83.1%, $p < 0.0001$), and the risk of major complications was higher (13.8% vs. 3.4%, $p = 0.003$). The rate of surgical cure decreased as the grade of Knosp increased ($p < 0.001$), whereas the risk of complications increased ($p < 0.001$). Patients with Knosp 3B PAs tended to achieve surgical cure less commonly than Knosp 3A PAs (30.0% vs. 56.0%, $p = 0.164$). Similar results were observed based on the invasion and extension of Hardy–Wilson classification (stage A–C 83.1% vs. E 28.8% $p < 0.0001$, grade 0–II 81.1% vs. III–IV 59.7% $p = 0.008$). The Knosp classification offered the greatest diagnostic accuracy for the prediction of surgical cure (AUC 0.820), whereas the invasion Hardy–Wilson classification lacked utility for this purpose (AUC 0.654).

OPEN ACCESS

Edited by:
Zhe Bao Wu, Shanghai Jiao Tong University, China

Reviewed by:
Matteo Zoli, IRCCS Institute of Neurological Sciences of Bologna (ISNB), Italy
Teresa Somma, Federico II University Hospital, Italy

***Correspondence:**
Marta Araujo-Castro
marta.araujo@salud.madrid.org
orcid.org/0000-0002-0519-0072

Specialty section:
This article was submitted to Neuro-Oncology and Neurosurgical Oncology, a section of the journal Frontiers in Oncology

Received: *01 November 2021*
Accepted: *08 December 2021*
Published: *20 January 2022*

Citation:
Araujo-Castro M, Acitores Cancela A, Vior C, Pascual-Corrales E and Rodríguez Berrocal V (2022) Radiological Knosp, Revised-Knosp, and Hardy–Wilson Classifications for the Prediction of Surgical Outcomes in the Endoscopic Endonasal Surgery of Pituitary Adenomas: Study of 228 Cases. Front. Oncol. 11:807040. doi: 10.3389/fonc.2021.807040

Conclusion: The Knosp classifications offer a good orientation for the estimation of surgical cure and the risk of complications in patients with PAs submitted to EET surgery. However, the invasion Hardy–Wilson scale lacks utility for this purpose.

Keywords: pituitary adenomas, invasive pituitary adenomas, Knosp classification, Hardy-Wilson classification, endoscopic endonasal transsphenoidal surgery

INTRODUCTION

Pituitary surgery aims to eliminate excess hormone production in functioning pituitary adenomas (PAs), avoid or ameliorate tumor mass effects, preserve both pituitary function and adjacent nerve structures, and eliminate or reduce the risk of future recurrences (1). Nevertheless, the operative approach of PAs is guided by the size and location of the tumor and its relation to surrounding anatomical structures. This way, invasion of cavernous sinus is a known limiting factor in the achievement of complete surgical resection and could lead to a higher risk of postoperative surgical complications (2–4). Pre-surgical information about status of cavernous sinus invasion and the invasion of other parasellar structures is a key factor to planning surgery and for the estimation of the chances of surgical cure in PAs.

The earliest universally accepted, radiographic and operative classification of local invasion was proposed by Hardy et al. in 1976 (5) and later modified by Wilson in 1979 to distinguish between different grades of extrasellar extension (6). In 1993, Knosp et al. described the classical radiological classification of cavernous sinus invasion based on the relations of the PAs with the line between the supraclinoid internal carotid artery (ICA) and intra-cavernous ICA on coronal magnetic resonance imaging (MRI) (7). Several studies have found that the Knosp grade is a good predictor of surgical outcomes (4, 8, 9). Later studies have found that the revised-Knosp classification (3), which includes the differentiation between superior or inferior cavernous sinus compartment invasion in grades 3A and 3B, provides a better prediction of gross total resection and endocrine remission in functioning PAs (10). However, to the best of our knowledge, no previous studies have compared the Hardy–Wilson, Knosp, and revised-Knosp classifications for the prediction of surgical cure and complications in PA surgery and analyzed the correlation of these radiological scales with histological findings.

The aim of our study was to evaluate whether the radiological Knosp, revised-Knosp, and Hardy–Wilson classifications are good predictors of surgical outcomes in PAs, and which of these classifications have a greater predictive value for this purpose. Moreover, we have evaluated the correlation of these radiological classifications with histological findings. This information could be useful for surgical planning and for the estimation of the chances of surgical cure in PAs.

METHODS

Patients

A retrospective, two-center study was conducted. A total of 309 pituitary surgeries of patients with pituitary tumors operated between January 2009 and December 2020 at the Department of Neurosurgery of the Hospital Universitario Ramón y Cajal (HURC) and Hospital Universitario HM Puerta del Sur (HUPS) were identified. Clinical and radiological information was collected retrospectively between 2009 and 2012 (n = 45) and prospectively since January 2012 (n = 264). Inclusion criteria in the present study were as follows: (1) patients with available information about preoperative clinical, hormonal, and radiological data, and (2) pathology reports confirming PA diagnosis. Patients with Rathke's cysts, craniopharyngioma, or pituicytoma diagnosis (n = 44), operated previously by the same or other neurosurgeons (n = 37), or operated by other neurosurgeons (n = 27) were excluded. A total of 228 patients met inclusion criteria and were enrolled (**Figure 1**). The local Ethical Committee of the HURC and HUPS reviewed and approved this study (approval date: October 4, 2019, code: ACTA 372).

Clinical and Hormonal Evaluation

The following demographic and clinical variables were included in our pituitary database: age, sex, diabetes mellitus, obesity, cardiovascular disease, hypertension, headache, visual impairment, and symptoms or signs of hypopituitarism, due to hormonal excess production. Visual involvement was defined as the presence of any degree of visual acuity compromise, from mild to severe visual acuity involvement and from partial to complete field conditions (9).

Hormonal assessment included preoperative measurement of 8am serum cortisol, ACTH, thyroid-stimulating hormone (TSH), free thyroxine (FT4), prolactin, follicle-stimulating hormone (FSH), luteinizing hormone (LH), insulin-like growth factor-1 (IGF-1), and total and free testosterone in males, as we have previously described (9). In those patients with 8am serum cortisol between 5 and 18 μg/dl, a 250-μg ACTH stimulating test was performed. The definitions of each pituitary hormone deficit were defined as we have previously described (11).

Biochemical cure was defined as normalization of urinary free cortisol in Cushing's disease (12), as IGF-1 level in age- and sex-adjusted normal range and random GH value <2.5 ng/ml or GH value <1 ng/ml during an oral glucose tolerance test (OGTT) (13), as normalization of prolactin levels in prolactinoma, and as FT4 and FT3 normal levels in TSH-secreting PAs.

Radiological Evaluation

Radiological evaluation was performed using an MRI of 1.5 T, GE 450w following our pituitary tumors protocol (1). The latero-lateral and craniocaudal diameters were assessed. PAs with maximum PA diameter <10, ≥10, ≥30 and <40, and ≥40 mm were defined as microadenomas, macroadenomas, very large, and giant PAs, respectively.

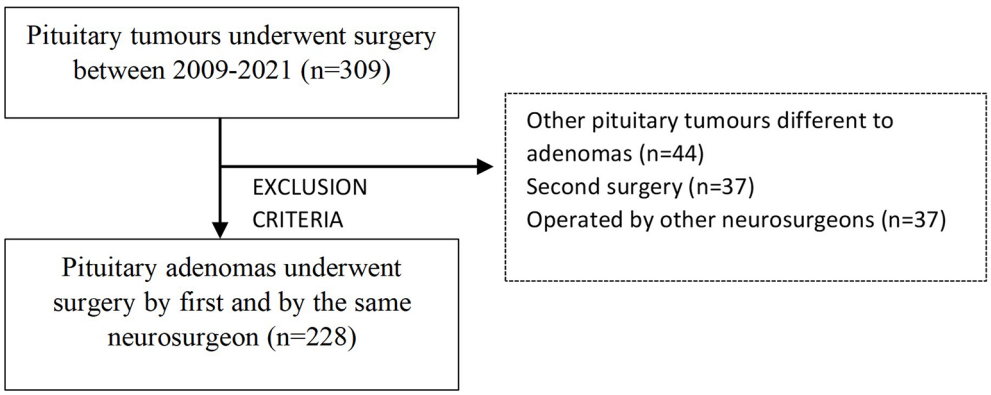

FIGURE 1 | Study population.

The Hardy–Wilson classification considered the degree of sellar destruction (grade) and extrasellar extension (stage) (14). Sellar destruction was divided into the following: Grade 0 when the enclosed adenoma is described as a tumor that remains within the anatomical confines of the osteoaponeural sheath of the sella turcica; Grade I: the sella turcica is within normal limits in size or focally expanded and the tumor is <10 mm; Grade II: tumor ≥ 10 mm and the sella turcica is enlarged but the floor remains intact; Grade III: a local erosion or destruction of the floor; Grade IV when the entire floor of the sella is diffusely eroded or destroyed, giving a characteristic "phantom sella" with all the boundaries barely visible. Extrasellar extension according to the Hardy–Wilson modified scale is divided into stage 0, with no suprasellar extension, A–C for progressive suprasellar extension (A: occupying cistern, B: recess of third ventricle obliterated, and C: third ventricle grossly displaced), and D–E grading parasellar extension (D: intracranial extension and E: cavernous sinus extension) (**Figure 2**).

Cavernous sinus invasion was evaluated using the Knosp–Steiner classification based on coronal T1-weighted contrasted imaging (15): Knosp 0 when PA is medial to medial tangent; Knosp 1 if PA extends to the space between the medial tangent and the intercarotid line; Knosp 2 when PA extends to the space between the intercarotid line and the lateral tangent; Knosp 3 if PA extends lateral to the lateral tangent; and Knosp 4 with a complete encasement of intracavernous ICA. Knosp score 3–4 were considered as invasive PA. Moreover, radiological reports were reviewed to include the revised-Knosp classification (3, 5). The revised-Knosp classification includes 2 subtypes of grade 3: Knosp 3A when PA is above the intracavernous ICA into the superior cavernous sinus compartment and Knosp 3B when PA is below the intracavernous ICA into the inferior cavernous sinus compartment (**Figures 2** and **3**).

The extent of tumor resection (EOR) was classified into total (100%) or subtotal 70%–100% based on the 3–6 months postoperative MRI. Surgical cure is defined as total EOR in non-functioning PAs and by biochemical remission in functioning PAs.

Surgical and Histological Evaluation

Pituitary surgery was performed by an experienced endoscopic pituitary surgeon (VB) with more than 300 endoscopic pituitary surgeries performed and an average of 35 pituitary surgeries/year in two high-volume centers (RyCUH and HMPSUH) during the last 10 years. The Endonasal Endoscopic Approach (EEA) was used in all surgeries included in this series. The approach included a binarial four-hand technique with wide anterior sphenoidotomy and partial posterior septectomy. In the cases with cavernous sinus invasion, an extended approach was performed. The macroscopic variables analyzed during pituitary surgery were tumor consistency (tumors difficult to remove with ring curettes and tumors that required sharp dissection, bipolar cautery, and/or surgical aspirator were termed hard tumors; the easily suckable were classified as soft tumors) and macroscopic information about dural, periosteal, or mucosal tissue invasion (defined as macroscopic invasiveness data). Complications have been divided into major [intrasellar bleeding (intra- or postoperative) requiring surgery, CSF fistula, meningitis, visual impairment with previously normal vision, new focal neurological deficit, carotid injury, stroke, or death] and minor (presence of diabetes insipidus, loss of the anterior pituitary hormonal axis, and medical complication).

The histological features evaluated were pituitary hormone immunostaining [ACTH, Prolactin and LH (polyclonal, Ventana), GH (clone A0570, Dako), TSH (clone 0042, Dako) and FSH (clone C10, Dako)] and the proliferation index based on Ki67 immunoexpression (clone MIB-1, Dako). Histological invasiveness was defined as invasion of sinus mucosa or adjacent bone in histopathologic sections.

Statistical Analysis

The statistical analysis was performed using STATA.15. In the descriptive analysis, categorical variables were expressed as percentages and (absolute values of variable) quantitative variables were expressed as mean ± standard deviation. The normality assumption was studied with Shapiro–Wilk test. Student's *t*-test was performed accordingly to compare

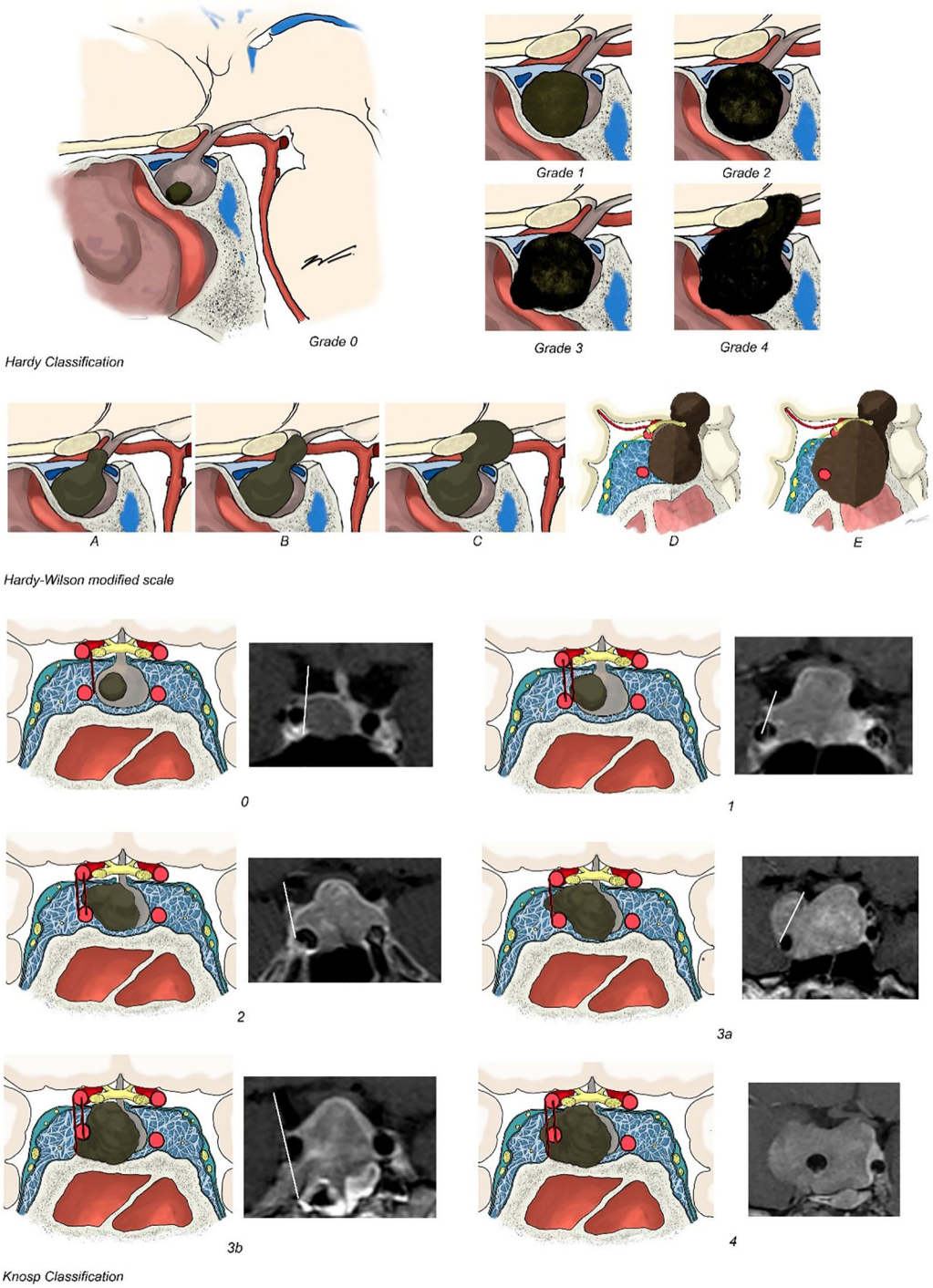

FIGURE 2 | Hardy–Wilson and Knosp classifications. Hardy–Wilson classification considered the degree of sellar destruction: Grade 0 when the adenoma remains within the anatomical confines of the osteoaponeural sheath of the sella turcica; Grade I: the sella turcica is within normal limits in size or focally expanded and the tumor is <10 mm; Grade II: tumor ≥ 10 mm and the sella turcica is enlarged but the floor remains intact; Grade III: a local erosion or destruction of the floor; Grade IV when the entire floor of the sella is diffusely eroded or destroyed. Extrasellar extension according to Hardy–Wilson is divided in stage 0, with no suprasellar extension, A–C for progressive suprasellar extension. Knosp–Steiner classification considered: Knosp 0 when PA is medial to medial tangent; Knosp 1 if PA extends to the space between the medial tangent and the intercarotid line; Knosp 2 when PA extends to the space between the intercarotid line and the lateral tangent; Knosp 3 if PA extends lateral to the lateral tangent; and Knosp 4 with a complete encasement of intracavernous ICA. Knosp score 3–4 were considered as invasive PA. The revised-Knosp classification includes Knosp 3A when PA is above the intracavernous ICA into the superior cavernous sinus compartment and Knosp 3B when PA is below the intracavernous ICA into the inferior cavernous sinus compartment.

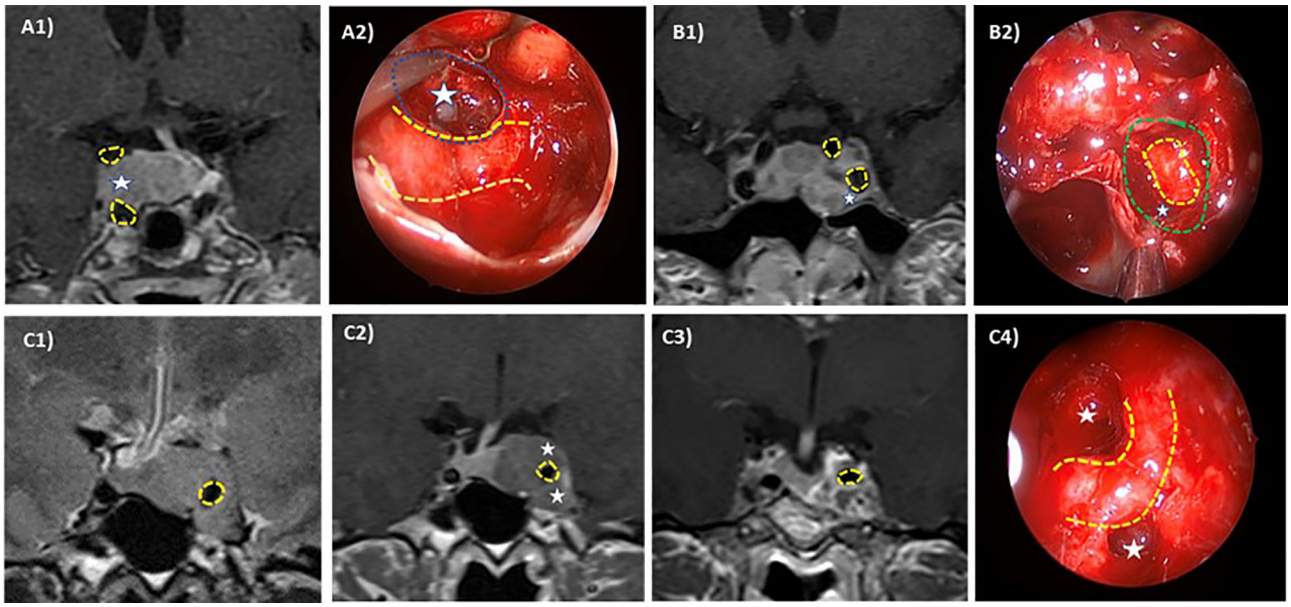

FIGURE 3 | Intraoperative–radiologic correlation of cavernous sinus invasion in pituitary adenomas. ICA is highlighted in yellow dotted line and differently affected CS compartments are pointed out (white stars). Case 1: Right superior compartment invasion of the cavernous sinus (Knosp 3A) in an acromegalic patient. Preoperative MRI **(A1)** and intraoperative view through a 45° endoscope **(A2)** after tumor resection (left cavernous sinus medial wall resected in blue dotted line). The patient was cured after surgery. Case 2: Left Inferior compartment invasion of the CS in a resistant prolactin-secreting PA (Knosp 3B). Preoperative MRI **(B1)** and intraoperative view through a 0° endoscope **(B2)** after tumor resection showing anterior CS wall resection (green dotted line). Case 3: Complete cavernous sinus invasion (Knosp 4) in an acromegalic patient. Preoperative MRI in T2 sequences **(C1, C2)** shows a complete ICA encasement and the postoperative coronal MRI **(C3)** shows a near total resection. Intraoperative view through a 45° endoscope **(C4)** after tumor resection showing ICA and superior and inferior compartment. No surgical cure was achieved.

differences in continuous parameters between two subgroups. The Chi-squared test was applied to compare categorical variables between independent samples. Kappa kohen index was used to evaluate the reliability between both classifications. ROC curves were performed to calculate the best predictive grade in the Knosp and Hardy classifications for surgical cure. The significance level was set at $p < 0.05$.

RESULTS

Baseline Characteristics

In the last 11 years, 228 patients with PAs underwent transsphenoidal endoscopic endonasal PA resection for the first time by the senior author (VB). Non-functioning PAs represent 61.4% (n = 140) of the cohort, 22.4% (n = 51) had acromegaly, 11.0% (n = 25) Cushing's disease, 4.8% (n = 11) prolactinoma, and one patient had a TSH-secreting PA. Forty patients were medically treated before surgery (8 patients with prolactinoma and 1 patient with acromegaly were treated with dopamine agonist, 24 patients with acromegaly were treated with somatostatin analogues, and 7 patients with Cushing's disease were treated with adrenal steroidogenesis inhibitors (ketoconazole and/or metyrapone)], and no patients had a history of previous pituitary radiotherapy. Baseline patient's characteristics are reported in **Table 1**.

Pre-Surgical Variables Associated With Radiological Invasiveness

Based on Knosp and extension Hardy classifications (stage), 35.1% (n = 80) presented cavernous sinus invasion. The Knosp grade distribution was as follows: grade 0 in 22.8% (n = 52), grade 1 in 15.4% (n = 35), grade 2 in 26.8% (n = 61), grade 3 in 16.2% (n = 37), and grade 4 in 18.9% (n = 43). Among the Knosp grade 3, 25 were grade 3A and 10 grade were 3B (in 2 patients, the images were not available for the classification in Knosp 3A and 3B) (**Figure 3**). Patients with invasive PAs presented larger tumors, which caused visual manifestations more commonly than non-invasive PAs (**Table 2**). Nevertheless, the higher prevalence of visual involvement in invasive PAs was related with their higher tumor size [adjusted OR: 1.0 (0.5–2.2)]. According to the Hardy invasion classification (n = 173), 5 were grade 0, 1 grade I, 38 grade II, 102 grade III, and 27 grade IV. Based on the Hardy extension classification, 148 were stage A–C (suprasellar extension) and 80 were stage E; 11 patients had intracranial extension of the PA although they were all considered grade E because of concomitant cavernous sinus invasion. As expected, when considered as dichotomic scales (Knosp 0–2 vs. 3–4 and Hardy stage A–C vs. E), there was an excellent accordance between the Knosp and extension Hardy classifications (kappa 1.00, global agreement 100%).

TABLE 1 | Patient and tumor characteristics of the study cohort at diagnosis.

Characteristic	Value
Age (years)	52.9 ± 15.4
Female sex	52.2% (*n* = 119)
Diabetes mellitus	13.2% (*n* = 30)
High blood pressure	30.7% (*n* = 70)
Obesity	10.5% (*n* = 24)
Heart disease	8.3% (*n* = 19)
Sleep apnea syndrome	7.9% (*n* = 18)
Headache	22.8% (*n* = 52)
Visual involvement	34.7% (*n* = 79)
Pituitary apoplexy	6.6% (*n* = 15)
Hypopituitarism	37.3% (*n* = 85)
Macroadenomas	86.3% (*n* = 196)
Knosp grade > 2/Hardy stage E	35.1% (*n* = 80)
Hardy grade > II (*n* = 173)	74.6% (*n* = 129)
Cranio-caudal diameter (mm)	20.7 ± 12.3
Latero-lateral diameter (mm)	19.0 ± 10.0
Total tumor resection in non-functioning PAs	69.3% (*n* = 88)
Biochemical cure in functioning PAs	65.9% (*n* = 58)
Postoperative permanent diabetes insipidus	4.8% (*n* = 11)
Cerebrospinal fluid leakage	5.3% (*n* = 12)
Postoperative new anterior pituitary deficits	13.3% (*n* = 19)
Hard consistency (*n* = 218)	28.9% (*n* = 63)

Invasion Hardy classification (sella destruction) was available only in 173 patients.

Knosp and Hardy Classifications: Correlation With Histological Invasiveness and Tumor Consistency

A clear association between the radiological Knosp and extension Hardy classifications and pathological invasiveness examination was found, as 7.6% of the Knosp 3–4 or stage E PAs had histological invasion compared to only one case of the non-invasive PAs (p = 0.004). Moreover, invasive PAs were more commonly of hard consistency than non-invasive PAs (**Table 2**).

Knosp, Modified Knosp, and Hardy–Wilson Classifications: Impact on Surgical Outcomes

Overall, surgical cure was achieved in 64.3% of the patients: complete surgical resection in 69.3% (n = 88) of non-functioning PA and biochemical remission in 65.9% (n = 58) of functioning PAs (80% of Cushing's disease, 66.7% of acromegaly, and 27.3% of prolactinomas and in the TSHoma). Complete surgical resection in non-functioning PAs and biochemical cure in functioning PAs were significantly higher in Knosp 0–2/Hardy stage A–C PAs than in Knosp 3–4/Hardy stage D–E PAs. Moreover, the risk of major complications and CSF leakage was lower in the group of non-invasive tumors (**Table 3** and **Figure 4**). No differences in the rate of surgical cure were observed between stage A and B (87.5% vs. 100%, p = 0.166), but patients of stage B achieved surgical cure more commonly than stage C patients (100% vs. 71.4%, p = 0.031). The rate of surgical complications was similar in stage A, B, and C (0%, 7.1% and 0%, $p > 0.05$). The higher risk chance of non-cure in radiological invasive PAs was independent of the tumor size [adjusted OR: 9.7 (4.7–20.2)], but the higher risk of major complications was related with the higher tumor size in these invasive PAs [adjusted OR: 2.0 (0.5–8.3)]. The overall rate of surgical cure decreased as the Knosp grade increased [MH Test for linear Trend: χ^2 = 66.8 ($p < 0.001$)], whereas the risk of complications increased [MH Test for linear Trend: $\chi^2(1)$ = 12.3 ($p < 0.001$)] (**Table 4** and **Figure 4**). A tendency to a lower rate of surgical remission was observed in Knosp 3B compared to 3A (30.0% vs. 56.0%, p = 0.164). Similar results were observed based on the invasion Hardy classification as 81.8% of Hardy 0–II vs. 59.7% in Hardy III–IV (p = 0.008) achieved surgical cure. Nevertheless, these differences disappeared after adjusting by tumor size [adjusted OR: 1.5 (0.6–3.8)] (**Table 5**). When comparing Hardy 0–III vs. IV, similar results were observed regarding surgical cure (70.6% vs. 37.0%, p = 0.001). However, in this case, the higher chance of surgical cure in grade 0–III persisted after adjusting by tumor size [adjusted OR: 2.8 (1.1–7.1)] (**Figure 4**). We found that the Knosp classifications considered as continuous scales (from grade 0 to 4) offered a greater diagnostic accuracy for the prediction of surgical cure [AUC 0.820 [0.760–0.879)], with the Knosp 3 and Knosp 3A being the ones that best predicted surgical failure (sensitivity 70.4%, specificity 84.2%). The AUC of the extension Hardy classification (grade A–C vs. grade D–E) was lower [AUC 0.769 [0.707–0.821)], especially the invasion Hardy classification (from I to IV) [AUC 0.654 [0.580–0.728)] (**Figure 5**).

TABLE 2 | Differences in clinical, hormonal, radiological, and histological features of invasive and non-invasive pituitary adenomas.

Variable	Knosp and extension Hardy classifications		
	Knosp ≤ 2/Hardy A–C (*n* = 148)	Knosp > 2/Hardy E (*n* = 80)	*p*-value
Age (years)	52.5 ± 15.3	53.5 ± 15.6	0.628
Female sex	54.7%	47.5%	0.297
Headache	19.6%	28.8%	0.116
Visual defect	24.3%	53.8%	<0.0001
L-L diameter	14.9 ± 7.4	26.5 ± 9.7	<0.0001
C-C diameter	16.2 ± 9.4	29.3 ± 12.7	<0.0001
Hormonal deficit	19.6%	21.3%	0.766
Functioning PA	41.9%	32.5%	0.164
Histological invasion	0.7% (*n* = 1)	7.5% (*n* = 6)	0.004
Hard consistency	23.6% (*n* = 33)	38.5% (*n* = 30)	0.020
Ki67 > 4%	7.4% (*n* = 11)	12.5% (*n* = 10)	0.207

L-L diameter, latero-lateral diameter; C-C diameter, cranio-caudal diameter; PA, pituitary adenoma.

TABLE 3 | Surgical outcomes according to cavernous sinus invasion based on Knosp and revised-Knosp classifications.

Variable	Knosp classification			Revised-Knosp classification		
	Knosp ≤ 2 (*n* = 148)	Knosp > 2 (*n* = 80)	*p*-value	Knosp 3A (*n* = 25)	Knosp 3B (*n* = 10)	*p*-value
Complete resection of NFPA	80.2% (69/86)	31.9% (19/54)	<0.0001	68.8% (11/16)	33.3% (3/9)	0.087
Biochemical cure of FPA	87.1% (54/62)	15.4% (4/26)	<0.0001	33.3% (3/9)	0% (0/1)	0.490
New hormonal deficits	10.3% (10/97)	20.0% (9/46)	0.115	16.7% (2/12)	12.5% (1/8)	0.798
Permanent DI	4.7% (7/148)	5.0% (4/80)	0.911	0% (0/25)	10% (1/10)	0.109
Any major complication	3.4% (5/148)	13.8% (11/80)	0.003	8.0% (2/25)	10.0% (1/10)	0.849
CSF leakage	2.7% (4/148)	10.0% (8/80)	0.017	4.0% (1/25)	10.0% (1/10)	0.490
Tumor recurrence	6.1% (9/148)	5.0% (4/80)	0.913	8.0% (2/25)	0% (0/10)	0.357

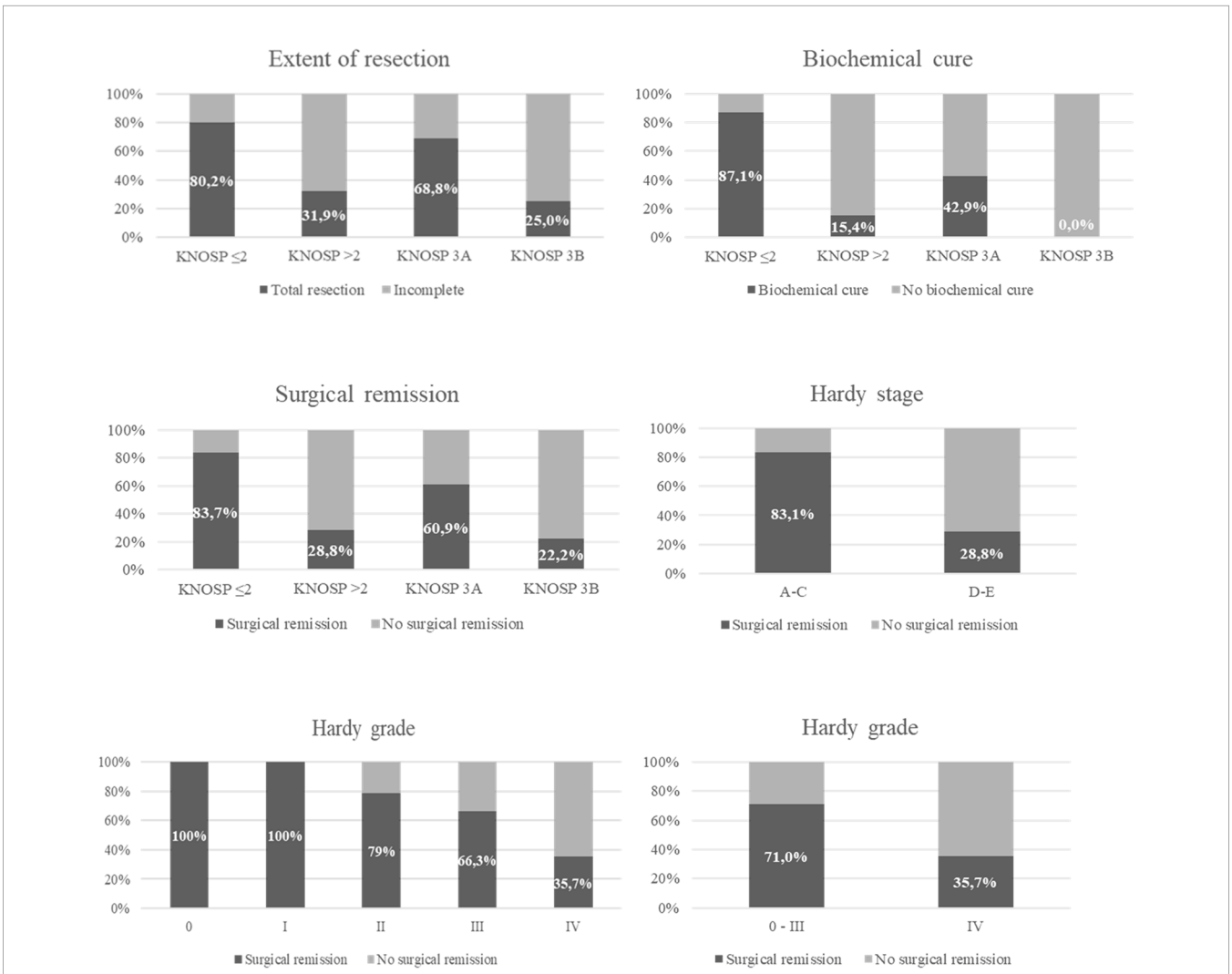

FIGURE 4 | Surgical remission in functioning pituitary adenomas and total resection in non-functioning pituitary adenomas based on Knosp and Hardy classifications.

DISCUSSION

Since the standardization of the transsphenoidal approach and the use of a surgical microscope in this approach by Jules Hardy in 1968 (15–17), attempts were performed to predict the resectability of pituitary tumors through this approach, based on their preoperative radiological image. The first attempt with great international acceptance was performed by Hardy himself, considering the characteristics of bone remodeling produced by these lesions in the imaging tests available at the time (x-ray and

TABLE 4 | Surgical outcome based on the Knosp and revised-Knosp classifications.

Knosp	Surgical remission	Major complications	Risk of non-cure, 95% CI (considering Knosp 0 as reference)
0	86.5% (45/52)	0% (0/52)	1
1	88.6% (31/35)	2.9% (1/35)	0.97 [0.25–3.72]
2	77.1% (47/61)	6.6% (4/61)	2.23 [0.79–6.32]
3	46.0% (17/37)	8.1% (3/37)	4.59 [2.05–10.31]
3A	56.0% (14/25)	8.0% (2/25)	5.89 [1.84–12.82]
3B	30.0% (3/10)	10.0% (1/10)	17.5 [3.54–86.54]
4	14.0% (6/43)	18.6% (8/43)	46.25 [13.76–155.46]
Total	64.3% (146/228)	7.0% (16/228)	

The chances of non-cure increased as the Knosp grade increased [MH Test for linear Trend: $\chi^2 = 73.1$ ($p = 0.0000$)].

TABLE 5 | Surgical outcome based on the invasion and extension Hardy classification.

	Surgical remission	Major complications
	Hardy invasion	
0	100% (5/5)	0% (0/5)
I	100% (1/1)	0% (0/1)
II	79.0% (30/38)	5.3% (2/38)
III	66.3% (67/101)	10.9% (11/101)
IV	35.7% (10/28)	7.1% (2/28)
	Hardy invasion	
A–D	83.1% (123/148)	3.4% (5/148)
E	28.8% (23/80)	13.8% (11/80)
Total	64.3% (146/228)	7.0% (16/228)

CT). He described four types of local invasion around the sella (visible on x-ray and CT), depending on whether it was more or less remodeled (18). He also added a staging for the suprasellar extension (17), which Wilson later modified (6).

It would not be until the 1980s when MRI was progressively introduced as a neuroimaging technique (19). So, together with a greater diffusion of the transsphenoidal approach, E. Knosp and others, intuiting that the main prognostic factor was the invasion of the cavernous sinus, proposed a new classification based solely on its degree of invasion, according to the MRI image characteristics (7). The Knosp classification is the most widely accepted and used, although the Hardy–Wilson classification continues to be cited and described on numerous occasions. Thanks to the most recent development and improvements in endoscopic techniques, which allow for a better visualization of the parasellar structures, several studies have correlated the intraoperative involvement of the medial wall of the cavernous sinus with the Knosp radiological classification (20, 21). Despite significant discrepancies involving the Knosp classification system for PAs and its correlation with the invasion observed intraoperatively (3, 22), no other pre-surgical classification has been validated to date, nor has it been shown to correlate better with surgical results and clinical prognosis than Knosp classification.

Cavernous sinus invasion is one of the most unfavorable features of PAs. The most widely used classification was proposed by Knosp in 1993 and revised in 2015. In accordance with the reported data in several previous series, we found that patients with PAs with invasion of the cavernous sinus, both based on the Knosp and extension Hardy–Wilson classifications, had a lower chance of surgical cure and a higher risk of surgical complications. However, the Knosp and revised-Knosp classifications were the best for the prediction of surgical failure, with an area under de ROC curve of 0.820, with the Knosp grade 3 and Knosp 3A being the ones that best predict surgical failure (sensitivity 70.4%, specificity 84.2%). Nevertheless, despite these findings, we observed that all the radiological classifications were poor predictors of histological invasiveness, as only 7.5% of radiological invasive PAs had histological invasion. This finding highlights the fact that surgical inspection remains the gold standard to predict cavernous sinus invasion and that Knosp or modified Knosp classification presents a relevant number of false positives, as it has been previously reported (23).

We found that 28.8% of invasive PAs based on Knosp and extension Hardy classifications achieved surgical remission. This is in accordance with the data reported by other authors (10, 24, 25). Buchy et al. showed that gross total resection was negatively correlated with Knosp grade, while rates were 55.8% for grade 3A and 30.0% for grade 3B (10). Similarly, Micko et al. (24) showed that grade 3A PAs have a significantly lower rate of invasiveness of the medial cavernous sinus wall than grade 3B and 4 adenomas. Furthermore, infiltration of and fibrous tumor texture within the space of the cavernous sinus were found more frequently in grades 3B and 4. Consequently, grade 3A adenomas had a higher rate of endocrine remission/gross total resection (64%) than grade 3B (33%, $p = 0.021$) and grade 4 (0%, $p < 0.001$) PAs (24). Therefore, parasellar adenoma growth should be classified into grades 3A, 3B, and 4 for prediction of adenoma invasion and surgical considerations and outcomes. Moreover, the differentiation in Knosp low-grade (grades 1 and 2) and high-grade (grades 3 and 4) adenomas is important since the rates of achievement of complete resection for Knosp high-grade tumors are poor in comparison to those for low-grade adenomas. Thus, PA volume and cavernous sinus invasion, classified with the Knosp and revised-Knosp scales, are tumor features that can be used as resection predictor variables in PA surgery (25). It should be noted that in our series, we found that invasive PAs were 10 mm larger and caused clinical manifestation two times more than non-invasive PAs. Nevertheless, cavernous sinus invasion was a predictor of surgical failure independent of tumor size, with a probability of non-cure of almost ten times higher in invasive PAs than in non-invasive PA after adjusted by tumor size. Although the endoscopic transsphenoidal approach provides a panoramic vision inside the surgical area, a superior close-up of the anatomy, an improved working angle, and the lower probability of cure in

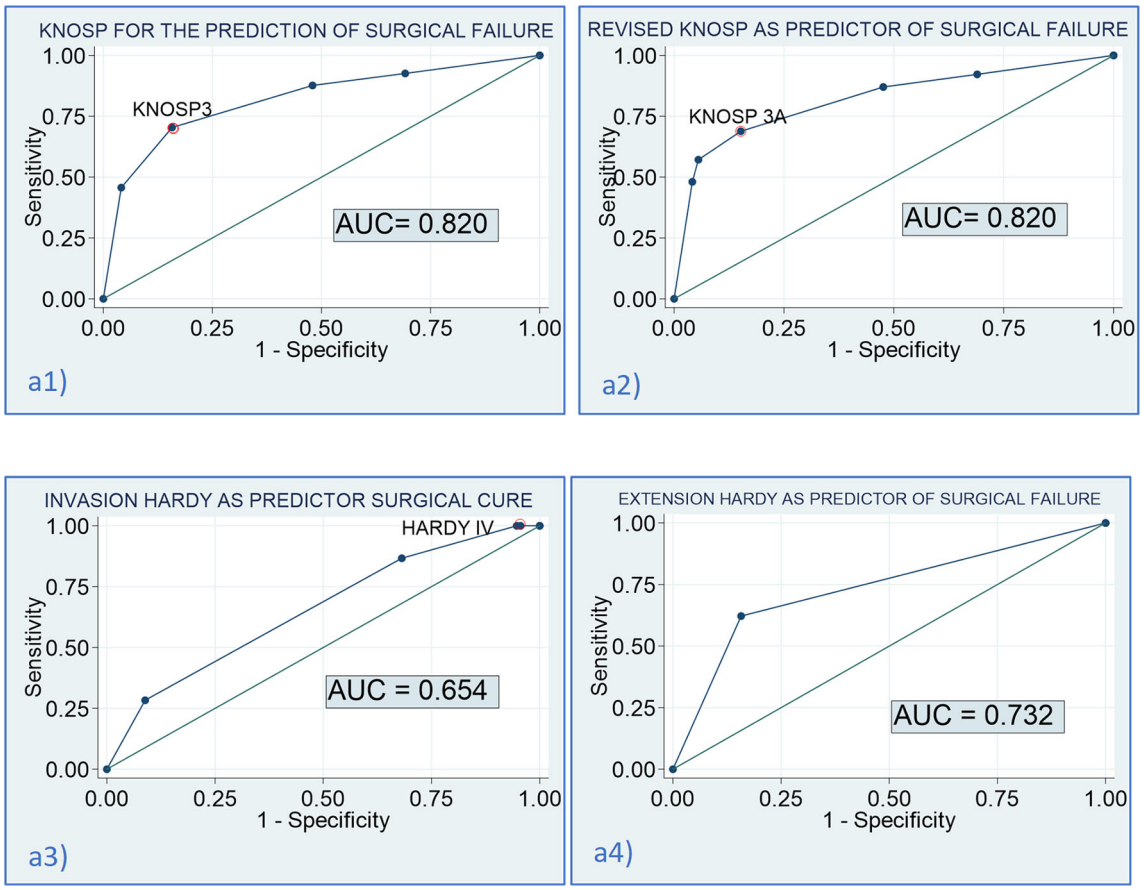

FIGURE 5 | Diagnostic accuracy of the Knosp and Hardy scales for the prediction of surgical cure. (a1) AUC of the Knosp scale for the prediction of surgical failure: 0.820 [0.760–0.879]; optimal cutoff for the prediction of failure: Knosp 3 [sensitivity (Se) = 70.4% (59.7–79.2), specificity (Sp) = 84.2% (77.5–89.3); a2] AUC of the revised-Knosp scale for the prediction of surgical failure: 0.820 [0.760–0.882]; optimal cutoff for the prediction of failure: Knosp 3A [Se= 68.8% (57.8–78.1), Sp = 84.8% (78.1–89.8); a3] AUC of the invasion Hardy scale for the prediction of surgical failure: 0.654 [0.580–0.728]; optimal cutoff for the prediction of failure: Hardy IV [Se = 86.7% (75.8–93.1), Sp = 31.9% (24.0–40.9); a4] AUC of the extension Hardy scale (A–D vs. E) for the prediction of surgical failure: 0.732 [0.672–0.793]; optimal cutoff for the prediction of failure: Hardy stage E [Se = 62.2% (51.4–71.9), Sp = 84.2% (77.5–89.3)].

invasive PAs could be related to the fact that gross total resection is usually more difficult in invasive PA than in non-invasive PA, especially if the tumor extends to the superior anterior clinoid process and posterior lateral ICA. In these cases, an expanded endonasal transcavernous approach should be considered (26). However, not only do anatomical characteristics play an important role in defining surgical planning and surgical goals, but also patient (age, comorbidities, symptoms) and tumor characteristics (acromegaly, Cushing disease or prolactin hypersecretion) are crucial, so the final decision must be individualized. Also, cavernous sinus invasion on preoperative imaging allows to predict higher surgical risk and lower cure rates, and this should be taken into account when giving informed consent to the patient. Different technical aspects have been described to improve the radiological accuracy of the diagnosis of cavernous sinus invasion, including 3-T MRI with the use of proton-density-weighted imaging or radiomics, among others (27).

Moreover, invasive PAs were more commonly of fibrous consistency than non-invasive PAs. Surgical outcomes seem to be associated with fibrous PA consistency. Up to 91% of adenomas are soft (meaning they are easily aspirated with conventional suction instruments), but approximately 10%–15% of patients will have tumors of fibrous consistency (requiring prior fragmentation with the use of a scalpel, forceps, or ultrasonic aspirators), associating a more significant number of incomplete resections and greater surgical risk (28–31). Fibrous PAs tend to be larger and invade neighboring structures, including the cavernous sinus. Some articles describe tumor remnants in cavernous sinus as fibrous, and this same consistency may be one of the causes of incomplete resection of the adenoma and ultimately implicating a higher number of recurrences (29, 24). It may be that the internal structure of the cavernous sinus itself, with trabeculae and ligaments, makes tumor removal difficult or a combination of this with the consistency of the adenoma (3, 32). A higher risk of

hypopituitarism or hyponatremia, RR = 6.75 (95% CI 3.23, 14.07), has also been described in those patients with fibrous adenomas (33). Several authors have suggested that preoperative radiological features of the PA in the MRI could be useful to predict tumor consistency, especially when radiomic and machine learning on T2-weighted MRI (34), diffusion-weighted imaging (35), or MR elastography were employed (36).

In our study, Hardy extension classification (considered A–D vs. E stage) showed a good concordance with Knosp classification (grades 0–II vs. III–IV) as they are considered equivalent since they evaluate the same items. Moreover, although the rate of surgical remission decreased as the grade in the extension and invasion Hardy classification increased, we found that the diagnostic accuracy of the Hardy classification, especially the invasive (sella destruction) Hardy classification, was quite low for the prediction of surgical outcomes. It was a first approach with the diagnostic tools available at that time (x-rays and CT), where they use some radiological characteristics visible in those images (invasion and destruction of sellar floor bone). Nevertheless, some previous series found that suprasellar extension less than 10 mm was associated with favorable remission and resection rates (37). Similarly, Yang et al. (38) described expressly that PAs with intracranial extension had increased surgical complications and a lower rate of gross total removal, although not describing Knosp grades. On the other hand, other authors found that the remission rate was not associated with sellar floor erosion according to the Hardy–Wilson system of grading, neither with supra- and parasellar extension (39, 40). Thus, it seemed that Hardy–Wilson classification is not a reliable marker of surgical remission. Moreover, the increase of risk as invasion Hardy increased was related with a larger tumor size in these tumors. When we adjusted the risk by tumor size, invasion Hardy classification lost its ability to predict surgical failure. Considering these data, we can affirm that the only reliable characteristic that predicts resectability is the invasion of the cavernous sinus, which is better systematized and in a more detailed way in the Knosp classifications. In fact, the Hardy classification is currently rarely used as it is considered not very precise for the evaluation of PAs. However, despite Knosp classification being the most universally accepted classification for this purpose, other more sophisticated scores have been proposed recently, including the Zurich Pituitary Score, which is based on two quantitative measurements: the maximum horizontal tumor diameter and the minimum inter-carotid distance at the intracavernous horizontal C4 segment of the ICA, according to the Bouthillier classification. This classification is a simple and reproducible tool that reliably predicts surgical outcomes including the extent of resection, residual volume, and gross total resection of PA patients undergoing transsphenoidal pituitary surgery (41). Moreover, it has been demonstrated as an excellent inter-rater agreement in three different external cohorts (42).

The most outstanding data of our research were that Knosp and revised-Knosp classifications showed a high diagnostic accuracy to predict surgical outcomes. The AUC of these two classifications for the prediction of surgical cure was 0.82, and a positive tendency to higher rate of complications and a lower rate of surgical cure was observed as the grade of Knosp classification increased. We found that the prediction of surgical failure was independent of tumor size. Similar results regarding surgical cure were reported in acromegaly series (overall remission rate 84.7% vs. 69.1%, $p < 0.001$ in invasive PAs) (43), Cushing's disease (77.1% in non-invasive vs. 53.0% in invasive PAs) (44), prolactinomas (95% in non-invasive vs. 20% in invasive PAs, $p < 0.001$) (45), and non-functioning PAs (92.5% non-invasive vs. 52.1% invasive PAs) (46). Although endoscopic surgery was considered to provide a better view for cavernous sinus invasion and superior structures and lesser nasal cavity injuries than microscopic surgery, the presence of invasion also seemed to clearly affect the surgical outcomes despite this supposed better visualization by the neurosurgeon. Moreover, the rate of surgical cure was as low as 28.8% in our cohort population. This figure is not lower than the one reported in previous endoscopic studies, with figures of even 5.9% having been described (47). Similar rates of approximately 30% have also been reported by other authors (48), and even a rate of 71% has been reported in a recent study evaluating the impact of an aggressive surgical approach that combined transsphenoidal transsellar and transmaxillary transpterygoidal approaches for the resection of grade 4 PAs (49). These differences in surgical remission rates probably depend on how conservative the surgical strategy regarding tumor resection was. Another important aspect to consider during pituitary surgery is complications. As previously reported (49, 50), we observed a higher proportion of surgical complications as higher Knosp grade of the PA. It is known that PAs invading the cavernous sinus are particularly surgically challenging due to their close proximity to critical neurovascular structures and their deep intracranial location.

In accordance with previous studies (8) and a recent meta-analysis (51), we found that patients with grade 3A showed a tendency to find a higher rate of surgical cure than those with grade 3B (56.0% vs. 30%). These results suggest that the revised-Knosp classification improves the accuracy of invasive PA diagnosis using surgical inspection. Nevertheless, the AUC of the ROC curve was equal to that of the classical Knosp classification. This could be related to the limited sample size of the Knosp 3 grade. In contrast, the Fang et al. meta-analysis (51) described that the modified Knosp had a remarkably higher AUC (0.91) than grades 3–4 (0.86) to predict cavernous sinus invasion, and thus probably for the prediction of surgical cure. Moreover, some studies have confirmed a high frequency of false positives in grade 3 in endoscopic series and recommended the addition of grades 3A and 3B into the existing parasellar classification (3, 52). We consider that although we did not find any differences in the diagnosis accuracy of the Knosp and revised-Knosp classification for the prediction of surgical cure, the differentiation between grades 3A and 3B is important as patients with grade A had a higher probability of surgical cure, which is more similar to grade 2 of Knosp, whereas the behavior of Knosp 3B is more similar to grade 4 of the classical Knosp. This information should be considered when surgery is being planned.

This study is not without limitations. One of them is related to its retrospective design, which must be considered when interpreting the results. Also, the operations performed in this series were also chiefly performed by a specialized skull base surgeon. Thus, the applicability of these results to centers with lower volume and experience performing endoscopic operations on invasive PAs may be limited.

CONCLUSION

Cavernous sinus invasion remains a significant determinant limiting EOR in PA surgery. That is why Knosp and revised-Knosp classifications offer an excellent orientation for the estimation of surgical cure and the risk of complications in patients with PAs submitted to EET surgery. However, the invasion Hardy scale lacks utility for this purpose.

DATA AVAILABILITY STATEMENT

The raw data supporting the conclusions of this article will be made available by the authors, without undue reservation.

ETHICS STATEMENT

The studies involving human participants were reviewed and approved by the Ethical Committee of the Ramón & Cajal Hospital. The patients/participants provided their written informed consent to participate in this study.

AUTHOR CONTRIBUTIONS

Conceptualization: MA-C. Methodology: MA-C. Formal analysis: MA-C. Data inclusion: VB and AC. Writing—original draft preparation: MA-C. Figure creation: CV. Writing—review and editing: MA-C, AC, CV, EP-C, and VB. All authors contributed to the article and approved the submitted version.

FUNDING

This research and APC were funded by Fundación para la Investigación Biomédica del Hospital Universitario Ramón y Cajal (FIBioHRC). IRYCIS. Ctra. Colmenar Viejo km 9,100. 28034. Madrid, Spain. VAT ES-G-83726984.

REFERENCES

1. Araujo-Castro M, Pascual-Corrales E, Martínez San Millan JS, Rebolleda G, Pian H, Ruz-Caracuel I, et al. Postoperative Management of Patients With Pituitary Tumors Submitted to Pituitary Surgery. Experience of a Spanish Pituitary Tumor Center of Excellence. *Endocrine* (2020) 69:5–17. doi: 10.1007/s12020-020-02247-y
2. Juraschka K, Khan OH, Godoy BL, Monsalves E, Kilian A, Krischek B, et al. Endoscopic Endonasal Transsphenoidal Approach to Large and Giant Pituitary Adenomas: Institutional Experience and Predictors of Extent of Resection - Clinical Article. *J Neurosurg* (2014) 121:75–83. doi: 10.3171/2014.3.JNS131679
3. Micko ASG, Wöhrer A, Wolfsberger S, Knosp E. Invasion of the Cavernous Sinus Space in Pituitary Adenomas: Endoscopic Verification and its Correlation With an MRI-Based Classification. *J Neurosurg* (2015) 122:803–11. doi: 10.3171/2014.12.JNS141083
4. Araujo-Castro M, Pascual-Corrales E, Martínez-Vaello V, Baonza Saiz G, Quiñones de Silva J, Acitores Cancela A, et al. Predictive Model of Surgical Remission in Acromegaly: Age, Presurgical GH Levels and Knosp Grade as the Best Predictors of Surgical Remission. *J Endocrinol Invest* (2020) 44:183–93. doi: 10.1007/s40618-020-01296-4
5. Mohr G, Hardy J, Comtois R, Beauregard H. Surgical Management of Giant Pituitary Adenomas. *Can J Neurol Sci/J Can Des Sci Neurol* (1990) 17:62–6. doi: 10.1017/S0317167100030055
6. Wilson CB. Neurosurgical Management of Large and Invasive Pituitary Tumors. In: GT Tindall, WF Collins (eds). *Clinical Management of Pituitary Disorders*. New York: Raven Press (1979) p. 335–42.
7. Knosp E, Steiner E, Kitz K, Matula C. Pituitary Adenomas With Invasion of the Cavernous Sinus Space: A Magnetic Resonance Imaging Classification Compared With Surgical Findings. *Neurosurg* (1993) 33:610–8. doi: 10.1227/00006123-199310000-00008
8. Zoli M, Milanese L, Bonfatti R, Sturiale C, Pasquini E, Frank G, et al. Cavernous Sinus Invasion by Pituitary Adenomas: Role of Endoscopic Endonasal Surgery. *J Neurosurg Sci* (2016) 60:485–94.
9. Braileanu M, Hu R, Hoch MJ, Mullins ME, Ioachimescu AG, Oyesiku NM, et al. Pre-Operative MRI Predictors of Hormonal Remission Status Post Pituitary Adenoma Resection. *Clin Imaging* (2019) 55:29–34. doi: 10.1016/j.clinimag.2019.01.020
10. Buchy M, Lapras V, Rabilloud M, Vasiljevic A, Borson-Chazot F, Jouanneau E, et al. Predicting Early Post-Operative Remission in Pituitary Adenomas: Evaluation of the Modified Knosp Classification. *Pituitary* (2019) 22:467–75. doi: 10.1007/s11102-019-00976-6
11. Araujo-Castro M, Pascual-Corrales E, Acitores Cancela A, García Duque S, Ley Urzaiz L, Rodríguez Berrocal V. Status and Clinical and Radiological Predictive Factors of Presurgical Anterior Pituitary Function in Pituitary Adenomas. Study of 232 Patients. *Endocrine* (2020) 70:584–92. doi: 10.1007/s12020-020-02455-6
12. Nieman LK, Biller BMKK, Findling JW, Newell-Price J, Savage MO, Stewart PM, et al. The Diagnosis of Cushing's Syndrome: An Endocrine Society Clinical Practice Guideline. *J Clin Endocrinol Metab* (2008) 93:1526–40. doi: 10.1210/jc.2008-0125
13. Giustina A, Barkan A, Casanueva FF, Cavagnini F, Frohman L, Ho K, et al. Criteria for Cure of Acromegaly: A Consensus Statement. *J Clin Endocrinol Metab* (2000) 85:526–9. doi: 10.1210/jc.85.2.526
14. Wilson CB. A Decade of Pituitary Microsurgery. The Herbert Olivecrona Lecture. *J Neurosurg* (1984) 61:814–33. doi: 10.3171/jns.1984.61.5.0814
15. Patel SK, Husain Q, Eloy JA, Couldwell WT, Liu JK. Norman Dott, Gerard Guiot, and Jules Hardy: Key Players in the Resurrection and Preservation of Transsphenoidal Surgery. *Neurosurg Focus* (2012) 33:E6. doi: 10.3171/2012.6.FOCUS12125
16. Hardy J. Transsphenoidal Hypophysectomy. *J Neurosurg* (1971) 34:582–94. doi: 10.3171/jns.1971.34.4.0582
17. Hardy J, Wigser SM. Trans-Sphenoidal Surgery of Pituitary Fossa Tumors With Televised Radiofluoroscopic Control. *J Neurosurg* (1965) 23:612–9. doi: 10.3171/jns.1965.23.6.0612
18. Mortini P, Albano L, Barzaghi LR, Spina A, Losa M. The Open Sella Technique for Surgical Treatment of Pituitary Macroadenomas: Safety and Efficacy in a Large Clinical Series. *Br J Neurosurg* (2021) 16:1–8. doi: 10.1080/02688697.2021.1950629
19. Hawkes R, Holland G, Moore WS, Worthington B. Nuclear Magnetic Resonance (NMR) Tomography of the Brain: A Preliminary Clinical Assessment With Demonstration of Pathology. *J Comput Assist Tomogr* (1980) 4:577–86. doi: 10.1097/00004728-198010000-00001
20. Truong HQ, Lieber S, Najera E, Alves-Belo JT, Gardner PA, Fernandez-Miranda JC. The Medial Wall of the Cavernous Sinus. Part 1: Surgical Anatomy, Ligaments, and Surgical Technique for its Mobilization and/or Resection. *J Neurosurg* (2018) 131:122–30. doi: 10.3171/2018.3.JNS18596

21. Cohen-Cohen S, Gardner PA, Alves-Belo JT, Truong HQ, Snyderman CH, Wang EW, et al. The Medial Wall of the Cavernous Sinus. Part 2: Selective Medial Wall Resection in 50 Pituitary Adenoma Patients. *J Neurosurg* (2018) 131:131–40. doi: 10.3171/2018.5.JNS18595
22. Koutourousiou M, Vaz Guimaraes Filho F, Fernandez-Miranda JC, Wang EW, Stefko ST, Snyderman CH, et al. Endoscopic Endonasal Surgery for Tumors of the Cavernous Sinus: A Series of 234 Patients. *World Neurosurg* (2017) 103:713–32. doi: 10.1016/j.wneu.2017.04.096
23. Dhandapani S, Singh H, Negm HM, Cohen S, Anand VK, Schwartz TH. Cavernous Sinus Invasion in Pituitary Adenomas: Systematic Review and Pooled Data Meta-Analysis of Radiologic Criteria and Comparison of Endoscopic and Microscopic Surgery. *World Neurosurg* (2016) 96:36–46. doi: 10.1016/j.wneu.2016.08.088
24. Micko A, Oberndorfer J, Weninger WJ, Vila G, Höftberger R, Wolfsberger S, et al. Challenging Knosp High-Grade Pituitary Adenomas. *J Neurosurg* (2020) 132:1739–46. doi: 10.3171/2019.3.JNS19367
25. Sanmillán JL, Torres-Diaz A, Sanchez-Fernández JJ, Lau R, Ciller C, Puyalto P, et al. Radiologic Predictors for Extent of Resection in Pituitary Adenoma Surgery. A Single-Center Study. *World Neurosurg* (2017) 108:436–46. doi: 10.1016/j.wneu.2017.09.017
26. Ji-Hu Y, Guo-Dong H, Tao J, Hai-Dong W, Yu-Fei L, Jian G, et al. Endoscopic Endonasal Surgery Treatment Strategies for Invasive Pituitary Adenoma: Analysis of Four Approaches. *World Neurosurg* (2018) 115:5–13. doi: 10.1016/j.wneu.2018.02.162
27. Serioli S, Doglietto F, Fiorindi A, Biroli A, Mattavelli D, Buffoli B, et al. Pituitary Adenomas and Invasiveness From Anatomo-Surgical, Radiological, and Histological Perspectives: A Systematic Literature Review. *Cancers (Basel)* (2019) 11:1–21. doi: 10.3390/cancers11121936
28. Acitores Cancela A, Rodríguez Berrocal V, Pian H, Martínez San Millán JS, Díez JJ, Iglesias P. Clinical Relevance of Tumor Consistency in Pituitary Adenoma. *Hormones* (2021) 20:463–73. doi: 10.1007/s42000-021-00302-5
29. Rutkowski MJ, Chang K-E, Cardinal T, Du R, Tafreshi AR, Donoho DA, et al. Development and Clinical Validation of a Grading System for Pituitary Adenoma Consistency. *J Neurosurg* (2020) 134:180–1807. doi: 10.3171/2020.4.jns193288
30. Cappelletti M, Ruggeri AG, Spizzichino L, D'Amico A, D'avella E, Delfini R. Fibrous Pituitary Macroadenomas: Predictive Role of Preoperative Radiologic Investigations for Proper Surgical Planning in a Cohort of 66 Patients. *World Neurosurg* (2019) 121:e449–57. doi: 10.1016/j.wneu.2018.09.137
31. Ciric I, Mikhael M, Stafford T, Lawson L, Garces R. Transsphenoidal Microsurgery of Pituitary Macroadenomas With Long-Term Follow-Up Results. *J Neurosurg* (1983) 59:395–401. doi: 10.3171/jns.1983.59.3.0395
32. Azab WA, Nasim K, Abdelnabi EA, Yousef W, Najibullah M, Khan T, et al. Endoscopic Endonasal Excision of Large and Giant Pituitary Adenomas: Radiological and Intraoperative Correlates of the Extent of Resection. *World Neurosurg* (2019) 126:e793–802. doi: 10.1016/j.wneu.2019.02.151
33. Schur S, Lasry O, Tewfik MA, Di Maio S. Assessing the Association of Tumor Consistency and Gland Manipulation on Hormonal Outcomes and Delayed Hyponatremia in Pituitary Macroadenoma Surgery. *Interdiscip Neurosurg Adv Tech Case Manag* (2020) 20:100628. doi: 10.1016/j.inat.2019.100628
34. Cuocolo R, Ugga L, Solari D, Corvino S, D'Amico A, Russo D, et al. Prediction of Pituitary Adenoma Surgical Consistency: Radiomic Data Mining and Machine Learning on T2-Weighted MRI. *Neuroradiology* (2020) 62:1649–56. doi: 10.1007/S00234-020-02502-Z
35. Ding W, Huang Z, Zhou G, Li L, Zhang M, Li Z. Diffusion-Weighted Imaging for Predicting Tumor Consistency and Extent of Resection in Patients With Pituitary Adenoma. *Neurosurg Rev* (2021) 44:2933–41. doi: 10.1007/S10143-020-01469-Y
36. Cohen-Cohen S, Helal A, Yin Z, Ball MK, Ehman RL, Van Gompel JJ, et al. Predicting Pituitary Adenoma Consistency With Preoperative Magnetic Resonance Elastography. *J Neurosurg* (2021) 1–8. doi: 10.3171/2021.6.JNS204425
37. Erkan B, Barut O, Akbas A, Akpinar E, Akdeniz YS, Tanriverdi O, et al. Results of Endoscopic Surgery in Patients With Pituitary Adenomas: Association of Tumor Classification Grades With Resection, Remission, and Complication Rates. *J Korean Neurosurg Soc* (2021) 64:608–18. doi: 10.3340/jkns.2020.0207
38. Yang YQ, Bao YY, Xie SH, Tang B, Wu X, Yang L, et al. Identification of the Extradural and Intradural Extension of Pituitary Adenomas to the Suprasellar Region: Classification, Surgical Strategies, and Outcomes. *Front Oncol* (2021) 11:723513. doi: 10.3389/fonc.2021.723513
39. Taghvaei M, Sadrehosseini SM, Ardakani JB, Nakhjavani M, Zeinalizadeh M. Endoscopic Endonasal Approach to the Growth Hormone–Secreting Pituitary Adenomas: Endocrinologic Outcome in 68 Patients. *World Neurosurg* (2018) 117:e259–68. doi: 10.1016/j.wneu.2018.06.009
40. Yildirim AE, Sahinoglu M, Divanlioglu D, Alagoz F, Gurcay AG, Daglioglu E, et al. Endoscopic Endonasal Transsphenoidal Treatment for Acromegaly: 2010 Consensus Criteria for Remission and Predictors of Outcomes. *Turk Neurosurg* (2014) 24:906–12. doi: 10.5137/1019-5149.JTN.11288-14.1
41. Serra C, Staartjes VE, Maldaner N, Muscas G, Akeret K, Holzmann D, et al. Predicting Extent of Resection in Transsphenoidal Surgery for Pituitary Adenoma. *Acta Neurochir (Wien)* (2018) 160:2255–62. doi: 10.1007/S00701-018-3690-X/TABLES/4
42. Staartjes VE, Serra C, Zoli M, Mazzatenta D, Pozzi F, Locatelli D, et al. Multicenter External Validation of the Zurich Pituitary Score. *Acta Neurochir (Wien)* (2020) 162:1287–95. doi: 10.1007/S00701-020-04286-W
43. Nishioka H, Ukuhara N, Horiguchi K, Yamada S. Aggressive Transsphenoidal Resection of Tumors Invading the Cavernous Sinus in Patients With Acromegaly: Predictive Factors, Strategies, and Outcomes: Clinical Article. *J Neurosurg* (2014) 121:505–10. doi: 10.3171/2014.3.JNS132214
44. Dai C, Feng M, Sun B, Bao X, Yao Y, Deng K, et al. Surgical Outcome of Transsphenoidal Surgery in Cushing's Disease: A Case Series of 1106 Patients From a Single Center Over 30 Years. *Endocrine* (2021). doi: 10.1007/s12020-021-02848-1
45. Zielinski G, Ozdarski M, Maksymowicz M, Szamotulska K, Witek P. Prolactinomas: Prognostic Factors of Early Remission After Transsphenoidal Surgery. *Front Endocrinol (Lausanne)* (2020) 11:439. doi: 10.3389/fendo.2020.00439
46. Kim JH, Lee JH, Lee JH, Hong AR, Kim YJ, Kim YH. Endoscopic Transsphenoidal Surgery Outcomes in 331 Nonfunctioning Pituitary Adenoma Cases After a Single Surgeon Learning Curve. *World Neurosurg* (2018) 109:e409–16. doi: 10.1016/j.wneu.2017.09.194
47. Hwang J, Seol HJ, Nam D-H, Lee J-I, Lee MH, Kong D-S. Therapeutic Strategy for Cavernous Sinus-Invading Non-Functioning Pituitary Adenomas Based on the Modified Knosp Grading System. *Brain Tumor Res Treat* (2016) 4:63. doi: 10.14791/btrt.2016.4.2.63
48. Zhu H, Li C, Gui S, Wang X, Zong X, Zhao P, et al. Experience of Endoscopic Endonasal Approach for 803 Pituitary Tumors With Cavernous Sinus Invasion. *J Craniofac Surg* (2021) Publish Ah:1–5. doi: 10.1097/scs.0000000000008049
49. Ouyang T, Zhang N, Xie S, Tang B, Li J, Xiao L, et al. Outcomes and Complications of Aggressive Resection Strategy for Pituitary Adenomas in Knosp Grade 4 With Transsphenoidal Endoscopy. *Front Oncol* (2021) 11:693063. doi: 10.3389/fonc.2021.693063
50. Van Gerven L, Qian Z, Starovoyt A, Jorissen M, Meulemans J, van Loon J, et al. Endoscopic, Endonasal Transsphenoidal Surgery for Tumors of the Sellar and Suprasellar Region: A Monocentric Historical Cohort Study of 369 Patients. *Front Oncol* (2021) 11:643550. doi: 10.3389/fonc.2021.643550
51. Fang Y, Pei Z, Chen H, Wang R, Feng M, Wei L, et al. Diagnostic Value of Knosp Grade and Modified Knosp Grade for Cavernous Sinus Invasion in Pituitary Adenomas: A Systematic Review and Meta-Analysis. *Pituitary* (2021) 24:457–64. doi: 10.1007/s11102-020-01122-3
52. Yamada S, Fukuhara N, Horiguchi K, Yamaguchi-Okada M, Nishioka H, Takeshita A, et al. Clinicopathological Characteristics and Therapeutic Outcomes in Thyrotropin-Secreting Pituitary Adenomas: A Single-Center Study of 90 Cases. *J Neurosurg* (2014) 121:1462–73. doi: 10.3171/2014.7.JNS1471

Conflict of Interest: The authors declare that the research was conducted in the absence of any commercial or financial relationships that could be construed as a potential conflict of interest.

this article, or claim that may be made by its manufacturer, is not guaranteed or endorsed by the publisher.

frontiers in Oncology

ORIGINAL RESEARCH
published: 08 February 2022
doi: 10.3389/fonc.2022.810234

Transsphenoidal Surgery of Corticotroph Adenomas With Cavernous Sinus Invasion: Results in a Series of 86 Consecutive Patients

Congxin Dai[1†], Ming Feng[2†], Lin Lu[3], Bowen Sun[1], Yanghua Fan[2], Xinjie Bao[2], Yong Yao[2], Kan Deng[2], Renzhi Wang[2] and Jun Kang[1*]*

[1] Department of Neurosurgery, Beijing Tongren Hospital, Capital Medical University, Beijing, China, [2] Department of Neurosurgery, Peking Union Medical College Hospital, Chinese Academy of Medical Sciences and Peking Union Medical College, Beijing, China, [3] Department of Endocrinology, Peking Union Medical College Hospital, Chinese Academy of Medical Sciences and Peking Union Medical College, Beijing, China

OPEN ACCESS

Edited by:
Qun Wu,
Zhejiang University, China

Reviewed by:
Wang Haijun,
The First Affiliated Hospital of Sun Yat-sen University, China
Run Yu,
UCLA David Geffen School of Medicine, United States

***Correspondence:**
Jun Kang
junkang2015@163.com
Renzhi Wang
wangrz@126.com

[†]These authors have contributed equally to this work

Specialty section:
This article was submitted to Neuro-Oncology and Neurosurgical Oncology, a section of the journal Frontiers in Oncology

Received: *06 November 2021*
Accepted: *03 January 2022*
Published: *08 February 2022*

Citation:
Dai C, Feng M, Lu L, Sun B, Fan Y, Bao X, Yao Y, Deng K, Wang R and Kang J (2022) Transsphenoidal Surgery of Corticotroph Adenomas With Cavernous Sinus Invasion: Results in a Series of 86 Consecutive Patients. Front. Oncol. 12:810234. doi: 10.3389/fonc.2022.810234

Objective: Transsphenoidal surgery (TSS) is the first-line treatment for corticotroph adenomas. Although most corticotroph adenomas are noninvasive microadenomas, a small subset of them invading cavernous sinus (CS) is notoriously difficult to manage. The aim of this study was to evaluate the surgical outcome of corticotroph adenomas with CSI from a single center.

Patients and Methods: The clinical features and outcomes of CD patients who underwent TSS between January 2000 and September 2019 at Peking Union Medical College Hospital were collected from medical records. The clinical, endocrinological, radiological, histopathological, and surgical outcomes, and a minimum 12-month follow-up of patients with corticotroph adenomas invading CS were retrospectively reviewed.

Results: Eighty-six patients with corticotroph adenomas invading CS were included in the study. The average age at TSS was 37.7 years (range, 12 to 67 years), with a female-to-male ratio of 3.1:1 (65/21). The median duration of symptoms was 52.6 months (range, 1.0 to 264 months). The average of maximum diameter of tumor was 17.6 mm (range, 4.5–70 mm). All included 86 patients underwent TSS using a microscopic or an endoscopic approach. Gross total resection was achieved in 63 patients (73.3%), subtotal resection was attained in 18 (20.9%), and partial resection was achieved in 5 (5.8%). After surgery, the overall postoperative immediate remission rate was 48.8% (42/86); 51.2% (44/86) of patients maintained persistent hypercortisolism. In 42 patients with initial remission, 16.7% (7/42) experienced a recurrence. In these patients with persistent disease and recurrent CD, data about further treatment were available for 30 patients. Radiotherapy was used for 15 patients, and 4 (26.7%) of them achieved biochemical remission. Repeat TSS was performed in 5 patients, and none achieved remission. Medication was administered in 4 patients, and one of them obtained disease control. Adrenalectomy was performed in 6 patients, and 5 (83.3%) achieved biochemical

remission. At the last follow-up, 10 of 30 patients (33.3%) were in remission, and 20 patients still had persistent disease.The remission rate in corticotroph adenomas with cavernous sinus invasion (CSI) that underwent gross total resection and first TSS was significantly higher than that in patients undergoing subtotal resection, partial resection, and a second TSS (all $p < 0.05$). However, there was no significant difference in the remission rate between patients with different tumor sizes, Knosp grades, and surgical approaches ($p > 0.05$).

Conclusion: The management of corticotroph adenomas with CSI remain a therapeutic challenge due to incomplete resection of invasive and/or a large adenoma. With the application of multiple techniques, approximately half of the patients could achieve gross total resection and biochemical remission *via* TSS by experienced neurosurgeons. The extent of tumor resection and the number of operations were associated with surgical remission rate in corticotroph adenomas with CSI. If the remission was not achieved by surgery, other treatments including radiotherapy, medical therapy, and even bilateral adrenalectomy are required.

Keywords: corticotroph adenomas, cavernous sinus invasion, transsphenoidal surgery, remission, recurrence

INTRODUCTION

Cushing disease (CD) is defined as chronic hypercortisolemia, which is mainly caused by corticotroph adenomas. CD is a relatively rare disease with an incidence of approximately 0.7–2.4 cases per million persons/year (1). If untreated or incompletely controlled, CD is associated with increased morbidity and higher mortality rate compared to the general population (2). Transsphenoidal surgery (TSS) is considered the first-line treatment for patients with CD. However, the remission rate after TSS has been reported to vary widely from 59% to 94% (3). Most corticotroph adenomas are non-invasive microadenomas with a tumor diameter of less than 8 mm (4, 5). The surgical remission rates in these patients with noninvasive visible microadenomas frequently exceed greater than 80% (6). However, surgery for corticotroph adenomas with cavernous sinus invasion (CSI) has represented challenge, and the remission rates tended to be extremely low. Because corticotroph adenomas with CSI are relatively rare, there is still no comprehensive study on large-scale cases of corticotroph adenomas with CSI. To date, surgical outcome and perioperative complications of corticotroph adenomas with CSI have not been clearly reported (7). The purpose of this study was to assess the surgical outcome and perioperative complications of corticotroph adenomas with CSI.

PATIENTS AND METHODS

We conducted a retrospective analysis of consecutive patients with corticotroph adenoma invading CS who underwent TSS at Peking Union Medical College Hospital (PUMCH) between January 2000 and September 2019. According to the guidelines of the PUMCH Medical Ethical Committee, clinical information on age, sex, clinical manifestation, preoperative biochemical parameters and imaging results, operative findings, postoperative hormone levels and pathology, long-term outcomes, and follow-up were collected for analysis.

Inclusion and Exclusion Criteria

The inclusion criteria for this study were as follows: (1) the CD was diagnosed based on the patient's history and results of a physical examination, laboratory tests, magnetic resonance imaging (MRI), and surgical findings; (2) a corticotroph adenomas was confirmed on immunohistopathological studies; (3) the CSI was recognized by both preoperative MRI results and intraoperative findings; and (4) with complete medical records and a minimum of 2 years of follow-up. According to the Knosp grade classification (8), if tumors were classified as Knosp grade of 2 based on preoperative MRI results, but the CSI was confirmed intraoperatively, these patients were also included in this study. If the tumors were classified as Knosp grade of 3 according to the preoperative MRI results, but no CSI was recognized intraoperatively, these patients were excluded from the study. Patients were excluded if the surgery was aborted because of carotid artery bleeding, surgery was *via* a transcranial approach, the medical records were not complete, or lack of pathological report or follow-up data.

Diagnosis of Corticotroph Adenomas with CSI

Most patients were diagnosed as having corticotroph adenomas with CSI by a pituitary multidisciplinary team (MDT) including members from the Departments of Neurosurgery, Endocrinology, Radiology, and Pathology, as we described in a previous study (9). All corticotroph adenomas with CSI were diagnosed based on clinical manifestation, endocrine examinations, radiological examinations, intraoperative

observation, and pathological results. In our center, all CD patients underwent comprehensive biochemical tests, including morning serum cortisol and ACTH, 24-h urine-free cortisol (UFC), and a combined low-dose and high-dose dexamethasone suppression test (LDDST and HDDST). The methods of LDDST and HDDST have been described in detail in our previous study (10). If 24-h UFC and cortisol were not suppressed on the LDDST but was suppressed on the HDDST, CD was diagnosed. Based on our previous research results, the sensitivity of combined LDDST and HDDST to diagnose CD is 88.53% in our center (11).

Preoperatively, all patients underwent pituitary contrast-enhanced MRI and/or dynamic gadolinium-enhanced MRI. Images were independently reviewed by one neuroradiologist and at least one neurosurgeon, to evaluate the invasiveness of tumors, and ensure that agreement was achieved on Knosp grade, which was described previously (8). Adenomas of Knosp Grade 0–2 were defined as non-invasive PAs, and adenomas of Knosp Grade 3–4 were defined as invasive PAs, respectively. However, preoperative diagnosis of CSI by PAs based on MRI has always been inconsistent with intraoperative exploratory results. With the advancement of endoscopic techniques, the medial wall of the CS can be exposed more clearly and directly observed. Therefore, whether a PA presents CSI was finally confirmed by preoperative Knosp grading combined with intraoperative observed results. According to the maximal diameter, adenomas were categorized as microadenoma (<1 cm), macroadenoma (<4 cm), and giant adenoma (≥4 cm).

Surgical Procedures

All TSSs were performed in the Department of Neurosurgery in PUMCH. Almost all the included patients were operated on by the same two experienced surgeons (RW and MF). The adenomas were removed via a transsphenoidal microscopic or an endoscopic approach, or a combination of them. The extended transsphenoidal approach assisted by multiple techniques was performed in some invasive macroadenomas or giant adenomas as previously described (12). In surgery, standard transsphenoidal PAs resection via a microscopic approach or an endoscopic approach was performed after broadly opening the sella floor. The tumor localized in the intrasellar and suprasellar region was removed first and then the residual tumor in the cavernous sinus (CS) was inspected. The medial wall of the CS was explored under direct vision, and soft tumor tissue was removed using suction and ring curettes. The ICA was located using intraoperative mini-Doppler. The anterior wall of the CS was opened carefully and then the soft tumors located lateral to the ICA was removed by suction and ring curettes. If the tumor was exposed insufficiently, the ICA could be gently pushed to increase visualization for further exposure. If the tumor was too hard to remove, or the tumor firmly adhered to the ICA or nerves, leave the tumor to avoid injuring the ICA or nerves. The residual tumors will be addressed via postoperative radiotherapy. Finally, the sella was reconstructed in all patients to avoid postoperative cerebrospinal fluid (CSF) leakage and CNS infection.

Classifications of Intraoperative Observed CSI

The CSI was determined by the experienced neurosurgeons during surgery based on the degree of invasion of the adenoma into the CS wall and the presence or absence of adenomas within the CS. After tumor removal, if the medial wall of CS was intact and smooth, absence of invasion was considered. If the medial wall was not intact, intracavernous ligaments, ICA, or nerve fibers were visible, and CSI was considered.

Extent of Tumor Resection

The extent of tumor resection was evaluated through MRI examinations within 3 days and on 3 months after initial surgery. The gross total resection (GTR) was defined as no residual tumor was identified. The subtotal resection (STR) was defined as more than 90% volume compared with when the preoperative volume was removed, or when a definite residual tumor volume less than 10% compared with when the preoperative volume was identified. Partial resection was defined as residual tumor volume greater than 10% (13).

Histological Analysis

The resected specimens of corticotroph adenomas were performed using routine H & E histological stains and immunohistochemical tests for ACTH. The diagnosis of CD was confirmed if pathology under light microscopy demonstrated an adenoma with immunohistological staining positive for ACTH.

Surgical Outcome Measures

After TSS, the endocrinological tests were performed within the first 7 days, 1 month, 3 months, and 12 months, respectively. As we described previously (14), immediate remission was defined as a serum cortisol level <5 μg/dl, and/or 24-h UFC level fell below 20 μg (56 nmol) within the first 7 days after TSS. Persistent disease was defined in patients as elevated postoperative cortisol levels and a need for additional therapy. Recurrence was defined in patients who achieved initial remission, followed by a rise in serum cortisol or 24-h UFC and associated with clinical symptoms of CD. To assess the degree of tumor resection, postoperative MRI was done within 3 days and on 3 months after the surgery.

Statistical Analysis

Statistical significance for continuous variables was determined using the Student's *t*-test or analysis of variance. Categorical variables were analyzed using either the Pearson χ^2 test or Fisher exact test. Pearson χ^2 testing for determination of statistical significance was performed by using either a $2 \cdot 2$ contingency table or test for independence if greater than 2 outcomes were being analyzed. Fisher exact test was used if any expected values were less than or equal to 5. Statistical significance was defined as a p-value less than.05. All statistical analyses were completed by using SPSS software, version 22 (SPSS, Inc., Chicago, Illinois).

RESULTS

Demographic and Clinical Characteristics of Included Patients

From January 2000 to September 2019, 1,381 patients with CD had TSS at the PUMCH, and the intraoperatively observed corticotroph adenomas invading CS accounted for 7.5% (104/1,381) of overall patients. Of these, 86 patients with complete medical records, pathological confirmation, and a minimum 2-year follow-up were included in this study. The detailed information is listed in **Table 1**. There are 21 male patients and 65 female patients, and the median duration of symptoms was 52.6 months (range, 1.0 to 264 months). The average age at TSS was 37.7 years (range, 12 to 67 years), and the mean follow-up time was 49.5 months (range, 24.0–159.0 months).

The median tumor diameter of overall patients was 17.6 mm (range 4.5–70.0 mm). Of these, 32.6% (28/86) of patients demonstrated microadenomas with a median tumor diameter of 6.9 mm, 62.8% (54/86) of patients demonstrated macroadenomas with a median tumor diameter of 20.0 mm, and 4.7% (4/86) of patients had giant adenomas with a median tumor diameter of 60.6 mm, respectively. Mean preoperative body mass index (BMI) was 26.6 (range, 18.9–36.7 kg/m^2). The median preoperative 24-h UFC levels, morning serum cortisol, and ACTH were 721.4 μg (range, 71.3–3,705.6), 28.9 μg/dl (range, 7.4–75.0), and 142.5 ng/L (range, 23.1–1,250.0), respectively. In these cases, 66 patients underwent first TSS, and 20 patients underwent repeated TSS, respectively. In 83.7% (72/86) patients, LDDST was not suppressed but HDDST was suppressed in the combined LDDST and HDDST test.

Prediction of Intraoperative CSI by Preoperative MRI-Based Knosp Grade

The radiological results represent the first essential step to evaluate CSI of PAs. However, the results of CSI evaluated using Knosp grade based on preoperative MRI are not always consistent with intraoperatively observed CSI. In this study, 1,273 patients were identified as Knosp Grade 0, 1 and 2, and 108 patients were classified into Knosp Grade 3 and 4, respectively, based on preoperative coronal MRI (**Table 2**). None of the Knosp Grade 0 and 1 based on preoperative coronal MRI had shown evidence of intraoperative CSI, and all the MRI-based Knosp Grade 4 patients demonstrated CSI intraoperatively. However, CSI was intraoperatively observed in 5.4% (4 of 74) of patients with MRI-based Knosp Grade 2, and no obvious CSI was found intraoperatively in 16.0% (8 of 50) patients with MRI-based Knosp Grade 3.

Surgical Outcome of Different Subgroups

Surgical outcomes of different subgroups based on different variables are shown in **Table 3**. Post-operatively, only 42/86 (48.8%) of overall included patients achieved immediate remission after TSS, whereas 44/86 (51.2%) patients still had persistent disease. Knosp grade was closely related to extent of tumor resection and biochemical remission. In this study, after TSS, only 55.6% (20/36) patients with Knosp Grade 3 and 41.3% (19/46) patients with Knosp grade 4 adenomas achieved biochemical remission, respectively. However, 75% (3/4) of patients with Knosp Grade 2 adenomas achieved remission, which were higher than that in the patients with Knosp grade 3 and 4 adenomas, but did not reach statistical significance (all $p > 0.05$).

Extent of tumor resection has been considered one of the most important factors affecting the surgical outcomes. In this study, GTR was achieved in 73.3% (63/86) patients, and remission was obtained in 60.3% (38/63) of these patients. STR was performed in 20.9% (18/86) patients, and 22.2% (4/18) of them achieved remission. PR were performed in 5 (5.8%) patients, and none achieved initial remission. The remission rate in patient performed with GTR was significantly higher than that in the patients with STR and RR (all $p < 0.05$).

Tumor size may be another important factor correlated with outcomes of surgery. In this study, a total of 86 included patients had 28 (32.6%) microadenomas, 54 (62.8%) macroadenomas, and 4 (4.7%) giant adenomas, and the postoperative remission rate in these patients were 60.7% (17/28), 42.6% (23/54), and 25.0% (1/4), respectively. However, there is no significant deference in remission rate among three groups (all $p > 0.05$).

TSS can be performed by microscopic or endoscopic approach, whether endoscopic approach yielded higher remission rate over the microscopic approach is still controversial. In this study,

TABLE 1 | Demographic and clinical characteristics of 86 patients with corticotroph adenomas invading cavernous sinus.

Characteristics	Value
Total	86
Gender	
Female (*n*, %)	65 (75.6%)
Male (*n*, %)	21 (24.4%)
Mean age, years (range)	37.7 (12–67)
Number of operations	
First (*n*, %)	66 (76.7%)
Repeat (*n*, %)	20 (23.3%)
Disease duration, months (range)	52.6 (1–264)
BMI	26.6 (18.9–36.7)
Tumor size (mean) (range)	17.6 mm (4.5–70.0 mm)
Microadenoma (*n*, %), Diameter (mm)	(28, 32.6%) 6.9 mm
Macroadenoma (*n*, %), Diameter (mm)	(54, 62.8%) 20.0 mm
Giant adenoma (*n*, %), Diameter (mm)	(4, 4.7%) 60.6 mm
Preoperative 24-h UFC level (μg)	721.4 (71.3–3705.6)
Preoperative serum cortisol level (μg/dl)	28.9 (7.4–75.0)
Preoperative ACTH level (ng/L)	142.5 (23.1–1250.0)
Combined LDDST and HDDST test	
Positive (*n*, %)	72 (83.7%)
Negative (*n*, %)	14 (16.3)
Follow-up time, months (range)	49.5 (24.0–159.0)

TABLE 2 | Comparison of results of Knosp grade based on preoperative MRI and surgically observed cavernous sinus invasion.

Knosp grade based on preoperative MRI	Surgically observed invasiveness		Total
	Invasive	Non-invasive	
0 and 1	0	1,199	1,199
2	4	70	74
3	42	8	50
4	58	0	58
Total	104	1,277	1,381

TABLE 3 | Rate of immediate remission and recurrence by subgroups based on different variables.

Variable	Number of patients	Remission	Persistence	*p*-value
Total patients Degree of invasion	86	42/86 (48.8%)	44/86 (51.2%)	
Knosp Grade 2 (a)	4 (4.7%)	3/4 (75%)	1/4 (25%)	a vs. b: $p = 0.46$
Knosp Grade 3 (b)	36 (41.9%)	20/36 (55.6%)	16/36 (44.4%)	a vs. c: $p = 0.19$
Knosp Grade 4 (c)	46 (53.5%)	19/46 (41.3%)	27/46 (58.7%)	b vs. c: $p = 0.20$
Extent of tumor resection				
GTR (d)	63 (73.3%)	38/63 (60.3%)	25/63 (39.7%)	d vs. e: $p = 0.004$
STR (e)	18 (20.9%)	4/18 (22.2%)	14/18 (77.8%)	d vs. f: $p = 0.008$
PR (f)	5 (5.8%)	0/5 (0%)	5/5 (100%)	e vs. f: $p = 0.25$
Tumor size				
Microadenomas (g)	28 (32.6%)	17/28 (60.7%)	11/28 (39.3%)	g vs. h: $p = 0.12$
Macroadenomas (h)	54 (62.8%)	23/54 (42.6%)	31/54 (57.4%)	g vs. i: $p = 0.18$
Giant adenomas (i)	4 (4.7%)	1/4 (25.0%)	3/4 (75.0%)	h vs. i: $p = 0.49$
Approach				
Microscopic approach (j)	31 (36.0%)	14/31 (45.2%)	17/31 (54.8%)	
Endoscopic approach (k)	55 (64.0%)	28/55 (50.9%)	27/55 (49.1%)	j vs. k: $p = 0.61$
Number of operations				
First TSS (l)	66 (76.7%)	38/66 (57.6%)	28/66 (42.4%)	
Repeat TSS (m)	20 (23.3%)	4/20 (20.0%)	16/20 (80.0%)	l vs. m: $p = 0.003$

31 patients underwent TSS using a microscopic approach and 55 patients had an endoscopic approach. However, no significant difference in the remission rate was observed between the two techniques in corticotroph adenomas with CSI ($p = 0.61$).

To further analyze the effect of the number of operations on the surgical outcome of corticotroph adenomas with CSI, patients were subclassified into two groups based on the status of first or repeated TSS. In this study, 66 patients underwent first TSS and 20 patients underwent repeated TSS, respectively. In the patients who underwent repeated TSS, only 20.0% (4/20) of them achieved immediate remission, which is significantly lower than the remission rate (57.6%, 38/66) in the patients who underwent first TSS ($p = 0.003$).

Perioperative Complications

The surgery for corticotroph adenomas with CSI usually was related to the high incidence of complications. In this series, the most common complication was intraoperatively CSF leakage, which occurred in in 24.4% (21/86) patients (**Table 4**). The sellar reconstruction was performed by packing of the sphenoid sinus and sella turcica with fat, muscle, and nasoseptal flap for all 21 patients with intraoperative CSF leakage. However, there were still 5 patients who have postoperative CSF leakage. Of these, 3 patients were successfully treated by repeated sellar reconstruction and external lumbar drain. Two patients who experienced CSF leakage and CNS infection were treated with antibiotics. After TSS, 15.1% (13/86) of the patients experienced transient diabetes insipidus. Of these, 9 of 13 recovered after medical therapy, and 4 patients developed permanent diabetes insipidus and needed lifelong treatment with desmopressin acetate. After surgery, 5.8% (5/86) of the patients experienced hypopituitarism and received hormone replacement therapy. Five patients (5.8%) experienced partial abducent nerve palsy and three patients (3.5%) experienced partial oculomotor nerve palsy, respectively, and all recovered completely within 1 year. Three patients showed visual deterioration after TSS, and two of them experienced various degrees of improvement of visual dysfunction. One patient who was undergoing repeated TSS experienced ICA rupture (which was controlled by direct compression) and underwent digital subtraction angiography immediately. The ICA rupture was blocked by the stent, and the patient recovered finally without neurological deficits.

Recurrence

Recurrence was observed in 16.7% (7/44) of all patients with initial remission, and the median time to recurrence for these patients was 33.0 months (range 2.0–105.0 months) (**Table 5**). However, no patients with Knosp Grade 2 were found to be

TABLE 4 | Perioperative complications of patients with corticotroph adenomas invading CS based on Knosp grade.

Results	Overall	Knosp Grade 2	Knosp Grade 3	Knosp Grade 4	*p*-value
Intraoperatively CSF leakage	21/86 (24.4%)	0/4 (0%)	8/36 (22.2%)	13/46 (28.3%)	$p > 0.05$
Postoperatively CSF leakage (%)	5/86 (5.8%)	0/4 (0%)	1/36 (2.8%)	4/46 (8.7%)	$p > 0.05$
Transient diabetes insipidus	13 /86 (15.1%)	1/4 (25.0%)	4/36 (11.1%)	8/46 (17.4%)	$p > 0.05$
Permanent diabetes insipidus	4/86 (4.7%)	0/4 (0%)	2/36 (5.6%)	2/46 (4.3%)	$p > 0.05$
Postoperative hypopituitarism	5/86 (5.8%)	1/4 (25.0%)	2/36 (5.6%)	2/46 (4.3%)	$p > 0.05$
Partial abducent nerve palsy (%)	5/86 (5.8%)	0/4 (0%)	2/36 (5.6%)	3/46 (6.5%)	$p > 0.05$
Partial oculomotor nerve palsy (%)	3/86 (3.5%)	0/4 (0%)	2/36 (5.6%)	1/46 (2.2%)	$p > 0.05$
Impaired vision	3/86 (3.5%)	0/4 (0%)	1/36 (2.8%)	2/46 (4.3%)	$p > 0.05$
CNS infection (%)	2/86 (2.3%)	0/4 (0%)	1/36 (2.8%)	1/46 (2.2%)	$p > 0.05$
ICA rupture (%)	1/86 (1.2%)	0/4 (0%)	0/36 (0%)	1/46 (2.2%)	$p > 0.05$

TABLE 5 | Recurrence outcome of included patients with initial remission based on Knosp grade.

MRI results	Overall	Knosp Grade 2 0/3 (0%)	Knosp Grade 3 3/20 (15.0%)	Knosp Grade 4 4/19 (21.1%)	*p*-value
Number of patients	7/42 (16.7%)				$p = 0.62$
Median time to recurrence (ms)	33.0 (2.00–105.0)	0	29.0 (6.0–56.0)	36.0 (2.0–105.0)	$p > 0.05$

recurrent. No significant difference in recurrence rate was observed between the patients with Knosp Grade 3 (15.0%, 3/20) and Knosp Grade 4 adenomas (21.1%, 4/19) ($p > 0.05$).

Further Treatments for Persistent and Recurrent Corticotroph Adenomas With CSI

For those patients with persistent disease (44) and recurrent corticotroph adenomas (7), data about further treatment were available for only 30 of 51 patients. Radiotherapy was used for 15 patients, and 4 (26.7%) of them achieved biochemical remission. Repeat TSS was performed in 5 patients, but none achieved remission. Medication was administered in 4 patients, and only one obtained disease control. Adrenalectomy was performed in 6 patients, and 5 (83.3%) achieved biochemical remission. At the last follow-up, 33.3% (10 of 30) of the patients were in remission, and 20 patients still had persistent disease (**Table 6**).

DISCUSSION

This study reports on the outcomes of TSS in 86 patients with corticotroph adenoma invading CS who underwent TSS at the PUMCH between 2000 and 2019. To our knowledge, this is one of the largest series on corticotroph adenomas with CSI published till now. This study demonstrated that the immediate remission of the surgical approach and the long-term outcome after adjuvant therapies for corticotroph adenomas with CSI are unsatisfactory. Additionally, CSI evaluated using Knosp grade based on preoperative MRI not always accurately predict intraoperatively observed CSI. Moreover, extent of tumor resection and number of operations significantly affected the surgical outcome of TSS for corticotroph adenomas with CSI. However, the Knosp grade, tumor size, and technical factor is not associated with the surgical outcome.

Preoperative MRI-based Knosp grade classifications play a crucial role in diagnosis of CSI of corticotroph adenomas. However, radiological results do not always discriminate between compression/extension and invasion of CS. In this study, only 84.0% (42 of 50) of the patients with MRI-based Knosp grade 3 was intraoperatively identified with CSI, and 8 other patients with Knosp grade 3 adenomas did not have CSI at surgery. Furthermore, 5.4% (4 of 74) of the patients with MRI-based Knosp grade 2 adenomas were found to have CSI during surgery. These findings are consistent with previous studies (15, 16). Dickerman and colleagues (17) demonstrated that dural invasion was directly observed at surgery and was confirmed histologically in 62% of the patients with no adenomas and interpreted based on preoperative MRI. Lonser also reported that preoperative MRI accurately predicted dural invasion in only 4 patients (22%) with CSI (18). Other previous studies also indicated that Knosp classification does not accurately predict the invasion of the Knosp grade 0–2 adenomas; thus, their application in the prediction of invasion among microadenomas is limited (19). A recent Meta-Analysis also reported that the prevalence of CSI radiographically (43%) was much higher than that (18%) intraoperatively, and the radiologic criteria of Knosp 3-4 had the highest correlation with intraoperative CSI (20). Therefore, although MRI-based Knosp grade can reliably define the degrees of CSI in Knosp 3–4 larger tumors, it is often unreliable to define the absence of CSI in Knosp 0–2 microadenomas. To define more accurately CSI beyond the lateral tangential line between ICA segments respectively, Knosp updated the original grading system of invasion in PAs by establishing the subtypes of grade 3a and 3b PAs in 2015 (15). However, up to 80% of CD patients present with a microadenoma, and there is no reliable grading system for microadenomas that accurately predicts CSI of corticotroph adenoma. Thus, more reliable grading systems of invasion for corticotroph adenomas are needed.

For corticotroph adenomas with CSI, complete surgical resection of tumor is difficult. Thus, lower remission rates of TSS have been reported in the patients with corticotroph adenomas with CSI. However, 48.8% of corticotroph adenomas with CSI in our center achieved remission after TSS, which was higher than that reported in previous studies (7, 21). The main reasons for the higher remission rate may include the experienced neurosurgeons, intraoperative multiple technique assistance, and aggressive surgical procedure.

Surgery for corticotroph adenomas with CSI has always been a challenge because of the highly complex anatomy of the CS and difficult in CS dissection. Thus, experienced neurosurgeon is essential to achieve complete tumor resection, biochemical remission, and avoid perioperative complications. In our center, almost all surgeries for CD patients were performed by RW and MF, who had experience with more than one thousand pituitary surgeries as previously described (9). Each year, more

TABLE 6 | Further treatments and remission rate in persistent and recurrent patients with invasive corticotroph adenomas.

Total/Remission Rate	Radiotherapy	Repeat TSS	Medical therapy	Adrenalectomy
Total (10/30, 33.3%)	4/15 (26.7%)	0/5 (0%)	1/4 (25.0%)	5/6 (83.3%)

than one hundred CD patients undergo pituitary surgery in PUMCH, and a large part of them are invasive macroadenomas and recurrent CD (22). The number of surgical patients with CD in PUMCH may be one of the largest centers. Therefore, large-scale surgical patients with CD have accumulated rich surgical experience in management of patients with corticotroph adenomas with CSI. Unfortunately, even in the hands of experienced surgeons, only about half of corticotroph adenomas with CSI could achieve remission after TSS. There are several studies that also found that biochemical remission rate is related to the number of years of neurosurgical experience. Yap and colleagues reported that the first decade of neurosurgery experience was associated with lower remission rates than that with the second and third decade of neurosurgery experience (23). A recent meta-analysis also demonstrated the possible association of neurosurgeons' experience with remission rates in CD patients (24). Therefore, neurosurgical experience may be one of main reasons for the higher remission rate of TSS in corticotroph adenomas with CSI.

Application of multiple techniques may be another important factor for the higher remission rate of TSS in corticotroph adenomas with CSI. In this study, multiple techniques including neuronavigation and intraoperative Doppler ultrasonography were used intraoperatively for surgical assistance in most patients, which resulted in maximum tumor removal and a relatively low rate of perioperative complications. For larger and recurrent corticotroph adenomas with CSI, neuronavigation and Doppler ultrasonography was used to determine the exact location of the ICA. These techniques can provide references for locating some important structures including the ICA, brainstem, and optic canal in real time during surgery (25). Precisely locating these structures can prevent injuries to them, thereby decreasing the frequency of perioperative complications. T. J. Owen also reported that using the neuronavigation system for localization, the rostral and caudal margins of the pituitary fossa during TSS may decrease morbidity and surgical time (26). Doppler ultrasonography has also been shown to determine the exact location of the ICA and whether an aneurysm exists, thereby avoiding injuring the ICA during surgery (27). Therefore, these multiple techniques used in surgery facilitate tumor resection and a safe operation and decrease perioperative complications in corticotroph adenomas with CSI.

In our center, an aggressive procedure was used to pursue a maximum safe removal of tumor. During the surgery, in order to accurately assess the CSI and to remove the tumor maximally, it is critical to widely expose the anterior and inferior sella dura, even the medial dural wall of the CS. Thus, endoscopic extended transsphenoidal surgery was used for most larger corticotroph adenomas with CSI, which provide direct visualization for resection of the tumors invading the CS and suprasellar (28). Recently, the incision of the CS wall has also been performed for PAs invading the CS, which resulted in a higher GTR rate (12). Therefore, rich surgical experience, wide exposure by endoscopic extended transsphenoidal surgery and incision of the CS, and intraoperative assistance of combined neuronavigation and intraoperative Doppler ultrasonography are the main reasons for the higher remission rate in our center.

Identification of the factors affecting surgical outcomes is very important for predicting the prognosis of patients with corticotroph adenomas invading CS. In this study, we found that the remission rate (75%) in patients with Knosp grade 2 adenomas is higher than that in patients with Knosp grade 3 adenomas (55.6%) and Knosp grade 4 adenomas (41.3%), but it did not reach statistical significance. This result indicated that the MRI-based Knosp grade classifications were not related to immediate remission in corticotroph adenomas with CSI, which is consistent with the results of most previous studies. Similarly, Wagenmakers (6) reported that the remission was achieved in 50.0% of patients with Knosp grade 2, 37.5% of patients with Knosp grade 3, and 33.3% of patients with Knosp grade 4, respectively. However, another study by Witek showed that the immediate postoperative remission depended on invasiveness based on Knosp grades 3 and 4 for macroadenomas (29). However, only 4 patients with Knosp grade 2 adenomas were included in the present study, and more large-scale studies are needed to further verify this conclusion.

Whether the adenoma size affects the surgical remission in corticotroph adenomas with CSI remains controversial. In our study, patients with microadenomas invading CS had higher immediate remission rates than patients with macroadenomas invading CS and giant adenomas invading CS; however, it does not reach statistical significance. This is consistent with the results from some previous studies. Starke reported that there was no significant difference in remission among patients with microadenomas and macroadenomas (30). Feng also reported that CD patients with macroadenomas and microadenomas had similar remission rate after TSS (11). On the contrary, a few studies have opposite conclusions; Blevins (31) indicated that CSI and the presence of a tumor diameter ≥ 2.0 cm were characteristics associated with an increased likelihood of residual disease after surgery. Other studies also demonstrated an inverse correlation between remission rates and tumor size in patients with CD (4, 32). However, most of the previous studies reported the effect of tumor diameter on remission rate in patients with CD, but not in patients with corticotroph adenoma invading CS. Therefore, more studies on potential factors predicting surgical outcomes in corticotroph adenomas with CSI are needed.

In this study, we found that the repeated TSS for corticotroph adenomas with CSI has shown significant lower remission rates compared with the first TSS. The main reasons for this result may be the destruction of the original anatomy and scar formation within the recurrent tumor. These factors make the surgery more difficult and dangerous. Valderrábano and colleagues (33) also demonstrated that the repeat TSS for CD is associated to a lower remission rate and a higher risk of recurrence, which is consistent with our results. However, the large-scale clinical study on results of repeat TSS for corticotroph adenomas with CSI is limited, and further studies are needed.

Depending on the neurosurgeon's preference, TSS for corticotroph adenomas with CSI could be performed using a

microscopic or endoscopic approach. Compared with the microscopic approach, the endoscopic approach provides a broader surgical view of the pituitary region, including lateral edges of the sella and CS. However, in this study, no significant difference was found in the remission rates among the patients with corticotroph adenomas invading CS who underwent microscopic TSS and endoscopic TSS. The microscopic and endoscopic techniques were used in combination for a subset of corticotroph adenomas with CSI, which might explain why an endoscopic versus a microscopic technique yielded a similar remission rate in our center. This result is in accordance with one recent meta-analysis, which indicated that comparisons of remission rates by endoscopic versus microscopic technique yielded the same results (34). However, another meta-analysis demonstrated that the endoscopic TSS reaches comparable results for microadenomas, and probably better results for macroadenomas than microscopic TSS for CD patients (35). To date, the data about comparisons of remission rates by an endoscopic versus a microscopic technique in corticotroph adenomas with CSI are limited, and more studies comparing the two techniques in corticotroph adenomas with CSI at the same institution are needed.

We have previously indicated that the number of operations, the duration of disease, tumor invasion, tumor size, and preoperative ACTH concentration could predict the immediate outcomes of TSS in patients with corticotroph adenomas (36). However, in this study, we found that neither Knosp grade nor tumor size affects the remission rate in corticotroph adenomas with CSI. The main reasons for the difference may be that all included corticotroph adenomas are invading CS in this study; therefore, the Knosp grade and tumor size did not affect the surgical outcomes. Compared with the first TSS, the repeated TSS for corticotroph adenomas with CSI is related to the lower remission rates, which is consistent with the results of previous studies (37, 38). Therefore, further research is needed to identify the factors affecting surgical outcomes of corticotroph adenomas with CSI.

It is difficult to manage patients with persistent or recurrent corticotroph adenomas with CSI. Therapy options include radiation therapy, repeated TSS, medical therapy, and, as a final step, bilateral adrenalectomy. These treatments have their own advantages and disadvantages; however, there is no consensus on which treatment is preferable. In our center, an individual-based comprehensive treatment was discussed by a multidisciplinary team (MDT) with collaborating experts. However, even if comprehensive treatments were used, the prognosis of these patients is still poor, and more effective treatments are needed.

LIMITATIONS

Although this study is a rather larger patient cohort regarding the results of TSS on corticotroph adenomas with CSI in a single institution, there are some limitations that deserve to be mentioned. First, because of the retrospective nature of the study, it is difficult to collect complete clinical information and long-term follow-up data for all patients. Some data on long-term follow-up and further treatments were missing, which may result in a bias of the results and conclusions on long-term outcomes and recurrence rate. Additional information of survival or death for half of the included patients cannot be obtained; thereby, the mortality results are not included and analyzed. Another limitation is that referral or selection bias must be taken into consideration because this was a single-center cohort study.

CONCLUSIONS

In summary, the remission rate of corticotroph adenomas with CSI was unsatisfactory due to incomplete resection of invasive and/or a large adenoma. With the application of multiple techniques, approximately half of the patients could achieve GTR and biochemical remission *via* TSS by experienced neurosurgeons. Extent of tumor resection and number of operations were associated with surgical remission rate in corticotroph adenomas with CSI. In contrast, Knosp grade, tumor size, and surgical approach did not affect the remission rate of TSS in corticotroph adenomas with CSI. In addition, further treatment including radiotherapy, repeated operation, medical therapy, and even bilateral adrenalectomy are required for persistent or recurrent corticotroph adenomas with CSI.

DATA AVAILABILITY STATEMENT

The raw data supporting the conclusions of this article will be made available by the authors, without undue reservation.

ETHICS STATEMENT

The studies involving human participants were reviewed and approved by the Ethics Committee of Peking Union Medical College Hospital (Reference number: S-K1423). Written informed consent to participate in this study was provided by the participants' legal guardian/next of kin.

AUTHOR CONTRIBUTIONS

All authors listed have made a substantial, direct, and intellectual contribution to the work, and approved it for publication.

FUNDING

Financial support for this study was provided by the Beijing Municipal Administration of Hospitals Incubating Program (grant number: PX2022004). The funding institutions had no role in the design of the study, data collection and analysis, decision to publish, or preparation of the manuscript.

REFERENCES

1. Steffensen C, Bak AM, Zøylner Rubeck K, Jørgensen JOL. Epidemiology of Cushing's Syndrome. *Neuroendocrinology* (2010) 92(1):1–5. doi: 10.1159/000314297
2. Clayton RN, Raskauskiene D, Reulen RC, Jones PW. Mortality and Morbidity in Cushing's Disease Over 50 Years in Stoke-On-Trent, UK: Audit and Meta-Analysis of Literature. *J Clin Endocrinol Metab* (2011) 96(3):632–42. doi: 10.1210/jc.2010-1942
3. Ioachimescu AG. Prognostic Factors of Long-Term Remission After Surgical Treatment of Cushing's Disease. *Endocrin Metab Clin* (2018) 47(2):335–47. doi: 10.1016/j.ecl.2018.02.002
4. Johnston PC, Kennedy L, Hamrahian AH, Sandouk Z, Bena J, Hatipoglu B, et al. Surgical Outcomes in Patients With Cushing's Disease: The Cleveland Clinic Experience. *Pituitary* (2017) 20(4):430–40. doi: 10.1007/s11102-017-0802-1
5. Solak M, Kraljevic I, Dusek T, Melada A, Kavanagh MM, Peterkovic V, et al. Management of Cushing's Disease: A Single-Center Experience. *Endocrine* (2016) 51(3):517–23. doi: 10.1007/s12020-015-0695-6
6. Wagenmakers MAEM, Boogaarts HD, Roerink SHPP, Timmers HJLM, Stikkelbroeck NMML, Smit JWA, et al. Endoscopic Transsphenoidal Pituitary Surgery: A Good and Safe Primary Treatment Option for Cushing's Disease, Even in Case of Macroadenomas or Invasive Adenomas. *Eur J Endocrinol* (2013) 169(3):329–37. doi: 10.1530/EJE-13-0325
7. Zhuang Z, Liu X, Bao X, Pan B, Deng K, Yao Y, et al. Invasive ACTH-Secreting Pituitary Macroadenoma in Remission After Transsphenoidal Resection: A Case Report and Literature Review. *Medicine* (2018) 97(46):e13148. doi: 10.1097/MD.0000000000013148
8. Knosp E, Steiner E, Kitz K, Matula C. Pituitary Adenomas With Invasion of the Cavernous Sinus Space: A Magnetic Resonance Imaging Classification Compared With Surgical Findings. *Neurosurgery* (1993) 33(4):610–7; discussion 617-8. doi: 10.1227/00006123-199310000-00008
9. Dai C, Fan Y, Liu X, Bao X, Yao Y, Wang R, et al. Predictors of Immediate Remission After Surgery in Cushing's Disease Patients: A Large Retrospective Study From a Single Center. *Neuroendocrinology* (2021) 111(11):1141–50. doi: 10.1159/000509221
10. Feng M, Liu Z, Liu X, Zhang X, Bao X, Yao Y, et al. Tumour Lateralization in Cushing's Disease by Inferior Petrosal Sinus Sampling With Desmopressin. *Clin Endocrinol* (2018) 88(2):251–7. doi: 10.1111/cen.13505
11. Feng M, Liu Z, Liu X, Bao X, Yao Y, Deng K, et al. Diagnosis and Outcomes of 341 Patients With Cushing's Disease Following Transsphenoid Surgery: A Single-Center Experience. *World Neurosurg* (2018) 109:e75–80. doi: 10.1016/j.wneu.2017.09.105
12. Bao X, Deng K, Liu X, Feng M, Chen CC, Lian W, et al. Extended Transsphenoidal Approach for Pituitary Adenomas Invading the Cavernous Sinus Using Multiple Complementary Techniques. *Pituitary* (2016) 19(1):1–10. doi: 10.1007/s11102-015-0675-0
13. de Paiva Neto MA, Vandergrift A, Fatemi N, Gorgulho AA, DeSalles AA, Cohan P, et al. Endonasal Transsphenoidal Surgery and Multimodality Treatment for Giant Pituitary Adenomas. *Clin Endocrinol* (2010) 72(4):512–9. doi: 10.1111/j.1365-2265.2009.03665.x
14. Dai C, Liang S, Liu X, Fan Y, Bao X, Yao Y, et al. Outcomes of Transsphenoidal Surgery in Cushing Disease Patients With Negative Pituitary Magnetic Resonance Imaging Findings: A Single-Center Experience. *Endocr Pract* (2020) 26(11):1320–30. doi: 10.4158/EP-2020-0177
15. Micko ASG, Wöhrer A, Wolfsberger S, Knosp E. Invasion of the Cavernous Sinus Space in Pituitary Adenomas: Endoscopic Verification and its Correlation With an MRI-Based Classification. *J Neurosurg* (2015) 122(4):803–11. doi: 10.3171/2014.12.JNS141083
16. Mastorakos P, Taylor DG, Chen C, Buell T, Donahue JH, Jane JA. Prediction of Cavernous Sinus Invasion in Patients With Cushing's Disease by Magnetic Resonance Imaging. *J Neurosurg* (2019) 130(5):1593–8. doi: 10.3171/2018.2.JNS172704
17. Dickerman RD, Oldfield EH. Basis of Persistent and Recurrent Cushing Disease: An Analysis of Findings at Repeated Pituitary Surgery. *J Neurosurg* (2002) 97(6):1343–9. doi: 10.3171/jns.2002.97.6.1343
18. Lonser RR, Ksendzovsky A, Wind JJ, Vortmeyer AO, Oldfield EH. Prospective Evaluation of the Characteristics and Incidence of Adenoma-Associated Dural Invasion in Cushing Disease. *J Neurosurg* (2012) 116(2):272. doi: 10.3171/2011.8.JNS11456
19. Dallapiazza R, Bond AE, Grober Y, Louis RG, Payne SC, Oldfield EH, et al. Retrospective Analysis of a Concurrent Series of Microscopic Versus Endoscopic Transsphenoidal Surgeries for Knosp Grades 0-2 Nonfunctioning Pituitary Macroadenomas at a Single Institution. *J Neurosurg* (2014) 121(3):511–7. doi: 10.3171/2014.6.JNS131321
20. Dhandapani S, Singh H, Negm HM, Cohen S, Anand VK, Schwartz TH. Cavernous Sinus Invasion in Pituitary Adenomas: Systematic Review and Pooled Data Meta-Analysis of Radiologic Criteria and Comparison of Endoscopic and Microscopic Surgery. *World Neurosurg* (2016) 96:36–46. doi: 10.1016/j.wneu.2016.08.088
21. Shin SS, Gardner PA, Ng J, Faraji AH, Agarwal N, Chivukula S, et al. Endoscopic Endonasal Approach for Adrenocorticotropic Hormone-Secreting Pituitary Adenomas: Outcomes and Analysis of Remission Rates and Tumor Biochemical Activity With Respect to Tumor Invasiveness. *World Neurosurg* (2017) 102:651–658.e1. doi: 10.1016/j.wneu.2015.07.065
22. Liu Y, Liu X, Hong X, Liu P, Bao X, Yao Y, et al. Prediction of Recurrence After Transsphenoidal Surgery for Cushing's Disease: The Use of Machine Learning Algorithms. *Neuroendocrinology* (2019) 108(3):201–10. doi: 10.1159/000496753
23. Yap LB, Turner HE, Adams CB, Wass JA. Undetectable Postoperative Cortisol Does Not Always Predict Long-Term Remission in Cushing's Disease: A Single Centre Audit. *Clin Endocrinol (Oxf)* (2002) 56(1):25–31. doi: 10.1046/j.0300-0664.2001.01444.x
24. Abu DA, Singh ON, Al NA, Farah WH, Barrionuevo P, Sarigianni M, et al. Predictors of Biochemical Remission and Recurrence After Surgical and Radiation Treatments of Cushing Disease: A Systematic Review and Meta-Analysis. *Endocr Pract* (2016) 22(4):466–75. doi: 10.4158/EP15922.RA
25. Dolati P, Eichberg D, Golby A, Zamani A, Laws E. Multimodal Navigation in Endoscopic Transsphenoidal Resection of Pituitary Tumors Using Image-Based Vascular and Cranial Nerve Segmentation: A Prospective Validation Study. *World Neurosurg* (2016) 95:406–13. doi: 10.1016/j.wneu.2016.06.008
26. Owen TJ, Chen AV, Frey S, Martin LG, Kalebaugh T. Transsphenoidal Surgery: Accuracy of an Image-Guided Neuronavigation System to Approach the Pituitary Fossa (Sella Turcica). *Vet Surg* (2018) 47(5):664–71. doi: 10.1111/vsu.12906
27. Solheim O, Selbekk T, Lovstakken L, Tangen GA, Solberg OV, Johansen TF, et al. Intrasellar Ultrasound in Transsphenoidal Surgery: A Novel Technique. *Neurosurgery* (2010) 66(1):173–85; discussion 185-6. doi: 10.1227/01.NEU.0000360571.11582.4F
28. Zhao B, Wei Y, Li G, Li Y, Yao Y, Kang J, et al. Extended Transsphenoidal Approach for Pituitary Adenomas Invading the Anterior Cranial Base, Cavernous Sinus, and Clivus: A Single-Center Experience With 126 Consecutive Cases. *J Neurosurg* (2010) 112(1):108. doi: 10.3171/2009.3.JNS0929
29. Witek P, Zielinski G, Szamotulska K, Maksymowicz M, Kaminski G. Clinicopathological Predictive Factors in the Early Remission of Corticotroph Pituitary Macroadenomas in a Tertiary Referral Centre. *Eur J Endocrinol* (2016) 174(4):539–49. doi: 10.1530/EJE-15-1226
30. Starke RM, Reames DL, Chen CJ, Laws ER, Jane JJ. Endoscopic Transsphenoidal Surgery for Cushing Disease: Techniques, Outcomes, and Predictors of Remission. *Neurosurgery* (2013) 72(2):240–7; discussion 247. doi: 10.1227/NEU.0b013e31827b966a
31. Blevins LJ, Christy JH, Khajavi M, Tindall GT. Outcomes of Therapy for Cushing's Disease Due to Adrenocorticotropin-Secreting Pituitary Macroadenomas. *J Clin Endocrinol Metab* (1998) 83(1):63–7. doi: 10.1210/jcem.83.1.4525
32. Valassi E, Biller BMK, Swearingen B, Pecori Giraldi F, Losa M, Mortini P, et al. Delayed Remission After Transsphenoidal Surgery in Patients With Cushing's Disease. *J Clin Endocrinol Metab* (2010) 95(2):601–10. doi: 10.1210/jc.2009-1672
33. Valderrábano P, Aller J, García-Valdecasas L, García-Uría J, Martín L, Palacios N, et al. Results of Repeated Transsphenoidal Surgery in Cushing's Disease. Long-Term Follow-Up. *Endocrinología y Nutrición* (2014) 61(4):176–83. doi: 10.1016/j.endonu.2013.10.008
34. Qiao N. Outcome of Endoscopic vs Microsurgical Transsphenoidal Resection for Cushing's Disease. *Endocrine Connections* (2018) 7(1):R26–37. doi: 10.1530/EC-17-0312
35. Broersen LHA, Biermasz NR, van Furth WR, de Vries F, Verstegen MJT, Dekkers OM, et al. Endoscopic vs. Microscopic Transsphenoidal Surgery for Cushing's Disease: A Systematic Review and Meta-Analysis. *Pituitary* (2018) 21(5):524–34. doi: 10.1007/s11102-018-0893-3
36. Dai C, Fan Y, Liu X, Bao X, Yao Y, Wang R, et al. Predictors of Immediate Remission After Surgery in Cushing's Disease Patients: A Large Retrospective

Study From a Single Center. *Neuroendocrinology* (2021) 111(11):1141–50. doi: 10.1159/000509221
37. Stroud A, Dhaliwal P, Alvarado R, Winder MJ, Jonker BP, Grayson JW, et al. Outcomes of Pituitary Surgery for Cushing's Disease: A Systematic Review and Meta-Analysis. *Pituitary* (2020) 23(5):595–609. doi: 10.1007/s11102-020-01066-8
38. Dai C, Feng M, Sun B, Bao X, Yao Y, Deng K, et al. Surgical Outcome of Transsphenoidal Surgery in Cushing's Disease: A Case Series of 1106 Patients From a Single Center Over 30 Years. *Endocrine* (2022) 75(1):291–27. doi: 10.1007/s12020-021-02848-1

Conflict of Interest: The authors declare that the research was conducted in the absence of any commercial or financial relationships that could be construed as a potential conflict of interest.

Publisher's Note: All claims expressed in this article are solely those of the authors and do not necessarily represent those of their affiliated organizations, or those of the publisher, the editors and the reviewers. Any product that may be evaluated in this article, or claim that may be made by its manufacturer, is not guaranteed or endorsed by the publisher.

frontiers in Oncology

ORIGINAL RESEARCH
published: 16 March 2022
doi: 10.3389/fonc.2022.846614

The Clinical and Pathological Characteristics of Refractory Pituitary Adenomas: A Single Center Experience

Xiaohai Liu[1,2†], Congxin Dai[2,3†], Xinjie Bao[2,4], Kan Deng[2,4], Yong Yao[2,4], Ming Feng[2,4], Mingchu Li[1,2], Ge Chen[1,2] and Renzhi Wang[2,4]*

[1] Department of Neurosurgery, Xuanwu Hospital Capital Medical University, Beijing, China, [2] Chinese Pituitary Specialists Congress, Beijing, China, [3] Department of Neurosurgery, Tongren Hospital Capital Medical University, Beijing, China, [4] Department of Neurosurgery, Peking Union Medical College Hospital, Chinese Academy of Medical Sciences and Peking Union Medical College, Beijing, China

OPEN ACCESS

Edited by:
Qun Wu,
Zhejiang University, China

Reviewed by:
Run Yu,
University of California, Los Angeles, United States
Yuan Shan,
Baylor Scott and White Health, United States

***Correspondence:**
Renzhi Wang
wangrz@126.com

[†]These authors have contributed equally to this work

Specialty section:
This article was submitted to Neuro-Oncology and Neurosurgical Oncology, a section of the journal Frontiers in Oncology

Received: *31 December 2021*
Accepted: *17 February 2022*
Published: *16 March 2022*

Citation:
Liu X, Dai C, Bao X, Deng K, Yao Y, Feng M, Li M, Chen G and Wang R (2022) The Clinical and Pathological Characteristics of Refractory Pituitary Adenomas: A Single Center Experience. Front. Oncol. 12:846614. doi: 10.3389/fonc.2022.846614

Background: Most of pituitary adenomas (PAs) are slow-growing benign tumors which can be cured or controlled by conventional therapies, including surgery, medical treatment or radiotherapy. A small set of PAs, usually known as aggressive PAs or refractory PAs, present with more aggressive behavior and lead to poorer prognosis than classical PAs.

Methods: We retrospectively analyzed the clinical and pathological characteristics of 44 patients who were diagnosed with refractory PAs by a multidisciplinary team (MDT). All the patients' demographic characteristics, radiological findings, Knosp grade, treatment details and clinical outcomes were abstracted from the medical records. Additionally, 44 patients with nonrefractory PAs (NRPAs) matched for age and gender were selected to serve as the control group.

Results: Despite using all combined treatments including surgery, radiotherapy and conventional medical treatments, all the refractory PAs showed tumor progression or hormone hypersecretion which caused increased morbidity and mortality and remained challenging to management. Compared with those of the non-refractory PAs, the tumor size, invasive rate and tumor growth rate (TGR) were significantly higher in the refractory PAs. TGR >2.2% per month may be considered as a preoperative indicator of refractoriness. The Ki-67 index in the refractory PAs were all ≥3%. EGFR, but not MMP2 or MMP9, was significantly overexpressed in refractory PAs compared with the corresponding levels in nonrefractory PAs.

Conclusion: Refractory PAs are unresponsive to surgery, radiotherapy and conventional medical treatments with a poor prognosis. Moreover, a TGR ≥2.2% per month, Ki-67 index ≥3% and EGFR overexpression may be independent predictors of clinical refractoriness.

Keywords: refractory pituitary adenoma, aggressive pituitary adenoma, tumor growth rate, Ki-67, EGFR

INTRODUCTION

Pituitary adenomas (PAs), accounting for 15% of all intracranial neoplasms, are monoclonal benign tumors arising from adenohypophyseal cells (1). With the development of imaging technology, the prevalence of clinically evident PAs has recently been reported to be 1/1000 in a Belgian population and 0.776/1000 (of which 0.542/1000 were hormone secreting) in a region of the United Kingdom (2, 3). Interestingly, according to a meta-analysis of radiology and pathology autopsy reports, incidental findings of pituitary lesions were commonly found in almost 16.7% of the population, indicating that most PAs were nonfunctional tumors which stopped growing or grew very slowly and needed no intervention after tumorigenesis (4). In contrast, a small set of PAs, usually known as aggressive PAs or refractory PAs, exhibit radiologically invasive and unusually rapid tumor growth rates (TGRs) or clinically relevant tumor growth despite maximal treatment with standard therapies, including surgery, radiotherapy and conventional medical treatments (5–8). At the extreme end of the spectrum, PAs accompanied with noncontiguous craniospinal or distant metastasis are called pituitary carcinomas, which are exceedingly rare, comprising only 0.1–0.2% of all PAs (9). Although it is not clear why most PAs are slowly-growing benign tumors while others exhibit aggressive or even malignant behavior are still obscure, it is ultimately urgent to get an accurate identification and early treatment for these refractory PAs to improve the patient outcomes.

To differentiate refractory PAs with aggressive even malignant behavior from benign PAs for early diagnosis and intensive therapy, the 2004 World Health Organization (WHO) classification system categorized PAs as typical tumors, atypical tumors and pituitary carcinomas (10). PAs with Ki-67 labeling index of >3% and excessive staining with p53 were diagnosed as atypical PA. However, the clinical impact of atypical PA is controversial as many studies have shown that some atypical PAs do not grow in a clinically aggressive mode and remain quiescent for years during follow-up or after the initial total resection (11, 12). Due to its low predictive value, the category of atypical PA is abnegated in the updated 2017 WHO classification of PAs (13), which also insisted on the evaluation of tumor proliferation potential by mitotic count and Ki-67 labeling index. According to the European Society for Endocrinology (ESE) guidelines, the diagnosis of an aggressive PA should be considered in patients with a radiologically invasive tumor and unusually rapid TGR, or clinically relevant tumor growth despite optimal standard therapies, including surgery, radiotherapy and conventional medical treatment (14). However, this definition may seem obscure and ambiguous as it does not define what represents "clinically relevant tumor growth" or an "unusually rapid TGR". Until now, no biomarkers have been used to predict the aggressiveness of PA and the outcome of patients.

During the last decade, we focused on the diagnosis and treatment of aggressive PAs and proposed a new category, "refractory PAs", to define these adenomas which exhibit a distinctive disease course compared with that of benign PAs (7, 8, 15). Although the definition of "aggressive" and "refractory" overlaps with each other, the definition of refractory PA emphasizes the importance of the Ki-67 index, TGR and the patient's response to the treatment from the standpoint of disease course. In order to optimize the definition of refractory PAs, here we investigated a series of 44 patients with refractory PAs to determine the clinical and pathological characteristics for early diagnosis and intensive intervention.

MATERIALS AND METHODS

Patients

Between Jan. 2014 and Dec. 2016, 2021 patients with PA underwent transsphenoidal surgery (TSS) or craniotomy at Peking Union Medical College Hospital (PUCMH, Beijing, China). Forty-four patients who were diagnosed with refractory PAs according to our diagnostic criteria by a multidisciplinary team (MDT) that included endocrinologists, neurosurgeons, pathologists, neuroradiologists, and oncologists were enrolled in this study (6). In our previous studies, the most important characteristics of refractory PAs included refractoriness to standard therapies, including surgery, radiotherapy and conventional medical treatment; tumor infiltration of the adjacent structures based on either radiological images or intraoperative findings; a cut-off value of > 3% for Ki-67; increasing TGR > 2% per month; and tumor recurrence within 6 months after surgery (7, 8). All the patients' demographic characteristics, radiological findings, Knosp grade, treatment details and clinical outcomes were abstracted from the medical records. Additionally, 44 patients with nonrefractory PAs (NRPAs) matched for age and gender were selected to serve as the control group. 40 cases in the NRPA group had been achieved total resection after the initial surgery, while 4 patients received subtotal resection and remained stable after external beam radiotherapy (EBRT). The study was approved by the Research Ethics Committee of PUMCH and all the patients provided their written informed consent for the research.

Clinical and Radiological Evaluation

Visual field and visual acuity assessments were performed by neuroophthalmologist for all patients. Regrading functional tumors, endocrine-related complications related to tumor were also evaluated. Endocrine assessment was performed for all patients, and once every 6 months to 1 year during the follow-up. All patients underwent pituitary magnetic resonance imaging (MRI) scans. Then the cases were classified according to the Knosp classification system. TGRs were determined by calculating the velocity of tumor volume increases using a stereological method based on the Cavalieri principle in the patients with at least 2 thin-slice magnetic resonance images (MRI) (16).

Immunohistochemical Staining

Immunohistochemical staining of all the PAs was performed on the paraffin blocks to test for adenohypophyseal hormones,

pituitary transcription factors including Pit-1, SF-1, and T-pit and other biomarkers including Ki-67, low molecular weight cytokeratin (CAM 5.2), EGFR, p53, MMP-2 and MMP-9. In brief, sections with 5-μm thickness were stained using Ki-67 (Chemicon, USA) antibodies, p53 (ZSGB-BIO, China), CAM 5.2 (ZSGB-BIO, China), MMP-2 and MMP-9 (Abcam, Cambridge, MA, USA), and EGFR (Cell Signaling Technology, Boston, MA). Sections incubated in phosphate-buffered saline alone served as negative controls. Three fields of view (400×) were randomly selected. The images were obtained under constant luminance without white balance. The integrated optical density (IOD) value was determined using Image-Pro Plus 6.0 software (Media Cybernetics, Inc., Silver Spring, MD, USA). The stained area was selected, and the other areas were hyalinized. The images were converted into grayscale images, and IOD values were calculated. A semiquantitative assessment of the immunohistochemical reactions for EGFR was used to score the staining as 0 (negative, IOD 0.1), 1+ (low, 0.1–0.4), 2+ (intermediate, 0.4–0.6), 3+ (high, 0.6–0.8), or 4+ (very high, >0.8). Quantification of Ki-67-labeled cells was assessed by counting more than 500 nuclei in four randomly selected high-power fields, excluding the nuclei of vascular components and hematological cells. Immunohistochemical protein expression was scored blindly by two observers using a conventional optical microscope (Olympus, Tokyo, Japan). p53 was considered positive if more than 10% of the nuclei stained densely. Negative staining was accepted when tumor cells were negative in areas with positive staining for endothelial and mesenchymal cells. Mitotic counts were performed by reviewing at least 20 high-power microscopic fields at × 400 magnification.

Statistical Analysis

Statistical analysis was performed with SPSS 15.0 software (SPSS, Inc., Chicago, IL, USA). Comparisons of categorical variables were carried out by Chi-square or Fisher's exact tests. Binary logistic regression was employed to analyze independent predicted variables of clinical refractoriness. When two-sided p values were ≤.05, the differences were considered statistically significant.

RESULTS

Clinical Characteristics of Refractory PA

Among the 2021 patients with PA who underwent TSS or craniotomy at PUCMH, 44 refractory PAs were diagnosed, with an incidence of 2.2%. The clinical and immunohistochemical characteristics of 44 refractory PAs with integrated clinical archives and effective follow-ups are shown in **Table 1**. Among the 44 patients with refractory PAs, male patients accounted for 56.9% (25 cases), while female patients accounted for another 43.1% (19 cases). There were 824 male patients (40.7%) and 1197 female patients (59.3%) in the whole cohort. Fisher's exact test revealed that the male sex distribution was significant ($p < 0.05$). The mean age at diagnosis in the refractory group was 46.6 years (range 21–80 years), while the mean age was 42.77 years (range 6–82 years) in the whole cohort, showing that patients with refractory PAs tended to be older than those with ordinary PAs ($p < 0.05$). Of the 44 patients with refractory PAs, 23 (52.3%) PAs were identified as clinically nonfunctional PAs, whereas 21 cases (47.7%) were functional PAs. Moreover, there were 4 gonadotroph adenomas (GAs), 5 lactotroph adenomas (LA), 6 somatotroph adenomas (SA), 8 corticotroph adenomas (CA), 7 Crooke's cell adenomas (CCAs), 12 null cell adenomas (NCAs), 1 pit-1 positive plurihormonal adenoma (PPPA) and 1 acidophilic stem cell adenoma (ASCA) according to the 2017 WHO classification of PAs.

At diagnosis, the most common symptom among patients with refractory tumors was impaired vision or visual deficit (n = 27, 61.4%), followed by headache (n = 26, 59.1%), hypopituitarism (n = 21, 47.8%) and cavernous sinus syndrome (n = 10, 22.8%). All 5 patients with lactotroph adenoma and 1 patient with acidophilic stem cell adenoma had been treated and resistant to bromocriptine, and 3 in 6 GH tumors had been treated and exhibited resistance to octreotide. Regarding surgery (including TSS and craniotomy), all the 44 patients received at least one operation: 1 patient (2.3%) had undergone six operations, 2 patients (4.5%) had undergone five operations, 6 patients (13.6%) had undergone four operations, 5 patients (11.4%) had undergone three operations, 10 patients (22.7%) had undergone two operations, and 20 patients (45.5%) had undergone one operation. Regarding radiotherapy [including stereotactic radiosurgery (SRS) and external beam radiotherapy (EBRT)], all the 44 patients received at least one radiotherapy: 1 patient (2.3%) receiving four courses of SRS, 1 patient (2.3%) receiving three courses of therapy (two courses of SRS and one course of EBRT), 8 patients (18.2%) receiving two courses of therapy and the remaining 34 patients (77.3%) receiving one course of therapy at diagnosis. Despite the use of these combinations of treatments, all the refractory PAs showed tumor progression or hormone hypersecretion which caused increased morbidity and mortality and remained challenging to management.

For most the refractory PAs, follow-up MRIs revealed rapid growth of the residual tumor with invasion of the suprasellar cistern and cavernous sinuses which could not be resected either through TSS or craniotomy. To measure "rapid growth", TGR was determined by calculating the velocity of tumor volume increases. TGR were calculated among the 28 refractory PAs with at least 2 thin-slice magnetic resonance images during follow-up, which varied from 2.2 to 12.4%/month. The mean TGR was 4.4%/month, which was significantly faster than that of nonrefractory PAs.

Refractory Versus Nonrefractory PAs

To investigate the clinical characteristics of the patients with refractory tumors, 44 patients with nonrefractory PAs (NRPAs) matched for age and gender were selected to serve as the control group (**Table 2**). There were 11 gonadotroph adenomas (GAs), 2 lactotroph adenomas (LA), 12 somatotroph adenomas (SAs), 8 corticotroph adenomas (CAs), 1 Crooke's cell adenomas (CCAs),

TABLE 1 | Clinical and immunohistochemical characteristics of the 44 refractory PAs.

Pat. No.	Sex/ Age	Tumor Type	SRS/ EBRT	TSS/ Craniotomy	Medical Therapy	Tumor Diameter (mm)	Ki67%	P53	Abundant Mitoses
1	M/59	SGLA	1/0	2/0	Bro	66.5	20	+	+
2	M/50	DGLA	1/0	2/2	Bro	57	20	+	+
3	F/60	SGLA	1/1	1/0	Bro	32	5	–	–
4	M/29	Acidophilic stem cell adenoma	1/0	0/1	Bro	57.5	3	–	–
5	M/60	SGLA	1/0	2/0	Bro	66	3	–	–
6	F/59	SGLA	1/0	1/0	Bro	38	20	–	+
7	F/67	NCA	0/1	1/0	–	58	3	–	–
8	F/30	NCA	0/1	1/0	–	42	3	–	–
9	F/21	NCA	0/1	1/1	–	50	5	–	+
10	F/56	GA	1/0	4/0	–	42	15	+	+
11	M/66	GA	0/1	1/0	–	128	10	+	–
12	F/55	NCA	0/1	1/0	–	56	3	–	–
13	M/80	NCA	1/0	1/0	–	45	3	–	–
14	M/32	SGSA	1/0	1/2	–	44	25	+	+
15	M/76	NCA	0/1	1/0	–	35	5	–	–
16	F/62	NCA	0/1	2/0	–	52	10	–	+
17	M/52	SGSA	1/0	3/0	–	18.4	5	–	–
18	M/40	NCA	1/0	3/0	–	52	3	+	+
19	M/24	SGSA	2/0	4/1	–	66	25	+	+
20	M/34	DGSA	0/1	3/1	–	72	5	–	–
21	F/26	NCA	0/1	1/0	–	14	3	+	+
22	F/55	NCA	2/0	3/1	–	69	3	–	–
23	M/66	NCA	1/0	1/0	–	53	3	–	–
24	F/27	NCA	0/1	1/0	–	82	3	+	–
25	M/25	PPPA	0/1	1/1	–	68	8	–	–
26	F/42	SGSA	1/0	1/1	–	32	3	–	+
27	F/29	SGSA	1/0	2/0	–	69	10	–	+
28	F/55	SGSA	1/0	1/0	Oct	12	3	–	–
29	F/42	DGSA	1/0	1/0	Oct	24	3	–	–
30	M/42	SGSA	1/0	1/0	Oct	16	3	–	–
31	M/76	SGSA	4/0	2/1	–	23	40	+	+
32	M/53	CCA	2/0	3/1	–	18	10	+	+
33	F/45	CCA	0/1	1/0	–	18	5	–	+
34	M/33	CCA	1/0	2/2	–	38	5	–	–
35	M/33	CCA	1/0	2/0	–	12	3	–	–
36	M/67	CCA	1/0	1/0	–	44	5	–	–
37	M/41	CCA	0/1	1/0	–	13	5	–	+
38	F/24	SGCA	2/0	1/0	–	12	3	–	–
39	M/39	CCA	1/0	1/0	–	26	3	–	–
40	M/30	SGCA	2/0	5/1	–	32	12	+	+
41	F/32	GA	2/0	0/5	–	64	25	+	+
42	F/63	SGCA	2/1	2/0	–	44	5	+	+
43	M/45	GA	1/0	1/2	–	39	5	–	–
44	M/50	SGCA	0/1	1/1	–	26	20	+	+

Bro, bromocriptine; CCA, Crooke's cell adenoma; DGCA, Densely granulated corticotroph adenoma; DGLA, Densely granulated lactotroph adenoma; DGSA, Densely granulated somatotroph adenoma; GA, Gonadotroph adenoma; NCA, Null cell adenoma; Oct, Octreotide; PPPA, Plurihormonal PIT-1 positive adenoma; SGCA, Densely granulated corticotroph adenoma; SGLA, Sparsely granulated lactotroph adenoma; SGSA, Sparsely granulated somatotroph adenoma.

10 null cell adenomas (NCAs) according to the 2017 WHO classification of PAs. The diameters of the tumors in the refractory group ranged from 12.0 to 128.0 mm, with a mean size of 43.0 mm. In contrast, the diameters of the tumors in the nonrefractory group ranged from 3.3 to 43.0 mm, with a mean size of 22.6 mm. There was a significant difference in the size of the refractory versus nonrefractory tumors (48.6 vs. 22.6 mm, $p < 0.01$, **Figure 1A**). In addition, 24 of the 44 (54.5%) refractory PAs presented as a giant tumor (> 40 mm), while only 1 of the 44 (2.3%) PAs was a giant tumor in the NRPA ($p < 0.01$). In the refractory group, 37 tumors (84.1%) invaded the cavernous sinus, 23 tumors (52.3%) demonstrated suprasellar extension and 14 tumors (31.8%) extended into the clival region. Five tumors (four cases of Knosp grade 4 and one case of Knosp grade 3) in the nonrefractory group demonstrated cavernous extension both on MRI and during the operation and received near-total resection (NTR). There was no suprasellar extension or clival region invasion in the NRPA group. Compared with nonrefractory tumors, refractory tumors were more likely to be invasive ($p < 0.01$), suggesting that invasiveness was an independent predictor in the binary logistic regression. Thirty-nine patients in the NRPA group had been achieved total resection after the initial surgery, while 5 patients received NTR and remained stable after radiotherapy for a follow-up

TABLE 2 | Clinical and immunohistochemical characteristics of the 44 non-refractory Pas.

Pat. No.	Sex/Age	Tumor Type	Knosp grade	Tumor Diameter	Ki67%	P53	Abundant Mitoses	Outcome
1	M/34	GA	2	24	1	–	–	CR
2	M/19	GA	2	21.9	10	+	+	CR
3	M/25	GA	2	24.8	2	–	–	CR
4	F/50	CCA	2	16	1	–	–	CR
5	M/63	NCA	4	38	1	–	–	SD after EBRT
6	F/35	NCA	3	29	1	+	+	CR
7	F/25	NCA	2	24	3	–	–	CR
8	F/53	NCA	2	20.3	2	+	+	CR
9	M/41	GA	3	31	3	–	–	CR
10	M/50	NCA	2	27.8	0.5	–	–	CR
11	M/22	GA	3	34	2	–	–	SD after EBRT
12	M/32	GA	3	29	3	–	–	CR
13	F/57	SGLA	1	18	1	–	–	CR
14	M/58	GA	4	34.2	3	–	–	SD after EBRT
15	F/43	SGSA	2	29	2	–	–	CR
16	M/30	DGSA	1	16	3	–	–	CR
17	F/36	DGSA	2	20	2	–	–	CR
18	F/67	GA	1	20	1	–	–	CR
19	M/53	DGSA	2	24	1	–	–	CR
20	F/40	DGLA	3	30	1	–	–	CR
21	M/33	SGSA	1	25	3	–	–	CR
22	M/72	DGSA	1	24	2	–	–	CR
23	F/51	NCA	1	22	4	–	+	CR
24	F/29	GA	2	27	10	+	–	CR
25	M/32	NCA	3	28	1	–	–	CR
26	F/39	NCA	2	21.2	1	–	–	CR
27	M/43	DGSA	2	25	1	–	–	CR
28	M/51	NCA	4	43	1	–	–	SD after EBRT
29	M/68	NCA	3	34	2	–	–	SD after EBRT
30	M/21	SGSA	1	11	1	–	–	CR
31	F/40	GA	3	36.7	2	–	–	CR
32	M/41	DGSA	2	22	2	–	–	CR
33	M/43	GA	2	25	2	–	–	CR
34	M/36	SGSA	1	19	5	+	–	CR
35	F/51	DGSA	1	15	3	+	–	CR
36	F/39	SGCA	1	3.3	2	–	–	CR
37	F/22	DGCA	1	13	5	–	–	CR
38	M/50	SGSA	3	30	1	–	–	CR
39	F/22	SGCA	1	10	1	–	–	CR
40	F/29	SGCA	1	18	2	–	–	CR
41	F/48	DGCA	1	11.1	1	–	–	CR
42	M/31	SGCA	1	6.2	3	–	–	CR
43	F/41	DGCA	1	10.2	2	–	–	CR
44	F/39	DGCA	1	3.5	1	–	–	CR

CCA, Crooke's cell adenoma; CR, Complete remission; DGCA, Densely granulated corticotroph adenoma; DGLA, Densely granulated lactotroph adenoma; DGSA, Densely granulated somatotroph adenoma; EBRT, external beam radiotherapy; GA, Gonadotroph adenoma; NCA, Null cell adenoma; Oct, Octreotide; PPPA, Plurihormonal PIT-1 positive adenoma; SD, Stable disease; SGCA, Densely granulated corticotroph adenoma; SGLA, Sparsely granulated lactotroph adenoma; SGSA, Sparsely granulated somatotroph adenoma.

time of 31 months (range, 24-57 months). In contrast, 3 patients died of tumor progression and 1 patient died of tumor metastasis even with temozolomide therapy in the refractory group at a follow-up time of 20 months (range, 14–62 months).

Pathological Characteristics and Predictors for Clinical Refractoriness

To investigate the pathological characteristics and identify the possible biomarkers predicting the refractoriness of PAs, immunohistochemical analysis was undertaken. In addition to biomarkers (such as Ki-67, mitotic index and p53 immunostaining) that were already used in the definition of atypical PAs investigated, but other biomarkers (such as MMPs and EGFR) were also assessed. For the histopathological examination, 13 of 44 (29.5%) refractory PAs displayed atypical features, including a Ki-67 labeling index above 3%, p53 staining and abundant mitosis, while none of the 44 nonrefractory PAs displayed atypical features ($p < 0.0001$). The Ki-67 index in the refractory group ranged from 3% to 40%, with a mean index of 8.6%, which was much higher than that among the nonrefractory tumors (1.2%, $p < 0.001$, **Figure 1B**). Binary logistic regression revealed that the Ki-67 index was an independent predictor of clinical refractoriness. Interestingly, the Ki-67 index increased over time in 12 of 14 (85.7%) cases whose tissues were available from repeat surgeries (**Figure 2**).

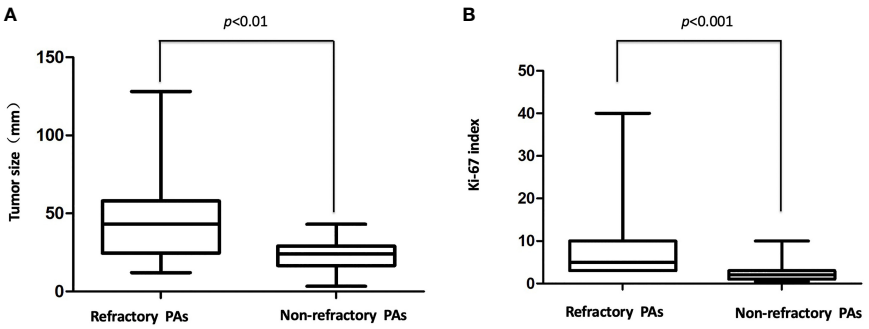

FIGURE 1 | **(A)** Tumor size in the refractory and nonrefractory groups. There was a significant difference in the size of the refractory versus nonrefractory tumors (48.6 vs. 22.6 mm, $p < 0.01$ **(B)**, The Ki-67 index in the refractory and nonrefractory groups. There was a significant difference in the Ki-67 index of the refractory versus nonrefractory tumors (6.9% vs. 1.2%, $p < 0.001$).

The increasing Ki-67 index indicated progression of tumor malignancy with an increasing number of operations. In addition, p53 immunostaining was positive in 15 of 44 refractory PAs (34.1%), while only 1 of 44 nonrefractory PAs (2.3%) was positive for p53, indicating a significant difference ($p < 0.001$). Abundant mitosis/nuclear pleomorphism was seen in 20 of 44 (45.5%) refractory PAs (41.0%), while 2 of 44 nonrefractory PAs (4.5%) displayed abundant mitosis ($p<0.001$).

IHC staining showed strong EGFR immunoreactivity in 33 of 44 (75.0%) refractory PAs and 7 of 44 (15.9%) nonrefractory PAs. Representative images of EGFR immunohistochemical staining of refractory PAs and nonrefractory PAs are shown in **Figure 3A**. The mean IOD values of the refractory PA group and nonrefractory PA group were 0.381 and 0.114, respectively. Using an unpaired t test, we found that EGFR was significantly increased in refractory PAs compared with nonrefractory PAs ($p < 0.01$, **Figure 3B**). Binary logistic regression revealed that EGFR was an independent predictor of clinical refractoriness. There was no significant difference between refractory PAs and nonrefractory PAs regarding MMP2 or MMP9 (0.086 vs. 0.92, 0.122 vs. 0.114, both $p >0.05$).

DISCUSSION

The use of the terms "aggressive" and "refractory" as descriptors for some PAs is intended to distinguish PAs with malignant behavior and a poor prognosis from PAs having benign characteristics. According to the European Society of Endocrinology (ESE) published guidelines on the management of aggressive pituitary tumors and carcinomas, an aggressive pituitary tumor should be considered in patients with a radiologically invasive tumor and unusually rapid TGR, or clinically relevant tumor growth despite optimal standard therapies (surgery, radiotherapy and conventional medical treatments) (14). However, there is no general agreement on the definition of aggressive PAs regarding their specific clinical and pathological characteristics and the guideline did not determine what represented"clinically relevant tumor growth" or an "unusually TGR". Therefore, the definition of aggressive PA relies mainly on subjective judgment of clinical characteristics but lacks objective diagnostic criteria and markers, leading to some confusion. Furthermore, "aggressive" and "invasive" are interpreted differently by different clinicians and are often used as interchangeable terms in the literature (17). In addition, there is a special situation in China where the Chinese words for "aggressive" and "invasive" are pronounced the same, which is more likely to lead to them being used interchangeably. Therefore, this was the initial reason for our proposal that a new term "refractory", be used to define these PAs.

In our previous studies, the most important characteristics of refractory PAs include refractoriness to standard therapies, including surgery, radiotherapy and conventional medical treatment; tumor infiltration of the adjacent structures based on either radiological images or intraoperative findings; a cut-off value of > 3% for Ki-67; increasing TGR > 2% per month; and tumor recurrence within 6 months after surgery (7, 8). Although the definitions of aggressive and refractory PAs overlap with each other, we retrospectively analyzed 44 patients with refractory PAs and investigated their clinical and pathological characteristics, emphasizing the importance of the Ki-67 index, tumor growth velocity, and other features for the early diagnosis.

In the present case series, all the 44 patients with refractory PAs showed radiological invasiveness at diagnosis, and binary logistic regression demonstrated that invasiveness was an independent predictor of refractoriness in the binary logistic regression. Although most refractory PAs were invasive, a small number of the refractory PAs were noninvasive tumors, even microtumors at the time of first diagnosis (especially CD), indicating that invasiveness alone is insufficient to define refractoriness. At the early stage of a refractory PA, the tumor can be noninvasive. With the passage of time, the tumors may develop more invasive or aggressive characteristics, even progressing to malignancy (18, 19). Nevertheless, some PAs extending into the cavernous sinus and that were radiologically invasive were not aggressive. Cavernous sinus extension of PAs may be caused by the weakness of the medial wall of the cavernous sinus, not by the nature of the tumor (19).

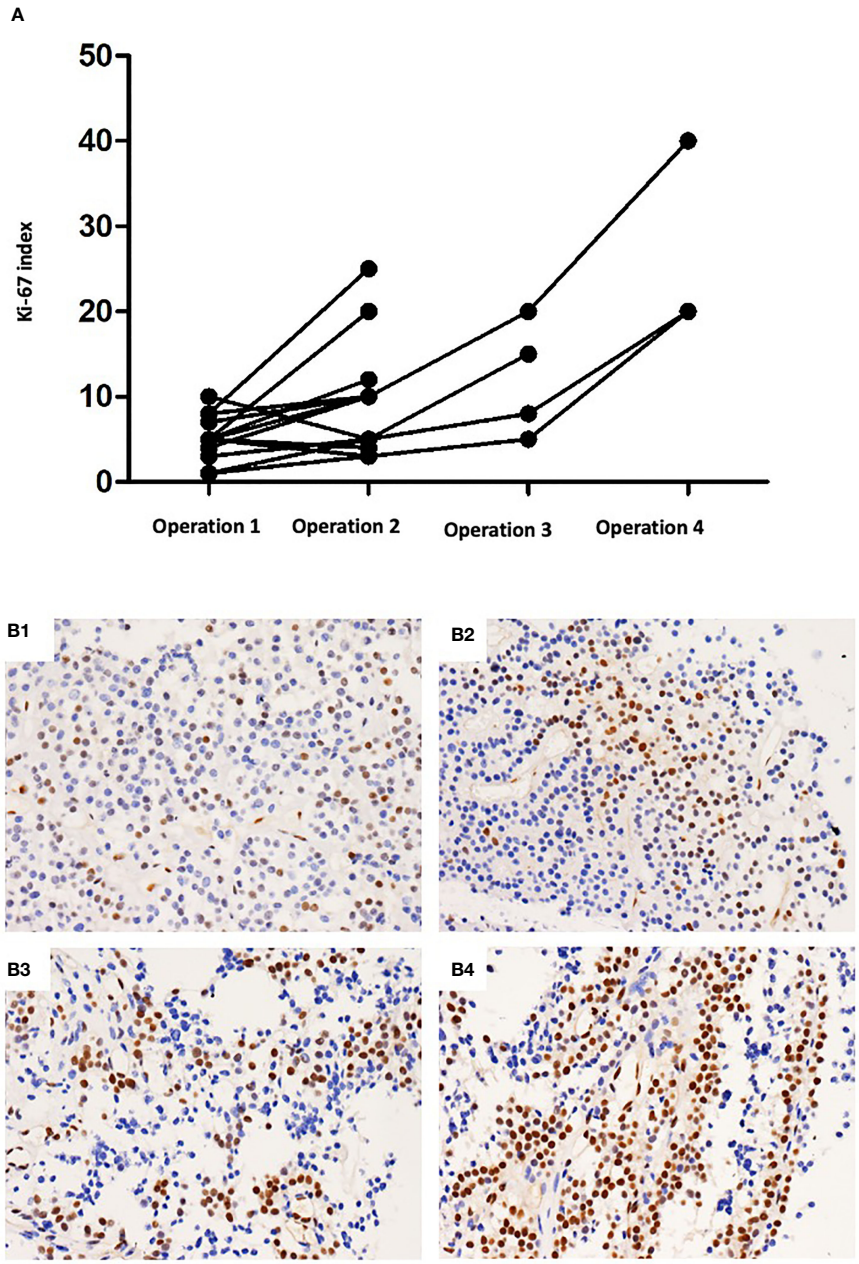

FIGURE 2 | **(A)**The Ki-67 index increased over operations in 11 of 14 (78.6%) cases whose tissues were available from repeat surgeries. **(B)** Immunohistochemical staining of Ki-67 in one patient with refractory PAs who received four operations. **(B1)** 5% (×100 magnification). **(B2)** 10% (×100 magnification). **(B3)** 20% (×100 magnification). **(B4)** 40% (×100 magnification).

Additionally, some invasive tumors can be totally resected by one or multiple operations or controlled by radiotherapy (20). In our control group, a substantial number of invasive PAs achieved total resection through extended transsphenoidal surgery and showed no recurrence after a long follow-up time (**Figure 1**). Herein, invasiveness is not the always related to aggressiveness, and objective diagnostic criteria are needed, such as TGR and pathological features.

All the patients with refractory PAs received at least one or more operation. For those 20 patients (45.5%) who had undergone only one operation, the tumors invaded the cavernous sinus and encompassed the internal carotid artery, which could not be totally removed in the operation. All 20 patients who underwent one operation received one or more radiotherapies and showed tumor progression. After a mean follow-up of 44.2 months (range 6–88 months), 2 patients died of tumor progression and 1 patient died

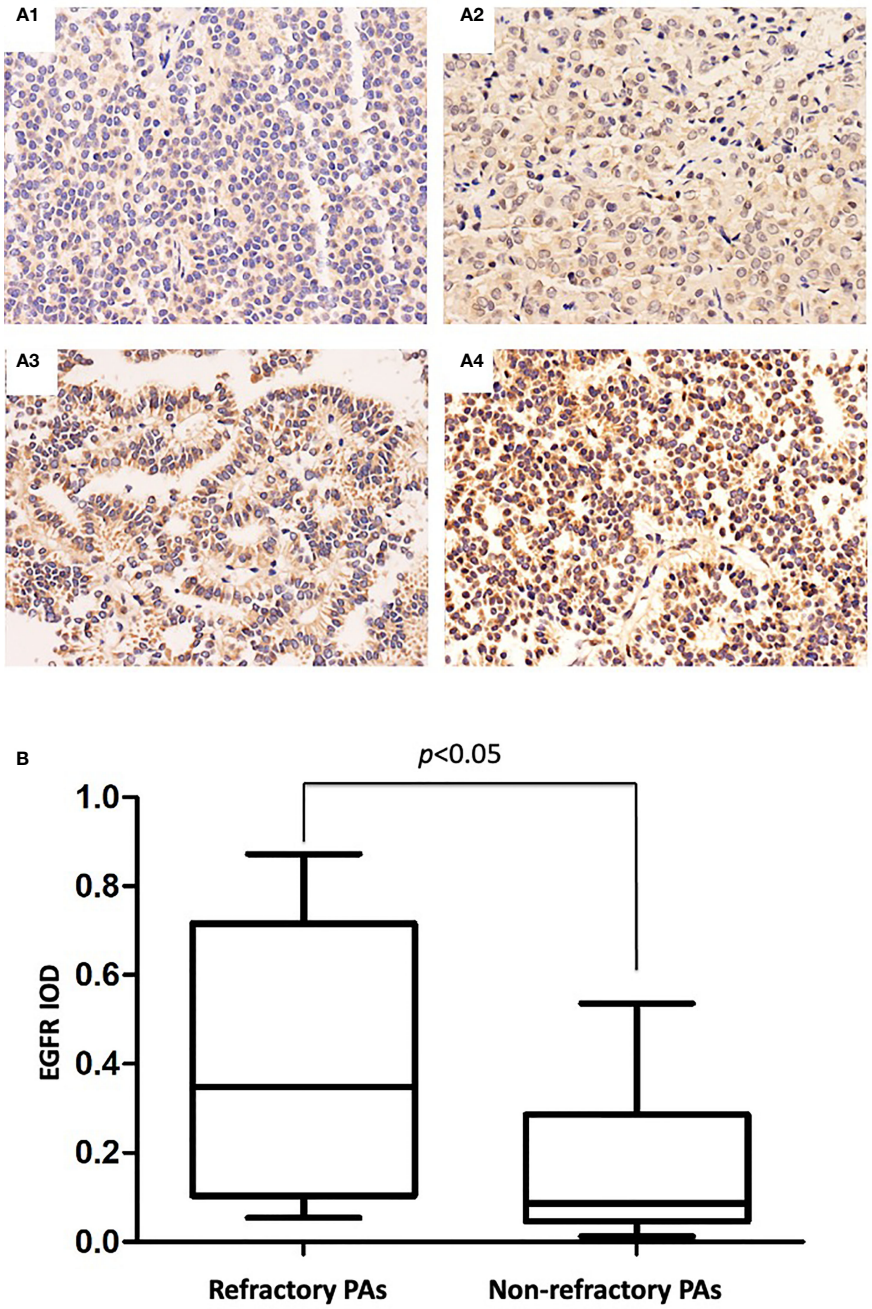

FIGURE 3 | **(A)** Immunohistochemical staining of EGFR in PAs. **(A1)** IOD: 0.036 (×100 magnification). **(A2)** IOD: 0.192 (×100 magnification). **(A3)** IOD: 0.466 (×100 magnification). **(A4)** IOD: 0.842 (×100 magnification). **(B)**, EGFR mean IODs of refractory PAs and nonrefractory PAs. The mean EGFR IOD of the refractory PAs was significantly increased compared with that of the nonrefractory PAs (0.381 vs. 0.114, $p < 0.05$).

of tumor metastasis even with temozolomide therapy in the refractory group, suggesting not only that the clinical manifestation was more aggressive but also that the life expectancy of these PA patients was also markedly reduced (21, 22). Therefore, the most important characteristic of refractory PAs is that they are unresponsive to surgery, radiotherapy and conventional medical treatments with a poor prognosis.

The definition for aggressive does not provide an objective criterion for rapid growth, which easily leads to different judgments from different clinicians (23, 24). Here, the definition of refractory includes a TGR ≥2.2% per month, which can be used to determine rapid growth. Although more data are needed, it does provide an objective criterion for rapid growth.

Beyond the Ki-67 index which is already used in the definition of refractory adenomas, other biomarkers have also been investigated as potential biomarkers of refractoriness. Such biomarkers include matrix metalloproteinases (MMPs; including MMP2 and MMP9) which degrade extracellular matrix for enabling tumor invasion and epidermal growth factor receptor (EGFR), one subtype of ErbB receptors, which is expressed in PAs and regulates cell motility and adhesion, tumor invasion, angiogenesis and tumor cell proliferation (25). Previous studies showed that EGFR overexpression in transgenic mice driven by tissue-specific promoters induced PA tumorigenesis (25, 26), indicating its important role in pituitary tumorigenesis. In this study, we found that EGFR could also be used to assess refractory behavior. MMPs, particularly MMP2 and MMP9, are thought to play a central role in the proteolytic process of the extracellular matrix and basement membrane degradation, an essential step in these processes (27). However, neither MMP9 nor MMP2 could be used as an independent predictor of clinical refractoriness in our study.

CONCLUSION

Refractory PAs are unresponsive to surgery, radiotherapy and conventional medical treatments with a poor prognosis. Moreover, a tumor growth rate ≥2.2% per month, Ki-67 index ≥3% and EGFR overexpression may be independent predictors of clinical refractoriness. Moreover, more cases and translational research are also needed to provide more insights into the definition of these refractory tumors.

DATA AVAILABILITY STATEMENT

The original contributions presented in the study are included in the article/supplementary material. Further inquiries can be directed to the corresponding author.

ETHICS STATEMENT

The study was approved by the Research Ethics Committee of PUMCH and all the patients provided their written informed consent for the research. Written informed consent to participate in this study was provided by the participants' legal guardian/ next of kin. Written informed consent was obtained from the individual(s) for the publication of any potentially identifiable images or data included in this article.

AUTHOR CONTRIBUTIONS

All the authors participated in the design, collection and assembly of data, data analysis, and manuscript writing.

FUNDING

The financial support for this study was provided by National Key R&D Program of China (grant number: 2021YFE0114300 to Renzhi Wang) and Beijing Hospitals Authority Youth Program (Code: QMS20210802 to Xiaohai Liu). The funding institutions had no role in the design of the study, data collection and analysis, decision to publish, or preparation of the manuscript.

REFERENCES

1. Lopes MBS. The 2017 World Health Organization Classification of Tumors of the Pituitary Gland: A Summary. *Acta Neuropathol* (2017) 134(4):521–35. doi: 10.1007/s00401-017-1769-8
2. Fernandez A, Karavitaki N, Wass JA. Prevalence of Pituitary Adenomas: A Community-Based, Cross-Sectional Study in Banbury (Oxfordshire, UK). *Clin Endocrinol (Oxf)* 72:377–82. doi: 10.1111/j.1365-2265.2009.03667.x
3. Daly AF, Rixhon M, Adam C, Dempegioti A, Tichomirowa MA, Beckers A. High Prevalence of Pituitary Adenomas: A Cross-Sectional Study in the Province of Liege, Belgium. *J Clin Endocrinol Metab* (2006) 91:4769–75. doi: 10.1210/jc.2006-1668
4. Ezzat S, Asa SL, Couldwell WT, Barr CE, Dodge WE, Vance ML, et al. The Prevalence of Pituitary Adenomas: A Systematic Review. *Cancer* (2004) 101:613–9. doi: 10.1002/cncr.20412
5. Heaney A. Management of Aggressive Pituitary Adenomas and Pituitary Carcinomas. *J Neurooncol* (2014) 117(3):459–68. doi: 10.1007/s11060-014-1413-6
6. Raverot G, Ilie MD, Lasolle H, Amodru V, Trouillas J, Castinetti F, et al. Aggressive Pituitary Tumours and Pituitary Carcinomas. *Nat Rev Endocrinol* (2021) 17(11):671–84. doi: 10.1038/s41574-021-00550-w
7. Dai C, Feng M, Liu X, Ma S, Sun B, Bao X, et al. Refractory Pituitary Adenoma: A Novel Classification for Pituitary Tumors. *Oncotarget* (2016) 7 (50):83657–68. doi: 10.18632/oncotarget.13274
8. Dai C, Liu X, Ma W, Wang R. The Treatment of Refractory Pituitary Adenomas. *Front Endocrinol* (2019) 10:334. doi: 10.3389/fendo.2019.00334
9. Melmed S. Pituitary-Tumor Endocrinopathies. *N Engl J Med* (2020) 382 (10):937–50. doi: 10.1056/NEJMra1810772
10. Delellis RA. *Pathology and Genetics of Tumours of Endocrine Organs*. Lyon: IARC Press (2004).
11. Zaidi HA, Cote DJ, Dunn IF, Laws ERJr. Predictors of Aggressive Clinical Phenotype Among Immunohistochemically Confirmed Atypical Adenomas. *J Clin Neurosci* (2016) 34:246–51. doi: 10.1016/j.jocn.2016.09.014
12. Chiloiro S, Doglietto F, Trapasso B, Iacovazzo D, Giampietro A, Di Nardo F, et al. Typical and Atypical Pituitary Adenomas: A Single-Center Analysis of Outcome and Prognosis. *Neuroendocrinology* (2015) 101(2):143–50. doi: 10.1159/000375448
13. RV Lloyd, RY Osamura, G Klöppel and J Rosai eds. *WHO Classification of Tumours of Endocrine Organs, 4th Edn*. Lyon: IARC Press (2017).
14. Raverot G, Burman P, McCormack A, Heaney A, Petersenn S, Popovic V, et al. European Society of Endocrinology Clinical Practice Guidelines for the Management of Aggressivepituitary Tumours and Carcinomas. *Eur J Endocrinol* (2018) 178(1):G1–G24. doi: 10.1530/EJE-17-0796
15. Dai C, Liu X, Feng M, Wang B. From "Aggressive" to "Refractory": Advances and Controversies in the Definition and Classification of Pituitary Tumors. *Endocr Pract* (2020) 26(11):1384–6. doi: 10.4158/EP-2020-0214
16. Anderson RC, Grant JJ, de la Paz R, Frucht S and Goodman RR. Volumetric Measurements in the Detection of Reduced Ventricular Volume in Patients With Normal-Pressure Hydrocephalus Whose Clinical Condition Improved After Ventriculoperitoneal Shunt Placement. *J Neurosurg* (2002) 97:73–9. doi: 10.3171/jns.2002.97.1.0073
17. Chatzellis E, Alexandraki KI, Androulakis II, Kaltsas G. Aggressive Pituitary Tumors. *Neuroendocrinology* (2015) 101(2):87–104. doi: 10.1159/000371806
18. Dai C, Sun B, Guan S, Wang W, Liu H, Li Y, et al. Evolution of a Refractory Prolactin-Secreting Pituitary Adenoma Into a Pituitary Carcinoma: Report of

a Challenging Case and Literature Review. *BMC Endocr Disord* (2021) 21 (1):217. doi: 10.1186/s12902-021-00874-8
19. Phillips J, East HE, French SE, Melcescu E, Hamilton RD, Nicholas WC, et al. What Causes a Prolactinoma to be Aggressive or to Become a Pituitary Carcinoma? *Horm (Athens Greece)* (2012) 11(4):477. doi: 10.14310/horm.2002.1380
20. Ouyang T, Zhang N, Xie S, Tang B, Li J, Xiao L, et al. Outcomes and Complications of Aggressive Resection Strategy for Pituitary Adenomas in Knosp Grade 4 With Transsphenoidal Endoscopy. *Front Oncol* (2021) 11:693063. doi: 10.3389/fonc.2021.693063.
21. Losa M, Bogazzi F, Cannavo S, Ceccato F, Curto L, De Marinis L, et al. Temozolomide Therapy in Patients With Aggressive Pituitary Adenomas or Carcinomas. *J Neurooncol* (2016) 126:519–25. doi: 10.1007/s11060-015-1991-y
22. Lasolle H, Cortet C, Castinetti F, Cloix L, Caron P, Delemer B, et al. Temozolomide Treatment can Improve Overall Survival in Aggressive Pituitary Tumors and Pituitary Carcinomas. *Eur J Endocrinol* (2017) 176:769–77. doi: 10.1530/EJE-16-0979
23. Ilie MD, Jouanneau E, Raverot G. Aggressive Pituitary Adenomas and Carcinomas. *Endocrinol Metab Clin North Am* (2020) 49:505–15. doi: 10.1016/j.ecl.2020.05.008
24. Ng S, Messerer M, Engelhardt J, Bruneau M, Cornelius JF, Cavallo LM, et al. Aggressive Pituitary Neuroendocrine Tumors: Current Practices, Controversies, and Perspectives, on Behalf of the EANS Skull Base Section. *Acta Neurochir (Wien)* (2021) 163(11):3131–42. doi: 10.1007/s00701-021-04953-6
25. Araki T, Liu X, Kameda H, Tone Y, Fukuoka H, Tone M, et al. Egfr Induces E2f1-Mediated Corticotroph Tumorigenesis. *J Endocr Soc* (2017) 1(2):127–43. doi: 10.1210/js.2016-1053
26. Liu X, Kano M, Araki T, Cooper O, Fukuoka H, Tone Y, et al. Erbb Recepaor-Driven Prolactinomas Respond to Targeted Lapatinib Treatment in Female Transgenic Mice. *Endocrinology* (2015) 156(1):71–9. doi: 10.1210/en.2014-1627
27. Horikawa T, Yoshizaki T, Sheen T, Lee S, Furukawa S. Association of Latent Membrane Protein 1 and Matrix Metalloproteinase 9 With Metastasis in Nasopharyngeal Carcinoma. *Cancer* (2000) 89:715–23. doi: 10.1002/1097-0142(20000815)89:4<715::AID-CNCR1>3.0.CO;2-9

Conflict of Interest: The authors declare that the research was conducted in the absence of any commercial or financial relationships that could be construed as a potential conflict of interest.

Publisher's Note: All claims expressed in this article are solely those of the authors and do not necessarily represent those of their affiliated organizations, or those of the publisher, the editors and the reviewers. Any product that may be evaluated in this article, or claim that may be made by its manufacturer, is not guaranteed or endorsed by the publisher.

frontiers | Frontiers in Oncology

ORIGINAL RESEARCH
published: 07 April 2022
doi: 10.3389/fonc.2022.739631

Drp1 Regulated Mitochondrial Hypofission Promotes the Invasion and Proliferation of Growth Hormone-Secreting Pituitary Adenomas *via* Activating STAT3

Yin Zhang[1,2†], Lei Zhang[3†], Kexia Fan[1], Yajun Gou[2], Zhenle Zang[1], Xiao Ding[1], Hui Yang[1,4] and Song Li[1,4*]*

[1] Multidisciplinary Center for Pituitary Adenomas of Chongqing, Department of Neurosurgery, Xinqiao Hospital, Army Medical University, Chongqing, China, [2] Department of Neurosurgery, People's Hospital of Shapingba District, Chongqing, China, [3] Department of Histology and Embryology, Chongqing Medical University, Chongqing, China, [4] Chongqing Institute of Brian and Intelligence, Guangyang Bay Laboratory, Chongqing, China

OPEN ACCESS

Edited by:
Zhixiong Liu,
Central South University, China

Reviewed by:
Zhaohui He,
Chongqing Medical University, China
Ramesh Kandimalla,
Indian Institute of Chemical Technology (CSIR), India

***Correspondence:**
Hui Yang
huiyangxinqiao@163.com
Song Li
dlisong3@163.com

[†]These authors have contributed equally to this work

Specialty section:
This article was submitted to Neuro-Oncology and Neurosurgical Oncology, a section of the journal Frontiers in Oncology

Received: 11 July 2021
Accepted: 10 March 2022
Published: 07 April 2022

Citation:
Zhang Y, Zhang L, Fan K, Gou Y, Zang Z, Ding X, Yang H and Li S (2022) Drp1 Regulated Mitochondrial Hypofission Promotes the Invasion and Proliferation of Growth Hormone-Secreting Pituitary Adenomas via Activating STAT3. Front. Oncol. 12:739631. doi: 10.3389/fonc.2022.739631

The invasiveness and high proliferation rate of growth hormone-secreting pituitary adenomas (GHPAs) are closely related to poor prognosis in patients. We previously reported that abnormal glycolysis participates in this process; however, the role of mitochondria in the invasion and proliferation of GHPAs remains unknown. In the current study, stereological methods were first used to quantitatively calculate the number and morphology of mitochondria. The results revealed that the numbers, volumes and membrane areas of mitochondria were decreased in invasive GHPAs (IGHPAs) samples compared to noninvasive GHPAs (NIGHPAs) samples. Furthermore, significantly downregulated mRNA and protein levels of dynamin-related protein 1 (Drp1) were detected in IGHPAs, but no notable changes in fusion related molecules (Mfn1, Mfn2 and OPA1) were detected, suggesting that the abnormal mitochondrial dynamics in IGHPAs are characterized by hypofission. Mitochondrial hypofission caused by Mdivi-1, a specific Drp1 inhibitor, enhanced the invasion and proliferation of GH3 cell lines and primary cells from patients with GHPAs *in vitro* and *in vivo*, while overexpression of Drp1 reversed these processes. Mechanistically, mitochondrial hypofission might activate signal transducer and activator of transcription 3 (STAT3). Specifically, elevated nuclear pSTAT3^{Y705} may promote GH3 cell invasion by upregulating the activity of matrix metalloproteinase 2/9, and elevated mitochondrial pSTAT3^{S727} may promote GH3 cell proliferation by inhibiting the mitochondria-dependent apoptotic pathway. Taken together, our findings suggest that mitochondrial hypofission induced by Drp1 might strengthen the invasion and proliferation of GHPA tumor cells by activating STAT3, providing us with a new perspective on how mitochondria regulate the development of IGHPAs.

Keywords: growth hormone-secreting pituitary adenomas, DRP1, mitochondrial fission, stat3, invasion, proliferation

INTRODUCTION

Growth hormone-secreting pituitary adenomas(GHPAs) are a common subtype of pituitary adenomas (PAs) that can cause neurological dysfunctions induced by the tumor mass effect, as well as endocrine symptoms induced by growth hormone (GH) hypersecretion, and increase the mortality of patients by approximate 2-fold (1). Surgery is regarded as the first-line treatment for GHPAs, and results in an initial endocrine remission rate of 80% for microadenomas and 50% for macroadenomas (1, 2).However, the remission rate for tumors invading the cavernous sinus drops to 35%, and five-year disease recurrence rates range from 2 to 8% (1, 2). Moreover, postsurgical pathological factors (e.g., Ki-67 index, sparsely granulated adenoma) are also correlated with the prognosis of GHPAs (1, 3). A multicenter case–control study found that invasive and highly proliferative tumors presented with an increased probability of tumor persistence or progression of 25- or 12-fold, respectively (4). Therefore, intensive study on invasive and highly proliferative GHPAs is essential for the development of new therapies.

Metabolic reprogramming is well recognized as a hallmark of cancer and plays important roles in tumorigenesis (5). Transcriptiomics data (6) and metabolomics investigations (7) supported the potential oncogenetic roles of metabolic dysregulation in PAs. Our group has reported that dysregulated glucose metabolism (8), cholesterol metabolism (9) and glutamine metabolism (10) might play important roles in the tumorigenesis of PAs. For example, we have reported that lactate dehydrogenase A (LDHA) enhances the glycolysis in pituitary GH3 cells, and then promotes the invasion and proliferation of GH3 cells (8). Recently, Zhang et al. further illustrated that overproduction of lactate promoted the invasion of tumor cells *via* M2-like macrophage polarization (11). Beyond abnormal glycolysis in cancer, mitochondrial dysfunction associated with energy metabolic reprogramming has also been confirmed (12).Several tricarboxylic acid cycle intermediates (e.g., 2-hydroxyglutarate, succinate and fumarate) induced by mutant metabolic enzymes in mitochondria are well recognized as oncometabolites (13–15). Oncocytoma, a special subset of pituitary adenoma, is characterized by mitochondrial hyperplasia. Kurelac reported that mitochondrial DNA (mtDNA) mutation might disrupt respiratory complex I and induce the oncocytic phenotype of pituitary adenoma (16). Feng et al. found that hyperplastic mitochondria were characterized by metabolic changes as a result of respiratory complex I dysfunction and inefficient oxidative phosphorylation in oncocytoma (17). However, whether mitochondrial dysfunction participates in the development of GHPAs is still unclear.

Mitochondrial succinate dehydrogenase (SDH) mutations were identified in familial patients with GHPAs. In animal models with $Sdh^{+/-}$ mice, the adenohypophysis presented dramatic hyperplasia, and pituitary cells displayed morphological abnormalities of mitochondria and high expression of HIF1a, which suggested the role of mitochondrial metabolic enzymes in the development of GHPAs (18). Mitochondrial function is not only affected by mitochondrial metabolic enzymes, but also determined by mitochondrial morphology to some extent (19). Mitochondrial morphology is highly dynamic between fission and fusion cycles, referred to as mitochondrial dynamics. Mitochondrial dynamics are crucial for cellular processes, such as apoptosis, cell cycle and cell death (19). Several studies have indicated that mitochondrial dynamics might regulate tumor growth and metastasis (20, 21). It has been reported that the underlying mechanism of dopamine agonists in treating GHPAs might activate the mitochondrial apoptosis pathway (22). These data provide instructive clues on the role of mitochondria in GHPAs. However, whether mitochondrial dynamics regulate the aggressive behavior and proliferation of GHPAs remains largely unknown.

In the current study, we investigated mitochondrial morphology and number in invasive GHPAs (IGHPAs) samples, and then explored the underlying mechanisms by which mitochondrial dynamics regulate the invasion and proliferation of GH3 cell lines and human primary GHPAs cells.

MATERIALS AND METHODS

Patient Selection

In this study, a total of 42 samples were obtained from patients with GHPAs, who underwent surgery in our department. IGHPAs and NIGHPAs samples accounted for 50% each. Among them, 14 GHPAs (7 IGHPAs, 7 NIGHPAs) were used for stereological study. Diagnoses of individual tumors were based on clinical signs, endocrine evaluation and postoperative pathological results. Tumor invasiveness was determined according to the Knosp classification combined with intraoperative findings (4). Grade III – IV tumors were defined as invasive tumors, and grade 0 - II tumors were noninvasive tumors. This study followed the Helsinki declaration and the supervision of the ethics committee of the Army Medical University. All patients provided written informed consent to participate in this study.

Electron Microscopic Observation and Stereology

Electron microscopic sectioning was performed at the Center for Biological Analysis and Testing at Army Medical University. A total of 2 slices were extracted for each case by equal distance at random. Twenty-five images were acquired from each slice magnified to 25 Kd using a Japanese projection electron microscope GEM 1400 plus in accordance with X, Y axis interval of 10 μm each. From these images, stereological analyses were performed by using the Standard Program Image Analysis System of the OLYMPUS microscope (23). The mitochondrial volume fraction(Vv) was obtained by stereological point measurement.

$$Vv = P/P'/V$$

P is the number of points to hit the mitochondria. P' is the total number of measuring points. V is the tumor volume measured by enhanced magnetic resonance imaging. The density of

mitochondrial surface area(Sv) was obtained using the linear intersection technique.

$$Sv = 2I/L'/V$$

I is the number of intersections between the lines and the boundary of the mitochondria. L is the total length of the line. The density of mitochondrial number (Nv) was obtained by means of the stereological box technique.

$$Nv = N/(S \times H)/V$$

N is the number of mitochondria in the stereological box by the forbidden line rule. S is the area of the forbidden line frame. H is the height of the forbidden line frame.

Reverse Transcription and Real-Time Quantitative PCR Technique

Total RNA of GHPAs was extracted using TRIzol (Toyobo, Osaka, Japan) and reverse transcribed into cDNA utilizing PrimeScript® RTase (Toyobo, Osaka, Japan). cDNA was amplified using SYBR premix Taq TM II (Toyobo, Osaka, Japan) and CFX96 real-time (Bio-Rad Laboratories, Hercules, CA, USA). The relative transcription level of the gene was calculated using the $2-^{\triangle\triangle}$ct method. The primer sequences (5'-3') used for qPCR were as follows: Mfn1 F-GTGGCAAA CAAAGTTTCATGTG, R-CACTAAGGCGTTTACTTCATCG; Mfn2 F- CTCTCGCAGAAGGCTTTCAAGT, R-TTCACGC ATTTCCTCGCAGTA; OPA1 F- TCTGCACACTCAGTT GAAGTAT, R-GCCTTTGTCATCTTTCTGCAAT; Drp1 F-CATGAGACTTTTGGGCGAACC, R-GGCACAAAT AAAGCAGGACGAG; β-actin F-GCACCACACCTTC TACAATGAGC, R-TAGCACAGCCTGGATAGCAACG.

Immunohistochemistry

GHPAs tissues were fixed in paraformaldehyde for 24 hours; and then embedded in paraffin. Paraffin sections were sliced at a thickness of 5 μm for subsequent immunohistochemical staining. Staining of sections was performed in accordance with the standard procedures described in our previous studies. The sections were incubated with anti-Drp1 (1:200; ab56788, Abcam, Cambridge, UK), anti-STAT3 (1:200; ab68153, Abcam), anti-phospho-STAT3 (S727) (1:150; ab32143, Abcam), and anti-phospho-STAT3 (Tyr705) (1:150; #9145, Cell Signaling Technology, Danvers, USA) primary antibodies overnight at 4°C. The sections were then incubated with secondary immunoglobulin conjugated to peroxidase-labeled dextran polymer for 1 h at 37°C. 3,3-Diaminobenzidine (Boster, Wuhan, China) was applied to view the immunoreactions. Finally, these slices were stained with hematoxylin, dehydrated, and covered with coverslips. Images of different sections were obtained by fluorescence microscopy (TSC-TIV; Leica, Nussloch, Germany). Negative control experiments lacked the primary antibodies.

Cell Lines and Primary Cells

Rat GH3 pituitary adenoma cell lines were purchased from the American Type Collection (ATCC, Manassas, VA, culture, USA). Cells were cultured in Ham's F-12K media containing 2.5% fetal bovine serum and 15% horse serum and placed in a humidified incubator with a 5% CO_2-humidified atmosphere at 37°C. Five primary GHPA cells were obtained from patients who were surgically treated at Xinqiao Hospital. The primary cells were maintained in 10% FBS–containing MEM and cultured in a 5% CO_2-humidified atmosphere at 37°C.

Lentivirus and Transfection

Lentiviral vectors (OBIO, Shanghai, China), including empty vector and Drp1 overexpression vector, were transfected into GH3 cells at a multiplicity of infection (MOI) of 100 according to the manufacturer's instructions. Stable colonies were identified by intense mCherry fluorescence. The upregulation efficacy of Drp1 protein was verified by western blotting.

Mitochondrial Division Inhibitor and STAT3 Inhibitor

Mdivi-1 (338967-87-6, Selleck, Shanghai, China), a mitochondrial division inhibitor, is a highly efficient small molecule that selectively inhibits the activity of Drp 1 GTPase by blocking the self-assembly of Drp1 (24). Mdivi-1 was formulated as 10 mM liquid storage with dimethylsulfoxide, and was used to inhibit Drp1 at a concentration of 10 μM. HO-3867(HY-100453, MCE, USA), an analog of curcumin, is a selective STAT3 inhibitor that inhibits STAT3 phosphorylation, transcription, and DNA binding activity without affecting the expression of other active STATs. HO-3867 was formulated as 10 mM liquid storage with dimethylsulfoxide, and was used to inhibit STAT3 at a concentration of 10 μM (25). Cryptotanshinone(Cry) (HY-N0174, MCE) is a STAT3 inhibitor, that strongly inhibits the phosphorylation of STAT3 Tyr705, and has a weak effect on STAT3 Ser727. Cry was formulated as 10 mM liquid storage with dimethylsulfoxide, and was used to inhibit STAT3 at a concentration of 7 μM (26).

Protein Extracts and Western Blotting

Total proteins were extracted from GHPAs tissue or GH3 cells using total protein extraction kits (Bestbio, Shanghai, China). Mitochondrial proteins and nuclear proteins were extracted with kits (Beyotime Biotech, Shanghai, China). Extracts equivalent to 50 μg of protein were integrated into SDS-PAGE gels and then transferred onto polyvinylidene difluoride membranes. The membranes were blocked in 5% nonfat milk with Tris-buffered saline containing 0.05% Tween 20 for 3 hours at room temperature and incubated with mouse antibodies against Drp1 (1:200; ab56788, Abcam) and β-Actin (1:1000; ab8227, Abcam) and with rabbit antibodies against Phospho-Drp1 (Ser616)(1:1000; #4494, Cell Signaling Technology), Phospho-Drp1 (Ser637)(1:1000; ab193216, Abcam), STAT3 (1:300; ab68153, Abcam), STAT3 (phospho S727) (1:250; ab32143, Abcam), STAT3 (phospho Tyr705) (1:250; #9145, Cell Signaling Technology), Bcl-2 (1:1000; ab59348, Abcam), Bax (1:1000; ab32503, Abcam), and Caspase 3 (1:500; #9662, Cell Signaling Technology). Then, the membranes were further incubated with horseradish peroxidase-conjugated goat anti-mouse (1:2000, ZB-2305, ZSGB-BIO, Beijing, China) and anti-

rabbit (1:2000; sc-2012, Santa Cruz Biotechnology) IgG secondary antibodies. The membrane signals were visualized using a gel imaging chemiluminescence system (Fluor Chem, ProteinSimp, USA).

Cell Counting Experiment

The number of cells was quantified using the WST-8 Cell Counting Kit-8 (Dojindo Laboratories, Mashiki-machi, Kumamoto, Japan) in accordance with the manufacturer's instructions. A total of $2.0*10^5$ cells were initially cultured in 96-well plates and harvested after drug intervention for 48 hours. Cell numbers were quantified according to the manufacturer's instructions.

Cell Invasion Assay

Cells were starved in serum-free medium for 12 hours. Then, cells (GH3, 5×10^5/well, primary tumor cells, 3×10^5) were suspended in 150 µl serum-free medium and placed into the upper chamber (8-mm pore; Costar, Bethesda, MD, USA) that had been precoated with 70 µl Matrigel at a concentration of 300 µg/ml (BD Biosciences, USA). Five hundred microliters of whole serum medium containing 2.5% FBS and 15% HS was added to the lower chamber. After incubation with the indicated treatments for 24 hours, the culture medium was removed, and the matrix adhesive on the bottom of the chamber was gently removed with cotton swabs. Next, the cells on the membrane were fixed in 5% paraformaldehyde for 15 min and stained with crystal violet solution (Boster). The cells on the membrane were imaged under an optical microscope (Leica, DMI3000 Bat) at a magnification of 10*20 for 10 images obtained according to random equidistant extraction.

Detection of Matrix Metalloproteinase 2/9 (MMP2/9)

MMP2/9 enzyme activities were detected using a cell MMP2/9 *in situ* zymography fluorescence staining kit (GMS80062.2, GenMed Scientifics Inc. USA). Then, the fluorescence intensity was observed under a fluorescence microscope (BX63, Olympus, Japan) and analyzed by Image-Pro Plus 6.0.

Cell Cycle Analysis

In total, 2.0×10^6 cells in each group were harvested and used for cell cycle analysis. The cells were washed with PBS three times and then incubated in 70% alcohol at 4°C overnight. Subsequently, the cells were stained in 0.05 mg/ml propidium iodide (PI; BD Biosciences Pharmingen) and analyzed by flow cytometry (FACScan; BD Biosciences Pharmingen, San Diego, CA, USA). Cell debris, cell doublets, and cell clumps were excluded from the analysis. DNA histograms were created using ModFit LT V2.0 software.

Apoptosis Analysis

In total, $2.0*10^6$ cells in each group were harvested and used for apoptosis analysis. Apoptosis was assessed using a FITC-Annexin V apoptosis detection kit (556547, BD Biosciences Pharmingen) according to the manufacturer's instructions. Cells were stained with FITC-Annexin V and PI. Apoptosis was detected by flow cytometry and analyzed further using ModFit LT V2.0 software.

Analysis of Mitochondrial Membrane Potential and Reactive Oxygen Species (ROS)

Approximately 1×10^6 GH3 cells were collected for mitochondrial membrane potential and ROS detection using flow cytometry. Mitochondrial membrane potential was detected by rhodamine 123 using a mitochondrial membrane potential detection kit (C2008S, Beyotime Biotech), and ROS was determined by a DCFH-DA reactive oxygen species assay kit (S0033S, Beyotime Biotech) according to the manufacturer's recommendations. Each sample was assessed by flow cytometry for fluorescence intensity. The results were analyzed by ModFit LT V2.0 software.

In Vivo Experiments

In vivo xenograft experiments were performed similar to our previous study (9). Twenty-eight 4 weeks old male BALB/cA-nu mice were purchased from Charles River (Beijing, China) and housed under SPF conditions. Then, the animals were randomly divided into 4 groups (7 mice/group). A total of 5×10^6 transfected GH3 cells suspended in 100 µl of solution (50% PBS and 50% Matrigel) were subcutaneously inoculated into the right flank of the mice. Treatment with Mdivi-1 was started 2 weeks after inoculation of the cells. The Mdivi-1-treated groups (VE+Mdivi-1, $Drp1^{++/++}$+Mdivi-1) received daily intraperitoneal injection of 50 mg/kg Mdivi-1 for the next 3 weeks until sacrifice, while the other two groups (VE, $Drp1^{++/++}$) received daily intraperitoneal injection of an equal volume of PBS only. The mice were monitored daily for any discomfort. The mice were weighed, and tumor volumes were also measured every three days. Tumor tissue was removed from tumor-bearing mice following the final treatment. Tumor volumes were calculated using the following formula: V (mm^3) = $[AB^2]/2$, where A is the tumor length and B is the tumor width. The excised tumors were weighted. All animal procedures were conducted according to protocols approved by the Institutional Animal Care and Ethics Committee.

Statistical Analysis

Data are expressed as the means ± SEM. A two-tailed Student's t-test was applied to determine statistical significance between the two groups. These analyses were performed using SPSS for Windows, version 18.0 (SPSS Inc., USA).

RESULTS

Mitochondrial Dynamics Were Dysregulated in IGHPAs

The morphology and number of mitochondria were visually observed under an electron microscope and contrasted objectively by stereological measurement, including contour counting, point counting and intersection counting. Several mitochondria with normal morphology and secretory granules

were observed in surgical noninvasive GHPAs (NIGHPAs) samples (**Figure 1A**). However, several swollen mitochondria were observed in IGHPAs samples (**Figure 1B**). Stereological analyses revealed that the density of mitochondrial number (Nv) and mitochondrial surface area (Sv) in IGHPAs were significantly lower than those in NIGHPAs (**Figures 1C, D**). Meanwhile, the mitochondrial volume fraction (Vv) in IGHPAs was significantly lower than that in NIGHPAs (**Figure 1E**). These stereological results suggest that mitochondrial fission and fusion might be dysregulated in IGHPAs.

Downregulation of Drp1 Induced Mitochondrial Hypofission Promotes the Invasion of GHPAs

The morphology and number of mitochondria are highly dynamic and determined by the processes of fusion and fission, which are affected by mitochondrial dynamics proteins, mainly mitofusin (Mfn), optic atrophy protein 1 (OPA1) and dynamin-related protein 1 (Drp1) (19). We detected the mRNA expression levels of the mitochondrial fusion related proteins (Mfn1, Mfn2 and OPA1), and observed no significant difference between NIGHPAs and IGHPAs samples (**Figures S1A–C**). However, the mRNA expression levels of the mitochondrial fission related protein Drp1 were significantly downregulated in IGHPAs samples (**Figure 2A**). Further western blotting experiments confirmed that the protein levels of Drp1 were also significantly downregulated in IGHPAs samples (**Figure 2B**). Accordingly, two main phosphorylation sites (Ser616 and Ser637) of Drp1 protein were detected significantly downregulated in IGHPAs samples (**Figure 2C**). These results indicate that the dysregulated mitochondrial dynamics confirmed by stereological measurement in IGHPAs might be a result of Drp1 induced mitochondrial hypofission. Furthermore, we verified the effect of Drp1 protein on mitochondrial fission and tumor cell invasion using GH3 cell lines *in vitro*. We successfully

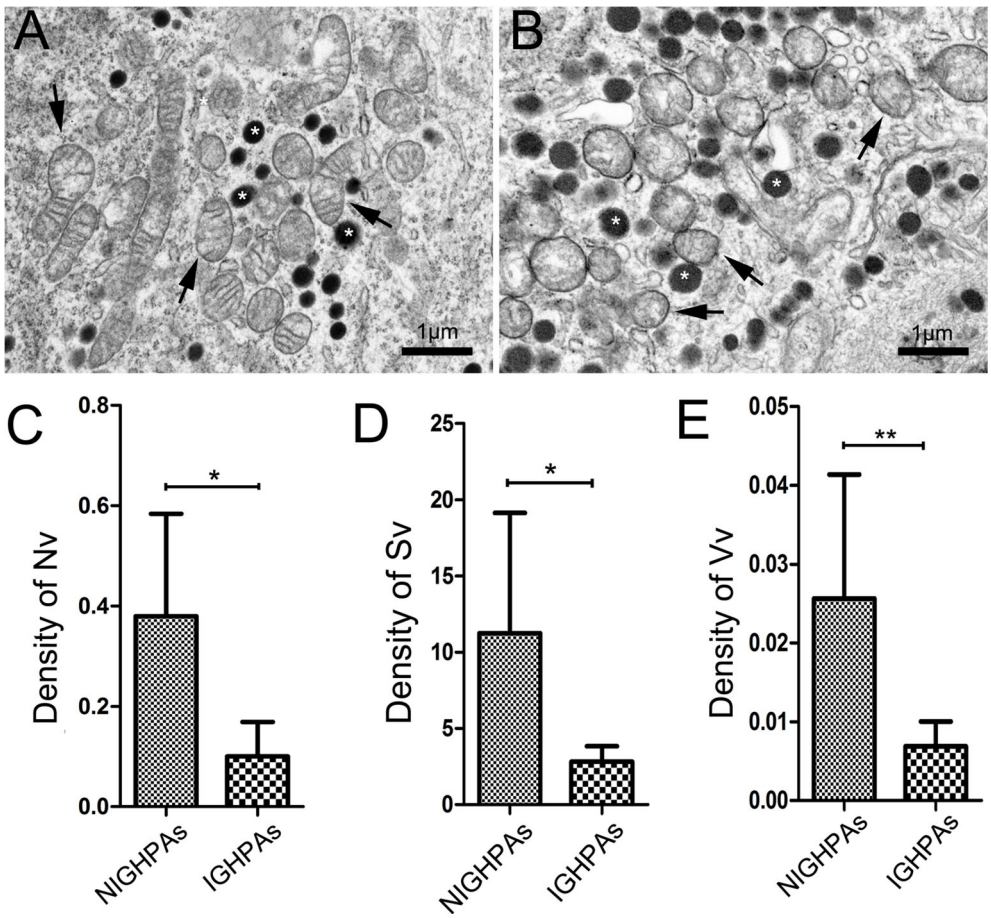

FIGURE 1 | Stereological analysis of mitochondria in NIGHPAs (n = 7) and IGHPAs (n = 7). The number density, bulk density and surface area density were corrected with tumor volume measured by nuclear magnetic resonance. Nonparametric tests were used for statistical analysis. **(A)** Representative electron microscopic image of tumor cells in NIGHPAs. Several mitochondria with normal morphology (arrows) and secretory granule (stars) were observed. **(B)** Representative electron microscopic image of tumor cells in IGHPAs. Several swollen mitochondria (arrows) and secretory granule (stars) were observed. **(C)** The density of mitochondrial number (Nv) in IGHPAs was significantly lower than that of NIGHPAs. **(D)** The density of mitochondrial surface area (Sv) in IGHPAs was significantly lower than that of NIGHPAs. **(E)** The mitochondrial volume fraction (Vv) in IGHPAs was significantly lower than that of NIGHPAs. Scale bar = 1um, *P < 0.05, **P < 0.01.

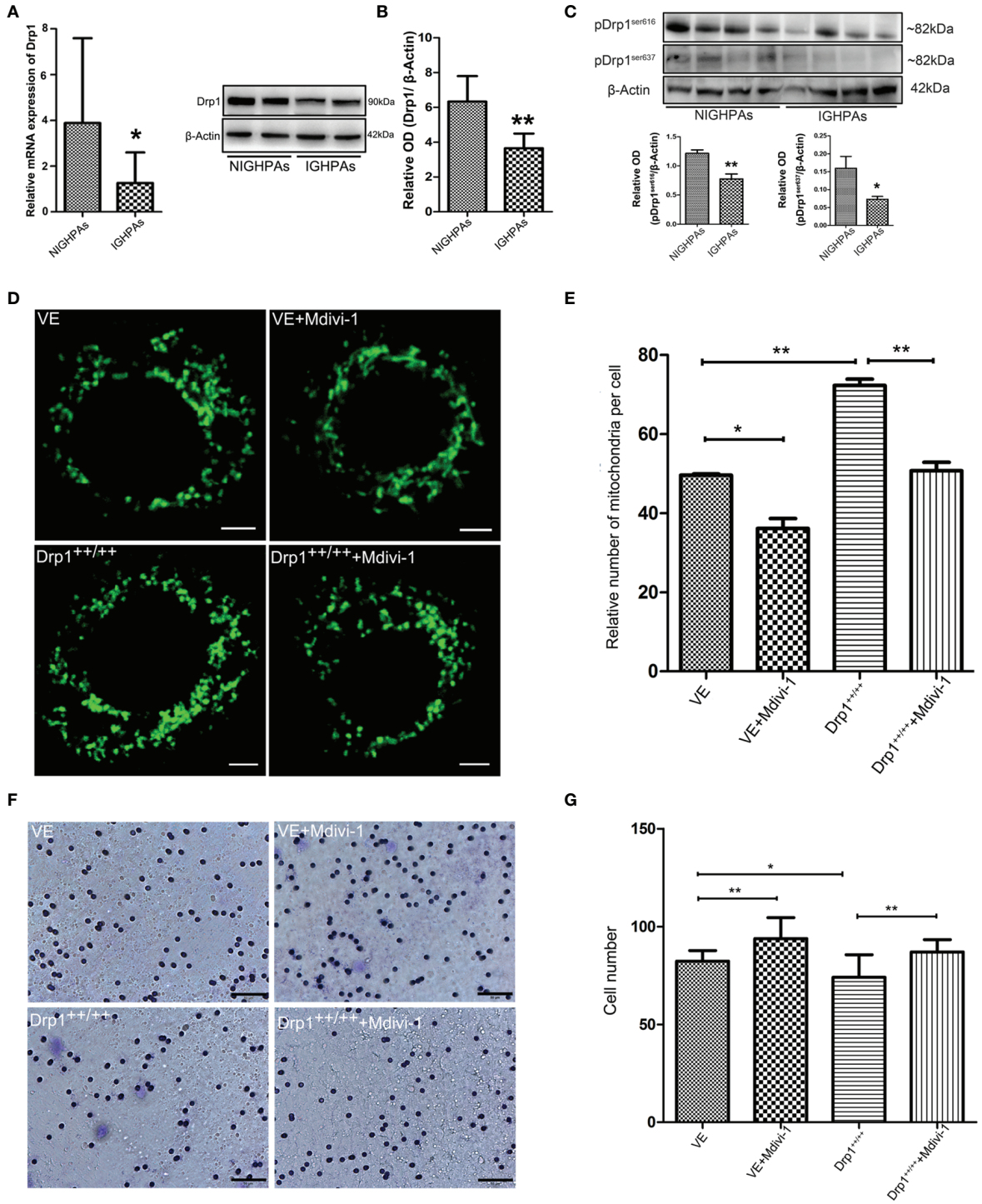

FIGURE 2 | The relationship between Drp1 regulated mitochondrial dynamics and tumor invasion. **(A)** Expression of Drp1 mRNA was assessed by RT-qPCR in NIGHPAs (n = 12) and IGHPAs (n = 13) samples. **(B)** Expression of Drp1 protein levels in NIGHPAs (n =8) and IGHPAs (n =8) samples was assessed by western blotting (left panel). Statistical analysis of the western blotting results (right panel). **(C)** Protein levels of phosphorylated Drp1at Ser616 and Ser637 in NIGHPAs and IGHPAs samples were assessed by western blotting (above panel). Statistical analysis of the western blotting results (below panel). **(D)** Mitochondria were stained with Mito-Tracker Green FM to display quantity and mitochondrial morphology in four GH3 cell lines groups, VE (transfected with empty vector) group, VE+Mdivi-1 group, $Drp1^{++/++}$(Drp1 over expression vector) group, $Drp1^{++/++}$+Mdivi-1 group. GH3 cells were observed after intervention with Mdivi-1 for 48 hours by confocal microscope. Scale bar = 2.5 um. **(E)** Statistical analysis of the relative number of mitochondria per cell (n = 25). **(F)** The invasive ability of GH3 cells was evaluated by transwell assay (n = 3). Scale bar = 50 um. **(G)** Statistical analysis of the invasive GH3 cell number. *P < 0.05, **P < 0.01.

constructed a Drp1 overexpression ($Drp1^{++/++}$) GH3 cell model (data not shown) by lentivirus transfection and used Mdivi-1 to specifically inhibit Drp1 (24). The number of mitochondria was significantly increased in response to overexpression of Drp1 in GH3 cells but decreased significantly in response to Mdivi-1 (**Figures 2D, E**), which were further confirmed by transmission electron microscopy (**Figure S1D**). Then, we evaluated whether inhibition of Drp1 might affect GH3 cell invasion. Transwell experiments demonstrated that overexpression of Drp1 attenuated the invasion of GH3 cells, while inhibition of Drp1 by Mdivi-1 promoted cell invasion (**Figures 2F, G**).

Inhibition of Drp1 Promotes GH3 Cells Invasion by Activating STAT3

The mitochondrial membrane has been well recognized as a platform that mediates the transduction of signals into and out of the mitochondria, which supports the role of mitochondrial dynamics in regulating cell signaling pathways (19). It is well known that the signal transducer and activator of transcription 3 (STAT3) signaling pathway is involved in cellular proliferation, invasion and apoptosis; thus, we detected whether Drp1 affects STAT3. We found that inhibition of Drp1 by Mdivi-1 upregulated the expression of total cell STAT3 protein, and downregulated STAT3 protein in $Drp1^{++/++}$ GH3 cells (**Figure 3A**). Moreover, the phosphorylated site of STAT3 at Y705 ($pSTAT3^{Y705}$), an active form of STAT3 that is primarily involved in STAT3 nuclear transcription, was upregulated in the nuclei of GH3 cells when Drp1 was inhibited by Mdivi-1. Accordingly, protein levels of $pSTAT3^{Y705}$ were downregulated in $Drp1^{++/++}$ GH3 cells (**Figure 3B**). Another active form of STAT3 that is primarily distributed in mitochondria, STAT3 phosphorylated at S727 ($pSTAT3^{S727}$), was also upregulated in the mitochondria of GH3 cells when Drp1 was inhibited by Mdivi-1 and downregulated in $Drp1^{++/++}$ GH3 cells (**Figure 3C**). Similarly, we found that expression levels of STAT3 protein were significantly higher in the IGHPAs samples (**Figure 3D**). Further immunohistochemical staining confirmed the overexpression of STAT3, $pSTAT3^{Y705}$ and $pSTAT3^{S727}$ in the IGHPAs samples (**Figures 3E–K**). STAT3 is known to activate matrix metalloproteinase 2/9 (MMP2/9) gene expression, which could mediate an enhancement effect on tumor invasiveness (27). We analyzed the enzyme activity of MMP2/9 in GH3 cells and found that the activity of MMP2/9 was increased by inhibition of Drp1. STAT3 inhibitors significantly reversed this effect, which was similar to the effect of Drp1 overexpression (**Figures 3L–R**). To explore the role of STAT3 in GH3 cells invasion induced by Mdivi-1, transwell assays were performed. We found that STAT3 inhibitors blocked GH3 cell invasion enhanced by inhibition of mitochondrial fission (**Figures 3S–V**).

Inhibition of Drp1 Enhances the Proliferation of GH3 Cells

To further investigate whether inhibition of Drp1 regulates GH3 proliferation, we inspected GH3 cell number by CCK-8, cell cycle and apoptosis by flow cytometry. The CCK-8 assay confirmed that inhibition of Drp1 enhanced the proliferation of GH3 cells (**Figure 4A**), which was due to promotion of the cell cycle (**Figure 4B**, **Figure S2A**) and protection from apoptosis (**Figure 4C**, **Figure S2B**). Moreover, we detected whether inhibition of Drp1 could directly affect the mitochondrial apoptosis pathway. GH3 cells treated with the Drp1 inhibitor Mdivi-1 presented reduced mitochondrial membrane potential, and $Drp1^{++/++}$ GH3 cells presented increased mitochondrial membrane potential, which could be reversed by Mdivi-1 (**Figure 4D**, **Figure S2C**). We also found that reactive oxygen species (ROS) underwent similar changes. (**Figure 4E** and **Figure S2D**). Then, we measured the expression of mitochondrial apoptotic pathway-related proteins, including Bcl-2, Bax and cleaved caspase-3. Western blotting results indicated that the proapoptotic protein levels of Bax/Bcl-2 (**Figure 4F**) and cleaved caspase-3 (**Figure 4G**) were significantly decreased by the Drp1 inhibitor Mdivi-1.

Drp1 May Regulate the Proliferation of GH3 Cells *Via* Mitochondrial STAT3 Signaling

To further investigate whether the STAT3 signaling pathway is involved in the process through which Drp1 regulates GH3 cell proliferation, we chose two STAT3 inhibitors, HO-3867 (a broad spectrum inhibitor of STAT3 phosphorylation) and Cry (a selective inhibitor of STAT3 phosphorylation at Tyr705), for *in vitro* experiments. The CCK-8 assay indicated that HO-3867 sufficiently reversed the proliferation of GH3 cells induced by Mdivi-1, but Cry had no effect (**Figure 5A**). Neither inhibitor affected the cell cycle (**Figure 5B** and **Figure S3A**). We further observed a higher rate of apoptotic cells treated with VE+Mdivi-1+HO-3867 while Cry had no effect compared to VE+Mdivi-1 (**Figure 5C** and **Figure S3B**). Moreover, HO-3867 significantly increased the mitochondrial membrane potential and ROS (**Figures 5D, E** and **Figures S3C, D**). Accordingly, western blotting results indicated that the proapoptotic protein levels of Bax/Bcl-2 (**Figure 5F**) and cleaved caspase-3 (**Figure 5G**) were significantly upregulated by HO-3867 but not Cry.

Inhibition of Drp1 Promotes the Invasion and Proliferation of MMQ Cell Lines and Human PAPCs

We further investigated whether inhibition of Drp1 affects the invasion and proliferation of MMQ cell lines and human primary GHPAs cells (PAPCs). Similar to GH3 cells, the Drp1 inhibitor Mdivi-1 significantly enhanced the invasion of MMQ cells (**Figures S4A, B**) and PAPCs (**Figures S4D, E**), and this effect was reversed by STAT3 inhibitors HO-3867 and Cry. The CCK-8 assay further confirmed that the Drp1 inhibitor Mdivi-1 significantly promoted the proliferation of MMQ cells (**Figure S4C**) and PAPCs (**Figure S4F**), and this pro-proliferative effect was reversed by the STAT3 inhibitor HO-3867.

Inhibition of Drp1 Promotes the Growth and Invasion of GH3 Cells *In Vivo*

To further investigate the effects of Drp1 on PA cells *in vivo*, a PA xenograft model was generated by subcutaneous injection of either vector control (VE) or $Drp1^{++/++}$ GH3 cells into nude mice. The

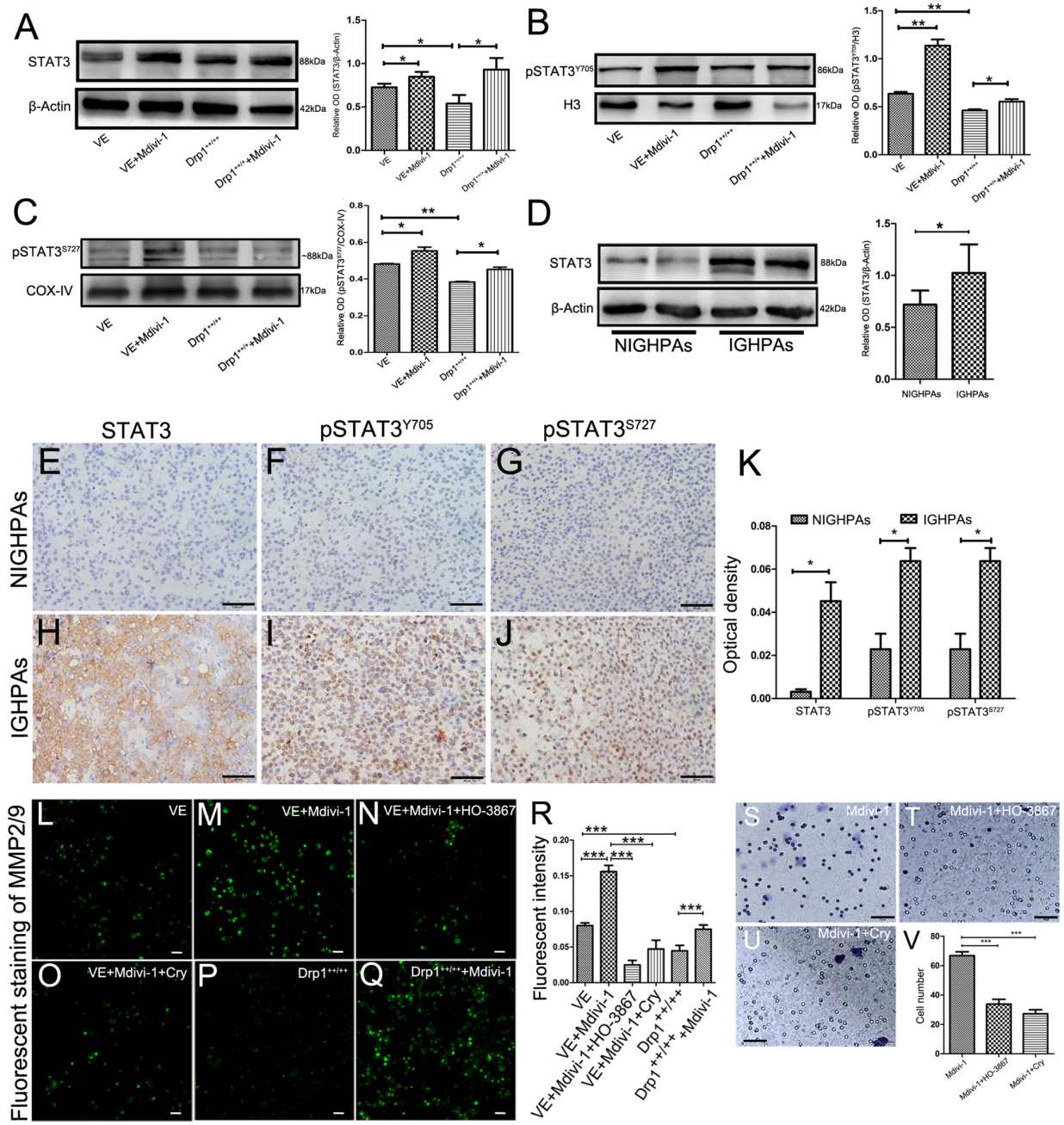

FIGURE 3 | Inhibition of Drp1 enhanced the invasion of GH3 cells *via* activating STAT3. **(A)** The expression of STAT3 protein was detected by western blotting in four GH3 cell groups (VE, VE+Mdivi-1, Drp1$^{+/+}$, Drp1$^{+/+}$+Mdivi-1) after 48 hours (n = 3) (left panel). Statistical analysis of the western blotting results (right panel). **(B)** Nuclear pSTAT3^{Y705}, a phosphorylated form of STAT3 and mainly involved in nuclear transcription, was detected by western blotting in the four groups. H3 was used as a reference (n = 3) (left panel). Statistical analysis of the western blotting results (right panel). **(C)** Mitochondrial p-STAT3^{S727}, another phosphorylated form of STAT3 and mainly distribute in mitochondria, was detected by western blotting in the four groups. COX-IV was used as a reference (n = 3) (left panel). Statistical analysis of the western blotting results (right panel). **(D)** Expression of STAT3 protein levels in NIGHPAs (n =8) and IGHPAs (n = 8) samples were assessed by western blotting (left panel). Statistical analysis of the western blotting results (right panel). **(E–G)** IHC staining of STAT3, pSTAT3^{Y705}, pSTAT3^{S727} in NIGHPAs samples (n = 10). **(H–J)** IHC staining of STAT3, pSTAT3^{Y705}, pSTAT3^{S727} in IGHPAs samples (n = 10). **(K)** Statistical analysis of the IHC results. **(L–Q)** Activity of MMP2/9 were detected by situ zymography fluorescence staining in six groups (VE, VE+Mdivi-1, VE+Mdivi-1+HO-3867, VE+Mdivi-1+Cry, Drp1$^{+/+}$, Drp1$^{+/+}$+Mdivi-1). **(R)** Statistical analysis of the MMP2/9 fluorescent intensity. **(S–U)** GH3 cell invasion were evaluated by transwell assay when treated with Mdivi-1, Mdivi-1+HO-3867, Mdivi-1+Cry. **(V)** Statistical analysis of the invasive GH3 cell number in the three groups. HO-3867, a broad spectrum inhibitor of STAT3 phosphorylation. Cry, a selective inhibitor of STAT3 phosphorylation at Tyr705. **(E–J, S-U)**, Scale bar =50 μm. L-Q, Scale bar =25 μm. *P < 0.05, **P < 0.01, ***P < 0.001. Data were expressed as mean ± SEM.

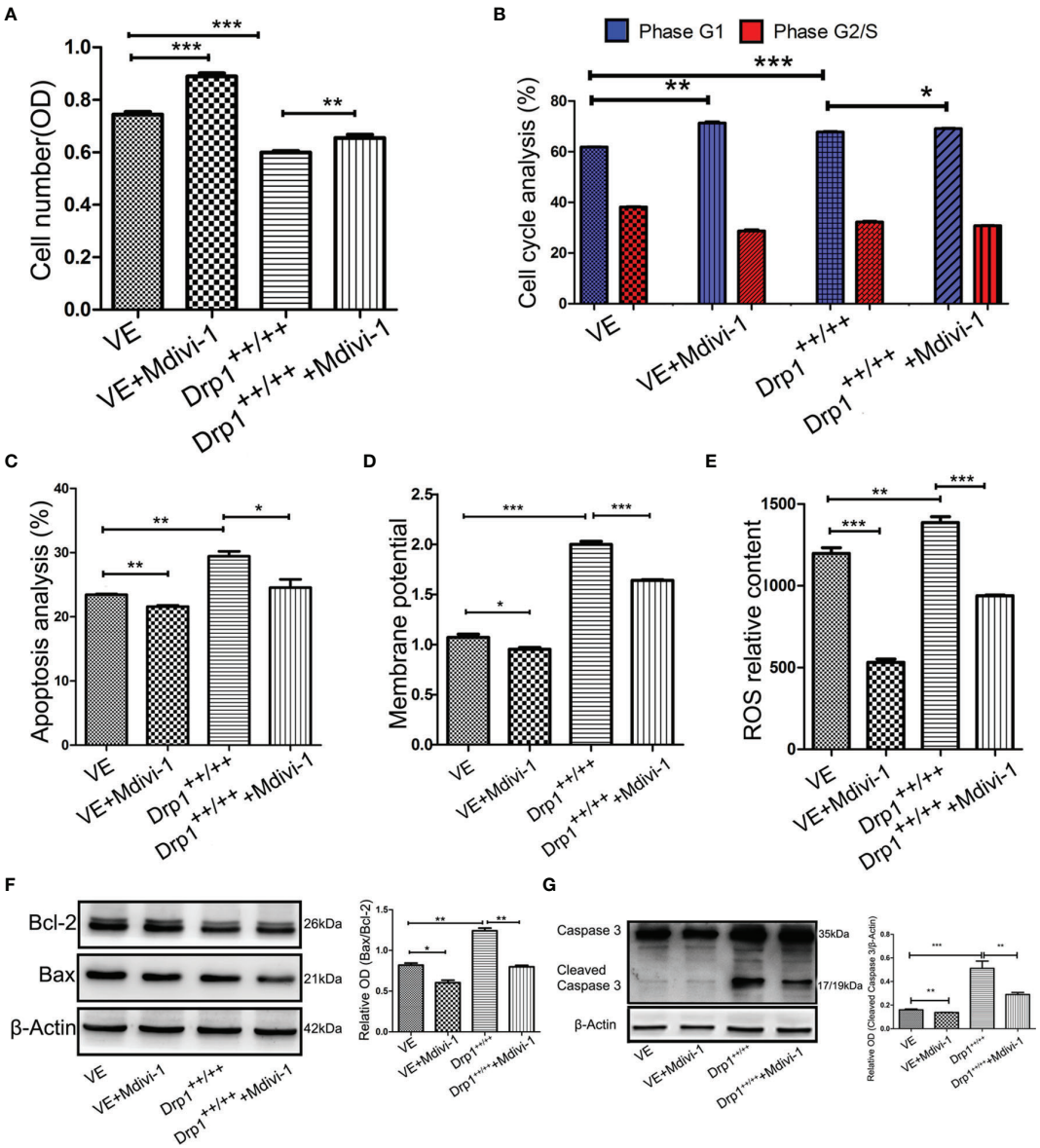

FIGURE 4 | Inhibition of Drp1 promoted proliferation of GH3 cells. **(A)** The number of GH3 cells in four groups (VE, VE+Mdivi-1, Drp1$^{++/++}$, Drp1$^{++/++}$+Mdivi-1) at 48 h were assessed by CCK-8 assay (n = 3). **(B)** Cell cycle at 48 h were analyzed by flow cytometry (n = 3). **(C)** Cell apoptosis at 48 h were analyzed by flow cytometry (n = 3). **(D)** Mitochondrial membrane potential of four GH3 cell groups were detected by flow cytometry using Rhodamine123 at 48 h (n = 3). **(E)** Reactive oxygen species (ROS) were detected by flow cytometry using DCF-DA fluorescence at 48 h (n = 3). **(F)** The expression of Bcl-2 and Bax proteins were detected by western blotting (n = 3) (left panel). Statistical analysis of the western blotting results (right panel). **(G)** The expression of cleaved caspase-3 protein was detected by western blotting (n = 3) (left panel). Statistical analysis of the western blotting results (right panel). *P < 0.05, **P < 0.01, ***P < 0.001. Data were expressed as mean ± SEM.

mice were randomly divided into four groups (VE, VE+Mdivi-1, Drp1$^{++/++}$, DRP1$^{++/++}$+Mdivi-1). We found that inhibition of Drp1 significantly promoted the growth of GH3 cells *in vivo*, and overexpression of Drp1 attenuated the tumor growth (**Figures 6A–C**). Further, HE staining confirmed that several tumor nodules were detected in tumor capsule in VE+Mdivi-1 group, but not in VE and Drp1$^{++/++}$ group, which indicated that inhibition of Drp1 enhanced the tumor invasion (**Figure 6D**).

DISCUSSION

Increasing evidence suggests that abnormal mitochondrial dynamics participate in the processes of tumorigenesis (28, 29). In the current study, stereological results confirmed dysregulated mitochondrial dynamics of IGHPAs. Furthermore, we identified that downregulation of Drp1 was responsible for the inhibition of mitochondrial fission and might be related to the invasion and

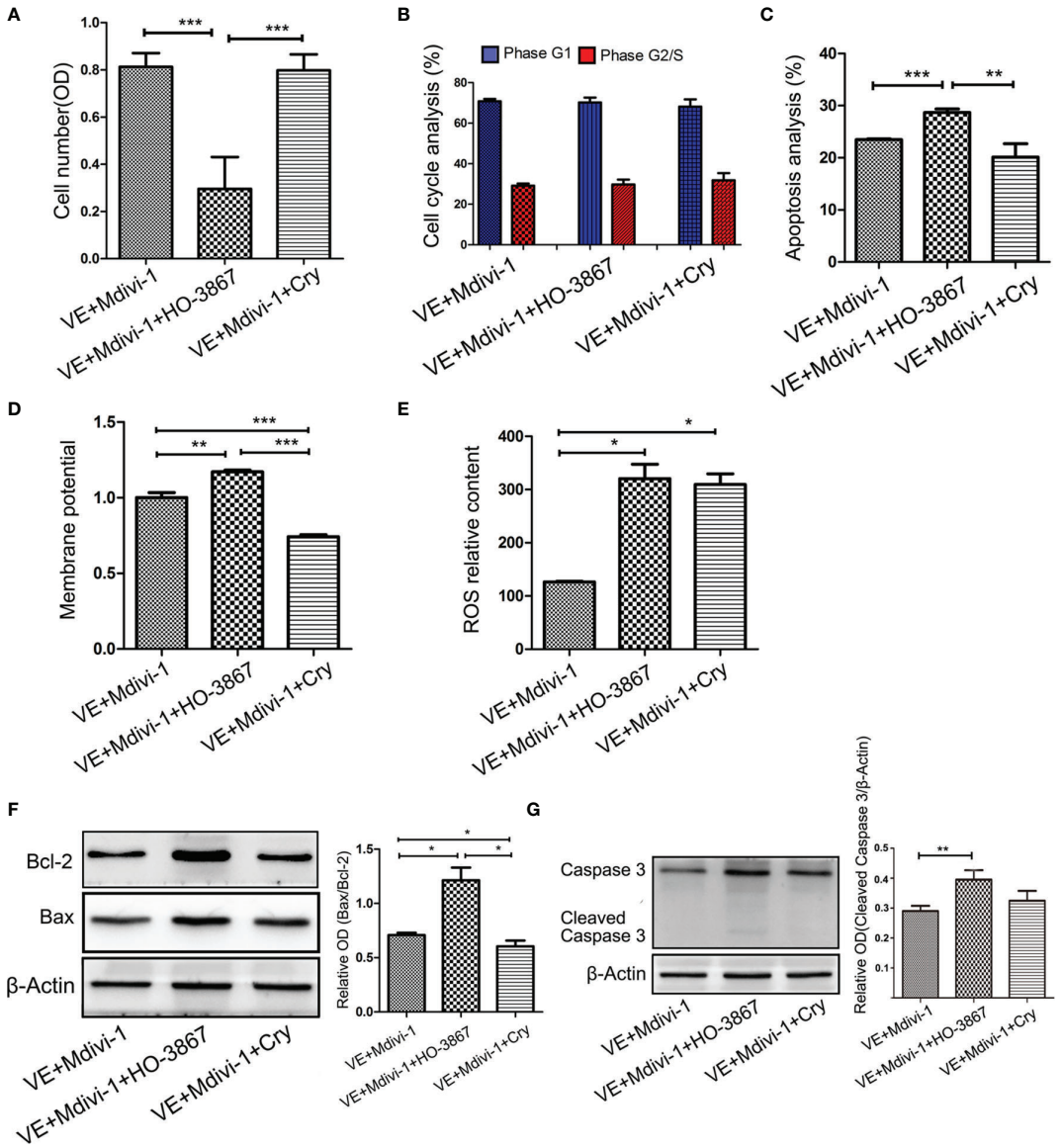

FIGURE 5 | Inhibition of STAT3 reversed the Drp1 regulating pro-proliferation of GH3 cells. **(A)** The number of GH3 cells in three groups (VE+Mdivi-1, VE+Mdivi-1 +HO-3867, VE+Mdivi-1+Cry) at 48 h were assessed by CCK-8 assay (n = 3). **(B)** Cell cycle at 48 h were analyzed by flow cytometry (n = 3). **(C)** Cell apoptosis at 48 h were analyzed by flow cytometry (n = 3). **(D)** Mitochondrial membrane potential of three GH3 cell groups were detected by flow cytometry using Rhodamine123 at 48 h (n = 3). **(E)** Reactive oxygen species (ROS) were detected by flow cytometry using DCF-DA fluorescence at 48 h (n = 3). **(F)** The expression of Bcl-2 and Bax proteins were detected by western blotting (n = 3) (left panel). Statistical analysis of the western blotting results (right panel). **(G)** The expression of cleaved caspase-3 protein was detected by western blotting (n = 3) (left panel). Statistical analysis of the western blotting results (right panel). *P < 0.05, **P < 0.01, ***P < 0.001. Data were expressed as mean ± SEM.

proliferation of IGHPAs. Inhibition of mitochondrial fusion enhanced the invasion and proliferation of GH3 cell lines and human primary GH-PA cells *in vitro* and *in vivo*, and overexpression of Drp1 reversed this process. Mechanistically, decreased mitochondrial fission inhibited mitochondrial pathway-mediated apoptosis and upregulated the activity of MMP2/9 in GH3 cells *via* activation of the transcription factor STAT3.

Despite supplying energy, mitochondria play a key role in tumor progression by regulating redox homeostasis, oncogenic signaling, innate immunity, and apoptosis of cancer cells (12). Mutations in *SDH* were detected in patients with GHPAs, and further animal models confirmed that *SDH* deficiency might contribute to tumorigenesis (18, 30). Mitochondrial function is affected not only by mitochondrial metabolism, but also by mitochondrial dynamics regulating mitochondrial morphology

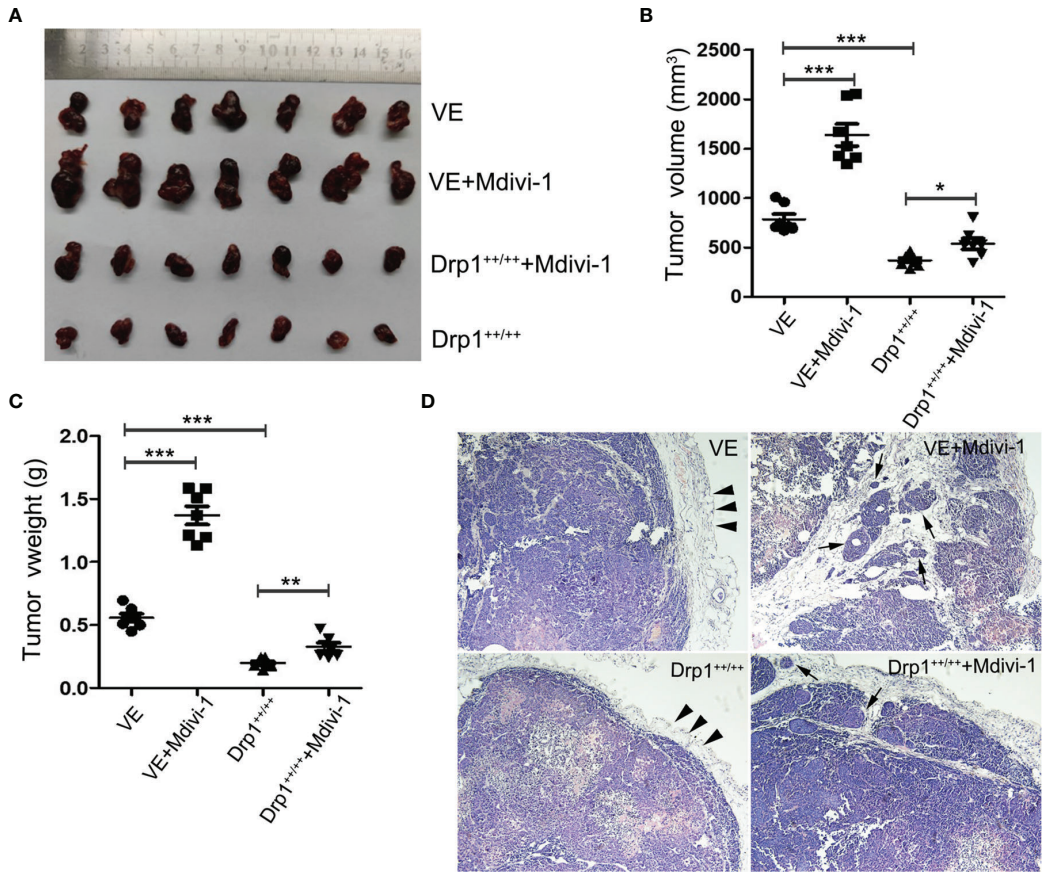

FIGURE 6 | Inhibition of Drp1 promoted the growth and invasion of GH3 cells *in vivo*. **(A)** Excised tumors in four groups (VE, VE+Mdivi-1, $Drp1^{++/++}$, $Drp1^{++/++}$+Mdivi-1) were shown. **(B)** Tumor volume in different groups. **(C)** Tumor weight in different groups. **(D)** HE staining of tumor(×100 magnification). Smooth tumor capsule (arrowheads) was detected in VE and $Drp1^{++/++}$ group. Tumor nodules (arrows) were detected in tumor capsule in VE+Mdivi-1 and $Drp1^{++/++}$+Mdivi-1 group. *P < 0.05, **P < 0.01, ***P < 0.001.

(19). In the current study, we found that the number, volume and membrane area of mitochondria were decreased in IGHPAs using stereological methods. Downregulation of mitochondrial membrane area referred to decreased mitochondrial ATP through oxidative phosphorylation (28), which seems consistent with our previous research on abnormal glycolysis in IGHPAs. Therefore, our stereological results first suggested a potential role of abnormal mitochondrial dynamics in the invasion of pituitary tumors.

The core mechanisms of mitochondrial membrane dynamics are fusion and fission, which are affected by mitochondrial dynamics proteins (19, 29). The mRNA expression levels of Mfn1, Mfn2 and OPA1 were similar between the IGHPAs and NIGHPAs sample, while the mRNA and protein levels of Drp1 were significantly downregulated in IGHPAs samples. These data suggest that the primary dysregulated mitochondrial dynamics event in IGHPAs might be hypofission, but not hyperfusion. Similar to our findings, Sabatino et al. observed downregulation of Drp1 protein levels and decreased mitochondrial fission during the development of estrogen induced experimental pituitary tumors *in vivo* (31, 32). However, upregulation of Drp1 has been reported in many cancers (e.g. breast cancer, glioblastomas) and may be a potential target for cancer treatment (21, 33). These data may seem contradictory and puzzled, however, we think they indicate the different role of mitochondria in tumorigenesis and development in various tumors (28). Furthermore, we investigated the role of mitochondrial dynamics in the invasion of GH3 cell lines *in vitro* and *in vivo*. We found that overexpression of Drp1 promoted the fission of mitochondria and attenuated the invasion of tumor cells, while inhibition of mitochondrial fission by Midiv-1 enhanced invasive behavior through upregulation of MMP2/9. The role of mitochondrial dynamics has been confirmed in the migration and invasion of different subtypes of cells. In neural stem cells, miR-137 accelerates mitochondrial fission and fusion and thereby promotes neuronal differentiation and migration (34). In a KRAS mutated carcinoma model, autophagy deficiency-induced mitochondrial hyperfission attenuated the invasion of tumor cells (35). Matrix metalloproteinase family members, primarily MMP-2 and

MMP-9, have been well-recognized as core molecules responsible for the invasion of pituitary adenomas by our previous studied (8, 36) and other studies (37). Taken together, our data indicate that mitochondrial hypofission might strengthen the invasiveness of IGHPAs tumor cells.

Considering that the IGHPAs generally accompanied by highly proliferative features, we further investigated whether Drp1 mediated mitochondrial hypofission affects the proliferation of tumor cells. We found that inhibition of mitochondrial fission promoted the proliferation of GH3 cell lines *in vitro* and *in vivo*, while overexpression of Drp1 reversed this pro-proliferative effect. Mechanistically, inhibition of mitochondrial fission decreased the mitochondrial membrane potential, reactive oxygen species (ROS) and internal apoptosis stimulator responses, which restrained the mitochondria-mediated apoptosis signaling pathway. Several proapoptotic (e.g., Bax and Bak) and antiapoptotic factors (e.g., Bcl-2 family members) were identified to colocalize with the fission sites of the mitochondrial outer membrane, and translocation of these factors in dysregulated mitochondrial dynamics triggers caspase-dependent apoptosis (38). In HeLa cells, Drp1 dependent mitochondrial fission might trigger intrinsic apoptosis *via* cytochrome c release (39). Mazumder et al. also reported that nonsteroidal anti-inflammatory drugs upregulated Drp1 expression and thereby promoted mitochondrial hyperfission, which resulted in apoptosis of gastric cancer cells (40). Thus, we hypothesized that inhibition of mitochondrial fission might restrain the Bax induced caspase 3 dependent apoptosis of GH3 cells. Conversely, Drp1 dependent mitochondrial hyperfission presents antiapoptotic effects and promotes the proliferation of tumor cells in pancreatic cancer (20) and glioblastoma (33). However, Zhao et al. found that regulation of mitochondrial dynamics by altering Drp1, Mfn1 and Mfn2 had no effect on the breast cancer cell cycle or cell viability (21). Thus, the diverse roles of mitochondrial dynamics in tumorigenesis are cell-type specific and may be dictated by various physiological or pathological conditions (28).

Mitochondria are characterized not only as cellular powerhouses but also as signaling organelles. Generally, the outer mitochondrial membrane (OMM) is regarded as a platform where cell signaling pathways converge, while the inner mitochondrial membrane (IMM) is more responsible for mitochondrial respiration (19). Thus, we speculated that Drp1 regulated OMM fission might affect some cellular signaling pathways. Upregulation of total cellular STAT3, mitochondrial $pSTAT3^{S727}$, and intranuclear $pSTAT3^{Y705}$ was detected in GH3 cells when mitochondrial fission was inhibited by the Drp1 inhibitor Mdivi-1. Similar overexpression of the three proteins was observed in IGHPAs samples. Activation of STAT3 signaling is well recognized in several cancers and promotes tumor cell proliferation, survival, invasion and immunosuppression (41, 42). Transcription of MMP2/9 is directly regulated by STAT3 in several cancers, especially the phosphorylation of STAT3 at Tyr705 (27, 43, 44). In our study, we found that inhibition of STAT3 and $pSTAT3^{Y705}$ significantly downregulated the expression of MMP2/9 and attenuated Mdivi-1-induced invasion of GH3 cell lines, PAPCs and MMQ cell lines, providing a probable mechanism by which STAT3 mediates mitochondrial hypofission induced invasion of IGHPAs. In addition to the canonical nuclear gene transcription regulation of STAT3, the role of noncanonical mitochondrial STAT3 signaling has been confirmed in tumorigenesis (42, 45). We found that inhibition of STAT3, but not $pSTAT3^{Y705}$, significantly decreased the mitochondrial hypofission induced proliferation of GH3 cell lines, PAPCs and MMQ cell lines. Moreover, inhibition of STAT3, but not $pSTAT3^{Y705}$, enhanced the mitochondria mediated apoptosis of GH3 cell lines. These data suggest a pro-proliferative role of mitochondrial $pSTAT3^{S727}$ in GHPAs *via* anti-apoptosis. Mitochondrial $pSTAT3^{S727}$ has been confirmed to regulate the activity of the electron transport chain, transcription of mtDNA and the mitochondrial permeability transition pore in several cell types, which could influence cellular proliferation by altering the production of ATP, ROS and mitochondrial transcripts (42, 45, 46). Ezzat et al. confirmed that fibroblast growth factor receptor 4 facilitates pituitary GH cell tumorigenesis *via* activation of mitochondrial $pSTAT3^{S727}$, and further experiments concluded that mitochondrial $pSTAT3^{S727}$ was a therapeutic target of pasireotide, which was approved for treating patients with GHPA (47, 48). Conclusively, mitochondrial hypofission in GHPA might enhance the invasion and proliferation of tumor cells *via* activation of intranuclear $pSTAT3^{Y705}$ and mitochondrial $pSTAT3^{S727}$, respectively.

In summary, this study revealed that mitochondrial hypofission caused by downregulation of Drp1 was responsible for the invasiveness and high proliferation of GHPAs. The underlying mechanisms might include activation of STAT3, which is especially dependent upon phosphorylation at S727 and Y705 in mitochondria and nuclei, respectively. Conclusively, our findings provide a new perspective on how mitochondria regulate the development of IGHPAs. However, whether the homozygous or heterozygous gene type is responsible for this alteration of Drp1, and the factors that trigger abnormal mitochondrial dynamics and consecutive dysregulation of mitochondrial metabolism in tumorigenesis requires further investigation.

DATA AVAILABILITY STATEMENT

The original contributions presented in the study are included in the article/**Supplementary Material**. Further inquiries can be directed to the corresponding authors.

ETHICS STATEMENT

The collection procedure of patient tissue samples in this study was approved by laboratory animal welfare and ethics committee of Xinqiao Hospital (the ethical review number: 2018-049-012). The patients/participants provided their written informed consent to participate in this study.

AUTHOR CONTRIBUTIONS

YZ, HY, and SL designed the experiments. YZ and LZ performed the stereological experiments. YZ, KF, and ZZ carried out the cell experiment *in vitro*. YZ and YJG performed the *in vivo* experiments. YZ and XD carried out the immunohistochemical staining and analyzed the data. YZ, LZ, and SL wrote the manuscript. All authors read and approved the final manuscript.

FUNDING

This work was supported by the Nursery Project of Army Medical University (No.2019R054),Natural Science Foundation of Chongqing (No.cstc2019jcyj-msxmX0475) and Basic Research Project of Army Military Medical University (2019XQN12).

SUPPLEMENTARY MATERIAL

The Supplementary Material for this article can be found online at: https://www.frontiersin.org/articles/10.3389/fonc.2022.739631/full#supplementary-material

Supplementary Figure 1 | (A–C) Expression of Mfn1, Mfn2 and OPA1 mRNA levels were assessed by RT-qPCR in NIGHPAs (n = 12) and IGHPAs (n = 13) samples. **(D)** Representative electron microscopic images of mitochondria in four GH3 cell groups (VE, VE+Mdivi-1, Drp1$^{++/++}$, Drp1$^{++/++}$+Mdivi-1). $^{\#}P > 0.05$. Scale bar = 0.5 um.

Supplementary Figure 2 | (A) Cell cycle of GH3 cells in four groups (VE, VE +Mdivi-1, Drp1$^{++/++}$, Drp1$^{++/++}$+Mdivi-1) at 48 h were analyzed by flow cytometry (n = 3). **(B)**. Cell apoptosis at 48 h were analyzed by flow cytometry (n = 3). **(C)** Mitochondrial membrane potential of four GH3 cell groups were detected by flow cytometry using Rhodamine123 at 48 h (n = 3). **(D)** Reactive oxygen species (ROS) were detected by flow cytometry using DCF-DA fluorescence at 48 h (n = 3).

Supplementary Figure 3 | (A) Cell cycle of GH3 cells in three groups (VE+Mdivi-1, VE+Mdivi-1+HO-3867, VE+Mdivi-1+Cry) at 48 h were analyzed by flow cytometry (n = 3). **(B)** Cell apoptosis at 48 h were analyzed by flow cytometry (n = 3). **(C)** Mitochondrial membrane potential of three GH3 cell groups were detected by flow cytometry using Rhodamine123 at 48 h (n = 3). **(D)** Reactive oxygen species (ROS) were detected by flow cytometry using DCF-DA fluorescence at 48 h (n = 3).

Supplementary Figure 4 | The invasion and proliferation of MMQ and PAPCs were affected by Drp1 *via* STAT3. **(A)** MMQ cell invasion were evaluated by transwell assay when treated with Mdivi-1, Mdivi-1+HO-3867, Mdivi-1+Cry (n = 3). **(B)** Statistical analysis of the invasive MMQ cell number in the four groups. **(C)** The number of MMQ cells in four groups were assessed by CCK-8 assay (n = 3). **(D)** PAPCs cell invasion were evaluated by transwell assay when treated with Mdivi-1, Mdivi-1+HO-3867, Mdivi-1+Cry (n = 5). **(B)** Statistical analysis of the invasive PAPCs cell number in the four groups. **(C)** The number of PAPCs cells in four groups were assessed by CCK-8 assay (n = 5). $^{*}P < 0.05$, $^{***}P < 0.001$. Data were expressed as mean ± SEM.

REFERENCES

1. Katznelson L, Laws ER Jr, Melmed S, Molitch ME, Murad MH, Utz A, et al. Acromegaly: An Endocrine Society Clinical Practice Guideline. *J Clin Endocrinol Metab* (2014) 99:3933–51. doi: 10.1210/jc.2014-2700
2. Almeida JP, Ruiz-Trevino AS, Liang B, Omay SB, Shetty SR, Chen YN, et al. Reoperation for Growth Hormone-Secreting Pituitary Adenomas: Report on an Endonasal Endoscopic Series With a Systematic Review and Meta-Analysis of the Literature. *J Neurosurg* (2018) 129:404–16. doi: 10.3171/2017.2.JNS162673
3. Lopes MBS. The 2017 World Health Organization Classification of Tumors of the Pituitary Gland: A Summary. *Acta Neuropathol* (2017) 134:521–35. doi: 10.1007/s00401-017-1769-8
4. Trouillas J, Roy P, Sturm N, Dantony E, Cortet-Rudelli C, Viennet G, et al. A New Prognostic Clinicopathological Classification of Pituitary Adenomas: A Multicentric Case-Control Study of 410 Patients With 8 Years Post-Operative Follow-Up. *Acta Neuropathol* (2013) 126:123–35. doi: 10.1007/s00401-013-1084-y
5. Hanahan D, Weinberg RA. Hallmarks of Cancer: The Next Generation. *Cell* (2011) 144:646–74. doi: 10.1016/j.cell.2011.02.013
6. Hu J, Yin H, Li B, Yang H. Identification of Transcriptional Metabolic Dysregulation in Subtypes of Pituitary Adenoma by Integrated Bioinformatics Analysis. *Diabetes Metab Syndr Obes* (2019) 12:2441–51. doi: 10.2147/DMSO.S226056
7. Pinzariu O, Georgescu B, Georgescu CE. Metabolomics-A Promising Approach to Pituitary Adenomas. *Front Endocrinol (Lausanne)* (2019) 9:814. doi: 10.3389/fendo.2018.00814
8. An J, Zhang Y, He J, Zang Z, Zhou Z, Pei X, et al. Lactate Dehydrogenase A Promotes the Invasion and Proliferation of Pituitary Adenoma. *Sci Rep* (2017) 7:4734. doi: 10.1038/s41598-017-04366-5
9. Ding X, Fan K, Hu J, Zang Z, Zhang S, Zhang Y, et al. SCP2-Mediated Cholesterol Membrane Trafficking Promotes the Growth of Pituitary Adenomas *via* Hedgehog Signaling Activation. *J Exp Clin Cancer Res* (2019) 38:404. doi: 10.1186/s13046-019-1411-9
10. Hu J, Chen Q, Ding X, Zheng X, Tang X, Li S, et al. Glutamine Metabolism in the Proliferation of GS-Expression Pituitary Tumor Cells. *Endocr Connect* (2020) 9:223–33. doi: 10.1530/EC-19-0515
11. Zhang A, Xu Y, Xu H, Ren J, Meng T, Ni Y, et al. Lactate-Induced M2 Polarization of Tumor-Associated Macrophages Promotes the Invasion of Pituitary Adenoma by Secreting CCL17. *Theranostics* (2021) 11:3839–52. doi: 10.7150/thno.53749
12. Zong WX, Rabinowitz JD, White E. Mitochondria and Cancer. *Mol Cell* (2016) 61:667–76. doi: 10.1016/j.molcel.2016.02.011
13. Dang L, White DW, Gross S, Bennett BD, Bittinger MA, Driggers EM, et al. Cancer-Associated IDH1 Mutations Produce 2-Hydroxyglutarate. *Nature* (2009) 462:739–44. doi: 10.1038/nature08617
14. Koivunen P, Lee S, Duncan CG, Lopez G, Lu G, Ramkissoon S, et al. Transformation by the (R)-Enantiomer of 2-Hydroxyglutarate Linked to EGLN Activation. *Nature* (2012) 483:484–8. doi: 10.1038/nature10898
15. Collins RRJ, Patel K, Putnam WC, Kapur P, Rakheja D. Oncometabolites: A New Paradigm for Oncology, Metabolism, and the Clinical Laboratory. *Clin Chem* (2017) 63:1812–20. doi: 10.1373/clinchem.2016.267666
16. Kurelac I, MacKay A, Lambros MB, Di Cesare E, Cenacchi G, Ceccarelli C, et al. Somatic Complex I Disruptive Mitochondrial DNA Mutations are Modifiers of Tumorigenesis That Correlate With Low Genomic Instability in Pituitary Adenomas. *Hum Mol Genet* (2012) 22:226–38. doi: 10.1093/hmg/dds422
17. Feng J, Zhang Q, Li C, Zhou Y, Zhao S, Hong L, et al. Enhancement of Mitochondrial Biogenesis and Paradoxical Inhibition of Lactate Dehydrogenase Mediated by 14-3-3eta in Oncocytomas. *J Pathol* (2018) 245:361–72. doi: 10.1002/path.5090
18. Xekouki P, Szarek E, Bullova P, Giubellino A, Quezado M, Mastroyannis SA, et al. Pituitary Adenoma With Paraganglioma/Pheochromocytoma (3pas) and Succinate Dehydrogenase Defects in Humans and Mice. *J Clin Endocrinol Metab* (2015) 100:E710–9. doi: 10.1210/jc.2014-4297
19. Giacomello M, Pyakurel A, Glytsou C, Scorrano L. The Cell Biology of Mitochondrial Membrane Dynamics. *Nat Rev Mol Cell Biol* (2020) 21:204–24. doi: 10.1038/s41580-020-0210-7
20. Kashatus JA, Nascimento A, Myers LJ, Sher A, Byrne FL, Hoehn KL, et al. Erk2 Phosphorylation of Drp1 Promotes Mitochondrial Fission and MAPK-Driven Tumor Growth. *Mol Cell* (2015) 57:537–51. doi: 10.1016/j.molcel.2015.01.002

21. Zhao J, Zhang J, Yu M, Xie Y, Huang Y, Wolff DW, et al. Mitochondrial Dynamics Regulates Migration and Invasion of Breast Cancer Cells. *Oncogene* (2013) 32:4814–24. doi: 10.1038/onc.2012.494
22. Li N, Zhan X. Mitochondrial Dysfunction Pathway Networks and Mitochondrial Dynamics in the Pathogenesis of Pituitary Adenomas. *Front Endocrinol (Lausanne)* (2019) 10:690. doi: 10.3389/fendo.2019.00690
23. Nyengaard JR. Stereologic Methods and Their Application in Kidney Research. *J Am Soc Nephrol* (1999) 10:1100–23. doi: 10.1681/ASN.V1051100
24. Manczak M, Kandimalla R, Yin X, Reddy PH. Mitochondrial Division Inhibitor 1 Reduces Dynamin-Related Protein 1 and Mitochondrial Fission Activity. *Hum Mol Genet* (2019) 28:177–99. doi: 10.1093/hmg/ddy335
25. Tierney BJ, McCann GA, Cohn DE, Eisenhauer E, Sudhakar M, Kuppusamy P, et al. HO-3867, a STAT3 Inhibitor Induces Apoptosis by Inactivation of STAT3 Activity in BRCA1-Mutated Ovarian Cancer Cells. *Cancer Biol Ther* (2012) 13:766–75. doi: 10.4161/cbt.20559
26. Shin DS, Kim HN, Shin KD, Yoon YJ, Kim SJ, Han DC, et al. Cryptotanshinone Inhibits Constitutive Signal Transducer and Activator of Transcription 3 Function Through Blocking the Dimerization in DU145 Prostate Cancer Cells. *Cancer Res* (2009) 69:193–202. doi: 10.1158/0008-5472.CAN-08-2575
27. Xie TX, Wei D, Liu M, Gao AC, Ali-Osman F, Sawaya R, et al. Stat3 Activation Regulates the Expression of Matrix Metalloproteinase-2 and Tumor Invasion and Metastasis. *Oncogene* (2004) 23:3550–60. doi: 10.1038/sj.onc.1207383
28. Chen H, Chan DC. Mitochondrial Dynamics in Regulating the Unique Phenotypes of Cancer and Stem Cells. *Cell Metab* (2017) 26:39–48. doi: 10.1016/j.cmet.2017.05.016
29. Anderson GR, Wardell SE, Cakir M, Yip C, Ahn YR, Ali M, et al. Dysregulation of Mitochondrial Dynamics Proteins are a Targetable Feature of Human Tumors. *Nat Commun* (2018) 9:1677. doi: 10.1038/s41467-018-04033-x
30. Xekouki P, Stratakis CA. Succinate Dehydrogenase (SDHx) Mutations in Pituitary Tumors: Could This be a New Role for Mitochondrial Complex II and/or Krebs Cycle Defects? *Endocr Relat Cancer* (2012) 19:C33–40. doi: 10.1530/ERC-12-0118
31. Sabatino ME, Petiti JP, Sosa Ldel V, Perez PA, Gutierrez S, Leimgruber C, et al. Evidence of Cellular Senescence During the Development of Estrogen-Induced Pituitary Tumors. *Endocr Relat Cancer* (2015) 22:299–317. doi: 10.1530/ERC-14-0333
32. Sabatino ME, Grondona E, Sosa LDV, Mongi Bragato B, Carreno L, Juarez V, et al. Oxidative Stress and Mitochondrial Adaptive Shift During Pituitary Tumoral Growth. *Free Radic Biol Med* (2018) 120:41–55. doi: 10.1016/j.freeradbiomed.2018.03.019
33. Xie Q, Wu Q, Horbinski CM, Flavahan WA, Yang K, Zhou W, et al. Mitochondrial Control by DRP1 in Brain Tumor Initiating Cells. *Nat Neurosci* (2015) 18:501–10. doi: 10.1038/nn.3960
34. Channakkar AS, Singh T, Pattnaik B, Gupta K, Seth P, Adlakha YK. MiRNA-137-Mediated Modulation of Mitochondrial Dynamics Regulates Human Neural Stem Cell Fate. *Stem Cells* (2020) 38:683–97. doi: 10.1002/stem.3155
35. Lin HH, Chung Y, Cheng CT, Ouyang C, Fu Y, Kuo CY, et al. Autophagic Reliance Promotes Metabolic Reprogramming in Oncogenic KRAS-Driven Tumorigenesis. *Autophagy* (2018) 14:1481–98. doi: 10.1080/15548627.2018.1450708
36. Zheng X, Li S, Zang Z, Hu J, An J, Pei X, et al. Evidence for Possible Role of Toll-Like Receptor 3 Mediating Virus-Induced Progression of Pituitary Adenomas. *Mol Cell Endocrinol* (2016) 426:22–32. doi: 10.1016/j.mce.2016.02.009
37. Yang Q, Li X. Molecular Network Basis of Invasive Pituitary Adenoma: A Review. *Front Endocrinol (Lausanne)* (2019) 10:7. doi: 10.3389/fendo.2019.00007
38. Youle RJ, Karbowski M. Mitochondrial Fission in Apoptosis. *Nat Rev Mol Cell Biol* (2005) 6:657–63. doi: 10.1038/nrm1697
39. Otera H, Miyata N, Kuge O, Mihara K. Drp1-Dependent Mitochondrial Fission *via* MiD49/51 is Essential for Apoptotic Cristae Remodeling. *J Cell Biol* (2016) 212:531–44. doi: 10.1083/jcb.201508099
40. Mazumder S, De R, Debsharma S, Bindu S, Maity P, Sarkar S, et al. Indomethacin Impairs Mitochondrial Dynamics by Activating the PKCzeta-P38-DRP1 Pathway and Inducing Apoptosis in Gastric Cancer and Normal Mucosal Cells. *J Biol Chem* (2019) 294:8238–58. doi: 10.1074/jbc.RA118.004415
41. Yu H, Lee H, Herrmann A, Buettner R, Jove R. Revisiting STAT3 Signalling in Cancer: New and Unexpected Biological Functions. *Nat Rev Cancer* (2014) 14:736–46. doi: 10.1038/nrc3818
42. Srivastava J, DiGiovanni J. Non-Canonical Stat3 Signaling in Cancer. *Mol Carcinog* (2016) 55:1889–98. doi: 10.1002/mc.22438
43. Xiang Y, Li JP, Guo W, Wang DQ, Yao A, Zhang HM, et al. Novel Interactions Between ERalpha-36 and STAT3 Mediate Breast Cancer Cell Migration. *Cell Commun Signal* (2019) 17:93. doi: 10.1186/s12964-019-0409-4
44. Jia ZH, Jia Y, Guo FJ, Chen J, Zhang XW, Cui MH. Phosphorylation of STAT3 at Tyr705 Regulates MMP-9 Production in Epithelial Ovarian Cancer. *PloS One* (2017) 12:e0183622. doi: 10.1371/journal.pone.0183622
45. Garama DJ, White CL, Balic JJ, Gough DJ. Mitochondrial STAT3: Powering Up a Potent Factor. *Cytokine* (2016) 87:20–5. doi: 10.1016/j.cyto.2016.05.019
46. Anisimov VN. Metformin for Prevention and Treatment of Colon Cancer: A Reappraisal of Experimental And Clinical Data. *Curr Drug Targets* (2016) 17(4):439–46. doi: 10.2174/1389450116666150309113305
47. Tateno T, Asa SL, Zheng L, Mayr T, Ullrich A, Ezzat S. The FGFR4-G388R Polymorphism Promotes Mitochondrial STAT3 Serine Phosphorylation to Facilitate Pituitary Growth Hormone Cell Tumorigenesis. *PloS Genet* (2011) 7:e1002400. doi: 10.1371/journal.pgen.1002400
48. Ezzat S, Wang R, Pintilie M, Asa SL. FGFR4 Polymorphic Alleles Modulate Mitochondrial Respiration: A Novel Target for Somatostatin Analog Action in Pituitary Tumors. *Oncotarget* (2017) 8:3481–94. doi: 10.18632/oncotarget.13843

Conflict of Interest: The authors declare that the research was conducted in the absence of any commercial or financial relationships that could be construed as a potential conflict of interest.

The reviewer ZH declared a shared affiliation with one of the authors LZ, to the handling editor at the time of review.

Publisher's Note: All claims expressed in this article are solely those of the authors and do not necessarily represent those of their affiliated organizations, or those of the publisher, the editors and the reviewers. Any product that may be evaluated in this article, or claim that may be made by its manufacturer, is not guaranteed or endorsed by the publisher.

frontiers | Frontiers in Oncology

ORIGINAL RESEARCH
published: 28 April 2022
doi: 10.3389/fonc.2022.882049

Development and Validation of a Prognostic Model for Post-Operative Recurrence of Pituitary Adenomas

*Liang Lu, Xueyan Wan, Yu Xu, Juan Chen, Kai Shu and Ting Lei**

Department of Neurosurgery, Tongji Hospital, Tongji Medical College, Huazhong University of Science and Technology, Wuhan, China

Background: We aimed to assess clinical factors associated with tumor recurrence and build a nomogram based on identified risk factors to predict postoperative recurrence in patients with pituitary adenomas (PAs) who underwent gross-total resection (GTR).

Methods: A total of 829 patients with PAs who achieved GTR at Tongji Hospital between January 2013 and December 2018 were included in this retrospective study. The median follow-up time was 66.7 months (range: 15.6–106.3 months). Patients were randomly divided into training (n = 553) or validation (n = 276) cohorts. A range of clinical characteristics, radiological findings, and laboratory data were collected. Uni- and multivariate Cox regression analyses were applied to determine the potential risk factors for PA recurrence. A nomogram model was built from the identified factors to predict recurrence. Concordance index (C-index), calibration curve, and receiver operating characteristic (ROC) were used to determine the predictive accuracy of the nomogram. Decision curve analysis (DCA) was performed to evaluate the clinical efficacy of the nomogram.

Results: Pseudocapsule-based extracapsular resection (ER), cavernous sinus invasion (CSI), and tumor size were included in the nomogram. C-indices of the nomogram were 0.776 (95% confidence interval [CI]: 0.747–0.806) and 0.714 (95% CI: 0.681–0.747) for the training and validation cohorts, respectively. The area under the curve (AUC) of the nomogram was 0.770, 0.774, and 0.818 for 4-, 6-, 8-year progression-free survival (PFS) probabilities in the training cohort, respectively, and 0.739, 0.715 and 0.740 for 4-, 6-, 8-year PFS probabilities in the validation cohort, respectively. Calibration curves were well-fitted in both training and validation cohorts. DCA revealed that the nomogram model improved the prediction of PFS in both cohorts.

Conclusions: Pseudocapsule-based ER, CSI, and tumor size were identified as independent predictors of PA recurrence. In the present study, we developed a novel and valid nomogram with potential utility as a tool for predicting postoperative PA recurrence. The use of the nonogram model can facilitate the tailoring of counseling to meet the individual needs of patients.

Keywords: pituitary adenoma, tumor recurrence, nomogram, pseudocapsule, extracapsular resection, cavernous sinus invasion

Edited by:
Zhixiong Liu,
Central South University, China

Reviewed by:
Teresa Somma,
Federico II University Hospital, Italy
Zhengwei Li,
Wuhan University, China

***Correspondence:**
Ting Lei
tlei@tjh.tjmu.edu.cn

Specialty section:
This article was submitted to Neuro-Oncology and Neurosurgical Oncology, a section of the journal Frontiers in Oncology

Received: *23 February 2022*
Accepted: *05 April 2022*
Published: *28 April 2022*

Citation:
Lu L, Wan X, Xu Y, Chen J, Shu K and Lei T (2022) Development and Validation of a Prognostic Model for Post-Operative Recurrence of Pituitary Adenomas. Front. Oncol. 12:882049. doi: 10.3389/fonc.2022.882049

INTRODUCTION

Pituitary adenomas (PAs), which represent 10–20% of all brain tumors, are benign tumors with a prevalence rate of 80–100/100,000 (1, 2). Further, the incidence of clinically related PAs is 4–7/100,000 per year (3). The prevalence and the incidence of PA are increasing due to the increased availability of MRI (4). Autopsy and radiological studies demonstrated that PAs have a prevalence rate of 17% (range: 14–23%), which is higher than expected (5). The primary treatment for PAs is transnasal-transsphenoidal surgery (TTS) (6); however, suprasellar or parasellar PAs are difficult to remove completely and result in residual adenoma relapse in 12–58% of patients (1). Even in adenomas achieving GTR, 10–20% recur within 5–10 years (1, 7). In patients who undergo repeated treatment for recurrent PAs, mortality rates are elevated and quality of life is significantly affected due to pituitary dysfunction, invasion-related risks, and complications (8). Therefore, the identification of predictive factors for recurrent PAs is needed.

A pseudocapsule is defined as the boundary between the pituitary gland and an adenoma, which results from compressed peritumoral cell cord basement membrane condensation (9). PAs often spread beyond the edge of the pseudocapsule and invade the surrounding pituitary tissue (10). These characteristics of PAs have resulted in an alteration of their operative approach including extending excision boundaries to achieve total tissue removal and providing special attention to complete pseudocapsule removal (11). Although some studies have reported that pseudocapsule-based ER may improve the resection rate and reduce the recurrence rate (11, 12), there have been few reports on the relationship between pseudocapsule-based ER and PA recurrence after GTR.

A nomogram is a convenient graphical representation of a model that includes various significant factors to predict a specific outcome. Two nomograms related to PA recurrence have been constructed for non-functional PAs and giant PAs, respectively (13, 14). Good performance has been verified in the two types of PAs in the above two nomograms, in which PA recurrence included regrowth of tumor remnants after subtotal resection or partial resection. In the present study, a nomogram was constructed and validated to predict all subtypes PA recurrence after GTR by combining clinical variables including pseudocapsule-based ER and clinical image data.

MATERIALS AND METHODS

Study Population and Design

We retrospectively assessed patients with PAs who underwent TTS at Tongji Hospital between January 2013 and December 2018. The median follow-up time was 66.7 months (range: 15.6–106.3 months). The criteria for inclusion were as follows: (1) PA patients confirmed histologically; (2) patients who underwent microscopic or endoscopic TTS; (3) patients who achieved GTR; and (4) patients followed up for more than one year post-GTR. Criteria for exclusion were as follows: (1) patients who did not undergo follow-up evaluations; (2) patients treated with chemotherapy or radiotherapy; and (3) patients with no data relating to variables assessed. The primary cohort was randomly assigned to the training and internal validation cohorts at a ratio of 2:1, respectively. A flowchart summarizing the enrollment strategy and design of the study is shown in **Figure 1**.

The following information was collected from all enrolled patients: baseline characteristics, radiological features, and preoperative laboratory tests. PA recurrence was defined as the reappearance of PAs, as observed *via* MRI examination after GTR. CSI status was determined according to MRI and operative records within which operating neurosurgeons documented their impressions. Pseudocapsule-based ER was conducted on patients with PAs within whom a pseudocapsule was identified during surgery. PFS in patients with PAs measured from the time of TTS to tumor recurrence. The study was approved by the Ethics Committee of Tongji Hospital. Due to the retrospective nature of the cohort study, the need for informed consent was waived.

Development and Validation of the Nomogram

There were no missing data among clinical characteristics. For radiological findings and laboratory data, mean imputation for missing data was applied. Patients were randomly assigned to the training and validation cohorts. Based on the rule of having at least 10 outcome events per variable (EPV) (15), we ensured no more than six features were retained for multivariate Cox regression analysis from 63 events in the training cohort.

All factors were filtered by least absolute shrinkage and selection operator (LASSO) algorithm using the R package glmnet (version 4.1). Uni- and multivariate Cox regressions were utilised to confirm independent risk factors related to recurrence level using the R package rms (version 6.2). Variables included in the multivariate Cox regression analysis were required to meet at least one criterion: confirmation as a significant predictor in comparison of recurrence and non-recurrence cohorts or univariate Cox regression analysis, or retention in LASSO analysis. Using the R packages rms and survival (version 3.2), identified risk factors were used to develop a nomogram. C-index, ROC curve analysis, and calibration curves were used to evaluate the accuracy of the nomogram model, and DCA was used to evaluate the clinical utility of the model.

Statistical Analysis

Model construction and validation were carried out on the basis of "Transparent Reporting of a Multivariable Prediction Model for Individual Prognosis or Diagnosis" (TRIPOD) guidance (**Table S1**) (15). R software (version 3.6.3) was used to perform statistical analysis and $p < 0.05$ was considered statistically significant. Categorical data were presented as percentages and continuous variables as means ± standard deviation (SD). The Student's t-test was used to compare two continuous variables, and the Chi-square test or Fisher's exact tests were used for categorised variables. The Spearman's correlation test was used to verify correlations between the quantitative variables and the Kaplan–Meier method was used for estimating PFS. Data were visualised using the "ggplot" R packages (version 3.3.3).

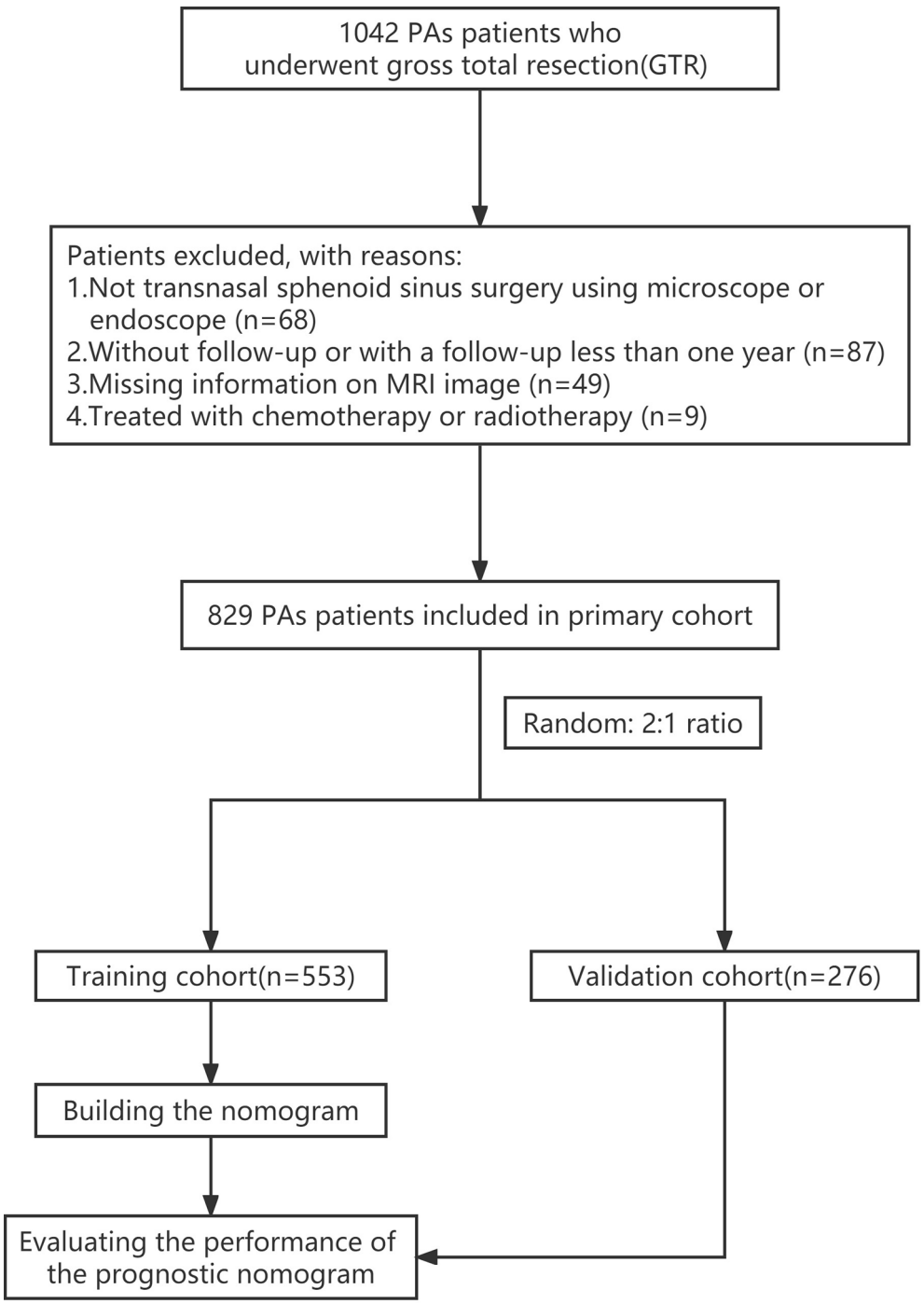

FIGURE 1 | Flowchart summarizing the enrollment strategy and design of the study. PAs, pituitary adenomas.

RESULTS

Clinical Characteristics

Detailed characteristics of patients with PAs in the recurrence and non-recurrence cohorts are summarized in **Table S2**, and the baseline characteristics of PA patients in the training and validation cohorts are summarised in **Table 1**. The training cohort included 315 male patients and 238 female patients, with an average age of 49.8 ± 12.36 years and a mean tumor size of 23.4 ± 5.5 mm. The validation cohort included 153 males and 123 females, with an average age of 49.5 ± 12.45 years and a mean tumor size of 23.7 ± 5.9 mm. Recurrence rates of the

TABLE 1 | Characteristics of patients with PAs in the training and validation cohorts.

Variable	Training cohort (n=553)	Validation cohort (n=276)	P value
Recurrence			0.945
YES	63 (11.4%)	31 (11.2%)	
NO	490 (88.6%)	245 (88.8%)	
Age, year	49.8 ± 12.36	49.5 ± 12.45	0.897
Gender			0.676
Female	238 (43.0%)	123 (44.6%)	
Male	315 (57.0%)	153 (55.4%)	
Headache			0.441
YES	148 (26.8%)	67 (24.3%)	
NO	405 (73.2%)	209(75.7%)	
Visual impairment			0.291
YES	273 (49.4%)	147 (53.3%)	
NO	280 (50.6%)	129(46.7%)	
Visual field defect			0.870
YES	125 (22.6%)	61 (22.1%)	
NO	428(77.4%)	215 (77.9%)	
Abnormal Menstruation			0.367
YES	42 (7.6%)	26 (9.4%)	
NO	511 (92.4%)	250 (90.6%)	
Acromegalia			0.567
YES	55 (9.9%)	31 (11.2%)	
NO	498 (90.1%)	245 (88.8%)	
Cushing's syndrome			0.314
YES	38 (6.9%)	14 (5.1%)	
NO	515 (93.1%)	262 (94.9%)	
Thyroid dysfunction			0.824
YES	7 (1.3%)	3 (1.1%)	
NO	546 (98.7%)	273 (98.9%)	
Pituitary apoplexy			0.471
YES	57 (10.3%)	24 (8.7%)	
NO	496 (89.7%)	252 (91.3%)	
Clinical subtype			0.904
Nonfunctional	304 (55.0%)	145 (52.5%)	
PRL secreting	117 (21.2%)	62 (22.5%)	
GH secreting	75 (13.6%)	31 (11.2%)	
ACTH secreting	18 (3.3%)	10 (3.6%)	
TSH secreting	2 (0.4%)	2 (0.7%)	
Plurihormonal	37 (6.7%)	18 (6.5%)	
Tumor size, mm	23.4 ± 5.5	23.7 ± 5.9	0.874
Cavernous sinus invasion			0.206
YES	151 (27.3%)	87 (31.5%)	
NO	402 (72.7%)	189 (68.5%)	
Knosp grading			0.587
0-2	348 (62.9%)	179 (64.9%)	
3-4	205 (37.1%)	97 (35.1%)	
Pseudocapsule-based extracapsular resection			0.817
YES	219 (39.6%)	107 (38.8%)	
NO	334 (60.4%)	169(61.2%)	
Intraoperative CSF leakage			0.574
YES	109 (19.7%)	59 (21.4%)	
NO	444 (80.3%)	217 (78.6%)	
Ki-67≥3			0.882
YES	82 (14.8%)	42 (15.2%)	
NO	471 (85.2%)	234 (84.8%)	
Prolacin (ng/mL)	20.5 ± 26.58	19.5 ± 22.39	0.714
Testosterone (ng/mL)	0.99 ± 1.293	0.99 ± 1.292	0.861
Estradiol (pg/mL)	43.1 ± 41.42	43.7 ± 42.85	0.292
Progesterone (ng/mL)	0.95 ± 2.045	1.15 ± 2.808	0.761
LH (IU/L)	4.61 ± 5.748	5.57 ± 7.377	0.535
FSH (IU/L)	12.2 ± 16.67	12.5 ± 18.75	0.595
TSH (mIU/L)	2.12 ± 2.799	2.35 ± 2.916	0.217
FT3 (pg/mL)	2.58 ± 0.651	2.49 ± 0.609	0.253
FT4 (ng/dL)	1.80 ± 3.183	1.68 ± 3.172	0.193
ACTH (pg/ml)	46.8 ± 25.33	50.3 ± 28.93	0.174
Morning cortisol (μg/dL)	7.48 ± 4.821	6.93 ± 5.297	0.251
Bedtime cortisol (μg/dL)	4.29 ± 2.625	4.03 ± 2.417	0.436
GH (μg/L)	4.23 ± 12.780	3.24 ± 9.498	0.493
IGF-1 (μg/L)	210 ± 244.1	198 ± 225.7	0.751

LH, luteinizing hormone; FSH, follicle-stimulating hormone; TSH, thyroid-stimulating hormone; FT3, free triiodothyronine; FT4, free tetraiodothyronine; ACTH, adrenocorticotropic hormone; GH, growth hormone;IGF-1, insulin-like growth factor-1.

training and verification cohorts were 11.4% and 11.2%, respectively. No statistically significant between-cohort differences in patient characteristics were observed.

Analysis of the Risk Factors of PA Recurrence

Univariate Cox regression and LASSO analysis were used to filter out clinical factors and multivariate Cox regression analysis was applied for further analysis (**Figure 2**, **Table S3**, and **Table S4**). As a result, ER (Hazard ratio [HR], 95% CI: 0.323, 0.141–0.741, P = 0.008), tumor size (HR, 95% CI: 1.043, 1.013–1.075, P = 0.005), and CSI (HR, 95% CI: 3.786, 1.222–11.726, P = 0.021) were incorporated into the multivariate model (**Figure 3**). Corresponding Kaplan–Meier survival curves are shown in **Figure 4**.

Development of a Nomogram for Postoperative Recurrence

A nomogram was developed to visualise the multivariate model (**Figure 5**). Tumor size was the largest contributor to a prognosis of recurrence, followed by the ER and CSI in the nomogram. To use the nomogram, the respective values were determined using the three factors of an individual patient, and the three values were added to obtain the total value. Subsequently, a line was drawn from the survival axis to determine 4-, 6-, and 8-year PFS probabilities.

Validation of the Nomogram

The nomogram for PFS prediction showed good predictive capacity with well-fitted calibration curves in both training and validation cohorts (**Figure 6**). The C-indices of the nomogram were 0.776 (95% CI: 0.747–0.806) and 0.714 (95% CI: 0.681–0.747) for the training and validation cohorts, respectively. The AUC of the nomogram was 0.770, 0.774 and 0.818 for 4-, 6-, and 8-year PFS probabilities in the training cohort, respectively; 0.739, 0.715 and 0.740 for 4-, 6-, and 8-year PFS probabilities in the validation cohort, respectively, attesting to the good performance of the nomogram model (**Figure 6**).

Evaluation of the Clinical Utility of the Nomogram

DCA was applied to evaluate the net benefit of the nomogram for assessing training and validation cohorts, which provided us with

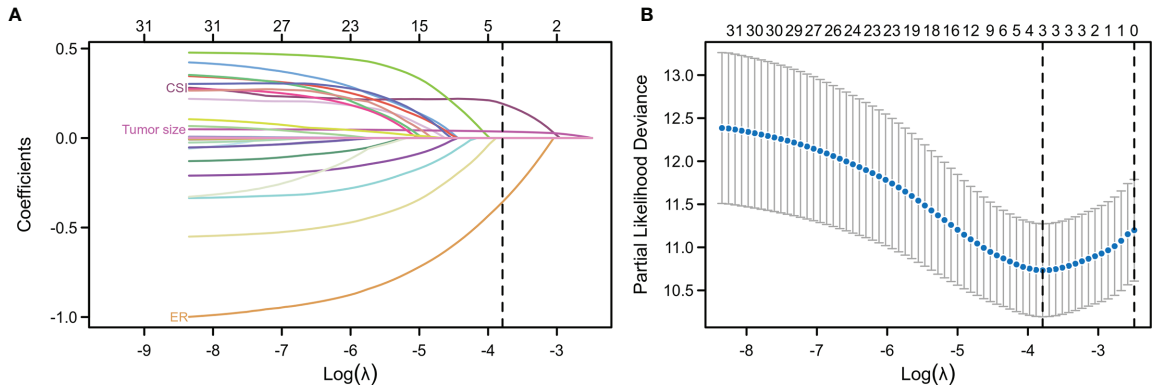

FIGURE 2 | Least absolute shrinkage and selection operator (LASSO) regression analysis for the selection of characteristic parameters. **(A)** Penalty diagram for coefficients of thirty-one characteristic variables. As the penalty coefficient lambda changes, the number of compression variable coefficients increases continuously. Finally, most of the variable coefficients are compressed to zero. **(B)** In the LASSO Logistic regression model, the optimal penalty coefficient lambda was selected by using 10-fold cross-validation and minimization criteria. The optimal lambda (lambda = 3) was selected at the lowest point of the curve, and three variables with non-zero coefficient were selected at the optimal lambda. The characteristic parameters without information were removed to realize automatic selection of characteristic parameters.

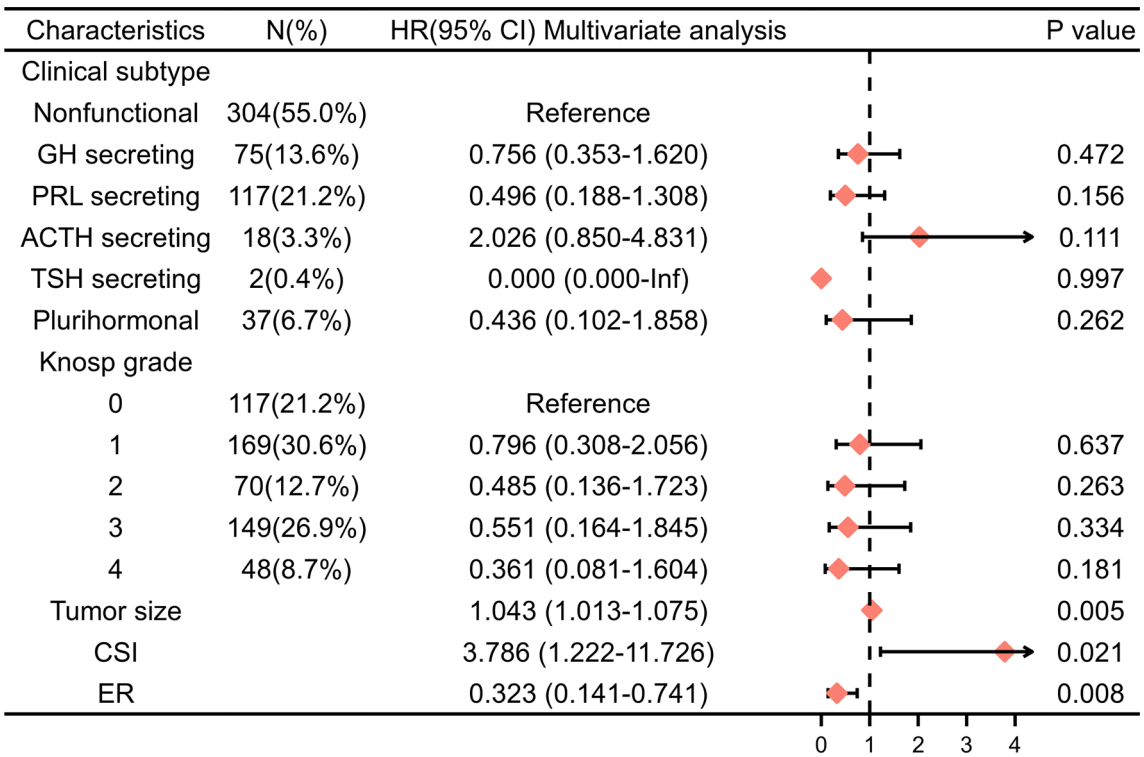

FIGURE 3 | Multivariable Cox regression analysis of PFS in the training cohort. HR, hazard ratio; CI, confidence interval; PRL, prolactin; GH, growth hormone; ACTH, adrenocorticotropic hormone; TSH,thyroid-stimulating hormone; CSI, cavernous sinus invasion; ER, extracapsular resection.

insights into the clinical benefit within a reasonable range of threshold probabilities. As a result, DCA revealed that using the nomogram for clinical application likely benefited patients when compared with treating either all or no patients of training and validation cohorts (**Figure 7**).

DISCUSSION

In the present study, we constructed a clinical nomogram based on pseudocapsule-based ER, tumor size, and CSI for the individualised evaluation of PA recurrence risk after GTR. C-

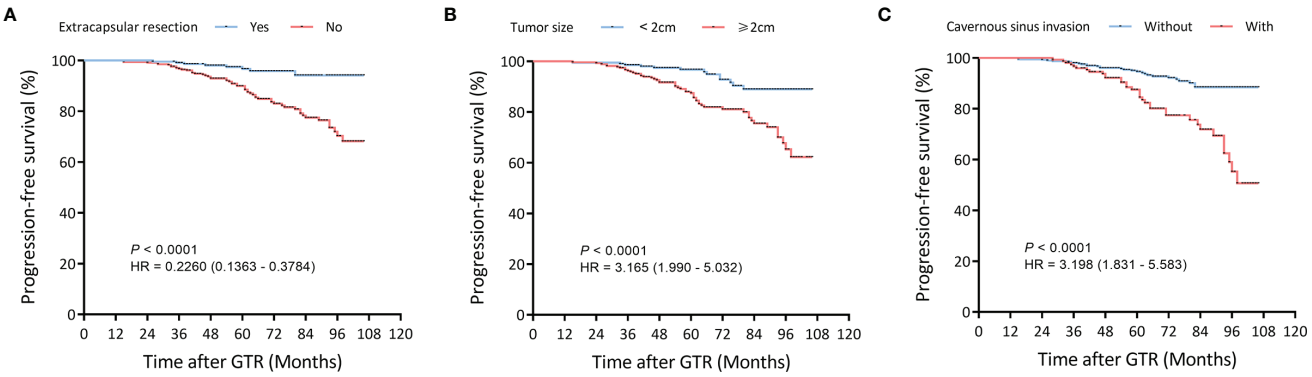

FIGURE 4 | Kaplan–Meier survival curves of filtered risk factors in the training cohort. **(A)** Kaplan–Meier survival curves of tumor size. **(B)** Kaplan–Meier survival curves of pseudocapsule-based extracapsular resection (ER). **(C)** Kaplan–Meier survival curves of cavernous sinus invasion (CSI). GTR, gross-total resection.

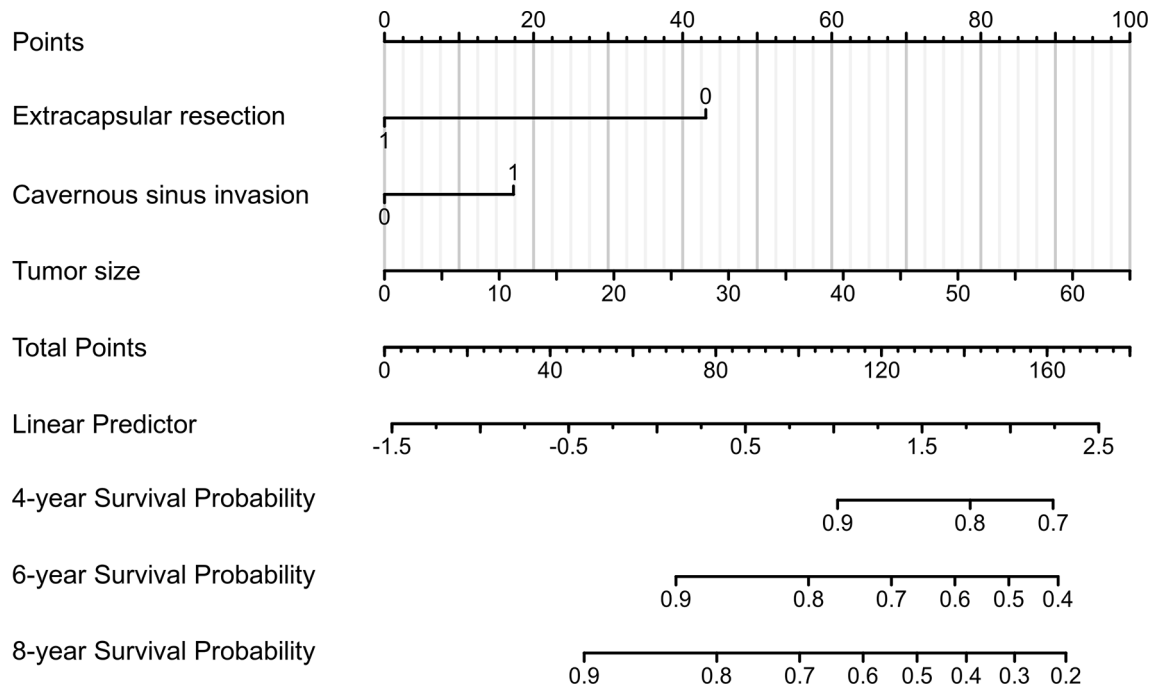

FIGURE 5 | A prognostic nomogram for predicting the 4-, 6-, and 8-year progression-free survival (PFS) probabilities in patients with pituitary adenomas (PAs) after gross-total resection (GTR).

indices, ROC, calibration curves, and DCA showed excellent predictive performance and clinical efficacy when using the nomogram models. Therefore, the nonogram can be used in clinical practice to improve the prediction accuracy of PA recurrence after GTR.

A major new finding from this study is the influence of pseudocapsule-based ER on the risk of PAs recurrence after GTR. The pseudocapsule is the important boundary between pituitary gland and adenoma. Oldfield EH began resecting PAs by dissecting the pseudocapsule from the mid-1980s (16). Kawamata described the important value of excising pseudocapsule when removing growth hormone-secreting tumors to improve rates of endocrine remission and tumor recurrence (11). Pseudocapsule, as a surgical capsule in TTS, may assist the operator in identifying the boundaries of PAs to achieve better resection and remission rates (12, 17). Furthermore, damage to normal pituitary tissue and occurrence of operative complications are reduced (16, 17). Adenoma cells frequently invade and infiltrate the pseudocapsule; as a result, a few tumor cells are easily retained

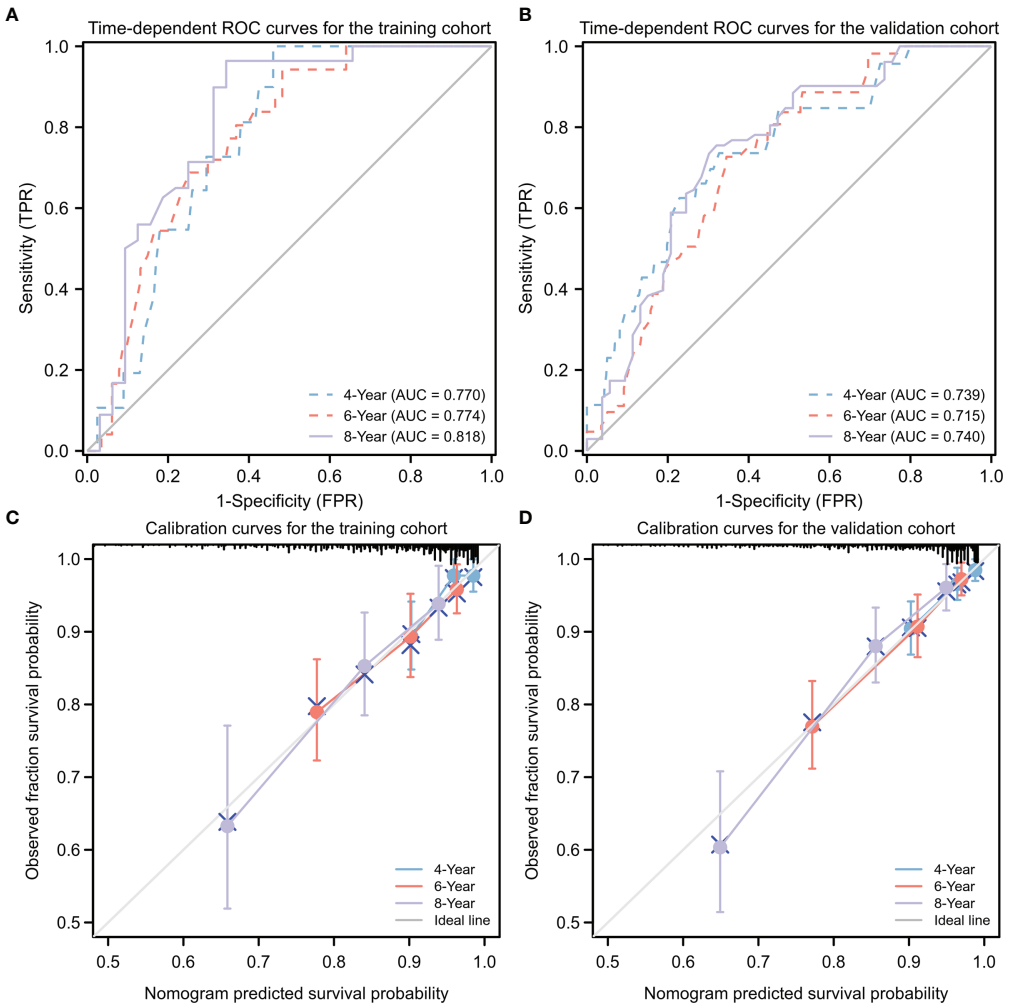

FIGURE 6 | Predictive performance for nomogram model. **(A, B)** Time-dependent ROC analysis of nomogram for 4-, 6-, and 8-year progression-free survival (PFS) probabilities in training cohort **(A)** and validation cohort **(B)**, respectively. **(C, D)** Calibration plots of the nomogram for the training **(C)** and validation **(D)** cohorts at 4, 6, or 8 years. ROC, receiver operating characteristic; TPR, true positive rate; FRR, false positive rate.

in the pseudocapsule during a conventional intracapsular resection (IR), thus promoting recurrence and preventing the achievement of complete remission (12). Therefore, ER should more completely involve the removal of residual or invasive tumors beyond IR, especially for portions not easily visible. Qu et al. reported that the ER method could be used to achieve higher resection and remission rates than those of IR, a finding consistent with results of prior studies (12, 17–19). Our study demonstrated that ER might reduce risk of PA recurrence after GTR (HR, 95% CI: 0.323, 0.141–0.741, P = 0.008), while careful inspection is essential with the suspicion that tumor cells may remain beyond the main tumor boundary when the pseudocapsule is not fully developed (12).

CSI is a prognostic indicator of the long-term prognosis of PAs (20). Some work has shown that CSI was associated with GTR and recurrence, and the revised Knosp radiological classification was recommended for prediction of surgical outcomes (21–23). GTR rates were negatively correlated with Knosp grade classification, with 56% for grade 3A and only 25% for grade 3B (21). Marta et al. reported that Knosp and revised-Knosp classification showed good diagnostic accuracy in predicting surgical cure (AUC, 0.820), whereas Hardy classification lacked practicality in this purpose (AUC, 0.654) (22), which may indicate that the main prognostic factor was CSI (24). In an 8-year, retrospective, multicenter, cohort study that included 410 patients, Trouillas et al. found that invasiveness was the main prognostic factor for predicting progression-free status (25). Furthermore, a clinicopathologic classification of PAs based on invasion and proliferation was generated to predict relapse/progression-free status (AUC, 0.814) in patients with PAs. They also validated this classification in a prospective single-center cohort comprising 374 postoperative patients followed up for 3.5 years (26).

Although all patients included in this study underwent GTR, complete removal of all adenomas was not guaranteed, especially

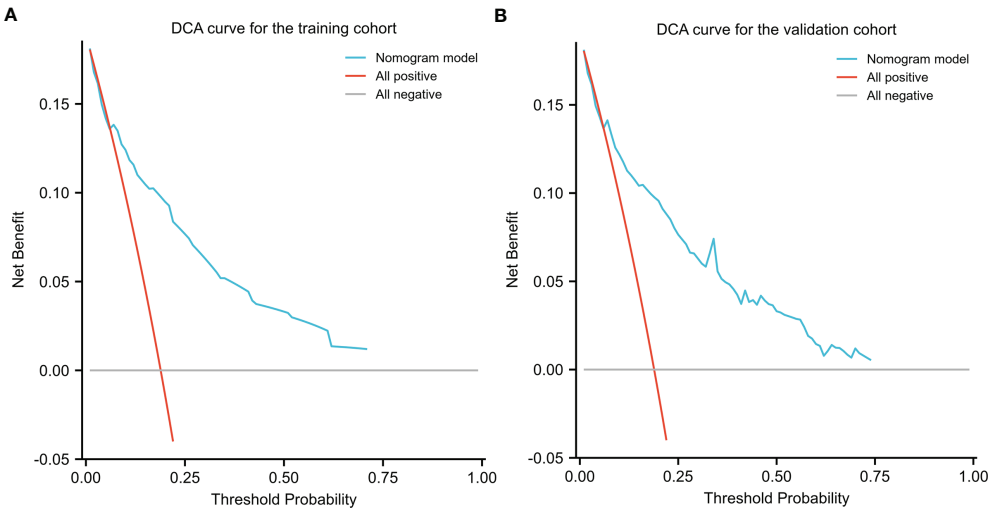

FIGURE 7 | Decision Curve Analysis (DCA) for the nomogram in the training **(A)** cohort and validation cohort **(B)**. Threshold probability and net benefit were represented by the X-axis and the Y-axis, respectively. The blue line represented the net benefit of the nomogram at different threshold probabilities. The area between the "All negative" (gray line) and "All positive" (red line) in the DCA curve indicated the clinical utility of the model.

for PAs with CSI that tended to be associated with invisible or infiltrating adenomas. Zhang et al. indicated that tumor size and CSI were important predictors of GTR in patients with PAs (27). Further, high-field intraoperative MRI facilitated the excision of PAs with CSI, increasing the rate of GTR and decreasing recurrence rates of PAs in endoscopic TSS (27). Thus, GTR improvement leads to improved PFS. CSI was also an independent prognostic indicator of PA recurrence (HR, 95% CI: 3.786, 1.222–11.726, P = 0.021) in our study. Our results suggest that PAs with CSI deserve more attention even after achieving GTR.

The large size of an adenoma may reduce the probability that it is completely resected, which may affect prognosis and recurrence. Hofstetter et al. assessed the effects of adenoma size on resection range, revealing that patients with PAs sized > 10 cm^3 are most likely to experience residual adenoma (28). GTR was achieved in 90.2% vs 40.0% of adenomas < and > 10 cm^3, respectively. Further, GTR was complete in 47.6% of a total of 166 patients with adenomas < 3cm versus 9.1% of a total of 77 patients with adenomas > 3 cm (28). Our study also suggested that PAs with larger tumor size are associated with a higher risk of recurrence (HR, 95% CI: 1.043, 1.013–1.075, P = 0.005). Considering its significant impact on the scope and extent of resection, more attention should be paid to the possibility of residual tissue and invasion of large PAs, even when GTR appears to be achieved *via* surgery.

There are several limitations to this study. The single-center study design and absence of external validation are the major limitations, which may introduce the possibility of selection bias and limit the predictive power of the nomogram model. In addition, the study design focuses on ER and PA patients after GTR, which may limit the clinical applicability of the model due to low recurrence rate after GTR and the fact that ER has not been put into use widely enough (1, 12). Despite these limitations, our nomogram was useful for predicting PA recurrence after GTR with good accuracy. Furthermore, pseudocapsule-based ER was introduced as an independent prognostic indicator of PA recurrence after GTR for the first time. This finding deserves more attention and may play a more important role in the treatment and prognosis of PAs. Using the nomogram model, clinicians can communicate more effectively with patients and adjust their treatment plans. Patients with pseudocapsules, for example, could be recommended to undergo pseudocapsule-based ER. Moreover, patients with macroadenomas and CSI should be reminded that they need long-term follow-up, as they are more likely to relapse compared to other patients with PAs, according to our study, even 8 years after GTR.

CONCLUSION

This study showed that pseudocapsule-based ER, CSI, and tumor size are independent risk factors for PA recurrence after GTR. Moreover, pseudocapsule-based ER was first introduced as an independent prognostic indicator of PA recurrence after GTR. The nomogram constructed in our study was effective and valuable for predicting PA recurrence after GTR, suggesting its potential utility for assisting neurosurgeons in the development of improved and individualised PA treatment strategies.

DATA AVAILABILITY STATEMENT

The original contributions presented in the study are included in the article/**Supplementary Material**. Further inquiries can be directed to the corresponding author.

ETHICS STATEMENT

The studies involving human participants were reviewed and approved by the Ethics Committee of Tongji Hospital. Written informed consent for participation was not required for this study in accordance with the national legislation and the institutional requirements.

AUTHOR CONTRIBUTIONS

Study design by TL and LL. Data acquisition and analysis by LL, XW, YX and JC. Interpretation of the data by KS and TL. Drafting of the manuscript by LL, XW, YX and JC. Revision of the manuscript by KS and TL. All authors contributed to the article and approved the submitted version.

FUNDING

This research was funded by National Natural Science Foundation of China (Grant numbers: 81270865, 82173136) and Transformation and Cultivation Project of Tongji Hospital (Grant number: 2016ZHYX21). The funding institutions had no role in the design of the study, data collection and analysis, the decision to publish, or the preparation of the manuscript.

SUPPLEMENTARY MATERIAL

The Supplementary Material for this article can be found online at: https://www.frontiersin.org/articles/10.3389/fonc.2022.882049/full#supplementary-material

REFERENCES

1. Chen Y, Wang CD, Su ZP, Chen YX, Cai L, Zhuge QC, et al. Natural History of Postoperative Nonfunctioning Pituitary Adenomas: A Systematic Review and Meta-Analysis. *Neuroendocrinology* (2012) 96(4):333–42. doi: 10.1159/000339823
2. Delgado-López PD, Pi-Barrio J, Dueñas-Polo MT, Pascual-Llorente M, Gordón-Bolaños MC. Recurrent Non-Functioning Pituitary Adenomas: A Review on The New Pathological Classification, Management Guidelines and Treatment Options. *Clin Trans Oncol* (2018) 20(10):1233–45. doi: 10.1007/s12094-018-1868-6
3. Day PF, Loto MG, Glerean M, Picasso MFR, Lovazzano S, Giunta DH. Incidence and Prevalence of Clinically Relevant Pituitary Adenomas: Retrospective Cohort Study in A Health Management Organization in Buenos Aires, Argentina. *Arch Endocrinol Metab* (2016) 60(6):554–61. doi: 10.1590/2359-3997000000195
4. Daly AF, Beckers A. The Epidemiology of Pituitary Adenomas. *Endocrinol Metab Clin North Am* (2020) 49(3):347–55. doi: 10.1016/j.ecl.2020.04.002
5. Aghi MK, Chen CC, Fleseriu M, Newman SA, Lucas JW, Kuo JS, et al. Congress of Neurological Surgeons Systematic Review and Evidence-Based Guidelines on the Management of Patients With Nonfunctioning Pituitary Adenomas: Executive Summary. *Neurosurgery* (2016) 79(4):521–3. doi: 10.1227/NEU.0000000000001386
6. Buchfelder M, Schlaffer SM, Zhao Y. The Optimal Surgical Techniques for Pituitary Tumors. *Best Pract Res Clin Endocrinol Metab* (2019) 33(2):101299. doi: 10.1016/j.beem.2019.101299
7. Brochier S, Galland F, Kujas M, Parker F, Gaillard S, Raftopoulos C, et al. Factors Predicting Relapse of Nonfunctioning Pituitary Macroadenomas After Neurosurgery: A Study of 142 Patients. *Eur J Endocrinol* (2010) 163(2):193–200. doi: 10.1530/EJE-10-0255
8. Greenman Y, Cooper O, Yaish I, Robenshtok E, Sagiv N, Jonas-Kimchi T, et al. Treatment of Clinically Nonfunctioning Pituitary Adenomas With Dopamine Agonists. *Eur J Endocrinol* (2016) 175(1):63–72. doi: 10.1530/EJE-16-0206
9. Farnoud MR, Kujas M, Derome P, Racadot J, Peillon F, Li JY. Interactions Between Mormal and Tumoral Tissues at the Boundary of Human Anterior Pituitary Adenomas. An Immunohistochemical Study. *Virchows Arch* (1994) 424(1):75–82. doi: 10.1007/BF00197396
10. Oldfield EH, Vortmeyer AO. Development of a Histological Pseudocapsule and Its Use as a Surgical Capsule in the Excision of Pituitary Tumors. *J Neurosurg* (2006) 104(1):7–19. doi: 10.3171/jns.2006.104.1.7
11. Kawamata T, Kubo O, Hori T. Surgical Removal of Growth Hormone-Secreting Pituitary Adenomas With Intensive Microsurgical Pseudocapsule Resection Results in Complete Remission of Acromegaly. *Neurosurg Rev* (2005) 28(3):201–8. doi: 10.1007/s10143-005-0384-7
12. Lee EJ, Ahn JY, Noh T, Kim SH, Kim TS, Kim SH, et al. Tumor Tissue Identification in the Pseudocapsule of Pituitary Adenoma: Should the Pseudocapsule be Removed for Total Resection of Pituitary Adenoma? *Neurosurgery* (2009) 64:(3 Suppl):ons62–9. doi: 10.1227/01.NEU.0000330406.73157.49
13. Lyu W, Fei X, Chen C, Tang Y. Nomogram Predictive Model of Post-Operative Recurrence in Non-Functioning Pituitary Adenoma. *Gland Surg* (2021) 10(2):807–15. doi: 10.21037/gs-21-47
14. Chen Y, Cai F, Cao J, Gao F, Lv Y, Tang Y, et al. Analysis of Related Factors of Tumor Recurrence or Progression After Transnasal Sphenoidal Surgical Treatment of Large and Giant Pituitary Adenomas and Establish a Nomogram to Predict Tumor Prognosis. *Front Endocrinol* (2021) 12:793337. doi: 10.3389/fendo.2021.793337
15. Moons KG, Altman DG, Reitsma JB, Ioannidis JP, Macaskill P, Steyerberg EW, et al. Transparent Reporting of a Multivariable Prediction Model for Individual Prognosis or Diagnosis (TRIPOD): Explanation and Elaboration. *Ann Intern Med* (2015) 162(1):W1–73. doi: 10.7326/M14-0698
16. Taylor DG, Jane JA, Oldfield EH. Resection of Pituitary Macroadenomas *via* the Pseudocapsule Along the Posterior Tumor Margin: A Cohort Study and Technical Note. *J Neurosurg* (2018) 128(2):422–8. doi: 10.3171/2017.7.JNS171658
17. Jagannathan J, Smith R, DeVroom HL, Vortmeyer AO, Stratakis CA, Nieman LK, et al. Outcome of Using the Histological Pseudocapsule as a Surgical Capsule in Cushing Disease. *J Neurosurg* (2009) 111(3):531–9. doi: 10.3171/2008.8.JNS08339
18. Monteith SJ, Starke RM, Jane JJA, Oldfield EH. Use of the Histological Pseudocapsule in Surgery for Cushing Disease: Rapid Postoperative Cortisol Decline Predicting Complete Tumor Resection. *J Neurosurg* (2012) 116(4):721. doi: 10.3171/2011.12.JNS11886
19. Qu X, Xu G, Qu Y, Song T. The Pseudocapsule Surrounding a Pituitary Adenoma and its Clinical Significance. *J Neurooncol* (2011) 101(2):171–8. doi: 10.1007/s11060-010-0247-0
20. Chang EF, Zada G, Kim S, Lamborn KR, Quinones-Hinojosa A, Tyrrell JB, et al. Long-Term Recurrence and Mortality After Surgery and Adjuvant Radiotherapy for Nonfunctional Pituitary Adenomas. *J Neurosurg* (2008) 108(4):736–45. doi: 10.3171/JNS/2008/108/4/0736
21. Buchy M, Lapras V, Rabilloud M, Vasiljevic A, Borson-Chazot F, Jouanneau E, et al. Predicting Early Post-Operative Remission in Pituitary Adenomas: Evaluation of the Modified Knosp Classification. *Pituitary* (2019) 22(5):467–75. doi: 10.1007/s11102-019-00976-6
22. Araujo-Castro M, Acitores Cancela A, Vior C, Pascual-Corrales E, Rodríguez Berrocal V. Radiological Knosp, Revised-Knosp, and Hardy–Wilson Classifications for the Prediction of Surgical Outcomes in the Endoscopic Endonasal Surgery of Pituitary Adenomas: Study of 228 Cases. *Front Oncol* (2022) 11:807040. doi: 10.3389/fonc.2021.807040
23. Ouyang T, Zhang N, Xie S, Tang B, Li J, Xiao L, et al. Outcomes and Complications of Aggressive Resection Strategy for Pituitary Adenomas in Knosp Grade 4 With Transsphenoidal Endoscopy. *Front Oncol* (2021) 11:693063. doi: 10.3389/fonc.2021.693063

24. Knosp E, Steiner E, Kitz K, Matula C. Pituitary Adenomas With Invasion of the Cavernous Sinus Space: A Magnetic Resonance Imaging Classification Compared With Surgical Findings. *Neurosurg* (1993) 33:610–8. doi: 10.1227/00006123-199310000-00008
25. Trouillas J, Roy P, Sturm N, Dantony E, Cortet-Rudelli C, Viennet G, et al. A New Prognostic Clinicopathological Classification of Pituitary Adenomas: A Multicentric Case-Control Study of 410 Patients With 8 Years Post-Operative Follow-Up. *Acta Neuropathol* (2013) 126(1):123–35. doi: 10.1007/s00401-013-1084-y
26. Raverot G, Dantony E, Beauvy J, Vasiljevic A, Mikolasek S, Borson-Chazot F, et al. Risk of Recurrence in Pituitary Neuroendocrine Tumors: A Prospective Study Using a Five-Tiered Classification. *J Clin Endocrinol Metab* (2017) 102 (9):3368–74. doi: 10.1210/jc.2017-00773
27. Zhang Z, Yang K, Xia Y, Meng X. High-Field Intraoperative Magnetic Resonance Imaging Increases Extent of Resection and Progression-Free Survival for Nonfunctioning Pituitary Adenomas. *World Neurosurg* (2019) 127:e925–31. doi: 10.1016/j.wneu.2019.04.001
28. Hofstetter CP, Nanaszko MJ, Mubita LL, Tsiouris J, Anand VK, Schwartz TH. Volumetric Classification of Pituitary Macroadenomas Predicts Outcome and Morbidity Following Endoscopic Endonasal Transsphenoidal Surgery. *Pituitary* (2012) 15(3):450–63. doi: 10.1007/s11102-011-0350-z

Conflict of Interest: The authors declare that the research was conducted in the absence of any commercial or financial relationships that could be construed as a potential conflict of interest.

Publisher's Note: All claims expressed in this article are solely those of the authors and do not necessarily represent those of their affiliated organizations, or those of the publisher, the editors and the reviewers. Any product that may be evaluated in this article, or claim that may be made by its manufacturer, is not guaranteed or endorsed by the publisher.

frontiers | Frontiers in Oncology

ORIGINAL RESEARCH
published: 05 May 2022
doi: 10.3389/fonc.2022.875219

Sprouting Angiogenesis in Human Pituitary Adenomas

Jie Zhou[1†], Yaomin Hu[1†], Wende Zhu[1†], Chuansheng Nie[1†], Wenxiu Zhao[1], Alexander T. Faje[1], Kay E. Labelle[1], Brooke Swearingen[2], Hang Lee[3], E. Tessa Hedley-Whyte[4], Xun Zhang[1], Pamela S. Jones[2], Karen K. Miller[1], Anne Klibanski[1], Yunli Zhou[1‡] and Roy J. Soberman[5‡]*

[1] Neuroendocrine Unit, Massachusetts General Hospital and Harvard Medical School, Boston, MA, United States, [2] Neurosurgery Department, Massachusetts General Hospital and Harvard Medical School, Boston, MA, United States, [3] Biostatistics Center, Massachusetts General Hospital and Harvard Medical School, Boston, MA, United States, [4] Department of Pathology (Neuropathology), Massachusetts General Hospital and Harvard Medical School, Boston, MA, United States, [5] Nephrology Division, Massachusetts General Hospital and Harvard Medical School, Boston, MA, United States

OPEN ACCESS

Edited by:
Zhe Bao Wu, Shanghai Jiao Tong University, China

Reviewed by:
Yan Gong, Wuhan University, China
Zhipeng Su, Wenzhou Medical University, China

***Correspondence:**
Yunli Zhou
yunli.zhou@mgh.harvard.edu

†Present addresses:
Jie Zhou, Neurosurgery Department, The Affiliated Hospital of Southwest Medical University, Luzhou, China
Yaomin Hu, Department of Endocrinology, Renji Hospital, School of Medicine, Shanghai Jiaotong University, Shanghai, China
Wende Zhu, Department of Neurosurgery, Union Hospital, Tongji Medical College, Huazhong University of Science and Technology, China
Chuansheng Nie, Department of Neurosurgery, Union Hospital, Tongji Medical College, Huazhong University of Science and Technology, China

‡These authors have contributed equally to the work and share senior authorship

Specialty section:
This article was submitted to Neuro-Oncology and Neurosurgical Oncology, a section of the journal Frontiers in Oncology

Received: 13 February 2022
Accepted: 05 April 2022
Published: 05 May 2022

Introduction: Angiogenesis in pituitary tumors is not fully understood, and a better understanding could help inform new pharmacologic therapies, particularly for aggressive pituitary tumors.

Materials and Methods: 219 human pituitary tumors and 12 normal pituitary glands were studied. Angiogenic genes were quantified by an angiogenesis qPCR array and a TaqMan probe-based absolute qPCR. Angiogenesis inhibition in pituitary tumors was evaluated *in vitro* with the endothelial tube formation assay and *in vivo* in RbΔ19 mice.

Results: 71 angiogenic genes, 40 of which are known to be involved in sprouting angiogenesis, were differentially expressed in pituitary tumors. Expression of endothelial markers CD31, CD34, and ENG was significantly higher in pituitary tumors, by 5.6, 22.3, and 8.2-fold, respectively, compared to in normal pituitary tissue. There was no significant difference in levels of the lymphatic endothelial marker LYVE1 in pituitary tumors compared with normal pituitary gland tissue. Pituitary tumors also expressed significantly higher levels of angiogenesis growth factors, including VEGFA (4.2-fold), VEGFB (2.2), VEGFC (19.3), PGF (13.4), ANGPT2 (9.2), PDGFA (2.7), PDGFB (10.5) and TGFB1 (3.8) compared to normal pituitary tissue. Expression of VEGFC and PGF was highly correlated with the expression of endothelial markers in tumor samples, including CD31, CD34, and ENG (endoglin, a co-receptor for TGFβ). Furthermore, VEGFR inhibitors inhibited angiogenesis induced by human pituitary tumors and prolonged survival of RbΔ19 mice.

Conclusion: Human pituitary tumors are characterized by more active angiogenesis than normal pituitary gland tissue in a manner consistent with sprouting angiogenesis. Angiogenesis in pituitary tumors is regulated mainly by PGF and VEGFC, not VEGFA and VEGFB. Angiogenesis inhibitors, such as the VEGFR2 inhibitor cabozantinib, may merit further investigation as therapies for aggressive human pituitary tumors.

Keywords: sprouting angiogenesis, angiogenic gene expression, angiogenesis inhibition, endothelial marker, Rb1 mice, VEGF inhibitor, cabozantinib, pituitary adenoma

INTRODUCTION

Approximately 15% of intracranial neoplasms are pituitary tumors, the vast majority of which are benign and slow-growing. Microadenomas (tumors < 1 cm) that are not hormone-secreting (i.e., nonfunctioning) can be monitored without intervention, whereas hormone-secreting tumors, except for prolactinomas for which dopamine agonist therapy is usually first-line therapy) are generally treated with surgery. Surgery is also the primary treatment modality for macroadenomas (tumors >1 cm), except for prolactinomas (1). Approximately 10% of pituitary tumors recur following surgery and are treated with repeat surgery, pharmacologic therapy and/or radiation (2). A very small percentage become locally invasive and/or metastasize despite standard therapies, including radiation (3, 4), and there are few effective therapies for these aggressive pituitary tumors. Temozolomide is first-line therapy for very aggressive tumors, including pituitary carcinomas, but escape usually occurs. Case reports suggest that checkpoint inhibitor therapy may have activity against a subset of such tumors, but preliminary reports indicate that responses are mixed. Therefore, new approaches are needed for the treatment of aggressive adenomas unresponsive to conventional therapies.

Multiple angiogenesis inhibitors targeting angiogenesis signaling pathways have been approved by the FDA to treat a wide range of human cancers (5, 6). Many more are currently under development or in clinical trials (5, 7). However, none of these drugs are approved for the treatment of pituitary tumors. To date, fewer than 20 patients with aggressive pituitary tumors have been reported to have been treated with antiangiogenic therapy, many following treatment with temozolomide (8, 9). Bevacizumab (Avastin®), a monoclonal antibody against VEGFA, has been most frequently reported in this context (N=11) (8, 9). Use of Sunitinib (Sutent®), a pan kinase inhibitor targeting VEGF receptors and PDGF receptors, and Apatinib, mainly targeting VEGFR2, have been reported in one case each (8). The treatment outcomes in these 13 patients ranged from a complete response to progressive disease (8). We suspect that one likely reason for the infrequent usage of angiogenesis inhibitors in pituitary tumor patients is the lack of data on angiogenesis in these tumors.

Angiogenesis is the process of forming new blood vessels from pre-existing ones (10) and has been implicated as a mechanism responsible for driving tumor growth, which is limited without neovascularization (11). Tumor vascularization can occur through vasculogenesis, vasculogenic mimicry, and intussusception, with endothelial sprouting identified as particularly important (12, 13). Vascular endothelial growth factors (VEGFs) are the master regulators of this process (14), which involves multiple signaling pathways (15) (16). The few studies examining angiogenesis specifically in pituitary tumors have demonstrated contradictory results. In contrast to the enhanced angiogenesis observed in many malignant tumors, Turner et al. demonstrated a lower density of blood vessels in benign pituitary tumors than in normal pituitary tissue, though macroadenomas demonstrated greater vascularity than microadenomas (17). In addition, most of the pituitary tumor angiogenesis literature focuses on microvessel density and endothelial markers, with McCabe et al. in addition observing an approximately 3-fold increase in VEGFA expression in nonfunctioning adenomas (NFAs) compared to normal pituitary tissue (18). We wanted to build on this literature by examining angiogenesis signaling pathways in pituitary tumors.

In this study, we used the TaqMan® probe-based absolute quantitative PCR method to assess expression of multiple growth factors from the major angiogenic signaling pathways in a large cohort of human pituitary tumors. We also examined expression of several vascular endothelial marker genes. Furthermore, we determined that VEGF signaling plays a major role in pituitary tumor angiogenesis and that blocking VEGF signaling significantly extended survival in a pituitary tumor mouse model.

MATERIALS AND METHODS

Human Subjects and Tumor Specimens for Gene Expression Assays

We studied 219 pituitary tumors: 151 clinically nonfunctioning adenomas (NFAs), 39 GH-secreting, 13 PRL-secreting, and 16 ACTH-secreting tumors (**Table 1**). Twenty-seven of these tumor samples were used in our previous experiments examining immune checkpoint molecules, which is unrelated to this study (19). Tumors from 132 males and 87 females were included. Patients ranged from 19 to 83 years, with a mean (SD) of 52 (16) years. Pituitary tumor samples were collected immediately following surgery and promptly used for primary tissue culture or stored in liquid nitrogen. Twelve control normal anterior pituitary glands were obtained from patients who died of non-endocrine causes. All glands were sampled for microscopy before

TABLE 1 | Clinical Characteristics.

Tumor Types	Number of Patients			Age at Surgery (mean ± SD)	Tumor Size[b](cm)(mean ± SD)	Ki67 index(%)(mean ± SD)
	Total	Male	Female			
All tumors	219	132	87	53 ± 16	2.3 ± 1.0	1.9 ± 1.6
Clinically non-functioning	151	105	46	57 ± 14	2.5 ± 0.9	1.7 ± 1.8
ACTH-producing	16	1	15	48 ± 13[c]	1.3 ± 0.8[c]	3.1 ± 2.7[c]
GH-producing	39	22	17	45 ± 15[c]	2.0 ± 1.0[c,d]	2.1 ± 1.6
PRL-producing[a]	13	6	7	34 ± 11[c,d,e]	2.1 ± 0.8[d]	2.1 ± 2.1

[a]*PRL-producing tumors were primarily resected from patients who were intolerant to medical treatment or had tumors that were resistant to medical treatment.*
[b]*Tumor size at baseline, measured in the largest dimension. Comparisons were performed using a one-way ANOVA multiple comparison test.* [c]$p < 0.05$ *vs NFA;* [d]$p < 0.05$ *vs ACTH-producing adenoma;* [e]$p < 0.05$ *vs GH-producing adenoma.*

donating the remainder of the unfixed tissue for research. They were considered to be normal if no abnormalities were observed. These tissues were fixed in RNAlater (Thermo Fisher Scientific, Waltham, MA) and stored at -80°C. The study was approved by the Mass General Brigham Institutional Review Board.

RNA Extraction and Reverse Transcription

Total RNA was extracted using Qiagen RNeasy® Mini Kits (#74104) following the manufacturer's instructions (Qiagen, Valencia, CA). Eluted RNA was treated with Qiagen RNase-free DNase and purified with Qiagen RNeasy MinElute Cleanup kit (#74204) following the manufacturer's instructions. Reverse transcription was performed with a specific amount of total RNA (ranging from 0.4 to 0.9 µg) using the ProtoScript® First Strand cDNA Synthesis Kit per the manufacturer's instructions (New England Biolabs, Ipswich, MA). The final volume of each RT reaction was 50 µl.

Angiogenesis RT^2 Profiler PCR Array Analysis

Human Angiogenesis RT^2 Profiler PCR array kits were used (Qiagen). RNA extracted from human pituitary tumors was pooled by combining 0.5 µg per sample. The pooled RNA contained equal quantities of RNA from 207 tumor samples, including 140 NFAs, 38 GH, 16 ACTH, and 13 PRL-secreting tumors. Reverse transcriptions were carried out with 1 µg pooled RNA per reaction as described above. The PCR with the array was performed following the protocol provided by Qiagen. PCR data were analyzed using Qiagen web-based PCR Array Data Analysis Software. The results from three experiments are presented as fold changes in tumor tissue compared to normal control tissue. P values < 0.05 were considered statistically significant.

Absolute TaqMan® Probe-Based Quantitative RT-PCR

Real-time PCR was performed using TaqMan® gene expression assays (Thermo Fisher Scientific, Waltham, MA). Briefly, real-time PCR was performed in triplicate in 20 µl per well containing 1 µl of RT reaction, 1 µl of specific TaqMan® probes, and 10 µl of TaqMan® Universal PCR Master Mix (Thermo Fisher Scientific, Waltham, MA). PCR was run on an Applied Biosystems® 7500 FAST Real Rime PCR System at 50°C for 2 min, followed by 95°C for 10 min, followed by 40 cycles at 95°C for 15 sec, and 60°C for 1 min. PCR data were analyzed by setting baseline auto and thresholds to 0.065.

To quantify gene expression, standard curves for TaqMan® probes were generated using linearized plasmid DNAs as templates. Real-time PCR was performed in quadruplicate containing 10^8, 10^7, 10^6, 10^5, 10^4, 10^3, 10^2, and 10 molecule copies of template DNA. Standard curves were generated in Excel using the XY-plot function, where x represents the log of copy number and y represents the cycle threshold (Ct) value. The y-intercept, slope, and coefficient of determination were computed. The amplification efficiency (€) was calculated using the following formula: $[10^{(-1/\text{slope})} - 1] \times 100$. Because one-fiftieth of the volume of an RT reaction was used for each PCR reaction, the expression of specific genes in tissue samples was calculated as $10^{[-A\ -\ \text{Intercept})/\text{Slope}]} \times 50/\text{RNA}_{\text{Input}}$, where A is the average of Ct values generated from triplicate PCR reactions and $\text{RNA}_{\text{Input}}$ the amount of total RNAs in µg used in the RT reaction. The resultant values are the numbers of transcript copies per µg total RNA. The genes, TaqMan® probes, plasmid DNA templates, and their corresponding qPCR standard curve parameters are provided in **Table 2**.

Detection of Protein by ELISA

To detect growth factors released by pituitary tumors, fresh tumor tissue was weighed and cultured with 2 ml DMEM/F12 medium containing 10% FBS. Forty-eight hours after incubation, medium supernatants were collected and stored as 100 µl aliquots at -80°C. ANGPT2 (Cat. #DANG20), PGF (#DPG00), and VEGFC (#DVEC00) were assayed using Quantikine® ELISA kits (R&D systems, Minneapolis, MN) per the manufacturer's instructions. The total quantity of each growth factor detected in 2 ml of medium was divided by the tissue weight to generate pg of each growth factor per mg tissue. To detect endothelial marker proteins, a small piece of tumor tissue was weighed, minced, and homogenized in 350 µl of RIPA lysis buffer containing a protease inhibitor cocktail from Sigma Aldrich (P8340, St. Louis, MO). The lysates were diluted with PBS and assayed with G-Biosciences ELISA kits for CD31 (#501482738) and CD34 (#501484437) (Thermo Fisher Scientific, Waltham, MA). ENG was assayed with Quantikine® ELISA kits (#DNDG00) (R&D systems, Minneapolis, MN). The total quantity of each endothelial marker detected in 350 µl of lysates was divided by the weight of the tissue to generate pg per mg tissue.

Endothelial Cell Tube Formation Assay

Human umbilical vein endothelial cells (HUVEC) were obtained from Lonza (Walkersville, MD) and maintained in the Lonza EBM™ basal medium plus SingleQuot™ growth factors (CC-4133) following the manufacturer's instructions. To obtain medium conditioned by human pituitary tumors, tumor tissue was washed with PBS, minced, and incubated with serum-free DMEM/F12 medium at 37°C and 5% CO_2 for 24 hours. The medium was collected and filtered through 0.45 µm filters before use. To ensure that the assay was not affected by the DMEM/F12 media, we cultured HUVEC cells with this media supplemented with the aforementioned growth factors for up to three days and observed no adverse effect on cell proliferation.

The tube formation assay was performed as described previously (20). Briefly, Matrigel® matrix (Corning Life Science, Tewksbury, MA) was added to 24-well plates (300 ul per well) and incubated in a 5% CO2, 37°C incubator for one hour. HUVECs (1.5×10^5) suspended in 300 µl of medium conditioned by human pituitary tumor tissue were seeded to the Matrigel® coated plates. To determine the effect of inhibition of the VEGF pathway on tube formation, conditioned media were supplemented with DMSO, regorafenib (S1178, Selleck Chemicals, Houston, TX), or cabozantinib (S1119) at a final concentration of 5 µM. After a 16-hour additional incubation,

TABLE 2 | Genes, TaqMan® Probes, and qPCR Standard Curve Performance.

Gene Symbol	Accession #	Gene Full Name	TaqMan® Assay ID	Standard Curve[a]			
				Template	I	€	R^2
ANGPT1	NM_001146.4	angiopoietin 1	Hs00919202_m1	pGEM-ANGPT1[c]	36.5	93.5%	0.998
ANGPT2	NM_001147.2	angiopoietin 2	Hs00169867_m1	pCR4-TOPO-ANGPT2[b]	36.4	97.3%	1.000
CD31	NM_000442.4	platelet and endothelial cell adhesion molecule 1	Hs01065279_m1	pCMV-Sport6-PECAM1[b]	35.2	95.7%	1.000
CD34	NM_001025109.1	CD34 molecule	Hs02576480_m1	pCMV-Sport6.1-CD34[b]	36.7	92.5%	0.999
ENG	NM_001114753.2	endoglin	Hs00923996_m1	pOTB7-ENG[b]	36.8	96.8%	1.000
FN1	NM_212482.2	fibronectin 1	Hs01549976_m1	pCR-XL-TOPO-FN1[b]	36.8	94.7%	0.999
HIF1A	NM_001530.3	hypoxia inducible factor 1 alpha subunit	Hs00153153_m1	pGEM-HIF1A[c]	36.6	94.6%	1.000
KDR	NM_002253.2	kinase insert domain receptor	Hs00911700_m1	pMD18-VER2[c]	36.4	92.8%	0.999
LYVE1	NM_006691.3	lymphatic vessel endothelial hyaluronan receptor 1	Hs01119300_g1	pDNR-LIB-LYVE1[b]	35.3	96.4%	0.999
PDGFA	NM_002607.5	platelet derived growth factor subunit A	Hs00234994_m1	pCMV6-Entry-PDGFA[d]	36.4	95.9%	1.000
PDGFB	NM_002608.3	platelet derived growth factor subunit B	Hs00966522_m1	pCMV-Sport6-PDGFB[b]	36.3	98.6%	1.000
PGF	NM_001207012.1	placental growth factor	Hs00182176_m1	pOTB7-PGF[b]	36.6	98.8%	1.000
TEK	NM_000459.4	TEK receptor tyrosine kinase	Hs00945150_m1	pCMV-Sport6-TEK[d]	36.0	94.7%	0.998
TGFB1	NM_000660.6	transforming growth factor beta 1	Hs00998133_m1	pCMV-Sport6-TGFB1[b]	35.4	92.6%	0.998
TGFB2	NM_001135599.3	transforming growth factor beta 2	Hs00234244_m1	pMD18-TGFB2[d]	36.0	98.9%	1.000
VEGFA	NM_001025366.2	vascular endothelial growth factor A	Hs00900055_m1	pCMV-Sport6-VEGFA[a]	36.6	94.6%	0.999
VEGFB	NM_001243733.1	vascular endothelial growth factor B	Hs00173634_m1	pCMV6-entry-VEGFB[d]	35.5	93.7	1.000
VEGFC	NM_005429.4	vascular endothelial growth factor C	Hs01099203_m1	pCMV-Sport6-VEGFC[b]	35.8	96.5%	1.000
GAPDH	NM_002046.5	glyceraldehyde-3-phosphate dehydrogenase	Hs03929097_g1	pCMV-Sport6-GAPDH[b]	35.8	96.5%	1.000

[a] *I is the y-intercept of the XY plots, where y is the cycle threshold (Ct) and x the log template amount; € is the amplification efficiency calculated as €=[10$^{(-1/slope)}$]-1; R^2 is the coefficient of determination. Template DNAs,* [b]*obtained from GE Dharmacon; Lafayette, CO,* [c]*from Sino Biological; Beijing, China;* [d]*from OriGene Technologies; Rockville, MD.*

tube formation was photographed under an inverted light microscope. Five images per well were captured. Tube lengths and branching points were quantified on the images using the online WimTube program (21).

Pituitary Tumor Mouse Model and Cabozantinib Treatment

The mice were housed at the animal facility of the Center for Comparative Medicine at Massachusetts General Hospital. The study was approved by the MGH Institutional Animal Care and Use Committee (IACUC).

Rb1^{tm2Brn} mice carrying a floxed exon 19 of the *Rb1* gene (also known as Rb1*fl/fl*) were obtained from the Jackson Laboratory (Bar Harbor, ME) (22). RbΔ19 mice were created by crossing *Rb1^{tm2Brn}* mice with CMV-Cre (BALB/c-Tg(CMV-cre)1Cgn/J, the Jackson Laboratory) and maintained as heterozygotes on C57BL/6 background. Mice used in the experiments were at least 8th generations subsequent to backcrossing with C57BL/6 mice. Thirty-two heterozygous RbΔ19 mice, as well as 27 wild-type (WT) littermates, were monitored. Mice were euthanized when they became moribund. The cause of death was determined by necropsy examination. Twenty-five RbΔ19 mice euthanized had large pituitary tumors. Other than thyroid tumors in eight mice, no apparent tumors or other significant anomalies were observed. For these mice, large pituitary tumors were the cause of death. Four RbΔ19 mice grew large neck masses affecting their breathing and had to be euthanized according to our IACUC policy. Necropsy examination showed that they had no or very small pituitary tumors. Three RbΔ19 mice died unexpectedly. No tumors were found in their pituitary glands. The cause of death was unknown. These mice were not included in the final survival analysis. Of the 27 WT littermates, only one died. This mouse had no pituitary tumor, and the cause of death was unknown. The survival curves were plotted, and median survival was determined using Prism 9 software.

Cabozantinib (XL184) (Cab), a potent inhibitor of VEGF receptor 2 (23), was obtained from Selleck Chemicals (Houston, TX). A suspension in sterile PBS of a final concentration of 5 mg/ml was prepared. The drug was administered once daily to mice *via* oral gavage at a concentration of 15 or 30 mg/kg body weight (designated as Cab-15 and Cab-30, respectively) for 14 days. After a 14-day break, the drug regimen was resumed for another 14 days. PBS was administered to another group of mice as controls. The number of mice receiving treatment in each group was as follows: 28 mice for the control PBS group, 26 for the cab-15 group, 28 for the cab-30 group, and 10 for the WT mice group, which was administered 30 mg Cab/kg body weight. The health of these mice was monitored, and they were euthanized when they reached a moribund state. After euthanasia, the mice underwent necropsy to determine the cause of death. Mice who died of causes unrelated to pituitary tumors were not included in the final analysis.

In the PBS group, five mice were removed from experiments because of large neck masses, which caused extreme difficulty with breathing. These neck masses were thyroid tumors. Necropsy revealed that these mice had very tiny pituitary tumors or no apparent pituitary tumors. In the Cab-15 group, one mouse was removed from the experiment because of severe conjunctivitis, one was removed because of a large neck mass, and two were removed due to sudden death soon after the treatment started, likely due to injuries caused by oral gavage. Necropsy revealed these mice had tiny pituitary tumors only. In the Cab-30 group, four mice were removed from experiments because of large neck masses. The rest of the mice in these groups ultimately became moribund. The moribund state was caused by

large pituitary tumors in all of these cases, and no apparent tumors were identified in other tissues.

Statistical Analyses

Data were analyzed using GraphPad Prism 9 software. The one-way ANOVA multiple comparison test was used to compare clinical characteristics. The Kruskal-Wallis nonparametric one-way ANOVA test was used to compare data from endothelial cell tube formation assays and gene expression levels between tumor groups and controls. Pearson's correlations were applied to determine relationships between expression levels among individual genes. The Kaplan-Meir method was applied to construct survival curves, and the log-rank (Mantel-Cox) test was used for between groups comparison. P values < 0.05 were considered significant.

RESULTS

Expression of Angiogenic Genes in Human Pituitary Tumors Determined by the RT² Profiler PCR Array

To evaluate the expression of angiogenesis-related genes in human pituitary tumors, we used the Qiagen human angiogenesis RT² profiler PCR array to evaluate RNA pooled from 207 pituitary tumor samples. RNA pooled from 12 normal human pituitary glands was used as the control. After PCR, we chose the RPLP0 gene as the internal control for Ct normalization following the manufacturer's instructions because the difference between Ct values from tumor plates and control plates was less than 1. The PCR array listed 84 angiogenesis-related genes (**Supplementary Table 1**). Four genes (IFNA1, IFNG, LEP, and PLG) were excluded from analysis because their PCR Ct values were greater than 32 for both tumor and control samples, indicating that the expression of these genes was extremely low and not reliable for comparison analysis. Among the remaining genes, seventy-one were expressed differentially between pituitary tumor and normal pituitary gland tissue with p values less than 0.05 (**Figure 1** and **Supplementary Table 1**). Sixty-four genes were upregulated, whereas seven were downregulated.

More than half of these differentially expressed genes (n=39) are known to regulate sprouting angiogenesis (14, 15, 24–28) (**Figure 1**). Most of these are components of signal transduction pathways regulating sprouting angiogenesis: VEGF pathway (VEGFA, VEGFB, VEGFC, PGF, KDR, FLT1, EFNB2, ITGAV, ITGB3, CDH5, EFNB2, NRP1, and NRP2) (26, 29), the angiopoietin-Tie pathway (ANGPT1, ANGPT2, and TEK) (30), the Notch pathway (NOTCH4 and JAG1) (27), the PDGF pathway (PDGFA) (31), and the TGFβ pathway (TGFB1, TGFB2, TGFBR1, and ENG) (32). Recently, Zegeye et al. reported that IL-6 inhibits sprouting angiogenesis by trans-signaling (33). We found that IL-6 expression was downregulated 17.1-fold in human pituitary tumor tissue compared to normal pituitary tissue (**Figure 1**). In addition, the expression of two well-known endothelial marker genes, *ENG* and *PECAM1* (34, 35) was increased in tumor tissue by 3.72 and 6.67-fold, respectively (**Figure 1**). The gene with the most elevated expression was *FN1*, which was nearly 100-fold higher in human pituitary tumor tissue than in normal pituitary samples (**Figure 1**). Products of the *FN1* gene are essential components of newly formed blood vessels (36). These data indicate that human pituitary tumors contain a more active angiogenesis program than normal pituitary tissue.

Expression of Vascular Endothelial Marker Genes in Human Pituitary Tumors

The PCR array showed that the expression of four out of five internal reference genes was approximately 4-fold higher in human pituitary tumor tissue than in normal pituitary tissue (**Figure 1** and **Supplementary Table 1**), suggesting that a relative quantitative PCR method would underestimate gene expression after normalization against these genes. Therefore, we employed an absolute quantitative PCR method to quantify the expression of these genes, using external DNA as a reference standard.

We quantified the expression of *ENG* and *PECAM* and also determined the expression levels of CD34 mRNA, which encodes a glycoprotein expressed in early, mature, and progenitor endothelial cells (37). We also quantified the expression of mRNA coding of LYVE1, a marker of lymphatic endothelial cells (38). The RNA transcripts detected in pituitary tumors for CD31, CD34 and ENG were 1.6×10^4, 3.3×10^4, and 1.0×10^5 copies/μg total RNA, respectively. Compared with normal pituitary tissue, RNA levels of CD31, CD34, and ENG were increased in pituitary tumors by 5.6 ($p<0.0001$), 22.6 ($p<0.0001$), and 8.2 ($p<0.0001$) fold, respectively (**Figure 2A**). In contrast, there were 1.9×10^3 copies/μg total RNA of LYVE1, which was not significantly different from that of controls (normal pituitary) ($p>0.9999$) (**Figure 2A**). These data indicate that the number of vascular endothelial cells, but not lymphatic endothelial cells, is significantly greater in all types of pituitary tumors than in normal pituitary tissue.

Because mRNA levels may not truly reflect their respective protein levels, we measured protein levels of CD31, CD34, and ENG in 12 additional pituitary tumors using ELISA assays. mRNA levels as determined by qPCR in these tumors were significantly higher than in normal pituitary tissue (**Figures 2B–D**, *left panels*). Their respective proteins were readily detected (**Figures 2B–D**, *middle panels*) and correlated well with mRNA levels (**Figures 2B–D**, *right panels*), suggesting that the mRNA levels we measured accurately reflect protein levels.

Expression of Angiogenic Growth Factors in Human Pituitary Tumors

The VEGF family of growth factors are master regulators of sprouting angiogenesis, as they stimulate proliferation and guide the migration of endothelial cells (24, 25, 27). VEGFA, VEGFB, VEGFC, and PGF, as well as their receptor, VEGFR2, also known as the kinase insert domain receptor (KDR), were examined. The genes with the highest to lowest levels of expression were: VEGFB (1.1×10^5 copies/μg total RNA), VEGFA (3.5×10^4), PGF (1.8 x

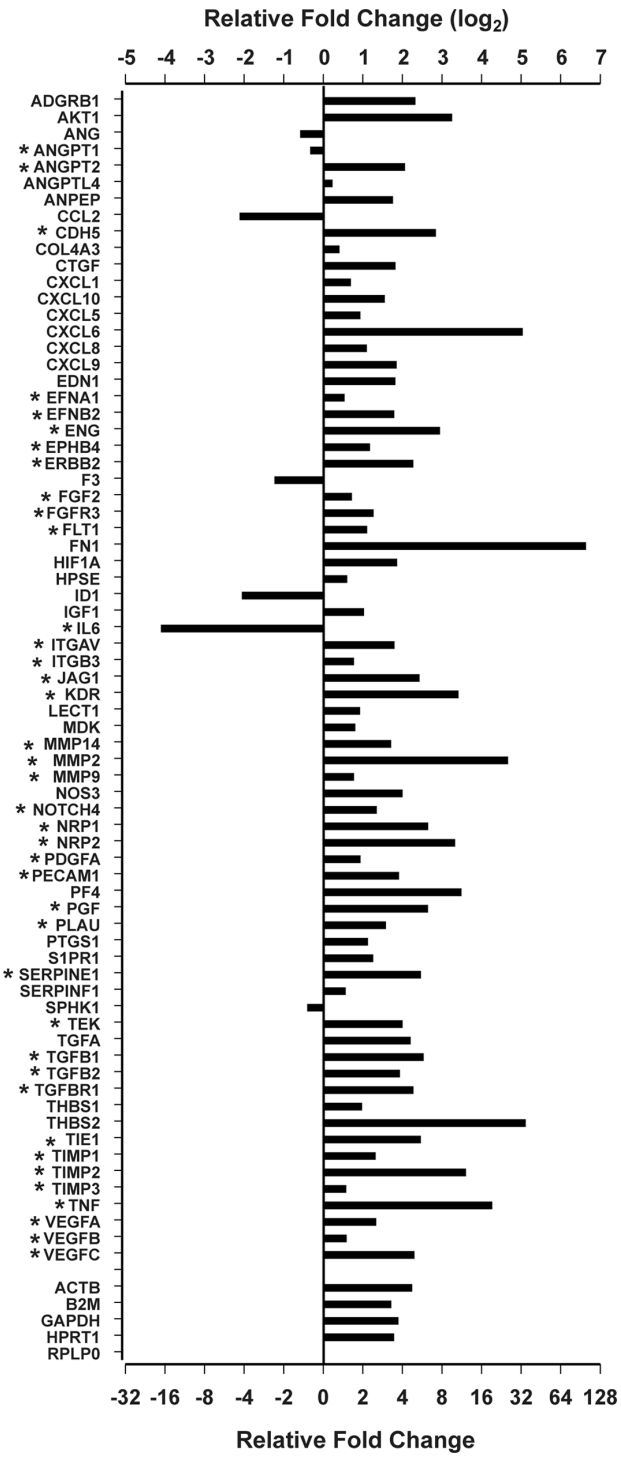

FIGURE 1 | Differentially expressed angiogenesis genes by the Qiagen RT^2 Profiler PCR Array. *Genes involved in sprouting angiogenesis.

10^4), and VEGFC (8.3 x 10^3), respectively. Compared with normal pituitary tissue, genes with the highest to lowest expression levels in pituitary tumor tissue were VEGFC (19.3-fold, p<0.0001), PGF (13.4-fold, p<0.0001), VEGFA (4.2-fold, p<0.0001) and VEGFB (2.2-fold, p=0.002) (**Figure 3A**). Moreover, elevated expression in all types of pituitary tumors was only observed with VEGFC and PGF. In contrast, VEGFA expression was increased in NFA and ACTH-secreting tumors but not in GH and PRL-secreting tumors (**Figure 3A**). KDR expression was 7.8-fold (p<0.0001) higher in all types of pituitary tumors combined than in normal pituitary tissue

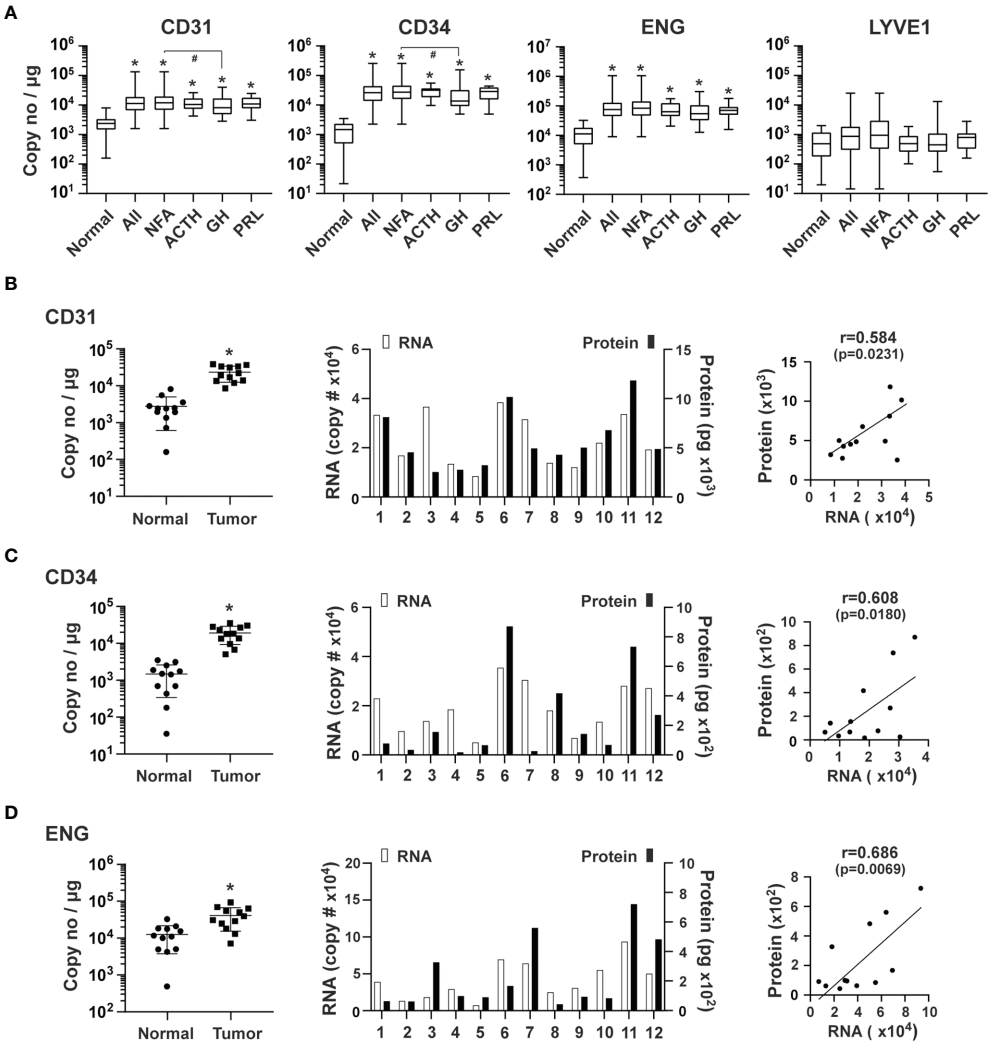

FIGURE 2 | Expression of endothelial markers in human pituitary tumors. **(A)** Expression of the indicated genes was quantified by the TaqMan® probe-based qPCR. A total of 207 human pituitary tumors, including 140 NFAs, 38 GH-producing, 16 ACTH-producing and 13 PRL-producing tumors, and 12 normal pituitaries were assessed. *p < 0.05 vs normal pituitaries; #p < 0.05 vs NFA. **(B)** CD31, **(C)** CD34 and **(D)** ENG: Correlation of their RNA and protein expression in an additional 12 pituitary tumors, including 11 NFA and 1 GH-secreting tumors. *Left panel*, RNA levels of endothelial markers in pituitary tumors and normal pituitary tissue. *p < 0.05 vs normal pituitaries. *Middle panel*, RNA and protein levels of individual pituitary tumors. RNA levels (open bars) are indicated on the left y-axis as copies of transcript/µg total RNA. Protein levels (solid bars) are indicated on the right y-axis as pg/mg of tumor tissue. *Right panel*, correlation between RNA levels determined by qPCR and protein levels determined by ELISA.

(**Figure 3A**). As a non-angiogenesis gene control, GAPDH expression was determined to be 7.6 x 10^6 copies/µg total RNA. Compared to the normal pituitary tissue, GAPDH expression was higher by 3.5-fold (p<0.0001) in tumors (**Figure 3A**), which confirmed the PCR array findings.

We next measured primary pituitary tumor production of PGF and VEGFC proteins. We cultured fresh tissue from 12 tumors for 48 hours and assessed PGF and VEGFC in culture media using ELISA. PGF and VEGFC proteins were readily detected in the culture medium (**Figure 3B**). Expression levels of mRNA and protein correlated well (**Figure 3B**).

Angiopoietin-Tie signaling regulates the homeostasis of blood vessels (5, 30). Angiopoietin 1 (ANGPT1) and 2 (ANGPT2) regulate angiogenesis *via* their common TEK tyrosine kinase receptor (TEK, also known as TIE2) (30, 39). ANGPT1, which is mainly produced from perivascular cells, such as pericytes and vascular smooth muscle cells, activates TEK resulting in endothelial cell survival and stabilization (30). ANGPT1 over-expression inhibits angiogenesis (40). ANGPT2, highly expressed in endothelial tip cells (41, 42), promotes angiogenesis in conjunction with VEGF by antagonizing ANGPT1 (30). The overall expression of ANGPT1 was 5.4 x 10^3 copies/µg total RNA in pituitary tumor tissue. Compared with normal pituitary tissue, the overall expression of ANGPT1 was significantly lower in pituitary tumor tissue by 2.1-fold (p=0.0043) (**Figure 4A**). The ANGPT1 downregulation was observed in all types of tumors

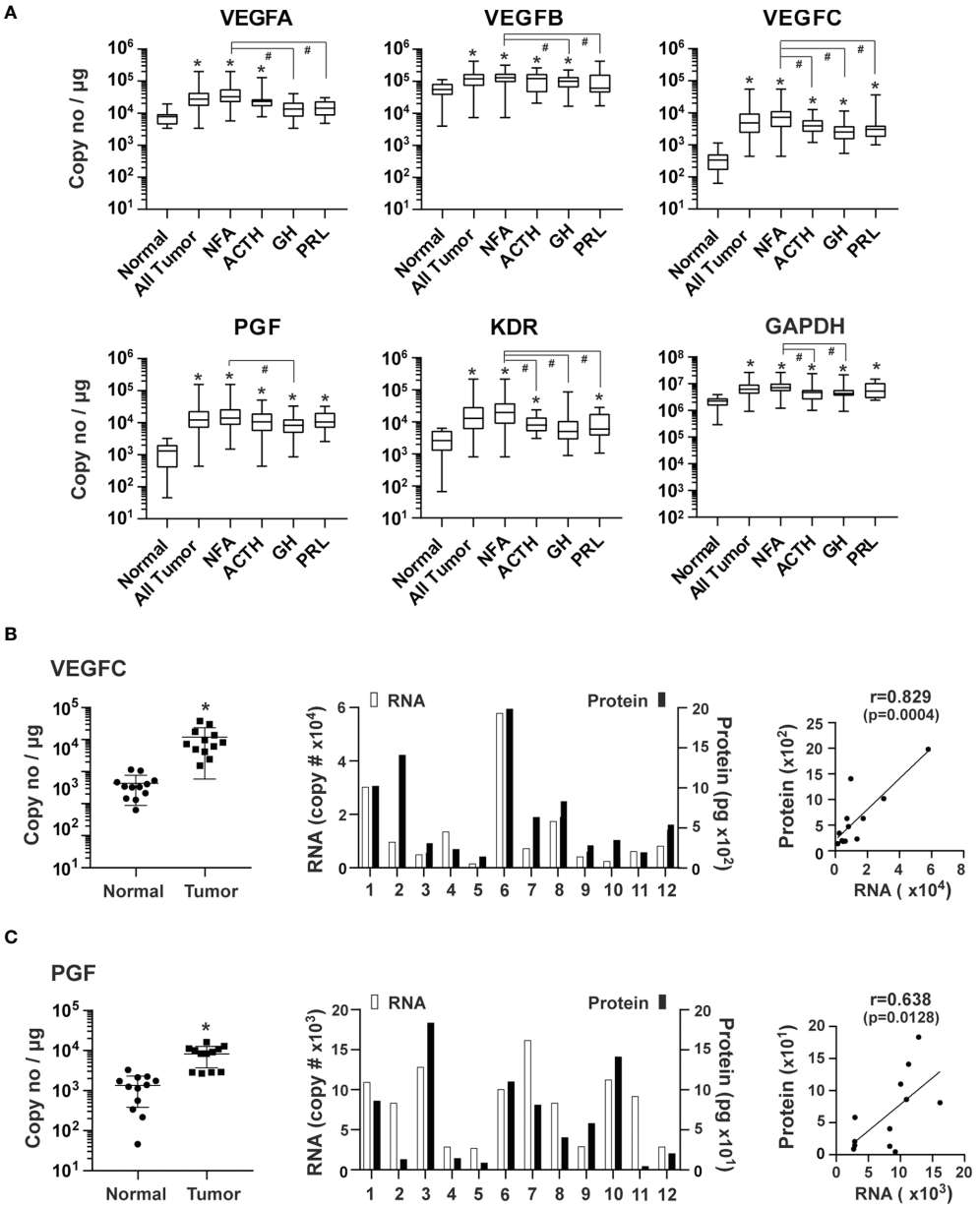

FIGURE 3 | Expression of VEGF family of growth factors in human pituitary tumors. **(A)** Expression of indicated genes was quantified by the TaqMan® probe-based qPCR. Normal pituitary tissue, n = 12; NFA, n = 140; ACTH, n = 16; GH, n = 38; PRL, n = 13. *p < 0.05 vs normal pituitary tissue; #p < 0.05 vs NFA. **(B)** VEGFC and **(C)** PGF, Correlation of RNA and corresponding protein expression in an additional 12 pituitary tumors, including 11 NFA and 1 GH-secreting tumors. *Left panel*, RNA levels of endothelial markers in pituitary tumors and normal pituitary tissue. *p < 0.05 vs normal pituitary tissue. *Middle panel*, RNA and protein levels of individual pituitary tumors. RNA levels (open bars) were indicated on the left y-axis as copies of transcript/µg total RNA. Protein levels (solid bars) were indicated on the right y-axis as pg/mg of tumor tissue. *Right panel*, correlation between RNA levels determined by qPCR and protein levels determined by ELISA.

except for PRL-producing tumors. In contrast, expression of ANGPT2 (3.6 x 10^3 copies/µg total RNA) and TEK (3.4 x 10^3) was significantly elevated in all types of pituitary tumors with an overall increase of 9.2 (p<0.0001) and 7.3-fold (p<0.0001), respectively (**Figure 4A**). The ANGPT2 protein was also detected in the culture medium of primary pituitary tumor tissue, and its protein levels correlated strongly with their corresponding RNA levels (**Figure 4B**).

The PDGF and TGFβ signaling pathways regulate blood vessel maturation (43, 44). The expression of PDGFA, PDGFB, TGFB1 and TGFB2 in pituitary tumor tissue was respectively 3.5 x10^4, 2.0 x 10^4, 1.3 x 10^5 and 6.6 x 10^3 copies/µg total RNA (**Figure 5A**). PDGFB expression in all types of pituitary tumors was, on average, 10.5-fold (p<0.0001) greater than that of normal pituitary tissue (**Figure 5A**). Significantly higher PDFA expression was only detected in NFA and ACTH-secreting tumors compared with

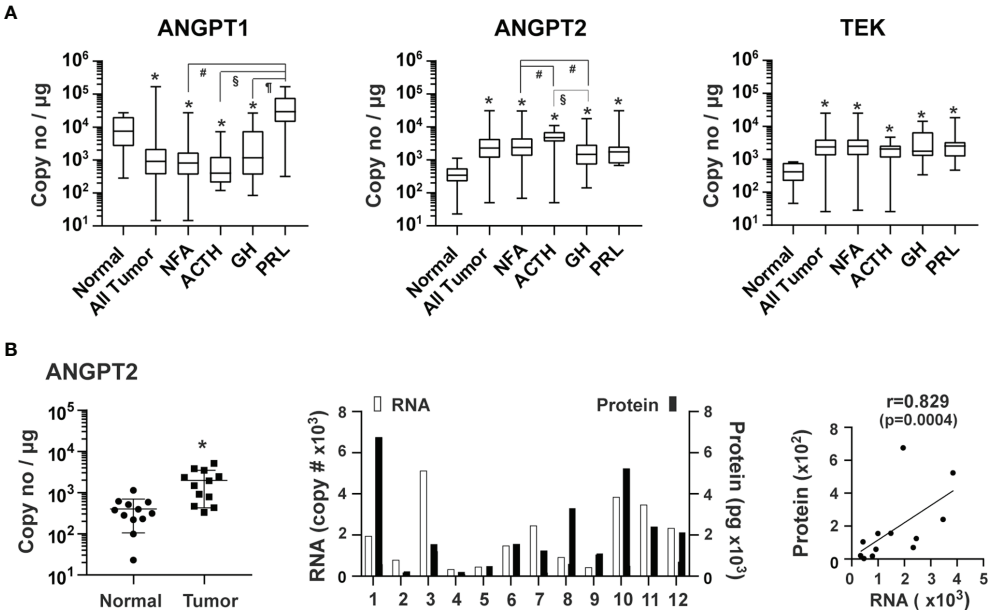

FIGURE 4 | Expression of angiopoietins and their receptor, TEK, in human pituitary tumors. **(A)** RNA expression of ANGPT1, ANGPT2 and TEK was quantified by TaqMan® probe-based qPCR. Normal pituitary tissue, n = 12; NFA, n = 140; ACTH, n = 16; GH, n = 38; PRL, n = 13. *p < 0.05 vs normal pituitary tissue; #p < 0.05 vs NFA; §p < 0.05 vs ACTH-secreting tumors; ¶p < 0.05 vs GH-secreting tumors. **(B)** Correlation of ANGPT2 RNA in tumor tissue and angiopoietin 2 released by the corresponding tumors. A total of 12 pituitary tumors, including 11 NFA and 1 GH-secreting tumors were assessed. *Left panel*, RNA levels of endothelial markers in pituitary tumors and normal pituitary tissue. *p < 0.05 vs normal pituitary tissue. *Middle panel*, RNA and protein levels of individual pituitary tumors. RNA levels (open bars) are indicated on the left y-axis as copies of transcript/µg total RNA. Protein levels (solid bars) are indicated on the right y-axis as pg/mg of tumor tissue. *Right panel*, correlation between RNA levels determined by qPCR and protein levels determined by ELISA.

normal pituitary tissue. TGFB1 was significantly higher in NFA (4.2-fold, p<0.0001), ACTH-secreting tumors (3.5-fold, p=0.0017), and GH-secreting tumors (2.96-fold, p=0.007), but not in PRL-secreting tumors (**Figure 5B**) compared with normal pituitary tissue. Conversely, TGFB2 expression was significantly higher in GH-secreting (4.2-fold, p<0.0001) and PRL-secreting tumor tissue (6.1-fold, p<0.0001), but not in NFA and ACTH-secreting tumor tissue (**Figure 5B**), than in normal pituitary tissue.

The alpha subunit of hypoxia-induced transcription factor 1 (HIF1A) is known to activate the expression of PGF, PDGFB, VEGFA, and VEGFC (45, 46). RNA levels of HIF1A were significantly higher in all tumor types compared with normal pituitary tissue, with an overall elevation of 2.4-fold (p=0.0004) (**Figure 5C**).

We also determined the expression of *fibronectin 1* (*FN1*) in pituitary tumor tissue. PCR products of *FN1* containing EDA and EDB domains are mainly found in newly formed blood vessels and overexpressed in many human tumors (47). We found that the FN1 transcript level in human pituitary tumors was 3.4 x 10^4 copies/µg total RNA, which was 89.6-fold (p<0.0001) that observed in normal pituitary tissue and significantly elevated in every tumor type (**Figure 5C**).

Sixteen of the 19 genes examined by absolute quantitative PCR in individual samples were included in the RT² Profiler PCR Array. The fold changes in pituitary tumors compared to normal pituitary gland tissue by these two methods correlated strongly (R=0.9815, p<0.0001). These data validate the RT² Profiler PCR Array findings and, more importantly, support the hypothesis that angiogenesis is enhanced in human pituitary tumors.

Correlation of Vascular Endothelial Markers and Angiogenic Growth Factors in Human Pituitary Tumors

We calculated the expression ratio between endothelial markers and the lymphatic endothelial marker LYVE1 based on data in **Figure 2** to determine the contribution of vascular endothelial cells and lymphatic endothelial cells to the increase in endothelial marker expression in pituitary tumor tissue. In normal pituitary tissue, the expression ratios of CD31, CD34, and ENG over LYVE1 were 3.9, 2.1, and 18.0, respectively. In pituitary tumor tissue, those ratios were increased substantially to 8.4, 17.9, and 55.7, respectively. This suggests that the elevated expression of endothelial markers is mainly due to a higher number of vascular endothelial cells, which reflects angiogenesis activity in pituitary tumors. Therefore, we reasoned that the contribution of angiogenic factors to angiogenesis in tumors could be evaluated by analyzing correlations between their expression and the expression of vascular endothelial markers. We performed a correlation analysis with data from NFAs and GH-producing tumors. Among 151 NFAs (**Table 1**), 140 tumor samples were used for analysis because expression data of all 19 genes (**Figures 2**–**5**) were available. For the same reason, 38 out of 39 GH-producing tumors (**Table 1**) were used for the analysis. The sample numbers of ACTH- and PRL-producing tumors were 16 and 13, respectively,

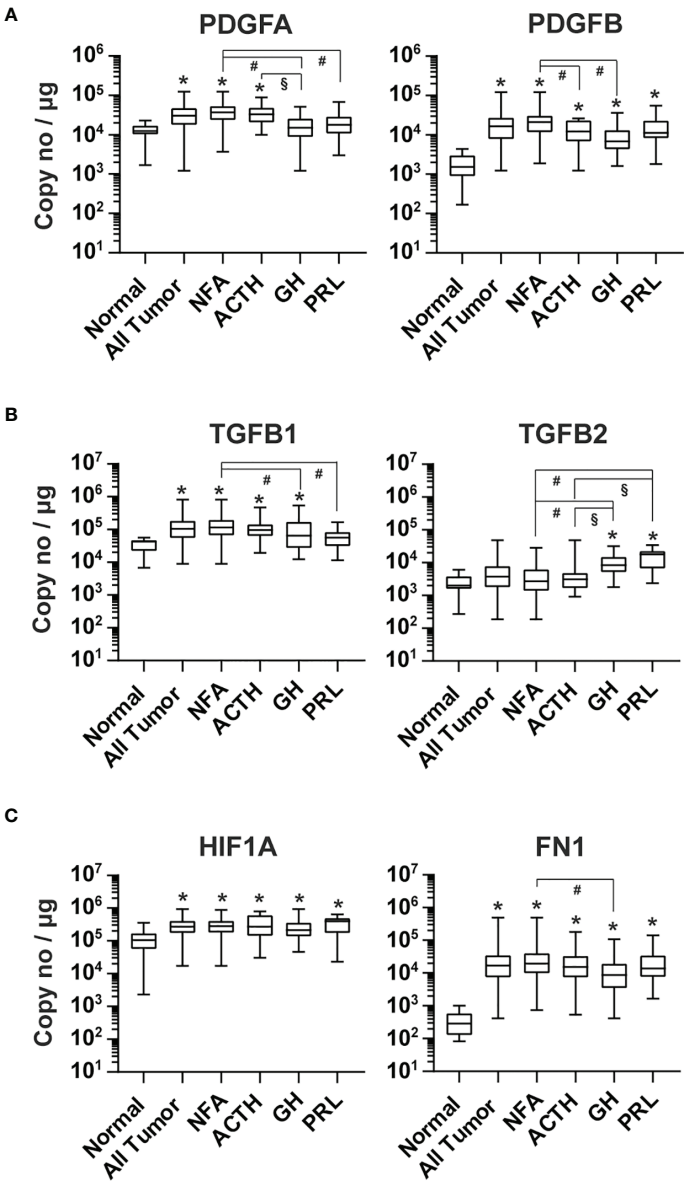

FIGURE 5 | Expression of other angiogenic growth factors in human pituitary tumors. RNA of **(A)** PDGFA and PDGFB, **(B)** TGFB1 and TGFB2, and **(C)** HIF1A and FN1 were quantified by TaqMan® probe-based qPCR. Normal pituitary tissue, n = 12; NFA, n = 140; ACTH, n = 16; GH, n = 38; PRL, n = 13. *p < 0.05 vs normal pituitaries; #p < 0.05 vs NFA; §p < 0.05 vs ACTH-producing tumors.

which were too small to perform meaningful correlation analyses. The full Pearson's correlation coefficient estimates for NFA and GH-secreting tumors are included in **Supplementary Figure S1** and **S2**.

In NFAs, CD31, CD34, and ENG levels correlated very strongly with each other (**Figure 6A**). The correlations between their expression and LYVE1 were much weaker. Endothelial marker levels did not correlate with GAPDH levels. Among angiogenic growth factors, PGF, ANGPT2, PDGFB, and TGFB2 correlated most strongly with each of the endothelial marker levels. These are members of four signaling pathways and play essential roles in angiogenesis sprouting and blood vessel maturation. A similar pattern was also observed in GH-producing tumors. Expression of at least one member from each of the four pathways positively correlated with endothelial marker expression (**Figure 6B**). Although both TGFB1 and TGFB2 correlated significantly with endothelial markers in NFAs (**Figure 6A**), only TGFB1, not TGFB2, positively correlated with endothelial markers in GH-producing tumors (**Figure 6B**). Moreover, neither expression of VEGFA nor VEGFB correlated with the expression of any endothelial marker. However, VEGFC expression correlated significantly with endothelial markers in both types of tumors (**Figures 6A, B**). Taken together, these data strongly suggest that human pituitary tumors maintain an active

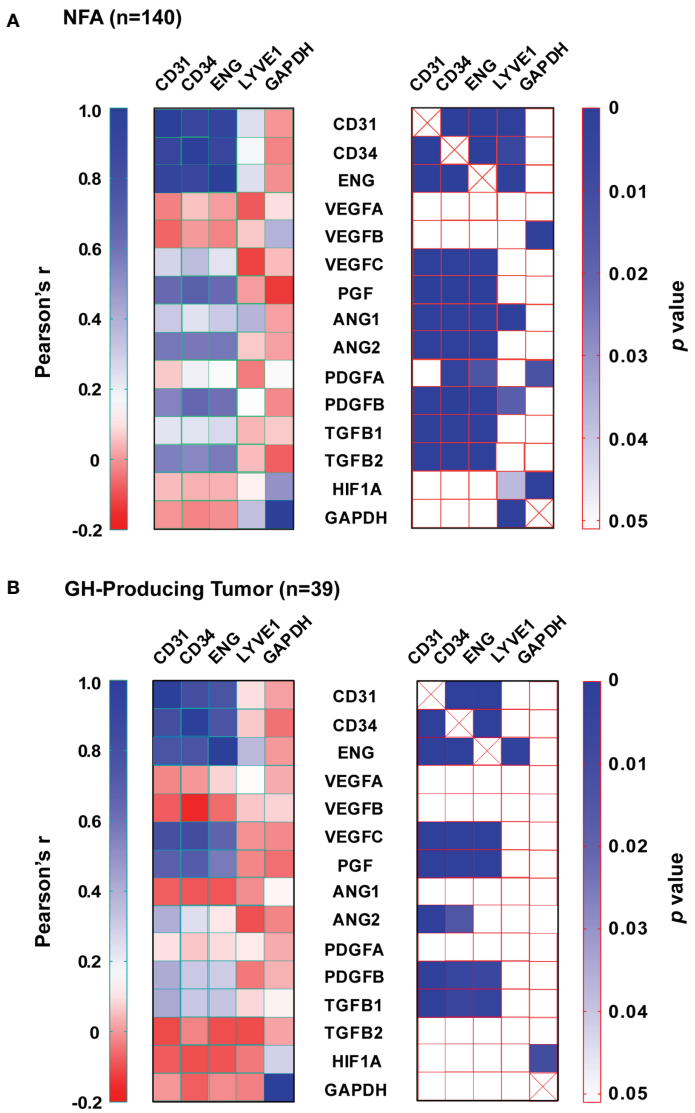

FIGURE 6 | Expression correlation between angiogenic growth factors and endothelial markers. **(A)** NFA and **(B)** GH-secreting tumors. Left panel, Pearson's correlation coefficients (*r*). Right panel, p value.

angiogenesis program. These data also suggest that VEGFC and PGF are the main members of VEGF family that regulate angiogenesis in human pituitary tumors.

Pituitary Tumors Stimulate Angiogenesis *via* the VEGF Signaling Pathway

We performed *in vitro* endothelial tube formation assays using culture media conditioned with primary human pituitary tissue. The assay is widely used to identify angiogenic and antiangiogenic factors by mimicking multiple steps in angiogenesis (48). Primary tumor tissue, which consists of both tumor cells and the tumor microenvironment (TME), was used. The TME is composed of non-tumor cells (such as fibroblast, folliculostellate, and immune cells) and extracellular matrix harboring enzymes, growth factors, and cytokines (49, 50). The TME is known to play an important role in tumor angiogenesis (51). Three tumors, including 2 NFAs and 1 GH-producing tumor, were included in the assay because we have observed that both types of tumors contain active angiogenesis programs (**Figure 6**). Media from primary pituitary tumor cultures increased endothelial tube formation in Matrigel by approximately 3-fold, measured as total tube length, and 4-fold as total branching points (**Figures 7A, B**). Regorafenib is an inhibitor of multiple receptor kinases, including VEGF receptors 1, 2, and 3 (52). Cabozantinib predominantly inhibits VEGF receptor 2 (23). When regorafenib (Reg) or cabozantinib (Cab) was added to the conditioned media, tube formation was significantly reduced (**Figures 7A, B**). These

experiments suggest that angiogenesis induced by human pituitary tumors is mediated by the VEGF signaling pathway.

Prolonged Survival by VEGF Receptor Inhibitor Cabozantinib in Mice With Pituitary Tumors

Inhibition of angiogenesis by anti-VEGF antibody or by VEGF receptor inhibitor was tested in prolactinoma mouse models (53–55). To test whether inhibition of angiogenesis suppressed a broader spectrum of pituitary tumors, we chose the Rb knockout mouse as our experimental model. The Rb pathway plays an important role in the pathogenesis of pituitary tumors (56). In humans, the RB pathway is silenced in approximately 90% of pituitary tumors (56). In mice, inactivation of the Rb pathway by deletion of the Rb gene, by overexpression of Rb inactivating oncogenes, or by deletion of CDK inhibitors promotes the development of pituitary tumors (57). For example, overexpression of the SV40 T-antigen in the pituitary gland resulted in GH-producing and null cell adenomas in mice (58, 59). For our study, we created *RbΔ19* mice in which the exon 19 of the *Rb1* gene had been deleted. The *RbΔ19 mice* were derived from $Rb1^{tm2Brn}$ mice, which carry a floxed exon 19 of the *Rb1* gene (22). We observed that heterozygous RbΔ19 mice all developed pituitary tumors, with a median survival of 412 days (**Figure 8A**). To determine when to initiate antiangiogenesis treatment in *RbΔ19* mice, we analyzed pituitary tumors from a set of apparently healthy mice at 345 days after birth. We observed that 16 out of 18 mice examined had visible pituitary tumors (**Supplementary Figure S3**). Histological staining confirmed that these tumors were adenomas. It also revealed that the other two

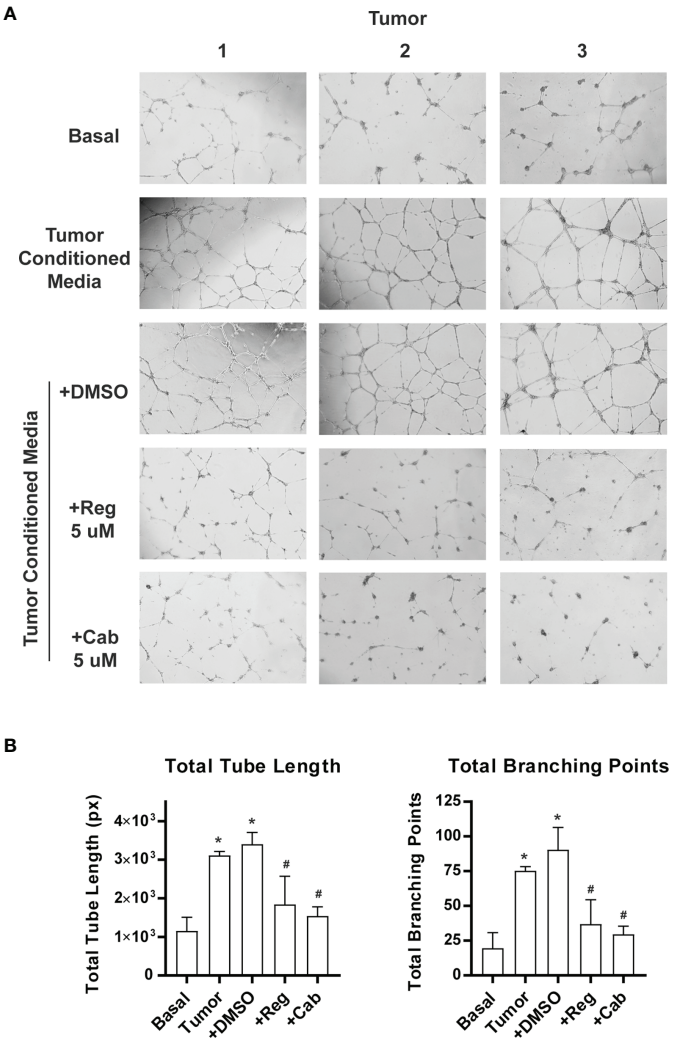

FIGURE 7 | Inhibition of pituitary tumor angiogenesis by VEGF receptor inhibitors. Angiogenesis was assayed by endothelial cell tube formation in Matrigel gel. The pictures were analyzed by WimTube online program. **(A)** A sample picture used for analysis by WimTube. **(B)** Tube formation is presented as total tube length (*left panel*) and total branching points (*right panel*) per field. The values are mean ± SD of experiments with three NFAs. *p < 0.05 vs basal medium; #p < 0.05 vs treatment with conditioned media.

pituitary glands contained micro tumors. Therefore, we chose 345 days as the age to begin antiangiogenesis treatment.

Three cohorts of *RbΔ19* mice were included in the experiments. Fifteen mg cabozantinib/kg body weight (Cab-15), 30 mg/kg body weight (Cab-30) and PBS, respectively, was administered. The drug has been approved for the treatment of human metastatic medullary thyroid cancer, advanced renal cell carcinoma, and hepatocellular cancer under the trade name COMETRIQ™. The health of all animals was monitored closely. They were euthanized when they became moribund. After euthanasia, causes of death were determined by necropsy. Mice that died of causes not related to pituitary tumors were excluded from the final analysis (see Materials and Methods). The mice in the PBS group (n=23) died between 9 to 204 days after the first dose was administered, with a median survival of 77 days (ranging from 9 to 204 days) after treatment initiation. In contrast, the median survival after the treatment was 101 days (16 to 279 days) for mice in Cab-15 group (n=22, vs PBS group, p = 0.0371) and 135 days (38 to 261 days) for mice in the Cab-30 group (n=24) vs the PBS group p = 0.0017) (**Figures 8B, C**).

There were no apparent adverse effects caused by Cab on wild-type mice. The WT mice administered 30 mg Cab/kg body weight lived well beyond 24 months, except for one mouse euthanized 365 days after treatment initiation. This animal developed a severe eye lesion and had to be euthanized following IACUC rules. A side effect that was only observed in *RbΔ19* mice treated with Cab was the development of grey patches on their fur. These patches slowly disappeared a few months after drug administration.

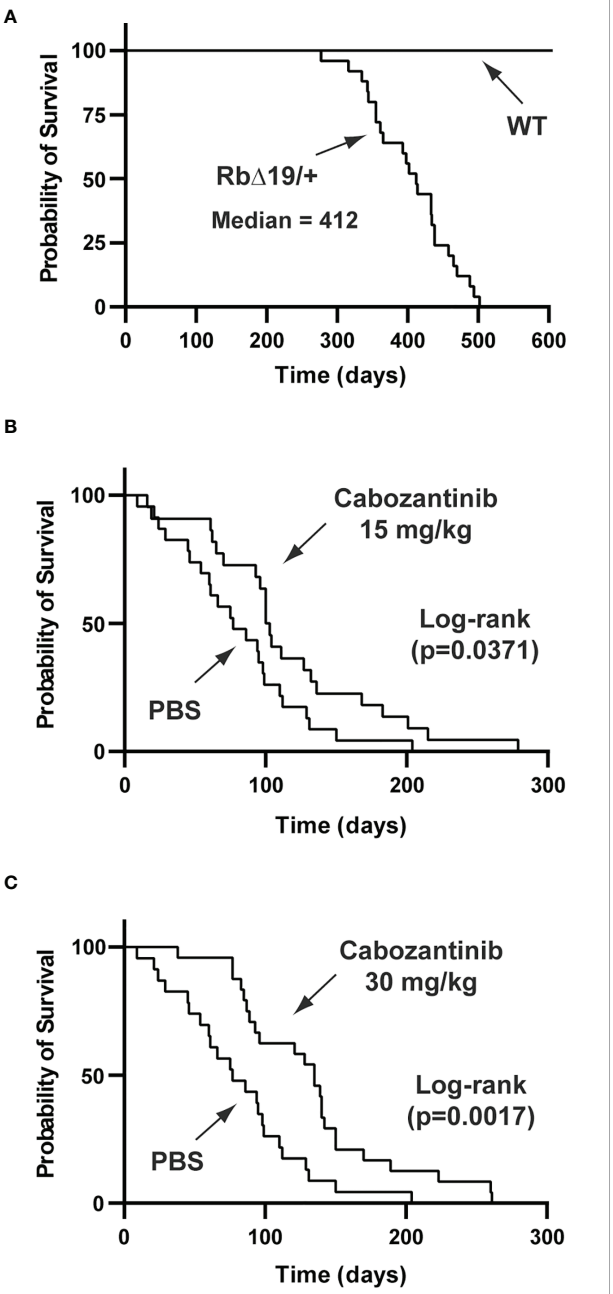

FIGURE 8 | Prolonged survival of *RbΔ19* mice by cabozanitinib treatment. **(A)** Survival of *RbΔ19* mice and their WT littermates in the absence of antiangiogenesis treatment. **(B)** Survival of *RbΔ19* mice treated with Cab at 15 mg/kg body weight for two two-week regimens. Mice treated with PBS were as controls. **(C)** Survival of *RbΔ19* mice treated with Cab at 30 mg/kg body weight for two two-week regimens. The treatment was initiated when mice reached 345 days old. Time designated as days after treatment initiation.

DISCUSSION

Our data suggest that human pituitary tumors, regardless of tumor type, are more vascular, have elevated expression of angiogenic growth factors, and upregulate angiogenic pathways more than normal pituitary gland tissue. In addition, we identified PGF and VEGFC as the major angiogenic growth factors regulating angiogenesis in human pituitary tumors. Furthermore, we show that targeting VEGF receptors significantly improves the survival of mice with pituitary tumors. These data provide a rationale for studying whether agents that target these pathways may be effective therapies for aggressive pituitary tumors.

In this study, we systematically quantified the expression of multiple endothelial markers and angiogenic genes in a large cohort of human pituitary adenomas. To the best of our knowledge, this is the first study employing the TaqMan® probe-based absolute qPCR technique to assess the expression of angiogenic genes in human pituitary tumors. One advantage of using the absolute qPCR is that it avoids biases introduced by internal reference genes. Another advantage is that data from absolute qPCR makes it possible to perform correlation analyses to analyze the roles individual angiogenic genes may play in pituitary tumor angiogenesis. In contrast, the large majority of reports in the literature investigating pituitary angiogenesis have examined vascularization by MVD assays. Using this method, some studies demonstrated decreased vascularization of pituitary tumors compared with normal pituitary glands, and others, even within the same papers, were contradictory. For example, Turner et al. demonstrated a lower density of blood vessels in benign pituitary tumors than in normal pituitary tissue; however, macroadenomas demonstrated greater vascularity than microadenomas (17). In

contrast, Takada et al. reported that the capillary vessel number per area in pituitary tumors was significantly higher than in normal pituitary gland tissue (60). However, if MVD were measured as the percentage of area, it was lower in the tumor tissue than in normal pituitary gland tissue (60), suggesting that pituitary tumors contain a greater number but smaller capillary vessels. Similarly, Perez-Millan et al. reported that human pituitary tumors contained more small blood vessels than normal pituitary glands (61). Other published studies have used endothelial markers to investigate angiogenesis in pituitary tumors. For example, Rotondo et al. observed a higher MVD in human pituitary tumors than in normal pituitaries when tissue sections were stained with an anti-CD105 antibody (62). CD105 is encoded by the ENG gene, which is believed to be expressed only in proliferating endothelial cells (35). Therefore, some, but not all, prior studies support our conclusion that angiogenesis is more active in human pituitary tumors than in normal pituitary glands.

Sprouting angiogenesis is a well-established mechanism of tumor angiogenesis (12). It is regulated by a signaling cascade of multiple angiogenic pathways involving VEGF, ANGPT2, PDGF, and TGFβ (15, 24). VEGF initiates the sprouting of endothelial cells by stimulating endothelial tip cell transformation and migration (16). ANGPT2 destabilizes vessels by antagonizing ANGPT1 to facilitate tip cell sprouting (30). TGFβ and PDGF signaling contribute to the growth and maturation of new blood vessels (24). Our data demonstrate that human pituitary tumors highly express these angiogenic growth factors (**Figures 3**–**5**). In addition, their expression levels strongly correlate with the expression of vascular endothelial markers (**Figure 6**). Therefore, our data strongly support that sprouting angiogenesis is an angiogenic mechanism for neovascularization in human pituitary tumors. Nevertheless, our data do not exclude the existence of other vascularization mechanisms in human pituitary tumors, such as vasculogenic mimicry (63).

A surprising finding was that expression levels of VEGFA and VEGFB did not correlate with the expression of endothelial markers (**Figure 6**). In contrast, Cristina et al. reported a positive correlation between VEGFA expression and CD31 in NFAs with an R^2 of 0.49 (p=0.010) (64). The discrepancy may be due to differences in data collection between the two studies. They quantified protein levels using Western blotting, and data were normalized against the internal control gene actin. In contrast, we quantified mRNA levels using absolute qPCR, and data are presented as copy numbers per ug total RNA. Our data indicate that PGF and VEGFC expression correlate strongly with endothelial marker expression (**Figure 6**). This suggests that PGF and VEGFC are the main angiogenic growth factors initiating angiogenesis in human pituitary tumors.

VEGF family of growth factor signaling is mediated by three receptors: VEGFR1 (encoded by the FLT1 gene), VEGR2 (KDR), and VEGFR3 (FLT4). These receptors form homo or heterodimers and are activated by autophosphorylation upon binding to VEGF ligands (29, 65). VEGF1 is predominantly expressed on blood vessel endothelial cells (66), and PGF binds only to VEGF1 (67). In addition to VEGFR2, VEGFA also binds to VEGFR1 with high affinity (67). Because it is characterized by very weak kinase activity, VEGFR1 is thought to be a negative regulator of the VEGF signaling by acting as a decoy receptor (29). We found that its expression in human pituitary tumors is approximately 2-fold that of normal pituitary tissue (FLT1 in **Figure 1**). VEGFR2 is expressed mostly in vascular endothelial cells (68). Both VEGFA and VEGFC bind to VEGFR2. VEGFR2 is the predominant receptor mediating VEGF-induced vascular angiogenesis (29, 68). Consistent with this, we found that VEGFR2 expression is more than 8-fold higher in pituitary tumors than in normal pituitary tissue (KDR in **Figure 3A**). Its expression correlated positively with levels of vascular endothelial markers in both NFAs and GH-secreting tumors (**Supplementary Figures S2** and **S3**), suggesting that VEGFR2 plays an important role in pituitary tumor angiogenesis. VEGFR3 only binds to VEGFC. VEGFC/VEGFR3 normally regulates lymphatic angiogenesis (69). We did not investigate VEGFR3 expression in our study, and its role in pituitary tumor angiogenesis is not known.

In pituitary tumors, PGF may regulate angiogenesis *via* several mechanisms. PGF binds to the VEGFR1 to free VEGFA from its receptor, thereby increasing interactions between VEGFA and VEGFR2 (70). PGF forms a heterodimer with VEGFA, which induces VEGFR1/VEGFR2 receptor dimers, thereby activating VEGFR2 by transphosphorylation (71). Therefore, VEGFA likely stimulates angiogenesis in human pituitary tumors in a PGF-dependent manner. PGF can also stimulate angiogenesis independently of VEGF by activating VEGFR1 (71). VEGFC has long been considered to be the main regulator of lymphangiogenesis (72). However, multiple studies indicate that it also plays an important role in regulating endothelial sprouting (73–75). These data raise the possibility that treatment with the anti-VEGFA antibody, bevacizumab, may not be sufficient to inhibit angiogenesis in pituitary tumors. VEGF-inhibition resistance has been reported in a number of cancers (76), and induction of PGF is believed to be one of the causes (76). Ideally, a panel of angiogenic factors could be assessed in surgically removed tumors and specific antiangiogenesis drugs selected according to the expression profile of the angiogenic growth factors observed in a specific tumor.

Anti-VEGF treatment has been demonstrated to successfully treat pituitary tumors in mouse models. Korsisaari et al. used the anti-VEGF antibody G6-31 to treat pituitary tumors in *Men1*$^{+/-}$ mice (53). After 67 days, they observed that G6-31 treatment reduced the tumor volume by 72% compared to the control group and significantly extended their survival. All pituitary tumors in *Men1*$^{+/-}$ mice were later identified as prolactinomas (53). The G6-31 antibody was also used to treat Drd2(-/-) mice with hyperplastic pituitary glands by Luque et al. (54). A group of female Drd2(-/-) mice were treated with G6-31 for six weeks (54). Pituitary hyperplasia was significantly reduced at the end of the treatment period compared to the placebo group. A reduction in MVD in G6-31 treated pituitary glands was also observed (54). Axitinib is a VEGF inhibitor targeting all three VEGF receptors (77), and it has been approved by the FDA to treat human renal cell carcinoma. Chauvet et al. tested axitinib on a transgenic mouse model expressing a truncated form of

Hmga2 protein (55). Hmga2 mice develop prolactinomas between 9-11 months. Axitinib was administered to animals with a high circulating prolactin level for six weeks. At the end of the treatment period, they observed a significant reduction in tumor size and improvement in vascular structure (55). The main shortcomings of these studies were: 1) all tumors included in the treatment were prolactinomas, and 2) a small number of mice were used. For example, the survival curves after treatment in the study by Korsisaari et al. only included 8 and 9 mice for G6-31 and the control group, respectively (53). However, these studies suggest that the efficacy of such agents may merit investigation for the treatment of aggressive pituitary tumors.

Mice carrying a heterozygous allele of the mutant *Rb1* gene are known to develop anterior pituitary tumors on the C57BL/6 background (78). We found that approximately 70% of *RbΔ19* mice of the 8th or greater generation after backcrossing with C57BL/6 developed anterior pituitary tumors, with about 25% of all tumors expressing ACTH, 25% PRL, 35% GH, 25% TSH, 10% LH and 25% expressing no hormones (data not shown). In addition, some tumors expressed more than one hormone. Therefore, the *RbΔ19* model may be seen as representative of all types of pituitary tumors. We also had a minimum of 22 mice in each treatment group, which is adequate for statistical analysis. Treatment with 15 mg or 30 mg Cab/kg body weight (the latter dose has been used previously to treat cancers in mouse models (23, 79)) for two two-week regimens significantly extended the survival of the *RbΔ19* mice (**Figure 8**). Interestingly, the prolonged survival appeared to be dose-dependent (**Figure 8**). However, there was no statistically significant difference in survival between the two doses. Although two two-week treatments did not seem to have resulted in any side effects in WT mice, we did not investigate whether mice with pituitary tumors could tolerate long-term administration of this agent. Another limitation of our study was our inability to randomize mice with similar tumor sizes to different treatments. Due to the prohibitive cost associated with scanning a large number of mice, it was impossible for us to select mice with tumors of specific sizes. Our goal was to determine whether inhibition of angiogenesis by targeting the VEGF pathway could suppress pituitary tumor growth, and we were able to show that this was the case by demonstrating prolonged survival. We also showed that inhibition of angiogenesis can shrink or slow tumor growth but does not entirely eradicate tumors. However, in practice, tumor eradication is not necessary, as shrinking or even arresting tumor growth can preserve vision, prevent mass effect and is often adequate treatment. Therefore, if such therapy were to achieve these goals in humans with aggressive pituitary tumors, it could have a significant impact.

In summary, our data indicate that human pituitary tumors are characterized by upregulation of angiogenesis compared with normal pituitary glands. Our data also suggest that pituitary tumor angiogenesis may follow the well-established sprouting angiogenesis model. Furthermore, we identified PGF and VEGFC, but not VEGFA or VEGFB, as the major angiogenic growth factors regulating angiogenesis in human pituitary tumors. Finally, we demonstrate that targeting VEGF receptors, thus inhibiting angiogenesis significantly improves the survival of mice with pituitary tumors. Our data suggest that angiogenesis inhibition as a therapy for the treatment of aggressive human pituitary tumors merits further investigation.

DATA AVAILABILITY STATEMENT

The original contributions presented in the study are included in the article/**Supplementary Material**. Further inquiries can be directed to the corresponding author.

ETHICS STATEMENT

The studies involving human participants were reviewed and approved by Mass General Brigham Institutional Review Board. Written informed consent for participation was not required for this study in accordance with national legislation and institutional requirements. The animal study was reviewed and approved by the Massachusetts General Hospital Institutional Animal Care and Use Committee.

AUTHOR CONTRIBUTIONS

YZ and AK conceptualized and designed the study. JZ, YH, WZhu, CN, WZhao, and KL collected experimental data. AF, BS, EH-W, and PJ collected the tumor samples and clinical data. JZ, XZ, HL, XZ, and YZ analyzed and interpreted data. JZ and YZ wrote the first draft manuscript. AF, KM, and RS critically reviewed and edited the manuscript. RJS and AK provided study funding. All authors reviewed the results and approved the final version of the manuscript.

FUNDING

This work was supported in part by the National Institutes of Health (R01 CA193520 to AK and RS) and the Jarislowsky Foundation (AK).

SUPPLEMENTARY MATERIAL

The Supplementary Material for this article can be found online at: https://www.frontiersin.org/articles/10.3389/fonc.2022.875219/full#supplementary-material

REFERENCES

1. Melmed S. Pituitary-Tumor Endocrinopathies. *N Engl J Med* (2020) 382:937–50. doi: 10.1056/NEJMra1810772
2. Chen Y, Wang CD, Su ZP, Chen YX, Cai L, Zhuge QC, et al. Natural History of Postoperative Nonfunctioning Pituitary Adenomas: A Systematic Review and Meta-Analysis. *Neuroendocrinology* (2012) 96:333–42. doi: 10.1159/000339823
3. Nakano-Tateno T, Lau KJ, Wang J, McMahon C, Kawakami Y, Tateno T, et al. Multimodal Non-Surgical Treatments of Aggressive Pituitary Tumors. *Front Endocrinol (Lausanne)* (2021) 12:624686. doi: 10.3389/fendo.2021.624686
4. Castinetti F. Radiation Techniques in Aggressive Pituitary Tumours and Carcinomas. *Rev Endocr Metab Disord* (2020) 21:287–92. doi: 10.1007/s11154-020-09543-y
5. Parmar D, Apte M. Angiopoietin Inhibitors: A Review on Targeting Tumor Angiogenesis. *Eur J Pharmacol* (2021) 899:174021. doi: 10.1016/j.ejphar.2021.174021
6. Available at: www.cancer.gov/about-cancer/treatment/types/immunotherapy/angiogenesis-inhibitors-fact-sheet (Accessed November 11, 2021).
7. Guryanov I, Tennikova T, Urtti A. Peptide Inhibitors of Vascular Endothelial Growth Factor A: Current Situation and Perspectives. *Pharmaceutics* (2021) 13:1337–52. doi: 10.3390/pharmaceutics13091337
8. Lamb LS, Sim HW, McCormack AI. Exploring the Role of Novel Medical Therapies for Aggressive Pituitary Tumors: A Review of the Literature-"Are We There Yet?". *Cancers (Basel)* (2020) 12:308–32. doi: 10.3390/cancers12020308
9. Osterhage K, Rotermund R, Droste M, Dierlamm J, Saeger W, Petersenn S, et al. Bevacizumab in Aggressive Pituitary Adenomas - Experience With 3 Patients. *Exp Clin Endocrinol Diabetes* (2021) 129:178–85. doi: 10.1055/a-1260-3975
10. Carmeliet P. Mechanisms of Angiogenesis and Arteriogenesis. *Nat Med* (2000) 6:389–95. doi: 10.1038/74651
11. Folkman J. What Is the Evidence That Tumors Are Angiogenesis Dependent? *J Natl Cancer Inst* (1990) 82:4–6. doi: 10.1093/jnci/82.1.4
12. Zuazo-Gaztelu I, Casanovas O. Unraveling the Role of Angiogenesis in Cancer Ecosystems. *Front Oncol* (2018) 8:248. doi: 10.3389/fonc.2018.00248
13. Potente M, Gerhardt H, Carmeliet P. Basic and Therapeutic Aspects of Angiogenesis. *Cell* (2011) 146:873–87. doi: 10.1016/j.cell.2011.08.039
14. Carmeliet P, Jain RK. Molecular Mechanisms and Clinical Applications of Angiogenesis. *Nature* (2011) 473:298–307. doi: 10.1038/nature10144
15. Duran CL, Howell DW, Dave JM, Smith RL, Torrie ME, Essner JJ, et al. Molecular Regulation of Sprouting Angiogenesis. *Compr Physiol* (2017) 8:153–235. doi: 10.1002/cphy.c160048
16. Gerhardt H, Golding M, Fruttiger M, Ruhrberg C, Lundkvist A, Abramsson A, et al. VEGF Guides Angiogenic Sprouting Utilizing Endothelial Tip Cell Filopodia. *J Cell Biol* (2003) 161:1163–77. doi: 10.1083/jcb.200302047
17. Turner HE, Nagy Z, Gatter KC, Esiri MM, Harris AL, Wass JA. Angiogenesis in Pituitary Adenomas and the Normal Pituitary Gland. *J Clin Endocrinol Metab* (2000) 85:1159–62. doi: 10.1210/jcem.85.3.6485
18. McCabe CJ, Boelaert K, Tannahill LA, Heaney AP, Stratford AL, Khaira JS, et al. Vascular Endothelial Growth Factor, its Receptor KDR/Flk-1, and Pituitary Tumor Transforming Gene in Pituitary Tumors. *J Clin Endocrinol Metab* (2002) 87:4238–44. doi: 10.1210/jc.2002-020309
19. Xi Z, Jones PS, Mikamoto M, Jiang X, Faje AT, Nie C, et al. The Upregulation of Molecules Related to Tumor Immune Escape in Human Pituitary Adenomas. *Front Endocrinol* (2021) 12:726448. doi: 10.3389/fendo.2021.726448
20. Kubota Y, Kleinman HK, Martin GR, Lawley TJ. Role of Laminin and Basement Membrane in the Morphological Differentiation of Human Endothelial Cells Into Capillary-Like Structures. *J Cell Biol* (1988) 107:1589–98. doi: 10.1083/jcb.107.4.1589
21. Wimasis. (2016). *WimTube: Tube Formation Assay Image Analysis Solution. Release 4.0.* Available from: https://www.wimasis.com/en/products/13/WimTube
22. Marino S, Vooijs M, van der Gulden H, Jonkers J, Berns A. Induction of Medulloblastomas in P53-Null Mutant Mice by Somatic Inactivation of Rb in the External Granular Layer Cells of the Cerebellum. *Genes Dev* (2000) 14:994–1004. doi: 10.1101/gad.14.8.994
23. You WK, Sennino B, Williamson CW, Falcon B, Hashizume H, Yao LC, et al. VEGF and C-Met Blockade Amplify Angiogenesis Inhibition in Pancreatic Islet Cancer. *Cancer Res* (2011) 71:4758–68. doi: 10.1158/0008-5472.CAN-10-2527
24. Welti J, Loges S, Dimmeler S, Carmeliet P. Recent Molecular Discoveries in Angiogenesis and Antiangiogenic Therapies in Cancer. *J Clin Invest* (2013) 123:3190–200. doi: 10.1172/JCI70212
25. Herbert SP, Stainier DY. Molecular Control of Endothelial Cell Behaviour During Blood Vessel Morphogenesis. *Nat Rev Mol Cell Biol* (2011) 12:551–64. doi: 10.1038/nrm3176
26. Hicklin DJ, Ellis LM. Role of the Vascular Endothelial Growth Factor Pathway in Tumor Growth and Angiogenesis. *J Clin Oncol* (2005) 23:1011–27. doi: 10.1200/JCO.2005.06.081
27. Gianni-Barrera R, Trani M, Reginato S, Banfi A. To Sprout or to Split? VEGF, Notch and Vascular Morphogenesis. *Biochem Soc Trans* (2011) 39:1644–8. doi: 10.1042/BST20110650
28. Siekmann AF, Affolter M, Belting HG. The Tip Cell Concept 10 Years After: New Players Tune in for a Common Theme. *Exp Cell Res* (2013) 319:1255–63. doi: 10.1016/j.yexcr.2013.01.019
29. Simons M, Gordon E, Claesson-Welsh L. Mechanisms and Regulation of Endothelial VEGF Receptor Signalling. *Nat Rev Mol Cell Biol* (2016) 17:611–25. doi: 10.1038/nrm.2016.87
30. Fagiani E, Christofori G. Angiopoietins in Angiogenesis. *Cancer Lett* (2013) 328:18–26. doi: 10.1016/j.canlet.2012.08.018
31. Heldin CH. Targeting the PDGF Signaling Pathway in Tumor Treatment. *Cell Commun Signal* (2013) 11:97. doi: 10.1186/1478-811X-11-97
32. Jin Y, Kaluza D, Jakobsson L. VEGF, Notch and TGFbeta/BMPs in Regulation of Sprouting Angiogenesis and Vascular Patterning. *Biochem Soc Trans* (2014) 42:1576–83. doi: 10.1042/BST20140231
33. Zegeye MM, Andersson B, Sirsjo A, Ljungberg LU. IL-6 Trans-Signaling Impairs Sprouting Angiogenesis by Inhibiting Migration, Proliferation and Tube Formation of Human Endothelial Cells. *Cells* (2020) 9:1414–27. doi: 10.3390/cells9061414
34. Lertkiatmongkol P, Liao D, Mei H, Hu Y, Newman PJ. Endothelial Functions of Platelet/Endothelial Cell Adhesion Molecule-1 (CD31). *Curr Opin Hematol* (2016) 23:253–9. doi: 10.1097/MOH.0000000000000239
35. Burrows FJ, Derbyshire EJ, Tazzari PL, Amlot P, Gazdar AF, King SW, et al. Up-Regulation of Endoglin on Vascular Endothelial Cells in Human Solid Tumors: Implications for Diagnosis and Therapy. *Clin Cancer Res* (1995) 1:1623–34.
36. Castellani P, Viale G, Dorcaratto A, Nicolo G, Kaczmarek J, Querze G, et al. The Fibronectin Isoform Containing the ED-B Oncofetal Domain: A Marker of Angiogenesis. *Int J Cancer* (1994) 59:612–8. doi: 10.1002/ijc.2910590507
37. Rakocevic J, Orlic D, Mitrovic-Ajtic O, Tomasevic M, Dobric M, Zlatic N, et al. Endothelial Cell Markers From Clinician's Perspective. *Exp Mol Pathol* (2017) 102:303–13. doi: 10.1016/j.yexmp.2017.02.005
38. Podgrabinska S, Braun P, Velasco P, Kloos B, Pepper MS, Skobe M. Molecular Characterization of Lymphatic Endothelial Cells. *Proc Natl Acad Sci USA* (2002) 99:16069–74. doi: 10.1073/pnas.242401399
39. Thomas M, Augustin HG. The Role of the Angiopoietins in Vascular Morphogenesis. *Angiogenesis* (2009) 12:125–37. doi: 10.1007/s10456-009-9147-3
40. Stoeltzing O, Ahmad SA, Liu W, McCarty MF, Wey JS, Parikh AA, et al. Angiopoietin-1 Inhibits Vascular Permeability, Angiogenesis, and Growth of Hepatic Colon Cancer Tumors. *Cancer Res* (2003) 63:3370–7.
41. Fiedler U, Scharpfenecker M, Koidl S, Hegen A, Grunow V, Schmidt JM, et al. The Tie-2 Ligand Angiopoietin-2 is Stored in and Rapidly Released Upon Stimulation From Endothelial Cell Weibel-Palade Bodies. *Blood* (2004) 103:4150–6. doi: 10.1182/blood-2003-10-3685
42. del Toro R, Prahst C, Mathivet T, Siegfried G, Kaminker JS, Larrivee B, et al. Identification and Functional Analysis of Endothelial Tip Cell-Enriched Genes. *Blood* (2010) 116:4025–33. doi: 10.1182/blood-2010-02-270819
43. Hellberg C, Ostman A, Heldin CH. PDGF and Vessel Maturation. *Recent Result Cancer Res* (2010) 180:103–14. doi: 10.1007/978-3-540-78281-0_7
44. Pardali E, Goumans MJ, ten Dijke P. Signaling by Members of the TGF-Beta Family in Vascular Morphogenesis and Disease. *Trends Cell Biol* (2010) 20:556–67. doi: 10.1016/j.tcb.2010.06.006
45. Schito L, Semenza GL. Hypoxia-Inducible Factors: Master Regulators of Cancer Progression. *Trends Cancer* (2016) 2:758–70. doi: 10.1016/j.trecan.2016.10.016

46. Morfoisse F, Kuchnio A, Frainay C, Gomez-Brouchet A, Delisle MB, Marzi S, et al. Hypoxia Induces VEGF-C Expression in Metastatic Tumor Cells *via* a HIF-1alpha-Independent Translation-Mediated Mechanism. *Cell Rep* (2014) 6:155–67. doi: 10.1016/j.celrep.2013.12.011
47. Kumra H, Reinhardt DP. Fibronectin-Targeted Drug Delivery in Cancer. *Advance Drug Delivery Rev* (2016) 97:101–10. doi: 10.1016/j.addr.2015.11.014
48. Benton G, Arnaoutova I, George J, Kleinman HK, Koblinski J. Matrigel: From Discovery and ECM Mimicry to Assays and Models for Cancer Research. *Advance Drug Deliv Rev* (2014) 79-80:3–18. doi: 10.1016/j.addr.2014.06.005
49. Ilie MD, Vasiljevic A, Raverot G, Bertolino P. The Microenvironment of Pituitary Tumors-Biological and Therapeutic Implications. *Cancers (Basel)* (2019) 11:1605–26. doi: 10.3390/cancers11101605
50. Marques P, Grossman AB, Korbonits M. The Tumour Microenvironment of Pituitary Neuroendocrine Tumours. *Front Neuroendocrinol* (2020) 58:100852. doi: 10.1016/j.yfrne.2020.100852
51. Jiang X, Wang J, Deng X, Xiong F, Zhang S, Gong Z, et al. The Role of Microenvironment in Tumor Angiogenesis. *J Exp Clin Cancer Res* (2020) 39:204. doi: 10.1186/s13046-020-01709-5
52. Wilhelm SM, Dumas J, Adnane L, Lynch M, Carter CA, Schutz G, et al. Regorafenib (BAY 73-4506): A New Oral Multikinase Inhibitor of Angiogenic, Stromal and Oncogenic Receptor Tyrosine Kinases With Potent Preclinical Antitumor Activity. *Int J Cancer* (2011) 129:245–55. doi: 10.1002/ijc.25864
53. Korsisaari N, Ross J, Wu X, Kowanetz M, Pal N, Hall L, et al. Blocking Vascular Endothelial Growth Factor-A Inhibits the Growth of Pituitary Adenomas and Lowers Serum Prolactin Level in a Mouse Model of Multiple Endocrine Neoplasia Type 1. *Clin Cancer Res* (2008) 14:249–58. doi: 10.1158/1078-0432.CCR-07-1552
54. Luque GM, Perez-Millan MI, Ornstein AM, Cristina C, Becu-Villalobos D. Inhibitory Effects of Antivascular Endothelial Growth Factor Strategies in Experimental Dopamine-Resistant Prolactinomas. *J Pharmacol Exp Ther* (2011) 337:766–74. doi: 10.1124/jpet.110.177790
55. Chauvet N, Romano N, Lafont C, Guillou A, Galibert E, Bonnefont X, et al. Complementary Actions of Dopamine D2 Receptor Agonist and Anti-Vegf Therapy on Tumoral Vessel Normalization in a Transgenic Mouse Model. *Int J Cancer* (2017) 140:2150–61. doi: 10.1002/ijc.30628
56. Zhou Y, Zhang X, Klibanski A. Genetic and Epigenetic Mutations of Tumor Suppressive Genes in Sporadic Pituitary Adenoma. *Mol Cell Endocrinol* (2014) 386:16–33. doi: 10.1016/j.mce.2013.09.006
57. Lines KE, Stevenson M, Thakker RV. Animal Models of Pituitary Neoplasia. *Mol Cell Endocrinol* (2016) 421:68–81. doi: 10.1016/j.mce.2015.08.024
58. Stefaneanu L, Rindi G, Horvath E, Murphy D, Polak JM, Kovacs K. Morphology of Adenohypophysial Tumors in Mice Transgenic for Vasopressin-SV40 Hybrid Oncogene. *Endocrinology* (1992) 130:1789–95. doi: 10.1210/endo.130.4.1312426
59. Kumar TR, Graham KE, Asa SL, Low MJ. Simian Virus 40 T Antigen-Induced Gonadotroph Adenomas: A Model of Human Null Cell Adenomas. *Endocrinology* (1998) 139:3342–51. doi: 10.1210/endo.139.7.6100
60. Takada K, Yamada S, Teramoto A. Correlation Between Tumor Vascularity and Clinical Findings in Patients With Pituitary Adenomas. *Endocr Pathol* (2004) 15:131–9. doi: 10.1385/EP:15:2:131
61. Perez-Millan MI, Berner SI, Luque GM, De Bonis C, Sevlever G, Becu-Villalobos D, et al. Enhanced Nestin Expression and Small Blood Vessels in Human Pituitary Adenomas. *Pituitary* (2013) 16:303–10. doi: 10.1007/s11102-012-0421-9
62. Rotondo F, Sharma S, Scheithauer BW, Horvath E, Syro LV, Cusimano M, et al. Endoglin and CD-34 Immunoreactivity in the Assessment of Microvessel Density in Normal Pituitary and Adenoma Subtypes. *Neoplasma* (2010) 57:590–3. doi: 10.4149/neo_2010_06_590
63. Di Michele J, Rotondo F, Kovacs K, Syro LV, Yousef GM, Cusimano MD, et al. Vasculogenic Mimicry in Clinically Non-Functioning Pituitary Adenomas: A Histologic Study. *Pathol Oncol Res* (2017) 23:803–9. doi: 10.1007/s12253-017-0196-4
64. Cristina C, Perez-Millan MI, Luque G, Dulce RA, Sevlever G, Berner SI, et al. VEGF and CD31 Association in Pituitary Adenomas. *Endocr Pathol* (2010) 21:154–60. doi: 10.1007/s12022-010-9119-6
65. Lohela M, Bry M, Tammela T, Alitalo K. VEGFs and Receptors Involved in Angiogenesis Versus Lymphangiogenesis. *Curr Opin Cell Biol* (2009) 21:154–65. doi: 10.1016/j.ceb.2008.12.012
66. Maslowska K, Halik PK, Tymecka D, Misicka A, Gniazdowska E. The Role of VEGF Receptors as Molecular Target in Nuclear Medicine for Cancer Diagnosis and Combination Therapy. *Cancers (Basel)* (2021) 13:1072–117. doi: 10.3390/cancers13051072
67. Shaik F, Cuthbert GA, Homer-Vanniasinkam S, Muench SP, Ponnambalam S, Harrison MA. Structural Basis for Vascular Endothelial Growth Factor Receptor Activation and Implications for Disease Therapy. *Biomolecules* (2020) 10:1673–97. doi: 10.3390/biom10121673
68. Miller B, Sewell-Loftin MK. Mechanoregulation of Vascular Endothelial Growth Factor Receptor 2 in Angiogenesis. *Front Cardiovasc Med* (2021) 8:804934. doi: 10.3389/fcvm.2021.804934
69. Secker GA, Harvey NL. Regulation of VEGFR Signalling in Lymphatic Vascular Development and Disease: An Update. *Int J Mol Sci* (2021) 22:7760–75. doi: 10.3390/ijms22147760
70. Carmeliet P, Moons L, Luttun A, Vincenti V, Compernolle V, De Mol M, et al. Synergism Between Vascular Endothelial Growth Factor and Placental Growth Factor Contributes to Angiogenesis and Plasma Extravasation in Pathological Conditions. *Nat Med* (2001) 7:575–83. doi: 10.1038/87904
71. Autiero M, Waltenberger J, Communi D, Kranz A, Moons L, Lambrechts D, et al. Role of PlGF in the Intra- and Intermolecular Cross Talk Between the VEGF Receptors Flt1 and Flk1. *Nat Med* (2003) 9:936–43. doi: 10.1038/nm884
72. Sainz-Jaspeado M, Claesson-Welsh L. Cytokines Regulating Lymphangiogenesis. *Curr Opin Immunol* (2018) 53:58–63. doi: 10.1016/j.coi.2018.04.003
73. Tammela T, Zarkada G, Wallgard E, Murtomaki A, Suchting S, Wirzenius M, et al. Blocking VEGFR-3 Suppresses Angiogenic Sprouting and Vascular Network Formation. *Nature* (2008) 454:656–60. doi: 10.1038/nature07083
74. Tammela T, Zarkada G, Nurmi H, Jakobsson L, Heinolainen K, Tvorogov D, et al. VEGFR-3 Controls Tip to Stalk Conversion at Vessel Fusion Sites by Reinforcing Notch Signalling. *Nat Cell Biol* (2011) 13:1202–13. doi: 10.1038/ncb2331
75. Jerafi-Vider A, Bassi I, Moshe N, Tevet Y, Hen G, Splittstoesser D, et al. VEGFC/FLT4-Induced Cell-Cycle Arrest Mediates Sprouting and Differentiation of Venous and Lymphatic Endothelial Cells. *Cell Rep* (2021) 35:109255. doi: 10.1016/j.celrep.2021.109255
76. Macarulla T, Montagut C, Sanchez-Martin FJ, Granja M, Verdaguer H, Sastre J, et al. The Role of PIGF Blockade in the Treatment of Colorectal Cancer: Overcoming the Pitfalls. *Expert Opin Biol Ther* (2020) 20:15–22. doi: 10.1080/14712598.2020.1677603
77. Hu-Lowe DD, Zou HY, Grazzini ML, Hallin ME, Wickman GR, Amundson K, et al. Nonclinical Antiangiogenesis and Antitumor Activities of Axitinib (AG-013736), an Oral, Potent, and Selective Inhibitor of Vascular Endothelial Growth Factor Receptor Tyrosine Kinases 1, 2, 3. *Clin Cancer Res* (2008) 14:7272–83. doi: 10.1158/1078-0432.CCR-08-0652
78. Leung SW, Wloga EH, Castro AF, Nguyen T, Bronson RT, Yamasaki L. A Dynamic Switch in Rb+/- Mediated Neuroendocrine Tumorigenesis. *Oncogene* (2004) 23:3296–307. doi: 10.1038/sj.onc.1207457
79. Torres KE, Zhu QS, Bill K, Lopez G, Ghadimi MP, Xie X, et al. Activated MET is a Molecular Prognosticator and Potential Therapeutic Target for Malignant Peripheral Nerve Sheath Tumors. *Clin Cancer Res* (2011) 17:3943–55. doi: 10.1158/1078-0432.CCR-11-0193

Conflict of Interest: The authors declare that the research was conducted in the absence of any commercial or financial relationships that could be construed as a potential conflict of interest.

Citation: *Zhou J, Hu Y, Zhu W, Nie C, Zhao W, Faje AT, Labelle KE, Swearingen B, Lee H, Hedley-Whyte ET, Zhang X, Jones PS, Miller KK, Klibanski A, Zhou Y and Soberman RJ (2022) Sprouting Angiogenesis in Human Pituitary Adenomas.*
Front. Oncol. 12:875219. doi: 10.3389/fonc.2022.875219

frontiers | Frontiers in Oncology

ORIGINAL RESEARCH
published: 13 May 2022
doi: 10.3389/fonc.2022.875122

High Histone Deacetylase 2/3 Expression in Non-Functioning Pituitary Tumors

Wenxiu Zhao[1†‡], Xiaobin Jiang[1†‡], Karrin Weisenthal[1†], Jun Ma[1], Erin M. Botticelli[1], Yunli Zhou[1], E. Tessa Hedley-Whyte[2], Baiyao Wang[1†], Brooke Swearingen[3], Roy J. Soberman[4], Anne Klibanski[1] and Xun Zhang[1]*

[1] Neuroendocrine Unit, Massachusetts General Hospital and Harvard Medical School, Boston, MA, United States,
[2] Neuropathology Unit, Massachusetts General Hospital and Harvard Medical School, Boston, MA, United States,
[3] Neurosurgical Service, Massachusetts General Hospital and Harvard Medical School, Boston, MA, United States,
[4] Nephrology Division, Massachusetts General Hospital and Harvard Medical School, Boston, MA, United States

Epigenetic modification of chromatin is involved in non-malignant pituitary neoplasia by causing abnormal expression of tumor suppressors and oncogenes. These changes are potentially reversible, suggesting the possibility of targeting tumor cells by restoring the expression of epigenetically silenced tumor suppressors. The role of the histone deacetylase (HDAC) family in pituitary tumorigenesis is not known. We report that HDAC2 and 3, Class I HDAC members, are highly expressed in clinically non-functioning pituitary adenomas (NFPAs) compared to normal pituitary (NP) samples as determined by RT-PCR and immunohistochemical staining (IHC). Treatment of a human NFPA derived folliculostellate cell line, PDFS, with the HDAC3 inhibitor RGFP966 for 96 hours resulted in inhibition of cell proliferation by 70%. Furthermore, the combination of RGFP966 with a methyltransferase/DNMT inhibitor, 5'-aza-2'-deoxycytidine, led to the restoration of the expression of several tumor suppressor genes, including STAT1, P16, PTEN, and the large non-coding RNA tumor suppressor MEG3, in PDFS cells. Our data support the hypothesis that both histone modification and DNA methylation are involved in the pathogenesis of human NFPAs and suggest that targeting HDACs and DNA methylation can be incorporated into future therapies.

Keywords: human clinically non-functioning pituitary adenomas, class I histone deacetylases, growth suppression, epigenetic modifications, regulation of tumor suppressor expressions

OPEN ACCESS

Edited by:
Zhe Bao Wu,
Shanghai Jiao Tong University, China

Reviewed by:
Lei Cao,
Capital Medical University, China
Anne Wierinckx,
Université Claude Bernard Lyon 1, France

***Correspondence:**
Xun Zhang
xzhang5@mgh.harvard.edu

***Present addresses:**
Wenxiu Zhao, Cardiovascular Division, Brigham and Women's Hospital and Harvard Medical School, Boston, MA, United States
Xiaobing Jiang, Department of Neurosurgery, Sun Yat-Sen University Cancer Center, State Key Laboratory of Oncology in South China, Guangzhou, China
Karrin Weisenthal, Emergency Medicine, Boston Medical Center, One Boston Medical Center Place, Boston, MA, United States
Baiyao Wang, Department of Radiation Oncology, Affiliated Cancer Hospital and Institute of Guangzhou Medical University, Guangzhou, China

‡*These authors have contributed equally to this work*

Specialty section:
This article was submitted to Neuro-Oncology and Neurosurgical Oncology, a section of the journal Frontiers in Oncology

Received: *13 February 2022*
Accepted: *13 April 2022*
Published: *13 May 2022*

INTRODUCTION

Pituitary adenomas are one of the most common intracranial neoplasms, comprising approximately 10% of all surgically resected intracranial tumors, with a prevalence of 22.5% in the general population (1). Cross-sectional studies have shown that the prevalence of symptomatic pituitary adenomas ranges from 7.76 in 10,000 to 9.4 per 10,000 individuals (2, 3). Non-functioning pituitary adenomas (NFPAs) that do not secrete hormones are common and are mainly derived from gonadotroph cells. The majority of these tumors are benign. However, patients can experience increased morbidity due to mass effect, causing neurologic complications, and a subset are aggressive (4–6). These tumors are

routinely treated with surgery and radiation. However, a subset of these requires additional therapies, such as temozolomide. The vast majority of these tumors escape from these temozolomide, and additional options are needed (7). There are no effective or FDA-approved pharmacologic therapies to treat these tumors. Therefore, it is critical to identify novel targets in NFPAs for the future development of medical therapy.

In sporadic pituitary adenomas, genetic mutations of oncogenes or tumor suppressors are extremely rare, and epigenetic dysregulation is the major factor dictating the expression of multiple tumor suppressor genes (8, 9). Studies have focused on how aberrant hypermethylation of CpG islands within promoters contributes to the inactivation of several important genes, including *RB1*, *CDKN1A(P21)*, *CDKN2A*, *CDKN2B*, *GADD45γ*, and *MEG3* (9). The role of histone modification, though firmly linked to the genesis of other tumors such as breast and colorectal cancer, has not been explored in pituitary tumorigenesis, especially in NFPAs.

Histone deacetylases (HDACs) are responsible for removal of acetyl groups from specific lysine residues located within the protein tails of histones (10, 11) as well as many non-histone proteins, including transcription factors (10, 11). The family of Class I HDAC includes HDAC1, HDAC2, HDAC3, and HDAC8. HDAC2 and HDAC3 are important for control of cell cycle regulation, cardiac function, and neural cell regulation (12, 13). Abnormal expression of HDAC1 has been reported in breast, gastric, colon, liver, renal and prostate carcinomas (14–16). High levels of HDAC2 expression have been shown in cervical, gastric (17, 18), breast, and other cancer types (16, 19). In addition, high levels of HDAC3 expression have been reported in colon cancer (20). Furthermore, the expression of HDAC1 has been reported to correlate with the progression and prognosis of gastrointestinal malignancies (21, 22); and HDAC3 also has been suggested as a prognostic marker in gastric (21), colorectal (23), and pancreatic cancer (24). *In vitro* experiments have shown that high levels of HDAC1 expression promotes migration and invasion of gallbladder (25) and breast tumor cell lines (26). Similarly, overexpression of HDAC2 has been shown to promote the migration and invasion of non-small cell lung cancer cell lines (27), and overexpression of HDAC3 has been reported to promote the proliferation of cholangiocarcinoma and pancreatic cancer cell lines (28, 29). Therefore, there is compelling evidence that high levels of HDAC1, 2 and 3 expression is implicated in the pathogenesis of several malignant tumors. However, there is no reported link between Class I HDAC and benign tumors such as NFPAs.

Because there is no reliably effective medical therapy for human clinically non-functioning pituitary adenomas, we focused our study on this type of pituitary tumor. We hypothesized that Class I HDAC RNA levels would be higher in NFPAs compared with normal human pituitary samples. We found that HDAC3 and HDAC2 RNA, but not HDAC1 RNA, were significantly higher in NFPAs compared to normal human pituitaries; increased HDAC3 protein expression was also confirmed by immunohistochemical (IHC) staining. The HDAC3-specific inhibitor RGFP966 suppressed PFDS [a folliculostellate cell line derived from a human NFPA (30),] cell proliferation by 70% at 96 hours after treatment. Treatment of PDFS cells with RGFP966 restored expression of MEG3, a long non-coding RNA tumor suppressor, whose expression is lost in NFPAs but not in hormone secreting pituitary adenomas (9). Furthermore, the combination of the DNA methyltransferase (DNMT) inhibitor 5'-aza-2'-deoxycytidine (5'-AZA) with RGFP966 further enhanced MEG3 expression and also activated expression of several well-known tumor suppressors including P16, PTEN, and STAT1. Therefore, we demonstrate that suppression of histone deacetylation and DNA methylation restores epigenetically silenced tumor suppressors such as MEG3, P16, PTEN and STAT1, resulting in inhibition of tumor cell growth. This study suggests HDAC3 inhibition may be a potential therapeutic approach for NFPAs.

MATERIAL AND METHODS

Tissue and Tumor Samples

Twenty-two human NFPA, as well as six GH-secreting, six ACTH-secreting, and six PRL-secreting human pituitary adenoma surgical samples were obtained at Massachusetts General Hospital and used for RT-PCR analysis. The diagnosis of NFPA was established by clinical, biochemical, and radiological findings and was confirmed by immunohistochemistry after surgery. Human pituitary tumors were collected in 0.9% saline after transsphenoidal surgery and immediately frozen in liquid nitrogen before analysis. Eleven normal human pituitary glands were obtained 2-16 hours postmortem from the Harvard Tissue Resource Center (Belmont, MA). This study was approved by the Partners Human Research Committee. Immunohistochemical staining on pituitary tumor slides was performed by Pathology Department of Massachusetts General Hospital on formalin-fixed, paraffin embedded sections for FSHβ, LHβ, TSHβ, prolactin, GH, ACTH, and glycoprotein hormone α-subunit, to confirm the tumor identities.

RNA Extraction, cDNA Synthesis and Quantitative Real-Time PCR

Total RNA was isolated using the RNeasy Mini Kit (QIAGEN, USA) according to the manufacturer's instructions. Extracted RNA samples were treated with DNase I to remove potential DNA contamination. One microgram of total RNA was subjected to reverse transcription using a ProtoScript®M-MuLV first-strand cDNA synthesis kit (New England Bio-Labs, Ipswich, MA, USA). All PCR reactions were performed in triplicate with an Applied Biosystems® 7500 Fast Thermocycler (Foster City, CA, USA) with the following protocol: 50°C for 2 minutes, 95°C for 5 minutes, followed by 40 cycles of 95°C for 30 seconds and 60°C for 1 minute. Melting curve analysis was performed and a no-template control was included in every qPCR using Invitrogen SYBR®PCR Master Mix (Thermo Fisher, Waltham, MA, USA). GADPH was used as internal controls. Expression levels for tested genes were calculated using the formula $2^{-\triangle Ct}$. The fold changes were determined by $2^{-\triangle\triangle Ct}$. The relative tumor expression levels for

genes were calculated by normalizing the value from the tumor against the mean average of values from the 11 normal pituitaries. Primers used in this study are listed in **Table S1**.

Immunohistochemistry Staining

A tissue microarray (TMA) containing 12 human NFPAs and 4 normal human pituitaries, which were distinct from the samples used in qRT-PCR, was constructed by the Department of Pathology Service Core Facility of Massachusetts General Hospital, and 4 μm sections were prepared from the TMA. Immunohistochemical staining was performed as previously described (25), with mouse monoclonal anti-HDAC3 (Abcam, ab219376, Cambridge, MA, USA) at 1:1000 dilution, or anti-HDAC2 (Abcam, ab16032) at 1:500 dilution. HDAC3/HDAC2 staining was considered positive only when showing definitive staining of tumor nuclei. Replacement of a primary antibody with PBS served as the negative control. Positive HDAC3/HDAC2 staining was assessed microscopically in 10 high-powered fields (×200) and quantified on the basis of the color intensity of photos (40x) converted to CYMK and split into green/red/yellow/blue channels. To collect data,100 nuclei were selected and averaged using CellProfiler3.0.0 software (Broad institute, Cambridge, MA, USA, http://cellprofiler.org/).

PDFS Cell Culture and Treatment With Inhibitors

The pituitary tumor-derived folliculostellate cell (PDFS) line (30) was maintained in DMEM (Life Technologies) supplemented with 10% FBS, 1% NEAA and PSG at 37°C with 10% CO_2. DNA methyltransferase inhibitor 5'-aza-2'-deoxycytidine (5'-AZA) was purchased from Sigma-Aldrich (Allentown, PA, USA). The HDAC3-specific inhibitor RGFP966 was purchased from Selleckchem (Houston, TX, USA) (31). To examine the effect of HDAC inhibition on the growth of PDFS, $1x10^6$ PDFS cells were plated on 100 mm cell culture dishes. After 24 hours, cells were treated with 10μM RGFP966 and/or 1μM 5'-AZA; with DMSO as a control. Culture medium was changed daily with fresh drug added. RNA was extracted from cells at Day 5. Cell proliferation was monitored at 24, 48, 72, and 96 hours by CCK8 Assay (see below).

Cell Growth (CCK8 Assay)

Cell proliferation was evaluated by a CCK8 Assay (Dojindo Molecular Technologies, Rockville, MD, USA). PDFS cells were plated into a 96-well plate in triplicate, with 100 l μL cell suspension (2000 cells/well) in each well. Cells were incubated for 24 hours at 37C, with 10% CO2, before the treatment drug was added. At each time point, 10 μL of CCK-8 Solution was added to each well of the plate. The plates were further incubated for 4 hours. The absorbance at 450 nm was measured using a Versamax Tunable Microplate Reader (Molecular Devices, San Jose, CA, USA). The experiment was repeated three times.

Statistical Analysis

Differences between quantitative parameters were expressed as mean ± SD (normal distribution) or medians with inter-quartile range (IQR). The statistical significance of gene expression was assessed by a two-tailed Student *t* tests. Associations between clinical, biological, imaging and HDAC3 expression were evaluated by Spearman's correlations, χ^2 tests, or Fisher's exact tests. A $p < 0.05$ was considered statistically significant. All statistical analyses were performed with Prism 6 (GraphPad Software, La Jolla, CA, USA).

RESULTS

Expression of HDAC2 and HDAC3 in NFPAs

We detected the expression of HDAC2 and HDAC3 in 22 human NFPA specimens and 11 normal pituitary specimens by qRT-PCR. As shown in **Figure 1A**, higher HDAC2 and HDAC3 mRNA expression was observed in 82% of NFPAs. When compared to the average HDAC3 mRNA level in the normal pituitary, there was a 64-fold higher HDAC3 mRNA expression in NFPAs (**Figures 1A, B**, 64.0 ± 20.5, $p < 0.0001$). The average HDAC2 mRNA level in NFPAs was by 45-fold higher than in the normal pituitary samples (**Figure 1B**, 44.7 ± 15.5, $p < 0.001$). HDAC1 mRNA expression was also observed by qRT-PCR; but there was no significant difference in its expression levels between NFPAs and the normal pituitary samples (**Figures 1A, B**). No HDAC8 expression was detected in either NFPAs or normal pituitaries (data not shown). Immunohistochemical staining revealed higher nuclear staining of HDAC3 protein in NFPAs compared with the HDAC3 staining in normal pituitary (**Figure 2A**), The HDAC3 staining results were quantified on the basis of color intensity (**Figure 2B**). Similar results were observed for HDAC2 immunostaining (**Figures 2C, D**). These findings demonstrate the upregulation of HDAC3 and HDAC2 in NFPAs.

HDAC2 and HDAC3 Expression in Hormone-Secreting Pituitary Adenomas

We also examined HDAC1, HDAC2, and HDAC3 expression by qRT-PCR in six GH-secreting, six ACTH-secreting, and six PRL-secreting human pituitary adenomas. Increased mRNA expression of Class I HDAC members was also found in a limited number of hormone-secreting human pituitary adenomas (**Figure 3**), although no statistically significant difference was found in RNA expression levels between normal human pituitaries and hormone-secreting pituitary tumors. Because the increase of HDAC2 and HDAC3 levels in pituitary tumors were similar, and there is no HDAC2-specific inhibitor available, we decided to focus our subsequent studies on HDAC3.

HDAC3 Inhibitor RGFP966 Suppressed PDFS Cell Growth

Because the high expression of HDAC3 RNA and protein in NFPAs suggested that HDACs could play a role in tumorigenesis of NFPAs, we examined whether RGFP966 (31), a specific HDAC3 inhibitor, could inhibit proliferation of PDFS; which also showed very high levels of HDAC3 expression (**Figure 4A**) compared with normal pituitary. Treatment of PDFS cells with

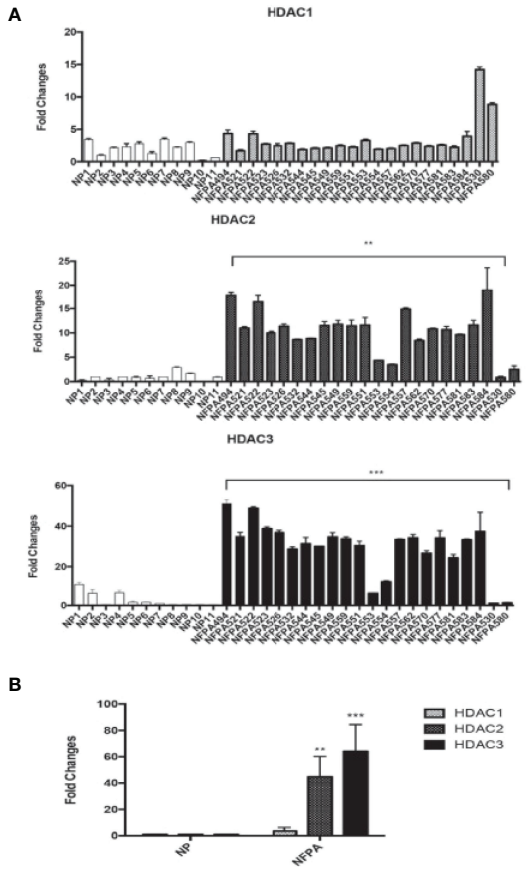

FIGURE 1 | HDAC1, 2, and HDAC3 mRNA expression in human NFPAs. **(A)** HDAC1 (Upper Panel), HDAC 2 (Middle Panel), and HDAC 3 (Bottom Panel) RNA expression were determined by qRT-PCR in 22 non-functioning pituitary adenomas. **(B)** The average expression levels of HDAC1, 2, and 3 mRNA in NFPAs compared to the average level in the normal pituitaries. Fold changes were determined by comparing the HDAC levels in tumors with that in normal pituitaries (NP, n = 11), which was set as 1. NFPA, non-functioning pituitary adenoma; **P < 0.001; ***P < 0.0001.

10 μM RGFP966 suppressed cell proliferation by 64 ± 2.8%, 55.2 ± 2.3%, and 72.1 ± 1.2% ($p<0.01$) at 48, 72, and 96 hours, respectively, comparing with PDFS treated with DMSO (**Figure 4C**). We also found that 5'-aza-2'-deoxycytidine (5'-AZA), a demethylation reagent, was also able to suppress proliferation of PDFS, although its effect was not as strong as RGFP966. As shown in **Figures 4B, C**, treatment of PDFS cells with 1 μM of 5'-AZA suppressed cell proliferation by and 41.3 ± 2.8%, 21.9 ± 4.8%, and 42 ± 3.5% at 48, 72, and 96 hours, respectively. A synergistic effect was observed when RGFP966 was combined with 5'-AZA, suppressing PDFS proliferation by 61.4 ± 2.4%, 82 ± 4.3% ($p<0.001$), and 92 ± 6.1% ($p<0.001$) at 48, 72, and 96 hours, respectively (**Figures 4B, C**).

Restoration of MEG3 Expression by HDAC3 Inhibition and DNA Demethylation

MEG3 is a large non-coding RNA (lncRNA) tumor suppressor whose expression is lost in NFPAs (32). PDFS cells lack expression of MEG3 due to gene silencing by DNA methylation (33, 34). To understand the molecular events related to growth suppression by RGFP966 and 5'-AZA, we examined the expression of MEG3 in PDFS cells treated with RGFP966 and 5'-AZA. As shown in **Table 1**, treatment of PDFS cells with 10 μM RGFP966 resulted in a 9-fold increase in MEG3 RNA expression compared to untreated cells. The demethylation reagent 5'-AZA (1μM) increased MEG3 RNA expression by approximately 28,000-fold. When RGFP966 and 5'-AZA were used together, MEG3 RNA expression increased by almost 140,000-fold compared to controls, confirming the synergistic effect of RGFP966 and 5'-AZA (**Table 1**).

Activation of the Retinoblastoma Pathway and Other Tumor Suppressors

RGFP966 functioned as a strong growth suppressor, but a weak inducer for MEG3 RNA. However, the demethylation reagent 5'-AZA was a strong inducer of MEG3 expression but a weak growth suppressor (**Figure 4** and **Table 1**). These data suggest that RGFP966 may also affect expression of additional tumor suppressors. It has been reported that the signaling pathways of retinoblastoma (Rb) have been compromised in human NFPAs (9). As shown in **Figure 5A**, treatment of PDFS cells with RGFP966 significantly increased the mRNA expression of two important components of Rb pathway, $p16^{ink4a}$ and E2F1, by 3.4- and 3.2-fold, respectively. Consistent with its strong growth suppressive function, RGFP966 was more potent than 5'-AZA in inducing $p16^{ink4a}$ and E2F1 mRNA expression, thus activating Rb signaling pathway. Treatment of PDFS cells with RGFP966 and 5'-AZA also significantly increased the mRNA expression of other tumor suppressors, including EGR1, PTEN, STAT1, and immune stimulatory receptor CD40 (**Figures 5B, C**). We also detected an increase in mRNA expressions of cell cycle related genes, such as *CCNB1*, *CDK1*, and *TSC1*, and transcriptional factors, such as C-Jun and C-Myc, upon RGFP966 and 5'-AZA treatment (**Table 2**). Therefore, change of chromosomal modifications in PDFS cells by HDAC3 inhibition and DNA demethylation led to activation of multiple tumor suppressors, resulting in growth suppression.

DISCUSSION

In this study, we investigated the expression of Class I HDAC family members in human NFPAs. We found a 40-60 fold elevation of the expression of HDAC2 and HDAC3 mRNA in NFPAs compared to normal pituitaries, suggesting their involvement in the pathogenesis of NFPAs. Increased mRNA expression of Class I HDAC members was also found in a limited number of hormone-secreting human pituitary adenomas, although no statistically significant difference was observed between hormone-secreting pituitary tumors and normal pituitaries. Further studies with a large number of such tumors are needed to verify this observation. Histone modification and abnormal expression of HDAC family members have been shown to be involved in the pathogenesis of many different human cancers. HDAC3 expression is not only elevated in these

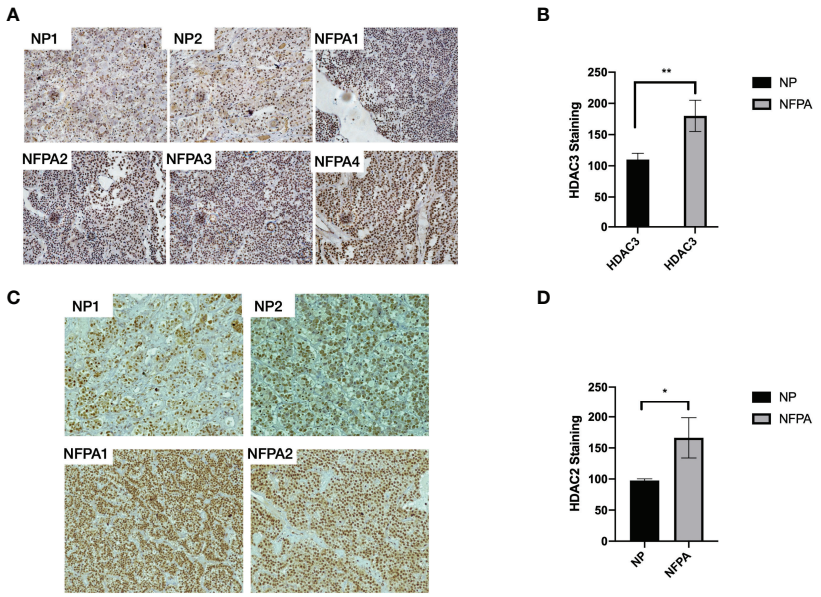

FIGURE 2 | HDAC3 protein staining in normal human pituitaries and NFPAs. **(A)** Representative immunohistochemical staining images of HDAC3 protein in 2 NPs and 4 NFPAs. **(B)** HDAC3 immunostaining was quantified on the basis of color intensity of converted photos (40x) to a subtractive color model CMYK and split into green/red/yellow/blue channels. The intensities were averaged from 100 selected nuclei. **(C)** Representative immunohistochemical staining images of HDAC2 protein in 2 NPs and 2 NFPAs. **(D)** HDAC2 immunostaining was quantified on the basis of color intensity of converted photos (40x) to a subtractive color model CMYK and split into green/red/yellow/blue channels. The intensities were averaged from 100 selected nuclei. NP, normal pituitary; NFPA, non-functioning pituitary adenoma; *P < 0.05; **P < 0.001.

cancers, but is also often associated with cancer cell dedifferentiation (12, 17) and overall survival rate of patients (35, 36). However, the role of HDAC family members in the pathogenesis of human pituitary adenomas, a non-malignant neoplasm, has not been previously studied to our knowledge. Our study revealed the involvement of histone deacetylation in the pathogenesis of human NFPAs for the first time and provides a rationale for pursuing HDAC suppression as a possible therapeutic target.

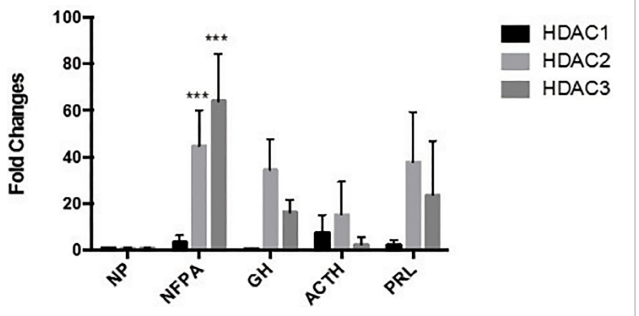

FIGURE 3 | The expression of HDAC family HDAC1, HDAC2 and HDAC3 in different types of pituitary tumors. HDAC family number HDAC1, HDAC2 and HDAC3 expressed in normal pituitary (NP, n = 11) and clinically non-functioning pituitary adenomas (NFPA, n = 22), growth hormone secreting tumors (GH, n = 6), adrenocorticotropic hormone secreting tumors (ACTH, n = 6) and prolactin secreting tumors (PRL, n = 6), ***P < 0.0001.

In our study, treatment of PDFS cells with the HDAC3 inhibitor RGFP966 resulted in a 70% suppression of cell proliferation at 96 hours. Consistently, HDACs have been shown to control cell growth, differentiation, and apoptosis by regulating histone modification and acetylation of transcription factors including as p53 and E2F (37, 38). Multiple mechanisms have been revealed for HDAC3-mediated growth regulation. In colon cancer cells, silencing of HDAC3 expression by RNA interference (RNAi) resulted in growth suppression, accompanied by increased expression of p21 and apoptosis (39). In acute myeloid leukemia (AML), oncogenic protein c-myc recruits HDAC3 to form a suppressive complex binding to the promoter of miR-451 gene, inhibiting the expression of this tumor suppressive microRNA (40). Wells et al. showed that in cutaneous T cell lymphoma cells, HDAC3 was associated with chromatin around DNA replication forks; and inhibition of HDAC3 significantly reduced DNA replication, disrupting cycling of tumor cells (41). Moreover, all Class 1 HDACs, including HDAC2 and HDAC3, are known to down-regulate p53 by deacetylation at KK373/K382, reducing the binding of p53 to the promoters of its downstream targets such as p21 (42, 43). Consistent with these results, we have shown here that HDAC3 inhibition led to activation of several tumor suppressors, including EGR1, PTEN, STAT1, all downstream targets of p53. In addition, suppression of HDAC3 also resulted in the upregulation of MEG3, a lncRNA tumor suppressor specifically silenced in NFPAs, as well as components in the Rb signaling pathway such as P16 and E2F1, both of which have been suggested to be involved in the pathogenesis of NFPAs.

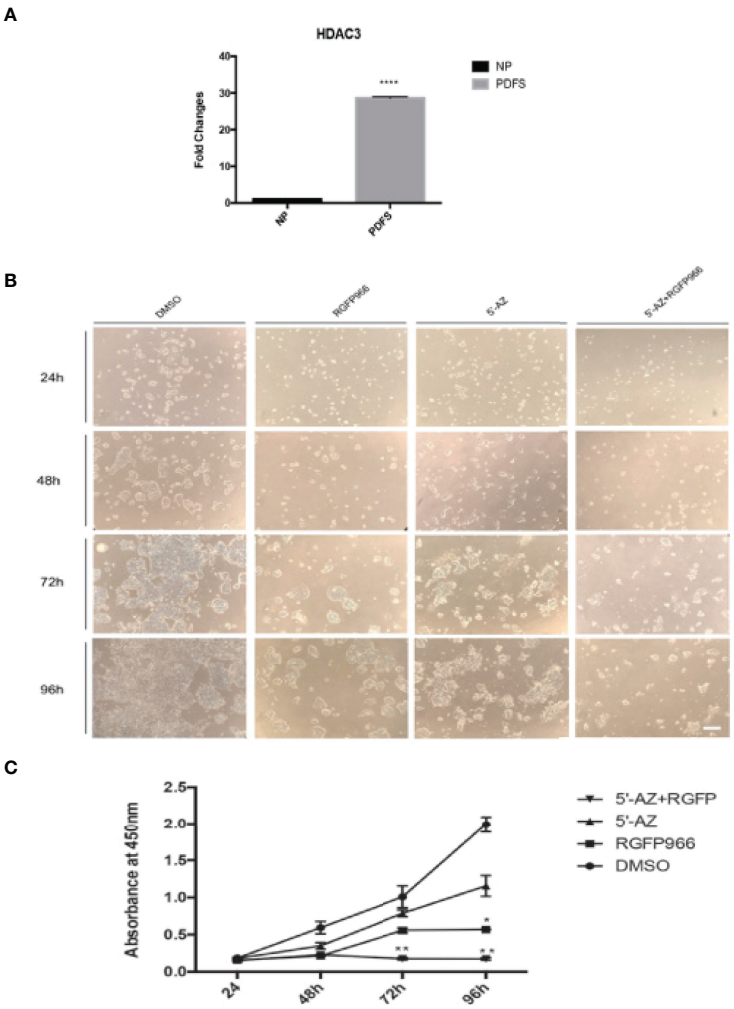

FIGURE 4 | HDAC3 inhibition and DNA demethylation decreases PDFS cell proliferation. **(A)** HDAC3 expression in PDFS cells and normal pituitary. ****p < 0.00001. **(B)** PDFS treated with HDAC3 inhibitor RGFP966 (10 μM) and DNMT inhibitor 5'-AZA (1 μM), alone and in combination, at 24, 48, 72, and 96 hours. DMSO was added as a control. **(C)** Growth curves of PDFS cells as determined by CCK8 Assays. *P < 0.01; **P < 0.001; ****P < 0.00001. Scale Bar = 100μm.

In addition, epigenetic regulation of protein expression of P16, PTEN, and STAT1 has been well documented (44–46). As deacetylation and demethylation are global events, several studies have explored the epigenomics of pituitary adenomas, as summarized in a few excellent recent reviews (47, 48). Our results are consistent with these global transcriptomic analyses. Taken together, our data strongly suggest a role of HDAC3 in the development of NFPAs.

TABLE 1 | Induction of MEG3 expression by 5'-AZA and RGFP966.

Treatment	MEG3(Mean Fold Change)	SD	*P* Value
DMSO	1	0.110	
5'-AZA	28842	585.362	<0.0001
RGFP966	9	2.890	0.0084
5'-AZA+RGFP966	135512	1709.604	<0.0001

Histone modifications and DNA methylations are two important layers of epigenetic regulation and are often connected. There are many studies exploring the involvement of DNA methylations in pituitary adenomas, but substantial investigations of histone modification are yet to be done in pituitary tumors. After we found the increase expression of HADC2/3 in these tumors and observed changes in gene expression by the inhibitor RGF966, it is logical to explore the combined effect of RGP966 and 5'-AZA so we would see the corporative or synergistical functions of histone modifications and DNA methylations in pituitary tumors. Indeed, the combination of HDAC3 inhibitor RGFP966 with a DNA demethylation reagent, 5-aza-2-deoxycytidine, synergistically enhanced the expression of several tumor suppressors such as p16, PTEN, STAT1, CD40, and large non-coding RNA MEG3, accompanied by growth suppression. These data further emphasize the importance of epigenetic abnormalities in

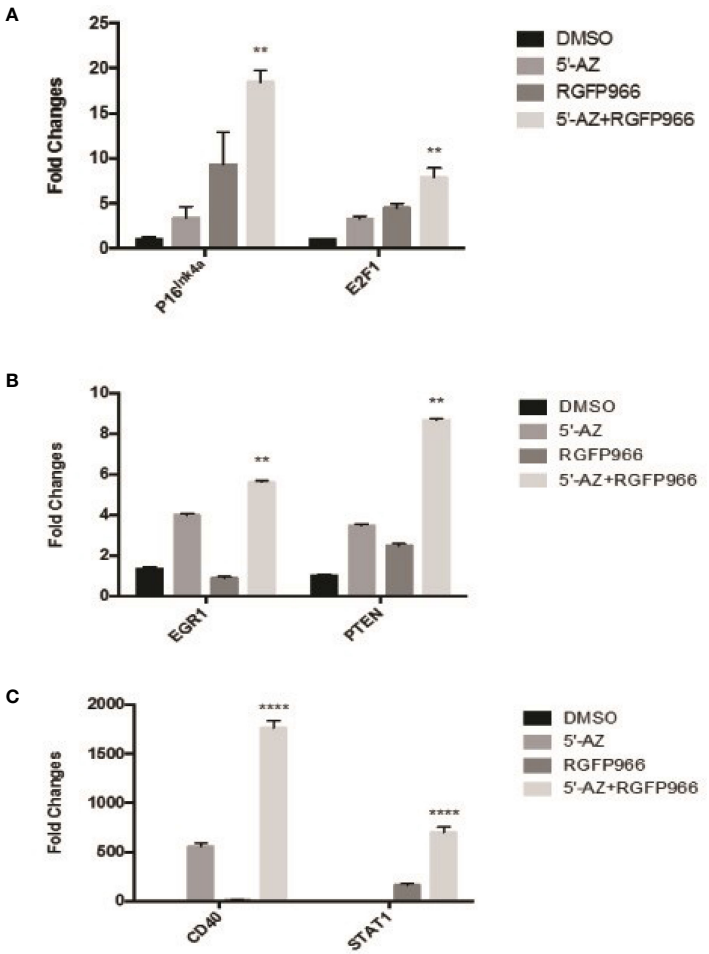

FIGURE 5 | The expression of tumor suppressors induced by HDAC3 and 5'-AZA. **(A)** Induction of E2F1, $P16^{Ink4a}$ by 5'-AZA and RGFP966. **(B, C)**: The expression of EGR1 and PTEN **(B)**, and CD40 and STAT1 **(C)** induced by 5'-AZA and RGFP966. **p < 0.001, ****p < 0.00001.

human NFPAs. A future study should investigate the combined effects of histone modification and DNA demethylation on global transcriptomic changes to understand the mechanisms by which histone modification and DNA demethylation regulate tumor growth. Because of the pivotal roles of HDACs in cancers, they have become targets for the development of novel cancer therapies. Indeed, Class 1 HDACs are targets for several cancer treatment drugs currently in use (49, 50). Some recently

TABLE 2 | Changes in gene expression changes by 5'-AZA and RGFP966 treatment.

Genes	Category	DMSO (Mean ± SD)	5'-AZA (Mean ± SD)	RGFP966 (Mean ± SD)	5'-AZA + RGFP966 (Mean ± SD)
CCNB1	Cell cycle	1.001 ± 0.071	1.732 ± 0.0484	1.194 ± 0.081	0.930 ± 0.0169
CDK1	Cell cycle	1.001 ± 0.030	0.396 ± 0.257	1.356 ± 0.113	1.051 ± 0.116
TSC1	Cell cycle	1.001 ± 0.037	1.327 ± 0.068	3.118 ± 0.532	1.791 ± 0.129
EGR1	TranscriptionFactor	1.340 ± 0.088	3.977 ± 0.097	0.884 ± 0.062	5.612 ± 0.077
C-JUN	TranscriptionFactor	1.038 ± 0.394	1.383 ± 0.049	2.322 ± 0.094	2.223 ± 0.072
STAT1	TranscriptionFactor	0.915 ± 0.001	1.920 ± 0.646	162.579 ± 14.801	698.954 ± 52.707
C-MYC	TranscriptionFactor	1.000 ± 0.014	2.604 ± 0.106	0.718 ± 0.069	2.074 ± 0.089
$P16^{Ink4a}$	CDK inhibitor	1.019 ± 0.247	3.417 ± 1.221	9.314 ± 3.570	18.485 ± 1.278
CD40	Membrane Receptor	1.264 ± 0.175	559.435 ± 31.045	9.534 ± 2.226	1762.570 ± 72.253
PTEN	Tumor suppressor	1.001 ± 0.053	3.473 ± 0.054	2.469 ± 0.101	8.676 ± 0.051
IL-6	Cytokine	1.008 ± 0.177	2.353 ± 0.055	3.730 ± 0.265	4.820 ± 0.0189
E2F1	P16 downstream	1.000 ± 0.0271	3.273 ± 0.280	4.484 ± 0.478	7.880 ± 1.051

developed HDAC inhibitors have shown promising results in preclinical studies, either working alone (51–55) or in combination with other compounds (56, 57). In addition, it has been reported that suppression of HDAC3 sensitized cancer cells that had developed resistance to chemotherapies (58, 59). These data, together with our data reported here, suggest that HDAC3 is a potential target for use in therapy of NFPAs. Further studies will be needed to confirm our findings, explore the mechanisms in detail, and validate our findings in animal models and other pre-clinical models.

DATA AVAILABILITY STATEMENT

The original contributions presented in the study are included in the article/**Supplementary Material**. Further inquiries can be directed to the corresponding author.

AUTHOR CONTRIBUTIONS

WZ: performing experiments, manuscript and figure preparations. XJ, KW, JM, EB, BW: performing experiments. E.TH-W, BS: critical clinical input and discussion. YZ, AK: study design, organization, and supervision. RS: critical scientific input and discussion, manuscript preparation. XZ: study design, organization, supervision, manuscript and figure preparation. All authors contributed to the article and approved the submitted version.

FUNDING

This work was supported in part by the National Institutes of Health (R01 CA193520 to AK and RS), and the Jarislowsky Foundation. None of the funding sources was involved in study design; in the collection, analysis and interpretation of data; in the writing of the report; and in the decision to submit the article for publication.

SUPPLEMENTARY MATERIAL

The Supplementary Material for this article can be found online at: https://www.frontiersin.org/articles/10.3389/fonc.2022.875122/full#supplementary-material

Supplementary Table 1 | Primers. *MGH-PGA Prime Bank: https://pga.mgh.harvard.edu/primerbank/.

REFERENCES

1. Ezzat S, Asa SL, Couldwell WT, Barr CE, Dodge WE, Vance ML, et al. The Prevalence of Pituitary Adenomas: A Systematic Review. *Cancer* (2004) 101 (3):613–9. doi: 10.1002/cncr.20412
2. Daly AF, Rixhon M, Adam C, Dempegioti A, Tichomirowa MA, Beckers A. High Prevalence of Pituitary Adenomas: A Cross–Sectional Study in the Province of Liege, Belgium. *J Clin Endocrinol Metab* (2006) 91(12):4769–75. doi: 10.1210/jc.2006-1668
3. Fernandez A, Karavitaki N, Wass JA. Prevalence of Pituitary Adenomas: A Community–Based, Cross–Sectional Study in Banbury (Oxfordshire, Uk). *Clin Endocrinol (Oxf)* (2010) 72(3):377–82. doi: 10.1111/j.1365-2265.2009.03667.x
4. Petersenn S. Management of Aggressive Pituitary Tumors – A 2019 Update. *Horm Metab Res* (2019) 51(12):755–64. doi: 10.1055/a-1060-1883
5. Kasuki L, Raverot G. Definition and Diagnosis of Aggressive Pituitary Tumors. *Rev Endocr Metab Disord* (2020) 21:203–8. doi: 10.1007/s11154-019-09531-x
6. Tatsi C, Stratakis CA. Aggressive pituitary tumors in the young and elderly. *Rev Endocr Metab Disord* (2020) 21:213–23. doi: 10.1007/s11154-019-09534-8
7. McCormack A, Dekkers OM, Petersenn S, Popovic V, Trouillas J, Raverot G, et al. Treatment of Aggressive Pituitary Tumours and Carcinomas: Results of a European Society of Endocrinology (ESE) Survey 2016. *Eur J Endocrinol* (2018) 178(3):265–76. doi: 10.1530/EJE-17-0933
8. Pease M, Ling C, Mack WJ, Wang K, Zada G. The Role of Epigenetic Modification in Tumorigenesis and Progression of Pituitary Adenomas: A Systematic Review of the Literature. *PloS One* (2013) 8(12):e82619. doi: 10.1371/journal.pone.0082619
9. Zhou Y, Zhang X, Klibanski A. Genetic and Epigenetic Mutations of Tumor Suppressive Genes in Sporadic Pituitary Adenoma. *Mol Cell Endocrinol* (2014) 386(1–2):16–33. doi: 10.1016/j.mce.2013.09.006
10. Minucci S, Pelicci PG. Histone Deacetylase Inhibitors and the Promise of Epigenetic (and More) Treatments for Cancer. *Nat Rev Cancer* (2006) 6 (1):38–51. doi: 10.1038/nrc1779
11. Stimson L, La Thangue NB. Biomarkers for Predicting Clinical Responses to HDAC Inhibitors. *Cancer Lett* (2009) 280(2):177–83. doi: 10.1016/j.canlet.2009.03.016
12. Morris MJ, Monteggia LM. Unique Functional Roles for Class I and Class II Histone Deacetylases in Central Nervous System Development and Function. *Int J Dev Neurosci* (2013) 31(6):370–81. doi: 10.1016/j.ijdevneu.2013.02.005
13. Lawlor L, Yang XB. Harnessing the HDAC–histone Deacetylase Enzymes, Inhibitors and How These Can be Utilised in Tissue Engineering. *Int J Oral Sci* (2019) 11(2):20. doi: 10.1038/s41368-019-0053-2
14. Muller BM, Jana L, Kasajima A, Lehmann A, Prinzler J, Budczies J, et al. Differential Expression of Histone Deacetylases HDAC1, 2 and 3 in Human Breast Cancer–Overexpression of HDAC2 and HDAC3 Is Associated With Clinicopathological Indicators of Disease Progression. *BMC Cancer* (2013) 13:215. doi: 10.1186/1471-2407-13-215
15. Halkidou K, Gaughan L, Cook S, Leung HY, Neal DE, Robson CN. Upregulation and Nuclear Recruitment of HDAC1 in Hormone Refractory Prostate Cancer. *Prostate* (2004) 59(2):177–89. doi: 10.1002/pros.20022
16. Ropero S, Esteller M. The Role of Histone Deacetylases (HDACs) in Human Cancer. *Mol Oncol* (2007) 1(1):19–25. doi: 10.1016/j.molonc.2007.01.001
17. Barneda–Zahonero B, Parra M. Histone Deacetylases and Cancer. *Mol Oncol* (2012) 6(6):579–89. doi: 10.1016/j.molonc.2012.07.003
18. Song J, Noh JH, Lee JH, Eun JW, Ahn YM, Kim SY, et al. Increased Expression of Histone Deacetylase 2 Is Found in Human Gastric Cancer. *APMIS* (2005) 113(4):264–8. doi: 10.1111/j.1600-0463.2005.apm_04.x
19. Weichert W, Roske A, Gekeler V, Beckers T, Ebert MPA, Pross M, et al. Association of Patterns of Class I Histone Deacetylase Expression With Patient Prognosis in Gastric Cancer: A Retrospective Analysis. *Lancet Oncol* (2008) 9(2):139–48. doi: 10.1016/S1470-2045(08)70004-4
20. Nakagawa M, Oda Y, Eguchi T, Aishima S-I, Yao T, Hosoi F, et al. Expression Profile of Class I Histone Deacetylases in Human Cancer Tissues. *Oncol Rep* (2007) 18(4):769–74. doi: 10.3892/or.18.4.769
21. Park YS, Jin MY, Kim YJ, Yook JH, Kim BS, Jang SJ. The Global Histone Modification Pattern Correlates With Cancer Recurrence and Overall Survival in Gastric Adenocarcinoma. *Ann Surg Oncol* (2008) 15(7):1968–76. doi: 10.1245/s10434-008-9927-9
22. Cao LL, Yue Z, Liu L, Pei L, Yin Y, Qin L, et al. The Expression of Histone Deacetylase HDAC1 Correlates With the Progression and Prognosis of Gastrointestinal Malignancy. *Oncotarget* (2017) 8(24):39241–53. doi: 10.18632/oncotarget.16843

23. Weichert W, Roske A, Niesporek S, Noske A, Buckendahl AC, Dietel M, et al. Class I Histone Deacetylase Expression has Independent Prognostic Impact in Human Colorectal Cancer: Specific Role of Class I Histone Deacetylases *In Vitro* and *In Vivo*. *Clin Cancer Res* (2008) 14(6):1669–77. doi: 10.1158/1078-0432.CCR-07-0990
24. Jiao F, Hu H, Han T, Zhuo M, Yuan C, Yang H, et al. Aberrant Expression of Nuclear HDAC3 and Cytoplasmic CDH1 Predict a Poor Prognosis for Patients With Pancreatic Cancer. *Oncotarget* (2016) 7(13):16505–16. doi: 10.18632/oncotarget.7663
25. He J, Shen S, Lu W, Zhou Y, Hou Y, Zhang Y, et al. HDAC1 Promoted Migration and Invasion Binding With TCF12 by Promoting EMT Progress in Gallbladder Cancer. *Oncotarget* (2016) 7(22):32754–64. doi: 10.18632/oncotarget.8740
26. Tang Z, Ding S, Huang H, Luo P, Qing B, Zhang S, et al. HDAC1 Triggers the Proliferation and Migration of Breast Cancer Cells *via* Upregulation of Interleukin–8. *Biol Chem* (2017) 398(12):1347–56. doi: 10.1515/hsz-2017-0155
27. Li L, Mei DT, Zeng Y. HDAC2 Promotes the Migration and Invasion of Non–Small Cell Lung Cancer Cells *via* Upregulation of Fibronectin. *BioMed Pharmacother* (2016) 84:284–90. doi: 10.1016/j.biopha.2016.09.030
28. Jiao F, Hu H, Yuan C, Jin Z, Guo Z, Wang L, et al. Histone Deacetylase 3 Promotes Pancreatic Cancer Cell Proliferation, Invasion and Increases Drug–Resistance Through Histone Modification of P27, P53 and Bax. *Int J Oncol* (2014) 45(4):1523–30. doi: 10.3892/ijo.2014.2568
29. Yin Y, Zhang M, Dorfman RG, Li Y, Zhao Z, Pan Y, et al. Histone Deacetylase 3 Overexpression in Human Cholangiocarcinoma and Promotion of Cell Growth *via* Apoptosis Inhibition. *Cell Death Dis* (2017) 8(6):e2856. doi: 10.1038/cddis.2016.457
30. Danila DC, Zhang X, Zhou Y, Dickersin GR, Fletcher JA, Hedley-Whyte ET, et al. A Human Pituitary Tumor–Derived Folliculostellate Cell Line. *J Clin Endocrinol Metab* (2000) 85(3):1180–7. doi: 10.1210/jc.85.3.1180
31. Malvaez M, McQuown SC, Rogge GA, Astarabadi M, Jacques V, Carreiro S, et al. HDAC3–Selective Inhibitor Enhances Extinction of Cocaine–Seeking Behavior in a Persistent Manner. *Proc Natl Acad Sci USA* (2013) 110(7):2647–52. doi: 10.1073/pnas.1213364110
32. Zhang X, Zhou Y, Mehta KR, Danila DC, Scolavino S, Johnson SR, et al. A Pituitaey–Derived MEG3a Isoform Functions as a Growth Suppressor in Tumor Cells. *J Clin Endocrinol Metab* (2003) 88(11):5115–62. doi: 10.1210/jc.2003-030222
33. Zhao J, Dahle D, Zhou Y, Zhang X, Klibansk A. Hypermethylation of the Promoter Region Is Associated With the Loss of MEG3 Gene Expression in Human Pituitary Tumors. *J Clin Endocrinol Metab* (2005) 90(4):2179–86. doi: 10.1210/jc.2004-1848
34. Gejman R, Batista DL, Ying Z, Zhou Y, Zhang X, Swearingen B, et al. Selective Loss of MEG3 Expression and Intergenic Differentially Methylated Region Hypermethylation in the MEG3/DLK1 Locus in Human Clinically Nonfunctioning Pituitary Adenomas. *J Clin Endocrinol Metab* (2008) 93 (10):4119–25. doi: 10.1210/jc.2007-2633
35. Minamiya Y, Ono T, Saito H, Takahashi N, Ito M, Motoyama S, et al. Strong Expression of HDAC3 Correlates With a Poor Prognosis in Patients With Adenocarcinoma of the Lung. *Tumour Biol* (2010) 31(5):533–9. doi: 10.1007/s13277-010-0066-0
36. Van Damme M, Crompot E, Meuleman N, Mineur P, Bron D, Lagneaux L, et al. HDAC Isoenzyme Expression is Deregulated in Chronic Lymphocytic Leukemia B–cells and has a Complex Prognostic Significance. *Epigenetics* (2012) 7(12):1403–12. doi: 10.4161/epi.22674
37. Marks PA, Richon VM, Rifkind RA. Histone Deacetylase Inhibitors: Inducers of Differentiation or Apoptosis of Transformed Cells. *J Natl Cancer Inst* (2000) 92(15):1210–6. doi: 10.1093/jnci/92.15.1210
38. Butler LM, Zhou X, Xu WS, Scher HI, Rifkind RA, Marks PA, et al. The Histone Deacetylase Inhibitor SAHA Arrests Cancer Cell Growth, Up–Regulates Thioredoxin–Binding Protein–2, and Down–Regulates Thioredoxin. *Proc Natl Acad Sci USA* (2002) 99(18):11700–5. doi: 10.1073/pnas.182372299
39. Wilson AJ, Byun DS, Popova N, Murray LB, L'Italien K, Sowa Y, et al. Histone Deacetylase 3 (HDAC3) and Other Class I HDACs Regulate Colon Cell Maturation and P21 Expression and Are Deregulated in Human Colon Cancer. *J Biol Chem* (2006) 281(19):13548–58. doi: 10.1074/jbc.M510023200
40. Su R, Gong JN, Chen MT, Song L, Shen C, Zhang XH, et al. C–Myc Suppresses Mir–451 Dash, verticalYWTAZ/AKT Axis *via* Recruiting HDAC3 in Acute Myeloid Leukemia. *Oncotarget* (2016) 7(47):77430–43. doi: 10.18632/oncotarget.12679
41. Wells CE, Bhaskara S, Stengel KR, Zhao , Sirbu B, Chagot B, et al. Inhibition of Histone Deacetylase 3 Causes Replication Stress in Cutaneous T Cell Lymphoma. *PloS One* (2013) 8(7):e68915. doi: 10.1371/journal.pone.0068915
42. Juan LJ, Shia WJ, Chen MH, Yang WM, Seto E, Lin YS, et al. Histone Deacetylases Specifically Down–Regulate P53–Dependent Gene Activation. *J Biol Chem* (2000) 275(27):20436–43. doi: 10.1074/jbc.M000202200
43. Zhao Y, Lu S, Wu L, Chai G, Wang H, Chen Y, et al. Acetylation of P53 at Lysine 373/382 by the Histone Deacetylase Inhibitor Depsipeptide Induces Expression of P21(Waf1/Cip1). *Mol Cell Biol* (2006) 26(7):2782–90. doi: 10.1128/MCB.26.7.2782-2790.2006
44. Xiao Z, He Y, Liu C, Xiang L, Yi J, Wang M, et al. Targeting P16INK4A in Uterine Serous Carcinoma Through Inhibition of Histone Demethylation. *Oncol Rep* (2019) 41(5):2667–78. doi: 10.3892/or.2019.7067
45. Stewart DJ, Nunez MI, Jelinek J, Hong D, Gupta S, Aldaz M, et al. Impact of Decitabine on Immunohistochemistry Expression of the Putative Tumor Suppressor Genes FHIT, WWOX, FUS1 and PTEN in Clinical Tumor Samples. *Clin Epigenet* (2014) 6(1):13. doi: 10.1186/1868-7083-6-13
46. Zhuang S. Regulation of STAT Signaling by Acetylation. *Cell Signal* (2013) 25 (9):1924–31. doi: 10.1016/j.cellsig.2013.05.007
47. Hauser BM, Lau A, Gupta S, Bi WL, Dunn IF. The Epigenomics of Pituitary Adenoma. *Front Endocrinol* (2019) 10:290. doi: 10.3389/fendo.2019.00290
48. Nadhamuni VS, Korbonits M. Novel Insights Into Pituitary Tumorigenesis: Genetic and Epigenetic Mechanisms. *Endocr Rev* (2020) 41(6):821–46. doi: 10.1210/endrev/bnaa006
49. Thangaraju M, Karunakaran SK, Itagaki S, Gopal E, Elangovan S, Prasad PD, et al. Transport by SLC5A8 With Subsequent Inhibition of Histone Deacetylase 1 (HDAC1) and HDAC3 Underlies the Antitumor Activity of 3–Bromopyruvate. *Cancer* (2009) 115(20):4655–66. doi: 10.1002/cncr.24532
50. Kikuchi J, Wada T, Shimizu R, Izumi T, Akutsu M, Mitsunaga K, et al. Histone Deacetylases are Critical Targets of Bortezomib–Induced Cytotoxicity in Multiple Myeloma. *Blood* (2010) 116(3):406–17. doi: 10.1182/blood-2009-07-235663
51. Fournel M, Bonfils C, Hou Y, Yan PT, Trachy-Bourget MC, Kalita A, et al. MGCD0103, A Novel Isotype–Selective Histone Deacetylase Inhibitor, has Broad Spectrum Antitumor Activity *In Vitro* and *In Vivo*. *Mol Cancer Ther* (2008) 7(4):759–6. doi: 10.1158/1535-7163.MCT-07-2026
52. Jin JS, Tsao TY, Sun PC, Yu CP, Tzao C. SAHA Inhibits the Growth of Colon Tumors by Decreasing Histone Deacetylase and the Expression of Cyclin D1 and Survivin. *Pathol Oncol Res* (2012) 18(3):713–. doi: 10.1007/s12253-012-9499-7
53. Minami J, Suzuki R, Mazitschek R, Gorgun G, Ghosh B, Cirstea D, et al. Histone Deacetylase 3 as a Novel Therapeutic Target in Multiple Myeloma. *Leukemia* (2014) 28(3):680–9. doi: 10.1038/leu.2013.231
54. Hsieh HY, Chuang HC, Shen FH, Detroja K. Targeting Breast Cancer Stem Cells by Novel HDAC3–Selective Inhibitors. *Eur J Med Chem* (2017) 140:42–51. doi: 10.1016/j.ejmech.2017.08.069
55. McLeod AB, Stice JP, Wardell SE, Alley HM, Chang CY, McDonnell DP. Validation of Histone Deacetylase 3 as a Therapeutic Target in Castration–Resistant Prostate Cancer. *Prostate* (2018) 78(4):266–77. doi: 10.1002/pros.23467
56. Peulen O, Gonzalez A, Peixoto P, Turtoi A, Mottet D, Delvenne P, et al. The Anti–Tumor Effect of HDAC Inhibition in a Human Pancreas Cancer Model is Significantly Improved by the Simultaneous Inhibition of Cyclooxygenase 2. *PloS One* (2013) 8(9):e75102. doi: 10.1371/journal.pone.0075102
57. Yoo GS, Yu JI, Park HC. Proton Therapy for Hepatocellular Carcinoma: Current Knowledges and Future Perspectives. *World J Gastroenterol* (2018) 24 (28):3090–100. doi: 10.3748/wjg.v24.i28.3090
58. Wood TE, Dalili S, Simpson CD, Sukhai MA, Hurren R, Anyiwe K, et al. Selective Inhibition of Histone Deacetylases Sensitizes Malignant Cells to Death Receptor Ligands. *Mol Cancer Ther* (2010) 9(1):246–56. doi: 10.1158/1535-7163.MCT-09-0495
59. Long J, Fang WY, Chang L, Gao WH, Shen Y, Jia MY, et al. Targeting HDAC3, A New Partner Protein of AKT in the Reversal of Chemoresistance

in Acute Myeloid Leukemia via DNA Damage Response. *Leukemia* (2017) 31 (12):2761–70. doi: 10.1038/leu.2017.130

Conflict of Interest: The authors declare that the research was conducted in the absence of any commercial or financial relationships that could be construed as a potential conflict of interest.

Publisher's Note: All claims expressed in this article are solely those of the authors and do not necessarily represent those of their affiliated organizations, or those of the publisher, the editors and the reviewers. Any product that may be evaluated in this article, or claim that may be made by its manufacturer, is not guaranteed or endorsed by the publisher.

Citation: *Zhao W, Jiang X, Weisenthal K, Ma J, Botticelli EM, Zhou Y, Hedley-Whyte ET, Wang B, Swearingen B, Soberman RJ, Klibanski A and Zhang X (2022) High Histone Deacetylase 2/3 Expression in Non-Functioning Pituitary Tumors. Front. Oncol. 12:875122. doi: 10.3389/fonc.2022.875122*

Advantages of publishing in Frontiers

OPEN ACCESS
Articles are free to read for greatest visibility and readership

FAST PUBLICATION
Around 90 days from submission to decision

HIGH QUALITY PEER-REVIEW
Rigorous, collaborative, and constructive peer-review

TRANSPARENT PEER-REVIEW
Editors and reviewers acknowledged by name on published articles

Frontiers
Avenue du Tribunal-Fédéral 34
1005 Lausanne | Switzerland

Visit us: www.frontiersin.org
Contact us: frontiersin.org/about/contact

REPRODUCIBILITY OF RESEARCH
Support open data and methods to enhance research reproducibility

DIGITAL PUBLISHING
Articles designed for optimal readership across devices

FOLLOW US
@frontiersin

IMPACT METRICS
Advanced article metrics track visibility across digital media

EXTENSIVE PROMOTION
Marketing and promotion of impactful research

LOOP RESEARCH NETWORK
Our network increases your article's readership